DEPARTMENT OF PURE & APPLIED CHEMISTRY

The Reconstruction of Fires Involving Highly Flammable Hydrocarbon Liquids

A Thesis Submitted in Fulfilment of the Requirements of

Doctor of Philosophy in Forensic Science

Forensic Science Unit

University of Strathclyde

Glasgow

April 1995

John David DeHaan

Advisors:

Prof. Brian Caddy, University of Strathclyde

Dr. Dougal Drysdale, University of Edinburgh

Prof. (Emeritus) Robert Anderson,

San Jose State University

ACKNOWLEDGEMENTS

This thesis would not have been possible without the contributions, support, and encouragement of many colleagues and friends, especially Prof. Brian Caddy of the Forensic Science Unit for taking the chance that a project could be carried out, not only as an external project by a full-time professional, but also one involving a singular aspect of forensic science that required the services of two external advisors. Those advisors, Dr. Dougal Drysdale of Edinburgh University and Prof. Robert Anderson of San Jose State University, and Prof. Caddy all generously provided invaluable support and encouragement. Peter Blevin of PBA Instruments, LaJolla, CA provided days of use of the Inframetrics Thermal Imaging System and considerable technical advice. Helmut Brosz of Helmut Brosz and Assoc. of Markham, Ontario provided access to that firm's Inframetrics system and operated it during both laboratory and field tests. Duane Matthews of the California Dept. of Consumer Affairs, Bureau of Home Furnishings Laboratory, loaned the YEW Thermocouple system, and Dr. Said Nurbakhsh, of the same laboratory conducted the fire studies of camping fuel. Fred Tulleners, Gary Davis, and Steve Scott of the Bureau of Forensic Services (BFS) and, especially, Laurence Harding provided irreplaceable assistance with data handling. Without them, all of this would still be held prisoner on floppy disks and computers across the State of California.

The California Criminalistics Institute staff, especially Nancy Masters, extended considerable efforts to allow me time to complete this study while maintaining a nearly normal schedule of CCI classes. Diane Conedy, Division of Law Enforcement Library Assistant, found all those obscure publications. Bureau of Forensic Services Chief Jan Bashinski and CCI Manager Victor Reeve allowed me the great flexibility in my schedule that made it possible to complete this project in the allotted time. Dr. Robin Holleyhead and his staff at Dr. J.H. Burgoyne and Partners provided welcome logistical support during my visits to Glasgow. The staffs of the forensic laboratories of San Diego PD and San Diego SO provided their facilities for some test sessions. Dr. J.H. Burgoyne, Dr. Georges Melhem, and John Lentini offered their advice and counsel on numerous occasions. Monty McGill and Joe Konefal of the State Fire Marshal provided the locations for many of the pool tests and both Monty and Ron Marley rendered assistance with those tests. My special thanks as well to Hugh Young and Jerry Chisum for their dedicated efforts in reviewing and editing the draft manuscript, to Annette Ayala for her assistance in preparing the manuscript, and to Stan Brown and Laurence Harding for their skillful help with graphics.

John David DeHaan

7 April 1995

Abstract

Highly flammable hydrocarbon liquids are involved in a high percentage of building fires, whether those fires are accidental or incendiary in origin. Their mere presence is often taken as proof of a particular fire cause by some investigators despite their limited knowledge of the behaviour of the vapours from these fuels as they spread and diffuse. They are sometimes assumed to vaporize completely and instantly upon exposure and to diffuse uniformly through any compartment. The available models address large scale spills in ambient conditions of sun and wind, which do not apply to typical building fires. This study addressed the problem of modelling the spread of vapours from small-scale (less than four litre) spills of highly flammable liquids by means of a series of overlapping and complementary experiments, all of which dealt with the conditions found in most interior building fires (moderate temperatures, still air, and no sun).

It was determined that the surface area produced by a given quantity of liquid could be predicted for smooth, flat floors whose surfaces could be classified as non-porous (vinyl or painted wood), semi-porous (unfinished concrete or wood), or porous (carpet or sand). The type of surface also controlled the evaporation rate (per unit area of the pool). Evaporation rates from surfaces such as carpet saturated with pentane were 1.5 times the rate for a free-liquid pool at the same temperature. A granular substrate such as sand produced a pentane evaporation rate twice that of a pentane liquid pool. This effect is not related to the roughness of the surface itself, but rather to the capillary drive within the matrix. Such a drive is stronger for granular matrices with a small void space (high packing density) and lower for those with larger void space.

The size of the pool also controls the evaporation rate (the mass loss rate per unit surface area). Smaller pools (0.05 – 0.1m diameter) exhibit much higher rates than do the larger ones (0.3m) in this study. This is due to the enhanced evaporation due to lateral flow of vapours from the edges of the pools. Larger pools have a large central quiescent area that does not contribute to the overall evaporation. Smaller pools have no such quiescent area and a higher initial rate. There are also predictable losses due to pouring and splashing of volatile fuels that are closely related to the vapour pressure of the liquid involved.

Vertical diffusion of n-pentane and hexane vapours is very slow when the vapours are being generated by evaporation from a pool. The heat lost to evaporative cooling results in a pronounced thermal gradient in the atmosphere above a pool that suppresses the vertical diffusion. The diffusion rates of pentane, hexane, and octane vapours can be predicted and the height at which an ignitable vapour/air mixture is present can be calculated. The vapours also exhibit a pronounced advective flow which spreads the vapours in a viscous, laminar fashion. The spread rate of this advective flow can be calculated and agrees well with experimental data.

The evaporation of n-pentane, hexane, and n-octane were found to be predictive of the evaporative behaviour of petrol and camping fuels, two of the consumer products more commonly encountered in fires. Petrol, with its high concentration of pentane-like hydrocarbons, evaporates at the same rate as does n-pentane, at least for the first 10 – 15min. Camping fuels are dominated by hexanes and their evaporative behaviour is very similar to that of the hexane studied in detail here. Octane contributes very little combustible

vapour at typical room temperatures due to its very low evaporation rates at these temperatures.

The behaviour of the flame propagation in vapour/air mixture layers is predictable. Layer ignition is found to produce some characteristic features that may be observed by a witness to the fire or that may produce burn patterns that survive the fire to be found by a diligent investigator. Unfortunately, estimates of the quantity of flammable liquid present and its distribution prior to the fire cannot be reliably made by examination of the burn patterns on carpet or floors after the fire, particularly if the fire was not suppressed for some time after ignition.

Finally, an operational model based on these findings is offered for the use of fire investigators. This model, while limited to incidents in closed compartments with no mechanical ventilation and limited activity, offers a means by which the physical distribution of ignitable vapours can be predicted as it varies with time. This enables the investigator to explore the viability of various hypotheses about the quantity and distribution of flammable liquids prior to a fire, the relative location (both vertical and horizontal) of a potential ignition source, and, most importantly, the time factors involved in the evaporation of a flammable liquid and distribution of its vapours.

Table of Contents

2 Experimental

Glossary

Advection: the horizontal transport (viscous flow) of vapours as a result of their density

Arson: the act of deliberately lighting a fire with malice and specific criminal intent; wilful fire raising with malice

Camping fuel: a straight-run naphtha fraction of petroleum distillation, typically ranging from n-pentane to n-undecane in range, flash point ≈–30°C

Evaporation rate: the rate at which volatile liquid is being lost from a pool or matrix per unit area (typically measured in g/min/m^2)

Flammable liquid: any ignitable liquid with a flash point (Tag closed cup) of 38°C or less, used here to describe most of the hydrocarbon fuels of interest

Highly flammable liquid: any ignitable liquid with a flash point below 32°C (U.K.)

Ignitable liquid: any volatile fuel with a flash point of less than 93°C (fuels categorized as either flammable or combustible liquids)

Mass loss rate: the rate at which volatile liquid is being lost from a pool or a matrix (typically measured in g/min)

Matrix: the combination of an substrate and the actively-evaporating liquid

Petrol: automotive motor fuel; automotive gasoline, a complex blend of alkanes, cycloparaffinic compounds, and aromatics, flash point below –40°C

Substrate: the absorptive material from which a volatile liquid can be evaporated

Key to Symbols Used

a = constant in Antoine relationship

A = constant in Wade

A_r = rate of absorption across surface

$\hat{A}$ = proportionality constant

b = constant in Antoine relationship

B = release rate

c = constant in Antoine relationship

c_o = initial concentration

C_a = concentration of species a

C_m = maximum molar concentration

C_p = specific heat capacity

d = depth of pool

D = diffusivity

e = base natural logarithm

Δ = buoyancy factor

e_d = evaporation rate in draught

e_s = evaporation rate in still air

E = constant in Antoine relationship

E_a = evaporation rate per unit area

E_t = total evaporation rate

F = constant in Antoine relationship

g = acceleration due to gravity

G_a = amount of gas absorbed

G_c = concentration of gas

h = heat transfer co-efficient

H_c = heat of combustion

H_v = heat of vaporization

J = mass diffusion rate

k_m = mass transfer co-efficient

k = thermal conductivity

K = draft parameter

L = leakage rate

m = mass

M = molecular weight

N = number of moles

n = constant

p = vapour pressure

p_0 = equilibrium vapour pressure

P = pressure

Ps = suction potential (capillarity)

Q = heat flux

q = heat flux

r = radius

r_0 = radius at time zero

R = gas constant

s = shape factor

S = speed of propagation of flame front

Sc = Schmidt number

t = time

T = temperature

u = average wind speed

U = overall (system) heat transfer co-efficient

v = velocity

V = volume

w = release rate

V.D. = vapour density

x = downwind dimension of rectangular pool

X = mole fraction

y = cross-wind dimension

z = distance from surface

σ = Stefan-Boltzmann constant

Δ = buoyancy

ϵ = emissivity

κ = von Karman constant

Ω = complex function defined by turbulent flow

I = complex gamma function

ρ = density

υ = kinematic viscosity

$\emptyset$ = conduction/convection balance factor

§ = constant

X = packing factor

μ = surface tension

$\sum$ = expansion factor

Note: The letter **A** preceding a Table or Figure number denotes location in Appendix A

INTRODUCTION

Section 1

1.1 Nature of Fire Losses Involving Flammable Liquids

1.1.1 Flammable Liquids in Accidental Fires

Fires involving flammable liquids constitute a significant problem for the fire service – both in their suppression and their investigation. Some of these fires are accidental, involving pre-existing pools of liquid (either in short-term storage or in use) in industrial or commercial situations. Some of them involve spills from leaks in pipes or tanks, overturned containers, structural failures, or even vehicular collisions. Because of the quantities of fuels involved, the extension of ignitable vapours into contact with ignition sources sometimes remote from the spill itself, and the intensity of the fire once ignited, these situations are very dangerous to the public and to responding fire service or emergency personnel and are very destructive to any residence, factory, store, or vehicle involved. The Fire Protection Association, for instance, reported that in 1992, of a total of 64,581 reported dwelling fires in the U.K., 1457 involved flammable liquids (and of those, 714 involved petrol). Of 42,856 fires in other types of buildings, 3141 were reported to involve flammable or combustible liquids.[Lewis, 1995] The California State Fire Marshal reported that over the period 1988 – 92, in California an average of 18,915 building fires of accidental origin were reported to have been initiated in flammable or combustible liquids each year (with petrol identified as the flammable liquid in about 75% of all these accidental fires). That number represents fully one-third of accidental fires, since over the same period, an annual average of 38,323 building fires of accidental origin were identified as having begun in wood, paper, cardboard, plastic, or other similar ordinary combustibles. [State Fire Marshal, 1995]

1.1.2 Flammable Liquids in Incendiary Fires

In addition, flammable liquids are involved in a large percentage of incendiary (deliberately set) and arson fires of buildings, vessels, and vehicles. (Arson is defined as the act of deliberately lighting a fire with malice and specific criminal intent.) Such fires are a massive national problem in the U.S.. The National Fire Protection Association (NFPA) reported an estimated total of 84,500 incendiary and suspicious building fires in the U.S. in 1993, representing some 13.6% of all reported building fires.[Karter, 1994] Extensive review of the literature, however, reveals a paucity of information about the fuels first ignited in incendiary (deliberately lit) fires. The NFPA reported that over the period 1987– 91, an average of 9400 homes in the U.S. each year suffered fires involving petrol (automotive gasoline) as the fuel first ignited. Of those, one-half were incendiary or suspicious in origin. [Miller, 1994] In addition, there were an estimated 800 – 900 home fires involving Class 1C (flash point between 22.8 and 38°C) flammable liquids, with nearly one-quarter being incendiary or suspicious in origin. Informal enquiries were made by the author among many fire investigators across the U.S. during 1992 – 94. The consensus was that flammable and combustible liquids (often referred to as ignitable liquids) were used in perhaps one-half of all incendiary fires, and in a higher percentage in arson fires (those involving identifiable specific criminal intent) .

Ignition of available ordinary combustibles is the most common scenario for problem fire-setters, children, and vandals but flammable liquids of various types are more widely used by those setting fires for fraud, revenge, intimidation, or even as a means of murder or assault. This is

confirmed by data from the California State Fire Marshal's California Fire Information Reporting System (CFIRS). In the period 1988 – 1992, CFIRS reported that, each year, approximately 3700 incendiary fires and 650 suspicious fires involving buildings of all types were identified as having been ignited using ignitable liquids. This can be compared to approximately 3875 incendiary and 3840 suspicious building fires (per year) where plastics, paper, cardboard, and/or wood were the first fuels ignited and another approximately 3950 incendiary and suspicious fires where the first fuel ignited was not identified or could not be determined.[State Fire Marshal, 1995]

In a 1988 study, the Home Office (U.K.) Standing Committee on Fire Prevention reported that 8.4% of deliberate or suspected deliberate fires began with the ignition of flammable liquids of some type.[Home Office, 1988] The NWFIU of the London Fire Brigades investigated 2469 fires in the years 1989 – 93, and determined 1252 to be deliberate. Of these, 225 fires involved the suspected use of a flammable liquid accelerant.[Gardiner, 1995]

Prince George's County, Maryland, which maintains one of the best local databases in the U.S., reports that in a typical year (1992), 404 set fires (involving 171 vehicles and 233 buildings) were reported where some 19% involve flammable liquids identified.[Estepp, 1993] In Los Angeles County, California, over the period 1989 – 92, 22.1% of the 16,849 incendiary fires (including trash dumpster fires) were identified as having been ignited with flammable or combustible liquids.[Reed, 1993]

Deliberately-set or incendiary flammable liquid fires are encountered in two predominant forms: the incendiary device, or a direct spill or pour followed by a separate ignition. An incendiary device may be defined as a container of flammable liquid or a chemical mixture capable of igniting

(generating heat or flames) with some means of ignition attached. It is nearly always some variant of a Molotov cocktail or petrol bomb — a breakable (glass) container with a source of ignition (open-flame fuse or wick, chemical incendiary, or electrical). It is intended to be launched by hand against the target, typically using less than one litre of liquid. One variation is a hybrid device using a larger metal container (4–20 litre) and a small explosive perforating device (high explosive or low-explosive pipe bomb). The explosion usually serves only to disperse the fuel (usually petrol) as a vapour and aerosol, since the fuel is being pushed away from a very short-lived ignition source. Hot (incandescent) metal fragments from the container serve to ignite the vapour produced.[DeHaan, 1991] Such devices are rare in the U.S. but are more common in terrorist attacks in the U.K. and other countries. Devices incorporating a quantity of flammable liquid in a drum, bottle, or plastic trash bag accompanied by a simple time-delay ignition device (such as time fuse or wick) are encountered more frequently. The U.S. Treasury Department reported 725 "actual and attempted" incendiary device incidents in the United States in 1993 (and a total of 2799 for the years of 1989 – 93). Virtually all of the "actual"devices (714 in 1993) involved flammable liquids in a device of some type.[U.S.Treasury Dept., 1994]

The second form of flammable liquid use is far more common than any "device": the direct pour or spillage of a quantity of flammable liquids followed by direct ignition. In one study by the author, only 12.3% of the arson cases examined involved the use of any type of identifiable ignition device. The most common scenario was the direct pour of liquid followed by match ignition, which was the mechanism identified in 61.2% of the arson cases submitted to the (Department of Justice) forensic laboratory over a three-year period.[DeHaan, 1979] Such cases typically involve the pouring of the

amount one person can carry easily without attracting undue attention, usually 3–20 litres.[DeHaan-1991] Such a quantity is more than enough to kindle a very large fire in a room with a "normal" fuel load of furnishings, carpet, draperies, and the like. If the fuel is adequately distributed, and the room is adequately ventilated, a fast-spreading, very destructive fire nearly always results. Fortunately for the fire investigator, such incidents often result in incomplete destruction of the target (at least for buildings) and subsequent detection of unburned flammable liquid accelerants in the fire debris. One study by the author revealed that in some 347 cases submitted to the forensic laboratory, petrol (automotive gasoline) was detected in 31% of them, other petroleum distillates were detected in 13%, and other highly flammable liquids (alcohols, ketones, lacquer thinners, etc.) were detected in 6%.[DeHaan, 1979]

1.2 Fire Investigation and Reconstruction

The complete investigation of a fire involves more than simply establishing its origin and cause; it entails reconstructing the circumstances of the fire's ignition and spread. It is well known that the pouring or spillage of a volatile fuel results in the evaporation of some quantity of that fuel into the vapour state. That vapour mixes with air to some degree. When that mixture reaches a certain concentration, i.e., falls within the flammability range for that fuel vapour in air, *and* comes into the vicinity of a suitable ignition source, ignition occurs. The flame front moves through the vapour/air mixture in a deflagration whose flame speed, extension, and overpressure resulting from the expanding gases depend on the shape, concentration, and extent of the vapour distribution, as well as on the shape,

complexity, and the confining effect of any surrounding enclosure. In those fires involving volatile liquid fuels, the vapours created by the evaporation of the liquid prior to ignition are the critical element of the ignition and initial spread of the fire. Only that fuel that is in the vapour state prior to ignition is available for contact with an ignition source, whether that source is intentional (such as a match) or accidental (such as a pilot light, hot water heater burner, electric motor brush arc, switch or thermostat spark, or hot surface).

The fire investigator is sometimes expected to determine the sequence and time interval between the exposure of a volatile fuel and its ignition. The ignition source responsible need not be in the immediate area of the liquid pool itself because the vapours can be spread by convection, diffusion, air currents, or mechanical movement. In fires occurring out of doors, the wind plays a dominant role in spreading volatile vapours and mixing them with air. Because the largest percentage of "cause unknown" fires occur indoors, wind is not often a factor. Except for areas in the near vicinity of doors or heating/ventilation/air conditioning (HVAC) openings, the expected linear air movement in a normal room is limited (<1m/s). Also, some incendiary fires and accidental fires start in basements (where thermal gradients may further reduce circulation) or in unoccupied buildings where there is no operating heating/ventilation equipment or power to run it. With limited mechanical movement of air, the predominant mechanisms for vapour spread will be diffusion and natural convection. The roles of diffusion and convection in spreading fuel vapours may not be appreciated by many fire investigators. The vapours of the most common fuels are heavier than air and will tend to form a layer at the floor of the compartment. The depth of this layer will depend on the quantity, vapour pressure, and temperature of

the fuel involved and the density of its vapour, as well as the time between release of the liquid fuel and the ignition of its vapours.

A mail survey of fire investigators in the U.S. and Australia conducted by this author yielded responses concerning some 50 cases in which flammable liquid vapours were identified as the cause of deflagrating explosions in structures (Appendix B). It was clear from the responses that, while it was a matter of routine to identify the fuel and its source and, in most cases, to identify a likely ignition source, efforts to establish the time lapse between the release of the fuel and its ignition were almost never successful. This will be explored in more detail in Section 4.10 of this thesis.

The statements of witnesses, victims, or persons suspected of involvement in setting a deliberate fire as to the circumstances of ignition and flame spread are sometimes invaluable in reconstructing the time sequence of a deflagration. It is the responsibility of the investigator to corroborate these statements with observed indicators and other information about the fire. Only by understanding the underlying mechanisms of evaporation, diffusion, and layer formation and movement can the investigator hope to predict the events and time factors involved in flammable liquid fires. The investigator must be able to answer a number of hypothetical challenges on the way to a solution. If a liquid is spilled at a certain time, how long will it be before it forms an ignitable vapour in the immediate vicinity? If there is a possible source of ignition some distance from the spill, can vapours reach it, and if so, how much time must elapse before they reach ignitable concentrations? If the ignition source is above or below the spill, can vapours reach the source? If various quantities are spilled, how large a pool will form? How much total vapour will be produced with time from spills of various quantities and at various temperatures? If a liquid is spilled on a tile floor, how quickly will it evaporate? Will it make a

difference if it is spilled on carpet, wood, or sand? These unknowns can be listed as follows:

1. Relationship between quantity of fuel and area of pool on various substrates.
2. Evaporation rate from that substrate.
3. Relationship between pool temperature and evaporation rate.
4. Volume of vapour generated by evaporation from pools of various sizes.
5. Volume of vapour generated by pouring and splashing.
6. Vertical diffusion of vapour in still air.
7. Horizontal spread of vapour in still air.
8. Underlying thermodynamics that control evaporation.
9. Evaporation of complex petroleum distillates.
10. Relationship between pools, fire behaviour, and post-fire indicators.

1.3 Limitations of Present Models

Sometimes the ignition source and time frame of a fire can be established from witnesses, video recordings, or other sources but the quantities cannot. Sometimes the effects of the resulting ignition and quantities of fuel used are known, but the ignition source and its location are not. The ability to estimate the time of formation, direction of movement, and height (depth) of ignitable vapour layers would be invaluable in the investigation of both accidental and incendiary fires. There is considerable material in the literature on the formation and spread of large vapour clouds from exterior spills.[Clancey,1977; Marshall,1977; VanUlden] and even models for their prediction.[Shaw/Briscoe, 1978; Fleischer,1980;

Melhem/Croce, 1995] These deal predominantly with large (1000 litre or more) spills of cryogenically liquified gases such as compressed natural gas (CNG) or pressurized fuels such as liquified petroleum gases (LPG) in exterior sites where wind is the dominant factor in the dispersion process. Such models also concentrate on deep spills on the ground or on water and not with shallow layers on wood, concrete, or carpet. The police or fire brigade fire investigator is more often faced with small (less than 20 litre) spills of liquids onto floor surfaces at ambient temperatures in still or nearly still environments where diffusion processes dominate. It is the objective of this study to provide fire investigators with a better understanding of accidental and incendiary flammable liquid fires by quantifying some of the factors influencing the formation of vapour layers of small spills of common flammable liquids at ordinary temperatures.

1.4 Fundamental Processes Involved in Layer Formation

The behavior of mixtures of vapours and gases, as well as the factors that influence their combustion, are well known. Most such fires involve a flame propagating though the vapour/air mixture from a single point source of ignition. Whether this fuel/air mixture is confined or not, such a deflagration produces quantities of heat (as both visible light and heat energy) and pressure that can be predicted based on the quantity of fuel involved and its concentration in the air. The effects of the pressure produced, of course, depend on the nature of the confinement. Deflagrating hydrocarbon vapour/air mixtures can produce devastating effects on structures, vessels, and vehicles. The processes that control the production and flammability of a vapour/air mixture will be reviewed briefly here.

1.4.1 Flammable Liquids

The flammable liquids under consideration in this study are those with a flash point below 22.8°C (73°F), i.e., those which constitute a fire hazard at ordinary indoor temperatures (10–30°C). Such liquids fall into NFPA classes 1A and 1B for flammable liquids, based upon NFPA No. 321, "Basic Classification of Flammable and Combustible Liquids". These classifications are based on flash point measured by Tagliabue (Tag) Closed Cup Tester (described in ASTM D56) as specified in NFPA No. 321.[McKinnon, 1976] Fuels with a flash point of 32°C or less are considered Highly Flammable Liquids under the U.K. classification scheme. The fuels under consideration are those that are liquids at ordinary temperatures and atmospheric pressure (1 Bar), and therefore, cryogenic liquids such as CNG or evaporating pressurized fuels such as LPG will not be considered here. The fuels most commonly encountered in structure and vehicle fires that meet these criteria are: acetone, methanol, petroleum ether, toluene, hexane, petrol (automotive gasoline), and camping fuel (an unleaded, straight-run naphtha fraction petroleum distillate used to fuel camping stoves and lamps). These will be the primary focus of this study.

Petrol (automotive gasoline) is the single most commonly encountered flammable liquid in accidental and incendiary fires (and found in both building and vehicular incidents). It is a complex mixture of more than 100 hydrocarbons (and often oxygenated compounds such as ketones, alcohols, and ethers in small quantities) that usually has a boiling point range of 40 – 190°C (100 – 400°F).[DeHaan,1991;Sanders/Maynard,1968] The boiling point range and vapour pressure (and therefore flash point) can vary with geographical location and time of year. Other sources list average ranges of

28 – 207°C for winter blends and 32 – 209°C for summer blends of unleaded petrols in the U.S.[Kirk-Othmer, 1985] Petrol sold in cold climates or at low altitudes has a higher concentration of light alkanes and iso-alkanes (including up to 8% butane in areas with severe winters) than those sold for use at high altitudes, in hot weather, or in pollution-controlled areas.[Melhem,1992] Other changes to basic formulation or additive packages are made to accommodate environmental restrictions. The elimination of lead additives from most automotive fuels in recent years is an example.

When petrol is exposed to air at ordinary temperatures, the evaporation is progressive with the lightest (lowest boiling point) compound evaporating first, followed successively by heavier and heavier compounds. At first, the evaporating species is almost entirely butane, iso-butane or n-pentane. As the process continues, the hexanes, benzene, toluene, xylenes, and heavier alkanes follow in sequence. As a result, the gas chromatographic profile of the remaining petrol changes dramatically with time. This effect is often seen in the partially evaporated petrol recovered from fire debris. [DeHaan/Fultz, 1992] The process is the same whether the petrol ignites or not. Mann, in his study of chromatographic profiles of petrol, determined that the sequence of loss proceeded in the same order in both burning petrol and in petrol evaporating at room temperatures. Only the time scale was affected by the radiant heat incident on the pool, the burning pool evaporating at a much faster rate.[Mann, 1990] Since it has such a significant effect on the evaporation rates of complex fuels, this progressive evaporation will be studied briefly as part of this enquiry. Each of the flammable liquids of concern to the fire investigator has a number of physical and chemical properties that critically influence their role as fuels.

1.4.2 Vapour Pressure

One of the major factors controlling the evaporation of a liquid is its vapour pressure. At equilibrium between liquid and vapour, the vapour pressure, p_o , is calculated from the Antoine relationship:

$\log_{10} p_o = a - b/(T+c)$ where T = temperature (°C) and a,b, and c are constants which have a different value for each compound [Dean, 1985] or in the form:

$\log_{10} p_o = (-0.2185\ E/T) + F$ where T is the temperature in K and E and F are constants which have a different value for each compound [Drysdale]

The a,b, and c factors commonly offered in the literature are:

n-pentane, a= 6.85296, b = 1064.84, c = 233.01

n-hexane, a = 6.87601, b = 1171.17, c = 224.41

n-octane, a = 6.91868, b = 1351.99, and c = 209.15).[Dean]

The vapour pressure of pentane, hexane, and octane were calculated over the temperature range of interest here using those values. (Fig. 1.1). These vapour pressure plots give generally accurate estimates for flash points and boiling points of these alkanes, and agree with the formulae and constants used in many references. For comparison, the average Reid vapour pressures for petrol in the U.S. are 645mm for winter grades and 502mm for summer grades (at 38°C).[Kirk-Othmer].

At equilibrium the Gibbs free energy of the substance is the same in both systems (liquid and vapour) but the Gibbs free energy at the interface is pressure, temperature, and surface contour dependent.[Fried, 1977] The vapour pressure of a liquid in any system is therefore dependent on the

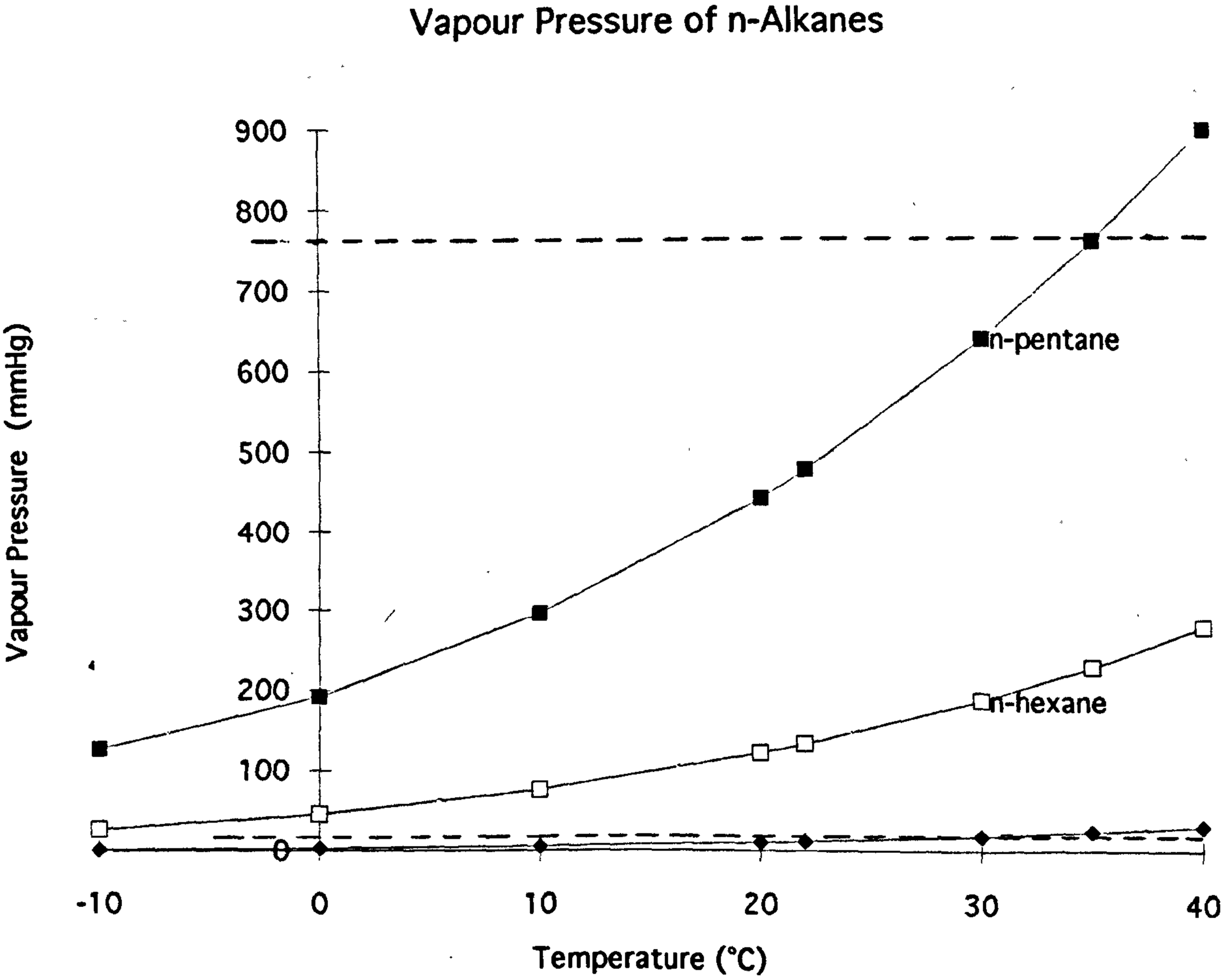

Fig.1.1 Vapour Pressure (mmHg) of n-pentane, n-hexane, and n-octane calculated for the temperature range –5 to 40°C. Vapour pressure corresponding to 760mmHg (boiling point) and 15mmHg (2% lower explosive limit) are dashed lines. (After Dean).

temperature, surface tension, and the shape of the surface. The higher the temperature, the lower the surface tension and thereby, the higher the vapour pressure. A flat surface has a higher vapour pressure than a concave one. A convex surface has a higher vapour pressure than a flat one and the smaller the radius of curvature of the surface, the higher the vapour pressure.[Fried] This is especially important in examining the combustion properties of mists and aerosols where the smaller the droplet, the faster its evaporation, and the less stable it is. In the present study, the fuel may be in a pool with a flat surface or it may be spread thinly across a convoluted surface with a large surface area having many elements of small radius, e.g., the filaments, threads, and yarns of a carpet or grains of sand. The capillary forces between a liquid and adjacent small elements of a complex matrix such as sand or carpet may also affect the vapour pressure.

1.4.3 Surface Area of Pools

The surface area of an exposed pool of an evaporating liquid will have a direct effect on the evaporation rate — the larger the surface area, the greater the total mass loss rate (g/ min). A model to predict pool size from the volume of liquid released would be useful. Such a model would depend on the relationship of gravity acting on a mass of liquid that represents the initial instantaneous release volume. Shaw and Briscoe claim that a pool of liquid that is simultaneously spreading and evaporating may be represented by the set of equations:

$$V_t = V_o + Bt - m_t/\rho$$

$$dm/dt = \pi r^2 \rho w$$

$h = V_t/\pi r^2$

$dr/dt = (2g\Delta h)^{0.5}$ [Shaw/Briscoe]

where r = radius of pool (m),

g = acceleration due to gravity ($m\text{-}s^{-2}$),

h = height of cylinder of liquid (m),

V_t = volume of liquid present at time t (m^3),

V_0 = volume of liquid present at time t = 0,

w = regression rate of the surface of the pool formed (m/s)

m_t = mass of liquid (kg) of density ρ (kg/m^3) which has evaporated to time t,

B = release rate (m^3/s),

Δ = buoyancy factor (when the release is onto a liquid surface)

It is difficult to solve these equations simultaneously. Approximate analytic solutions are possible, and one approach uses the numerical technique of the SPILL program.[Fleischer] A simpler approach is to assume that the spread can take place before there is substantial evaporation, and treat r and m_t as independent variables.

Since the buoyancy factor, $\Delta = g[1 - \rho_l / \rho_w]$, this simplifies to g for liquid spills on land.

Integrating dr/dt for an instantaneous spill of volume V_0 yields:

$r^2 = (8g\Delta V_0/\pi)^{0.5}t + r_0^2$ where r_0 is the initial radius.

Depending on the nature of the viscosity of the spreading liquid, there are two flow regimes that can influence the spread rate, according to Melhem.[Melhem/Croce] In the first regime, the force of gravity and liquid

inertia are dominant. In the second, the viscous drag becomes important and must be taken into account. Melhem introduces a shape factor, s, which defines the liquid pool height at its edge. A value of s = 0 corresponds to a pool edge depth of zero. Values of s between 0 and 1 indicate a pool that is thick in the middle and thin at the edge. Values of s between 1 and 2 indicate a pool that is thin in the middle and thick at the edge, and values of s greater than 2 indicate a pool with a hole in the middle. With this correction factor for acceleration, the equation above for a liquid spreading on a non-absorbent solid surface becomes:

$$r^2 = [8g(1-s)V_0/\pi]^{0.5}t + r_0^2$$

With liquids of low viscosity such as pentane, hexane, or petrol, the shape of the pool quickly becomes almost uniform in depth (s =1), but that solution is trivial for this equation. Correlation of pool area versus initial volume and time depends on experimentally determining a value of s which fits the data. This model is only valid for spills of non-volatile liquids on non-porous surfaces.

Spills of volatile fuels require use of the more complex solution where V_0 is reduced by the evaporation term , mt/ρ. For large spills, the time required to reach maximum area will be large and the term mt/ρ will be significant. For small spills of low viscosity liquids of the type being considered here, the time of most significant spread will be short, less than two minutes, and the correction term may be disregarded.

For spills on porous surfaces, the volume of spreading liquid is also reduced by the volume being absorbed into the surface covered by the pool. Melhem discusses penetration into soil, and concludes that a simplified model that assumes liquid penetration to behave as saturated piston flow

influenced only by gravitational forces is adequate for most situations. This results in the penetration depth being directly dependent on the intrinsic permeability of the soil and elapsed time. [Melhem/Croce] While values of permeability are available for sands and soils under various conditions, they are not available for floors of wood or concrete, or floor coverings such as carpet. Therefore, penetration into such surfaces cannot be modelled by this method. Once again, since the time of spread for small spills is likely to be very short, this penetration may be disregarded or may be determined empirically. For purposes of this discussion, pools may be defined as the area covered by a free-standing liquid atop a substrate, or as the area of a porous substrate that has been visibly wetted by the absorbed liquid.

1.4.4 Evaporation Rate

Only the fuel that is in the vapour state at the time of ignition can contribute to the initial spread of the fire. Once the area of the pool can be established, the controlling factor of vaporization from the surface is the evaporation mechanism. The evaporation rate of volatile liquids has been the subject of numerous studies over a period of many years. Early studies focused on establishing empirical mathematical formulas relating evaporation rate to surface area and wind speed.

Wade examined in great detail the limited case of a fixed area of an evaporating liquid exposed to a moving air stream.[Wade, 1942] It was claimed that in still air (described as natural convection) evaporation, e_s, could be described as:

$$e_s = A\,(p_e - p_d)^{1.25}$$

and E_t, total evaporation in a draught, would be:

$$E_t = e_s + W(p_e - p_d)v^n = A(p_e - p_d)^{1.25} + W(p_e - p_d)v^n$$

where v = velocity of the imposed draught,

p_e = equilibrium vapour pressure,

p_d = vapour pressure in incoming draught,

and A, W, and n are constants to be determined empirically.

It was argued that the role e_s plays is not constant with increasing draught and suggested the form:

$$E_t = Ke_s + W(p_e - p_d)v^n = K[A(p_e - p_d)^{1.25}] + W(p_e - p_d)v^n$$

where K is a suitable parameter that is a function of the forced draft. He gathered a great deal of data in wind-tunnel tests of water, acetone, benzene, ethyl acetate, toluene, trichloroethylene, and carbon tetrachloride at various temperatures (and thereby at different vapour pressures) and at different wind speeds. He did demonstrate that for natural convection (no draft) where $p_d = 0$, the linearity of log e_s v. log vapour pressure (p_e) reflected the relationship

$$e_s = K\ p_e^{1.25} \quad .$$

Taking the ratio of rate of evaporation per unit pressure against molecular weight (M), he empirically derived the relationship:

$$e_s = (9.8 \times 10^{-7})\ M^{0.71} p_e^{1.25} \quad \text{for still air.}$$

With forced convection with a draft of velocity v, the same process yielded:

$$e_d = (1.57 \times 10^{-7})\, M^{0.71}\ p_e v^{0.85}.$$

It should be noted that all Wade's data and calculations dealt with the

condition of a fixed pool 8.9cm x 8.9 cm. The final relationship was generalized to include situations where the "incoming" draft would have significant quantities of the evaporating liquid already in it (such as the relative humidity of air when examining the evaporation of water), i.e., where $p_d > 0$. The final expression was :

$$E_t = 10^{-7} M^{0.71} \{[9.8 \log^{-1}(-0.011v)](p_e - p_d)^{1.25} + 1.57 v^{0.85}(p_e - p_d)\}$$

When Pasquill examined the evaporation of liquids in turbulent air flows, he pointed out that the "...molecular weight term $M^{0.71}$ [was] a form of expression which cannot be regarded as possessing physical significance".[Pasquill, 1944] Studying evaporation of water and complex organic chemicals from saturated filter paper, based on first principles and Sutton's extensive work on turbulent flow [Sutton, 1934] he offered the relationship for evaporation from a pool of dimensions x and y into moving air:

$$E_t = \Gamma u^{[(2-n)/(2+n)]} x^{2/(2+n)} y$$

where E_t = total evaporation rate,

u = the average wind speed ,

x = down-wind dimension of a rectangular pool,

y = cross-wind dimension of pool,

n = an empirical constant,

Γ = a complex gamma function that depends on ν , the kinematic viscosity of air, and a turbulence factor related to the height above the surface.

He showed that the relationship between evaporation rate, E_t and T could be approximated as:

E_t proportional to $[M(p_s - p_a)]/T$

where p_s = saturation vapour pressure of the liquid, and

p_a = vapour pressure of the species in ambient (incoming) air but the fit to the data gathered by numerous investigators (including Wade) was better if a correction factor based on the diffusivity of the vapour in air (D_a) was incorporated:

$$E \text{ proportional to } \{M(p_s - p_a) D_a^{[2n/(2+n)]}\}/T$$

Correlating this to experimental results, the best fit for this equation was with n = 0.25. This value "...was appropriate to the customary one-seventh power law velocity profile" for turbulent flow above a plane surface.[Pasquill] This resulted in the final form of the relationship:

$$E = \Omega u^{0.78} x^{0.89} y \quad \text{for } n = 0.25$$

where Ω is a complex function determined by the kinematics of turbulent flow.

Pasquill cited work by Powell that showed the vapour pressure at the surface of water-saturated filter paper and similar materials was not appreciably different from that at a surface of free water. [Powell, 1942] That may be true for water, which presented an exception to every evaporation rate study, but not for hydrocarbons of much lower surface tensions and it may be the reason why the predictions of even Pasquill's corrected formula did not fit the experimental data. He also pointed out that the diffusion of heat, matter, and momentum can be regarded as being controlled by the movement of eddies or masses of fluid, which depends on molecular diffusion. He drew a parallel between the Peclet number for thermal diffusion : $\bar{u}z/\alpha$, where α is the thermal diffusivity and $\bar{u}z/D$, where D is the molecular diffusivity. He cites Elias who showed that thermal flux Q

from a flat heated plate into a moving air stream was proportional to $u^{0.8}x^{0.89}$ [Pasquill]

Clancey [1974] used the same formula in describing evaporation from a pool (of dimensions x and y) of volatile liquid:

$$E_t = \hat{A}\, u^{0.78}\, x^{0.89}\, y \quad \text{again with } n = 0.25$$

u = velocity of moving air stream.

x = down-wind dimension of pool,

y = cross-wind dimension of pool, and

$\hat{A}$ = proportionality constant

This constant, $\hat{A}$, is proportional to $B\upsilon^{[2n/(2+n)]\ [4(1-n)/(2+n)]}$

where $B = MpD^{[2n/(2+n)]}/RT$,

υ = kinematic viscosity of air (cm^2/s),

κ = von Karman constant (0.4),

M = molecular weight,

p = vapour pressure (mmHg),

R = gas constant,

T = absolute temperature (K), and

D = diffusivity (cm^2/s).

He inserted numerical values into these, again with n = 0.25, and concluded:

$$E_t = (1.2 \times 10^{-10})(Mp/T)u^{0.78}x^{0.89}\, y$$

with all quantities in CGS units.[Clancey, 1974]

This relationship is often cited in the literature as the controlling model for a flammable liquid evaporating in an air stream. Unfortunately, it is only

valid for situations where the draught-induced evaporation dominates over diffusion, i.e., where u is greater than one m/s. It also assumes that the vapour pressure of the evaporating liquid is sufficiently low for heat transfer from the air and ground to be sufficient to replace the heat lost to vaporization and that the surface temperature of the liquid is the same as that of the bulk liquid. These assumptions may not be valid for many volatile fuels of interest to fire investigators.

In their extensive evaluation of evaporative models, Melhem and Croce described the evaporation of a volatile liquid as dependent on two regimes within the liquid pool: a surface region and a bulk liquid below it as in Fig. 1.2.[Melhem/Croce] Energy lost to the evaporating phase cools the surface and heat must come from the bulk liquid to replace it. Heat is, in turn, transferred from the supporting surface to the bulk liquid. As the pool surface temperature decreases so does the vapour pressure of the evaporating liquid. It is the vapour pressure of the liquid that is the driving force behind evaporation, so any predictive model must take the surface temperature factor into account. The surface temperature is a function of the total heat balance of the pool. For a pool of liquid that is initially at ambient temperature with the surrounding air and ground, the heat received via solar radiation, atmospheric long-wave radiation, and direct heat transfer from the air and substrate must balance the heat lost by radiation, direct heat transfer, and evaporative cooling if the temperature is to remain constant. The effects of the last two factors are most significant for volatile liquids of interest here, due to the significant depression of surface and bulk temperatures that can be caused by evaporation of fuels such as n-pentane. If more heat is lost than is gained, the temperature and, therefore, the evaporation rate will drop. One experiment cited by Kawamura and Mackay

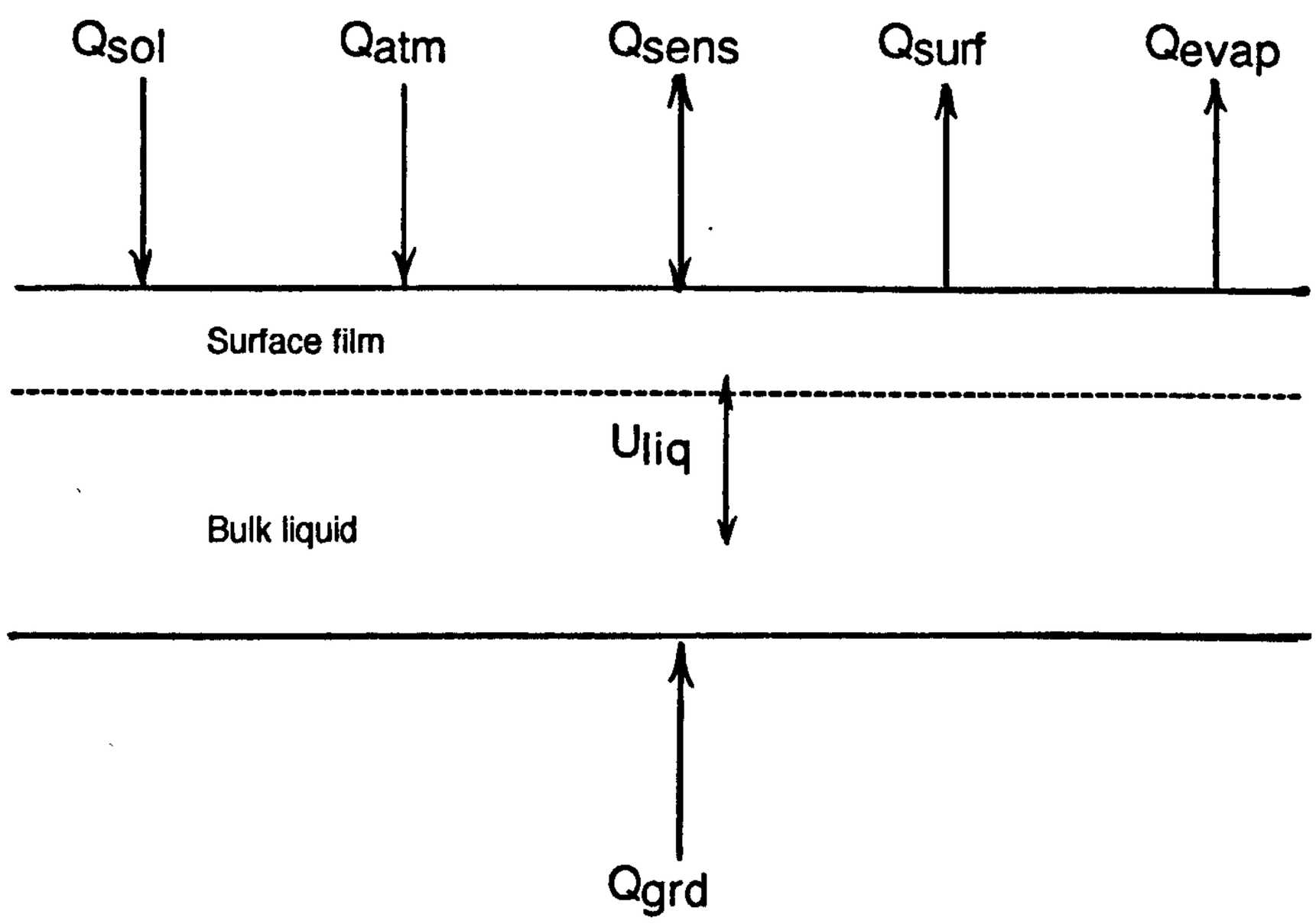

Fig. 1.2 Heat balance for a pool of evaporating liquid. Q_{sol} is the heat input from solar radiation. Q_{atm} is the heat input from atmospheric radiation. Q_{sens} is the sensible heat transfrered between the pool and the atmosphere by conduction and convection. Q_{surf} is the heat lost by radiation from the pool surface. Q_{evap} is the heat lost due to evaporation. Q_{grd} is the heat conducted into the pool from the ground.

U_{liq} is the heat transfer co-efficient within the liquid. For an interior pool $Q_{sol} = 0$ and $Q_{atm} = Q_{surf}$ when $T_{pool} = T_{atm}$.

over-estimated the evaporation rate of pentane evaporating from a flat pan by a factor of four because it did not take into account the cooling effect. [Kawamura/Mackay] They suggest an energy-balancing formula based on the basic relationship of:

$$E_a = k_m M p_s / RT$$

where E_a = the evaporation rate per unit area (g/m^2 h) (*sic.*),

k_m = the mass transfer co-efficient (m/h),

M = the molecular weight,

p_s = the vapour pressure at the actual surface temperature (Pa),

R = the gas constant, (8.34 Pa-m^3/mol K), and

T = the absolute temperature.

They correlated k as:

$$k_m = 0.029u^{0.78}{}_x{}^{-0.11}Sc^{-0.67}$$

where u = wind velocity at 10m (m/h),

x = downwind dimension (m), and

Sc= the Schmidt number, defined as the dimensionless ratio of the kinematic viscosity of air to the diffusivity of the vapour into air, ν/D. Kinematic viscosity is defined as the ratio of dynamic viscosity to density.

Kawamura and Mackay derive the relationship:

$$E_t = E_r [1/(1+B)] + E_a [B/(1+B)]$$

where E_r (the evaporation rate due to solar radiation) = Q_{sol} M/H_v,

E_a = the evaporation rate assuming the liquid temperature stays the

same as the ambient temperature, and

B = a correction factor which depends on the Schmidt number of the vapour, and the molecular weight, and heat of vaporization of the liquid involved.

This correction factor is inversely proportional to vapour pressure. It is small for volatile compounds like pentane where the difference in temperature between the ground (ambient) and the evaporating surface is large. As a result, E_t comes to be dominated by E_r . Such substances (such as pentane) have significant evaporative cooling effects unless a great deal of heat is being received from radiative sources.

The authors also derive a more elaborate alternate method, based on the same heat balance whose solution is the equation:

$$Q_{sol} + Q_{atm} + T_a(U_{liq} + U_{grd}) = T_S\,(U_{liq} + U_{grd}) + kH_v\, p_S/RT_S + \epsilon\sigma T_S^4$$

where T_S = actual temperature of the evaporating liquid surface

p_S = vapour pressure at the actual temperature, T_S,

ϵ = emissivity,

k = thermal conductivity,and

σ = Stefan-Boltzmann constant.

This equation, which takes into account the surface temperature reduced by evaporative cooling of volatile fuels, may be solved for the actual surface temperature using standard root determining methods such as the Newton's method.[Kawamura/Mackay, 1987]

It is interesting to note that their derivation includes the overall heat transfer co-efficient, U_{grd}, defined as $U_{grd} = 1/[(1/h_{grd}) + 1/h_{liq})]$ where h_{grd} is the heat transfer co-efficient from the surface to the bulk liquid and

h_{liq} is the heat transfer co-efficient that accounts for the thermal resistance between the surface of the ground to the surface of the liquid pool. Because heat transfer within the pool can be achieved by both conduction and convection (eddy turbulence),they offer the derivation of: $h_{liq} = k_{liq} / Ød$. The term k_{liq} is the thermal conductivity of the liquid itself. The term d denotes the average depth of the liquid layer, where Ø takes into account the relative roles of heat transfer by conduction and turbulence. If only conduction takes place, Ø will equal unity; if there is convection, Ø is smaller than unity and h_{liq} will be larger. This is especially important in evaluating liquids evaporating from very thin films or from absorptive surfaces. In a deep pool of non-viscous liquid, there will be eddy circulation and general convection where the cooler liquid will sink, being denser, to be replaced by warmer, less dense liquid from beneath. This convective circulation helps maintain the energy balance within the pool. In the absence of actual convection, some turbulent mixing will occur. As the evaporating layer becomes very thin, or if the liquid is absorbed into a solid inert matrix such as sand, carpet, or concrete, the convective or eddy transfer will become negligible. This would be marked by the factor Ø approaching unity, with corresponding changes in h_{liq} and, thereby, in U_{liq}. If the substrate is heat conductive, the heat losses at the surface are more likely to be compensated in part by heat transfers from the bulk liquid or substrate. If the substrate is not heat conductive, the evaporative heat losses will produce a very large difference in temperature between the supporting surface and the evaporating surface of the liquid. The resulting low surface temperature will result in a very low vapour pressure and thereby a low evaporation rate.

Their experimental results, using seven volatile liquids, ranging from toluene to Freon 11, in an experimental form that minimized ground conduction effects, showed good correlation to both models. The best correlation for their "direct evaporation" model (0 – 37% different from experimental results) was for the less volatile liquids tested (toluene, cyclohexane,hexane, methanol, and dichloromethane) as contrasted with the estimates for pentane and Freon 11, which were 10 – 40% low. It was suggested that this error may have been due to the approximation made in their derivation that the slope of the vapour pressure curve was a constant. For very volatile liquids, this is not true (as seen in Fig. 1.1 of this study).

Their results for the more elaborate surface temperature model were uniformly more accurate for all liquids tested, with predictions falling within 1– 32% of the experimental values. They further tested their models against a more involved experimental procedure that included ground conduction effects, with similar accuracy. [Kawamura/Mackay]

The evaporation rate of complex fuels such as petrol or camping fuel is not linear with time. The early stages are dominated by the loss of the pentanes, hexanes, and similar compounds, and the loss of volatiles from the surface must be compensated by diffusive and convective transport of those species from the bulk liquid. Burgoyne first noted the non-linearity of evaporating petrol in pools under both draft and still-air conditions. [Burgoyne,1944] This has been confirmed by recent work by DeHaan and Greenfield. [DeHaan/Greenfield, 1992] The diffusion processes of mass transfer within the material are thought to play a significant role in the large differences in evaporation rate observed in very thin layers compared to deep pools. The complexity of the thermal transfer and mass transfer relationship has made it very difficult to model. In this study, the situation is simplified

due to the short time intervals of evaporation that usually elapse between the release of a flammable fuel and the ignition of its vapours. The short-term evaporation of both petrol and camping fuel will be examined to determine whether it is dominated by one or two species.

1.4.5 Vapour Density

The end result of evaporation is the production of a layer of vapour whose properties depend on the liquid source. The density of the vapour is directly related to the molecular weight of the evaporating liquid. Vapour density (V.D.) is the ratio of the molecular weight of the liquid to the molecular weight of air. The molecular weight of air is usually assumed to be 29. The vapour densities of the liquids of interest are tabulated in Table 1.1. Note that all of the vapours of interest are significantly denser than air (which has a density of 1.205g/l at 20°C). Only methane, (V.D. =0.55), acetylene (V.D. = 0.90), and ethane (V.D. = 1.1) are lighter or nearly equal to air in density. The higher the vapour density , the less likely the vapour is to mix with air and the more likely it is to form a dense layer at the floor of the compartment.

1.4.6 Vertical Diffusion

Diffusion of one gaseous material into another is controlled by the Gibbs free energy, which forces molecules to move from an area of high energy to an area of lower energy. Graham's Law of Diffusion says that the rate of diffusion of a gas is inversely proportional to the square root of its density (ρ) as $[3P/p]^{0.5}$, or to its molecular weight (M) as $[3PV/M]^{0.5}$

Table 1:1: Properties of Selected Highly Flammable Liquids

[McKinnon, 1976]

Compound	Flammability Range % at 20°C	Vapour Density (relative to air:1.20g/l)	AIT (°C)	Flash Point (°C)
n-Pentane	1.5 – 7.8	2.5	260	–40
n-Hexane	1.2 – 7.5	3.0	225	–22
n-Octane	1.0 – 7.0	3.9	220	13
Benzene	1.4 – 7.1	2.8	560	–11
Methanol	6.7 – 36.0	1.1	385	11
Acetone	2.6 – 12.8	2.0	465	–18
Diethyl Ether	1.9 – 36.0	2.6	160	–45
Petrol (100)	1.4 – 7.6[1]	3–4[1]	456[1]	<–40
Petroleum Ether	1.1 – 5.9	2.5	288	<–18
Toluene	1.2 – 7.1	3.1	480	4
Camping Fuel	1.5 – 7.4[2]	na	335[2]	–28

Notes:
1. The properties of petrol depend on the grade and seasonal variations.
2. Properties of Coleman© brand camping fuel. [May,1995]

(where P = pressure, V = volume). If two gases interdiffuse at equal pressures, their fluxes are in the inverse ratio of the square roots of their molecular weights. For the case of a gas interdiffusing with air:

$$J_{gas}/J_{air} = [M_{air}/M_{gas}]^{0.5}$$

where J is the mass diffusion rate of that species. [Mason/Kronstadt,1967] This ratio can also be expressed as (Vapor Density)$^{-0.5}$. The diffusivity is usually defined as flux of one species into another, and represented as D_{ab}. This is in accordance with Fick's first law of diffusion, usually expressed (in one dimension) as:

$$J_{A,x} = -c_o D_{ab} (\partial X_a/\partial x)$$

where $J_{A,x}$ = molecular flux of species A in x direction,

X_a = molar fraction of species A.

c_o = initial concentration [Welty,et al., 1979]

This expression is analogous to Fourier's law of heat conduction:

$$Q_y = -\alpha [d(\rho C_p T)/dy]$$

where Q_y = heat flux in y direction,

α = thermal diffusivity,

C_p = specific heat capacity, and

ρ = density. [Szekely/Themelis, 1971]

The diffusivity of various gases and vapours into air has been measured experimentally and is recorded in the literature. Sherwood and Pigford demonstrated a simple derivation of diffusion coefficients by first principles from mechanics of number of molecules per unit volume, the molecular speeds, the distance between the centres of molecules of the two

types of molecules involved and the weights of the molecules involved.[Sherwood/Pigford, 1952] This takes the form of:

$$D_{ab} = 0.0069\ T^{1.5}\ (\ 1/M_a + 1/M_b\ )^{0.5}/\ P(V_a^{0.3} + V_b^{0.3})2$$

for T in Rankine, P = 1 atm, and molecular volumes (V_a,V_b) as calculated from a table of atomic volumes. Solving this for pentane at 20°C gives 0.074 cm^2/s, which compares favorably with the 0.071 used in the example in Kawamura and Mackay. Repeating this calculation for pentane, hexane and octane at different temperatures yields the results in Table 1.2.

Reid, Prausnitz, and Poling cited a modification of this formula by Fuller et al.:

$$D_{ab} = 0.000143\ T^{1.75}\ (\ 1/M_a + 1/M_b\ )^{0.5}/\ P(V_a^{0.3} + V_b^{0.3})2$$

(where T is in K and atomic diffusion volume increments are given in a table) saying that it gave better agreement with experimental values. For the limited temperature span of interest here, the temperature correction will not be significant, and either formula could be used.[Reid, et al., 1987]

1.4.7 Concentration Gradients

The vapour concentration above a pool of evaporating liquid is not constant with respect to height above the pool surface. Where the vapour is free to diffuse into the atmosphere, Drysdale describes the concentration gradient as one "...which decreases monotonically with height." but offers no specific determination.[Drysdale, 1985]

Ishida and Iwama in their study of divergent flash point and flame point measurements show a similar gradient; however, no mathematical

Table 1.2 Diffusivities of n-Alkanes In Air (Calculated) – (cm^2/s)

Alkane/Air	5°C	20°C	35°C
Pentane	0.067	0.074	0.080
Hexane	0.061	0.067	0.072
Octane	0.053	0.058	0.062

relationships are offered. [Ishida/Iwama, 1982] The concentration profiles of methanol vapour above liquid methanol were measured by Suzuki, Mashiko, et al. at three different temperatures.[Suzuki, et al.,1981] Their plots of equivalency ratio against height above surface showed similar profiles, displacing upwards with increasing temperature, as in Figure 1.3.

In discussing diffusion of a gas into a vacuum, Glasstone offers the relationship:

$$\ln (p_0 / p_i) = Mgh_i / RT$$

where g = the acceleration due to gravity,

p_0 = the equilibrium vapour pressure at the vapour/liquid interface,

p_i = the vapour pressure at height h_i.[Glasstone, 1946]

While this relationship is mathematically suitable (limiting conditions are $p_i = p_0$ at height = 0, and p_i approaches zero as height becomes very large), it is valid only for an equilibrium state of diffusion. Therefore, its usefulness to predict the relationship of vapour pressure (concentration) as a function of height above the liquid surface in a dynamic, real-world situation is limited.

The variation of vapour concentration with height above a pool of liquid in a non-steady (real-world) state is dependent on time. Theoretically, in a static, sealed environment, diffusion would eventually result in a uniform concentration throughout the airspace, but a fire or explosion will often occur long before this state is reached. The diffusion is limited by the molecular weight (and thereby, the diffusivity) of the evaporating species. Danckwerts demonstrated that, for the case of a gas diffusing into a liquid, the rate of absorption across the surface, A_r, could be expressed as:

$$A_r = -D_A(\partial c_a / \partial z)$$

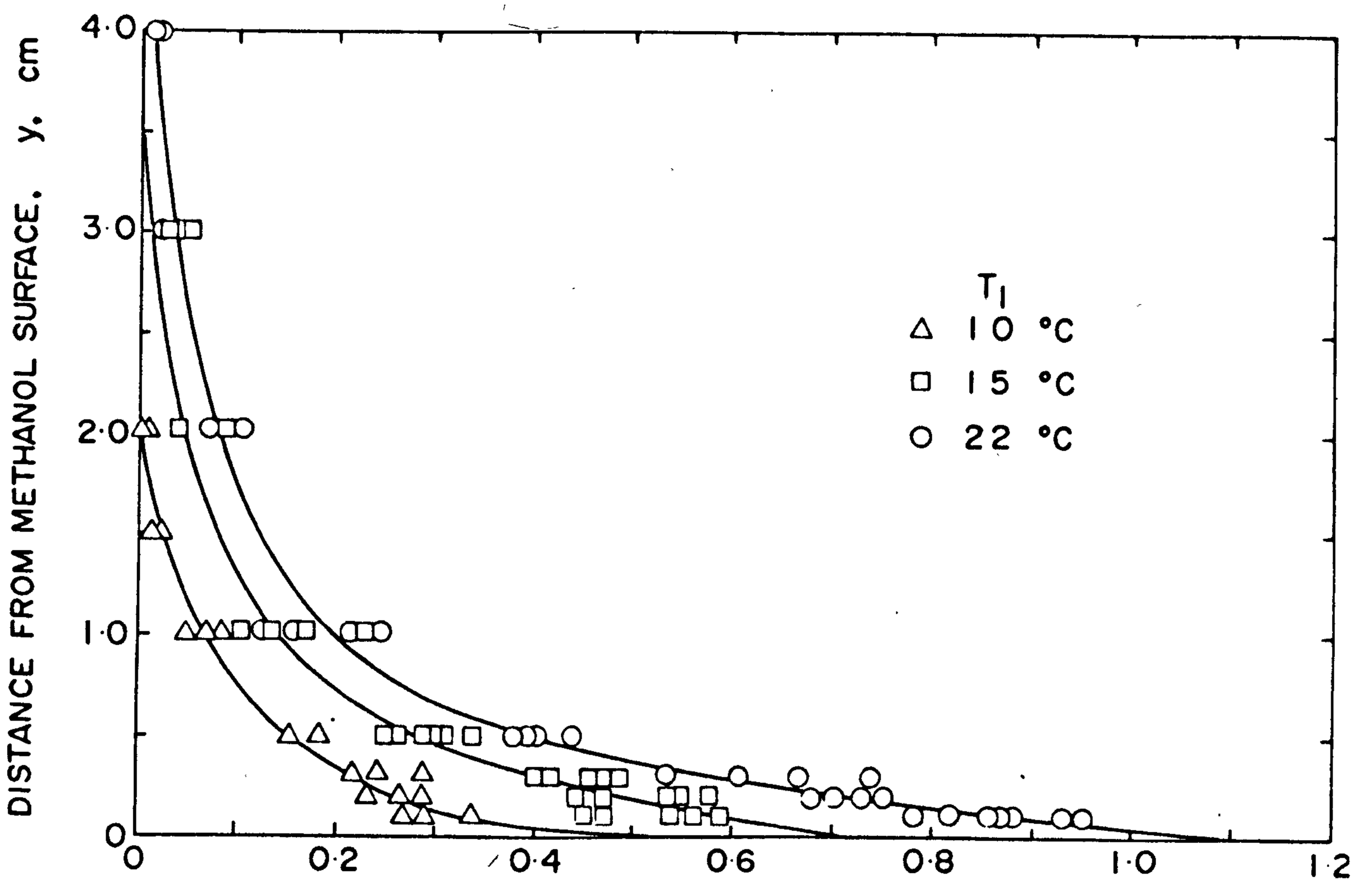

Fig. 1.3 Relationship between vapour concentration and height above methanol pool at three different temperatures. (Suzuki et al.)

where c_a = concentration of species A, and

z = distance from the surface.

For limiting conditions of:

c_a = G_0 initial concentration of gas in the liquid (uniform throughout the liquid) at $t = 0$,

c_a remains = G_0 at distances remote from the surface ($x = \infty$, $t > 0$), and $c_a = G^*$ (the initial concentration of the species in the gas at the surface, $z = 0$), the concentration gradient can be represented as:

$$c_a - G_0 = (G^* - G_0)\ \mathrm{erfc}[x/2(D_A t)^{0.5}] = (G^* - G_0)\{1 - \mathrm{erf}\ [x/2(D_A t)^{0.5}]\}$$

where erf, the error function, is:

$$\mathrm{erf}\ x/2(D_a t)^{0.5} = 2(\pi^{-0.5}) \int e^{-z_2}\, dz.$$

The gradient can be expressed as:

$$(c_a - G_0)/(G^* - G_0) = 1 - \mathrm{erf}\ [x/2(D_A t)^{0.5}].$$

The rate of absorption becomes:

$$A_r = (G^* - G_0)\,(D_a/\pi t)^{0.5},$$

and the amount of gas, G_t, absorbed by a unit area of surface in time t is then:

$$G_t = \int R\, dt = 2(G^* - G_0)\,(D_a t/\pi)^{0.5}$$

The absorption rate, by this, is infinite when the liquid and the gas first come into contact (t=0) and decreases with time. Danckwerts applied this approach to a gas dissolving into a liquid and obtained concentration profiles as a function of depth at various times that match Suzuki's for vapour concentrations above a diffusing source, as in Fig.1.4.[Danckwerts,1970] It

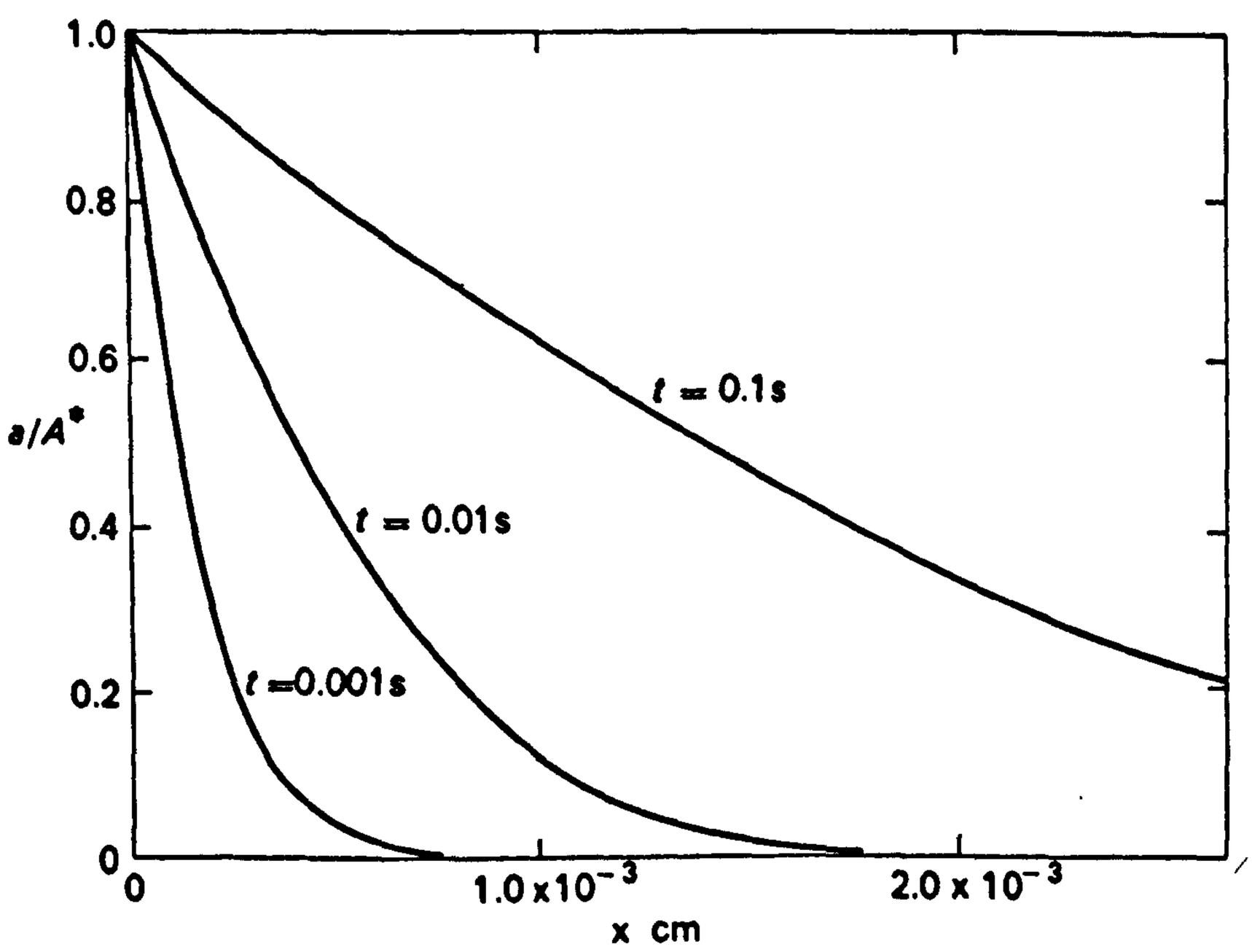

Fig. 3-2 Concentration-profiles for the absorption of a gas into water

Fig. 1.4 Relationship between gas concentration and depth for absorption of gas into liquid at various times using error function calculation. (Danckwerts)

can be argued that this an exact parallel to a volatile liquid coming into contact with the atmosphere for the first time, with the diffusion going from the liquid into the air rather than from a gas into a liquid, and using c_a as the concentration of the vapour in air. The same form can be used to calculate the temperature of a semi-infinite slab (in parallel with the Fourier conduction relationship shown in Sect. 1.4.6). In that case, the ratio of temperature differences becomes:

$$(T - T_0)/(T - T_a) = 1 - \text{erf } z/2(\alpha t)^{0.5}$$

where α = thermal diffusivity of the material [Drysdale]

Rabinkov demonstrated that a stratified layer of gas/air mixture is formed at the floor of a compartment when the gas is heavier than air and the source is at or near floor level, even when there is the non-steady-state continuous (but presumably non-turbulent) change of room air.[Rabinkov, 1988] He derived a complex relationship between the diffusivity, gas concentration, height, rate of gas introduction (per unit surface area), room-air changes, and time, and offered experimental validation using propane (vapour density = 1.52) at three different times, as in Figure 1.5. Note the steep concentration gradient and gradual deepening of the flammable layer (lower explosive limit – LEL – for propane = 2.2%) with time. If one were to substitute the evaporation rate for the rate of gas introduction, this model could serve for predicting the concentration of vapour from an evaporating pool at floor level. Unfortunately, the mathematics of the calculation are very difficult to use.

Valentine and Moore modelled a heavy flammable vapour (propane) leaking into the base of a semi-infinite column of stable, still air applying Fick's Law to a differential control volume representing a cross-section of the

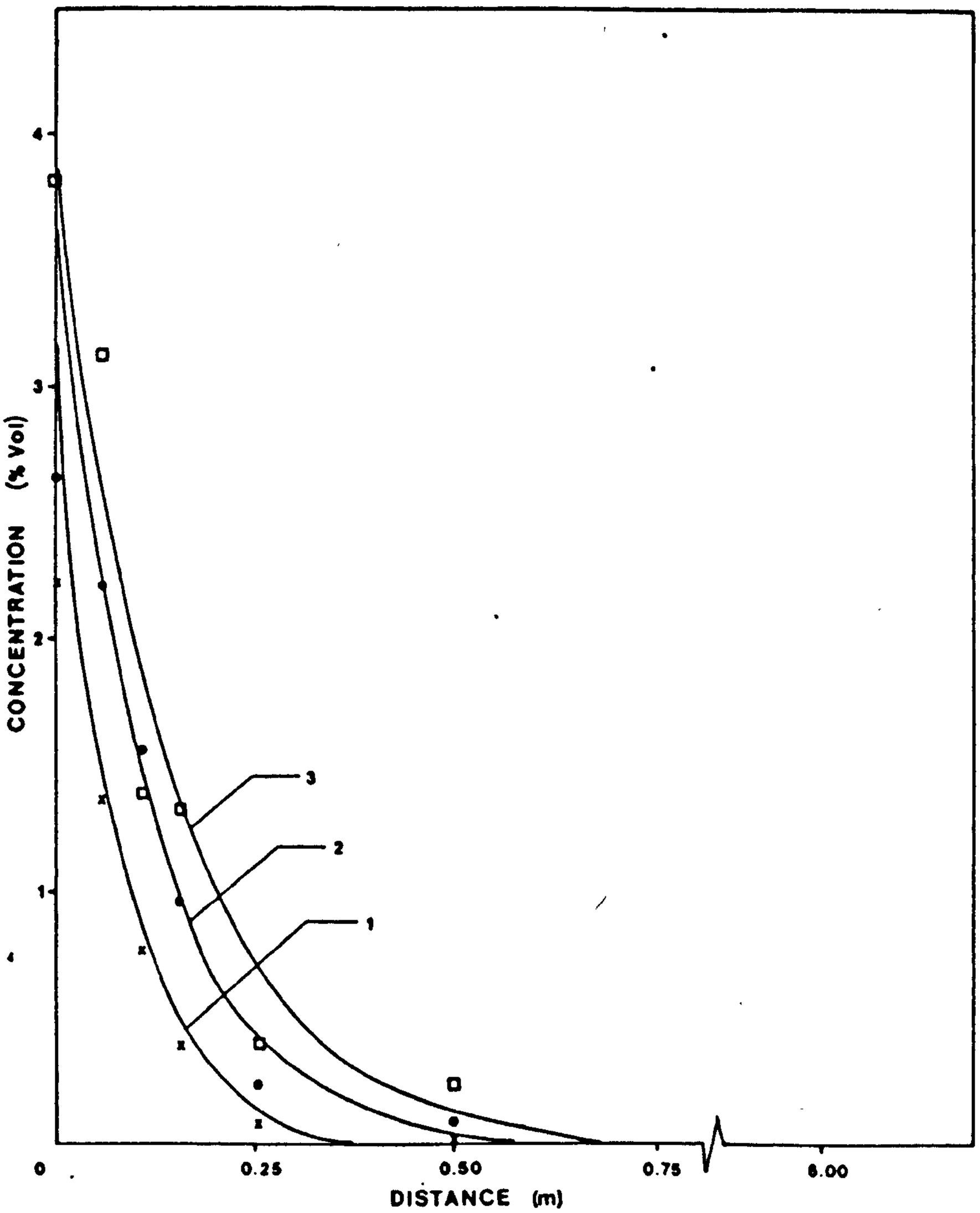

Fig. 3. The spreading of propane in the building with the leak position at floor level. Gas volume flow rate 0.3 m^3/h; $K = 2/h$. Gas concentrations shown as a function of height after 0.25 h (x), 0.5 h (●), and 1.0 h (□). Solid lines 1, 2 and 3 refer to the solutions of eqn. (4) at 0.25 h, 0.5 h and 1.0 h, respectively.

Fig. 1.5 Propane concentration v. distance from floor at various times for propane leaking into a room at floor level with two changes of room air per hour. (Rabinkov)

column. [Valentine/Moore, 1974] They showed that the governing diffusion equation for such a column would be:

$$\partial^2 X/\partial z^2 - (L/DC_m)\,\partial X/\partial z = (1/D)\,\partial X/\partial t$$

where X = mole fraction of propane in propane-air mixture,

z = height in column (above base), (m)

L = propane leakage flux rate, (mol/m^2-s)

D = diffusion co-efficient of propane in air, (m^2/s)

C_m = maximum propane molar concentration, (mol/m^3) and

t = time, (s).

They developed a finite-difference numerical solution using methods adapted from non-steady-state heat conduction problems. [Kreith, 1973] They were able to calculate the molar concentration of propane at any height in the column at different times for various filling (leakage) rates. Experimental data was collected using an open vertical column, 2.5m high and 0.15m in diameter being filled with propane through a sintered plate at its base. It was found to fit the calculated concentrations for times of 1 – 4 hours very well. The shapes of their concentration curves, Fig. 1.6, are very similar to those of Rabinkov, Ishida and Iwama, and Danckwerts. It demonstrates a very steep concentration gradient rather than a linear one, that becomes steeper at faster flow (leakage) rates. Their tests involved introduction of gaseous propane into a column of still air that was all at the same ambient temperature. Valentine and Moore point out that in the presence of a thermal gradient, such as in a basement where cooler temperatures dominate at lower levels of the compartment, the concentration gradient would be even steeper, producing a situation where the gas (with its

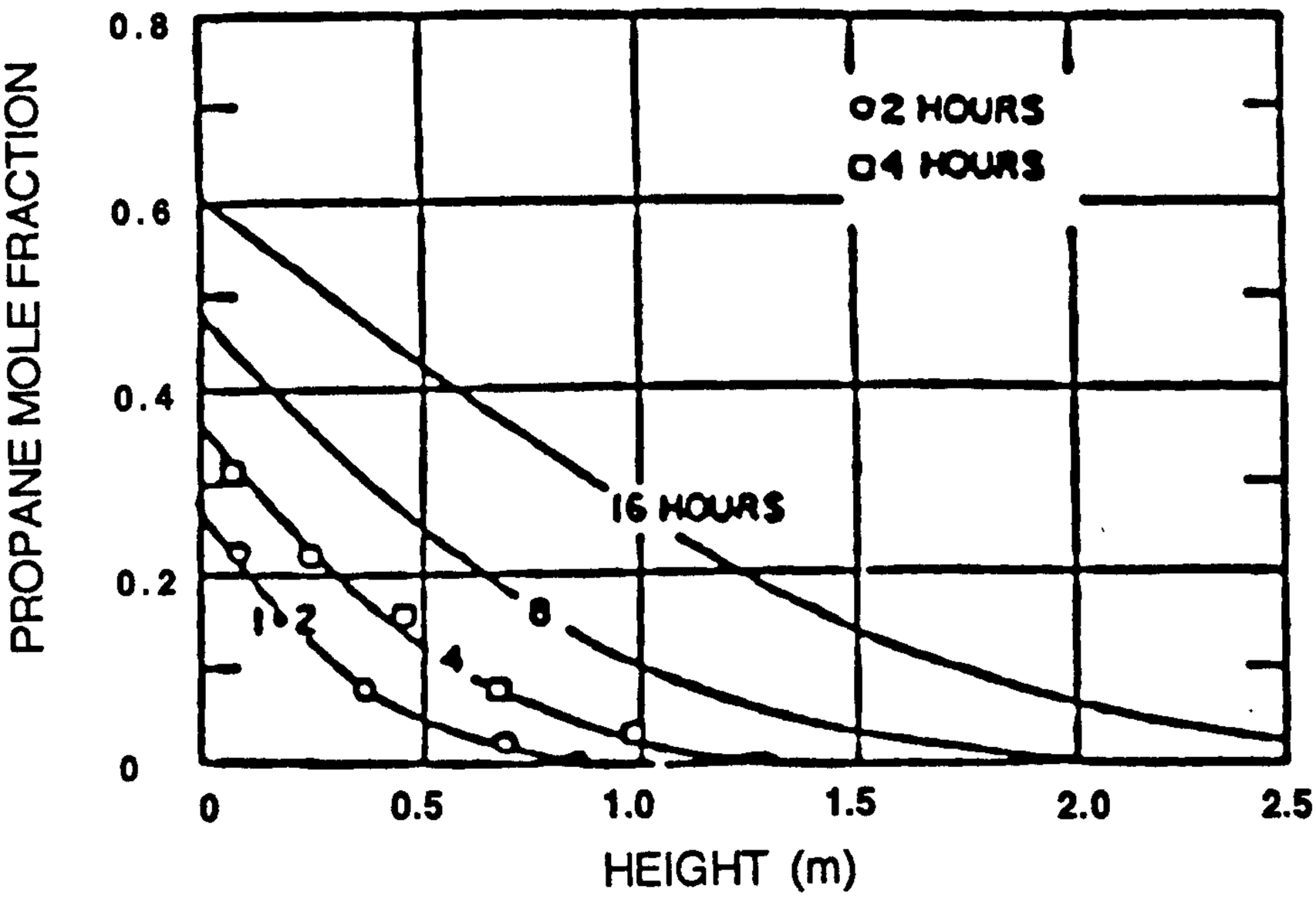

Calculated curves and experimental data points of propane concentration as a function of height and time for a flux rate of 0.02g/s-m^2

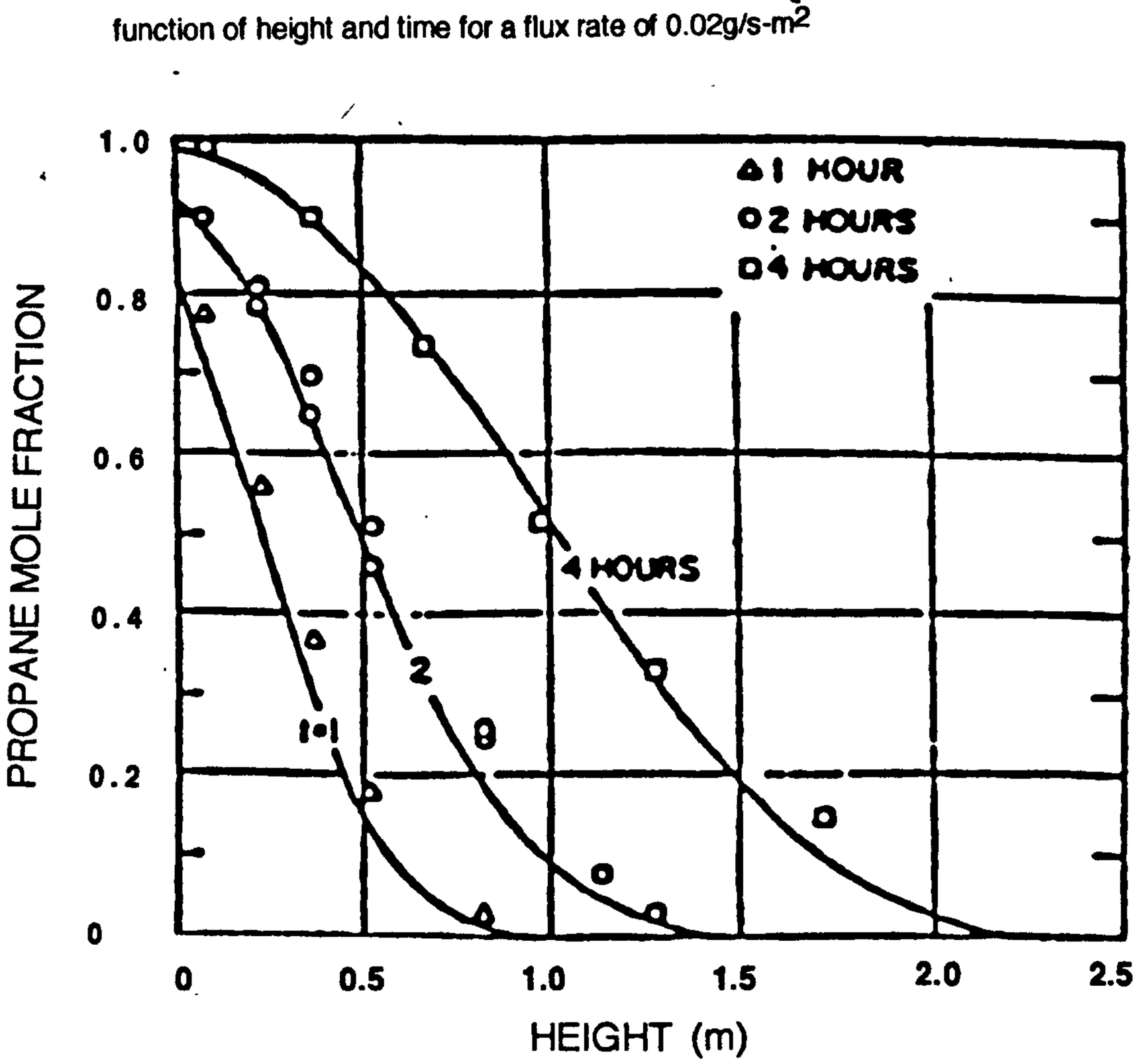

Calculated curves and experimental data points of propane concentration as a function of height and time for a flux rate of 0.135 g/s-m^2

Fig. 1.6 Propane concentration v. height at various times for different rates of leakage into a room at floor level using finite-difference calculation. (Valentine and Moore)

accompanying odorant) might be undetectable at nose height (1.5m) and yet a substantial quantity of fuel/air mixture within its flammable range might be present immediately beneath that level.

Instead of propane seeping into the base of a column at a uniform temperature, if a flammable liquid pool at the base of the column were the source of vapours, the evaporative cooling would produce a thermal gradient that would accentuate the steepness of the concentration profile. The nature and extent of any such thermal gradient has not been explored. In addition, the situation treated in all of these studies was that of a source that filled the entire base of the compartment, producing movement in the vertical direction only. In real-world incidents, it is much more common for a compartment to have a source of vapours that is much smaller than the "floor area" of the compartment. The generation of a layer of vapour in an enclosure is more complex when the source takes the form of a small pool or series of small pools, which produce vapours that are free to move vertically by diffusion but also horizontally by advection (viscous flow).

1.4.8 Advection

Diffusion of the vapour from a liquid pool into static air can be visualized as producing initially a layer or puddle of vapour of some height and approximately the same horizontal dimensions as the evaporating pool. Some diffusion in the horizontal plane will take place but it will be dependent on the vapour density. For many fuel vapours, this vapour density will be in the range of 2.5 to 4 and horizontal diffusion will be very limited. It was for this reason that most investigators discounted diffusive transfer in the

horizontal plane as negligible when compared to the spread caused by even a moderate wind. There is another mechanism that accounts for some horizontal transport, and that is advective or laminar viscous flow, described by Mason and Evans as being controlled by the viscosity of the vapour and a viscous flow parameter. [Mason/Evans,1969] As the layer or puddle of vapour achieves any significant height, it can slump sideways and produce lateral spread. This is the mechanism explored by Van Ulden, who showed that the area covered by such density-driven slumping from an instantaneous release of volume V_0 is a linear function with time, t:

$$r^2 - r_0^2 = 2\,c\{[g\,(\rho_0 - \rho_a)V_0]/[\pi\rho_0]\}0.5\,t$$

where r = radius of gas cloud at time t

g = acceleration due to gravity

ρ_0 and ρ_a are the densities of the gas and of air, and

c = unknown constant. [Van Ulden]

This spread is of the same form as that given earlier for spreading of liquid pools, but now a buoyancy factor must be included, $(\rho_0 - \rho_a)/\rho_0$. This is the factor, Δ, introduced by Melhem regarding liquid spreading on water.[Melhem/Croce] This approach assumes that there is no mixing with air to change the density of the gas and applies to an instantaneous release. This viscous flow is more pronounced with vapours of higher vapour density (which mix very little with air over short time frames) and should be valid for vapours of petrol, camping fuels, and similar fuels of interest to the fire investigator. Melhem points out that the initial rate of spreading or slumping can be significant and is dependent on the difference between the mean vapour density and the air density. [Melhem/Croce] If mixing occurs where the

"front" of heavy gas rolls through the surrounding air, the mean vapour density decreases quickly. There is, however, little mixing in the vertical direction and the vapour cloud hugs the ground. Using Melhem's formula for the area spread rate (shown earlier):

$$r^2 = [8\Delta(1 - s)V_0/\pi]^{0.5}t + r_0^2$$

the equivalent formula for a continuous release, with $V_0 = 0$ and r_0 = at time $t = 0$, is:

$$r^2 = (2/3)^{0.5}\{[8\Delta (1 - s)L]/\pi\}^{0.25} t^{0.75}$$

where L is the leakage (release) rate in m^3/s.[Melhem/Croce]

Burgoyne's experiments also demonstrated a barrier effect related to this slumping. The evaporation rate was slower when the petrol pool was evaporated in a deep pan than when a pool of the same depth was tested in a shallow pan. Limited circulation produces a dense layer of vapour over the pool and if that cloud cannot slump sideways, the increased vapour concentration over the pool slows the evaporation.[Burgoyne, 1944] This implies that advection of vapours plays a role in both the horizontal dispersion of heavy vapours and in the evaporation rate of the liquid.

1.5 Ignition of Flammable Vapour/Air Mixtures

Once the layer is formed, the attention focuses on the properties that control its flammability. These properties are reviewed briefly here.

1.5.1 Flammability Limits

Every fuel/air mixture has a range of concentrations within which it is flammable. If the fuel is at too low a concentration in air to be ignited, it is said to be too lean or under its lower flammability limit (LFL) or lower explosive limit (LEL). If it is too concentrated or too rich to ignite, it is above its upper flammability limit (UFL) or upper explosive limit (UEL). The concentration range between the two limits constitutes the flammability range for that fuel. The range for each material is affected by the ambient temperature: the LFL decreases with increasing temperature, and the UFL rises, producing a wider flammability range. The initial conditions in most fire scenes, however, will not cause significant changes in flammability range. At ordinary temperatures, the ranges for the fuels of interest here are shown in Table 1.1.

As described above, the vapour layer above a liquid displays a gradient of vapour pressure from saturation just above the surface to zero some finite distance above it. If this gradient includes a vapour pressure equivalent to a concentration within the flammability range of that vapour, then the layer is ignitable. For n-hexane at 25°C, the equilibrium vapour pressure just above a flat, liquid pool surface is approximately 150mmHg. Against a standard atmospheric pressure of 760mmHg, this vapour pressure represents a concentration of 150/760 = 19.7%. This is well above hexane's LFL of 1.2% (and also above its UFL of 7.5%), so the vapours of hexane (at static equilibrium) are readily ignitable at some height above the surface. If a suitable ignition source is brought into contact with the vapours in their flammability range, ignition can occur. Thus, at normal temperatures in the space above a flammable liquid there will be a layer within its flammability range. The higher the temperature of the liquid, the deeper this layer will

be,i.e., the further it will extend above the surface. As the temperature decreases, the vapour pressure above the liquid drops (if all other conditions remain the same). Eventually, at some temperature, the vapour pressure (even close to the surface) drops below 9mm, which is the LFL (1.2%), and the vapour is no longer ignitable. This temperature is defined as the flash point of the hexane under those test conditions. The height above the liquid surface at which the ignition source is offered can make a significant difference (three degrees) in the observed flash point. [Ishida/Iwama, 1982] This is due to the gradient in vapour pressure immediately above the surface. As Fried, et al. pointed out, a convex liquid surface produces a higher vapour pressure than a flat surface of the same liquid, and the smaller the radius of curvature, the higher the pressure [Fried,et al., 1977]. In his discussion of evaporation of fuel droplets, Kanury showed that mass transfer rate from the droplet surface is inversely proportional to the radius of the droplet [Kanury, 1975] As can be appreciated from the foregoing arguments, any change in the conditions, such as a textured substrate which may create a higher vapour pressure by creating a convex-contour surface, will change the flash point as it is measured.

1.5.2 Ignition Temperatures and Energies

One of the properties that contribute to the hazard of vapour/air mixtures is the low energies necessary to ignite them. The minimum ignition energy is that required to establish a flame of the critical minimum size needed to produce flame propagation and, for the hydrocarbon fuels under consideration here, is 0.25mJ for a stoichiometric mixture of fuel/air. [Harris, 1983] The ignition temperature, or auto-ignition temperature (AIT), is a

function of the reactivity of the fuel/air mixture, and is independent of the ignition energy. It is distinct from the piloted ignition temperature of a fuel (that being the temperature necessary for there to be sufficient ignitable vapours to sustain a flame when an external or pilot ignition source is offered). The auto-ignition temperature of any fuel is dependent on the time, geometry, and dynamics of the contact between the fuel and the heat source. The auto-ignition temperatures of vapour/air mixtures are usually measured by introducing a mixture into a chamber pre-heated to a particular temperature. If ignition occurs within a set time interval of the introduction, the process is repeated at successively lower temperatures until ignition does not occur within that time. A material's auto-ignition temperature is dependent on the concentration of the vapour in air and the shape, size, and material of the containment vessel used for the determination. Typical ignition temperatures (AIT) for simple alkanes are inversely related to the molecular weight (Table 1.1).

For ignition to take place, there must be a source of ignition of adequate energy in contact with the fuel. The fuel must be in an ignitable form at the place of contact, and the contact has to be of sufficient duration to allow adequate energy to be transferred to the fuel. In the case of vapour/air mixtures of hydrocarbons, the required energy is so low that many ignition sources have more than enough energy and the contact does not have to be of long duration for there to be ignition. The vapour/air mixture does, however, have to be within its flammability range at the point of contact with the ignition source. One can have a very hot surface (at a temperature well above the measured AIT for that fuel), spark, or even an open flame exposed to a mixture and not have ignition if that mixture is above or below its flammability limits. Because of the localized turbulence caused by most

ignition sources (especially flames and arcs), and the changes in flammability limits induced by changes in temperature, localized ignition can occur if the mixture is just outside its normal ambient temperature flammability range.

1.5.3 Flame Speed

If the fuel/air concentration is within its flammability range, the flame front will proceed radially outward from the ignition source at a speed characteristic of the fuel involved. This speed is not constant, however, throughout the range. It reaches a maximum for each fuel at a concentration just over its stoichiometric ratio (Fig. 1.7). [Harris] The flame front moving through a gradient of vapour/air concentrations above a liquid fuel is curved in vertical contour, and not a vertical straight-line.[Hirano, 1977] Flame progression itself will not be addressed by this study, but it is useful to examine some of the basic relationships between flame propagation and vapour concentration to better appreciate the effects of both combustion and any resulting overpressures produced.

The speed at which the flame front propagates through a uniform fuel/air mixture, S_f, is related to the burning velocity, S_0, the rate at which the flame front moves relative to the unburned mixture immediately in front of it and to the expansion factor $\sum$ as in:

$$S_f = S_0 \sum.$$

For a reaction where all starting products and all final products are gases, the expansion factor $\sum$ is dependent on the change in the number of moles of gas from initial condition to final, and to the change in temperature as:

$$\sum = (T_f / T_i)(N_f / N_r), \text{ where}$$

EFFECT OF GAS CONCENTRATION ON BURNING VELOCITY
Results from Gibbs and Calcote[10]–see table 1.2 for recommended maximum values for different fuels

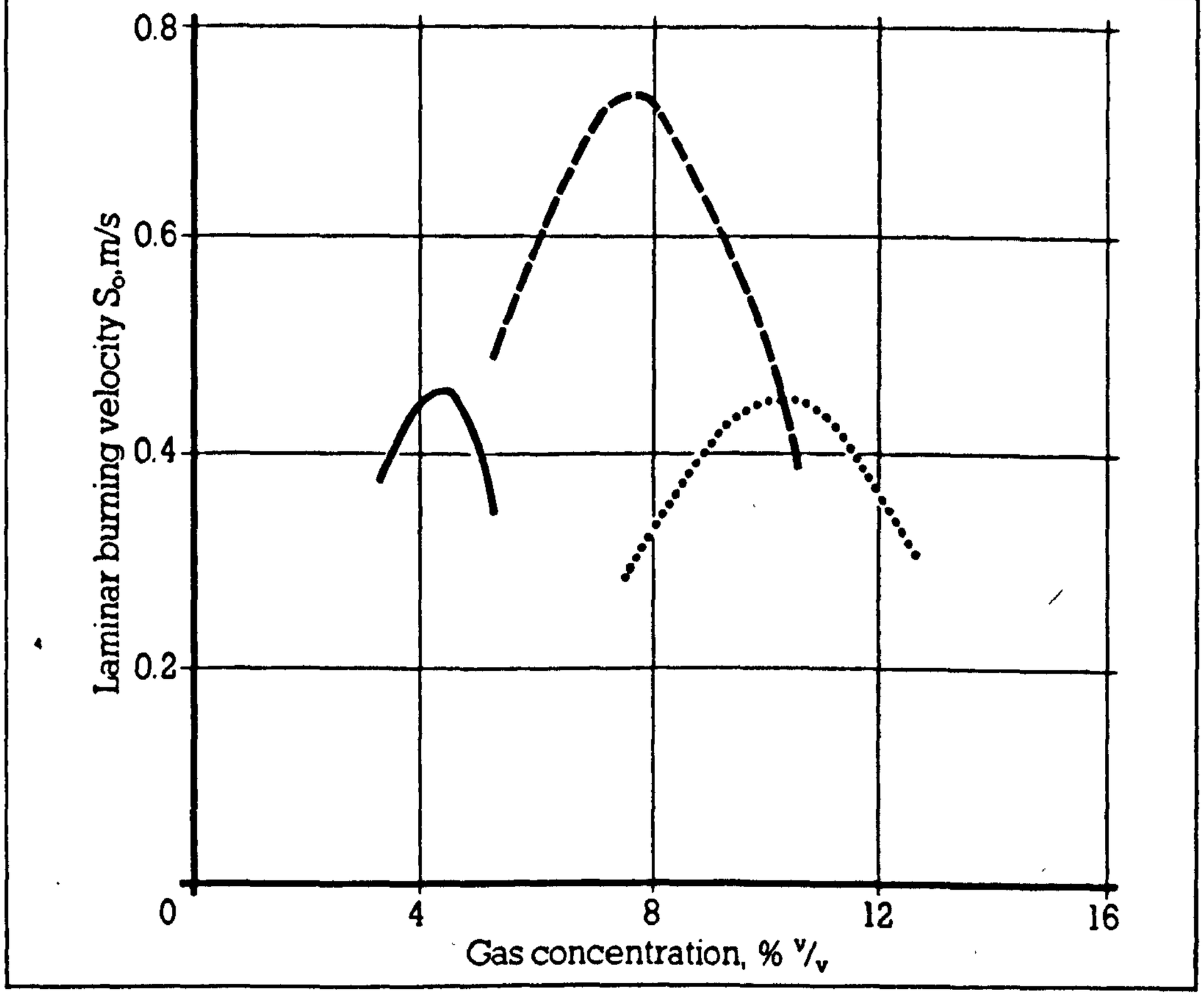

Fig. 1.7 Laminar burning velocity v. fuel gas concentration for three different fuels. (Harris)

T_f = final temperature (K),

T_i = initial temperature (K)

N_r = number of moles of reactant gas and

N_f = number of moles of final gaseous product.[Harris]

For n-pentane burning in air, the stoichiometry is:

$$C_5H_{12} + 8\,(O_2 + 3.76\,N_2) = 6\,H_2O + 5\,CO_2 + 30.08\,N_2$$

and $N_r = 39.08$ and $N_f = 41.08$.

N_f/N_r = mole number ratio = 1.05

If T_i = 288 K and T_f is assumed to be the adiabatic flame temperature, 2232 K (per Harris), the temperature ratio is 2232/288 = 7.7. Therefore, under ideal conditions this reaction would produce a volume of gas (based on $\sum$) of: 7.7 x 1.05 = 8.08 times the original volume.

According to Harris, the maximum laminar burning velocity for n-pentane in air (S_o) is 0.52 m/s and therefore the maximum laminar flame speed (S_f) is of the order of 4.0 m/s. If the deflagration is proceeding uniformly under adiabatic conditions and in laminar fashion, the expansion ratio is on the order of 8 and if the reaction occurs in a compartment whose volume cannot change, a maximum pressure is developed on the order of 8 Bar or 120 psi. [Harris]

One important note is that the layered fuel/air mixture does not necessarily behave according to this prediction. It has been noted that a layered combustible gas mixture can support flame propagation speeds four to five times the normal laminar flame speed of the stoichiometric mixture. Burgoyne and Roberts observed flames propagating across a liquid fuel surface at 220 cm/s for propanol and 190 cm/s for butanol, compared to a

maximum laminar flame speed of about 45 cm/s for alcohols. [Burgoyne/Roberts, 1968] Flame speeds of 185 – 220 cm/s have been observed in propagation tests above porous (but unsaturated) beds containing hexane and benzene, which produced a vertical concentration gradient of vapours.[Kaptein/Hermance, 1977] Feng, Lam, and Glassman in their study of methane-air mixtures layered along the top of a gallery model showed that the ratio of the propagation speed to the laminar flame speed was equal to the square root of the ratio of the unburned to burned gas density when the corridor was of infinite height. [Feng, et al., 1975] This is the same geometry as a layer of dense vapour lying above a pool of highly flammable liquid.

Since flame speeds are dependent on vapour concentration, the concentration gradient above a pool will produce a characteristic flame front that is curved in vertical cross-section. The leading portion of the curved front will be in the portion of the layers whose concentration is closest to the stoichiometric mixture for that fuel where the combustion has the highest speed. The upper and lower edges will trail behind as they progress through the mixtures closer to the LEL or UEL for the fuel, where the flame speeds are lower than they are for those mixtures close to stoichiometry.

The mass reaction rate is dependent on the surface area of the combustion zone volume. Turbulence on the interface between the burning volume and the unburned gases surrounding it creates a larger surface area and therefore higher reaction rates. This effect is pronounced in structures where furniture, doorways, and other irregularities create localized turbulence, which enhances the deflagration by creating more surface area for the flame front. In fact, the propagation rate is determined by the product

of $S_o\Sigma$ and the surface area in contact with the unburned mixture. Harris has suggested an area correction term, A_f/A_m, where A_m is the minimum surface area achievable in the geometry of the fuel/air mixture and A_f is the actual area of the flame front (which will generally increase with time). [Harris]

The effects of deflagrating explosions can be devastating. As shown above, the theoretical maximum pressures that can be developed at ordinary temperatures are on the order of 8 Bar, well in excess of the failure pressures of common building systems and components. Overpressures caused by the deflagration of even limited quantities of vapour inside a room (such as partial room volumes) can do serious structural damage to typical residential and commercial properties. Pressures in excess of 300 mBar (5 psi) can severely damage ordinary buildings (flattening walls and lifting roofs) and such pressures can be produced by deflagrating explosions in vapours that occupy only a small percentage (<10%) of the volume of the room.[Harris] In addition, if there are pockets of overly-rich fuel/air mixture, the turbulence created by the initial combustion stirs air into this excess fuel, promoting post-blast burning, which can be as destructive as the blast itself. This is especially true of heavier-than-air vapours such as those from petrol where pools of vapour can sustain combustion for many seconds. If there is an excess of liquid fuel present, the heat from the deflagration induces on-going evaporation of the fuel, which supports continuous burning. This effect has been documented in a number of full-scale fire tests using petrol and other flammable liquids conducted by this author. [DeHaan, 1990]

1.5.4 Actual Fire Tests

This author has participated in numerous tests under a variety of conditions where a highly flammable liquid has been allowed to evaporate at normal temperatures inside a room to form an ignitable layer of vapour/air mixture at floor level. The circumstances of these tests did not permit the measurement of flame speed; however, the general behavior of the propagating flame was as predicted above. In the best documented series of tests, the flame front can be seen to progress radially outward from the centrally-located electric match ignition source, with a curved flame front whose shape reflects the difference in flame speed produced by the concentration gradient above the pool. The initial ignition proceeds throughout the layer first, reaching the limits of the 4m x 5m compartment within 1–2 seconds, followed by localized vertical flames where the turbulence created by objects in the room encourage vertical mixing of the burning gases. Typically, within 20 seconds of ignition upon completion of the combustion of the fuel already in the vapour state, the flames retreated to isolated areas surrounding the irregular pools of liquid on the floor. [DeHaan, 1990]

1.6 Statement of Problem

A fire involving flammable liquid vapours from any source poses a variety of problems for safety professionals: predicting and controlling the risks; suppression of a fire once ignited; and for investigators, who must accurately determine the origin and cause after the fire or explosion. Such

fires may be encountered in a variety of situations: from vehicle accidents, industrial mishaps, or as the mechanism for intentionally-set fires. Because of the mobility of flammable liquid vapours and the ease with which they may be ignited, the fuel source and the ignition source need not be in the same location and spillage, and ignition need not occur at the same time. The prediction of the factors involved require a comprehensive knowledge of fluid dynamics of both gases and liquids, as well as ignition mechanisms.

The ability to estimate the time of formation, extent of horizontal movement, and height (depth) of ignitable vapour layers would be invaluable in the investigation of both accidental and incendiary fires. The available models for the production of layers and/or plumes of vapours, while useful for large industrial incidents out-of-doors occurring over hours or days, are of very limited use for interior spills of small quantities of highly flammable liquids at ordinary ambient temperatures and atmospheric pressure, particularly when the spill is on a complex surface such as carpet.

It is the objective of this study to explore the numerous mechanisms that influence the formation and distribution of vapour layers from small spills of common flammable liquids at ordinary temperatures by quantifying the factors involved. It is hoped that this study will provide fire investigators with a better understanding of these factors in both accidental and incendiary fires involving such fuels. The study here will proceed in several inter-related steps:

1. Determine the relationship between volume of a spill and the surface area of pool for a variety of surfaces. Most accidental and intentional spills of small quantities take only seconds and can be assumed to be an instantaneous event. Starting from a given quantity of fuel, it will be

important to estimate how large a surface area is going to represent a source for the vapour, since all evaporation is directly dependent on the surface area of the pool.

2. Establish the evaporation rates for selected compounds from various substrates and compare those rates against the evaporation rates for pools of the same compounds. Depending on the thermal and physical characteristics of the substrate, it will be important to predict what the strength (mass release rate) of the source of vapour is when compared to a pool of equal size. As part of this section, it will be useful to evaluate existing models (such as Kawamura and Mackay's) for evaporation rates from pools. These models apply to volatile liquids in exterior locations under normal ambient conditions, but they may yield the basic structure of a predictive model for evaporation of simple pure compounds (n-pentane and n-hexane) in still air from pools and from various substrates.

3. Establish the effect of ambient temperature on evaporation rate.

4. Establish the effect of pool size on evaporation rate.

5. Establish the contributions from pouring and splashing of volatile fuels to the amount of vapour present.

6. Establish the depth of the vapour layer as a function of time given the area of the spill and the source strength of the spill on the substrate in question.

7. Establish the speed of lateral movement of the established layer in a room as a function of the flammable liquid involved and the drafts normally encountered in rooms.

8. Correlate the behaviour of pure compounds such as pentane and hexane with those of typical fuels such as petrol and camping fuel.

9. Determine the reliability of using post-fire indicators such as burn patterns to estimate the area of a pre-fire pool of flammable liquid.

10. Correlate the predictions with empirical data collected from real fire and explosion scenes.

The final product will give fire investigators a better understanding of the many factors that control the formation of ignitable layers of highly flammable liquid vapours and provide them with a model by which some of them may be quantified and predicted. Such factors as typical interior temperatures and conditions of air changes and draughts, small quantities (less than 20 litres), short time frames (less than one hour), complex substrates such as carpet, and the potential roles of accidental or intentional ignition sources will be considered.

EXPERIMENTAL

Section 2

The multi-aspect nature of this enquiry necessitated a number of separate but related experiments: Pool size v. quantity; Evaporation rate v. substrate; Evaporation rate v. temperature; Evaporation rate v. pool size; Losses from pouring and splashing; Vertical diffusion; Horizontal transport; Thermodynamics of evaporating pools; Relation of single compound evaporation rates to those of multi-component petroleum products; and Relation of pool and vapour-layer characteristics to ignition and flame spread properties. Each of these will be treated in separate sections to follow.

2.1 Pool Size v. Quantity

To study the relationship between quantity of liquid poured and the surface area of the resulting pool for various substrates, quantities of volatile liquids were poured onto interior floor substrates: polished marble, smooth-finished concrete, plywood (painted and unpainted), and carpets of various types and pile depths. Most of the pours involving larger quantities of liquids (larger than 200ml) were conducted using methanol (methyl alcohol) or methylated spirits (denatured ethyl alcohol) due to environmental (air pollution) considerations and also to minimize personal safety hazards of inhaling hydrocarbon vapours. Methanol and denatured ethanol were selected for these tests as substitutes because their surface tensions and viscosities, the physical properties that control spreading more than any other, were more similar to those of the hydrocarbons being studied here, as well as to those of petrol, than that of water as seen in Table 2.1. Several experiments were conducted using one- and two-litre quantities of n-pentane and petrol on the

Table 2.1: Surface Tensions and Viscosities of Common Flammable Liquids

	Surface Tension (dynes/cm @ 20°C)	Viscosity (cp @20°C)
Methanol/air	22.61	0.597 (0.55mPa[3])
Ethanol/vapour	22.75	1.200
n-pentane/vapour	16.3[1]	0.24 (0.24[2]) (0.24mPa[3])
n-hexane/air	18.43 (18.99[1])	0.326 (0.31mPa[3])
n-octane/vapour	21.8 (22.0[1])	0.542
Toluene/vapour	28.5	0.59[2] (0.59 mPa[3])
Xylenes/air	28-30	0.65[2] (0.81mPa[3])
Water/air	73.05	1.05[2] (1.00mPa[3])
Petrol/air	≈23[4]	≈0.5[4]

Notes: 1. Calculated after the method of Macleod, as described in Perry/Green, p.3-288.

2. Calculated from the nomograph for liquid viscosities in Perry/Green, pp3-250-251.

3. Lide, 1991, p.8-64.

4. Estimated from data in the CRC Aviation Handbook [CRC].

same floor surfaces as methanol to determine the suitability of the methanol pool size data for predicting hydrocarbon pool sizes. All liquids were poured by hand from a large plastic beaker from a low height (less than 15cm) to minimize losses from splashing and turbulent pouring. (Fig.2.1.1) The actual pouring rate was not strictly controlled but was monitored visually to minimize splashing and to maintain a symmetrical starting pool. Pour times ranged from 10 – 20 s. A manually operated digital stop watch was triggered with the initiation of pouring to record elapsed time. The pool to be measured was defined by the edges of the free-standing liquid visible on non-porous surfaces or by the visibly wetted areas of absorbent substrates where there was no free-standing liquid. The dimensions of the pools were measured at one minute intervals after pouring began. The contours of all pools were recorded by hand-drawn diagram. The larger pours were also recorded using a 35mm still camera and by a hand-held VHS videotape camera to capture their shape (Fig. A.2.1.1). Due to the variety of locations used, control of ambient temperature was not possible. Ambient temperatures were measured using an alcohol thermometer. They ranged from 15 to 25°C. The depths of free-standing pools were measured by insertion of a plastic centimetre scale or by visual estimate. Control samples of carpets involved were recovered for later identification of the fibre content by polarizing light microscopy

The pours (as they appeared 2min after pouring) were then reproduced by freehand drawing onto newsprint paper in the laboratory using the diagrams, video images and size data as guides. Each replicated pool was then cut from the newsprint and the paper weighed. Comparison of this weight against the weight of a one-metre-square panel cut from the same material yielded the area of the pool directly in square metres. The same newsprint

Fig. 2.1.1: Typical pool pour test – one litre methanol on concrete.

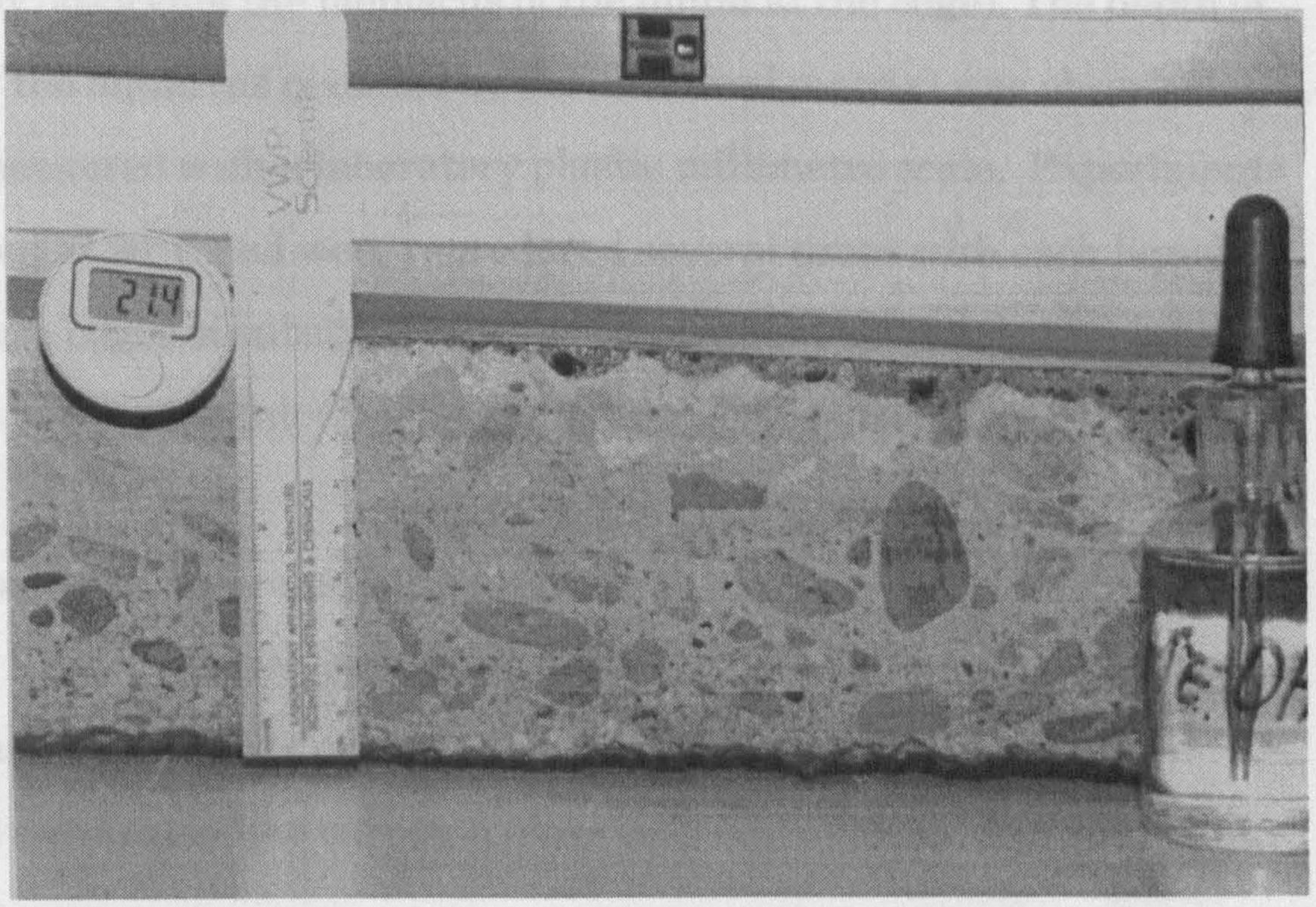

Fig. 2.1.2: Typical depth penetration – methanol on concrete.

paper was used for the measurement of all larger pools. Three one-metre-square panels were cut and weighed to establish the accuracy of the method. Each panel weighed 49.16 ± 0.21g. This simple quantitative method has been shown in the past to yield reproducibility of better than ±1% (roughly equal to manual planimetry methods). For the smaller pools, the process was repeated three times, with the final area being based on a numerical average of the three weights. The larger pools were reproduced on newsprint only once.

2.1.1 Penetration into Substrates

To supplement this information, a limited study was conducted to estimate the penetration of flammable liquids into concrete. A smooth-finished, uncoated section of concrete, 13 x 42cm in size, was sawn from an interior floor slab (Fig. 2.1.2). A small quantity of liquid was pipetted by hand onto the surface sufficient to flood the surface but not to run over the edge under observation (by observing the meniscus of the liquid at the edge). The depth of penetration of the liquid (as revealed by the darkened matrix) was observed directly and measured with a laboratory plastic millimetre scale. Experiments were carried out at 20°C and were reproduced several times with each liquid. Due to the rough edges of substrates like wood, similar experiments on other surfaces were not successful. (See Sect. 3.1.1 for results.)

2.1.2 Transport within Porous Substrates

To examine the role of spread of pentane driven by capillary action within porous substrates like carpet, a glass thin-layer chromatography tank

was fitted with a metal rack that would hold 5 x 20cm strips of carpet in vertical orientation (Fig. 2.1.3). A quantity of n-pentane was placed in the bottom of the tank at 20°C, and the tank closed and allowed to equilibrate at saturation for one hour. The rack was then lowered into the tank so that the lower 1cm of each carpet strip was immersed in the liquid pentane while the upper portion was immersed in a saturated pentane/air mixture to reduce evaporative losses. The absorption of pentane by the carpet against gravitational pull was observed by visually noting the progress of a wetted area moving up the carpet strip. The height was measured against a plastic 15 centimetre scale which had been affixed to the metal frame, and was recorded at time intervals of 5 min., 30 min., and 60 min. (See Sect. 3.1.2 for results.) Two primary types of common carpet were examined: (1) a commercial-type short-loop pile with an integral backing of synthetic rubber or urethane foam rubber and (2) a residential-type plush pile with a jute or polypropylene backing but without an integral pad. Typical cross-sections of both types are shown in Fig. A.2.1.2.

2.2 Evaporation Rate v. Substrate (Source Strength)

To compare the evaporation rates from complex substrates like carpet to that of a pool and to isolate some of the contributing factors, it was decided to evaporate small (80 – 220ml) quantities of pentane, hexane, and octane from shallow glass Petri dishes in still air and measure the loss of mass over a period of time. To accomplish this, an experimental system as shown in Fig. 2.2.1 was assembled. The heart of the system was a Sartorius "Basic" Model electronic pan balance operated by a Compaq® LTE386s portable personal

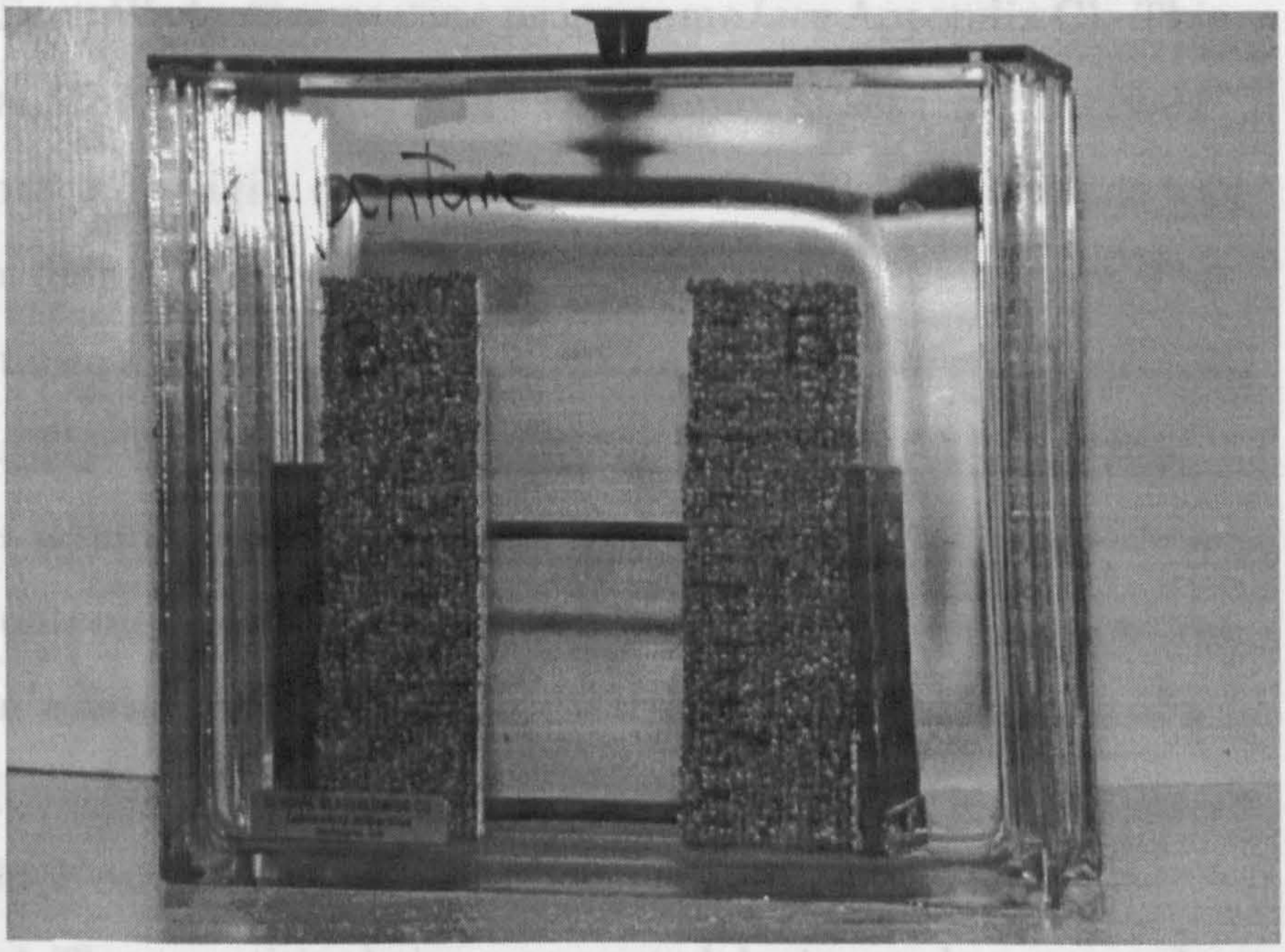

Fig. 2.1.3: Porosity (capillarity) tests – carpet in pentane tank.

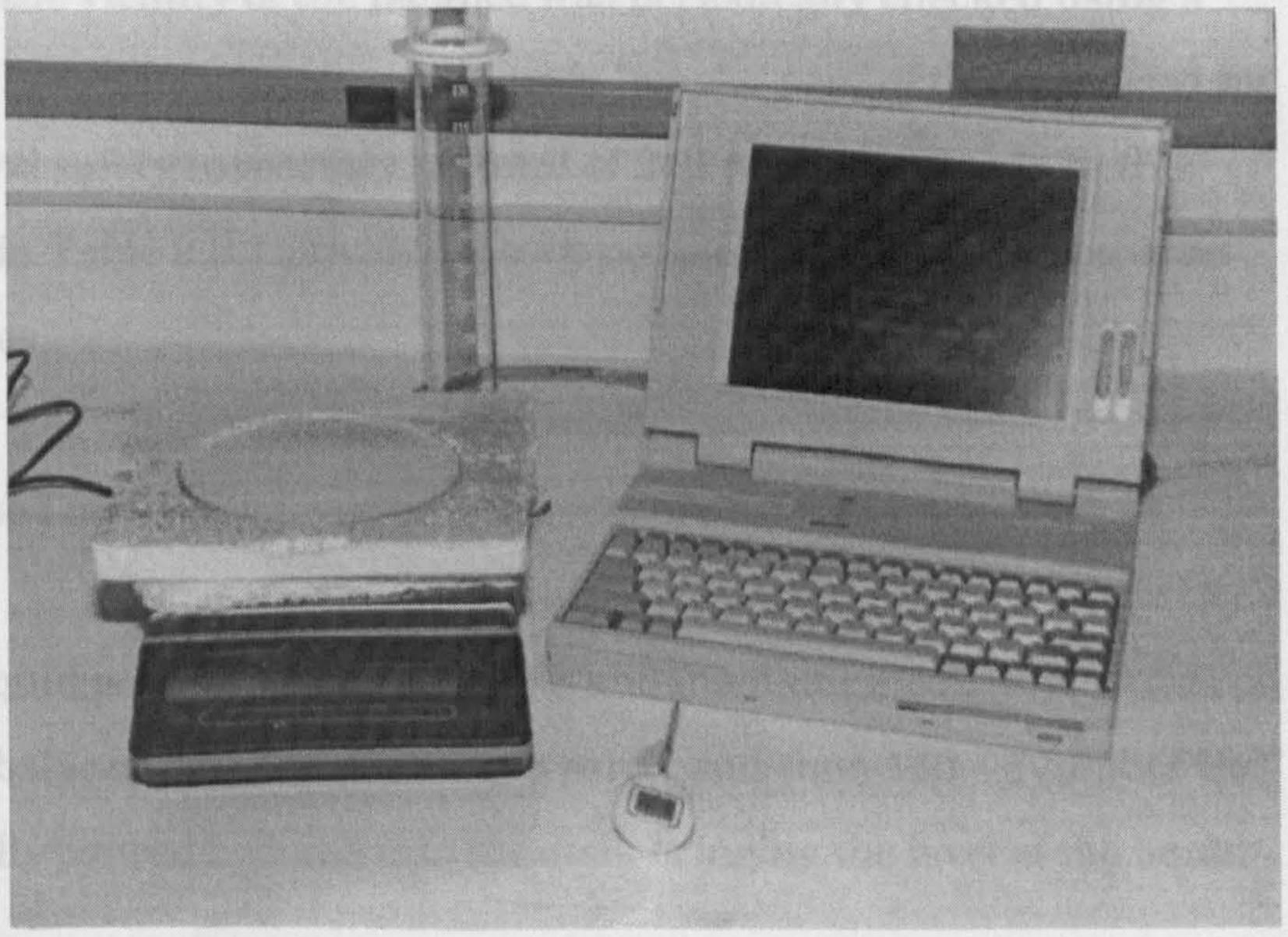

Fig. 2.2.1: Sartorius pan balance with insulated Petri dish and Compaq© portable computer.

computer with a SartoWedge® operating programme (see Appendix C). This programme allowed the computer to query the balance at set time intervals and record the time and weight on the balance in a data file. The balance was fitted with a 15cm diameter glass Petri dish, approximately 13mm deep. The Petri dish was set into a block (12mm thick, 220mm square) of rigid expanded polystyrene foam (Styrofoam) so that its rim was flush with the top of the foam. A separate 12mm block of Styrofoam was used to thermally insulate the dish and its contents from the balance pan for most of the data gathering. The entire system was assembled on a laboratory bench placed in front of a large laboratory fume hood (1.2 m in width), which was not operated during the actual run but which could be started at the end of each run to remove the vapours generated. The quantities being evaporated during each run were kept small so as to minimize the risk of accidental ignition of accumulated vapours in the laboratory. The doors to the laboratory were kept closed, and foot traffic in the vicinity of the system prohibited to minimize drafts. The extent of natural drafts in the vicinity of the balance was periodically checked using a GasTec® stannic chloride/ stannic oxychloride "smoke pen" of the type used by environmental and safety inspectors. A total of 242 runs were made in this manner (as seen in Table 2.2.1) involving both pools of free liquid and pools on various substrates.

2.2.1 Pools – Free Liquid

For free liquid pool runs, the Petri dish and insulator block were placed on the balance, the balance was tared (reset to zero), and then 150 – 170ml of the liquid was carefully poured by hand into the dish, bringing the level of the liquid

Table 2.2.1: Master List of Evaporation Rate Experiments

Number	Volume	Liquid	Substrate	Diameter	Conditions		Amb. Temp.
1	80 ml	PENTANE	Pool	15 cm			18.0
2	100 ml	PENTANE	Pool	15 cm	B		18.0
3	115 ml	PENTANE	Pool	15 cm			24.0
4	150 ml	PENTANE	Pool	15 cm			22.0
5	150 ml	PENTANE	Pool	15 cm	B		23.0
6	150 ml	PENTANE	Pool	15 cm	B		24.0
7	150 ml	PENTANE	Pool	15 cm		I	23.0
8	100 ml	PENTANE	Pool	15 cm	B	I	24.0
10	100 ml	PENTANE	on Sand	15 cm			25.0
11	100 ml	PENTANE	on Sand	15 cm		I	25.0
12	100 ml	PENTANE	on Sand	15 cm		I	22.0
13	100 ml	PENTANE	on Sand	15 cm	B	I	22.0
14	100 ml	PENTANE	on Sand	15 cm	B	I	22.0
15	150 ml	PENTANE	Pool	15 cm	B	I	23.0
16	220 ml	PENTANE	on Carpet	15 cm		I	23.0
17	220 ml	PENTANE	on Carpet	15 cm		I	22.0
18	225 ml	PENTANE	on Carpet	15 cm		I	22.0
19	225 ml	PENTANE	on Carpet	15 cm	B	I	22.5
20	100 ml	PENTANE	Pool	15 cm		I	22.0
21	122 ml	PENTANE	Pool	15 cm		I	22.0
22	120 ml	PENTANE	Pool	15 cm	B	I	21.4
23	124 ml	PENTANE	Pool	15 cm	B	I	21.0
24	225 ml	PENTANE	on Carpet	15 cm		I	22.0
25	110 ml	PENTANE	on Sand	15 cm		I	22.6
26	219 ml	PENTANE	on Carpet	15 cm		I	22.5
27	110 ml	PENTANE	on Sand	15 cm		I	22.7
28	100 ml	PENTANE	on Sand	15 cm	B	I	22.6
29	221 ml	PENTANE	on Carpet	15 cm	B	I	22.0
30	85 ml	PENTANE	on Al	15 cm		I	21.0
31	85 ml	PENTANE	on Al	15 cm		I	21.0
32	90 ml	PENTANE	on Al	15 cm		I	20.0
33	88 ml	PENTANE	on Al	15 cm	B	I	20.0
34	88 ml	PENTANE	on Al	15 cm	B	I	20.0
35	100 ml	PENTANE	on Sand	20 cm			22.0
36	50 ml	PENTANE	on Al	20 cm			22.0
37	100 ml	OCTANE	Pool	15 cm		I	22.0
38	230 ml	OCTANE	on Carpet	15 cm		I	21.8
39	108 ml	OCTANE	on Sand	15 cm		I	21.8
40	105 ml	OCTANE	on Al	15 cm		I	21.7
41	100 ml	OCTANE	on Al	15 cm		I	21.7
43	100 ml	OCTANE	on Al	15 cm	B	I	22.0

Conditions Key:

B - 0.6m high acrylic barrier in place during run
I - Petri dish insulated from pan of balance
O - High temperature runs in oven at 35-37°C
L - Barrier runs with lid

Table 2.2.1: Master List of Evaporation Rate Experiments

(Cont.)

Number	Volume	Liquid	Substrate	Diameter	Conditions		Amb. Temp.
44	100 ml	OCTANE	on Sand	15 cm	B	I	22.1
45	240 ml	OCTANE	on Carpet	15 cm	B	I	21.8
46	140 ml	PENTANE	Pool	15 cm		I	23.2
47	150 ml	PENTANE	Pool	15 cm		I	24.0
48	90 ml	PENTANE	on Sand	15 cm		I	24.5
49	100 ml	PENTANE	on Al	15 cm		I	24.1
50	240 ml	PENTANE	on Carpet	15 cm		I	24.6
51	150 ml	OCTANE	Pool	15 cm		I	24.6
52	250 ml	OCTANE	on Carpet	15 cm		I	25.3
53	150 ml	PENTANE	Pool	15 cm	B	I	25.6
54	95 ml	PENTANE	on Sand	15 cm	B	I	25.8
55	150 ml	HEXANE	Pool	15 cm		I	21.7
56	100 ml	HEXANE	on Sand	15 cm		I	21.5
57	95 ml	HEXANE	on Al	15 cm		I	21.4
58	220 ml	HEXANE	on Carpet	15 cm		I	21.2
59	100 ml	HEXANE	on Sand	15 cm	B	I	21.5
60	150 ml	HEXANE	Pool	15 cm	B	I	21.0
61	240 ml	HEXANE	on Carpet	15 cm	B	I	21.2
65	108 ml	PENTANE	Pool	15 cm		I	24.1
66	130 ml	PENTANE	Pool	15 cm		I	24.1
67	135 ml	PENTANE	on Al	15 cm		I	24.6
68	100 ml	PENTANE	on Sand	15 cm		I	24.5
70	180 ml	PENTANE	Pool	15 cm		I	21.9
71	180 ml	PENTANE	Pool	15 cm		I	22.2
72	190 ml	HEXANE	Pool	15 cm		I	23.2
73	190 ml	HEXANE	Pool	15 cm		I	23.3
74	190 ml	OCTANE	Pool	15 cm		I	23.0
75	190 ml	OCTANE	Pool	15 cm		I	23.4
76	190 ml	PENTANE	Pool	15 cm		I	23.6
77	50 ml	PENTANE	Pool	15 cm		I	22.5
78	50 ml	PENTANE	Pool	15 cm		I	23.0
79	190 ml	HEXANE	Pool	15 cm		I	23.0
80	190 ml	PENTANE	Pool	15 cm		I	23.0
81	190 ml	PENTANE	Pool	15 cm			23.5
82	190 ml	HEXANE	Pool	15 cm			24.0
83	180 ml	HEXANE	Pool	15 cm			24.0
85	180 ml	PETROL	Pool	15 cm		I	22.0
86	150 ml	PETROL	Pool	15 cm		I	22.9
87	180 ml	PETROL	Pool	15 cm		I	22.4
90	185 ml	PENTANE	Pool	15 cm		I	22.0
92	150 ml	PENTANE	on Carpet A	25 cm		I	22.0

Conditions Key:

B - 0.6m high acrylic barrier in place during run
I - Petri dish insulated from pan of balance
O - High temperature runs in oven at 35-37°C
L - Barrier runs with lid

Table 2.2.1: Master List of Evaporation Rate Experiments

(Cont.)

Number	Volume	Liquid	Substrate	Diameter	Conditions	Amb. Temp.
93	100 ml	PENTANE	on Carpet A	22x26 cm	I	22.0
94	150 ml	HEXANE	on Carpet A	25 cm	I	22.5
95	150 ml	HEXANE	on Carpet B	28 cm	I	22.5
96	145 ml	PENTANE	on Carpet A	27 cm	I	22.0
97	146 ml	PENTANE	on Carpet A	27 cm	I	22.0
98	20 ml	PENTANE	Film	15 cm	I	21.0
99	20 ml	PENTANE	Film	15 cm	I	22.0
100	20 ml	PENTANE	Film	15 cm	I	22.0
101	20 ml	PENTANE	Film	15 cm	I	22.0
102	20 ml	PENTANE	Film	15 cm	I	22.2
103	20 ml	HEXANE	Film	15 cm	I	22.0
104	20 ml	HEXANE	Film	15 cm	I	21.5
105	20 ml	HEXANE	Film	15 cm	I	21.5
106	20 ml	HEXANE	Film	15 cm	I	21.5
107	20 ml	HEXANE	Film	15 cm	I	21.5
108	150 ml	PENTANE	on Carpet E	12 cm	I	21.0
109	151 ml	PENTANE	on Carpet D	11 cm	I	20.8
110	150 ml	PENTANE	on Carpet C	11 cm	I	21.0
111	150 ml	PENTANE	on Carpet E	12 cm	I	21.5
112	150 ml	PENTANE	on Carpet D	10 cm	I	21.3
113	151 ml	PENTANE	on Carpet C	13 cm	I	20.2
114	150 ml	PENTANE	on Carpet E	13 cm	I	20.5
115	150 ml	PENTANE	on Carpet A	27 cm	I	20.5
116	151 ml	PENTANE	on Carpet B	28 cm	I	21.5
117	150 ml	PENTANE	on Carpet D	12 cm	I	21.4
118	300 ml	PENTANE	on Carpet E	18 cm	I	21.0
119	10 ml	PENTANE	Film	15 cm	I	5.0
120	11 ml	PENTANE	Film	15 cm	I	4.5
121	11 ml	PENTANE	Film	15 cm	I	4.5
122	10 ml	PENTANE	Film	15 cm	I	3.1
123	10 ml	HEXANE	Film	15 cm	I	4.2
124	10 ml	HEXANE	Film	15 cm	I	4.3
125	10 ml	HEXANE	Film	15 cm	I	5.0
126	20 ml	PENTANE	Film	15 cm	I	3.0
127	190 ml	PENTANE	Pool	15 cm	I	3.3
128	190 ml	PENTANE	Pool	15 cm	I	5.1
129	190 ml	PENTANE	Pool	15 cm	I	6.1
130	110 ml	PENTANE	on Al	15 cm	I	3.6
131	100 ml	PENTANE	on Sand	15 cm	I	6.0
132	200 ml	PENTANE	on Carpet	15 cm	I	5.4
133	100 ml	PENTANE	on Sand	15 cm	I	6.5

Conditions Key:

B - 0.6m high acrylic barrier in place during run
I - Petri dish insulated from pan of balance
O - High temperature runs in oven at 35-37°C
L - Barrier runs with lid

Table 2.2.1: Master List of Evaporation Rate Experiments

(Cont.)

Number	Volume	Liquid	Substrate	Diameter	Conditions	Amb. Temp.
134	115 ml	PENTANE	on Al	15 cm	I	3.0
135	110 ml	PENTANE	on Sand	15 cm	I	5.5
136	15 ml	OCTANE	Film	15 cm	I	4.5
137	350 ml	PENTANE	on Carpet	20.5 cm	I	20.5
138	175 ml	PENTANE	Pool	20.5 cm	I	21.9
139	112 ml	PENTANE	on Sand	20.5 cm	I	21.5
140	118 ml	PENTANE	on Al	20.5 cm	I	20.5
141	115 ml	PENTANE	on Al	20.5 cm	I	20.1
142	120 ml	PENTANE	on Sand	20.5 cm	I	20.8
143	375 ml	PENTANE	on Carpet C	20.5 cm	I	21.2
144	90 ml	PENTANE	on Carpet A	15 cm	I	21.6
146	100 ml	PENTANE	on Carpet A	24 cm	I	22.0
147	100 ml	PENTANE	on Carpet B	21x28 cm	I	22.0
148	100 ml	PENTANE	on Carpet C	8x10 cm	I	22.5
149	100 ml	PENTANE	on Carpet D	13x18 cm	I	23.0
150	100 ml	PENTANE	on Carpet E	10x13 cm	I	22.5
155	190 ml	HEXANE	Pool	15 cm	B I	20.9
156	188 ml	HEXANE	Pool	15 cm	B I	19.0
157	190 ml	HEXANE	Pool	15 cm	B I	20.1
158	190 ml	HEXANE	Pool	15 cm	B I	20.5
159	185 ml	HEXANE	Pool	15 cm	B I	21.5
160	220 ml	HEXANE	on Carpet	15 cm	I	21.2
161	190 ml	HEXANE	Pool	15 cm	B I	21.0
162	190 ml	HEXANE	Pool	15 cm	B I	22.0
163	190 ml	HEXANE	Pool	15 cm	L I	21.5
164	225 ml	HEXANE	on Carpet	15 cm	I	22.0
165	190 ml	HEXANE	Pool	15 cm	L I	22.0
166	190 ml	OCTANE	Pool	15 cm	I	22.0
167	190 ml	OCTANE	Pool	15 cm	B I	22.0
169	190 ml	PENTANE	Pool	15 cm	I	22.0
170	190 ml	PENTANE	Pool	15 cm	I	22.0
171	220 ml	PENTANE	on Carpet	15 cm	I	22.0
172	105 ml	PENTANE	on Sand	15 cm	I	22.0
173	114 ml	PENTANE	on Al	15 cm	I	22.3
174	100 ml	PENTANE	on Sand	15 cm	I	23.0
175	110 ml	PENTANE	on Al	15 cm	I	23.5
176	215 ml	PENTANE	on Carpet	15 cm	I	22.5
177	190 ml	PENTANE	Pool	15 cm	I	23.7
178	190 ml	PENTANE	Pool	15 cm	O	36.6
179	185 ml	PENTANE	Pool	15 cm	O	35.5
180	100 ml	PENTANE	on Al	15 cm	O	35.5

Conditions Key:

B - 0.6m high acrylic barrier in place during run
I - Petri dish insulated from pan of balance
O - High temperature runs in oven at 35-37°C
L - Barrier runs with lid

Table 2.2.1: Master List of Evaporation Rate Experiments

(Cont.)

Number	Volume	Liquid	Substrate	Diameter	Conditions	Amb. Temp.
181	185 ml	HEXANE	Pool	15 cm	O	35.1
182	190 ml	HEXANE	Pool	15 cm	O	36.5
183	190 ml	HEXANE	Pool	15 cm	O	36.0
184	100 ml	HEXANE	on Al	15 cm	O	35.0
185	100 ml	HEXANE	on Sand	15 cm	O	35.0
186	90 ml	PENTANE	on Sand	15 cm	O	36.0
187	90 ml	PENTANE	on Al	15 cm	O	36.0
188	190 ml	PENTANE	on Carpet	15 cm	O	33.5
189	190 ml	PENTANE	Pool	15 cm	B I	22.0
190	192 ml	PENTANE	Pool	15 cm	B I	22.2
191	190 ml	HEXANE	Pool	15 cm	B I	22.4
192	190 ml	PENTANE	Pool	15 cm	B I	22.6
193	100 ml	PENTANE	on Sand	15 cm	B I	22.1
194	350 ml	PENTANE	on Carpet C	18 cm	I	20.0
195	300 ml	PENTANE	on Carpet E	20 cm	I	20.0
196	300 ml	PENTANE	on Carpet D	15 cm	I	21.0
197	210 ml	PENTANE	on Ur. Foam	15 cm	I	21.0
198	250 ml	PENTANE	on Ur. Foam	15 cm	I	21.5
199	250 ml	PENTANE	on Ur. Foam	15 cm	I	22.3
200	250 ml	HEXANE	on Ur. Foam	15 cm	I	22.5
201	250 ml	PENTANE	on Lg. Pan	33 cm	I	19.7
202	275 ml	PENTANE	on Lg. Pan	33 cm	I	20.5
203	275 ml	PENTANE	on Lg. Pan	33 cm	I	20.5
204	272 ml	PENTANE	on Lg. Pan	33 cm	I	20.8
205	20 ml	PENTANE	on Petri Dish	5.2 cm	I	19.6
206	20 ml	PENTANE	on Petri Dish	5.6 cm	I	20.7
207	270 ml	PENTANE	on Lg. Pan	33 cm	I	20.1
208	200 ml	PENTANE	on Beaker	6 cm	I	21.5
209	25 ml	PENTANE	on Petri Dish	6 cm	I	20.6
210	25 ml	PENTANE	on Petri Dish	5 cm	I	20.5
211	300 ml	PENTANE	on Rect. Pan	26x38 cm	I	20.4
212	30 ml	PENTANE	on Petri Dish	6 cm	I	21.2
213	30 ml	PENTANE	on Petri Dish	5 cm	I	20.5
214	300 ml	PENTANE	on Rect. Pan	26x38 cm	I	20.5
215	230 ml	PENTANE	on Ur. Foam	15 cm	I	21.2
216	250 ml	PENTANE	on Ur. Foam	15 cm	I	20.5
217	190 ml	CAMP FUEL 1	Pool	15 cm	I	19.7
218	20 ml	CAMP FUEL 1	Film	15 cm	I	20.2
219	38 ml	BP PETROL	Film	15 cm	I	20.5
220	195 ml	CAMP FUEL 2	Pool	15 cm	I	20.5
221	190 ml	BP PETROL	Pool	15 cm	I	19.5

Conditions Key:

B - 0.6m high acrylic barrier in place during run
I - Petri dish insulated from pan of balance
O - High temperature runs in oven at 35-37°C
L - Barrier runs with lid

Table 2.2.1: Master List of Evaporation Rate Experiments

(Cont.)

Number	Volume	Liquid	Substrate	Diameter	Conditions	Amb. Temp.
222	190 ml	CAMP FUEL 2	Pool	15 cm	I	20.0
223	192 ml	CAMP FUEL 3	Pool	15 cm	I	20.2
224	230 ml	PENTANE	on Ur. Foam	15 cm	I	20.0
225	230 ml	PENTANE	on Ur. Foam	15 cm	I	21.0
226	240 ml	PENTANE	on Ur. Foam	15 cm	I	20.5
227	9 ml	PENTANE	on Plaster	15 cm	I	20.0
228	10 ml	PENTANE	on Plaster	15 cm	I	20.5
229	10 ml	PENTANE	on Plaster	15 cm	I	20.5
230	190 ml	OCTANE	Pool	15 cm		36.0
231	190 ml	OCTANE	Pool	15 cm		36.5
232	190 ml	OCTANE	Pool	15 cm		36.0
233	190 ml	OCTANE	Pool	15 cm		36.0
234	15 ml	HEXANE	on Plaster	15 cm	I	22.0
235	25 ml	HEXANE	on Plaster	15 cm	I	22.0
236	22 ml	HEXANE	on Plaster	15 cm	I	22.0
237	220 ml	HEXANE	on Ur. Foam	15 cm	I	23.0
238	23 ml	HEXANE	on Plaster	15 cm	I	22.0
239	240 ml	HEXANE	on Ur. Foam	15 cm	I	22.0
240	25 ml	HEXANE	on Plaster	15 cm	I	23.0
241	230 ml	HEXANE	on Ur. Foam	15 cm	I	22.0
242	25 ml	HEXANE	on Plaster	15 cm	I	23.0

Conditions Key:
B - 0.6m high acrylic barrier in place during run
I - Petri dish insulated from pan of balance
O - High temperature runs in oven at 35-37°C
L - Barrier runs with lid

to just below the rim of the dish to minimize edge effects. Elapsed time was measured from the time interval in which the pour was completed, (which typically required 6 – 9s to complete). The start then corresponded to maximum mass of liquid. Several modifications of this protocol were used to gather additional data about the vaporization process. In one, a small quantity (50ml) of liquid was poured into an empty Petri dish, producing a shallow pool (3 – 4mm deep) at the bottom of a shallow well (9 – 10mm deep) formed by the sides of the Petri dish. The evaporation tests were then carried out as for other pool tests. In the second, approximately 170ml of distilled water were placed in the Petri dish and then a small quantity (10 – 20ml) of liquid was added to float atop the water. This produced a thin film of liquid (1 – 2mm thick) flush with the rim of the dish, i.e., without the walls of the dish to affect the dispersion of vapours. (See Sect. 3.2 for results.)

2.2.2 Substrates

To attempt to isolate some of the mechanical and thermal effects that may result from different substrates, dry silica sand of 20 – 30 mesh and granulated aluminium of the same mesh size were used as substrates. The 15cm Petri dishes used for most of the tests contained 0.37 ± 0.02kg of sand or aluminium granules. In addition, one dish was filled nearly to the brim with plaster of Paris that was allowed to harden in place, for solid porous-matrix tests. Panels of jute-backed synthetic pile carpet and light-weight urethane foam were cut to fit snugly in the same 15cm Petri dishes and were used for the carpet and foam matrix tests. The carpet was of 12mm thickness, so its top surface was flush with the rim of the Petri dish when flooded with liquid. The

foam was tested in both 22mm and 12mm thicknesses. For all other substrate runs, the substrate was placed in the dish with its top surface nearly level with the rim of the dish and the liquid added until the surface was just covered with liquid and even with or just below the rim of the Petri dish, thus ensuring that the same surface area was exposed as for the liquid pool tests. (Figs. A2.2.2.1(a) –(d))

For each substrate test, the insulated Petri dish with its substrate was placed on the balance pan, the balance tared, and then enough liquid was added to saturate the substrate and generate a slight excess of liquid to bring the pool surface as level as possible with the rim of the dish. Starting time was recorded as the time interval in which pouring was completed (maximum mass). Care was taken to store all materials together so that the starting temperatures (of substrate and liquid) would be the same as ambient for all tests. The weight of the sample was recorded approximately* every 20 seconds for 30 – 60 minutes for most of the experiments. When it became apparent that the evaporation rate may have been changing so quickly during the first minute of each run that measurements every twenty seconds may not have been detecting important data, the sampling rate was changed to approximately* once every five seconds. Starting weights varied from run to run due to minor differences in volume between Petri dishes and irregularities in packing and settling of the granular substrates. Since the focus of this study was the rate of mass loss, such discrepancies were not considered important. The starting ambient temperature was measured using a mercury thermometer and the final bulk

*In the SartoWedge® operating programme, the time interval is set in 1/18th second increments, which resulted in slight variations from true 5s or 20s intervals.

temperature of the liquid pool or of the matrix was measured at the end of each run by insertion of a digital electronic thermometer. This thermometer had a small (1mm diameter) tip, which minimized contact with the surface to be measured. Its thermal mass appeared to be quite low as its insertion had no detectable effect on measurements conducted simultaneously via thermocouples in later tests. Changes in the physical appearance of the substrate were noted during each run. Any unevaporated liquid was recovered for later re-use when the substrate (such as sand, aluminium, or foam) would not create contamination that could interfere with subsequent tests..

At the end of each run, the adjacent fume hood was operated for a short time to vent any accumulated vapours. The recorded time and mass data captured by the SartoWedge® programme on the portable computer were transferred to floppy disc for analysis by manipulation using standard Microsoft Excel® spreadsheet operations. This allowed the calculation of rate of mass loss per unit time, which could then be plotted using the Excel ChartWizard® programme. The entire process was repeated for n-pentane several times, and most of the experiments were repeated using hexane and n-octane to study the effect of vapour pressure.

A limited number of evaporation rate studies were conducted using carpets of various types, cut into 28 x 28cm panels and each glued to a panel of 12mm rigid Styrofoam. Each carpet/insulator block was placed on the balance pan, the balance tared, and then a pre-measured quantity of liquid was poured by hand onto the centre of the carpet panel. (Fig. 2.2.2.2) The liquid was allowed to seek its own limits, which were recorded by measuring the dimensions of the visibly wetted area of the carpet surface using a laboratory centimetre scale, as in Fig.2.2.2.3. The collection of weight data was conducted

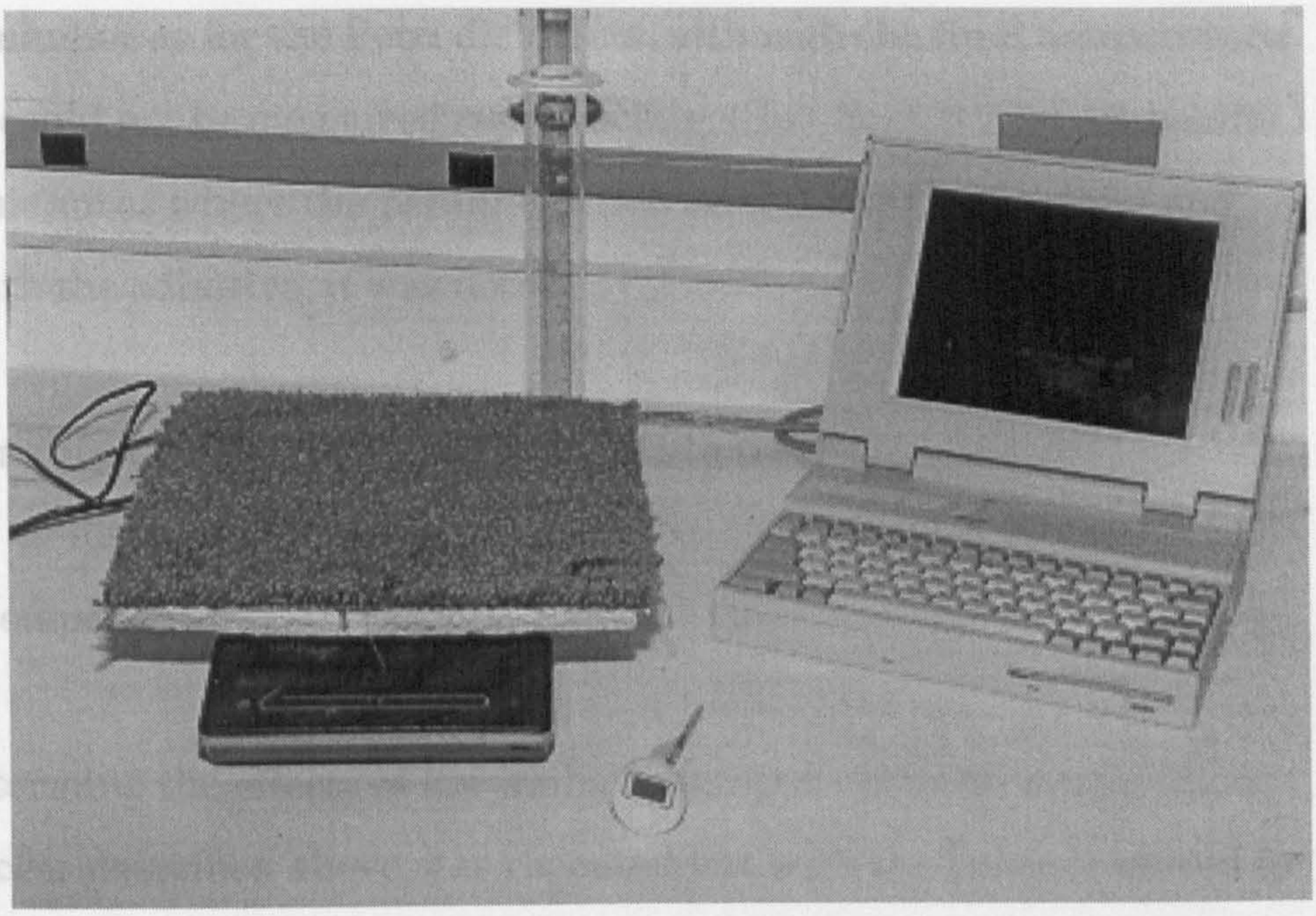

Fig. 2.2.2.2: Balance with insulated carpet test panel.

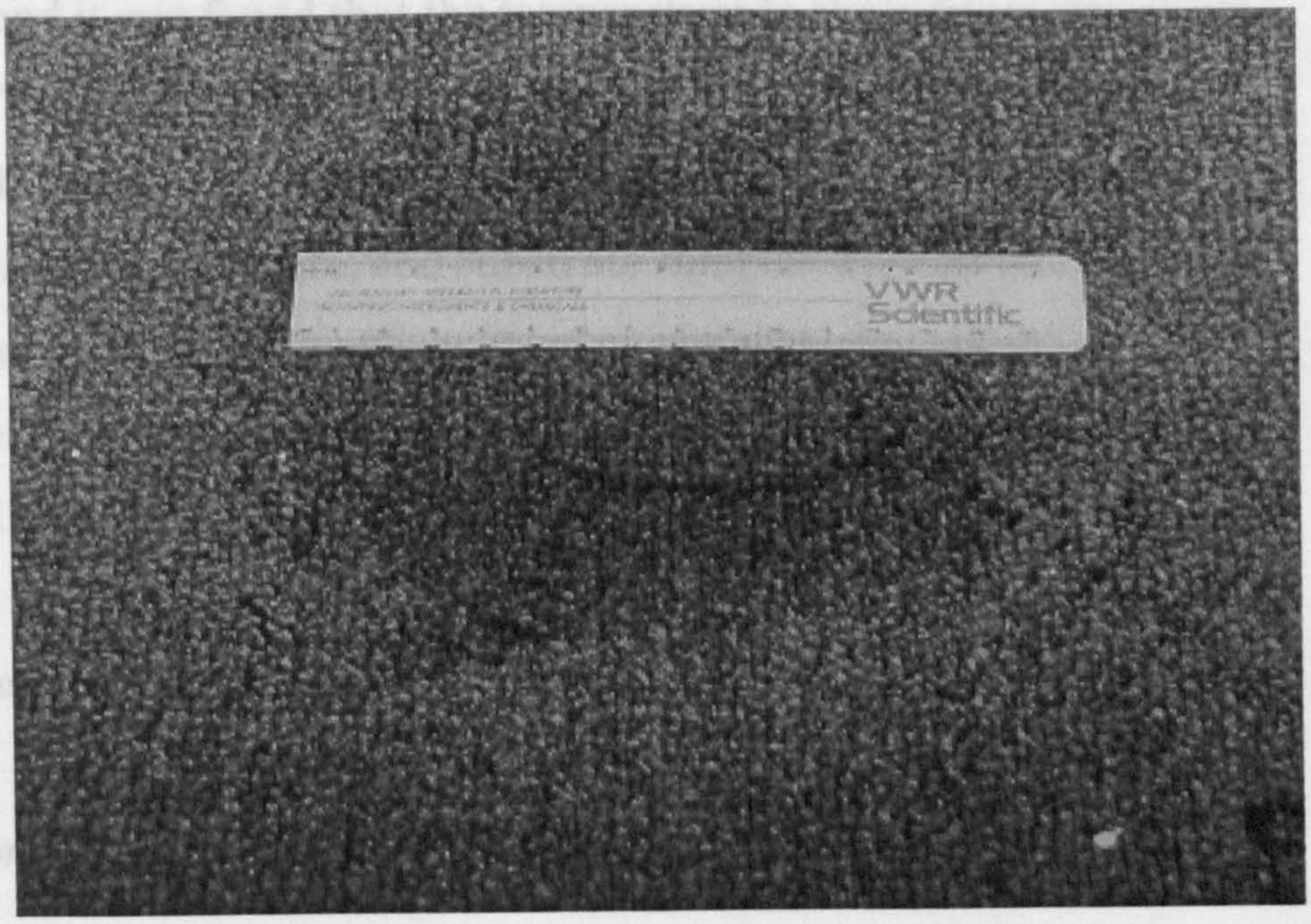

Fig. 2.2.2.3: Typical pour on carpet with wetted area 0.14m in diameter.

in the same manner as for the Petri dish tests, although the final temperature of the carpet could not be measured reproducibly. (See Sect. 3.2 for all results.) In the rare instances where the pentane penetrated the carpet backing and interacted with the adhesive, it was noted.

2.3 Relationship of Initial Evaporation Rate to Temperature

2.3.1 Low Temperature

To determine the effects of low ambient temperatures on evaporation rate, the process described above was repeated but with the balance moved to the floor of a walk-in refrigerator for the data runs. The refrigerator could be cooled to ≈4°C and then turned off to minimize air currents. Mass data were collected every 5s but runs were conducted only over ten minute intervals. The ambient temperatures were monitored with a mercury laboratory thermometer and it was found that the temperature in the refrigerator would only rise 2 – 3°C over a ten minute interval. The computer could be operated from outside the refrigerator by means of an umbilical connection to the balance. The liquids, glassware, and substrate samples were all stored in the same refrigerator to ensure a uniform starting temperature. All other procedures were the same as for normal ambient temperature runs. (See Sect. 3.3 for results.)

2.3.2 High Temperature

To determine high temperature effects, the balance was moved to the

interior of a convection-type laboratory oven designed for serological testing. The computer was kept outside the oven and the control umbilical fed to the balance through the thermometer port/vent in the top of the oven. This oven had an internal glass door, which made it possible to establish a temperature of 36 – 37°C inside, and then for the oven to be shut off for up to 15 minutes and still maintain an interior temperature ≥34°C. This was essential since the oven was not explosion-proof and it was necessary to conduct each evaporation test with the power off to minimize the risk of a vapour explosion within the oven. At the end of each run, the oven was vented before being energized to resume its preset temperature. All other procedures were the same as normal ambient temperature runs.

As with normal ambient runs, the data gathered from these runs were analyzed using the Microsoft Excel® spreadsheet programme to allow calculation of mass loss and then rate of mass loss. The results were then plotted using the Microsoft Excel® ChartWizard® plot programme. The process was repeated several times for each liquid and each substrate. The results will be presented in the Data section to follow. (See Sect. 3.3 for results.)

2.4 Evaporation Rates v. Pool Size

The data gathering process described above was repeated using glass Petri dishes ranging in diameter from 5 to 15cm (producing pools of 0.006 – 0.016m^2 in area). For larger pools, it was necessary to use a shallow plastic dish, 20.5cm in diameter (0.033m^2 in area) (Fig. A2.4.1), a shallow (9mm

deep), circular, light-gauge metal pan of 33cm diameter (0.045m^2 in area), and a shallow (15mm deep), rectangular metal pan 28 x 38cm in size (0.11m^2 in area). While the thermal properties of these pans were not the same as those of the glass Petri dishes, the most important data were their initial evaporation rates. Each pan was supported by a Styrofoam panel, 12mm in thickness. The edges of these larger pans were not insulated. Their different thermal capacities and conductivities would be expected to play a role only in later stages of the evaporation process, and could be disregarded for these tests.

Pool sizes of varying sizes were created on carpet by pouring different quantities of fuels onto carpet panels (28 x 28cm) that had been glued to solid panels of Styrofoam (see Sect. 2.2.2). The different quantities and pile heights resulted in wetted areas ranging from 6 to 28cm in diameter (0.005 – 0.07 m^2 in area). (See Sect. 3.4 for results for both pools and carpets.)

2.5 Evaluation of Losses from Pouring and Splashing

For these tests, a plastic pan, approximately 12cm in depth and 24cm in diameter was filled with an expanded aluminium foil mesh designed for flash suppression in fuel cans (Fig.2.5.1). This mesh allowed the trapping of virtually all the liquid that entered the pan without splashing. A series of experiments was conducted by pouring 250ml quantities of n-pentane and n-hexane at various heights from a 250ml graduated cylinder to produce a laminar flow, and a 250ml (TC) volumetric flask to produce a turbulent flow. The weight of the cylinder or flask was measured on the Sartorius electronic pan balance, then tared. The starting weight of the liquid was recorded. The pan with its mesh

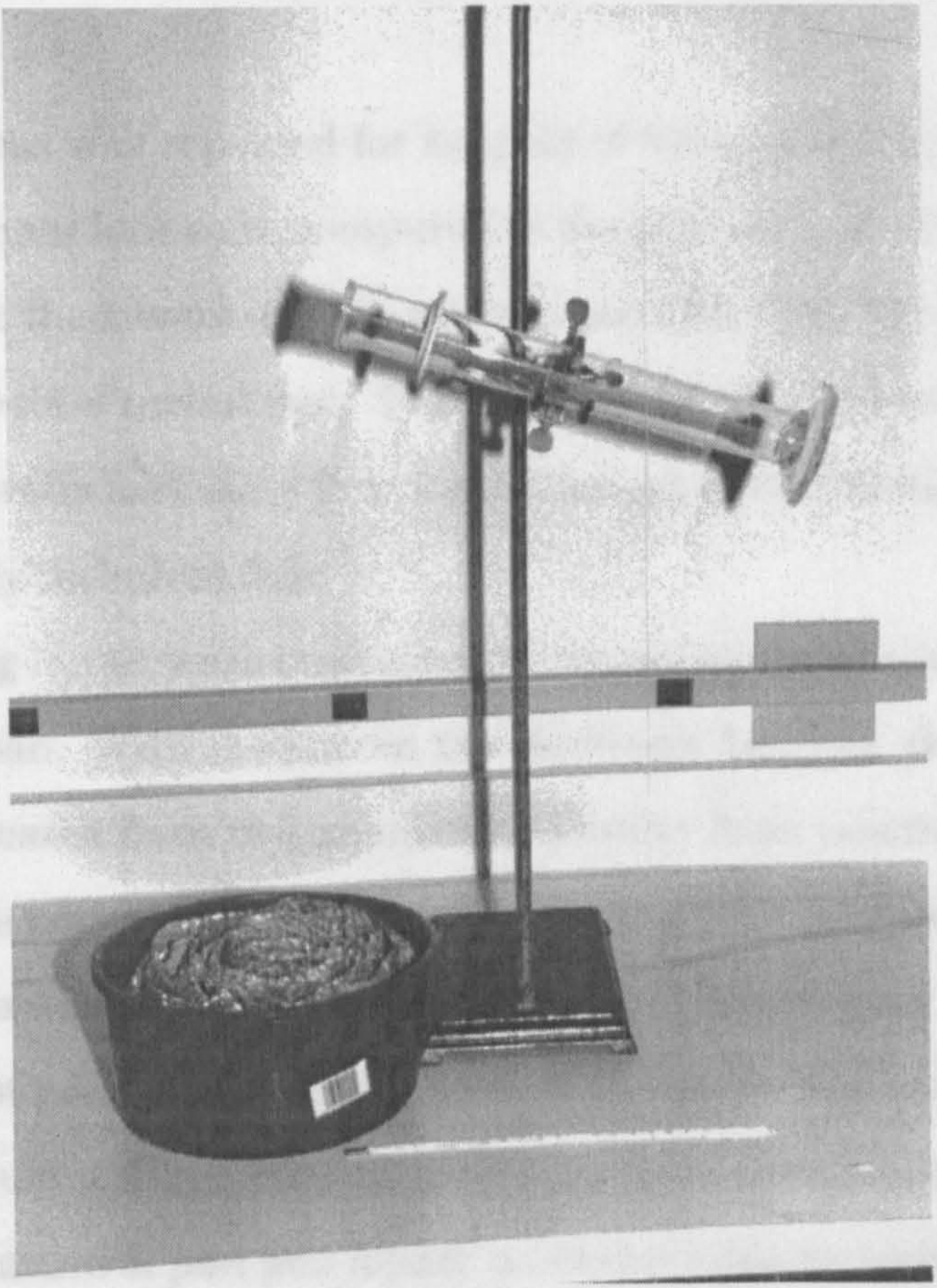

Fig. 2.5.1: Pouring loss experiment – laminar flow into mesh-filled pan.

filler was similarly weighed and tared. The liquid was first poured by hand into the pan from 0cm (level with the rim of the pan) and the accumulated weight was measured immediately at the completion of the pour. The time needed to pour was measured by manually operated digital stopwatch and recorded. This yielded a control measure of loss caused by transfer from one container to the other.

The process was repeated for heights of 50cm and 100cm, and the percentages of mass loss were compared to the control loss. Two orientations of the volumetric flask were used to achieve two different, but generally reproducible, levels of turbulence. The flask emptied nearly horizontally produced a generally turbulent flow but a flask up-ended vertically over the pan produced a highly turbulent flow.

Splashing losses were evaluated by removing the aluminium splash mesh from the pan. With the pan on the electronic balance, the pouring process was repeated from the graduated cylinder from positions 50cm and 100cm above the bottom of the pan, allowing the pour to splash into the centre of the pan from a uniform and reproducible height. Each pour was controlled manually so that pour time was reproduced at 10±1 s. The weight of the accumulated liquid was recorded immediately upon completion of the pour. The starting temperature of pan and liquid were the same as ambient, 20±1°C. The recovered liquid was allowed to return to ambient temperature before re-use. (See Sect. 3. 5 for results.)

2.6 Vertical Diffusion of Hydrocarbon Vapours

2.6.1 Barrier Tests

As a volatile liquid evaporates, it produces a layer of vapour by diffusion. Since the vapour densities (V.D.) of these liquids are greater than 1.0 (V.D. of pentane = 72/29 = 2.48), and the layer is cooler than the surrounding ambient air , the vapours are much denser than the surrounding air. As a result, they tend to flow off the edge of the Styrofoam block and cascade onto the floor of the fume hood (which is not in operation during the actual data run). This effect was documented in preliminary fashion by placing an electronic hydrocarbon detector on the bench top some 20cm from the balance and observing a response within 30s of beginning a run.

To investigate the effect of this convective and advective flow of the vapour generated, a number of runs were conducted with an acrylic plastic barrier placed on the benchtop concentric with the balance and evaporating sample, as shown in Fig. 2.6.1.1 . This barrier was 0.4m in inner diameter and 0.61m in height. There was a foam seal at the base that allowed the passage of the power and data cables for the balance, while minimizing the loss of vapours. The cylindrical barrier was open at the top for most of the tests. This barrier allowed the vapours being produced to establish some sort of equilibrium condition in the vicinity of the balance. Lighter vapours (pentane) would be expected to escape from the top of the barrier and while the resulting evaporation rate would be slowed in comparison to un-barricaded tests, evaporation would continue at some reduced rate. Heavier vapours (hexane and octane) would not be expected to escape as readily and the evaporation rate would be affected to a greater degree as an equilibrium is established. Each

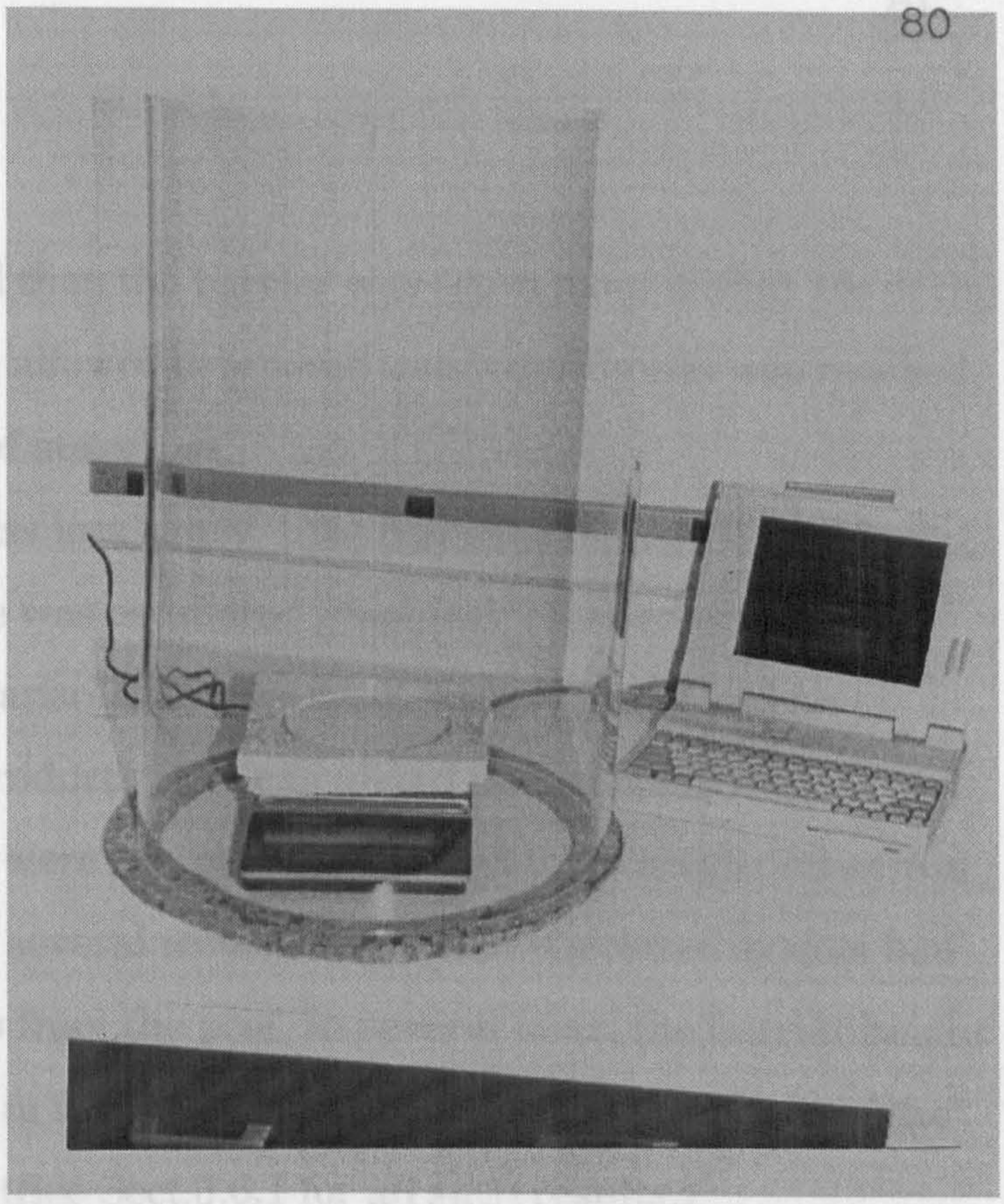

Fig. 2.6.1.1: Balance with 0.6m acrylic barrier in place.

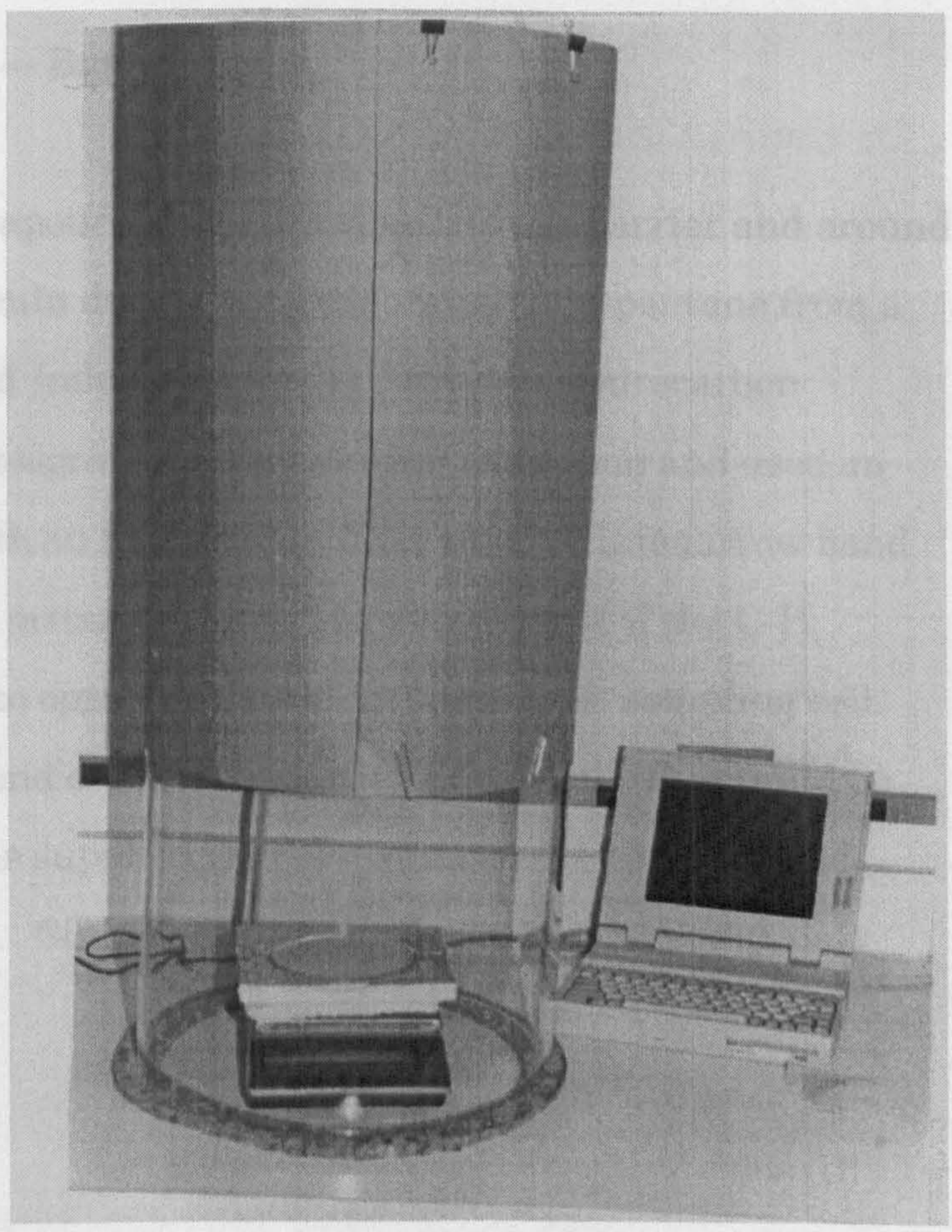

Fig. 2.6.1.2: Balance with 0.6m acrylic barrier and extension tube in place.

run was begun as before and then the barrier was set in place within 10s of the start of the run. The run was allowed to proceed until equilibrium was reached, marked by a constant rate of mass loss.

Using the plots of mass loss rate v. time collected in Sect. 2.2, the equilibrium evaporation rate was estimated graphically for each run. The differences in equilibrium evaporation rates between barricaded and un-barricaded tests of similar products were calculated for a number of fuels and substrates. Additional tests were run placing a 0.5m x 0.5m acrylic lid across the top of the barrier during several tests to determine if a closed system had any effect on mass loss rates from the pool. In several tests, the barrier height was extended from 0.6m to 1m using a cardboard sleeve on the outside of the acrylic barrier (Fig. 2.6.1.2). (See Sect.3.6.1 for all such results.)

2.6.2 Hydrocarbon Detector — Barrier Tests

The concentration of vapours above the mouth of the barrier and around its base were measured at 10min during the evaporation of n-pentane from a pool at 21°C using an Infrared Industries IR-711 Portable Hydrocarbon detector. This detector was designed for fire scene investigation and used an infrared light source fitted with an interference filter to provide a narrow band of IR in the region of 3.39μ (a primary absorption wavelength of the C-H stretch) and a detector fitted to opposite ends of an open-sided sampling cell. The cell was mounted in one end of a baton-like sampling probe that could be easily moved, while power was supplied via cable from a remote power and control unit, as in Fig. 2.6.2.1. Since the cell had no mechanical pump, only

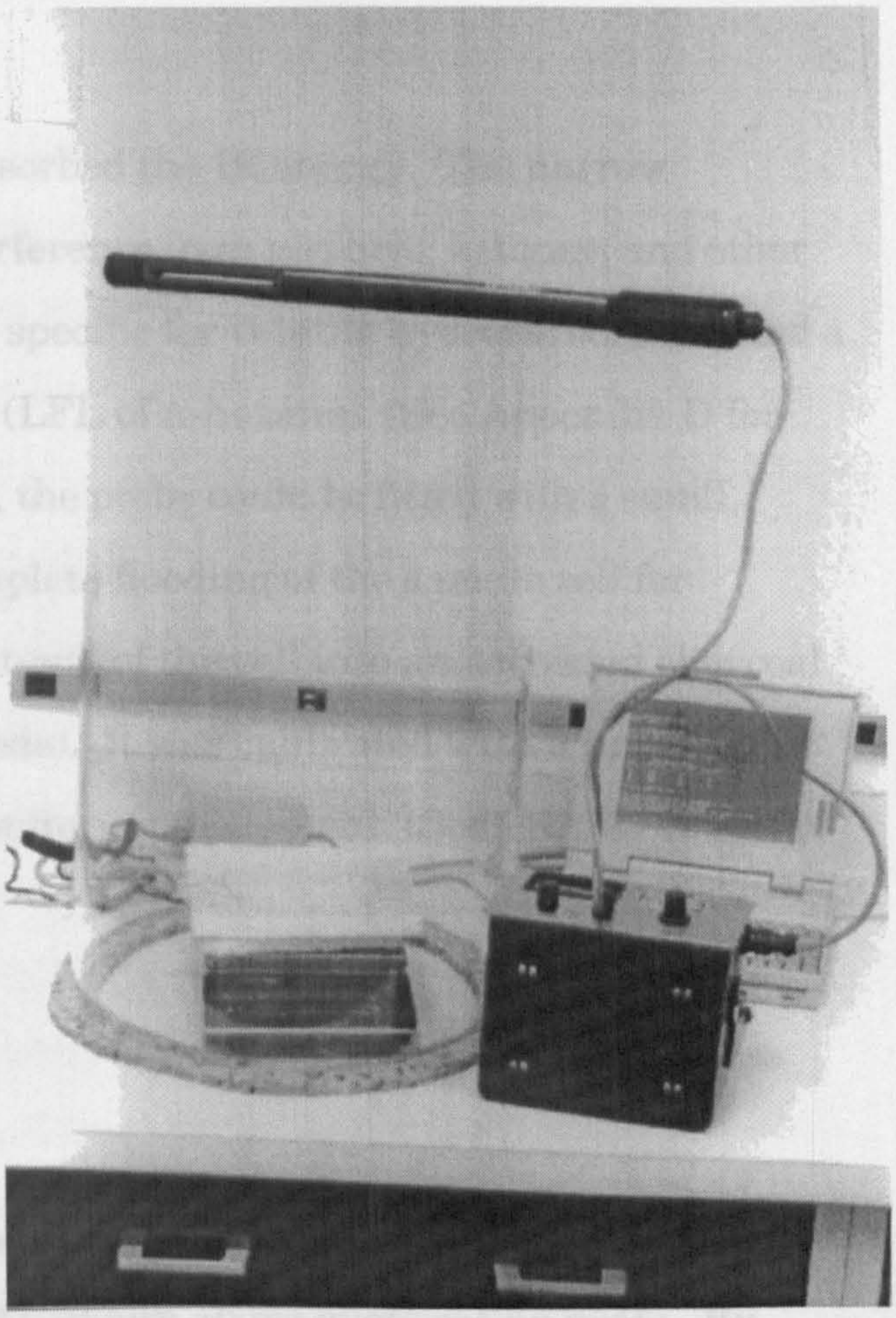

Fig. 2.6.2.1: Barrier with IR-711 Hydrocarbon Detector at top opening.

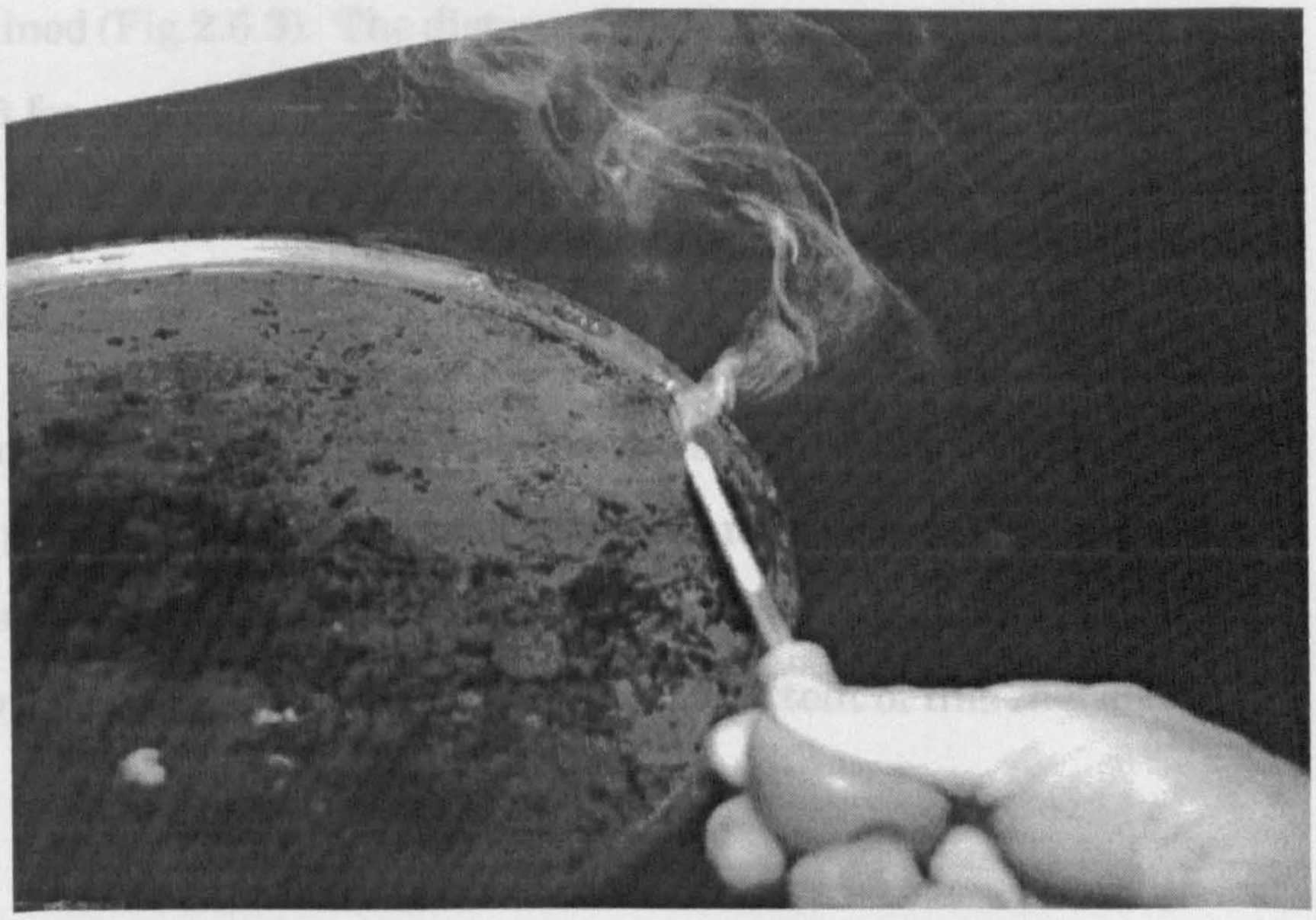

Fig. 2.6.3: GasTec© smoke pen test at edge of pan.

vapours that drifted into the cell absorbed the IR energy. The narrow wavelength band used reduced interference from alcohols, ketones, and other species and made the detector very specific for volatile hydrocarbons. It had a usable range of 20ppm to 2000ppm (LFL of n-hexane). (See Appendix D for additional information.) In addition, the probe could be fitted with a small, battery-powered pump to allow complete flooding of the sample cell for calibration (or for sweeping the contents of the cell into an activated charcoal trap for gas chromatographic analysis). It was calibrated with a hexane/air cylinder used for environmental monitoring equipment. (See Sect. 3.6.2 for results.)

2.6.3 Smoke Pen Tests

In addition, the GasTec® stannic chloride smoke pens described earlier were used to test the distribution of vapours above evaporating pools. By releasing a gentle stream of smoke at various positions and heights above the pool, the movement of the vapours could be visually monitored as the smoke trail was entrained (Fig.2.6.3). The distances involved were estimated visually. (See Sect. 3.6.3 for results.)

2.6.4 Thermal Gradient Tests

The evaporative cooling of volatiles such as pentane and hexane would be expected to produce vapours that were significantly cooler than ambient conditions. This would result in a thermal gradient that would reduce the vertical distribution of the vapours. To explore the extent of this thermal

gradient, an experimental rig was designed and constructed (Fig.2.6.4.1). An array of ten iron-constantan thermocouples of 0.45mm (0.018") diameter wire were arranged to monitor the temperature of air or vapours, at 1,2,3, and 4 cm above the surface of the evaporating liquid or of sand saturated with the same liquid, as well as the temperature of air or vapour 1cm above the surface of the insulating panel adjacent to the pool and 1cm above the surface of the adjacent benchtop. Small quantities of n-pentane and hexane were evaporated under ambient conditions of still air at 21.0±0.5°C both as pools in Petri dishes and as a sand/pentane matrix. The temperatures of the evaporating liquid and the ambient air were monitored as controls. The temperatures were collected using the YEW Model 3081 Hybrid 30-channel data recorder (provided by the Bureau of Home Furnishings Laboratory) (Fig. 2.6.4.2). (See Appendix E for additional information.) The data collected were converted to Celsius equivalents and processed using a Microsoft Excel© spreadsheet programme. (See Sect. 3.6.4 for results.)

2.6.5 Hydrocarbon Detector — Bench Tests

In addition, the IR-711 Hydrocarbon Detector was used to estimate the depth of the vapour layer being produced by n-pentane evaporating at 21°C in still air from a 15cm Petri dish in the middle of a large benchtop. The probe was hand-held above the Petri dish, parallel to the surface of the pentane pool, and slowly moved downward until it yielded a signal indicating a concentration of 500ppm (Fig.2.6.5). At that point, the distance above the surface of the liquid was estimated visually with reference to a laboratory centimetre scale. The experiment was repeated a number of times. (See Sect. 3.6.5 for results.)

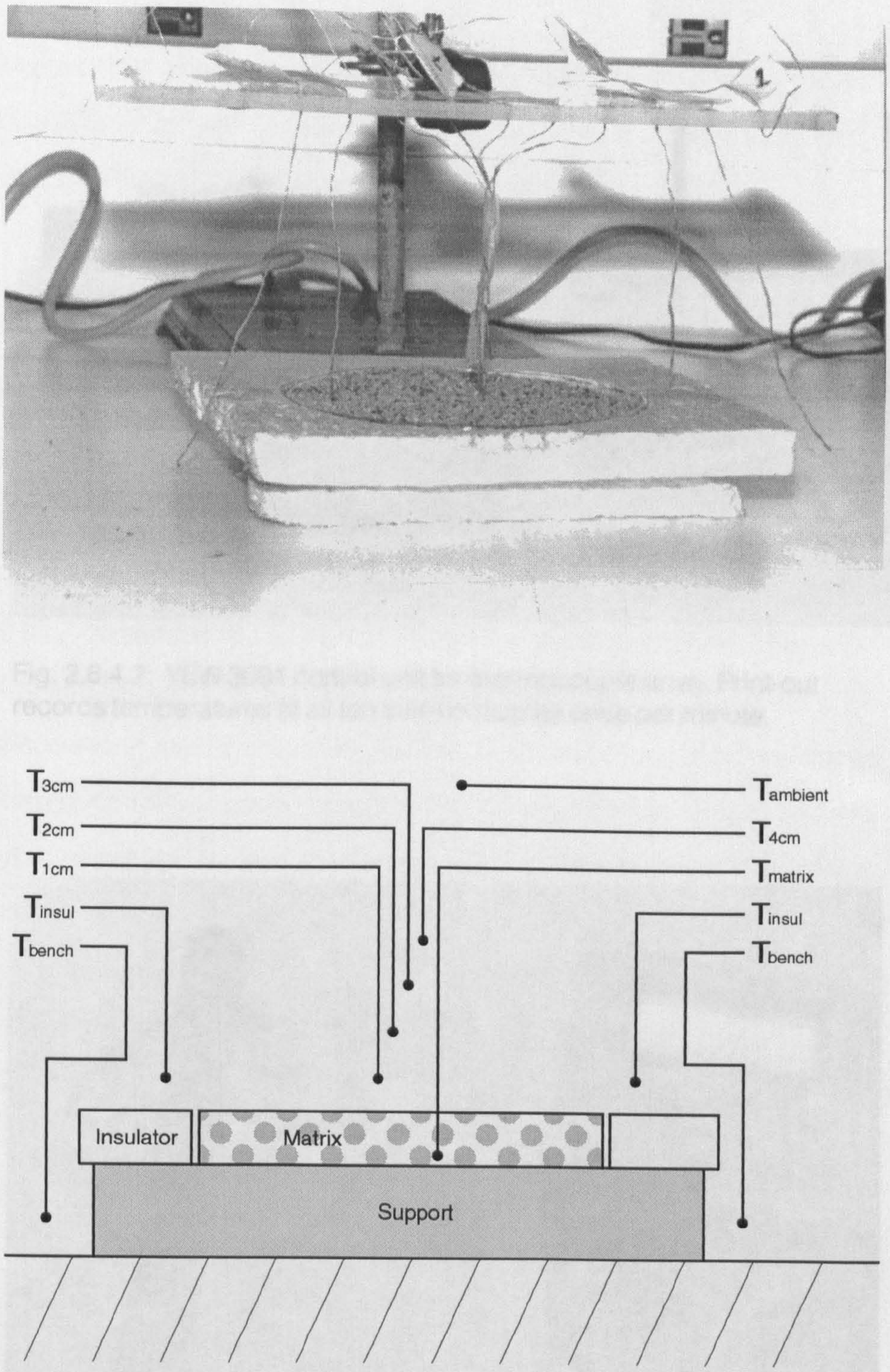

Fig. 2.6.4.1(a): Iron-constantan thermocouple array for measuring thermal layers above evaporating pools.

(b): Schematic diagram of thermocouple array. One central thermocouple is buried in the matrix, the others are positioned 1,2,3, and 4cm above its surface.

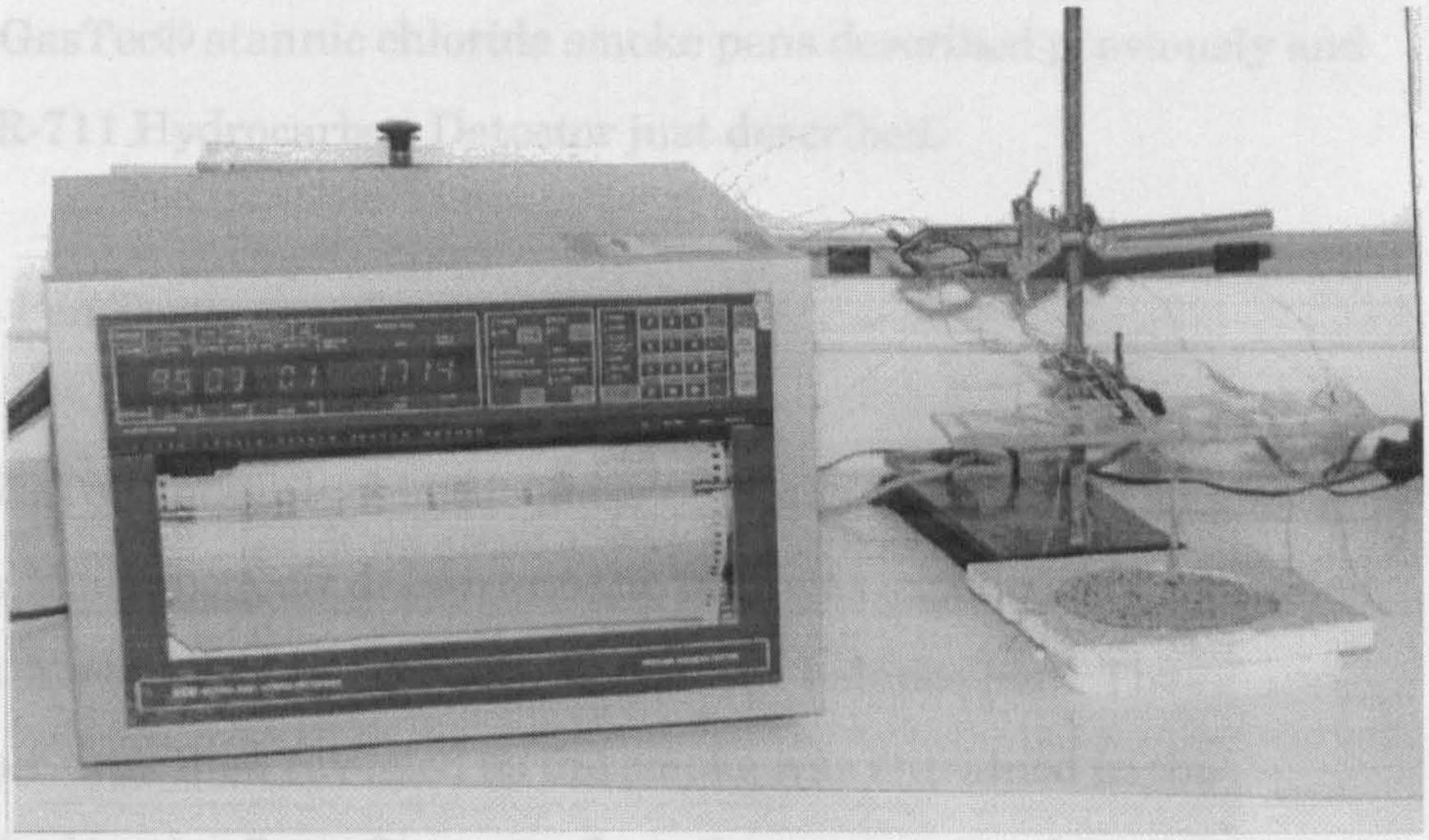

Fig. 2.6.4.2: YEW 3081 control unit for thermocouple array. Print-out records temperatures at all ten thermocouples once per minute.

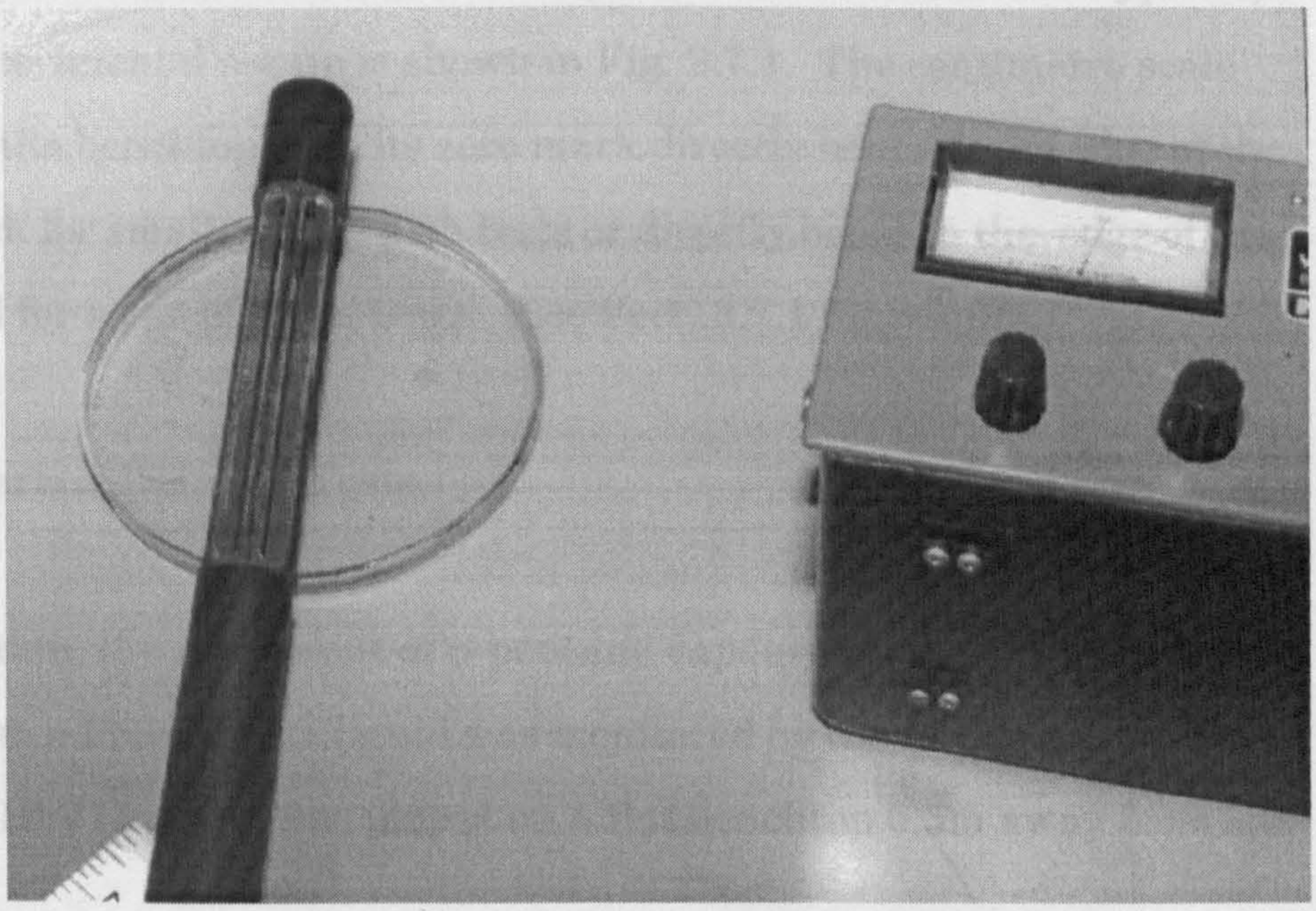

Fig. 2.6.5: IR-711 Hydrocarbon Detector above pool in Petri dish.

2.7 Advective Flow of Vapours — Horizontal Transport

The movement of vapours during evaporation runs were monitored by the use of the GasTec® stannic chloride smoke pens described previously and by using the IR-711 Hydrocarbon Detector just described.

2.7.1 Smoke Pen Tests

Each GasTec® stannic chloride glass tube was fitted with a small aspirator bulb. Moist room air drawn into the tube was expelled in a controlled puff or stream of white smoke in the vicinity of the balance pan. The movement of air was then revealed as the smoke was entrained in the convective and advective flow of vapours from the evaporating liquid. The movement of the smoke could be observed directly for some 10 – 20s before dispersing and becoming too dilute to see. Horizontal motion could be measured by measuring (via manually-operated digital stopwatch) the time required for a wave or front of smoke to be carried the length of a known reference (typically 30cm). The experimental set-up is shown in Fig. 2.7.1. The centimetre scale was placed on the benchtop with its zero mark directly beneath the edge of the insulating block for smaller Petri dish tests or directly beneath the edge of the large pan used for some of these tests. (See Sect. 3.7.1 for results.)

2.7.2 Hydrocarbon Detector Tests

In addition, the movement of n-pentane vapours across a flat benchtop originating from a Petri dish of liquid was monitored by the IR-711 Hydrocarbon Detector. The IR-711 probe was placed on a flat benchtop 0.5m away from the

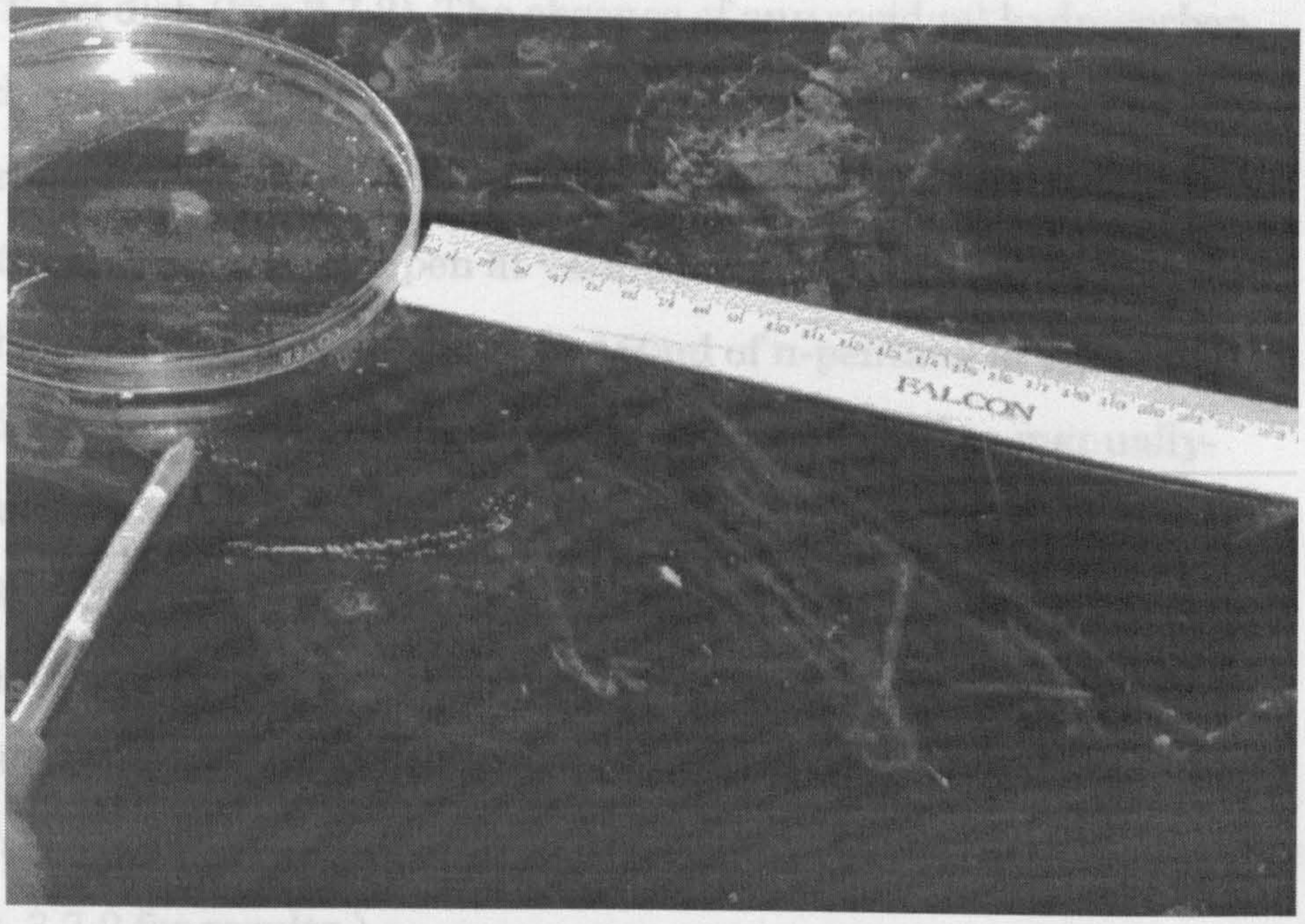

Fig. 2.7.1: Smoke test for horizontal movement of pentane vapours from Petri dish.

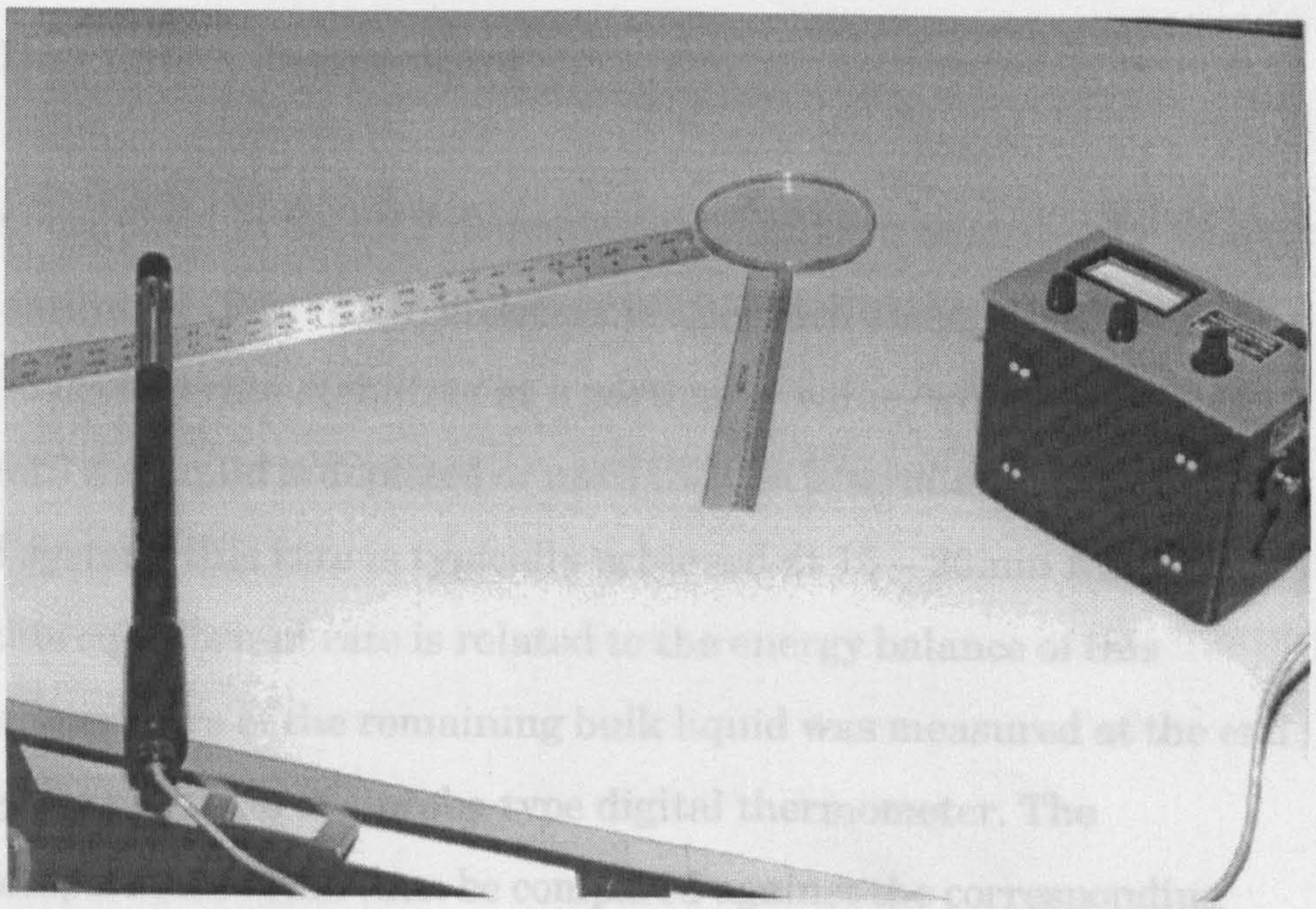

Fig. 2.7.2: IR-711 Hydrocarbon Detector on table 0.5m from pentane pool.

rim of a 15cm Petri dish (Fig.2.7.2). The absence of any residual hydrocarbon vapours was checked with the probe prior to the start of each experiment. The absence of significant prevailing drafts in the room air at bench level was then checked with the GasTec® smoke pen at various locations around the periphery of the Petri dish. Approximately 150ml of n-pentane at ambient temperature (21°C) was poured slowly into the Petri dish while a manually-operated digital stop watch recorded the time elapsed from the moment of first pouring. The time required for vapours to reach the probe and produce a signal of 500ppm was then recorded for a variety of probe positions relative to the pan. When a signal was recorded, the probe was then slowly moved around the Petri dish at various distances to establish (if possible) the extent of the vapour pool. (See Sect. 3.7.2 for results.)

2.8 Thermodynamics of Evaporation from Pools

2.8.1 Mass Loss Rate v. Temperature

The data plots acquired in Sect.2.2 demonstrate a uniform tendency for nearly all pools and saturated (Petri dish) matrices to approach an equilibrium state at which the mass loss rate stabilizes at a particular value, which is maintained until the liquid is depleted or until the run is terminated. In this experimental system, this rate is typically achieved at 15 – 20min from the start. Since this equilibrium rate is related to the energy balance of this system, the temperature of the remaining bulk liquid was measured at the end of each run by the insertion of a probe-type digital thermometer. The equilibrium temperature could then be compared against the corresponding

equilibrium mass loss rate. This was carried out for pools of both n-pentane and hexane evaporating in still air both with and without a barrier, as in Sect.2.6.1. (See Sect. 3.8.1 for results.)

2.8.2 Surface Temperature Measurements

The evaporation rate of a volatile hydrocarbon is closely related to the temperature of the evaporating liquid, particularly at its surface. It was decided that a non-invasive means of measuring the surface temperature of the liquid alone or that of the substrate/liquid matrix was needed. An Inframetrics Model 760 Infrared Imaging video system radiometer was generously provided by PBA Instruments, LaJolla, CA. This video system, as shown in Fig. 2.8.2.1, captures the infrared radiation being emitted or reflected in the 8 – 12 micron region by a target, and converts it to a false-colour or grey-scale video image that allows the measurement of temperatures in any temperature range and discrimination of temperatures as close as 0.25°C. This image can be captured continuously as a VHS videotape record or as a colour image from the display screen. (See specifications, Appendix F.) The system will also monitor the temperatures at three different locations within the camera's field of view and record them as a datafile and as a plot on the video display terminal, using the ThermaGram® data analysis system (see Appendix G), as shown in Fig. 2.8.2.2. This system was also used to record the surface temperatures of carpets, concrete, and tile surfaces where very shallow pools of pentane were evaporating.

Fig. 2.8.2.1: Inframetrics Model 760 Infrared Video Radiometer camera and control unit, along with the balance and computer used for the evaporation experiments.

Fig. 2.8.2.2: Video display of ThermaGram© Data System showing the thermal video (false-colour) image of the evaporating sample along with overlying traces recording the temperatures at three selected sampling points within the image. The image is of pentane on sand. Note the irregularities in the surface temperature.

2.8.2.1 Infrared Imaging of Liquid Pools

It was suggested that the IR video system may not capture the temperature of the actual surface of a liquid such as pentane that is transparent to visible light and has no strong absorption bands in the $8-12\mu$ region of the infrared. To test this, the experimenter's hand was imaged in the video and then a polythene bag containing a quantity of n-pentane was laid over it. (Polythene was selected when it was determined that two layers did not obscure the thermal image of the hand.) An examination of the video image showed where the hand (with its surface temperature of 33°C) was visible and areas where the pentane (at a starting ambient temperature of 23°C) blocked the image of the hand. The areas where the image was obscured were inspected visually to establish whether even thin layers of n-pentane would block the thermal signals from warmer surfaces beneath them. (See Sect. 3.8.2.1 for results.)

2.8.2.2 Thermal Imaging Calibration

The calibration of the infrared thermal imaging system is dependent on the setting of the detector's emissivity level, which should match that of the target. Because these experiments were dealing with non-luminous sources at temperatures close to ambient and experimental conditions (room interiors) where there were no strong exterior sources of infrared, differences in emissivity or reflectivity of the targets involved (carpet, sand, liquid pool, aluminium granules) would not be expected to make a large difference in the temperatures observed. This was tested by observing several targets: an empty glass Petri dish, a sample of dry carpet, a Petri dish of sand, a Petri dish

of aluminium granules, a dish containing diesel fuel, along with the adjoining benchtop and the ceiling of the laboratory, all at ambient conditions, with the emissivity calibration of the IR system set for an emissivity, ϵ, of 1.0. The Inframetrics image was then examined to detect systematic errors in temperature measurements. See Sect. 3.8.2.2 for results.

2.8.3 Temperature Distribution in Evaporating Liquids and Matrices

The surface temperatures of n-pentane evaporating as a pool and from various substrates as measured by infrared video imaging were recorded for a variety of situations, in some cases with simultaneous recording of the mass loss. In any liquid pool, a temperature difference between the top layer and lower layers will cause some circulation by convection as the surface layer, cooled by evaporative losses, becomes denser than the layers beneath and sinks. This circulation may be accomplished through a generalized circulation or localized eddies, depending on the amount of temperature difference and the viscosity of the liquid. To test the extent of this condition in the relatively shallow pools being studied here, as well as the validity of the conclusion about the depth of the observable layer, a series of tests were carried out in which the test dish was instrumented with iron-constantan thermocouples as previously described. One thermocouple (#3) was mounted so that it was maintained at surface level, and two thermocouples were mounted so that their junctions were maintained within the mass. For liquids, both were mounted against the bottom of the dish; for the sand or aluminium granules, one was at the bottom, while one was maintained near the center of the solid mass (see Fig.2.8.3). A fourth thermocouple was affixed to the benchtop near the balance to record ambient conditions.

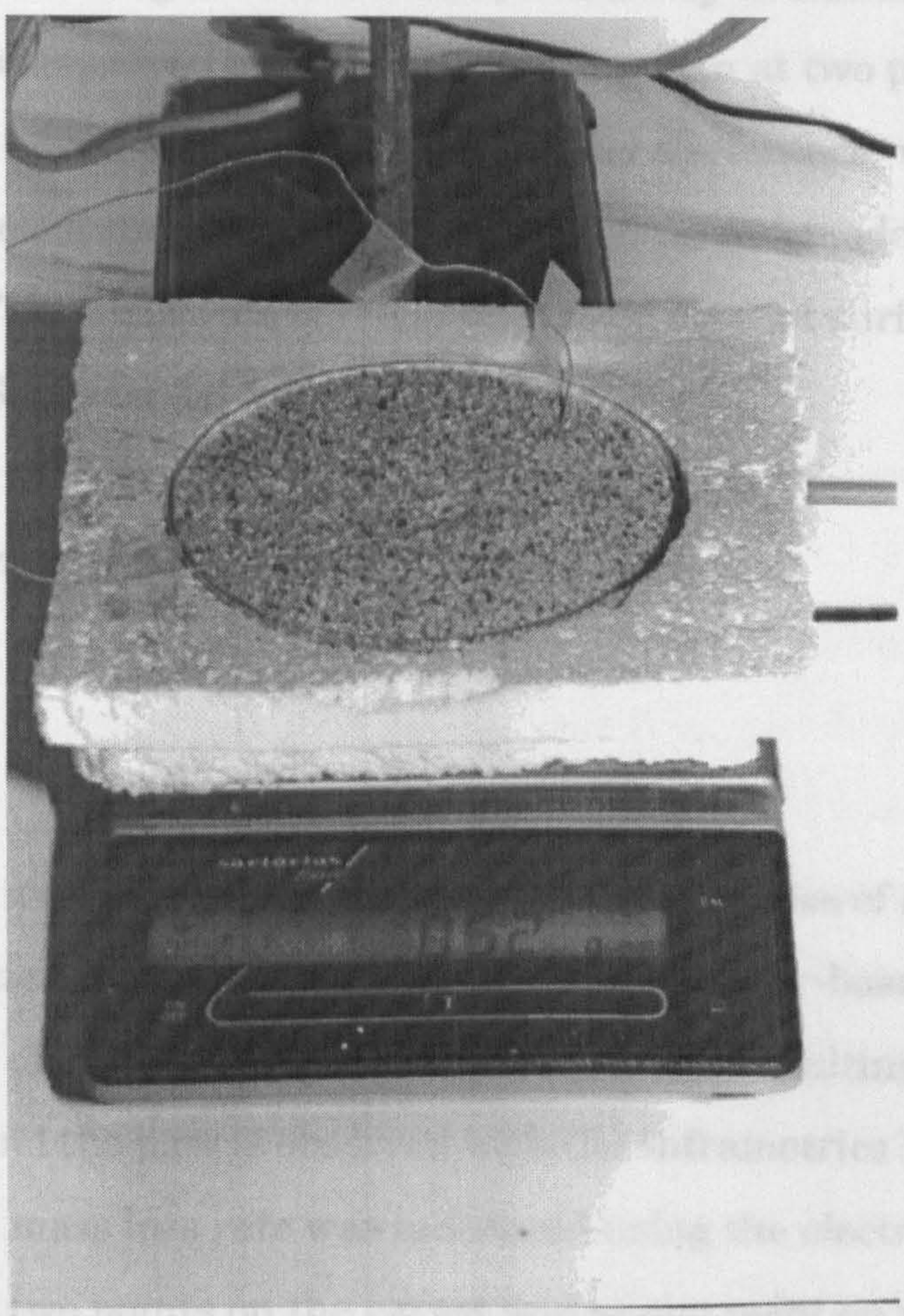

Fig. 2.8.3: Thermocouples in sand/pentane matrix. One is positioned at surface, two others are located at the bottom of the Petri dish beneath the sand.

The data gathered were recorded as Fahrenheit temperatures on hard-copy print-outs. This necessitated manual conversion of the data to Celsius, followed by manual entry into Microsoft Excel® for plotting and manipulation. Four runs were made with pentane and hexane with various substrates while simultaneously recording the surface temperature by IR thermal imaging. Temperatures as measured by the IR imaging system at two points on the pool or substrate and at one point on the benchtop (as a reference) were recorded continuously for each run, and a videotape recording was made of the IR image for later review. The evaporation rate was plotted against surface temperature for these runs. (See Sect. 3.8.3 for results.)

2.8.4 Thermodynamics of Evaporation from Matrices

2.8.4.1 Carpets

Five tests were carried out pouring 100ml quantities of n-pentane on panels of synthetic carpet that had been glued with water-based contact cement to panels of 12mm thick rigid Styrofoam. The resulting wetted areas were measured and the panels observed with the Inframetrics IR imaging system while the mass loss rate was measured using the electronic balance. Temperatures at two points on the carpet and at one point on the benchtop (as a reference) were recorded continuously for each 30min run, and a videotape recording was made of the IR image for later review. (See Sect. 3.8.4.1 for results.)

2.8.4.2 Other Matrices

Five tests were carried out to examine the thermal effects of a small quantity spill of a volatile liquid on a massive substrate such as concrete, or vinyl floor tile on a concrete floor. In each test, the Inframetrics system was set up to monitor the temperature of a segment of floor, both as a continuous image and at three discrete points on the surface: two within the area of the spill and one outside it as a reference. Small (10 – 25ml) quantities of n-pentane were poured on the target surface, and the thermal response was noted. Results are presented in Sect.3.8.4.2.

2.9 Evaporation of Pure Compounds v. Complex Mixtures

Pure compounds such as pentane and hexane are rarely encountered in fire investigations. Consumer products such as petrol are much more common, but are also much more complex to evaluate due to their multi-component composition. It was thought that comparing the evaporation properties of two of the most common complex fuels to those of pentane and hexane would yield data predictive of their behaviour. As described in Sect. 1, petrol is typically comprised of aliphatic, aromatic and cyclo-paraffinic hydrocarbons in the range of butane (C_4H_{10}) to n-dodecane ($C_{12}H_{26}$) (Fig. 2.9.1). Camping fuel is a flammable liquid sometimes encountered in accidental as well as incendiary fires. It is typically a "straight-run naphtha fraction" petroleum distillate with a flash point of –30°C, which contains normal- and iso-alkanes ranging from hexane to undecane and which does not produce significant soot when burned (Fig.2.9.2).

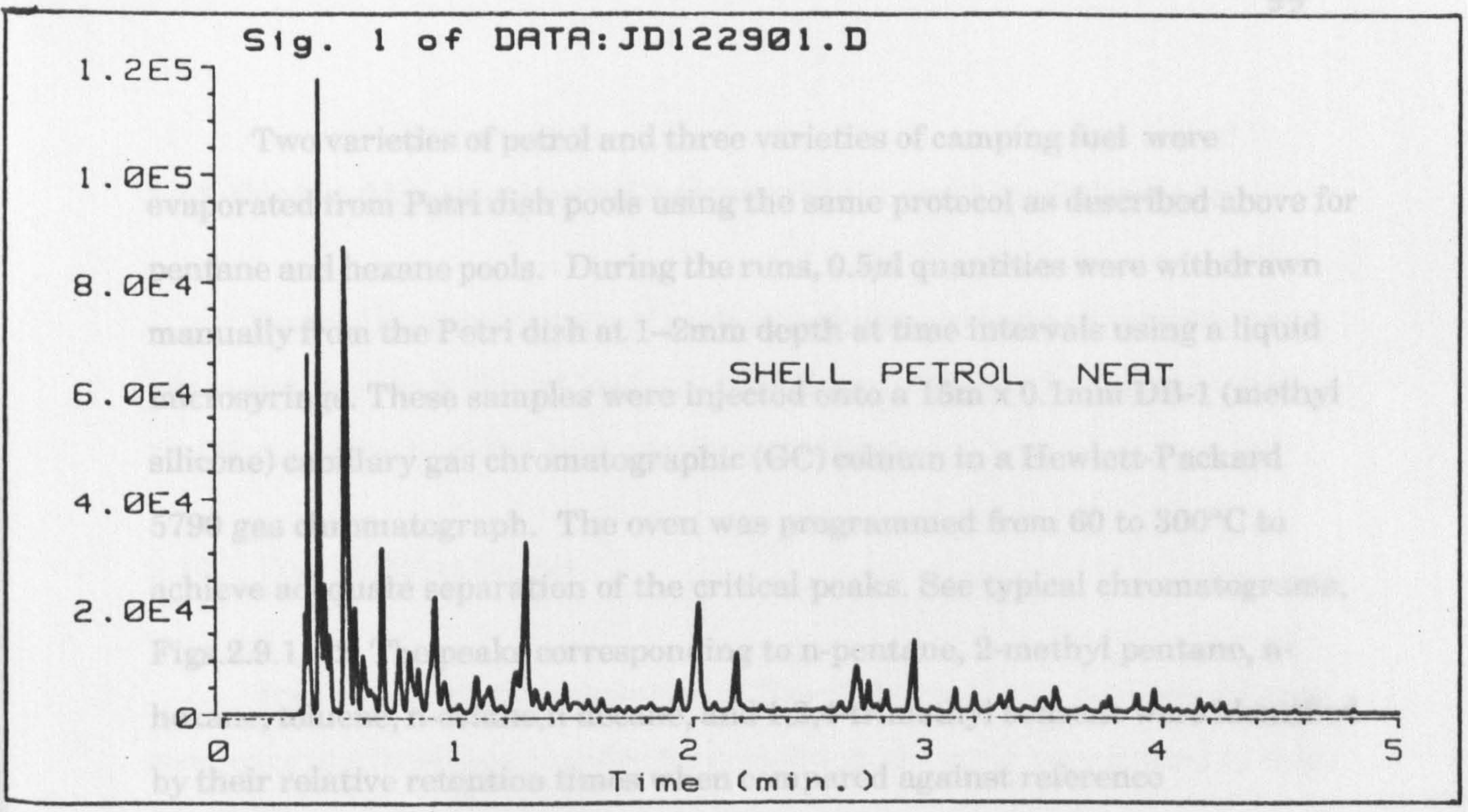

Fig. 2.9.1: Typical gas chromatogram of Shell brand petrol.

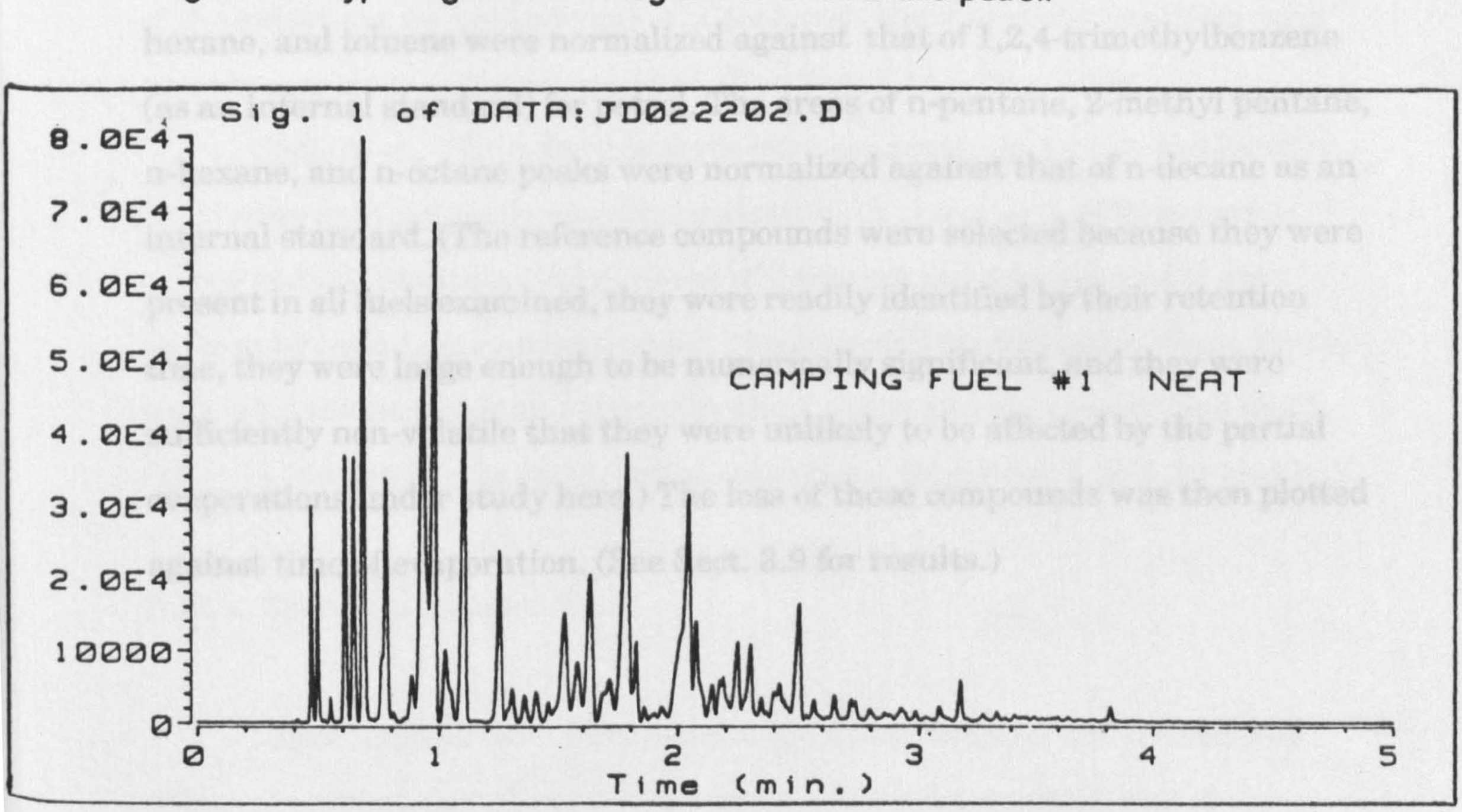

Fig. 2.9.2: Typical gas chromatogram of camping fuel.

Two varieties of petrol and three varieties of camping fuel were evaporated from Petri dish pools using the same protocol as described above for pentane and hexane pools. During the runs, 0.5μl quantities were withdrawn manually from the Petri dish at 1–2mm depth at time intervals using a liquid microsyringe. These samples were injected onto a 15m x 0.1mm DB-1 (methyl silicone) capillary gas chromatographic (GC) column in a Hewlett-Packard 5790 gas chromatograph. The oven was programmed from 60 to 300°C to achieve adequate separation of the critical peaks. See typical chromatograms, Figs.2.9.1 – 2. The peaks corresponding to n-pentane, 2-methyl pentane, n-hexane, toluene, n-octane,n-decane, and 1,2,4-trimethyl benzene were identified by their relative retention times when compared against reference chromatograms of pure reference compounds and mixtures.

The areas under the selected peaks were quantified using the H-P Data Station system, and the areas representing pentane, 2-methyl pentane, hexane, and toluene were normalized against that of 1,2,4-trimethylbenzene (as an internal standard) for petrol. The areas of n-pentane, 2-methyl pentane, n-hexane, and n-octane peaks were normalized against that of n-decane as an internal standard. (The reference compounds were selected because they were present in all fuels examined, they were readily identified by their retention time, they were large enough to be numerically significant, and they were sufficiently non-volatile that they were unlikely to be affected by the partial evaporations under study here.) The loss of those compounds was then plotted against time of evaporation. (See Sect. 3.9 for results.)

2.10 Pool and Vapour Layer Characteristics and Fire Behaviour

Tests of flaming ignition of pools of methanol, petrol and camping fuel were conducted on a limited basis to study the relationship between pre-fire pool size and the post-fire burn patterns, as follows.

2.10.1 Pool Tests on Carpet

Tests 1 – 5. At the conclusion of five of the methanol pool-spread tests conducted in a building scheduled for demolition, the pools were ignited by open flame. The carpet was identified (by later microscopic examination) as acrylic-loop pile. The resulting fires were recorded by hand-held video camera, and the behaviour of the fire and its spread were noted and recorded on the audio track of the videotape. At the conclusion of each test, the size of the resulting burn pattern was measured and recorded. (See Sect 3.10.1 for results.)

Tests 6 – 8. Three further tests were conducted in an exterior location by pouring approximately one-litre quantities of petrol onto different types of carpet/pad combinations. The extent of flame spread from each pool upon ignition by open flame were recorded by colour still photography. Since these tests were conducted in an exterior location, there was an uncontrolled wind factor in the fire effects on the adjacent carpets. (See Sect. 3.10.1 for results.)

2.10.2: Room Calorimeter Tests

Three ignition tests were carried out using camping fuel poured onto nylon-pile carpeted surfaces in the room-size furniture calorimeter at the

California Dept. of Consumer Affairs - Bureau of Home Furnishings in North Highlands, CA. The test room was 3m by 3.6m x 2.4m high and was fitted with thermocouples at ceiling level and at mid-level (1.2m) height, and gas-sampling probes to measure O_2, CO_2, and CO levels. Ventilation was supplied by a single door opening 0.95m wide x 2m in height. A panel of carpet was laid down over a sheet of galvanized metal over a non-combustible insulating panel of gypsum wall board. The fuel (1.9 litres) was poured without turbulence onto the carpet and allowed to equilibrate for 30 seconds at a temperature of 18°C before being ignited with a wooden match. The ventilation system for the heat release rate (HRR) measurement was not turned on until well after ignition so as not to cause excessive or non-reproducible evaporation. The resulting fire was recorded through an open door by tripod-mounted video camera for later evaluation.

Three tests were conducted at this facility: (9) camp fuel over loose, unpadded carpet; (10) camp fuel over carpet fixed over a rubber pad, open door throughout; and (11) camp fuel over fixed, padded carpet, door closed for six minutes, then opened. All tests used the same quantity of flammable liquid and the same type of synthetic carpet and pad. (See Fig.A. 2.10.2) The heat release rate, recorded in kilowatts (kW), from each fire was calculated by the oxygen depletion method measuring the oxygen concentration in the gases exhausted into a duct above the doorway of the test room. For Test 11, the doorway was blocked about 15 seconds after ignition by inserting a panel of gypsum wallboard over the opening. This largely limited the oxygen available to that which was in the room at the start of the fire and simulated a flash fire in a closed room, but it also prevented direct calculation of rate of heat release, until the door was opened at six minutes after ignition. Other thermal and gas analysis data were still reliable. (See Sect 3.10.2 for results.)

2.10.3 Room Tests (Non-Instrumented)

In each of three additional tests, approximately 2.5 litres of camping fuel was poured directly from the metal can (with a standard 18mm screw-cap opening) onto the nylon-pile carpeted floor of a bedroom compartment, in a random pattern. Each room was approximately 3m x 4m x 2.4m in height. Room temperatures were on the order of 25°C. In each case, the door to the compartment was closed and the vapours allowed to stabilize for 30 – 40s after pouring was completed and before ignition. Each of these tests was conducted in a building scheduled for demolition, so a viewport was cut into one wall of the compartment and covered with clear plastic. A tripod-mounted video camera recorded through the viewport the development of the fire from a point 1 – 2 m away from the point of ignition . Ignition was carried out remotely using an electric match ignition device. The resulting videotapes were used for later evaluation. In two of these tests, an Inframetrics 600 Infrared imaging system, donated and operated by Helmut Brosz and Associates, was mounted in an adjacent building so that it viewed the test room through an exterior window. The glass exterior window failed upon ignition in each test, and the Inframetrics system was able to collect some data on the temperatures of gases within the room. Prior to each test, control samples of the carpet and the underlying "rebond" polyurethane pad were recovered from each room for later evaluation.

2.10.4 Post-Fire Indicators

In addition, observations were made when possible of the extent of damage to the carpet and pad in the vicinity of the poured liquid after the fire was extinguished in each of the fire behaviour tests conducted. These observations were supplemented with the results of flammable liquids on a variety of floor surfaces. The extent of visibly detectable correlations between the location of the liquid and the burn damage was noted. (See Sect. 3.10.4 for results.)

EXPERIMENTAL RESULTS

Section 3

The results of the experiments described in Section 2 will be presented in the same order.

3.1 Pool Size v. Quantity

It should be remembered that the pool to be measured was defined by the edges of the free-standing liquid visible on non-porous surfaces or by the visibly wetted areas of absorbent substrates where there was no free-standing liquid. The results of a total of some fifty pour/pool size experiments are presented in Table 3.1.1 and summarized in Table 3.1.2. They are presented by surface type (Non-porous: marble, linoleum,vinyl tile, sealed ceramic tile; Semi-porous: concrete, plywood; and Porous: carpet).

It was noted that hydrocarbons (pentane or petrol) produced consistently larger pools per litre than ethanol on all surfaces. The pool sizes for methanol were consistent with those for hydrocarbons for all surfaces except wood. These differences suggest that the surface tension and viscosity of the liquid play an important role in determining the pool area, and that the polar nature of alcohols can influence their spreading properties on some surfaces such as wood.

Estimates of pool area appear to be valid for methanol and light (low viscosity) hydrocarbons for pours of less than 4 litres, since interpolations and modest extrapolations produce consistent results. Ethanol pools are 50% smaller in area, per litre of liquid, than methanol pools of equal volume most probably due to its significantly higher surface tension.

Table 3.1.1: Pool Size v. Quantity

Liquid	Quantity	Substrate	Pool Area(m^2)	m^2/l	Comments
		Non-Porous			
Methanol	1000ml	Smooth marble	2.12 (Ir)	2.12	Level.Sealed seam
Methanol +Ethanol[1]	950ml 50ml	Smooth marble	2.72 (Ir)	2.72	Level.Sealed seam
Methanol	1000ml	Smooth linoleum	2.62 (Ov)	2.62	Waxed. No seams
Methanol	1000ml	Vinyl floor	3.54 (Ov)	3.54	Textured.No seams
Methanol	500ml	Ceramic tile	1.34 (Ov)	2.68	Sealed grout
Pentane	25ml	Vinyl tile	0.10 (Sq)	4.0	Waxed. Seams

Table 3.1.1: Pool Size v. Quantity (continued)

Semi-Porous

Liquid	Quantity	Substrate	Pool Area(m^2)	m^2/l	Comments
Methanol	1000ml	Rough plywood	1.83(Ir)	1.83	Unfinished. Seams
Methanol	1000ml	Rough plywood	2.17 (Ir)	2.17	Unfinished. Seams
Methanol	1000ml	Smooth plywood	1.40 (Sq)	1.40	Lightly painted
Methanol	2000ml	Smooth plywood	2.56 (Ov)	1.28	Lightly painted
Petrol	1000ml	Smooth plywood	1.30 (Ov)	1.30	Lightly painted
Methanol	1000ml	Smooth concrete	2.81 (Ir)	2.81	Level. Unsealed
Methanol	1000ml	Smooth concrete	2.08 (Ir)	2.08	Level. No cracks
Methanol	1000ml	Smooth concrete	1.81 (Ir)	1.81	Not level
Pentane	10ml	Smooth concrete	0.044 (Ir)	4.4	Level. Unsealed
Pentane	1000ml	Smooth concrete	2.85 (Ir)	2.85	Level. Unsealed
Petrol	1000ml	Smooth concrete	3.04 (Ir)	3.04	Level. Unsealed
Ethanol	1000ml	Smooth concrete	1.14 (Ir)	1.14	Level. No cracks
Ethanol	1000ml	Smooth concrete	1.42 (Ir)	1.42	Not level

Table 3.1.1: Pool Size v. Quantity (continued)

Carpets

Liquid	Quantity	Substrate	Pool Area(m^2)	m^2/l	Comments
Pentane	150ml	Carpet A	0.05 (Cr)	0.40	5mm nylon loop. Rubber-backed
Pentane	100ml	Carpet A	0.04 (Cr)	0.40	Same
Pentane	100ml	Carpet A	0.044 (Cr)	0.44	Same
Pentane	150ml	Carpet A	0.06 (Cr)	0.42	Same
Methanol	250ml	Carpet A	0.08 (Cr)	0.32	Same
Methanol	250ml	Carpet A	0.08 (Cr)	0.32	Same
Pentane	150ml	Carpet B	0.07 (Cr)	0.47	5mm loop, polypropylene. Foam-backed
Pentane	100ml	Carpet B	0.045 (Cr)	0.45	Same
Methanol	250ml	Carpet B	0.08 (Cr)	0.32	Same
Methanol	250ml	Carpet B	0.09 (Cr)	0.36	Same
Methanol	250ml	Carpet B	0.085 (Cr)	0.34	Same
Methanol	250ml	Carpet B	0.09 (Cr)	0.36	Same
Methanol	500ml	Carpet B	0.18 (Cr)	0.36	Same

Table 3.1.1: Pool Size v. Quantity (continued)

Liquid	Quantity	Substrate	Pool Area(m^2)	m^2/l	Comments
Pentane	150ml	Carpet C	0.0095 (Cr)	0.07	11mm nylon plush pile
Pentane	100ml	Carpet C	0.006 (Ov)	0.06	Same
Pentane	350ml	Carpet C	0.025 (Cr)	0.07	Same
Pentane	150ml	Carpet D	0.009 (Cr)	0.06	14mm sculptured nylon pile
Pentane	100ml	Carpet D	0.005 (Ov)	0.05	Same
Pentane	300ml	Carpet D	0.016 (Cr)	0.05	Same
Pentane	150ml	Carpet E	0.011 (Cr)	0.08	10mm plush nylon pile
Pentane	100ml	Carpet E	0.01 (Ov)	0.10	Same
Pentane	300ml	Carpet E	0.031 (Cr)	0.10	Same
Methanol	250ml	Carpet E	0.018 (Cr)	0.07	Same
Methanol	250ml	Carpet E	0.018 (Cr)	0.07	Same
Methanol	250ml	Carpet E	0.025 (Cr)	0.10	Same
Methanol	500ml	Carpet E	0.05 (Cr)	0.10	Same
Pentane	150ml	Short Pile carpet	0.02 (Cr)	0.14	Larger "pool" on reverse (0.06m^2)

Table 3.1.1: Pool Size v. Quantity (continued)

Liquid	Quantity	Substrate	Pool Area(m^2)	m^2/l	Comments
Pentane	150ml	Medium pile carpet	0.01 (Cr)	0.07	Unbacked. Large "pool" on reverse
Methanol	2000ml	Short-loop carpet	0.48 (Ov)	0.24	3mm acrylic loop pile. Rubber-backed
Methanol	2000ml	Short-loop carpet	0.34 (Ir)	0.17	Same carpet. Worn
Methanol	1000ml	Tight-loop carpet	0.47 (Cr)	0.47	3mm loop. Bonded foam back.Similar to B
Methanol	1000ml	Tight-loop carpet	0.40 (Cr)	0.40	Same
Methanol	1000ml	Medium pile carpet	0.10 (Cr)	0.10	12mm nylon pile. Rebond foam pad.Similar to E

Notes: 1. Mixture of methyl and ethyl alcohols was used to maintain consistency of pour volumes despite insufficient quantity of methyl alcohol on hand at test site.

KEY: Cr = approximately circular pool
Ov = approximately oval in shape
Ir = irregular in shape
Sq = approximately square pool

Table 3.1.2: Summary of pool size tests

Surface	Pool Depth (mm)	Measured pool areas (m^2)	Average (m^2/litre)
Non-porous	0.1 – 0.2 (film)	2.12	MeOH: 2.7 ± 0.7
		2.62	Pentane: 4.0 *
		2.68	
		2.72	
		3.54	
		4.0	
			*for small quantity with almost instantaneous spread
Semi-porous Concrete	1 – 2		
		MeOH	2.5 ± 0.5
		1.81	
		2.08	
		2.81	
		Pentane	2.95 ± 0.1
		2.85	
		3.04	
		4.4 *	
			*for small quantity with rapid spread)
		Ethanol	
		1.14	1.3 ± 0.15
		1.42	
Plywood			
		Methanol	
		1.28	1.7 ± 0.4
		1.40	
		1.83	
		2.17	
		Pentane	
		1.3	

Table 3.1.2: Summary of pool size tests (Cont.)

Porous (carpets):

Methanol

5mm pile: 0.32 – 0.47 0.3 – 0.5

10mm pile: 0.07 – 0.10 0.07 – 0.1

Pentane

5mm pile: 0.40 – 0.47

10mm pile: 0.08 – 0.10

11mm pile: 0.06 – 0.07

14mm pile: 0.05 – 0.06

3.1.1 Penetration into Substrate

Tests included flooding the surface of a smooth-finished concrete slab with various liquids and observing the penetration of that liquid into the surface of the concrete (along a smooth vertically-cut edge). Results are shown in Table 3.1.1.1.

3.1.2 Transport within a Substrate

Liquids absorbed into wood were sometimes seen to exhibit limited extension beyond their original pool limits, but the additional surface areas produced would be expected to have little effect on the evaporation rates. It was thought that the woven, porous nature of carpets would promote extensive absorptive or capillary-action spread. The vertical absorption tests showed that, at saturation pentane rose only 3 – 4cm in loop-pile synthetic carpets (5mm pile height) and less than 2cm in plush pile synthetic carpets (10 – 14mm pile height). Most of this absorption was noted to have taken place in the first five minutes after insertion into the pentane reservoir, with very little advancement up to one hour after immersion. The results are summarized in Table 3.1.2.1. These results are for carpet, and results for underlayments (carpet pad) may be different. It is rare, however, that an underlayment will be the upper (evaporating) surface.

3.1.3 Spread Rates

Measurement of maximum pool dimensions revealed that on non-porous surfaces, spread occurs for up to 3 min, while on semi-porous materials, spread occurs for 1 – 2 min and on porous materials, spread occurs for less than 1 min. It was consistently observed that spreading

Table 3.1.1.1: Penetration into Concrete

Liquid	Penetration Range	Predominant Range (@ 1min)
Xylene	0.5 – 2mm	≈1mm
Hexane	1 – 2mm	≈ 1.5mm
Petrol	2 – 4mm	≈ 2mm
Methanol	2 – 4mm	≈ 3mm

Table 3.1.2.1: Capillarity (Vertical Transport) in Carpets

Carpet	Time (min)	Height of wetted area (cm above pentane pool)
Polypropylene loop, 5mm pile (Carpet B)	6	4
	40	5
	60	5
Polypropylene loop, 5mm pile (Carpet B)	0.1	3
	4	4
	25	5
	60	5.5
Nylon plush pile, 10mm pile (Carpet D)	2	2
	60	2
Nylon plush pile (Carpet C)	2	2
	60	3
Nylon loop , 5mm pile (Carpet A)	0.5	4
	3	5
	60	6
Nylon plush pile (Carpet E)	2	2
	60	3

occurred until evaporation or absorption reduced the depth of the advancing pool so that inadequate free liquid was available to sustain further spread. On non-porous surfaces, where there was no absorption, the spread of all tested liquids continued for a longer period of time than on semi-porous surfaces. In all cases observed, the rate of spread after the first minute was on the order of 2 – 5cm per min. For a pool with a radius of 1m, an increase in radius of 2 – 5cm would result in the pool area increasing by less than 20% over two minutes. On porous surfaces where there is rapid, maximum absorption, there was no significant spread after the first minute. This is further supported by the observation of pool areas of very small quantities (10 – 50ml) of liquids which were observed to attain their maximum areas almost instantaneously. The larger equivalent pool sizes (4 – 4.4 m^2/litre) were extrapolated from very small pours on non-porous or semi-porous surfaces, which achieved maximum pool size in seconds, before any significant absorption or evaporation could occur. Attempts to quantify the horizontal spread rate by laboratory (bench-scale) experiments were not successful.

3.2 Evaporation Rates v. Substrates

To study the effects of substrates on evaporation rates, over 200 analytical runs were conducted in which small quantities of n-pentane, hexane, n-octane, petrol, and camping fuel were evaporated from pools (of various depths) of free-standing liquid. The mass loss rates (g/min) were calculated from the recorded weight of the liquid as it was measured every 5 or 20s. The resulting mass loss rates were then plotted against time. The

initial rate was estimated graphically from the intercept on the y-axis corresponding to zero elapsed time. The rates observed were then compared against the rates observed for the same fuels evaporating from a variety of substrates. The evaporation rates (mass loss/min/m^2) from various pools and matrices were then calculated from the mass loss rates and pool areas. Due to the volume of raw data and individual plots, it is impractical to present all of it here. A summary list of all the experiments conducted is shown in Table 3.2.1. Typical data plots are shown in Figs. 3.2.1 – 3.2.8.

Each plot demonstrates the same general behaviour: an initial rate which decreases with time — sharply for volatile compounds like pentane, less sharply for less volatile hexane, and very slowly for octane. Occasionally, erratic initial rates (very high or very low) would be produced when the rate measured in the first time interval captured some of the movement of the liquid in the Petri dish. This was especially apparent in the runs where the time interval between data points was 5s. All tabular data for initial mass loss rate was checked against a graphical estimation of the initial rate and also against a spreadsheet manipulation to check the initial rate against the average of the rate calculated from data in the first 3 or 4 intervals of each run.

3.2.1 Pools

The data in Table 3.2.1.1 represent a summary of the initial rates (0 – 30s) observed for liquid pools. The diameter and area of each pool are shown. The mass loss rate per unit area calculated by dividing the net rate by the surface area of the pool is shown under 'Rate'. The number of runs conducted that yielded data are shown under 'n'. Data on the changes in

Table 3.2.1 Master List of Evaporation Rate Experiments

Number	Volume	Liquid	Substrate	Diameter	Conditions	Amb. Temp.
221	190 ml	BP PETROL	Pool	15 cm	I	19.5
219	38 ml	BP PETROL	Film	15 cm	I	20.5
217	190 ml	CAMP FUEL 1	Pool	15 cm	I	19.7
218	20 ml	CAMP FUEL 1	Film	15 cm	I	20.2
220	195 ml	CAMP FUEL 2	Pool	15 cm	I	20.5
222	190 ml	CAMP FUEL 2	Pool	15 cm	I	20.0
223	192 ml	CAMP FUEL 3	Pool	15 cm	I	20.2
55	150 ml	HEXANE	Pool	15 cm	I	21.7
60	150 ml	HEXANE	Pool	15 cm	B I	21.0
72	190 ml	HEXANE	Pool	15 cm	I	23.2
73	190 ml	HEXANE	Pool	15 cm	I	23.3
79	190 ml	HEXANE	Pool	15 cm	I	23.0
82	190 ml	HEXANE	Pool	15 cm		24.0
83	180 ml	HEXANE	Pool	15 cm		24.0
155	190 ml	HEXANE	Pool	15 cm	B I	20.9
156	188 ml	HEXANE	Pool	15 cm	B I	19.0
157	190 ml	HEXANE	Pool	15 cm	B I	20.1
158	190 ml	HEXANE	Pool	15 cm	B I	20.5
159	185 ml	HEXANE	Pool	15 cm	B I	21.5
161	190 ml	HEXANE	Pool	15 cm	B I	21.0
162	190 ml	HEXANE	Pool	15 cm	B I	22.0
163	190 ml	HEXANE	Pool	15 cm	L I	21.5
165	190 ml	HEXANE	Pool	15 cm	L I	22.0
181	185 ml	HEXANE	Pool	15 cm	O	35.1
182	190 ml	HEXANE	Pool	15 cm	O	36.5
183	190 ml	HEXANE	Pool	15 cm	O	36.0
191	190 ml	HEXANE	Pool	15 cm	B I	22.4
57	95 ml	HEXANE	on Al	15 cm	I	21.4
184	100 ml	HEXANE	on Al	15 cm	O	35.0
58	220 ml	HEXANE	on Carpet	15 cm	I	21.2
61	240 ml	HEXANE	on Carpet	15 cm	B I	21.2
160	220 ml	HEXANE	on Carpet	15 cm	I	21.2
164	225 ml	HEXANE	on Carpet	15 cm	I	22.0
94	150 ml	HEXANE	on Carpet A	25 cm	I	22.5
95	150 ml	HEXANE	on Carpet B	28 cm	I	22.5
103	20 ml	HEXANE	Film	15 cm	I	22.0
104	20 ml	HEXANE	Film	15 cm	I	21.5
105	20 ml	HEXANE	Film	15 cm	I	21.5
106	20 ml	HEXANE	Film	15 cm	I	21.5
107	20 ml	HEXANE	Film	15 cm	I	21.5
123	10 ml	HEXANE	Film	15 cm	I	4.2

Conditions Key:
B - 0.6m high acrylic barrier in place during run
I - Petri dish insulated from pan of balance
O - High temperature runs in oven at 35-37°C
L - Barrier runs with lid

Table 3.2.1 Master List of Evaporation Rate Experiments
(Cont.)

Number	Volume	Liquid	Substrate	Diameter	Conditions	Amb. Temp.
124	10 ml	HEXANE	Film	15 cm	I	4.3
125	10 ml	HEXANE	Film	15 cm	I	5.0
234	15 ml	HEXANE	on Plaster	15 cm	I	22.0
235	25 ml	HEXANE	on Plaster	15 cm	I	22.0
236	22 ml	HEXANE	on Plaster	15 cm	I	22.0
238	23 ml	HEXANE	on Plaster	15 cm	I	22.0
240	25 ml	HEXANE	on Plaster	15 cm	I	23.0
242	25 ml	HEXANE	on Plaster	15 cm	I	23.0
56	100 ml	HEXANE	on Sand	15 cm	I	21.5
59	100 ml	HEXANE	on Sand	15 cm	B I	21.5
185	100 ml	HEXANE	on Sand	15 cm	O	35.0
200	250 ml	HEXANE	on Ur. Foam	15 cm	I	22.5
237	220 ml	HEXANE	on Ur. Foam	15 cm	I	23.0
239	240 ml	HEXANE	on Ur. Foam	15 cm	I	22.0
241	230 ml	HEXANE	on Ur. Foam	15 cm	I	22.0
37	100 ml	OCTANE	Pool	15 cm	I	22.0
51	150 ml	OCTANE	Pool	15 cm	I	24.6
74	190 ml	OCTANE	Pool	15 cm	I	23.0
75	190 ml	OCTANE	Pool	15 cm	I	23.4
166	190 ml	OCTANE	Pool	15 cm	I	22.0
167	190 ml	OCTANE	Pool	15 cm	B I	22.0
230	190 ml	OCTANE	Pool	15 cm		36.0
231	190 ml	OCTANE	Pool	15 cm		36.5
232	190 ml	OCTANE	Pool	15 cm		36.0
233	190 ml	OCTANE	Pool	15 cm		36.0
40	105 ml	OCTANE	on Al	15 cm	I	21.7
41	100 ml	OCTANE	on Al	15 cm	I	21.7
43	100 ml	OCTANE	on Al	15 cm	B I	22.0
38	230 ml	OCTANE	on Carpet	15 cm	I	21.8
45	240 ml	OCTANE	on Carpet	15 cm	B I	21.8
52	250 ml	OCTANE	on Carpet	15 cm	I	25.3
136	15 ml	OCTANE	Film	15 cm	I	4.5
39	108 ml	OCTANE	on Sand	15 cm	I	21.8
44	100 ml	OCTANE	on Sand	15 cm	B I	22.1
1	80 ml	PENTANE	Pool	15 cm		18.0
2	100 ml	PENTANE	Pool	15 cm	B	18.0
3	115 ml	PENTANE	Pool	15 cm		24.0
4	150 ml	PENTANE	Pool	15 cm		22.0
5	150 ml	PENTANE	Pool	15 cm	B	23.0
6	150 ml	PENTANE	Pool	15 cm	B	24.0
7	150 ml	PENTANE	Pool	15 cm	I	23.0
8	100 ml	PENTANE	Pool	15 cm	B I	24.0
15	150 ml	PENTANE	Pool	15 cm	B I	23.0

Conditions Key:

B - 0.6m high acrylic barrier in place during run
I - Petri dish insulated from pan of balance
O - High temperature runs in oven at 35-37°C
L - Barrier runs with lid

Table 3.2.1 Master List of Evaporation Rate Experiments
(Cont.)

Number	Volume	Liquid	Substrate	Diameter	Conditions		Amb. Temp.
20	100 ml	PENTANE	Pool	15 cm		I	22.0
21	122 ml	PENTANE	Pool	15 cm		I	22.0
22	120 ml	PENTANE	Pool	15 cm	B	I	21.4
23	124 ml	PENTANE	Pool	15 cm	B	I	21.0
46	140 ml	PENTANE	Pool	15 cm		I	23.2
47	150 ml	PENTANE	Pool	15 cm		I	24.0
53	150 ml	PENTANE	Pool	15 cm	B	I	25.6
65	108 ml	PENTANE	Pool	15 cm		I	24.1
66	130 ml	PENTANE	Pool	15 cm		I	24.1
70	180 ml	PENTANE	Pool	15 cm		I	21.9
71	180 ml	PENTANE	Pool	15 cm		I	22.2
76	190 ml	PENTANE	Pool	15 cm		I	23.6
77	50 ml	PENTANE	Pool	15 cm		I	22.5
78	50 ml	PENTANE	Pool	15 cm		I	23.0
80	190 ml	PENTANE	Pool	15 cm		I	23.0
81	190 ml	PENTANE	Pool	15 cm			23.5
90	185 ml	PENTANE	Pool	15 cm		I	22.0
127	190 ml	PENTANE	Pool	15 cm		I	3.3
128	190 ml	PENTANE	Pool	15 cm		I	5.1
129	190 ml	PENTANE	Pool	15 cm		I	6.1
138	175 ml	PENTANE	Pool	20.5 cm		I	21.9
169	190 ml	PENTANE	Pool	15 cm		I	22.0
170	190 ml	PENTANE	Pool	15 cm		I	22.0
177	190 ml	PENTANE	Pool	15 cm		I	23.7
178	190 ml	PENTANE	Pool	15 cm	O		36.6
179	185 ml	PENTANE	Pool	15 cm	O		35.5
189	190 ml	PENTANE	Pool	15 cm	B	I	22.0
190	192 ml	PENTANE	Pool	15 cm	B	I	22.2
192	190 ml	PENTANE	Pool	15 cm	B	I	22.6
30	85 ml	PENTANE	on Al	15 cm		I	21.0
31	85 ml	PENTANE	on Al	15 cm		I	21.0
32	90 ml	PENTANE	on Al	15 cm		I	20.0
33	88 ml	PENTANE	on Al	15 cm	B	I	20.0
34	88 ml	PENTANE	on Al	15 cm	B	I	20.0
36	50 ml	PENTANE	on Al	20 cm			22.0
49	100 ml	PENTANE	on Al	15 cm		I	24.1
67	135 ml	PENTANE	on Al	15 cm		I	24.6
130	110 ml	PENTANE	on Al	15 cm		I	3.6
134	115 ml	PENTANE	on Al	15 cm		I	3.0
140	118 ml	PENTANE	on Al	20.5 cm		I	20.5
141	115 ml	PENTANE	on Al	20.5 cm		I	20.1
173	114 ml	PENTANE	on Al	15 cm		I	22.3
175	110 ml	PENTANE	on Al	15 cm		I	23.5
180	100 ml	PENTANE	on Al	15 cm	O		35.5

Conditions Key:

B - 0.6m high acrylic barrier in place during run
I - Petri dish insulated from pan of balance
O - High temperature runs in oven at 35-37°C
L - Barrier runs with lid

Table 3.2.1 Master List of Evaporation Rate Experiments
(Cont.)

Number	Volume	Liquid	Substrate	Diameter	Conditions	Amb. Temp.
187	90 ml	PENTANE	on Al	15 cm	O	36.0
208	200 ml	PENTANE	on Beaker	6 cm	I	21.5
16	220 ml	PENTANE	on Carpet	15 cm	I	23.0
17	220 ml	PENTANE	on Carpet	15 cm	I	22.0
18	225 ml	PENTANE	on Carpet	15 cm	I	22.0
19	225 ml	PENTANE	on Carpet	15 cm	B I	22.5
24	225 ml	PENTANE	on Carpet	15 cm	I	22.0
26	219 ml	PENTANE	on Carpet	15 cm	I	22.5
29	221 ml	PENTANE	on Carpet	15 cm	B I	22.0
50	240 ml	PENTANE	on Carpet	15 cm	I	24.6
132	200 ml	PENTANE	on Carpet	15 cm	I	5.4
137	350 ml	PENTANE	on Carpet	20.5 cm	I	20.5
171	220 ml	PENTANE	on Carpet	15 cm	I	22.0
176	215 ml	PENTANE	on Carpet	15 cm	I	22.5
188	190 ml	PENTANE	on Carpet	15 cm	O	33.5
92	150 ml	PENTANE	on Carpet A	25 cm	I	22.0
93	100 ml	PENTANE	on Carpet A	22x26 cm	I	22.0
96	145 ml	PENTANE	on Carpet A	27 cm	I	22.0
97	146 ml	PENTANE	on Carpet A	27 cm	I	22.0
115	150 ml	PENTANE	on Carpet A	27 cm	I	20.5
144	90 ml	PENTANE	on Carpet A	15 cm	I	21.6
146	100 ml	PENTANE	on Carpet A	24 cm	I	22.0
116	151 ml	PENTANE	on Carpet B	28 cm	I	21.5
147	100 ml	PENTANE	on Carpet B	21x28 cm	I	22.0
110	150 ml	PENTANE	on Carpet C	11 cm	I	21.0
113	151 ml	PENTANE	on Carpet C	13 cm	I	20.2
143	375 ml	PENTANE	on Carpet C	20.5 cm	I	21.2
148	100 ml	PENTANE	on Carpet C	8x10 cm	I	22.5
194	350 ml	PENTANE	on Carpet C	18 cm	I	20.0
109	151 ml	PENTANE	on Carpet D	11 cm	I	20.8
112	150 ml	PENTANE	on Carpet D	10 cm	I	21.3
117	150 ml	PENTANE	on Carpet D	12 cm	I	21.4
149	100 ml	PENTANE	on Carpet D	13x18 cm	I	23.0
196	300 ml	PENTANE	on Carpet D	15 cm	I	21.0
108	150 ml	PENTANE	on Carpet E	12 cm	I	21.0
111	150 ml	PENTANE	on Carpet E	12 cm	I	21.5
114	150 ml	PENTANE	on Carpet E	13 cm	I	20.5
118	300 ml	PENTANE	on Carpet E	18 cm	I	21.0
150	100 ml	PENTANE	on Carpet E	10x13 cm	I	22.5
195	300 ml	PENTANE	on Carpet E	20 cm	I	20.0
98	20 ml	PENTANE	Film	15 cm	I	21.0
99	20 ml	PENTANE	Film	15 cm	I	22.0
100	20 ml	PENTANE	Film	15 cm	I	22.0
101	20 ml	PENTANE	Film	15 cm	I	22.0

Conditions Key:

B - 0.6m high acrylic barrier in place during run
I - Petri dish insulated from pan of balance
O - High temperature runs in oven at 35-37°C
L - Barrier runs with lid

Table 3.2.1 Master List of Evaporation Rate Experiments
(Cont.)

Number	Volume	Liquid	Substrate	Diameter	Conditions	Amb. Temp.
102	20 ml	PENTANE	Film	15 cm	I	22.2
119	10 ml	PENTANE	Film	15 cm	I	5.0
120	11 ml	PENTANE	Film	15 cm	I	4.5
121	11 ml	PENTANE	Film	15 cm	I	4.5
122	10 ml	PENTANE	Film	15 cm	I	3.1
126	20 ml	PENTANE	Film	15 cm	I	3.0
201	250 ml	PENTANE	on Lg. Pan	33 cm	I	19.7
202	275 ml	PENTANE	on Lg. Pan	33 cm	I	20.5
203	275 ml	PENTANE	on Lg. Pan	33 cm	I	20.5
204	272 ml	PENTANE	on Lg. Pan	33 cm	I	20.8
207	270 ml	PENTANE	on Lg. Pan	33 cm	I	20.1
205	20 ml	PENTANE	on Petri Dish	5.2 cm	I	19.6
206	20 ml	PENTANE	on Petri Dish	5.6 cm	I	20.7
209	25 ml	PENTANE	on Petri Dish	6 cm	I	20.6
210	25 ml	PENTANE	on Petri Dish	5 cm	I	20.5
212	30 ml	PENTANE	on Petri Dish	6 cm	I	21.2
213	30 ml	PENTANE	on Petri Dish	5 cm	I	20.5
227	9 ml	PENTANE	on Plaster	15 cm	I	20.0
228	10 ml	PENTANE	on Plaster	15 cm	I	20.5
229	10 ml	PENTANE	on Plaster	15 cm	I	20.5
211	300 ml	PENTANE	on Rect. Pan	26x38 cm	I	20.4
214	300 ml	PENTANE	on Rect. Pan	26x38 cm	I	20.5
10	100 ml	PENTANE	on Sand	15 cm		25.0
11	100 ml	PENTANE	on Sand	15 cm	I	25.0
12	100 ml	PENTANE	on Sand	15 cm	I	22.0
13	100 ml	PENTANE	on Sand	15 cm	B I	22.0
14	100 ml	PENTANE	on Sand	15 cm	B I	22.0
25	110 ml	PENTANE	on Sand	15 cm	I	22.6
27	110 ml	PENTANE	on Sand	15 cm	I	22.7
28	100 ml	PENTANE	on Sand	15 cm	B I	22.6
35	100 ml	PENTANE	on Sand	20 cm		22.0
48	90 ml	PENTANE	on Sand	15 cm	I	24.5
54	95 ml	PENTANE	on Sand	15 cm	B I	25.8
68	100 ml	PENTANE	on Sand	15 cm	I	24.5
131	100 ml	PENTANE	on Sand	15 cm	I	6.0
133	100 ml	PENTANE	on Sand	15 cm	I	6.5
135	110 ml	PENTANE	on Sand	15 cm	I	5.5
139	112 ml	PENTANE	on Sand	20.5 cm	I	21.5
142	120 ml	PENTANE	on Sand	20.5 cm	I	20.8
172	105 ml	PENTANE	on Sand	15 cm	I	22.0
174	100 ml	PENTANE	on Sand	15 cm	I	23.0
186	90 ml	PENTANE	on Sand	15 cm	O	36.0
193	100 ml	PENTANE	on Sand	15 cm	B I	22.1
197	210 ml	PENTANE	on Ur. Foam	15 cm	I	21.0

Conditions Key:
B - 0.6m high acrylic barrier in place during run
I - Petri dish insulated from pan of balance
O - High temperature runs in oven at 35-37°C
L - Barrier runs with lid

Table 3.2.1 Master List of Evaporation Rate Experiments
(Cont.)

Number	Volume	Liquid	Substrate	Diameter	Conditions	Amb. Temp.
198	250 ml	PENTANE	on Ur. Foam	15 cm	I	21.5
199	250 ml	PENTANE	on Ur. Foam	15 cm	I	22.3
215	230 ml	PENTANE	on Ur. Foam	15 cm	I	21.2
216	250 ml	PENTANE	on Ur. Foam	15 cm	I	20.5
224	230 ml	PENTANE	on Ur. Foam	15 cm	I	20.0
225	230 ml	PENTANE	on Ur. Foam	15 cm	I	21.0
226	240 ml	PENTANE	on Ur. Foam	15 cm	I	20.5
85	180 ml	PETROL	Pool	15 cm	I	22.0
86	150 ml	PETROL	Pool	15 cm	I	22.9
87	180 ml	PETROL	Pool	15 cm	I	22.4

Conditions Key:

B - 0.6m high acrylic barrier in place during run
I - Petri dish insulated from pan of balance
O - High temperature runs in oven at 35-37°C
L - Barrier runs with lid

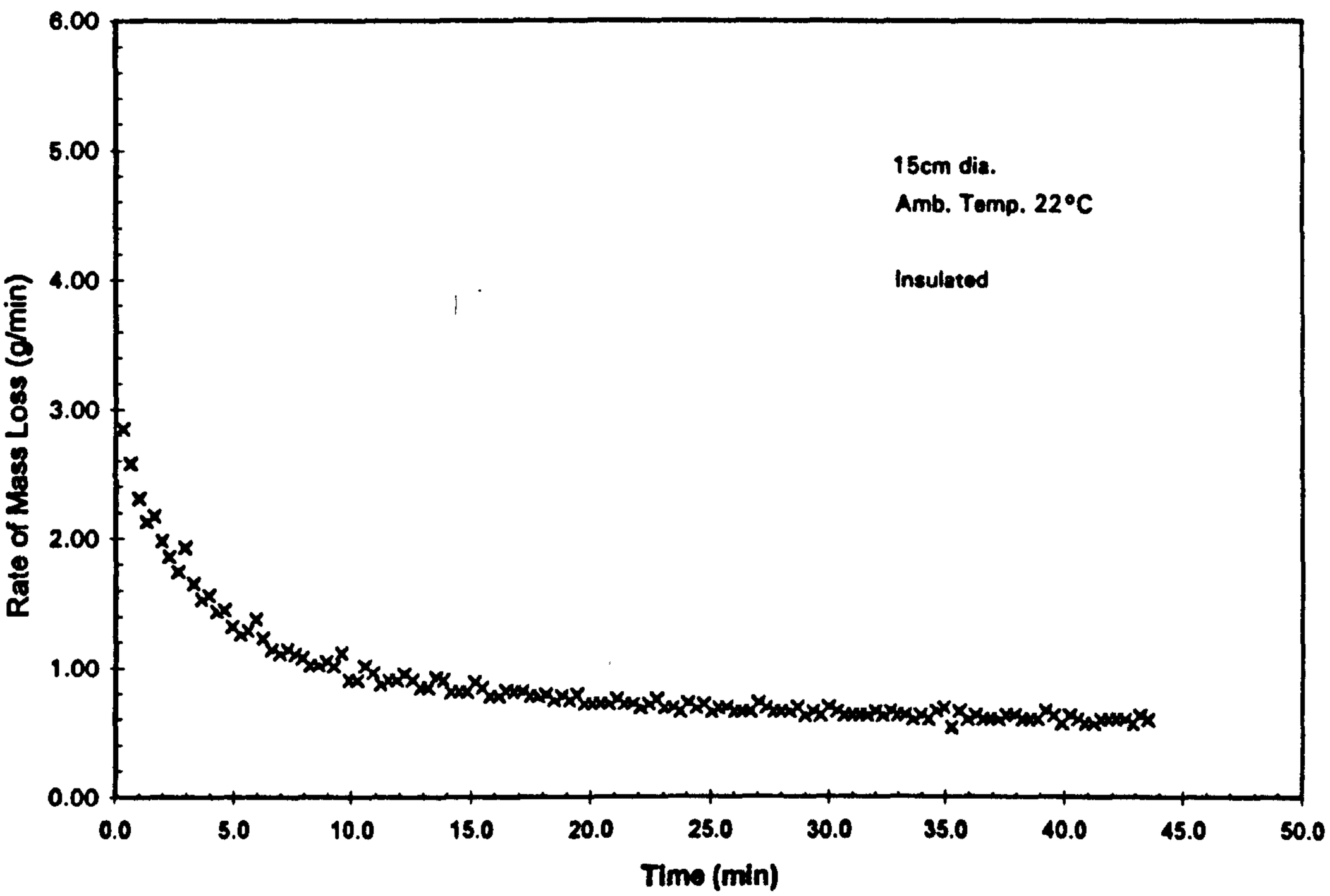

Fig. 3.2.1: Typical mass loss rate v. time plot for pentane pool (D=0.15m) at 22°C ambient.

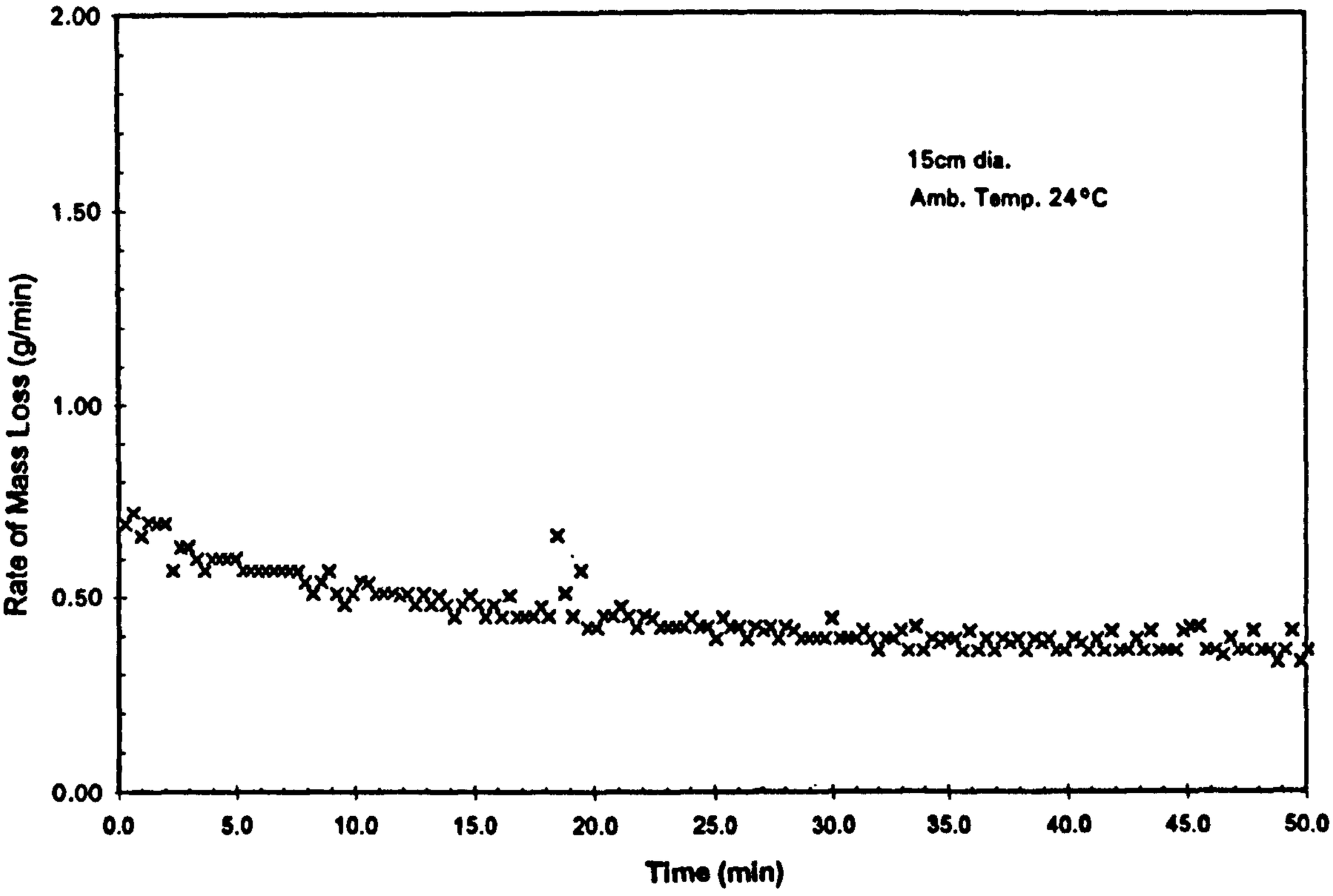

Fig. 3.2.2: Typical mass loss rate v. time plot for hexane pool (D=0.15m) at 22°C ambient.

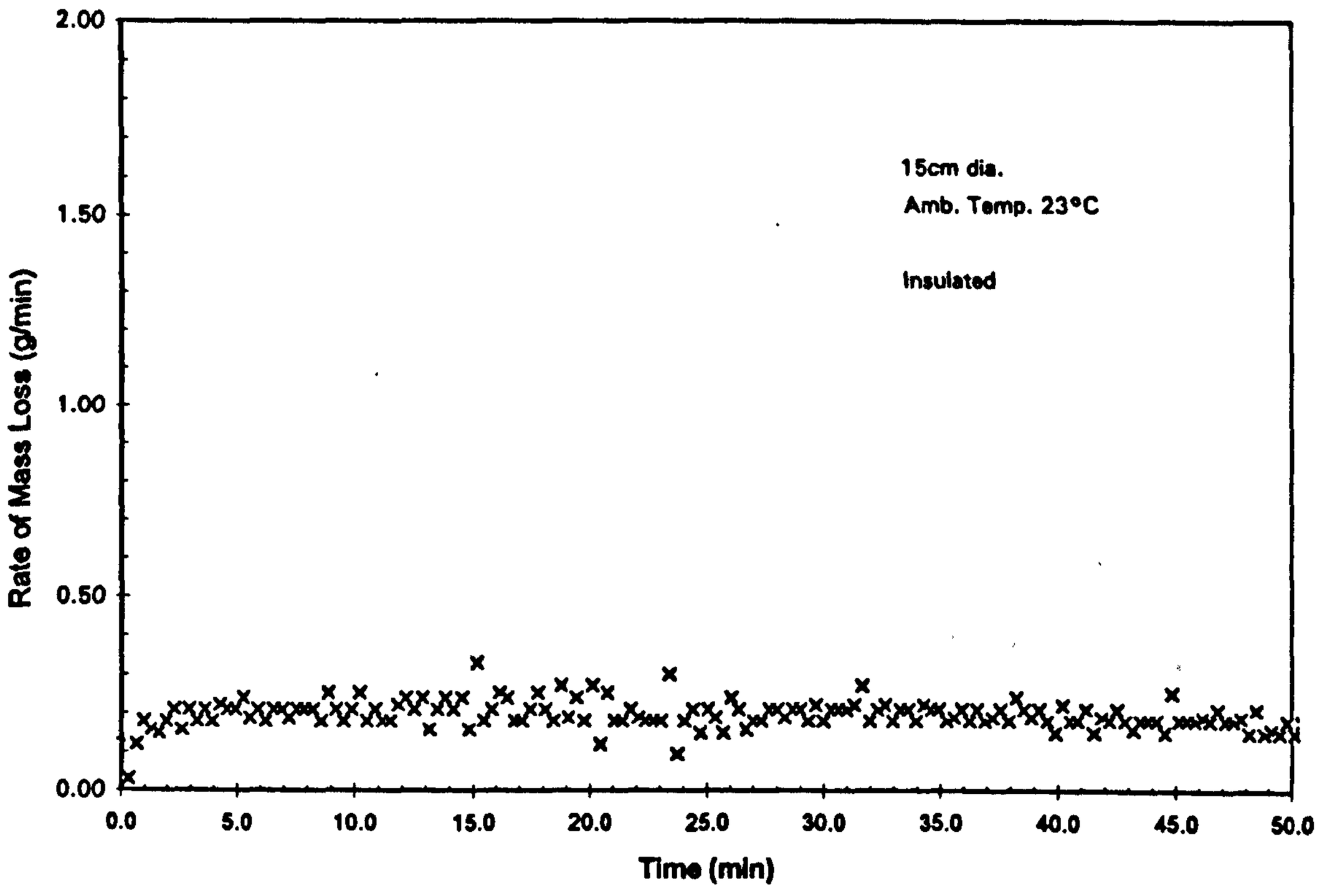

Fig. 3.2.3: Typical mass loss rate v. time plot for octane pool (D=0.15m) at 22°C ambient.

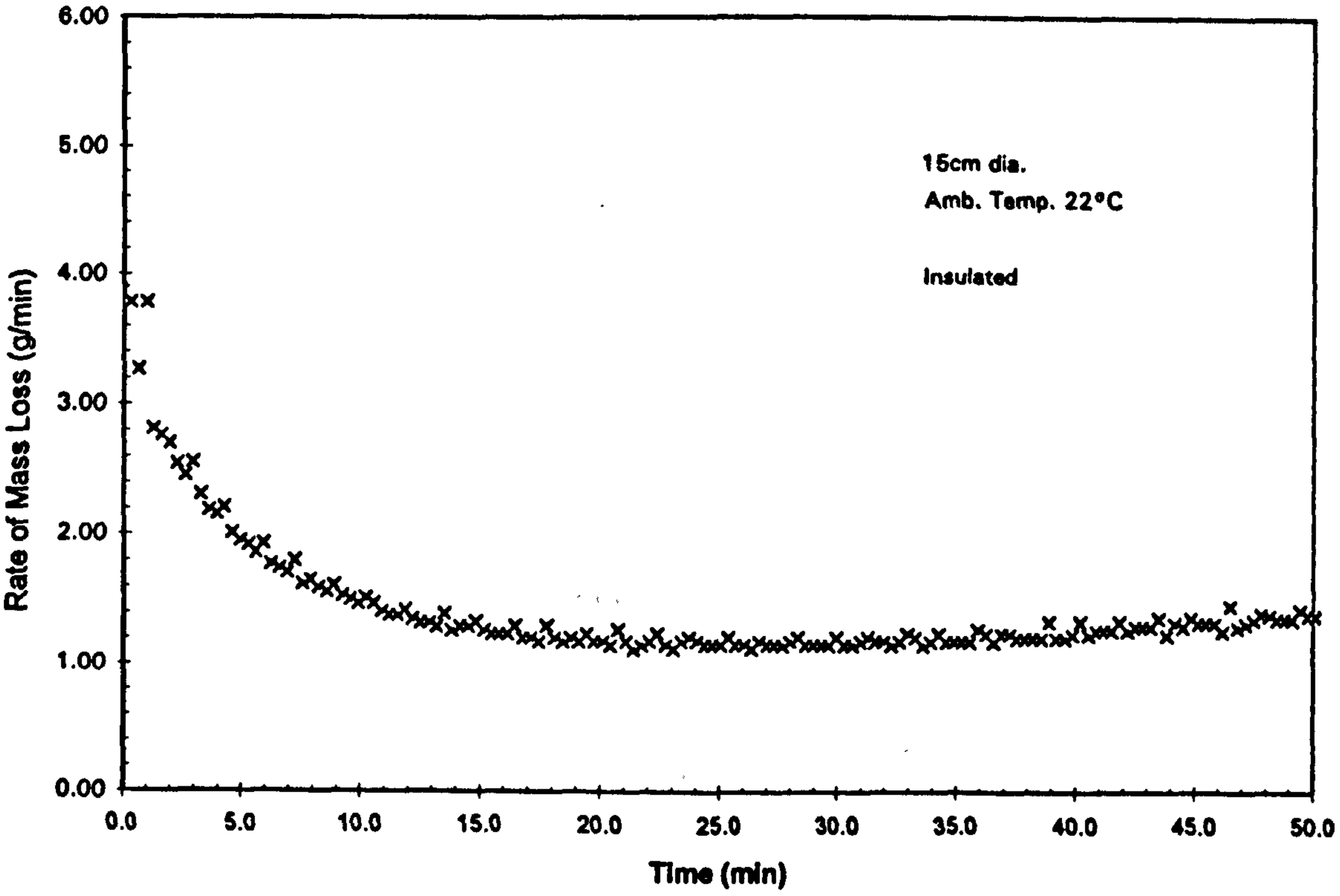

Fig. 3.2.4: Typical mass loss rate v. time plot for pentane on carpet (D=0.15m) at 22°C ambient.

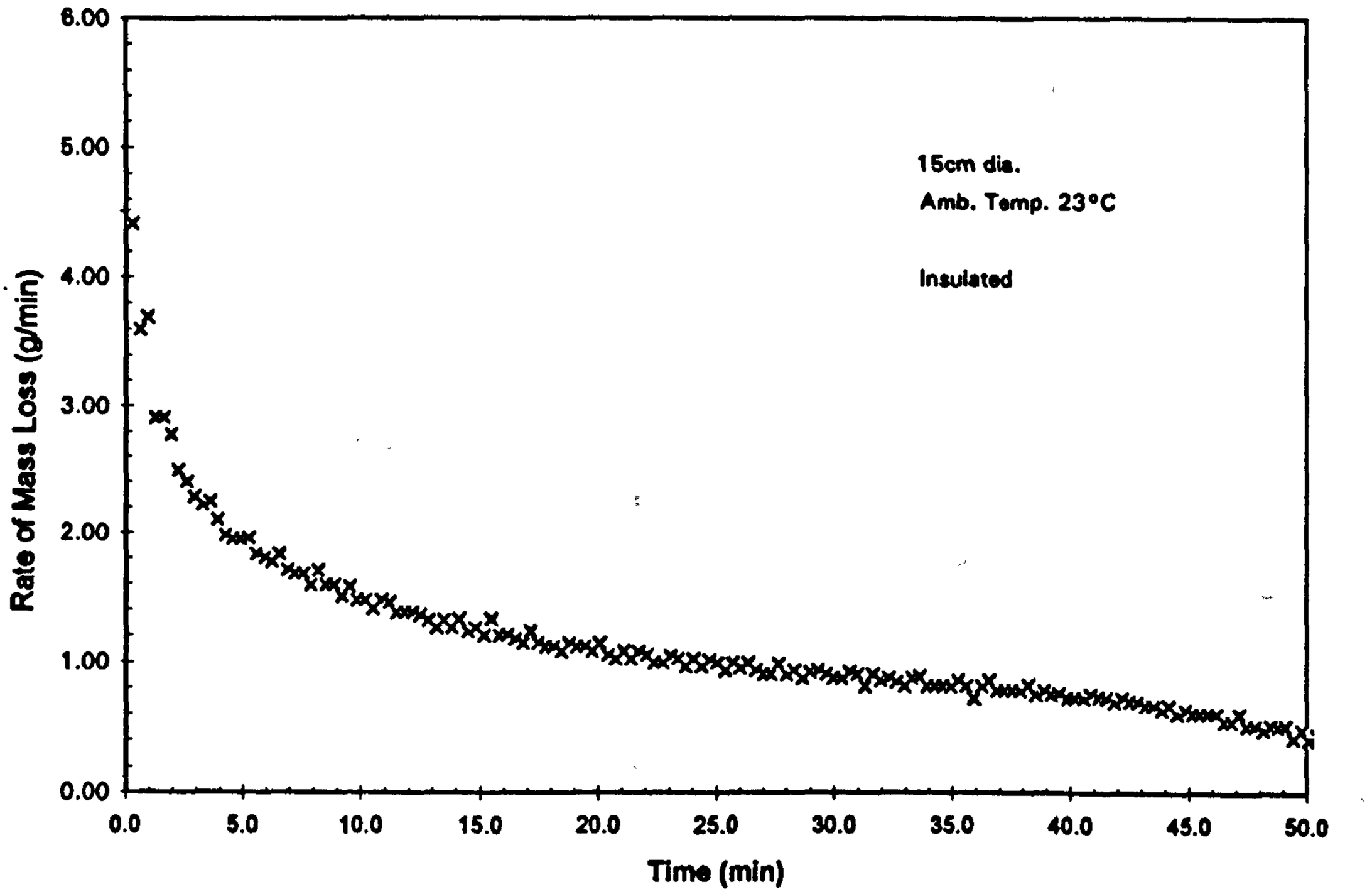

Fig. 3.2.5: Typical mass loss rate v. time plot for pentane on sand (20-30 mesh) (D=0.15m) at 22°C ambient.

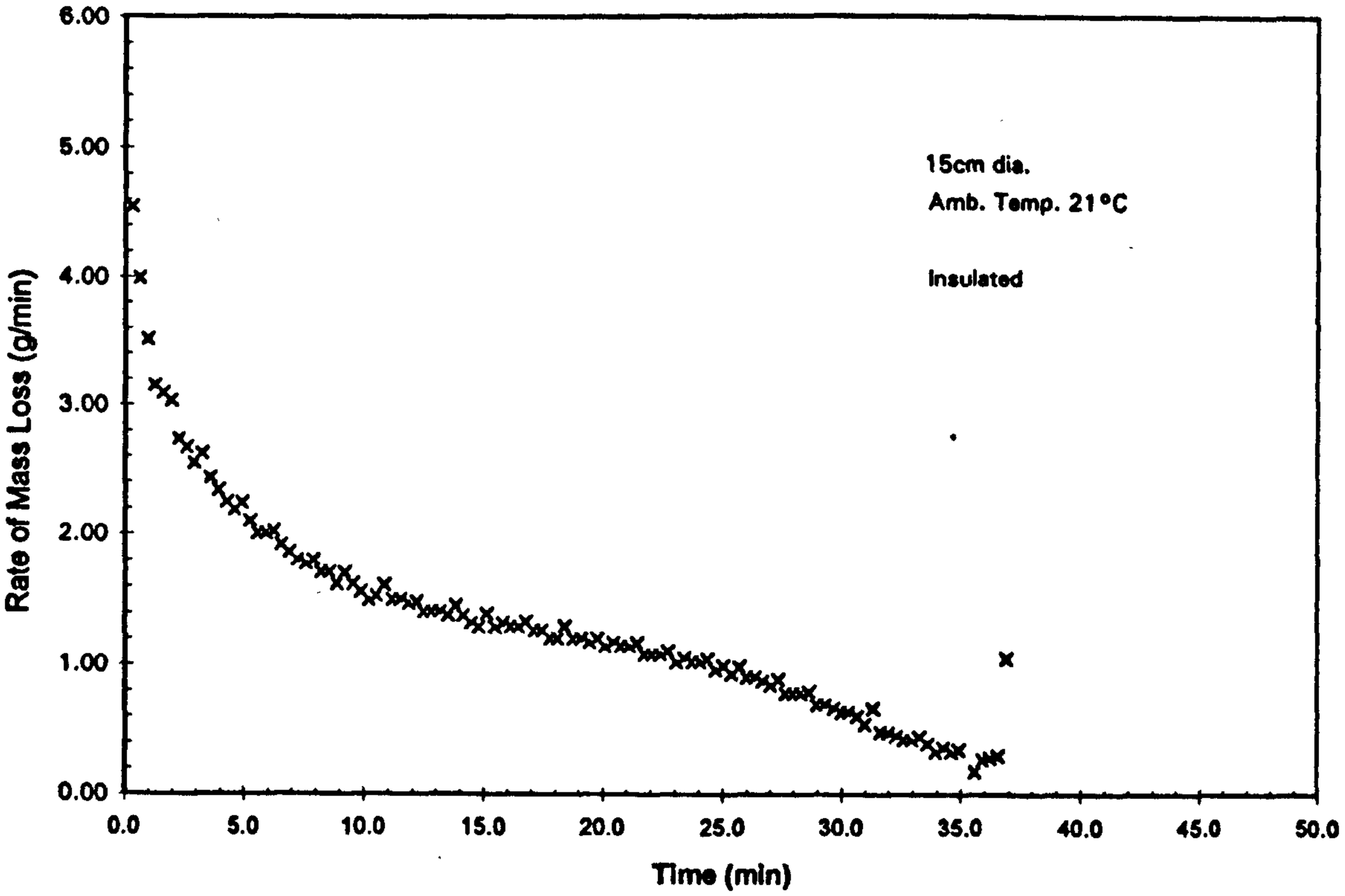

Fig. 3.2.6: Typical mass loss rate v. time plot for pentane on aluminium granules (D=0.15m) at 22°C ambient.

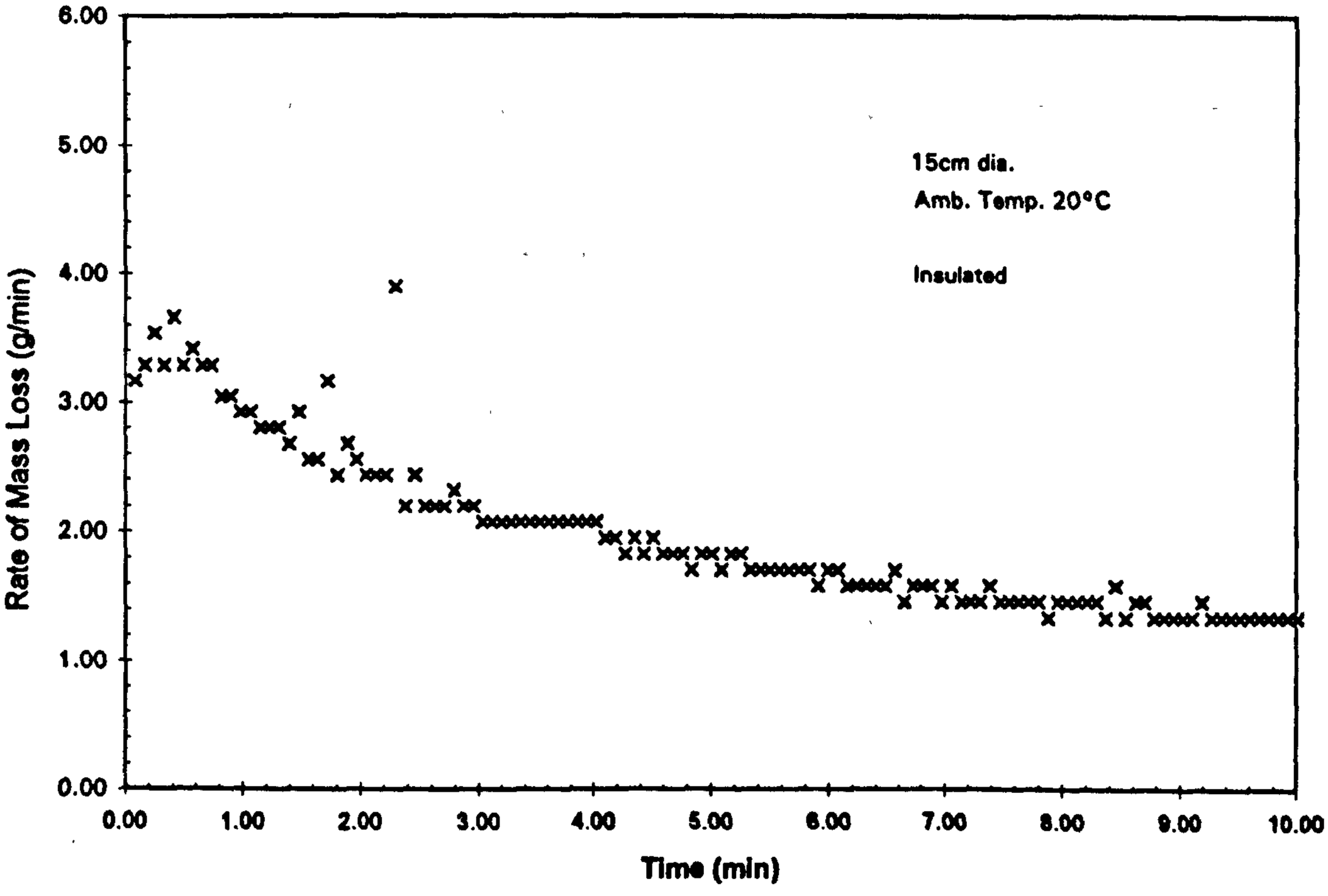

Fig. 3.2.7: Typical mass loss rate v. time plot for pentane on polyurethane foam (D=0.15m).

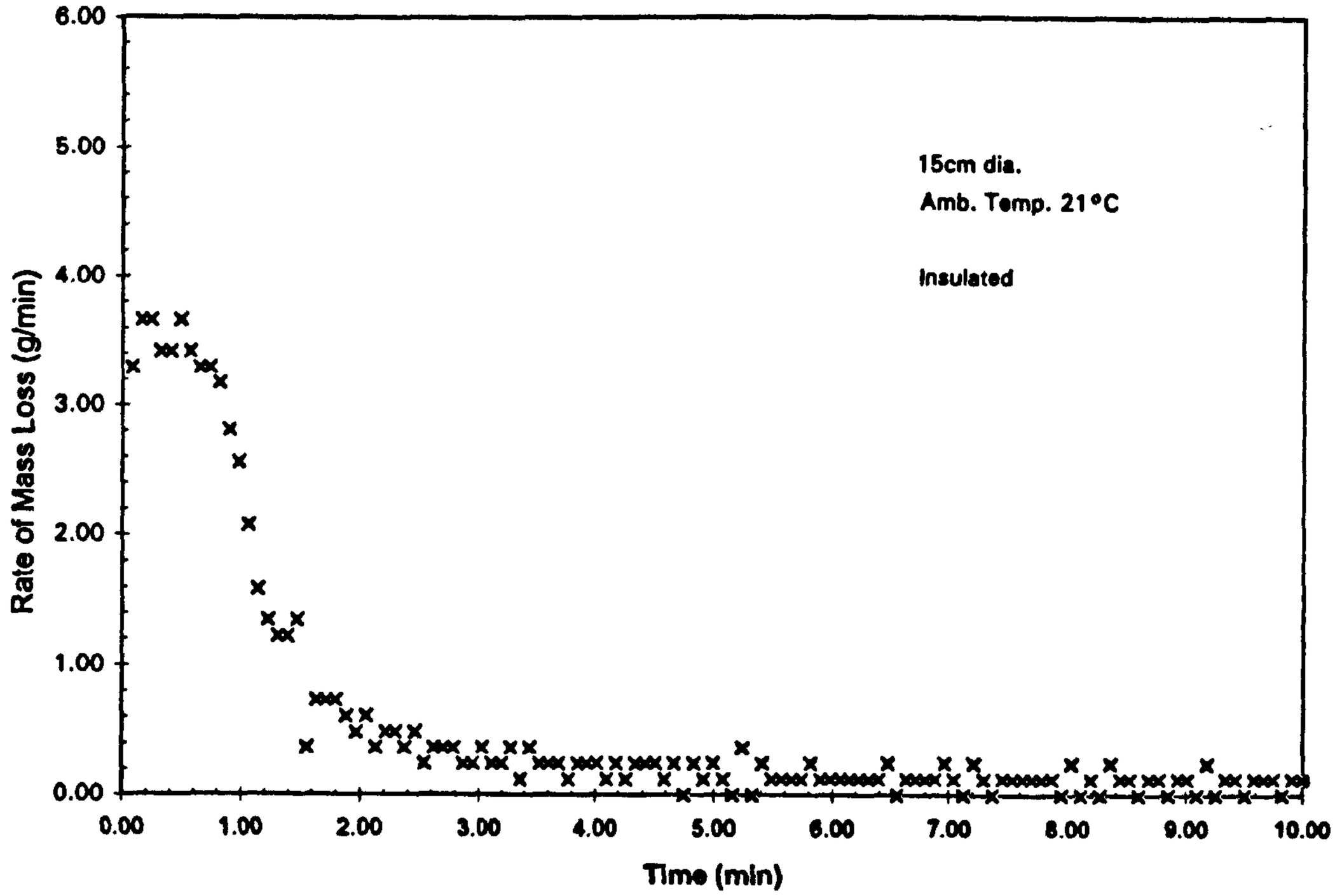

Fig. 3.2.8: Typical mass loss rate v. time plot for pentane on plaster of Paris (D=0.15m) at 22°C ambient. Small quantity of pentane evaporates very quickly.

Table 3.2.1.1: Initial Evaporation Rates for Pools at 20 – 21°C

Pentane: (Vapour pressure = 441mmHg @ 20°C)

Depth	Diameter	Area	Rate of Mass Loss	Mass Flux	n
mm	cm	m^2	g/min	$g/min/m^2$	
12	15	0.016	1.4 – 2.8	90 –175	24
4	15	0.016	1.3	81	2
Film(1mm)	15	0.016	2.3 – 2.4	143 –150	5
5	33	0.085	8.5 – 10	100 –117	5
4	35	0.096	7 – 7.4	73 – 77	2

Hexane: (Vapour pressure = 121mmHg @ 20°C)

Depth	Diameter	Area	Rate of Mass Loss	Mass Flux	n
mm	cm	m^2	g/min	$g/min/m^2$	
12	15	0.016	0.5 – 0.7	31 – 44	20
Film(1mm)	15	0.016	0.6 – 0.7	38 – 44	5

Octane: (Vapour pressure = 11mmHg @ 20°C)

Depth	Diameter	Area	Rate of Mass Loss	Mass Flux	n
mm	cm	m^2	g/min	$g/min/m^2$	
12	15	0.016	0.1 – 0.2	6 – 12	6

evaporation rate with time will be presented in Sect.3.8. Prior to their use, the n-pentane and hexane stocks used were analyzed by capillary gas chromatography with FID and peak area integration to establish their composition. The n-pentane was found to be: n-pentane 99.85%, 2-methyl pentane 0.15%. The hexane was identified as containing: n-hexane 85.0%, methyl hexane 12.7%, 3-methyl pentane 2.1%, other alkanes 0.3%.

It was noted that the initial evaporation rates for the films for each liquid fell in the same range as the mean rate observed for the deep pools of the same size. The initial rate for a shallow pool (4mm) in a deep (12mm) dish, i.e., having a pool surface that was not flush with its surroundings, thus surrounded by a low barrier, was considerably lower than either a deep pool or a shallow pool (film) flush with its surroundings.

3.2.2 Substrates

The data in Tables 3.2.2.1, 3.2.2.2, and 3.2.2.3 represent the initial mass loss rates (0 – 30s) for alkanes evaporating from both free pools (liquids poured onto carpet and allowed to seek their own maximum sizes) and from substrates confined to a 15cm Petri dish and saturated with enough liquid to come level with the top of the substrate and the rim of the Petri dish. The area of each pool (or visibly wetted area of the free pool) and the pile height of the carpet is shown under 'Condition'. The mass loss rate per unit area calculated by dividing the net rate by the surface area of the pool is shown under 'Rate'. The number of runs conducted that yielded data are shown under 'n'. To facilitate comparisons between pools and substrates, the data from those tables were summarized in Table 3.2.2.4.

Table 3.2.2.1: Initial Evaporation Rates – Pentane Matrices

Type	Area m^2	Condition	Rate of Mass Loss (g/min)	Mass Flux (g/min/m^2)	n
Carpet A	0.045–.057	Free Pool 5mm	6.3 – 9.5	140–184	5
Carpet B	0.044–.071	Free Pool 5mm	9.0 – 9.5	127–155	2
Carpet C	0.006–.013	Free Pool 14mm	4.2 – 5.5	340–650	4
Carpet D	0.008–.011	Free Pool 12mm	2.5 – 3.2	370–500	5
Carpet E	0.011–.013	Free Pool 11mm	3.1 – 3.6	350–420	4
	0.025–.031	Free Pool 11mm	5.5 – 6.5	216–268	2
Carpet G	0.016	Saturated. 12mm	2.4 – 4	150–250	12
Carpet G	0.033	Saturated. 12mm	5.2 – 7.5	158–227	2
Sand	0.016	Saturated. Dish	4.0 – 5.5	250–344	19
Aluminium	0.016	Saturated. Dish	4.0 – 5.5	250–344	14
Urethane Foam		22mm	2.1 – 2.4	131–150	5
Urethane Foam		Saturated.12mm	3.2 – 3.5	200–220	3
Plaster of Paris		Saturated. Film	3.5 – 4.5	220–262	3

Table 3.2.2.2: Hexane (Initial Rates)

Type	Area m^2	Conditions	Rate of Mass Loss g/min	Mass Flux $g/min/m^2$	n
Carpet A	0.047	Free Pool 5mm	3.0	64	1
Carpet B	0.07	Free Pool 5mm	2.8	40	1
Carpet G	0.016	Saturated 12mm	0.8 – 1.5	50 –94	4
Sand	0.016	Saturated. Dish	1.5 - 2.0	94 –125	2
Aluminium	0.016	Saturated. Dish	1.75	109	1
Urethane Foam		22mm	0.75	46	1

Table 3.2.2.3: Octane (Initial Rates)

Type	Area m^2	Conditions	Rate of Mass Loss g/min	Mass Loss $g/min/m^2$	n
Carpet G	0.016	Saturated 12mm	0.1 – 0.3	6 – 19	3
Sand	0.016	Saturated. Dish	0.25 – 0.7	16 – 40	2
Aluminium	0.016	Saturated. Dish	0.2 – 0.3	12 –19	3

Table 3.2.2.4: Initial Rates for Pools/Matrices of Same Sizes and Types

($g/min/m^2$)

Liquid	Pool	Saturated Carpet	Sand	Aluminium	Foam	Plaster
Pentane	90–175	200–250	250–344	250–344	200–206	220–262
Hexane	31–50	50 –75	94 –125	109	46	75 –94
Octane	3 – 9	6 –12	16 –22	12 – 19	na	na

3.2.3 Comparison

Fig. 3.2.3.1 demonstrates in bar graph form the distribution of initial mass loss rates for 15cm (0.016m^2) pools of pentane evaporating as a free liquid pool and from various matrices. It can be seen that the rates for films overlay the norms of distributions for pools and that the rates for matrices are consistently higher than those for pools at the same temperatures.

Fig. 3.2.3.2 demonstrates in bar graph form the distribution of initial mass loss rates for 15cm (0.016m^2) pools of hexane and octane evaporating from free liquid pools and from various matrices. The rates for octane are very low and are scattered due to the statistical variation of results when measuring rates (≈0.1g/min) since it is close to the detection limit of the equipment used.

From these data, it can be seen that for all three liquids, the mass loss rates per unit area from free liquid pools are the lowest of all the forms, with liquids saturated onto urethane foam, plaster, and carpet having similar rates, all approximately 1.5 times those of free liquids. The granulated matrices like sand and aluminium granules have rates twice those of free liquid for n-pentane and three times the rate for hexane.

3.3 Relationship of Initial Evaporation Rate to Temperature

3.3.1 Low Temperatures

The data in Table 3.3.1 represent evaporation tests of n-alkanes conducted in ambient temperatures of 3 – 5°C.

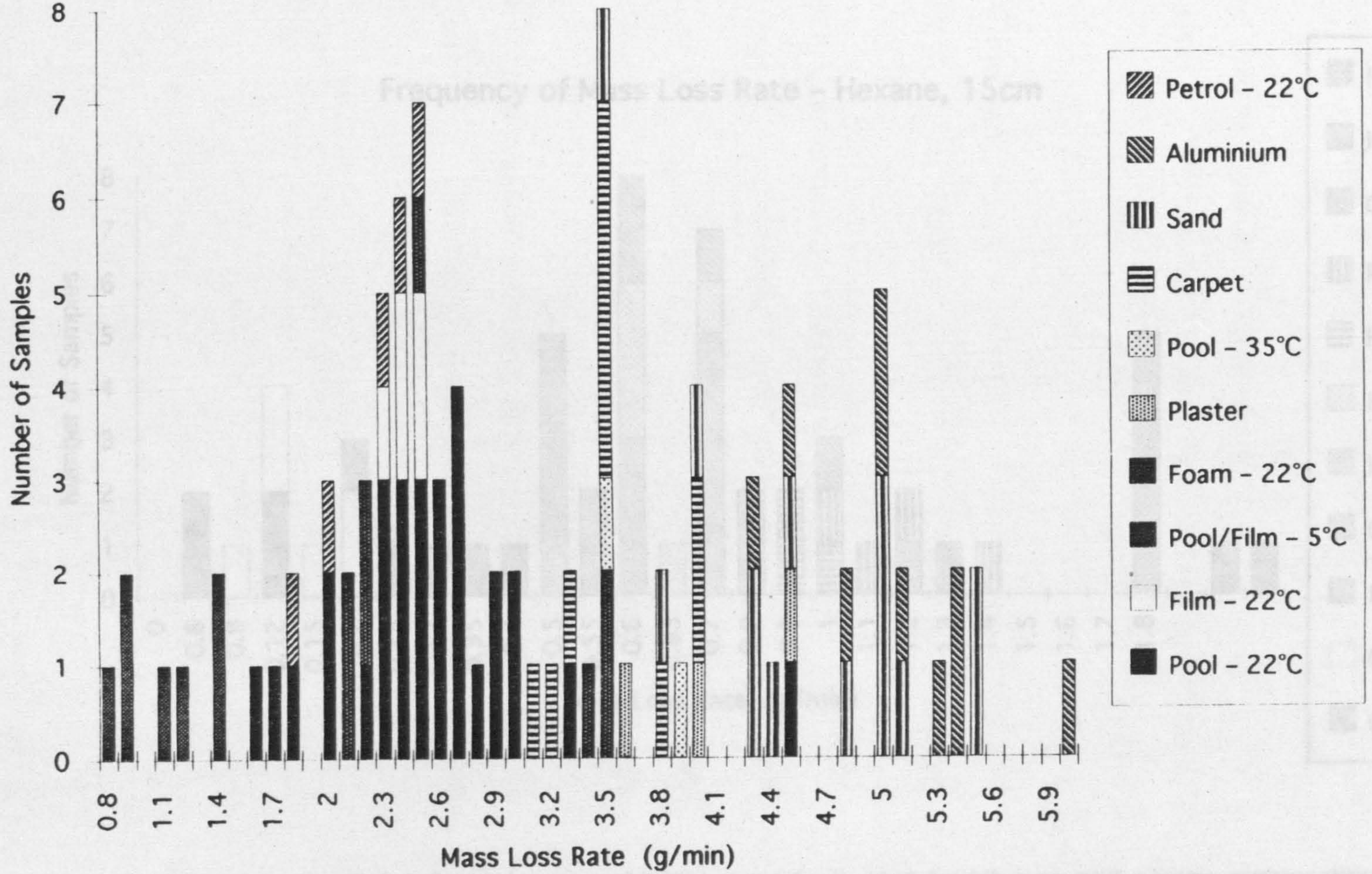

Fig. 3.2.3.1: Histogram of initial mass loss rates for n-pentane evaporating from liquid pools and matrices at various temperatures (all from 0.016m^2 pools). Note that the rates for evaporation of pentane from a film and for petrol fall on top of rates for pentane pools at the same temperatures and that the rates for all matrices are significantly higher than for pools.

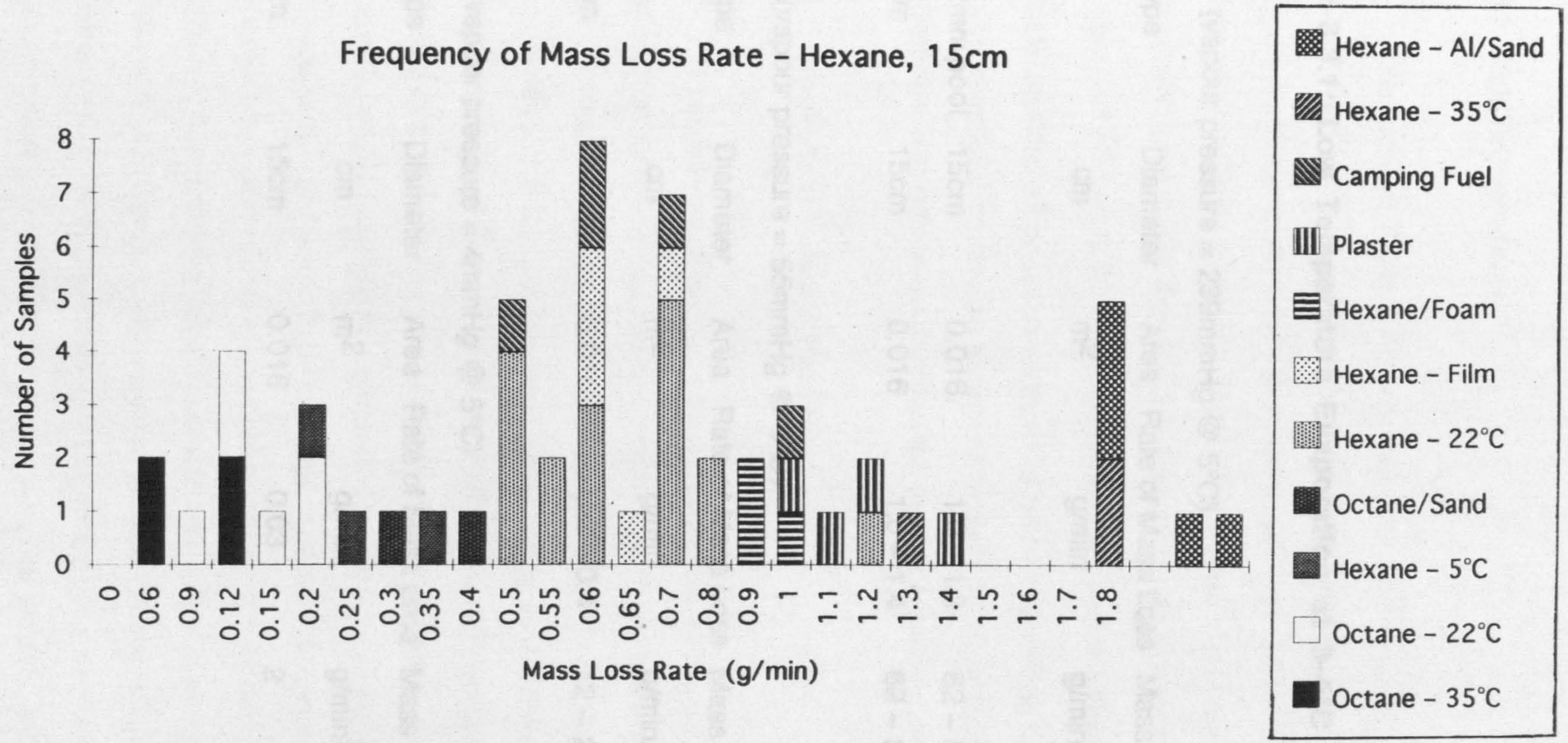

Fig. 3.2.3.2: Histogram of initial mass loss rates for hexane and octane evaporating from liquid pools and matrices at various temperatures (all from 0.016m^2 pools). Note that the rates for evaporation of hexane from a film and for camping fuel fall on top of rates for hexane pools at the same temperatures and that the rates for matrices are significantly higher than for pools.

Table 3.3.1: Low Temperature Evaporation at 3–5°C (Initial Rates)

Pentane: (vapour pressure = 239mmHg @ 5°C)

Type	Diameter	Area	Rate of Mass Loss	Mass Flux	n
	cm	m^2	g/min	$g/min/m^2$	
12mm pool	15cm	0.016	1.0 – 1.3	62 – 81	3
Film	15cm	0.016	1.0 – 1.4	62 – 88	5

Hexane: (vapour pressure = 55mmHg @ 5°C)

Type	Diameter	Area	Rate of Mass Loss	Mass Flux	n
	cm	m^2	g/min	$g/min/m^2$	
Film	15cm	0.016	0.2 – 0.4	12 – 25	3

Octane: (vapour pressure = 4mmHg @ 5°C)

Type	Diameter	Area	Rate of Mass Loss	Mass Flux	n
	cm	m^2	g/min	$g/min/m^2$	
Film	15cm	0.016	0.03	2	1

3.3.2 High Temperatures

The data in Table 3.3.2 represent the initial evaporation rates of n-alkanes from pools at ambient temperatures of 35 – 36°C. Using the Antoine equation to calculate the vapour pressure of these alkanes at these temperatures (Sect. 1.4.2, also Fig.1.1), and plotting evaporation rate v. vapour pressure yields Fig. 3.3.2.1. Plotting evaporation rate v. vapour pressure $v^{1.25}$ to test Wade's prediction of the relationship yields Fig. 3.3.2.2. Plotting a line between the pool rates and adding the evaporation rates for various substrates along the projection show that the net effect of a substrate is to increase the effective vapour pressure, as in Fig. 3.3.2.3.

3.4 Evaporation Rates v. Pool Size

It can be seen from the data presented in Section 3.3 that the initial evaporation rate does not remain constant with changes in pool surface area. Plotting the initial mass loss rate per unit area v. the surface area for pools yields Fig. 3.4.1 and for carpets yields Fig. 3.4.2. There is an observed non-linearity for pools of both very small areas and very large areas. It is observed that the rate does not approach zero as pool surface area approaches zero as would be expected. One of the approaches to evaluating combustion rates of liquid fuels burning as pools is to determine the regression rate of the level of the pool (dividing the volume loss rate by the pool area). Using the initial evaporation (mass loss rates) and dividing by the density of pentane (0.6262 g/cc) to get the volume of fuel being consumed in the first minute, regression rates (mm/min) were calculated for deep pools of various diameters and different pool sizes on carpets and plotted v. diameter. (See Figs 3.4.3 and 3.4.4.) The regression rate holds steady for

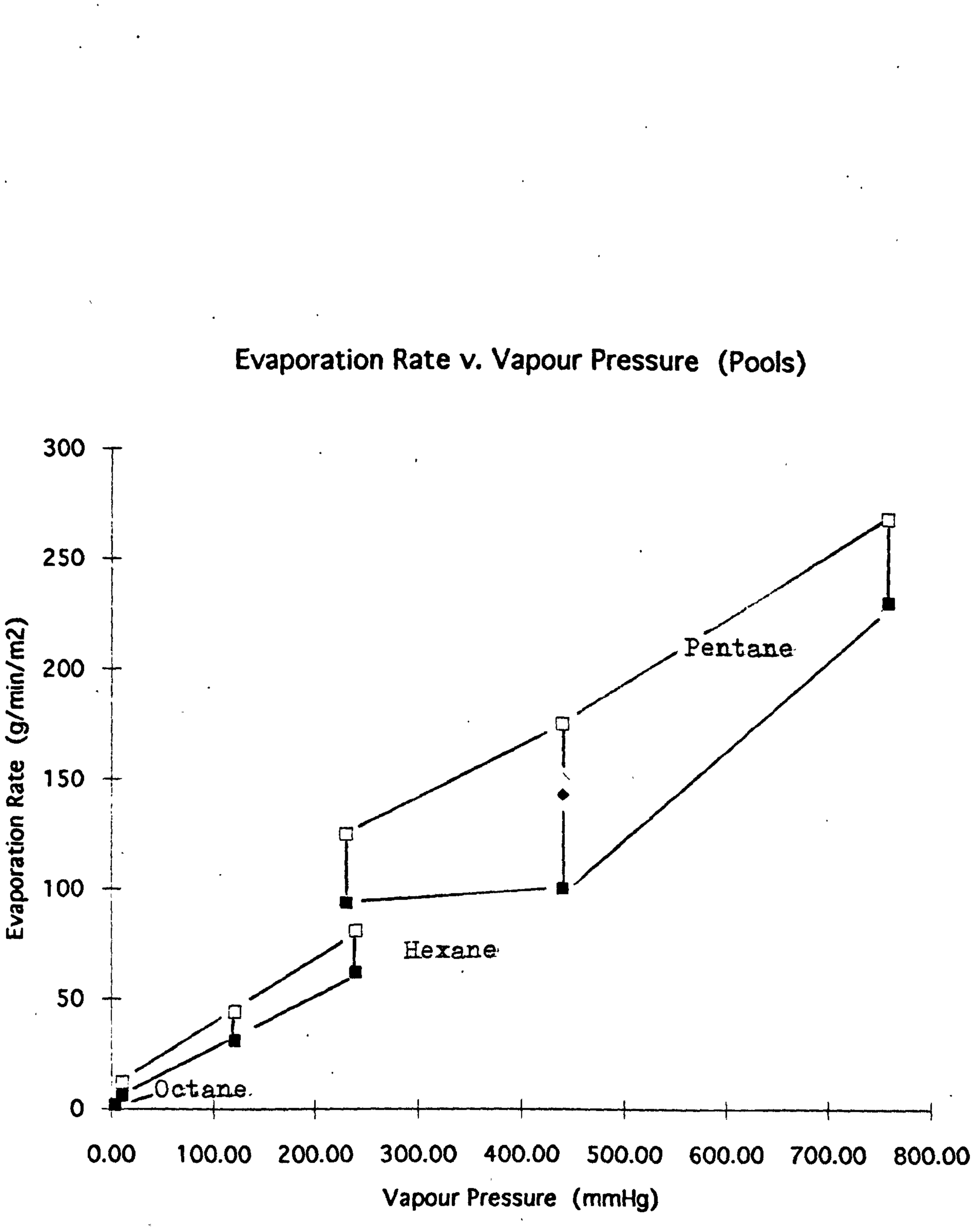

Fig. 3.3.2.1: Evaporation rate (per unit area) v. vapour pressure (for n-pentane, hexane and n-octane as calculated , per Dean, for temperatures of 5, 22, and 35°C)

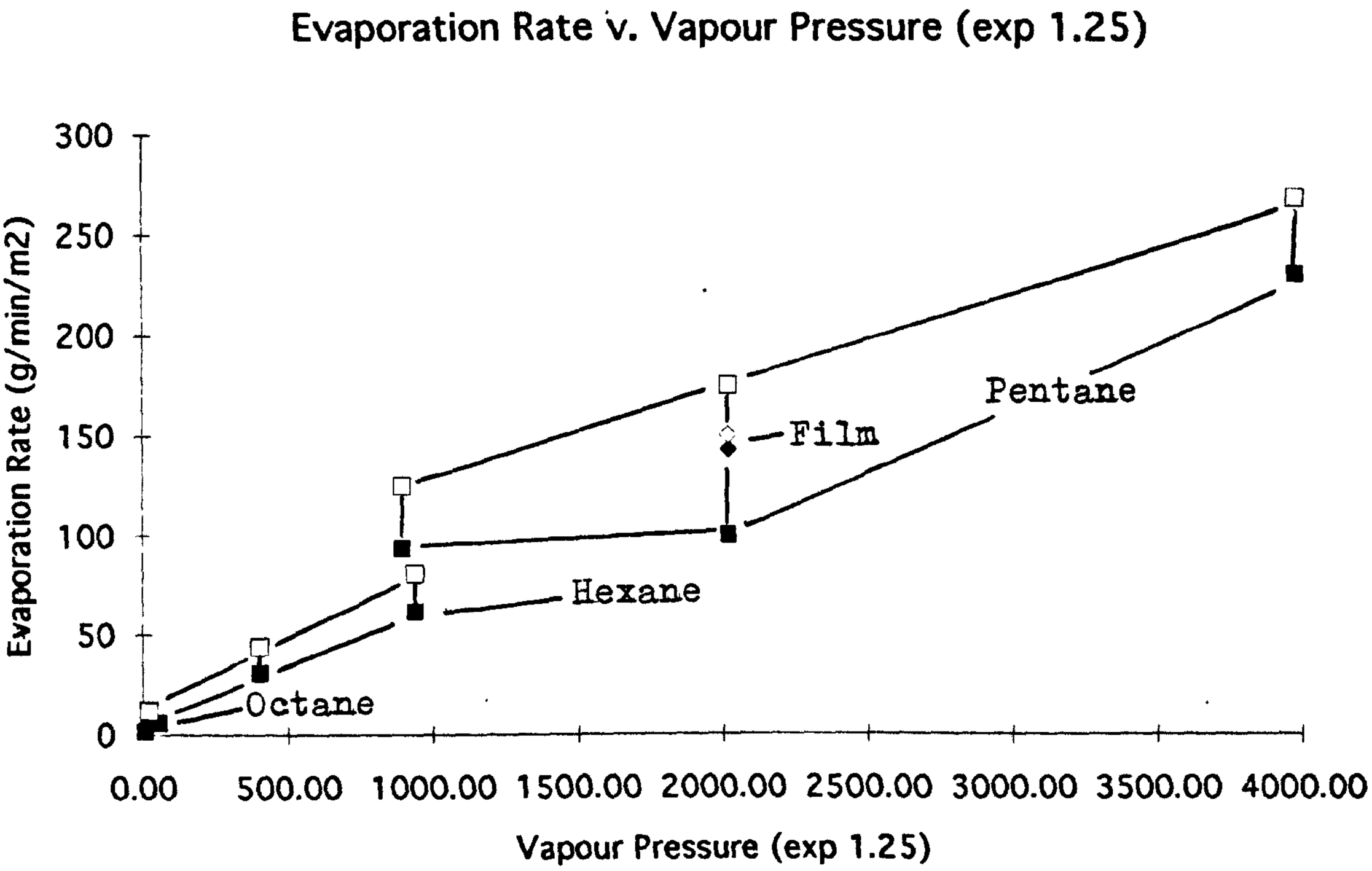

Fig. 3.3.2.2: Evaporation rate (per unit area) v. vapour pressure (exp. 1.25) for pentane, hexane, and octane demonstrate the relationship as predicted by Wade – $e_S = Kp_S^{1.25}$ (See Sect. 1.4.4.)

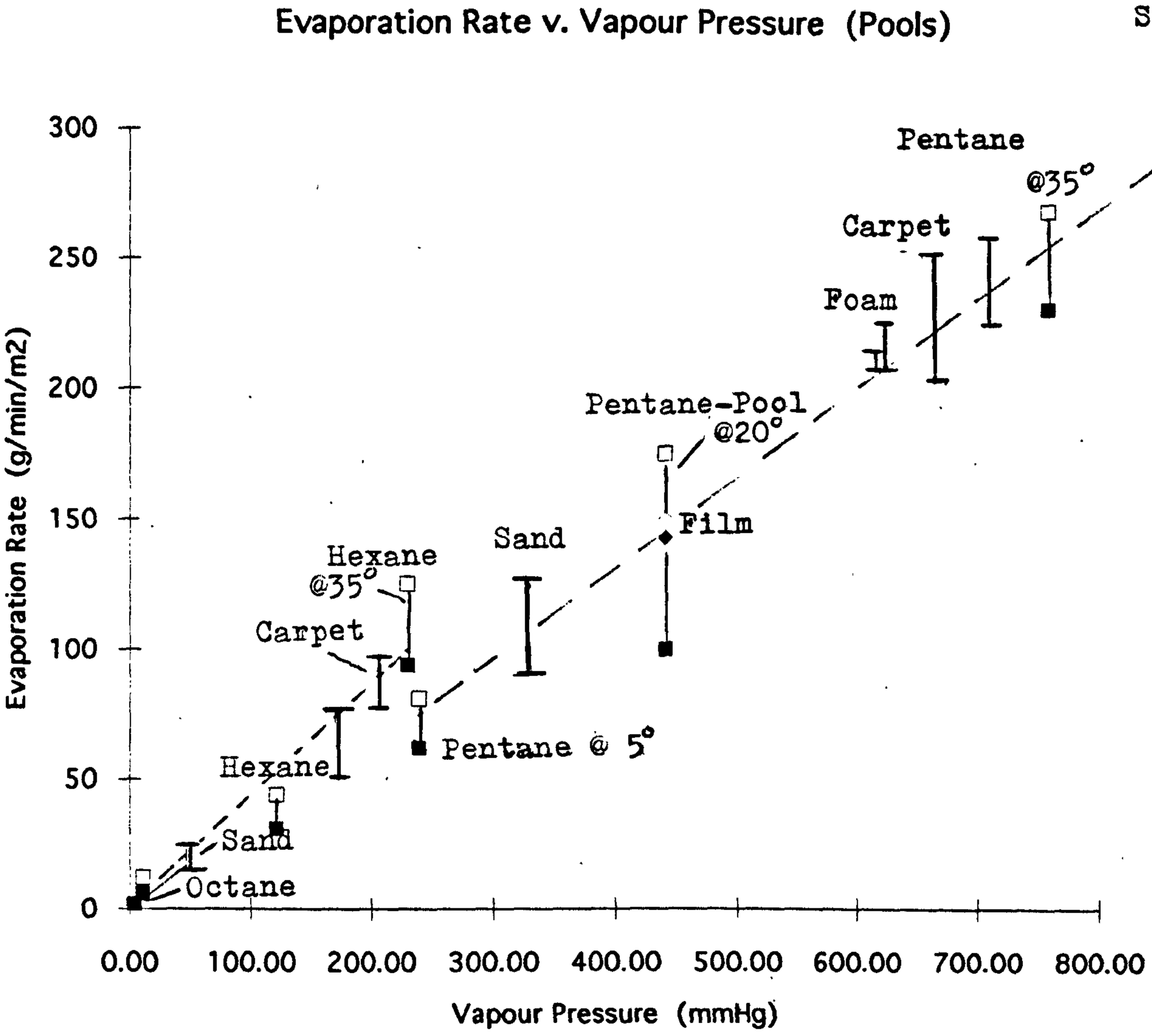

Fig. 3.3.2.3: Evaporation rate (mass loss per unit area) v. vapour pressure for pentane, hexane, and octane with evaporation rates for pentane-, hexane-, and octane matrices plotted along the same trend line. Fig. 3.3.2.1 demonstrated the relationship between evaporation rate and vapour pressure. The equivalent vapour pressure for each matrix shows the effect of the substrate is to effectively increase the vapour pressure.

Table 3.3.2 High Temperature Evaporation at 35–36°C (Initial Rates)

Pentane: (vapour pressure = 758mmHg @ 35°C)

Type	Diameter	Area	Rate of Mass Loss	Mass Flux	n
	cm	m^2	g/min	$g/min/m^2$	
12mm pool	15cm	0.016	3.7 – 4.3	231 – 269	2

Hexane: (vapour pressure = 230mmHg @ 35°C)

Type	Diameter	Area	Rate of Mass Loss	Mass Flux	n
	cm	m^2	g/min	$g/min/m^2$	
12mm pool	15	0.016	1.5 – 2.0	94 – 125	3
Aluminium	15	0.016	2.0	125	1
Sand	15	0.016	2.0	125	1

Octane: (vapour pressure = 24mmHg @ 35°C)

Type	Diameter	Area	Rate of Mass Loss	Mass Flux	n
	cm	m^2	g/min	$g/min/m^2$	
12mm pool	15	0.016	0.09	6	4

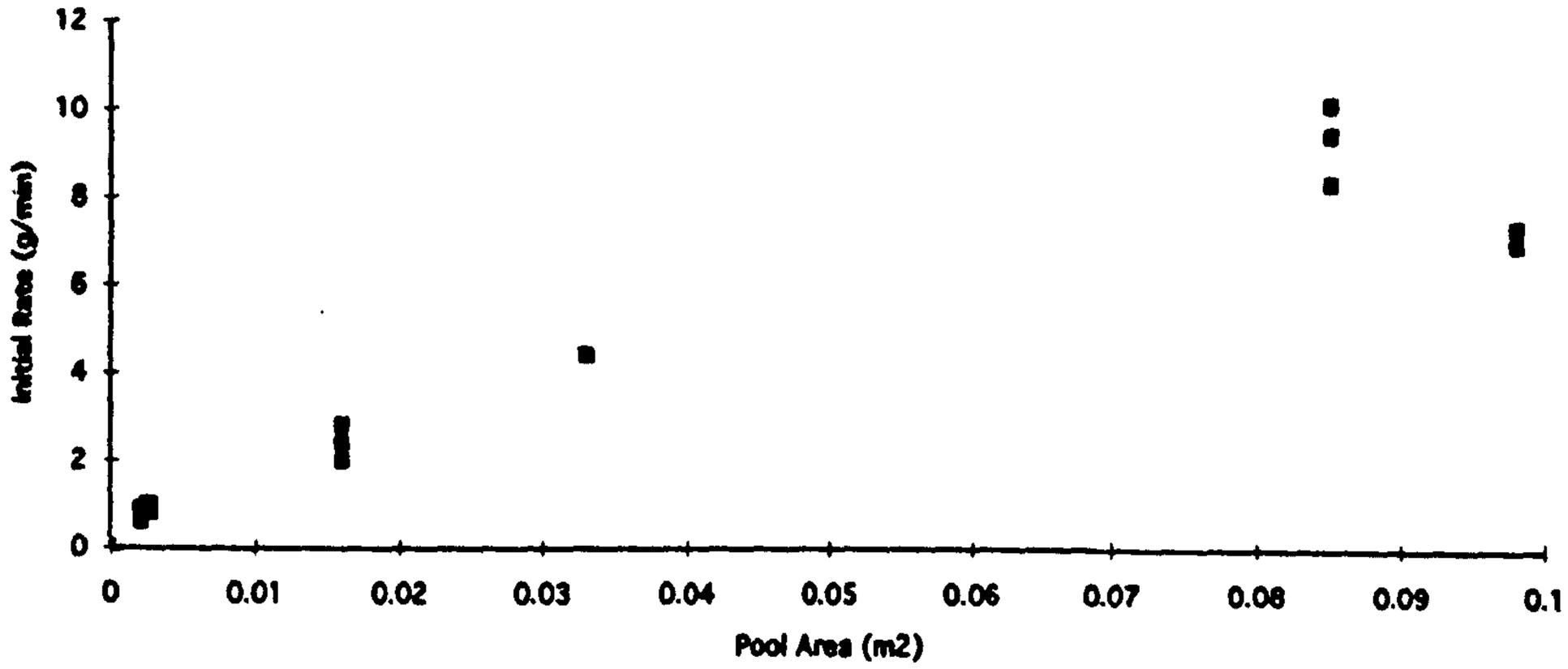

Fig. 3.4.1: Initial mass loss rate (g/min) v. pool area – pentane at 20-22°C.

Initial Evaporation Rate (g/min) vs Area (m2)

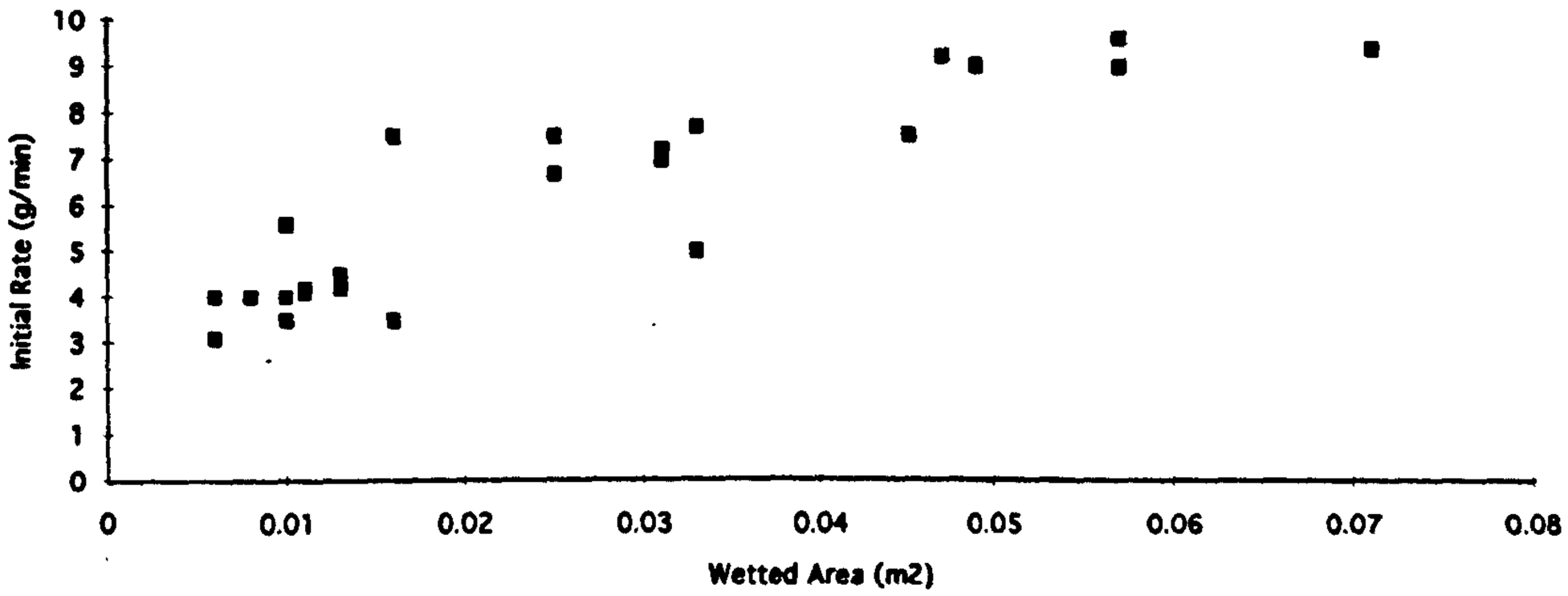

Fig. 3.4.2: Initial mass loss rate (g/min) v. pool (visibly wetted) area – pentane on carpet.

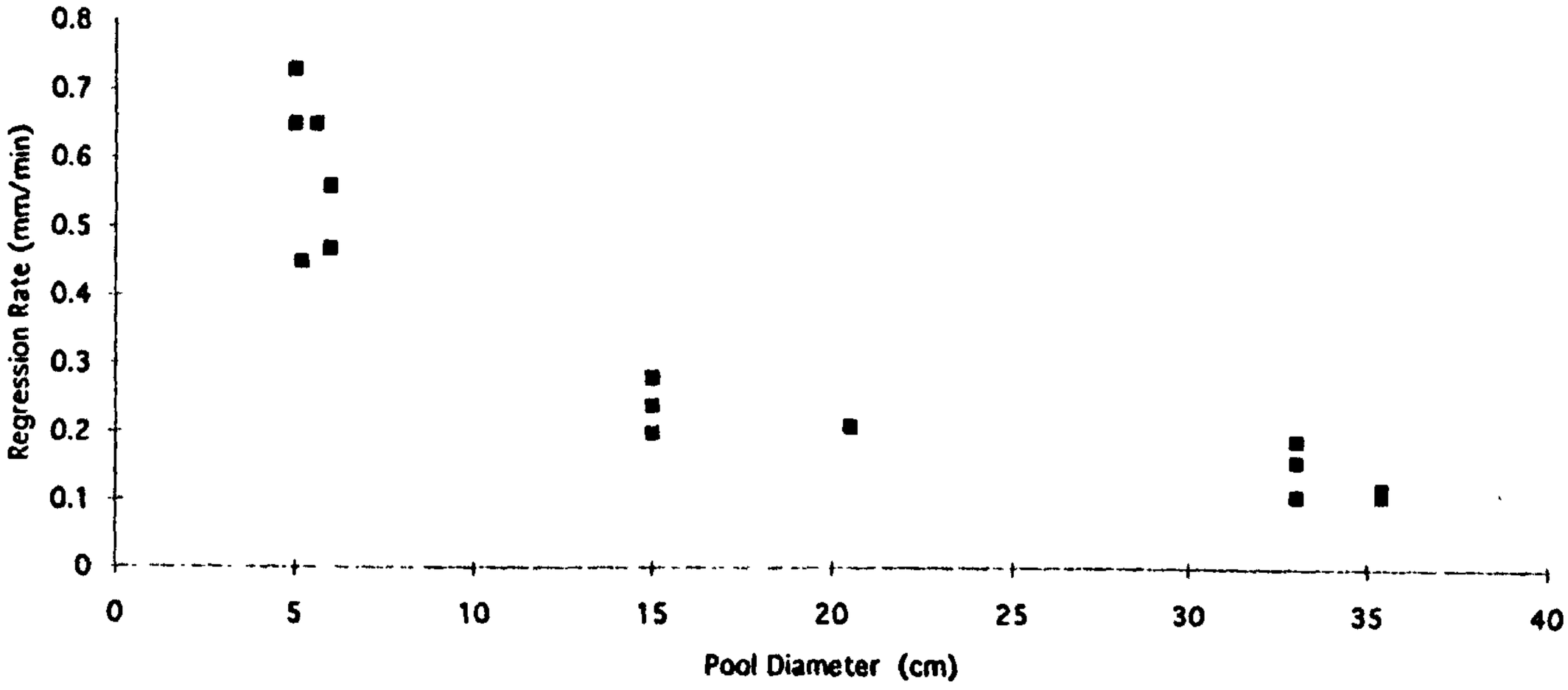

Fig. 3.4.3: Initial regression rate (mm/min) v. pool area – pentane pools only, at 20-22°C.

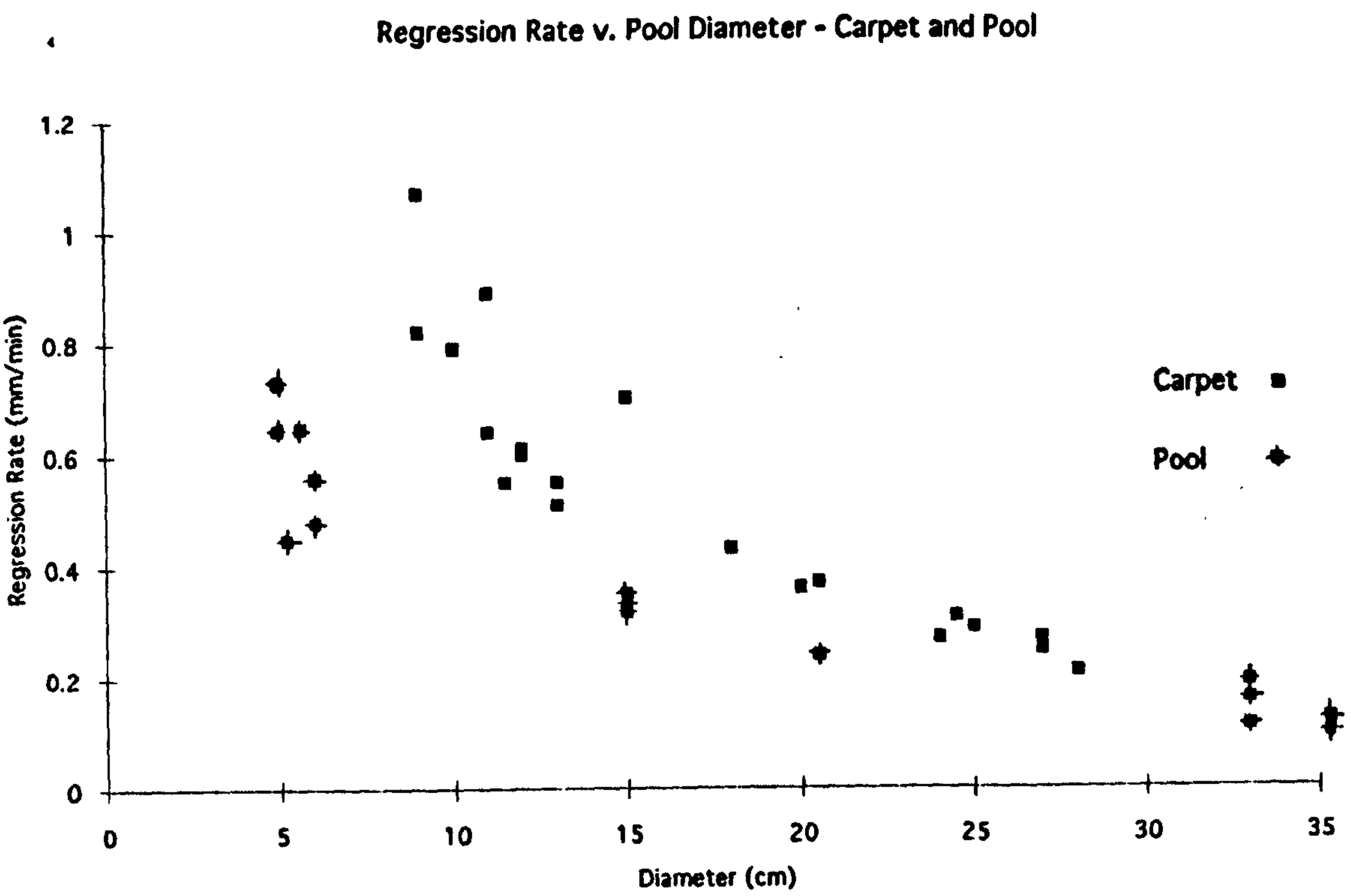

Fig. 3.4.4: Initial regression rate (mm/min) v. pool area for pentane at 20-22°C. Rates for both pools and carpets are shown for comparison.

pools of 15 – 30cm (0.15 – 0.3m) diameter but smaller pools have a markedly higher regression rate. As pool diameters reached 35cm, the regression rate appears to level off at 0.1 – 0.15mm/min. This effect was observed in the regression rates for small pool fires cited in Drysdale. That relationship will be explored in Sect.3.10.

3.5 Evaluation of Losses from Pouring and Splashing

3.5.1 Pour Tests

The data in Table 3.5.1 represent the results of tests of pentane and hexane poured into a non-splash receptacle from various heights in still air at 20 – 21°C ambient temperatures. It was observed that laminar pours became turbulent within 25cm of the graduated cylinder from which they were poured. Pouring from volumetric flasks produced fully turbulent pours (Fig. 3.5.1).

3.5.2 Splash Tests

The data in Table 3.5.2 represent the results of tests in which pentane and hexane were poured from a graduated cylinder (semi-laminar pour) into a splash-prone receptacle from a height of 50cm at ambient temperatures of 19 – 20°C in still air.

Table 3.5.1: Pour Tests at 20°C. 250ml

Laminar Pour: (from graduated cylinder), 8 – 10s in duration

Pentane: 155. 5 ± 0.3 g start weight

Pour Height	Mass Loss(net)	%Loss	
0cm:	1.4 ± 0.2g loss	0.9%	n = 6
50cm: *	7.9 ± 1 loss	5.1%	n = 8
100cm:*	20.3 ± 1 loss	13.1%	n = 5

Hexane: 162.5 ± 0.3g start weight

Pour Height	Mass Loss(net)	%Loss	
0 cm:	0.4 ± 0.2 loss	0.2%	n = 6
50cm:*	3.7 ± 0.7 loss	2.3%	n = 5
100cm:*	8.4 ± 1.5 loss	5.2%	n = 5

*Note: Flows became turbulent after ≈25cm

Turbulent Pour: (from volumetric flask)

Pentane: 156 ± 0.3g start weight

Pour Height	Mass Loss(net)	%Loss	
0 cm	3.2 ± 1.2g loss	2.0%	n = 6
50cm	12.4 ± 0.6g loss	7.9%	n = 6
100cm	19.2 ± 1 g loss	12.3%	n = 4

Hexane: 164.2 ± 0.2g

Pour Height	Mass Loss(net)	%Loss	
50cm	4.8 ± 0.3g loss	2.9%	n = 3
100cm	8.2 ± 0 g loss	5.0%	n = 1

Highly Turbulent Pour:

Pentane: 156 ± 0.2g start weight

Pour Height	Mass Loss(net)	%Loss	
30cm	18.8 ± 1.6g loss	12.1%	n = 4

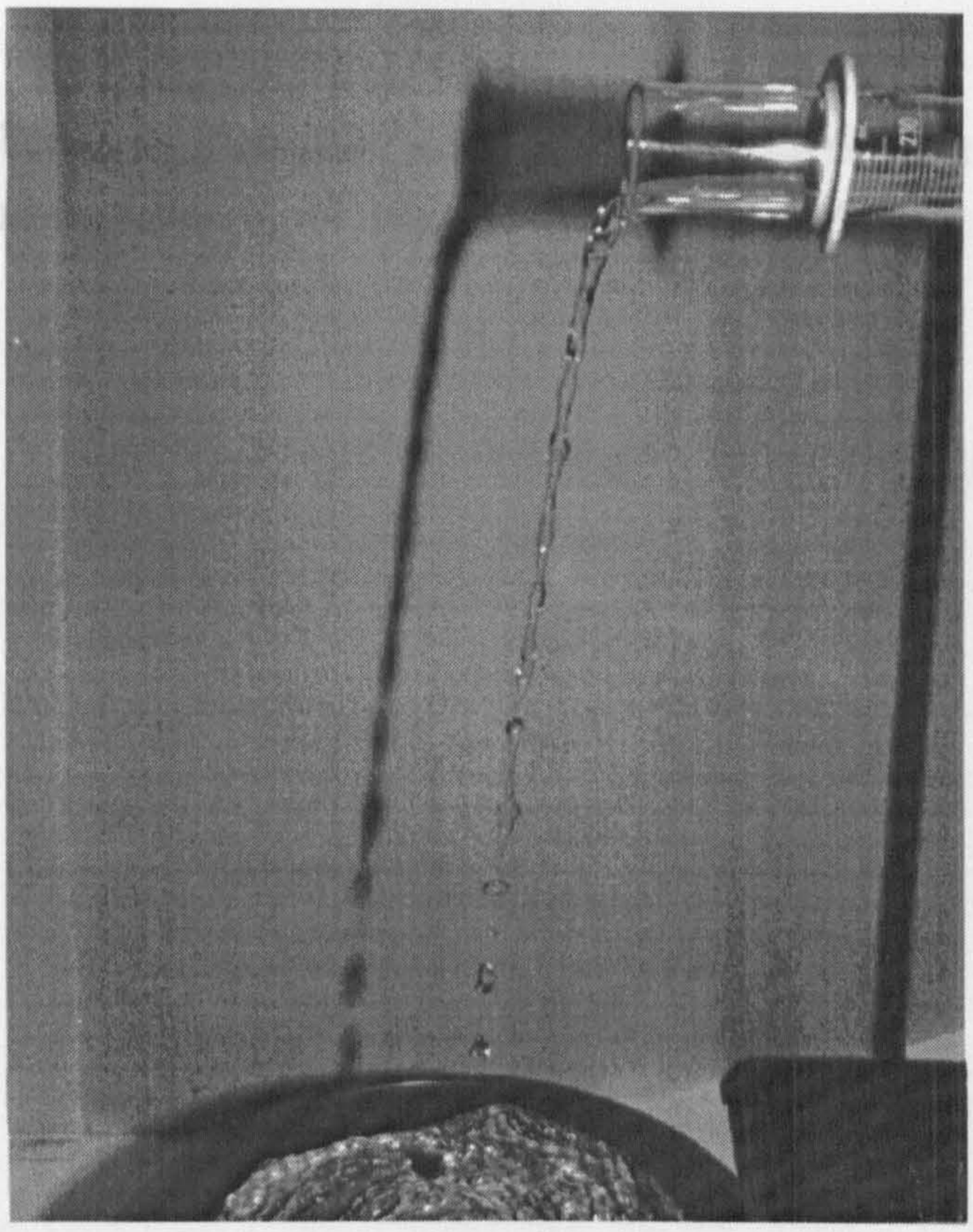

Fig. 3.5.1: Typical pours:
(a) Laminar pour from graduated cylinder becoming turbulent. *above*
(b) Turbulent pour from volumetric flask. *below*

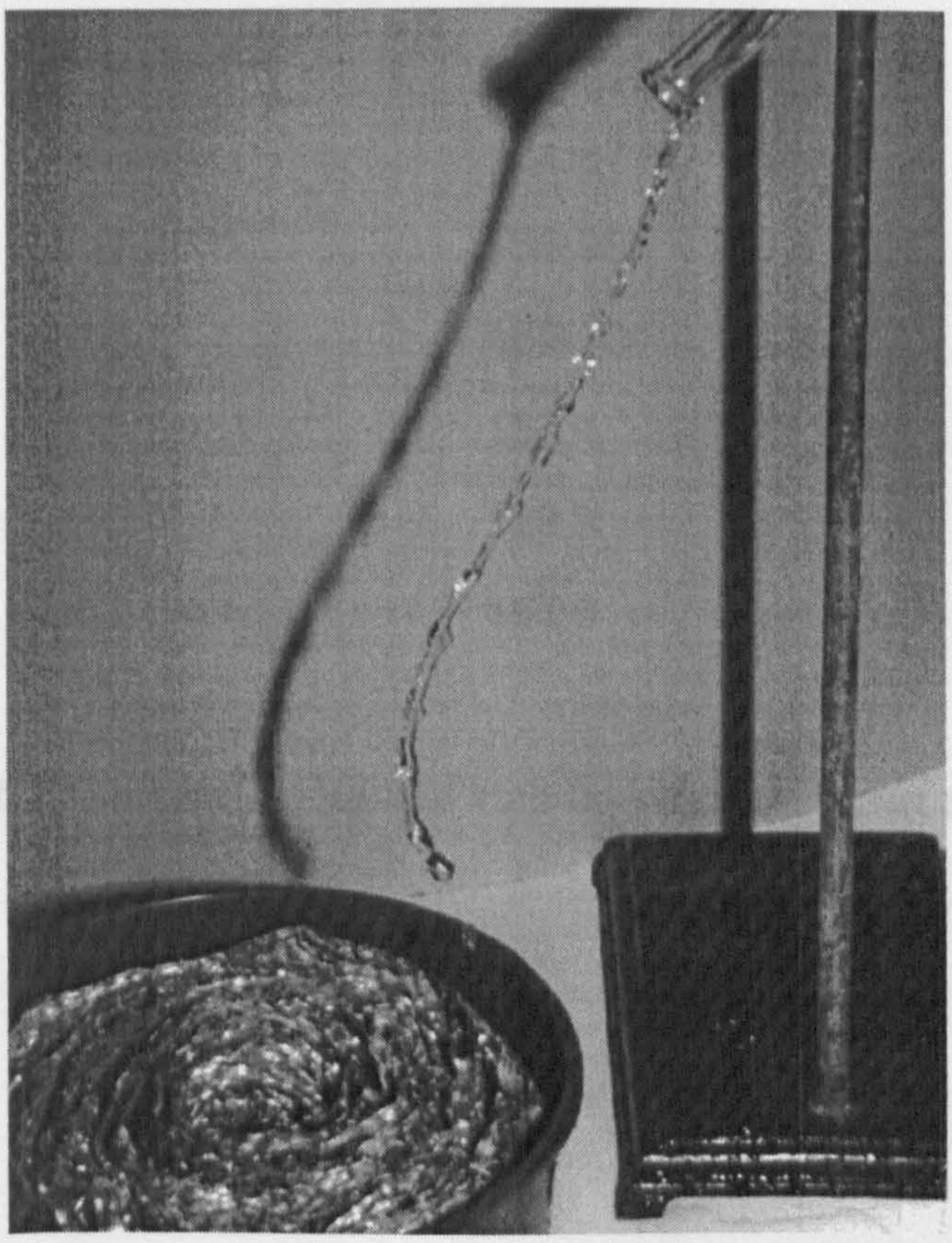

Table 3.5.2: Splash Tests – Pentane and Hexane poured at 50cm above bottom of plastic pan, at 19–20°C

Pentane (250ml)

Starting Weight	End Weight	Loss(net)	Loss(percent)
155.00	142.2	12.8	8.2
155.47	144.1	11.4	7.3
154.85	142.1	12.8	8.2
154.63	144.2	10.5	6.8
155.00	147.1	7.9	5.1
155.34	146.1	9.2	5.9
155.36	146.4	9.0	5.9
155.68	147.0	8.7	5.6
154.65	145.7	9.0	5.8
			Avg: 6.5%

Hexane

156.45 *	152.66*	3.8	2.4
156.09 *	152.62*	3.5	2.2
155.55 *	151.87*	3.7	2.4
157.40 *	153.95*	3.4	2.2
156.14 *	152.70*	3.4	2.2
163.05	158.4	4.6	2.8
163.17	158.9	4.3	2.6
162.54	157.9	4.6	2.8
			Avg: 2.5%

*240ml pours, instead of 250ml, due to weight limit on electronic pan balance

3.6 Vertical Diffusion of Hydrocarbon Vapours

3.6.1 Barrier Tests

The data in Table 3.6.1 represent the equilibrium mass loss rates observed in evaporation tests from 15cm Petri dish pools and matrices of n-pentane, hexane and n-octane at 20 – 22°C, in which a cylindrical barrier was placed around the balance within 10s of the start of each run compared to the equilibrium rates observed in still air at 20 – 22°C without the barrier.

3.6.2 Hydrocarbon Detector Tests

The data in Table 3.6.2 are the results of measuring the hydrocarbon concentration using the IR-711 Portable Hydrocarbon detector immediately above the open mouth of the 0.4m x 0.6m barrier and near its base. Tests were conducted using n-pentane evaporating from a Petri dish at 21°C. Measurements were made 10min after the start of each run.

3.6.3 Smoke Pen Tests

Stannic oxychloride smoke released at various positions and heights above pentane pools of various sizes produced results as seen in Figs.3.6.3.1 and 3.6.3.2 and yielded the following observations:

Large Pans (0.33 – 0.35m diameter, 0.085 – 0.1m^2 area):

Releases above pans produced only random eddy diffusion until the smoke was 1 – 2cm above the liquid surface at which point it formed a quiescent layer above the entire central area of the pan. Smoke within approximately

Table 3.6.1: Barrier Tests

Equilibrium Mass Loss Rate (Net) at 40min for Pentane @ 20–22°C,

Area = 0.016m^2. All rates are in g/min.

Substrate	Without Barrier	With Barrier	Difference
Pool	0.5 – 0.6	0.4 – 0.5	0.1 – 0.2
Carpet	1.2 –1.4	0.8	0.4 – 0.6
Sand	0.5 – 1.5	0.5 – 0.6	0 – 0.9
Aluminium Granules	1.3 –1.5	0.7	0.6 – 0.8

Equilibrium Mass Loss Rate (Net) at 40min for Hexane @ 20–22°C, Area = 0.016m^2

All rates are in g/min.

Substrate	Without Barrier	With Barrier	Difference
Pool	0.35	0.2*	0.15
Carpet	0.5 – 0.6	0.35	0.15 – 0.25
Sand	0.4 – 0.5	0.35	0.05 – 0.15

*0.15 with lid

Equilibrium Mass Loss Rate (Net) at 40min for Octane @ 20–22°C, Area = 0.016m^2

All rates are in g/min.

Substrate	Without Barrier	With Barrier	Difference
Pool	0.05 – 0.15	0	0.05 – 0.15
Carpet	0.1	0	0.1
Sand	0.25 – 0.35	0.1	0.15 – 0.25
Aluminium Granules	0.2	0.1	0.1

Table 3.6.2: Hydrocarbon Concentrations (in ppm)

Exterior to Barrier. Pentane at 21°C

Test	Top of 0.6m high barrier	Near Base Gasket
189	≤7ppm	40 – 50ppm
190	≤5ppm	40 – 50ppm
191	≤25ppm	----
192	25-50ppm	200 – 300ppm

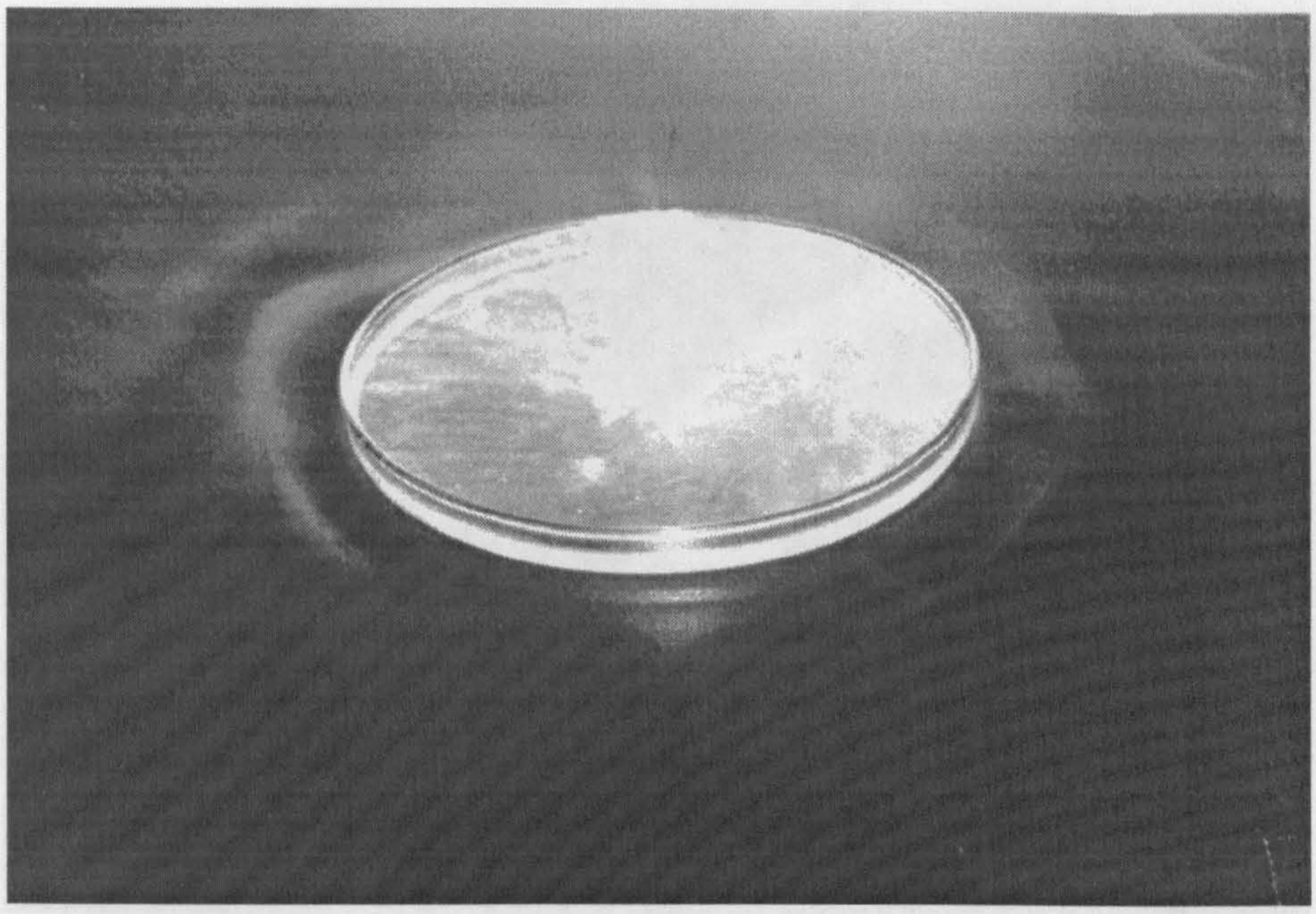

Fig. 3.6.3.1: Typical smoke tests:
(a) 0.15m pentane pool at 21° C. Note quiescent area at centre and smoke entrained at edges.
(b) 0.35m pentane pool at 21° C. Smoke within 2cm of edge is entrained and swept away.

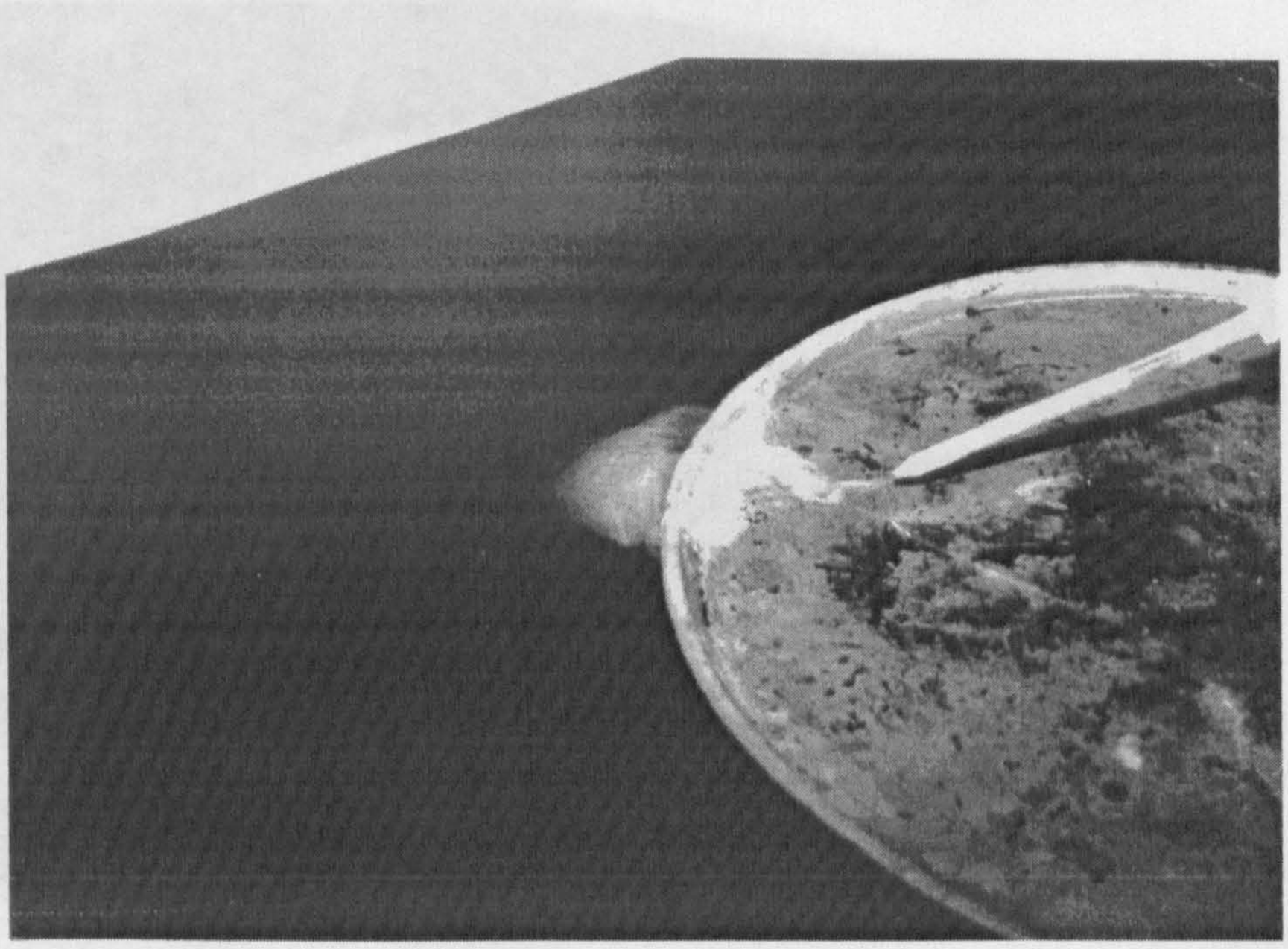

Fig. 3.6.3.2: Typical smoke tests for large pentane pools. *above & below* Large quiescent area visible above centre of pan. Only smoke within 2cm of edge is entrained.

2 – 5cm of the perimeter of the pan was entrained and swept over the edge of the pan to cascade onto the benchtop 10 – 12cm below. Mass loss rates: 7 – 9g/min.

Small Pans (Petri dishes, 0.05 – 0.15m diameter, 0.002 – 0.016m^2 area): Releases above pans produced only random eddy diffusion until the smoke was ≤1cm above surface at which point it was entrained and swept over the edge of the pan to cascade onto the benchtop 10 – 12cm below. There was no central quiescent area visible. Mass loss rates: 0.5 – 2.4 g/min.

3.6.4 Thermal Gradients above Volatile Liquids

Thermocouple array data from tests in which n-pentane was evaporated from a 15cm diameter pool in a Petri dish in still air at 21°C were used to generate a profile of temperatures at various points above and around the pool. At equilibrium, pentane pools produced a thermal gradient extending some 3 – 4cm above the surface of the liquid, as shown in Fig. 3.6.4.1.

Temperatures 4cm above the surface were depressed 0.5 – 0.8°C from ambient once an equilibrium condition was established (typically requiring 2min from the time of pouring). Temperatures 3cm above the surface were depressed 0.8 –1.0°C from ambient, while temperatures 2cm above the surface were depressed by 1.0 – 3.0°C from ambient. Temperatures at 1cm above the surface ranged in temperature from 5 to 14°C below ambient. The pools producing these vapors began at 21.5°C ambient, and reached temperatures of 7.3 – 8.0°C during the course of these runs. It was noted that the layers were very sensitive to disturbance by

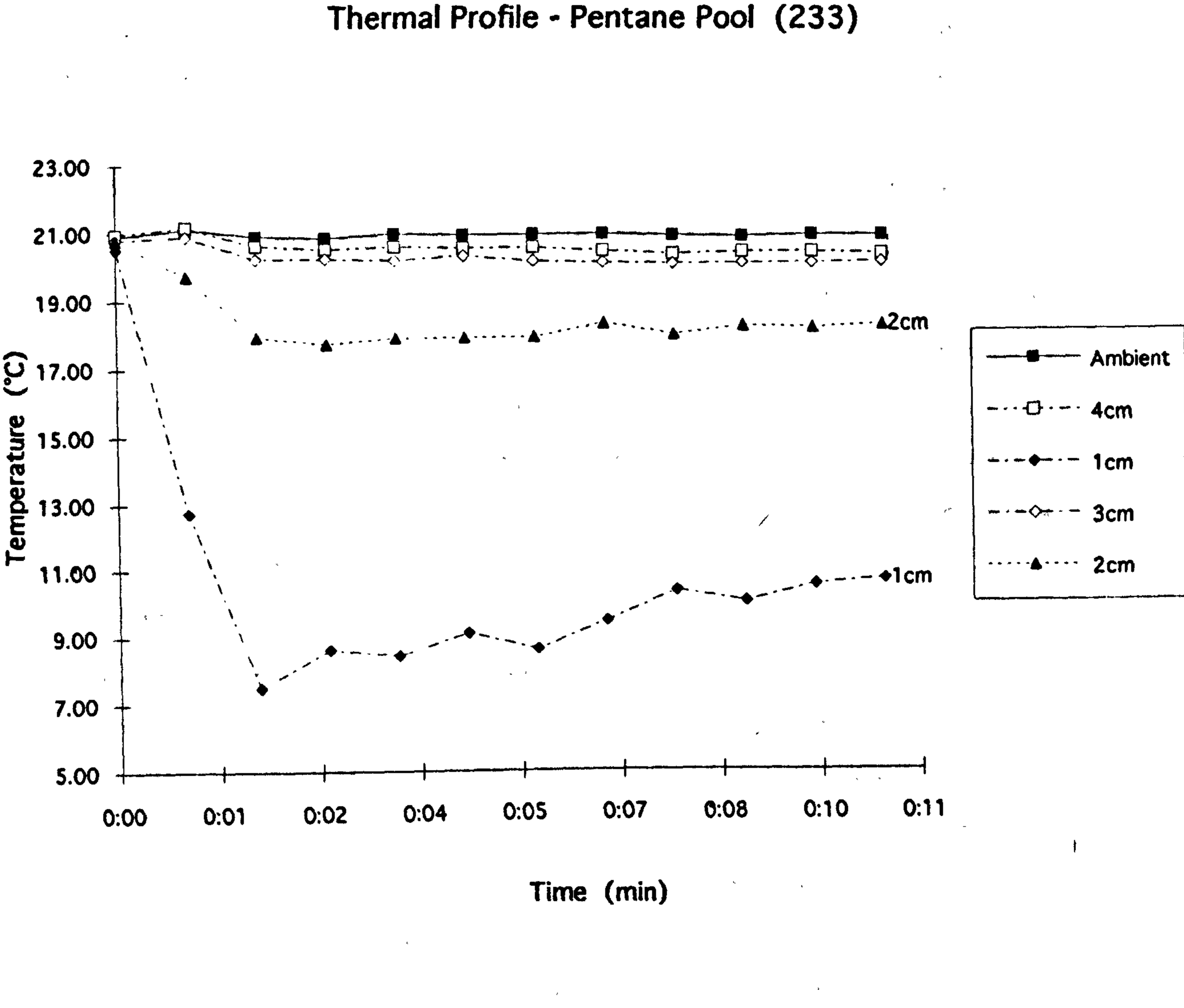

Fig. 3.6.4.1: Thermal profile by thermocouple array for pentane pool (0.15m diameter).

mechanical movement in the immediate area and by random draughts from the fumehood duct nearby. This sensitivity will limit the applicability of the resulting predictive model to still air situations and will be discussed in Sect. 4.6.

Experiments in Sect. 3.2.2 of this study revealed that pentane evaporated from a saturated sand substrate at a rate approximately twice that from a liquid pool of the same area at the same temperature. Here, n-pentane was evaporated from sand in a Petri dish of 15cm diameter, beginning at an ambient temperature of 21.2 –21.5°C. A typical temperature profile from a pentane/sand matrix evaporation run is shown in Fig.3.6.4.2. Temperatures 4cm above the surface of the sand were depressed 0.6 –1.0°C from ambient, while temperatures at 3cm above the pool were 1.0 –2.0°C below ambient, and those at 2cm were 2 – 2.5°C below ambient. Temperatures 1cm above the sand were 6 –11°C below ambient. During this time, the temperature of the sand/pentane substrate decreased from ambient to 1.9 –3.7°C. Temperatures to each side of the pool were 0.5 – 0.9°C lower than ambient, while those of the benchtop under the edges of the Styrofoam insulating panel were 0.2 – 0.5°C below ambient.

Evaporation of hexane under the same conditions had previously been shown to be significantly slower than that of pentane, and, therefore the thermal gradient would be expected to be correspondingly less marked. Hexane evaporating as a pool from an uninsulated Petri dish 15cm in diameter produced a thermal gradient of the type seen in Fig.3.6.4.3. It may be seen that temperatures 4cm above the pool were unchanged from ambient, while those 3cm above the pool were typically 0.4 – 0.5°C below ambient. Those at 2cm were 0.9 – 2.0°C below ambient, and those at 1cm

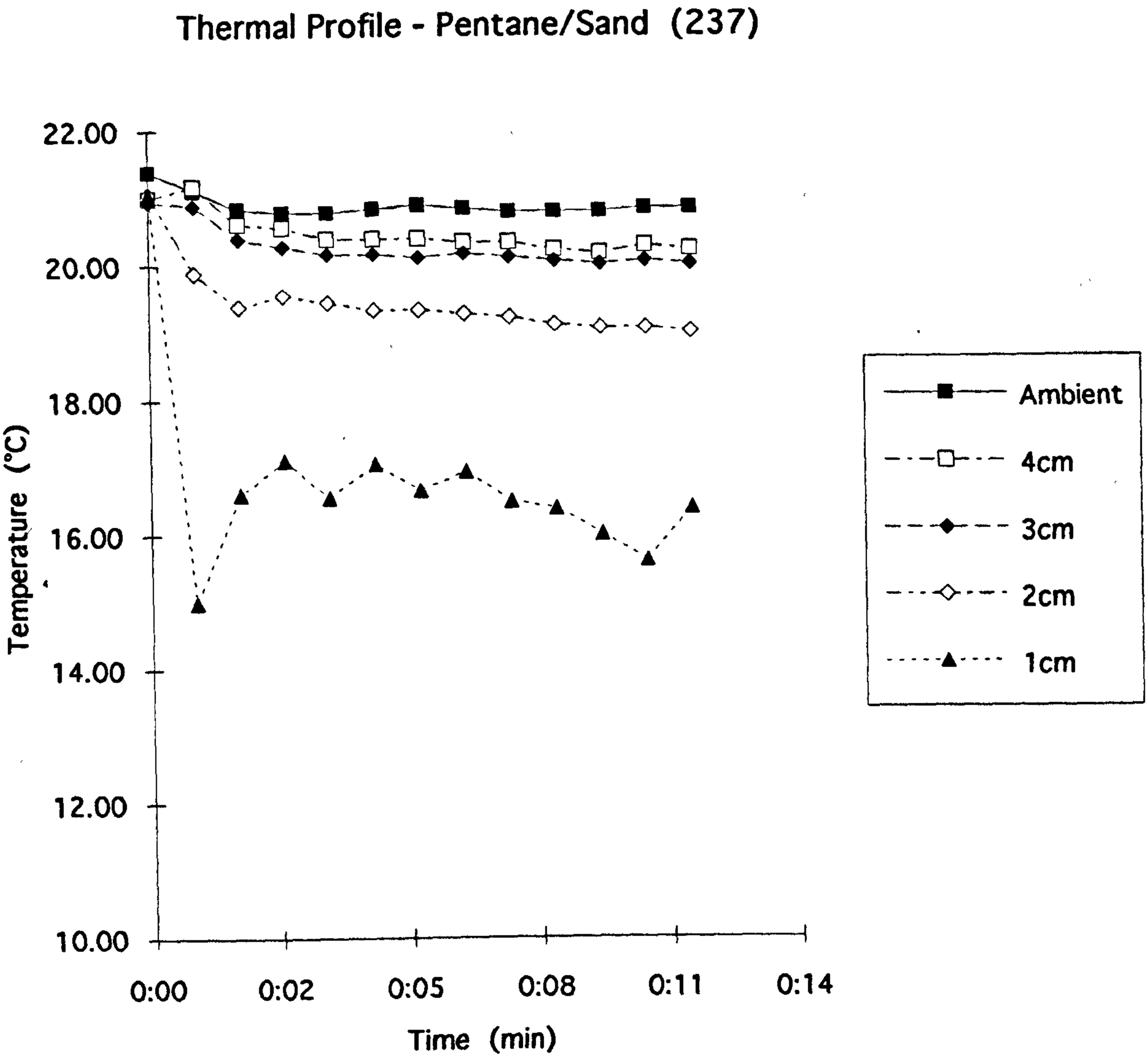

Fig. 3.6.4.2: Thermal profile by thermocouple array for pentane/sand matrix (0.15m diameter).

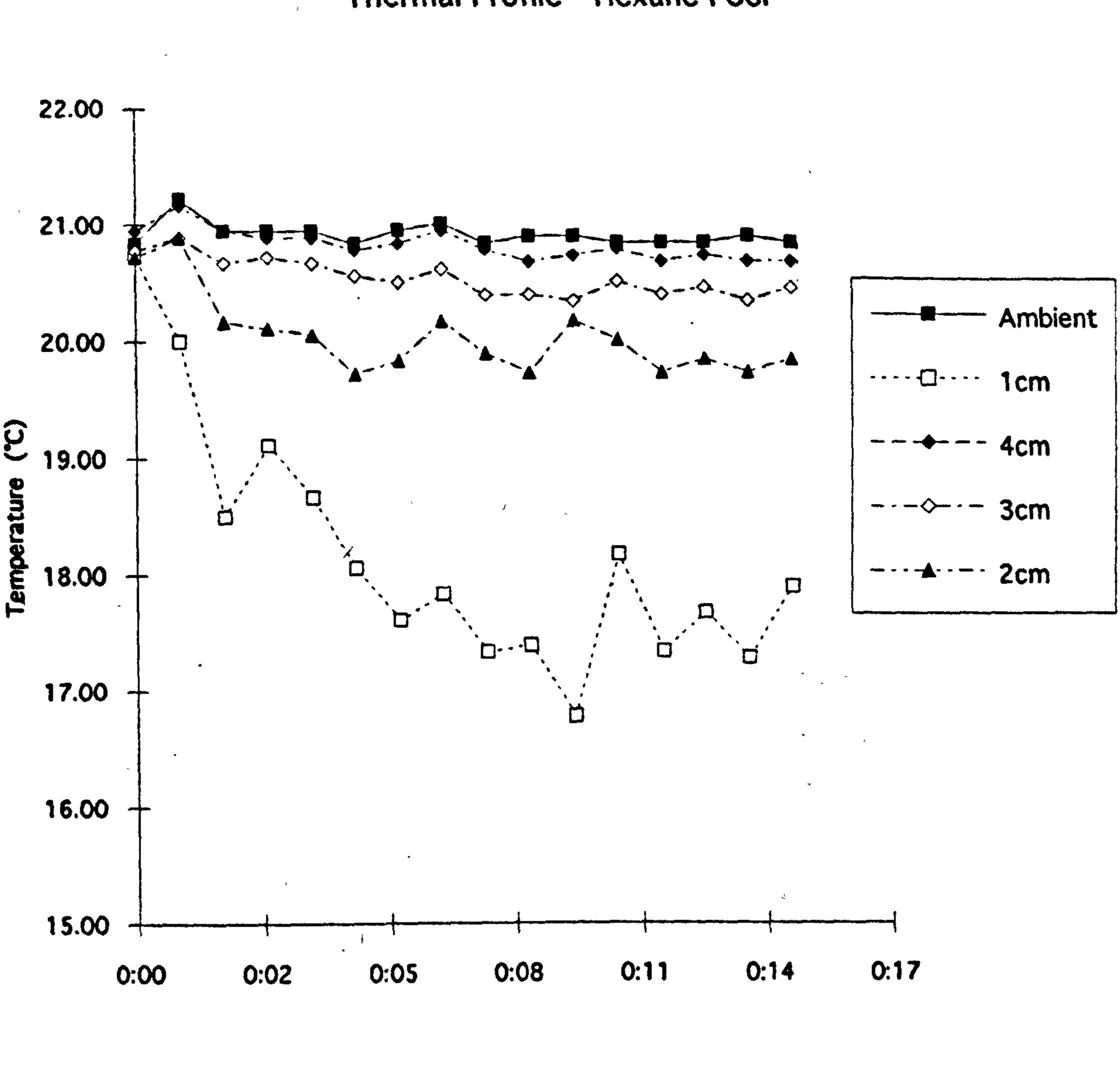

Fig. 3.6.4.3: Thermal profile by thermocouple array for hexane pool (0.15m diameter).

ranged from 2.4 to 9°C below ambient. During each run, the temperature of the hexane pool decreased from ambient to 13.7 – 16.8°C in the 12min run. Temperatures on the insulating panel adjacent to the hexane pool were 0 – 0.3°C below ambient, while those on the benchtop below were indistinguishable from ambient.

As previously seen, hexane evaporates from sand at twice the rate it evaporates from a liquid pool under the same conditions. A temperature profile for a hexane/sand matrix is shown in Fig.3.6.4.4. Temperatures at 4cm above the sand surface were typically only 0.2°C below ambient, while those at 3cm were 0.5°C lower than ambient. Temperatures at 2cm were 0.8 –1.1°C below ambient and those at 1cm were 2.5 –3.5°C below ambient. Temperatures to each side of the sand/hexane matrix were only 0.2 –0.3°C below ambient, while those on the benchtop below were about the same. During a 12min run, temperatures of the sand/hexane matrix decreased from ambient to 13.7 – 14.6°C.

As with pentane, hexane evaporations required 1 – 2min to achieve equilibrium after pouring was initiated. In each case, the minimum temperatures of all positions above the pools were typically reached at mid-test (4 – 6min), with a slight increase as the test continued, corresponding to the drop in temperature of the matrix, which resulted in a levelling off of the mass loss rate. The slower mass loss rates for hexane resulted in a shallower, less marked gradient for hexane, both as a pool and above sand. If one arbitrarily assigns a threshold of 0.5°C change to represent the layer of vapour being generated by the liquid, the heights noted in these tests (3cm above pentane pools, 2cm above hexane) agreed with the results of the smoke pen tests described in the previous section.

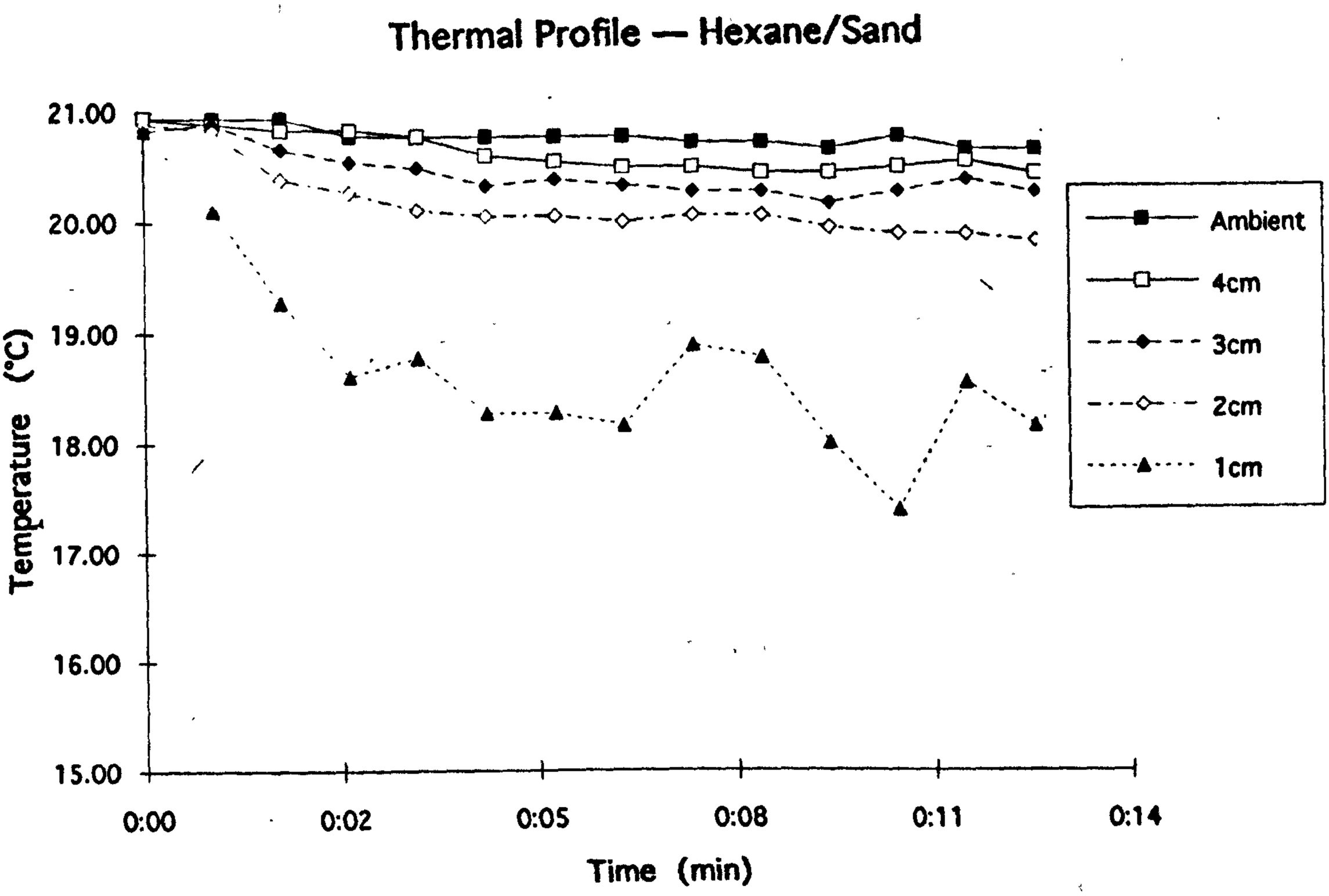

Fig. 3.6.4.4: Thermal profile by thermocouple array for hexane/sand matrix (0.15m diameter).

3.6.5 Hydrocarbon Detector – Bench Tests

The heights at which a signal of 500ppm was recorded by the detector above a pool of pentane in a Petri dish, observed and recorded in ten duplicate trials, are shown in Table 3.6.5. The height recorded in this experiment is the distance between the surface of the pool and the bottom of the IR-711 probe. Since the active IR absorption cell is centered in the probe casing, it is located 1– 2cm above this lower periphery. These results, then, are consistent with the estimates for the 2 – 4cm depth of unrestrained pentane vapours above a liquid pool resulting from experiments in Sections 3.6.3 and 3.6.4 above.

3.7 Advective Flow of Vapours – Horizontal Transport

Tests to measure the advective flow of pentane vapours were conducted by two different methods: one using the entrainment of stannic oxychloride smoke to track the movement, and the other using the IR-711 Portable Hydrocarbon Detector described previously.

3.7.1 Smoke Pen Tests

These tests were conducted by the same method as used for the evaporation tests described in Sect. 2.2. The balance with its Petri dish pool was located in a large fume hood for these tests with a 30cm laboratory scale fixed to the benchtop having its zero mark directly beneath the edge of the insulator (Fig. 3.7.1). Smoke was released over the edge of the Petri dish and the time required for a trace to move from one end of the scale to the other was recorded . The rear wall of the enclosure was less than 0.3m from the

Table 3.6.5: Detection of Pentane Vapors above Liquid Pool

Conditions: n-pentane 15cm petri dish pool 21°C in still air

Threshold of Detection: ≥500ppm

Height: 1-2cm above surface of pool n =10 trials.

Fig. 3.7.1: Smoke pen advection test. Smoke released at edge of pan is swept along centimetre scale. Time to travel 0.3m is recorded.

perimeter of the larger pans. The hood was not operated during the tests, but it was noted that a very slight cold air stream could be detected coming down the hood exhaust during these tests. As a result, the observed movement of vapours towards the rear of the hood was probably reduced (and movement towards the front of the hood and into the room enhanced) from what would be encountered in absolutely still air with walls a symmetrical distance away from the vapour source. The results of vapour advection tests using the smoke pen are shown in Table 3.7.1.

3.7.2 Hydrocarbon Detector

Using an IR-711 hydrocarbon detector on a benchtop to detect the arrival of pentane vapours from a Petri dish pool created on the same benchtop in still air yielded the results shown in Table 3.7.2. It appears that the additional momentum provided by the vapours falling 10cm from the edge of the insulator panel to the benchtop produced slightly higher velocities than those exhibited by vapours issuing from a Petri dish at bench level. In either case, these data demonstrate that horizontal transport of pentane vapours by advection is very slow and its role in spreading fuel vapours such as pentane and hexane will be very limited.

3.8 Thermodynamics of Evaporation from Pools

It can be seen from the sample mass loss rate plots (Figs. 3.2.1, 3.2.4, and 3.2.6) that the initial evaporation rate begins to change almost immediately. Since evaporation rate is known to be directly related to vapour pressure, and therefore, to the temperature of the evaporating liquid, any

Table 3.7.1: Smoke Pen Tests – Advection of Pentane Vapors @ 20°C. Still air.

Test #	Time to Move 0.3m (s)			Calculated Velocity (m/s)		
	To Front	To Rear	To Side	Front	Rear	Side
202	3.6	5.6	4.5	0.08	0.05	0.07
(0.3m pan)	4.4	6.2	5.1	0.07	0.05	0.06
	4.9	6.3	5.0	0.06	0.05	0.06
	4.9			0.06		
	5.0			0.06		
204	5.0	5.7	5.0	0.06	0.05	0.06
(0.3m pan)	4.0	4.1	5.5	0.08	0.07	0.05
	6.4	8.0	7.5	0.05	0.04	0.04
203[1]	3.5	5.2	na	0.08	0.06	
(0.3m pan)	5.5	5.8		0.05	0.05	
	4.8			0.06		
	3.8			0.08		
208[1]	4.0			0.08		
(0.06m	6.7			0.04		
beaker)						
214[1]	3.6	6.7		0.08	0.04	
(0.35m pan)	5.3	7.0		0.06	0.04	

Table 3.7.2: Hydrocarbon Detector Tests

Advection of Pentane Vapours @ 21°C. Still air.

Time to Move 0.5m (s)		Calculated Velocity (m/s)	
To Right	To Left	Right	Left
49.2	17.4	0.01	0.03
60.7	19.2	0.008	0.03
16.1	24.6	0.03	0.02
14.5	15.6	0.03	0.03
37.6	17.8	0.01	0.03

decrease in the temperature of the liquid will cause a decrease in the rate. This is especially important with volatile fuels like pentane, where the heat lost to evaporative cooling can quickly depress the evaporation rate. To establish the amount of cooling taking place under the experimental conditions here, the temperature of the bulk liquid remaining at the end of each experimental run was measured. In addition, the surface temperature of the liquid or of the substrate involved was measured continuously during evaporation runs using both infrared thermal imaging and conventional thermocouple array.

3.8.1 Bulk Temperature Measurements

The data in Table 3.8.1 reflect the temperatures of the remaining bulk liquid at the termination of pentane and hexane evaporation tests (as measured by insertion of a probe-type digital thermometer) and the corresponding mass loss rates for both barrier and non-barrier tests.

3.8.2 Surface Temperature Measurements

3.8.2.1 Infrared Imaging of Liquid Pools

Areas of the experimenter's hand that were blocked from view by the infrared video imaging system were observed to be covered by between 1–2mm (or more) of liquid within the bag. Any more than 2mm of pentane completely blocked the hand image. This empirically demonstrated that while pentane has no strong absorption bands in the 8 –12 micron range of the infrared, it is sufficiently absorptive that the temperature being recorded is of the top 2mm layer of the pool, even if a source beneath it is substantially warmer.

Table 3.8.1 Bulk Equilibrium Temperatures v. Mass Loss Rates from Pools at 20–22°C

	Non-Barrier		Barrier	
Liquid	Temp.	Mass Loss Rate	Temp.	Mass Loss Rate
	°C	g/min	°C	g/min
Pentane	3.2	0.6	5.4	0.4
	4.0	0.5	6.0	0.4
	2.3	0.6	5.0	0.5
	2.1	0.6		
	3.8	0.5		
	3.7	0.5		
	2.7	0.25		
	3.3	0.28		
10min	7.8[1]	0.8	8.6[1]	0.8
	11.0[1]	1.0	8.8[1]	0.8
	6.0[1]	0.8	9.3[1]	0.8
Hexane	12.2	0.3	14.6	0.2
	13.4	0.3	13.7	0.2
	13.7	0.35	14.3	0.2
			13.9	0.2
			14.8	0.2
			16.3[2]	0.15
			16.0[2]	0.15

Notes: 1. These temperatures and rates were recorded at the end of 10min runs, not at equilibrium.

2. These temperatures and rates were recorded for barrier tests with a lid.

3.8.2.2 Thermal Imaging Calibration

The accuracy of measuring the surface temperatures of targets of different emissivity was tested by observing several targets at ambient conditions, with the emissivity calibration of the IR system set at 1.0 (Fig. 3.8.2.2). The results of these tests are summarized in Table 3.8.2.

3.8.3 Temperature Distributions in Evaporating Liquids and Matrices

The surface temperature of a typical 15cm pentane pool (12mm deep) evaporating under ambient conditions of still air at 23.4°C insulated from its surroundings is shown in Fig. 3.8.3.1. The apparent difference in starting temperature between the surface temperature (measured at two different spots on the pool) and the reference temperature (measured on the benchtop background) is due in part to the 20s delay between the start of the run and the taking of the first data point. The liquid was checked by mercury thermometer and digital thermometer to ensure it was at ambient temperature prior to its being poured. The rapid cooling of the pool is exacerbated by the thermal losses induced by pouring and agitation as it fills the Petri dish. Time is recorded from the start of the pour (typically 7 – 9s in duration). This pool initially evaporated at 2.5g/min. This rate decreased monotonically until ≈20min, after which it stabilized at 0.66g/min. The final temperature was 1°C.

The temperature history of a 15cm hexane pool (12mm deep) evaporating under ambient conditions of still air at 24°C, insulated from its surroundings, is shown in Fig. 3.8.3.2. A smaller difference between pool temperature and ambient is recorded via thermocouple array, as would be expected from hexane's lower volatility. This is accompanied by a much

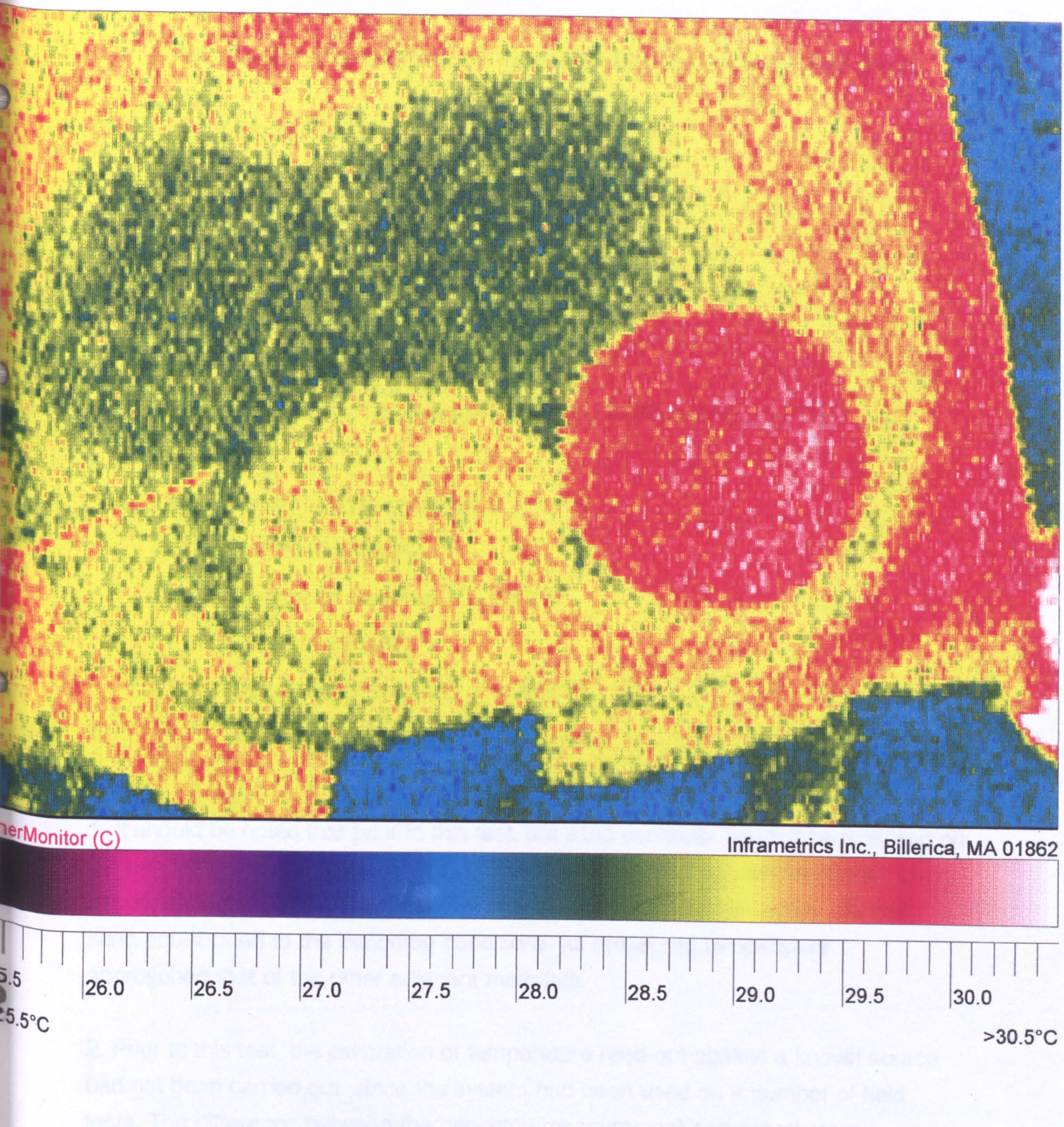

Fig. 3.8.2.2: False-colour Inframetrics image of test targets of Petri dishes containing sand (upper left), diesel fuel (upper right), aluminium granules (lower right), and carpet (lower left), all at ambient temperature showing sensitivity of thermal imaging. Despite differences in reflectivity and emissivity, the temperature readings are very close; ($T_{background} = 30.1$, $T_{diesel} = 28.6$, $T_{al} = 29.9$, $T_{carpet} = 29.3$, and $T_{sand} = 28.6$).

Table 3.8.2 : Correlation of Temperatures by Infrared Imaging:

Test 1: Empty Petri dish: T = 24.7°C

Carpet: T = 24.7°C

Benchtop Surface T= 23.8°C

Ceiling T= 25.0°C

Aluminium granules: T = 24.2°C

Sand : T = 23.2 (rising with time)[1]

Ambient Air Temperature (by digital thermometer): 24.7°C

Test 2: Background (benchtop): T = 30.1°C

Carpet: T = 29.3°C

Aluminium granules: T = 29.9°C

Sand: T =28.6°C

Diesel fuel (Petri dish): T = 28.6°C

Ambient Air Temperature: 23.0°C[2]

Notes:

1. It should be noted that prior to this test, the sand container had not been stored on the benchtop with the other materials. It had been on the floor, where contact with the concrete floor had cooled it below prevailing ambient temperatures. As the sand equilibrated to the benchtop conditions, its measured temperature approached that of the other adjacent materials.

2. Prior to this test, the calibration of temperature read-out against a known source had not been carried out since the system had been used on a number of field tests. The difference between the benchtop measurement and actual room temperature indicates that the temperature read-out was off by 7.0 degrees. This would have no effect on the reliability of comparing the indicated temperatures of various targets or recording changes in temperature, which was the focus of this experiment.

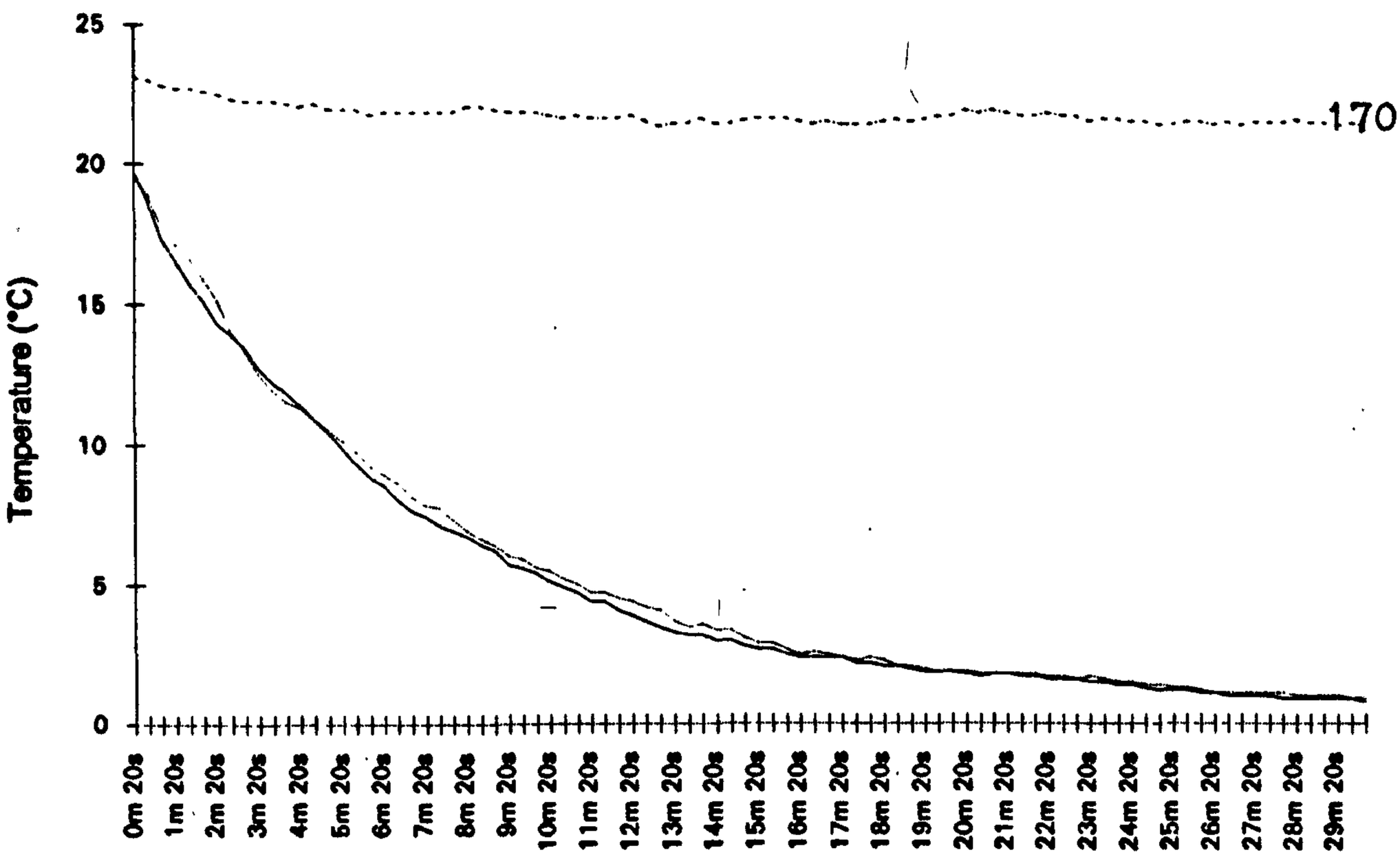

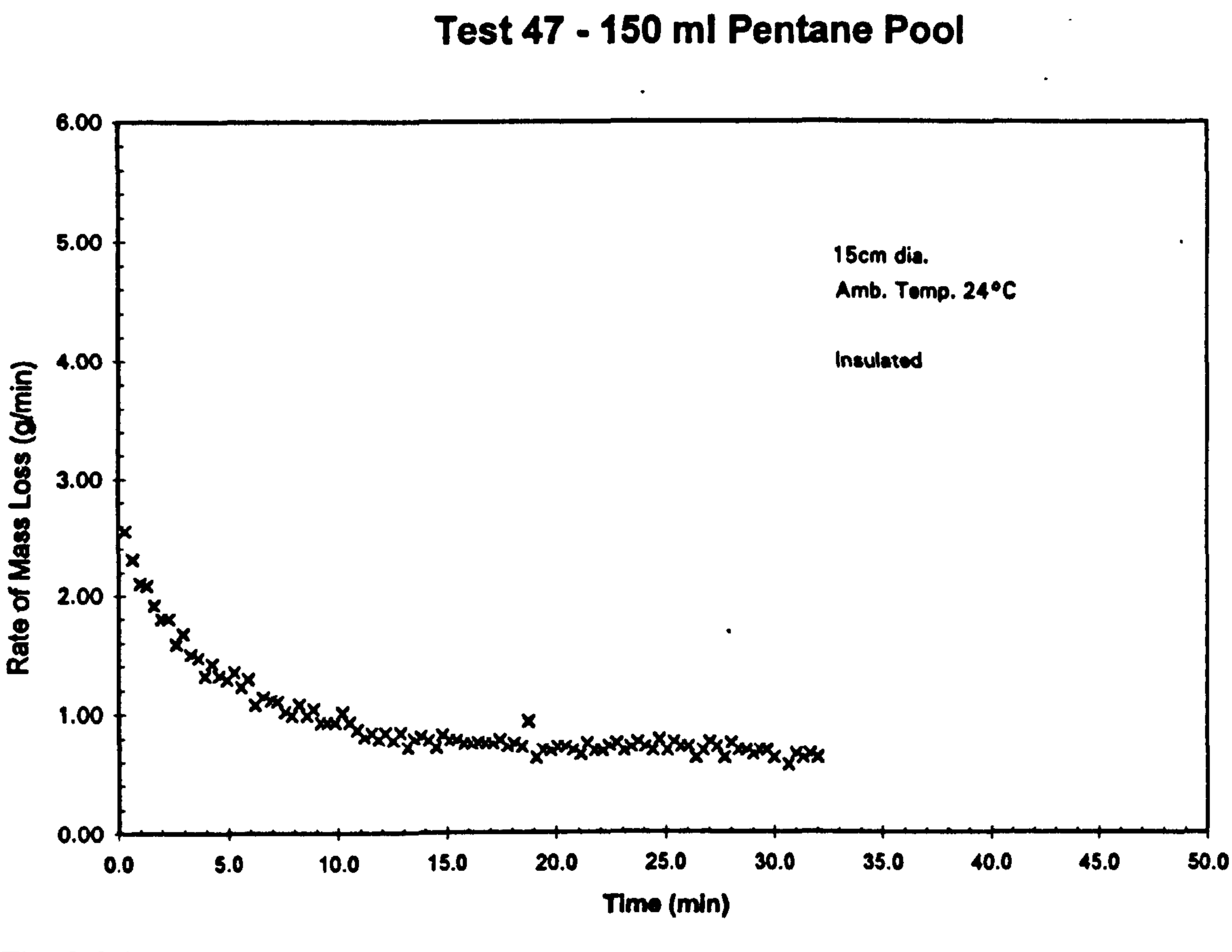

Fig. 3.8.3.1: (a) Typical surface temperature plot of n-pentane evaporating from a 0.15m pool as measured by the Inframetrics system. The dashed line represents the ambient temperature. The dotted and solid lines represent the temperatures of two different points on the pool surface. All materials started at ambient temperature, 23.4°C, but a delay in capturing the first data point causes an apparent difference in starting temperature, exacerbated by some circulation and cooling of the pentane as it is poured into the dish.

(b) Accompanying mass loss rate plot. Note sharp decrease in mass loss rate matched closely by decrease in surface temperature.

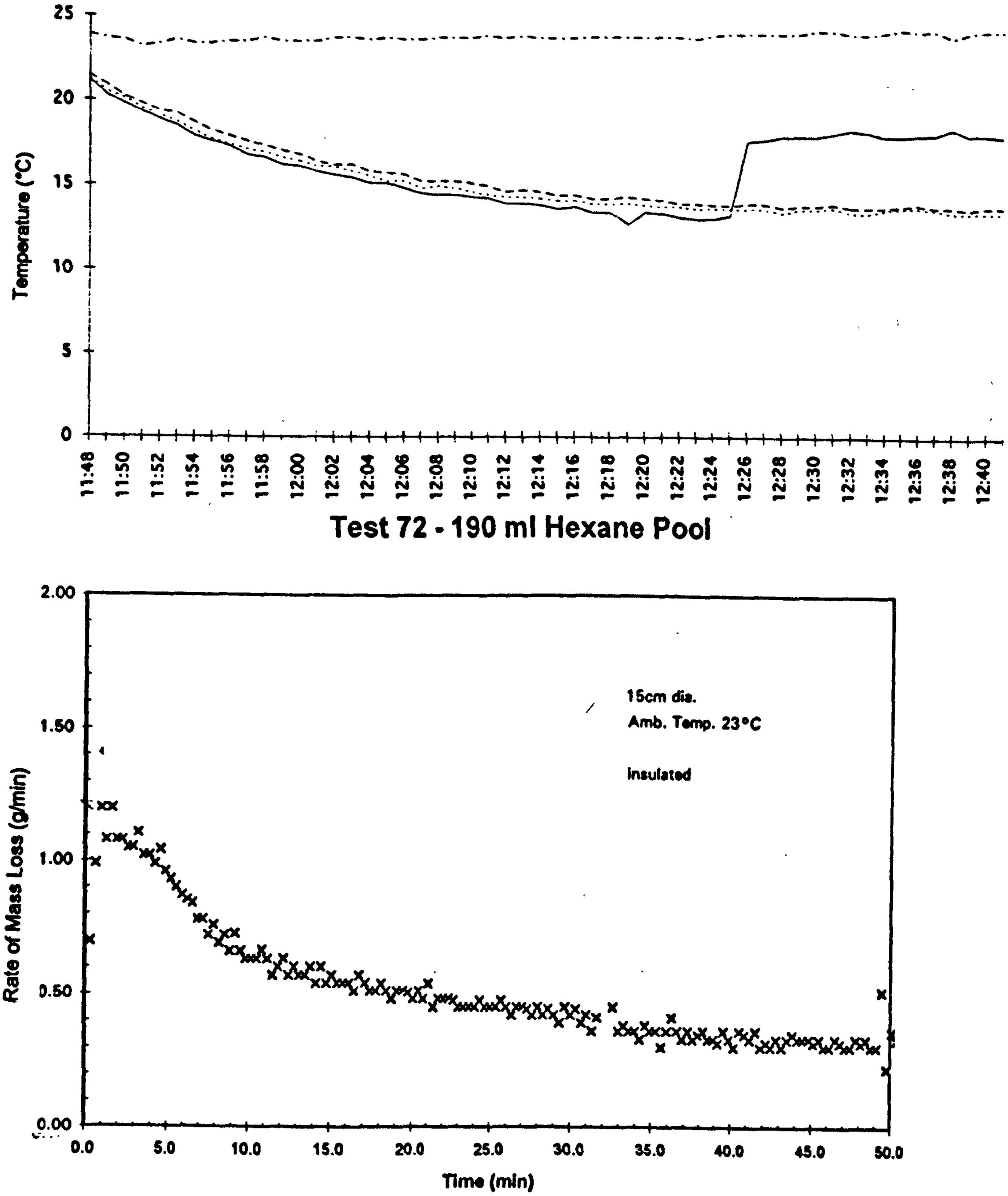

Fig. 3.8.3.2: Typical plot of temperature (as recorded by thermocouple array) of hexane evaporating from a 0.15m pool with accompanying mass loss rate data. Decreases in both mass loss rate and temperature are less dramatic than for more volatile pentane. Abrupt change in temperature of one thermocouple at 37min (12:25) is the result of it coming adrift and pulling clear of the pool and into the vapour above the pool.

slower decrease in temperature. This pool initially evaporated at 1.2g/min. The rate decreased rapidly for the first 10min, then dropped gradually over the next 40min. The final rate was ≈0.3g/min at a temperature of 13°C. The abrupt change in one thermocouple channel at 12:26 (38min from pour) was due to one of the thermocouples coming loose and rising free of the pool surface. It then began to report the temperature of the vapour layer above the pool (which is cooler than the ambient air).

The surface temperature of a 15cm n-octane pool (12mm deep) evaporating under similar ambient conditions is shown in Fig. 3.8.3.3. This data is from an Inframetrics observation. There is a very slow decrease in temperature over the 30min run. This corresponds to an initial mass loss rate of 0.15g/min which remains essentially constant throughout the entire run.

The surface temperature of n-pentane evaporating from sand in a 15cm Petri dish is shown in Fig. 3.8.3.4. An even greater difference in temperature is visible in the first sampling interval than for a pentane pool. This parallels the extremely rapid evaporation of pentane from sand as seen in the mass loss rate plot (measured at 4.0 g/min initially in this run). Differences in temperature at the two sampling points are caused by local irregularities in the sand surface, which can be seen in the fixed thermal images of this test. Note that the surface temperature at one location drops below 0°C at 23min. The evaporation rate dropped quickly for the first 2min and then decreased much more gradually but steadily for the next 30min. The final mass loss rate was 0.63g/min, at which time the surface temperature was 0 – 1°C.

The surface temperature of n-pentane evaporating from aluminium granules in a 15cm Petri dish is shown in Fig. 3.8.3.5. A difference in

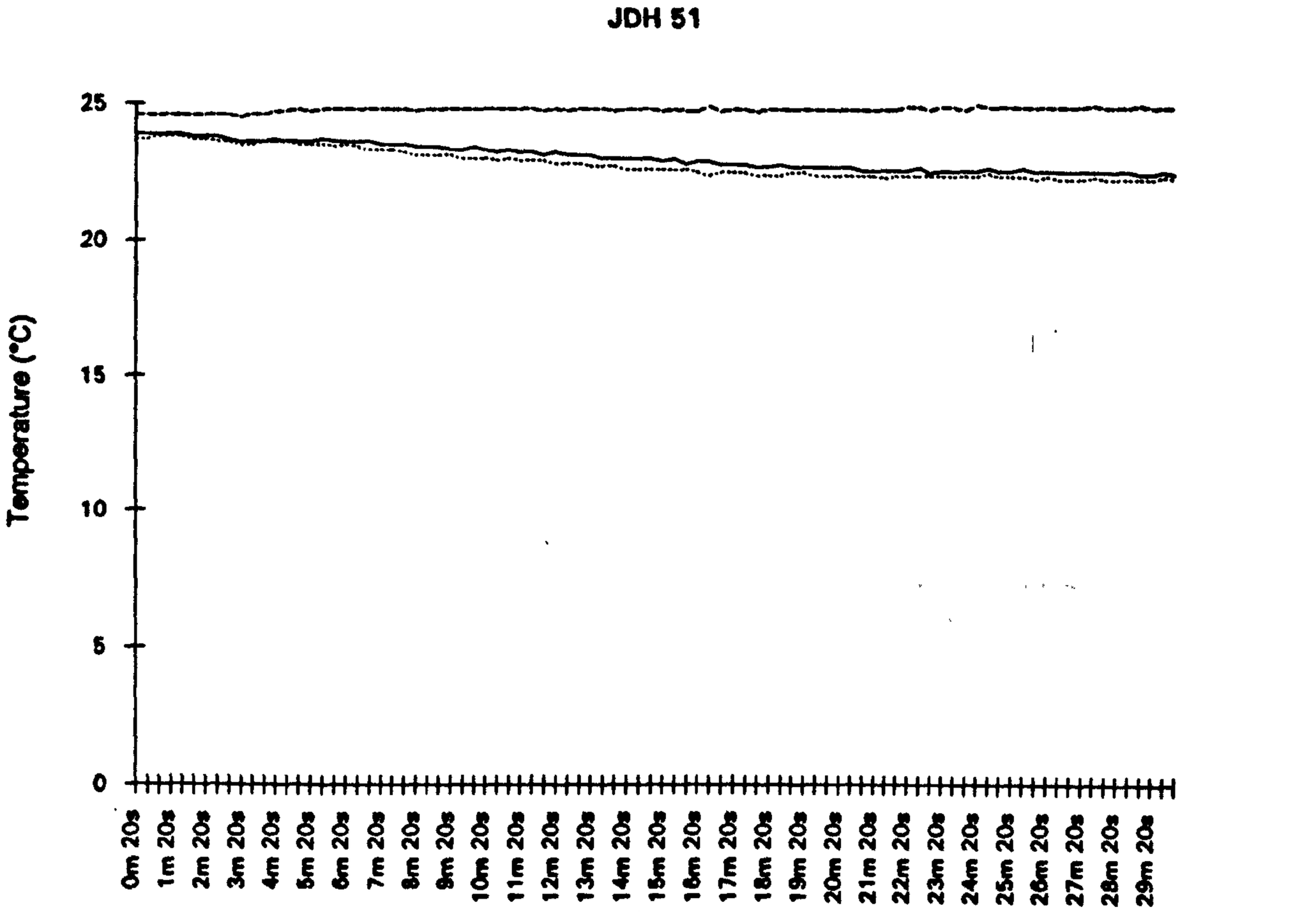

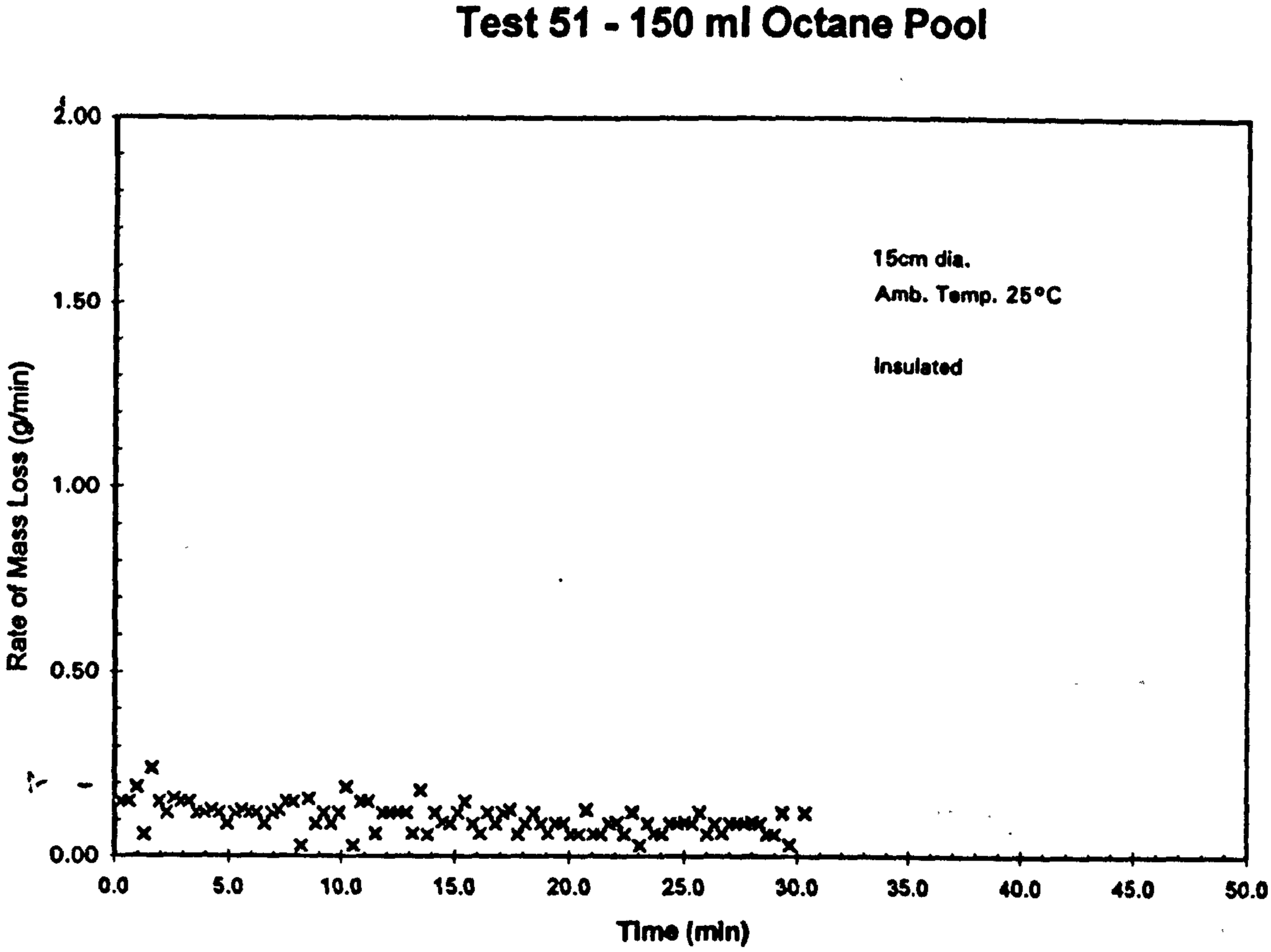

Fig. 3.8.3.3: Plot of temperature (measured by the Inframetrics system) of n-octane evaporating from a 0.15m pool with accompanying mass loss rate plot. Initial mass loss rate is very low and decrease only slowly with time. Temperature decreases in same manner.

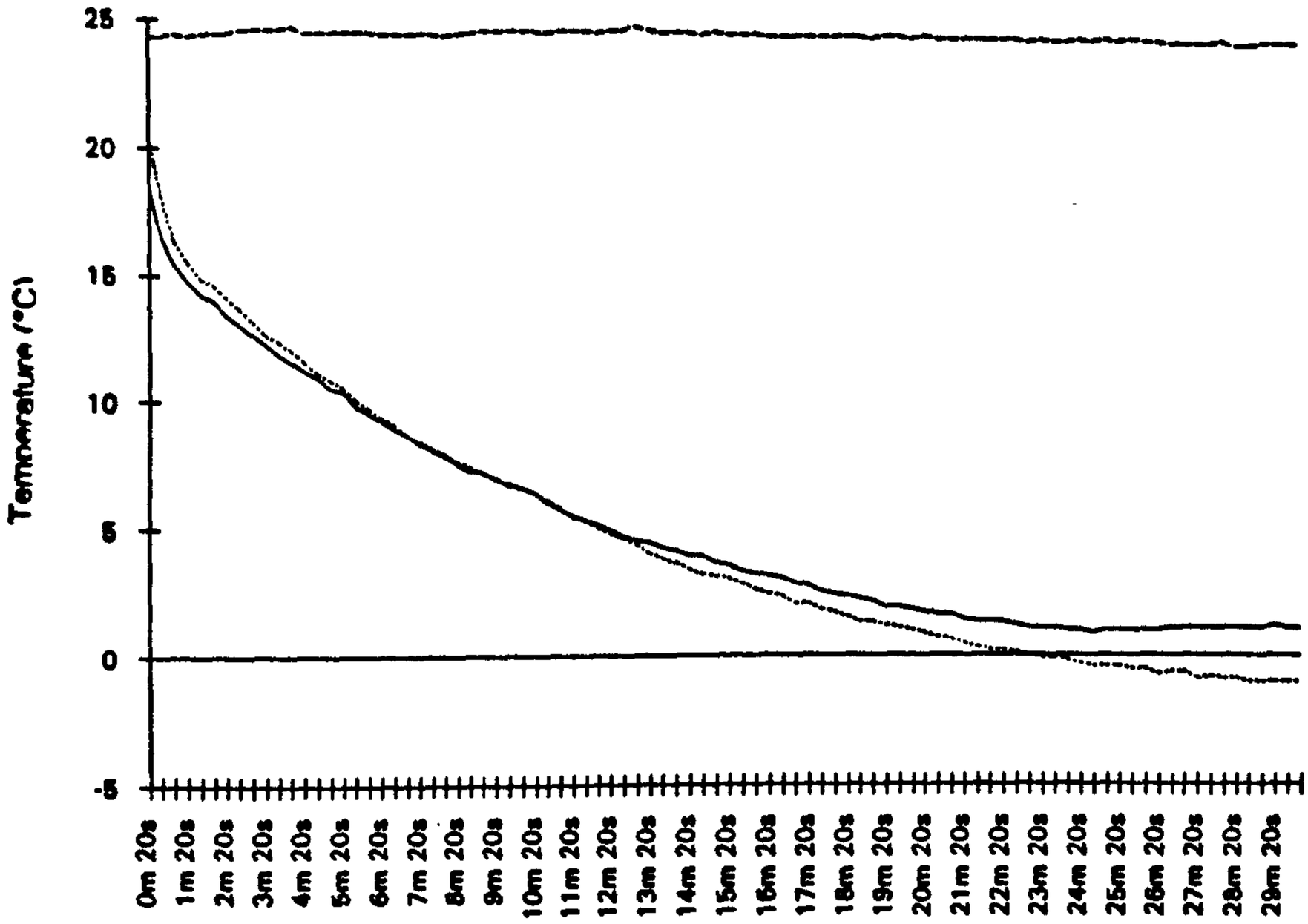

Test 48 - 90 ml Pentane on Sand

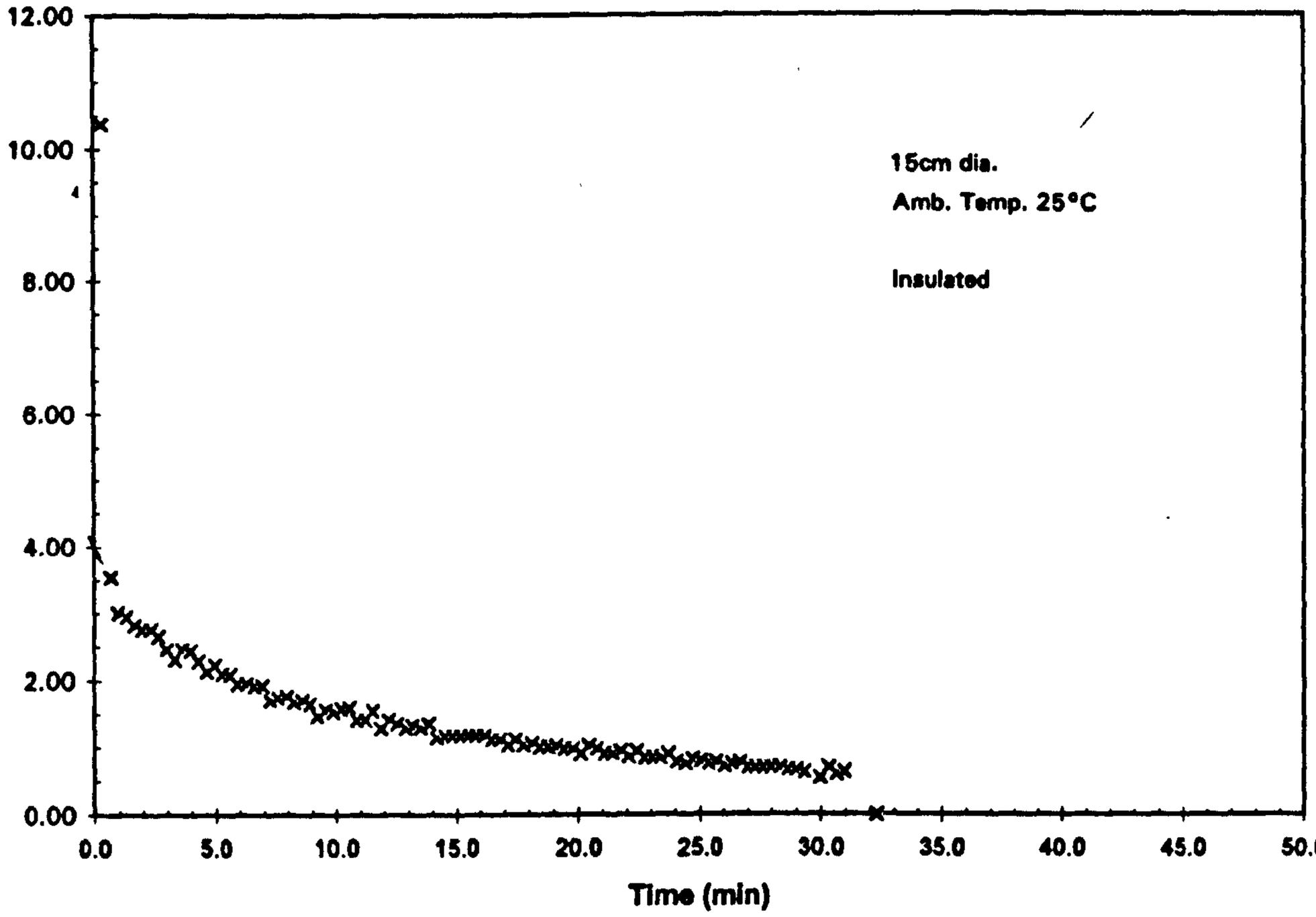

Fig.3.8.3.4: Surface temperature plot of n-pentane evaporating from sand (D=0.15m) as measured by the Inframetrics system. Note the extremely rapid drop in surface temperature in the first minute and the differences in temperature caused by irregularities in the surface of the sand (localized variations). Accompanying mass loss rate plot shows a very rapid decrease in the first minute, then a slower, steady decrease, closely paralleling the temperature.

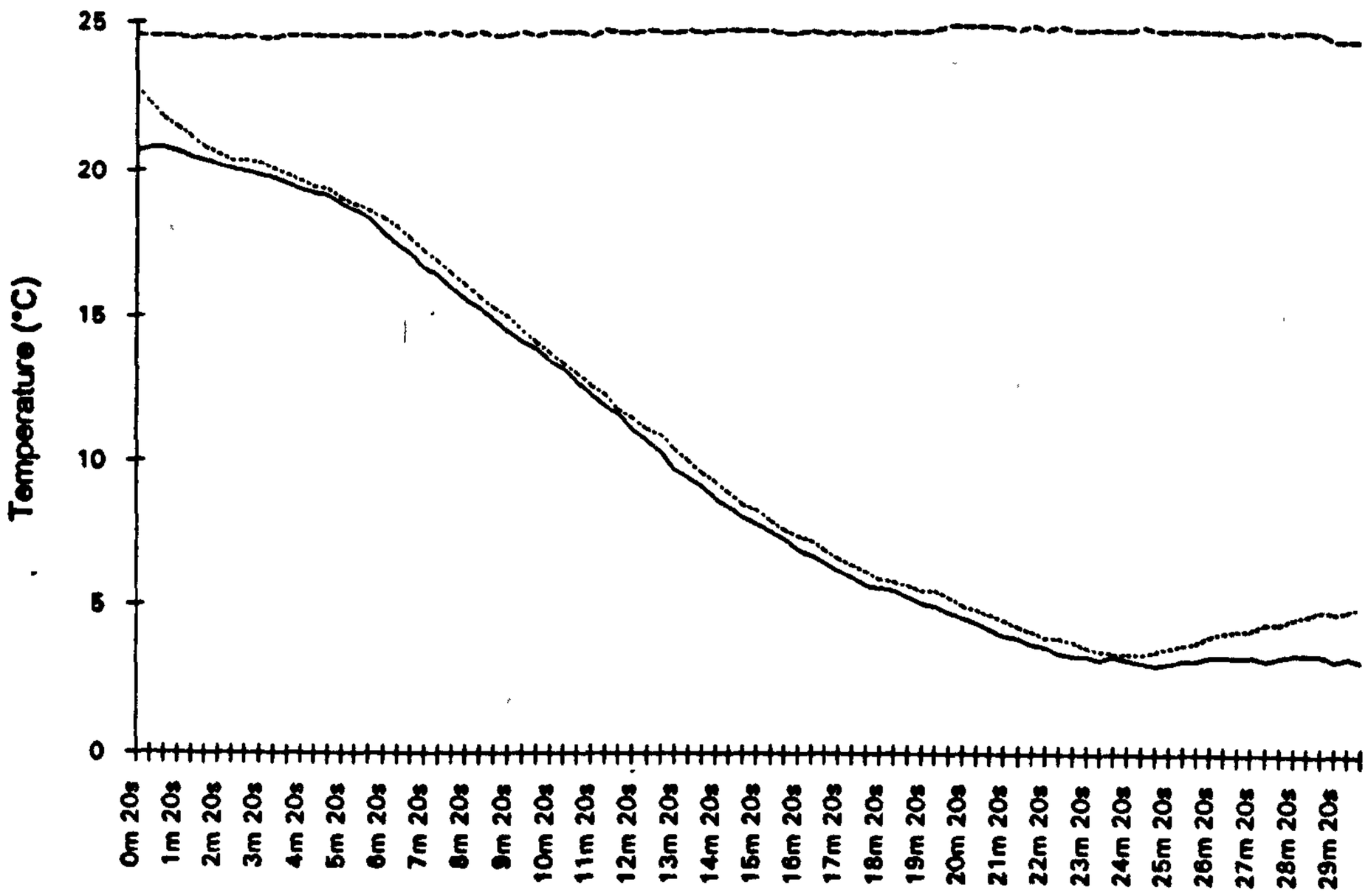

Test 49 - 100 ml Pentane on Al

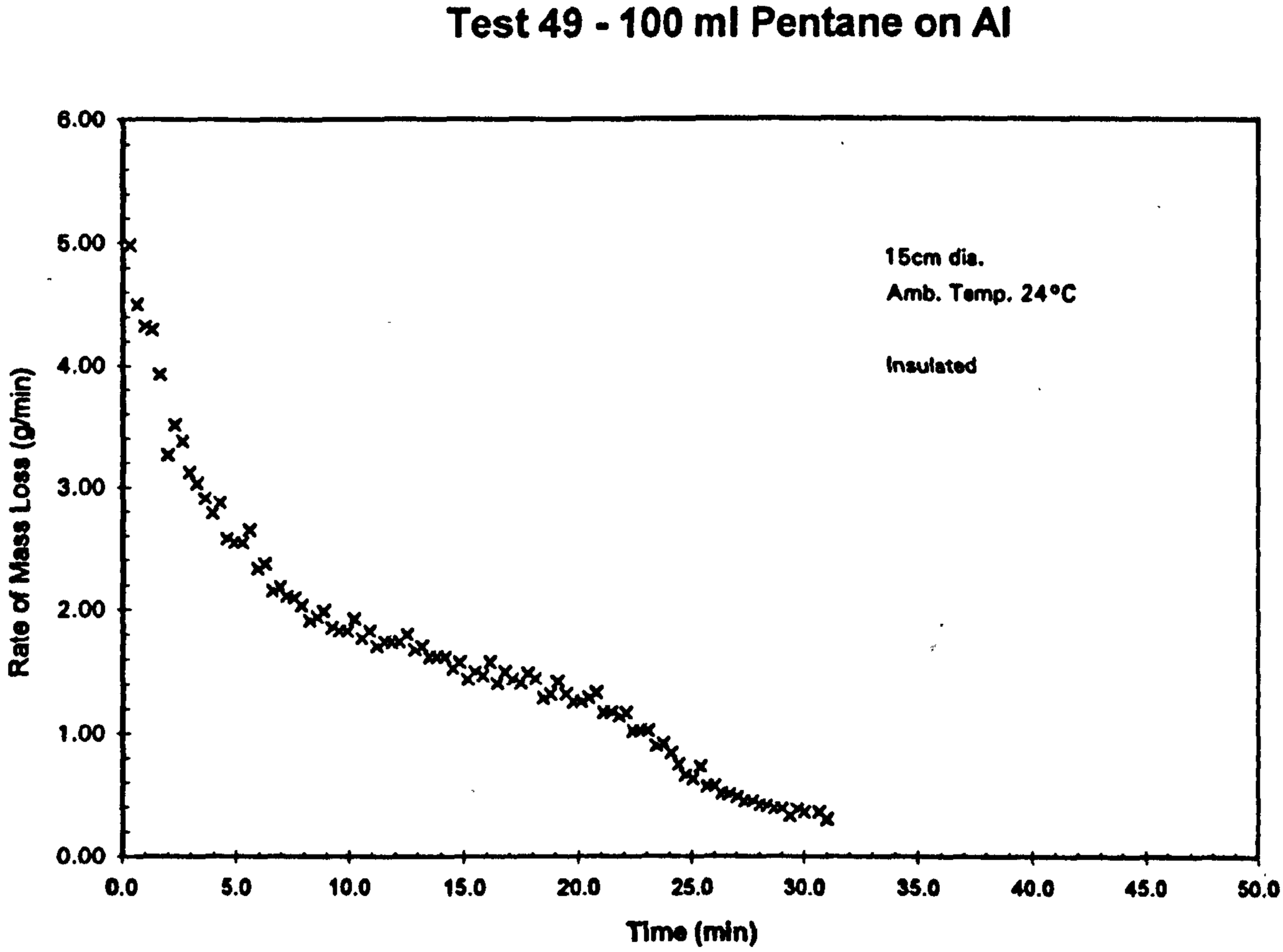

Fig. 3.8.3.5: Surface temperature plot of n-pentane evaporating from aluminium granules (as measured by the Inframetrics system). Rapid change in temperature as seen in the case of sand. Temperature begins to rise at 24min at the same time the mass loss rate drops to near zero, due to exhaustion of the pentane.

temperature is again visible in the first sampling interval. This parallels the extremely rapid evaporation of pentane on this substrate seen in the mass loss rate plot (initially 4.8g/min in this run). Differences in temperature at the two sampling points are caused by local irregularities in the granular surface, which can be seen in fixed thermal images of the test. At approximately 24min, some of the matrix has lost some 47g of its original 55.56g of pentane and its temperature begins to rise as heat from the room is absorbed in its vicinity, which is no longer being cooled as much by evaporation. This point is also marked by a sharp discontinuity in the evaporation rate curve, which makes a sharp drop from 1.0g/min to 0.4g/min, proving the lack of available pentane.

The surface temperature of n-pentane evaporating from carpet in a 15cm Petri dish is shown in Fig. 3.8.3.6. A drop in temperature similar to that seen in the sand/pentane matrix is visible in the first sampling interval. This parallels the very rapid evaporation of pentane from carpet (initially 4.0g/min here). Differences in temperature at the two sampling points are caused by local irregularities in the carpet surface, which can be seen in fixed thermal images of the test. Note that at approximately 12min, the temperature dips below 0°C. The final temperature was –5°C, and frost condensed from the moisture in the room air was visible on portions of the carpet surface. The evaporation rate decreased monotonically to about 15min, at which point it stabilized at ≈1.2g/min. The accumulating frost may have decreased the loss rate, but the carpet surface was still dissipating pentane at a significant rate (1g/min) even while at –5°C.

A series of experiments were conducted in which the Inframetrics thermal imaging system was used to capture the surface temperature of a matrix while iron-constantan thermocouples captured the temperature of

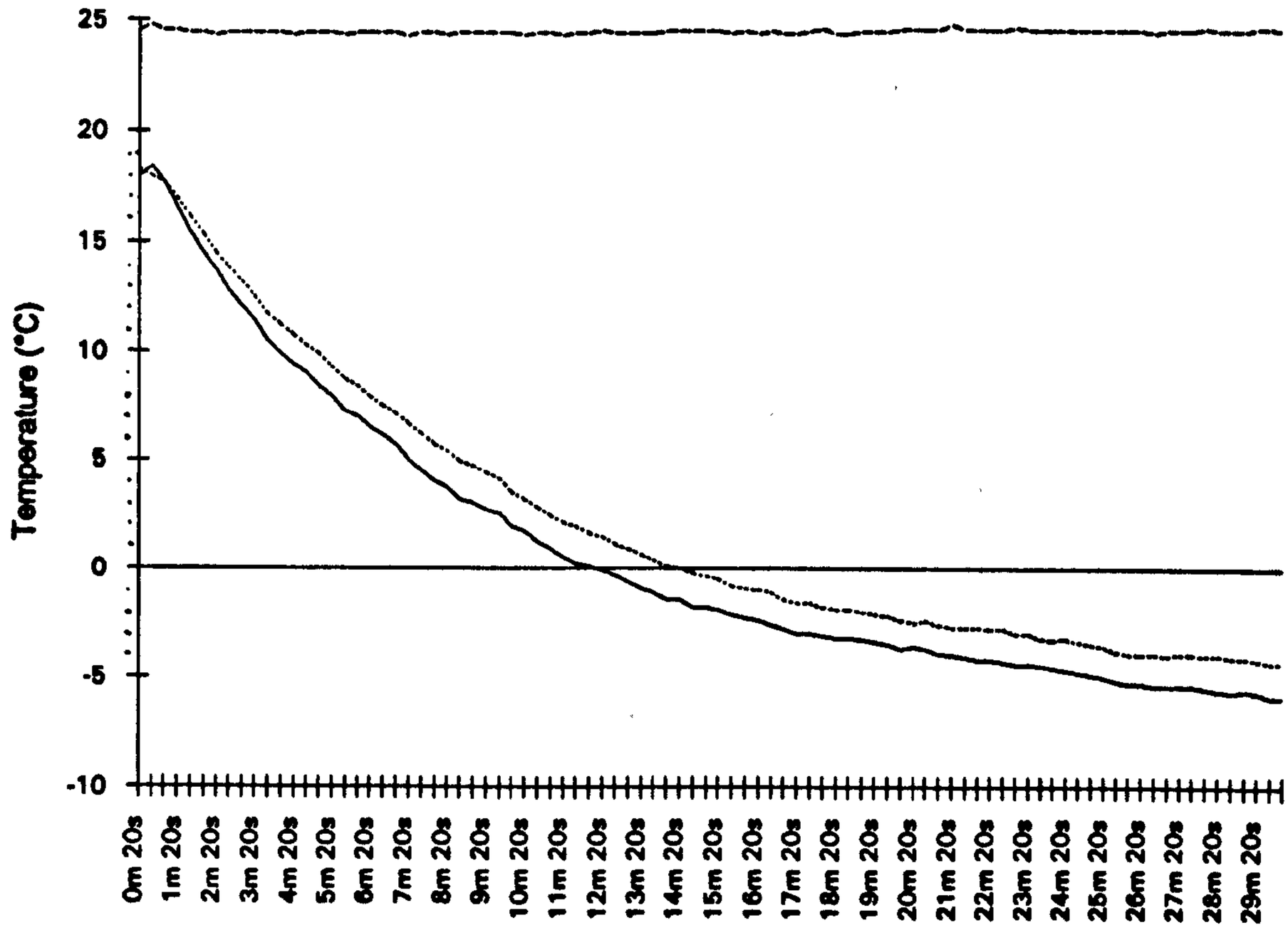

Test 50 - 240 ml Pentane on Carpet

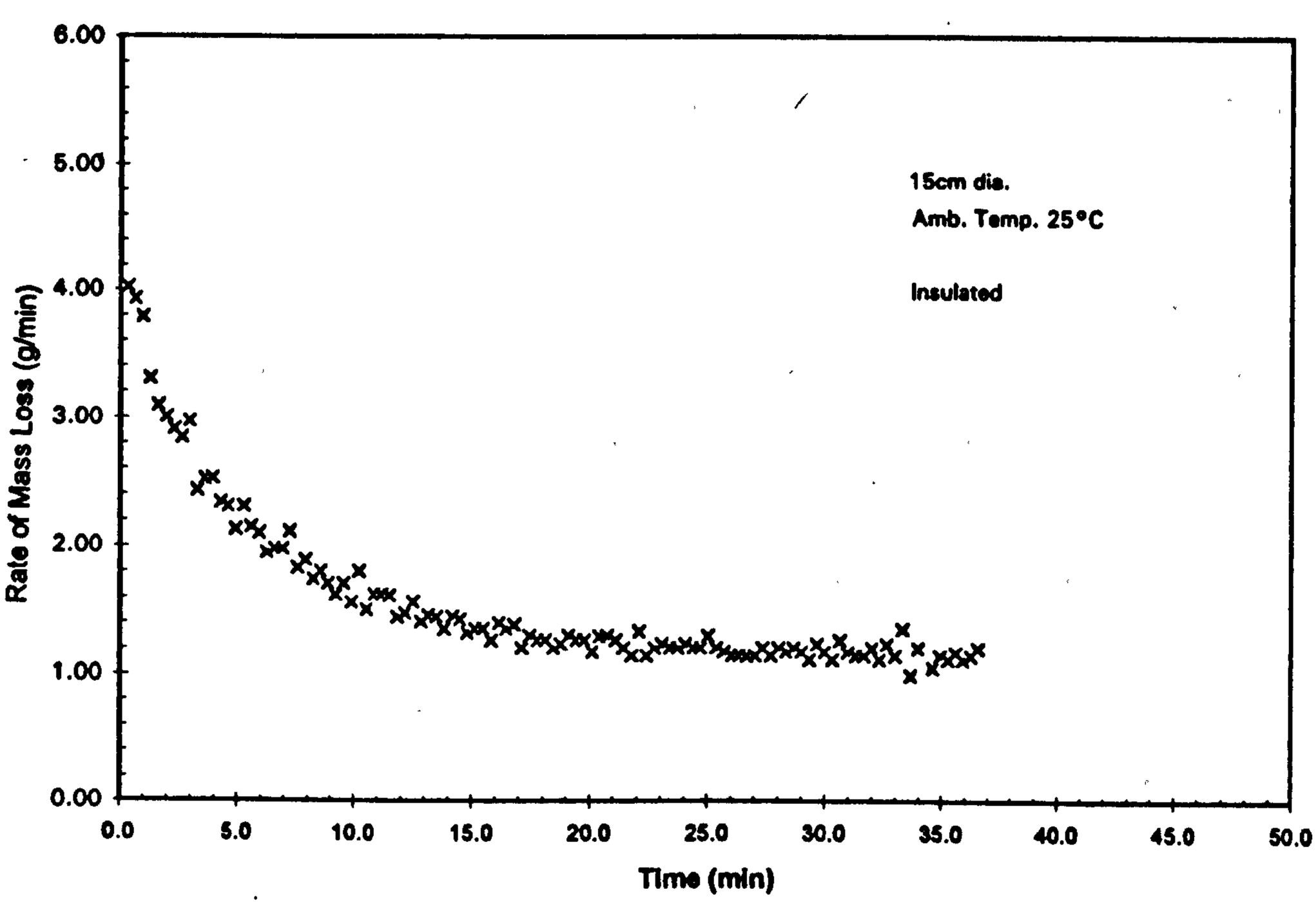

Fig. 3.8.3.6: Surface temperature plot of n-pentane evaporating from carpet and the accompanying mass loss rate plot. Note close parallel between the two. The final temperature was -5°C and frost was visible on the surface of the carpet at the end of the run. Despite the low temperature, the mass loss rate remains at 1g/min.

the matrix. In Figs. 3.8.3.7 and 3.8.3.8, the upper graph displays the Inframetrics record of an evaporating pentane pool, and the lower graph displays the thermocouple measurements. While there are some minor variations in local measurements, there is very good agreement between the two sets of measurements. Note that both record the abrupt change in temperature at the start of the run. The sampling time for the thermocouple system was every 60s (beginning at the start of pouring), so its first data point shows a very significant drop of some 3°C. The sampling time for the Inframetrics system was changed to every 3s, but the image was obscured by the graduated cylinder being used for the pouring and the hands of the experimenter (which produced the 'spikes' in the IR temperature record of Fig.3.8.3.7). The rapid decrease in temperature is still detectable. This corresponds to an initial mass loss rate of 2g/min in both runs. The rate decreased monotonically and approached 0.6 – 0.66g/min at a temperature of ≈4.5°C.

The irregular changes in the thermocouple data of both figures were the result of the thermocouples coming loose from their positions in the pool and drifting free of the liquid. In one test, the thermocouple came completely free of the liquid and its temperature recorded the temperatures of the vapour/air layer above the pool (cooler than the ambient air). In the other, two of the thermocouples loosened but remained (trapped by surface tension) at the air/liquid interface. The cooling produced by the enhanced evaporation is reflected in the abrupt drop in temperature recorded.

The thermal data from two 15cm, shallow (3 – 4mm) pool pentane experiments are shown in Figs.3.8.3.9 and 3.8.3.10. The mass loss rates for both runs began at 1.3g/min, decreasing rapidly to ≈0.5g/min at 10min, then decreasing much more gradually to 0.3g/min (even with a temperature of

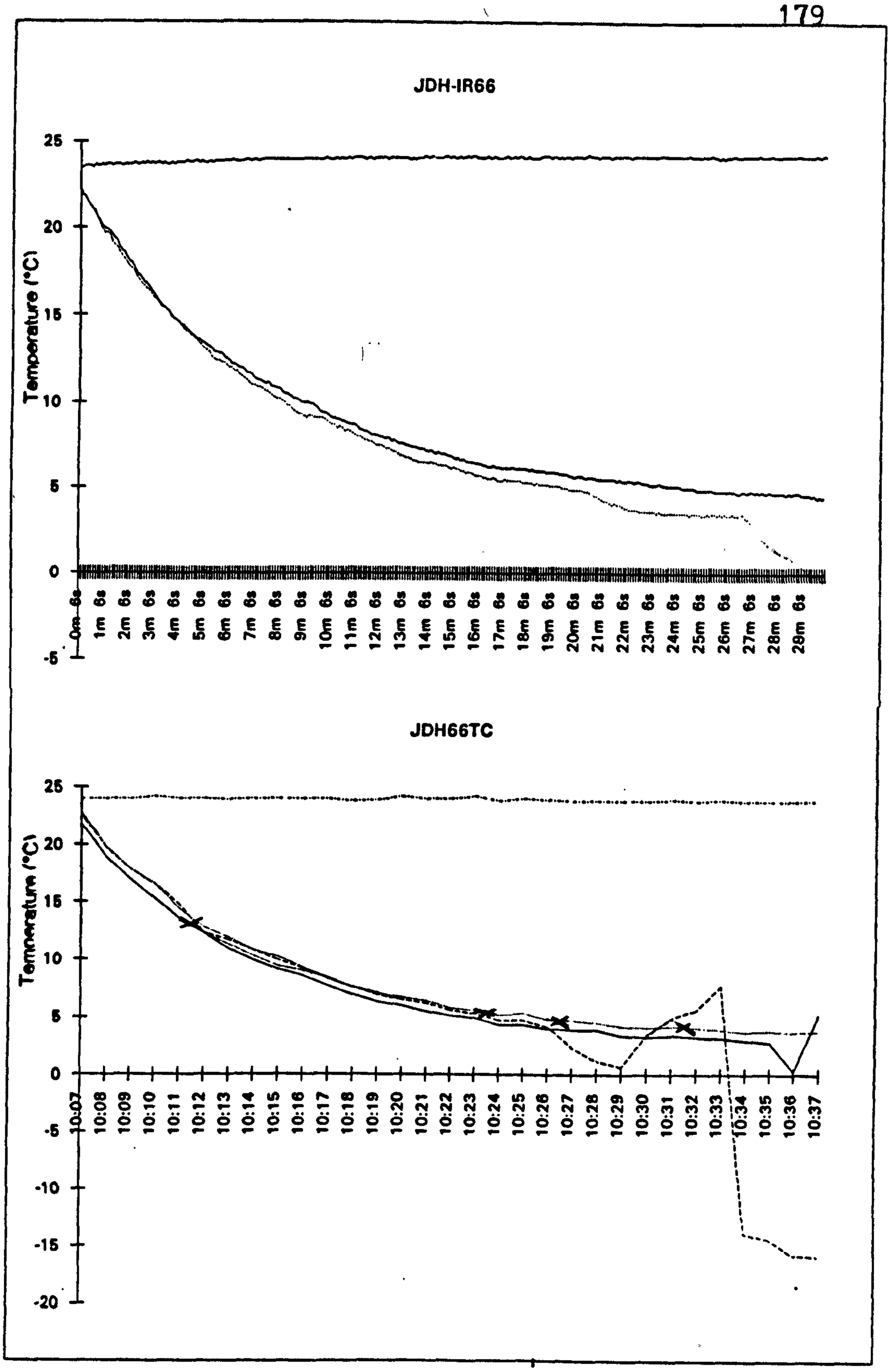

Figure 3.8.3.8: Repeat of pentane pool experiment. In this case, the temperature being measured by the Inframetrics system was inserted as isolated data points on the thermocouple data plot, showing excellent correlation. One thermocouple began to rise from the pool at 10:26, and enhanced evaporation caused its reading to drop before the wire came completely free of the pool. Note minimal difference between surface temperature and the bulk pool temperature.

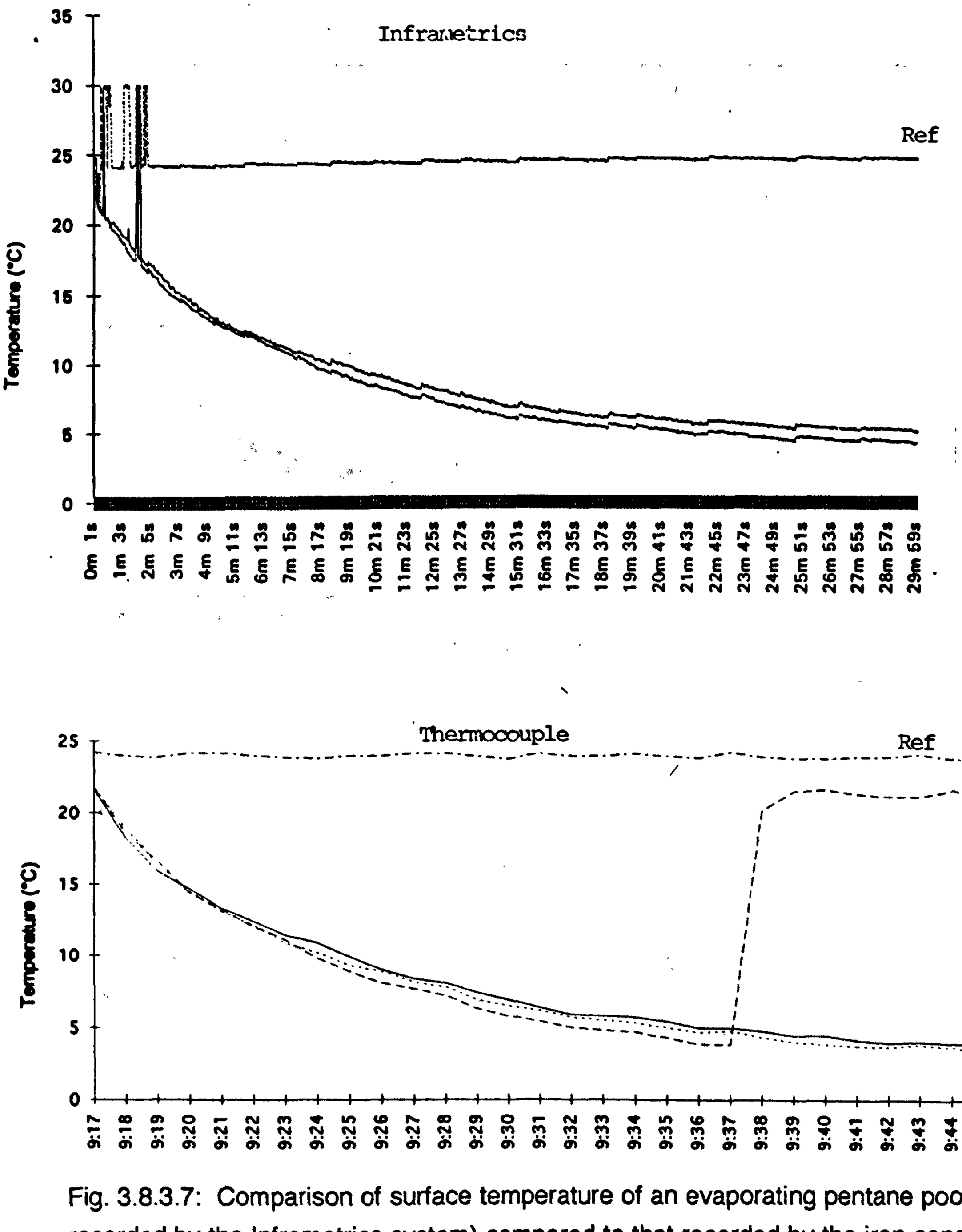

Fig. 3.8.3.7: Comparison of surface temperature of an evaporating pentane pool (as recorded by the Inframetrics system) compared to that recorded by the iron-constantan thermocouple array. There is good correlation between the two, with very little difference in temperatures at the surface and at the bottom of the pool. The spikes in the IR image record were the result of the experimenter's hands being in the sampling area, and the periodic steps were apparently the result of the cycling on-and-off of the room's HVAC system. The abrupt change in one TC trace was the result of it coming adrift and out of the pool.

Test 77 - 50 ml Pentane Pool

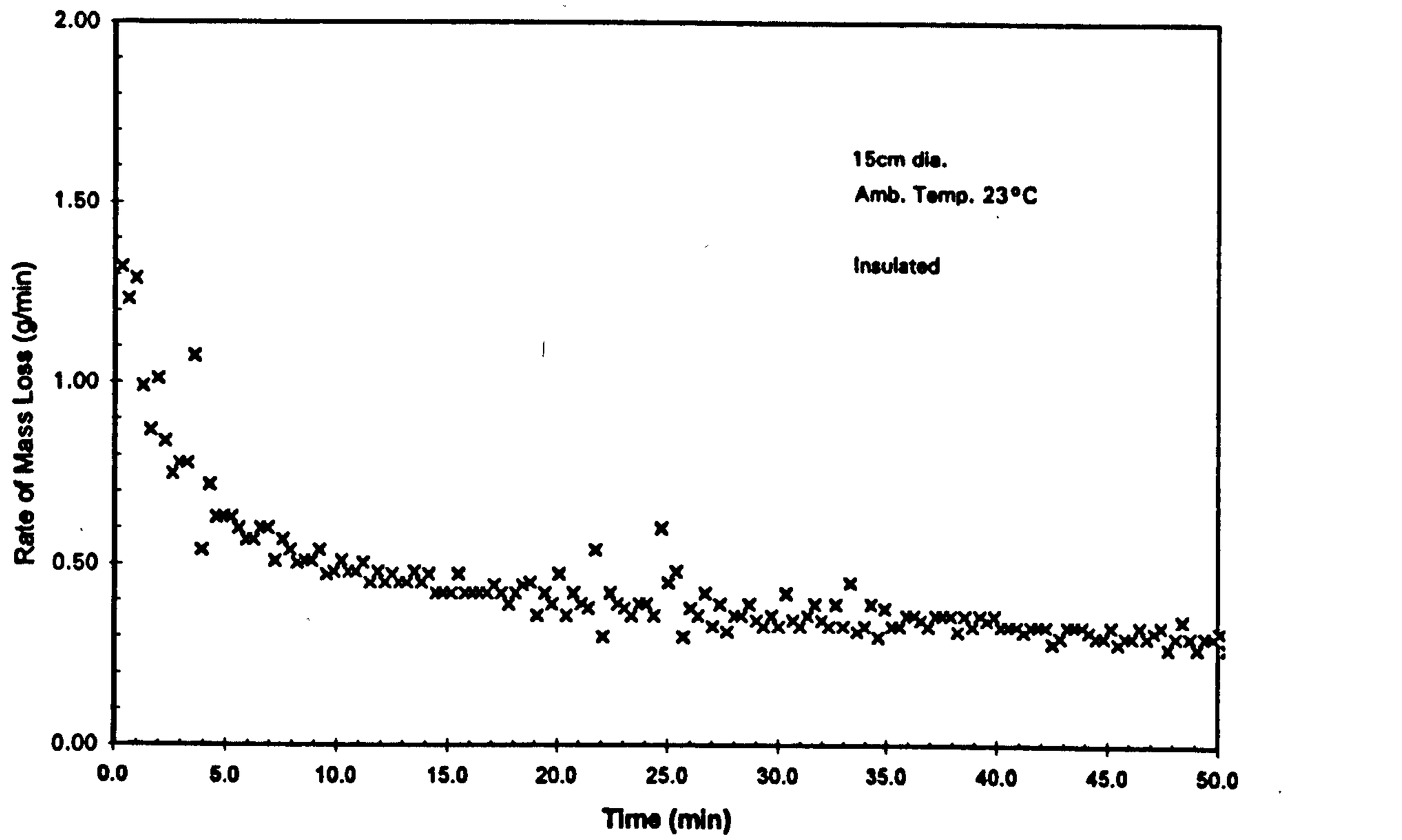

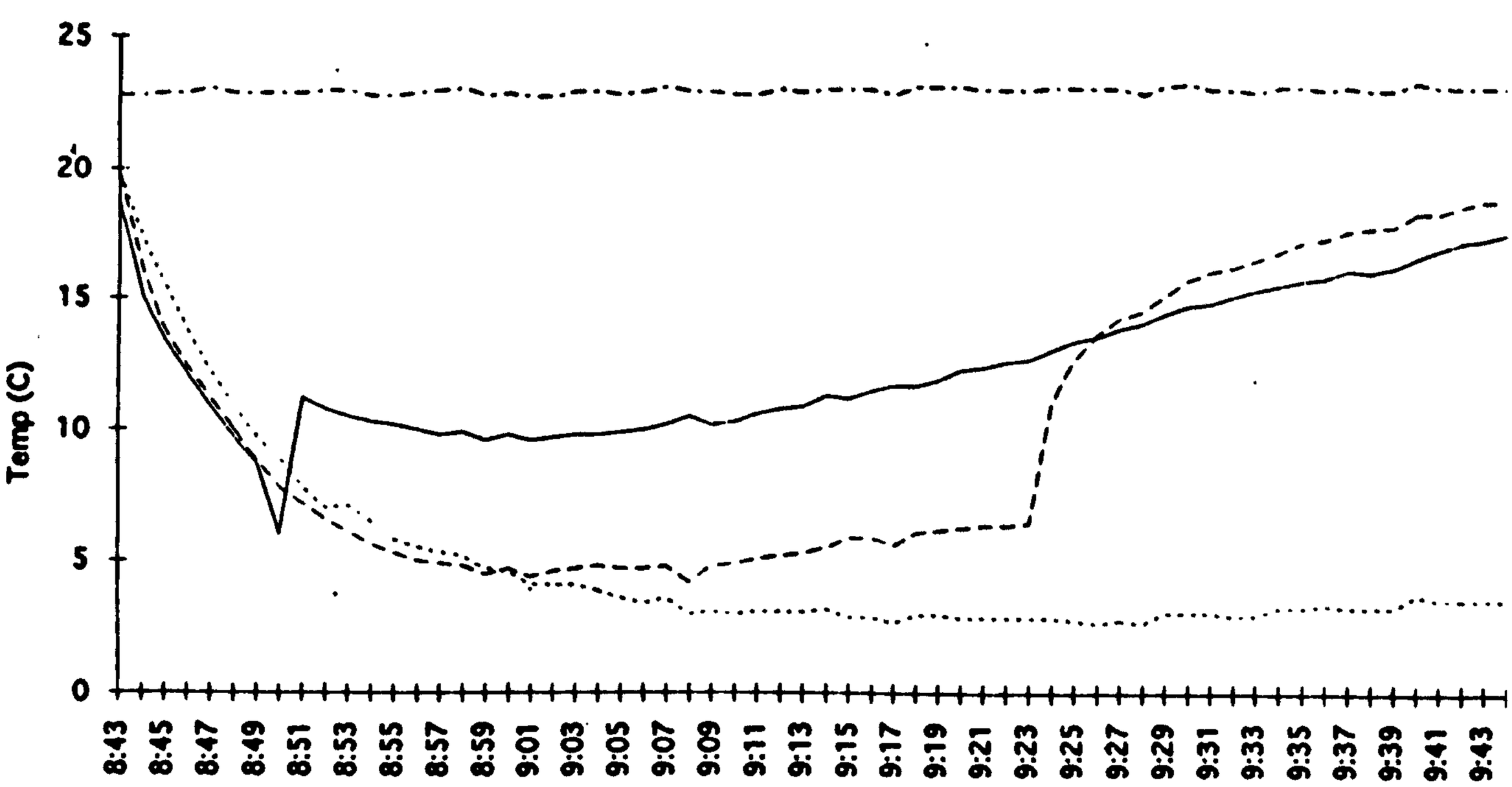

Fig. 3.8.3.9: Thermocouple data plot for a shallow (<4mm) pool of n-pentane. Note extremely rapid drop in temperature of all three data points and the change in temperature as first the surface thermocouple (#3) comes free of the surface (at 8:50), followed by another on the bottom of the dish going "dry" at 9:23 (t = 40min). The last thermocouple remained wetted by a localized pool of pentane until the end of the run. Compare to the mass loss data for the same run.

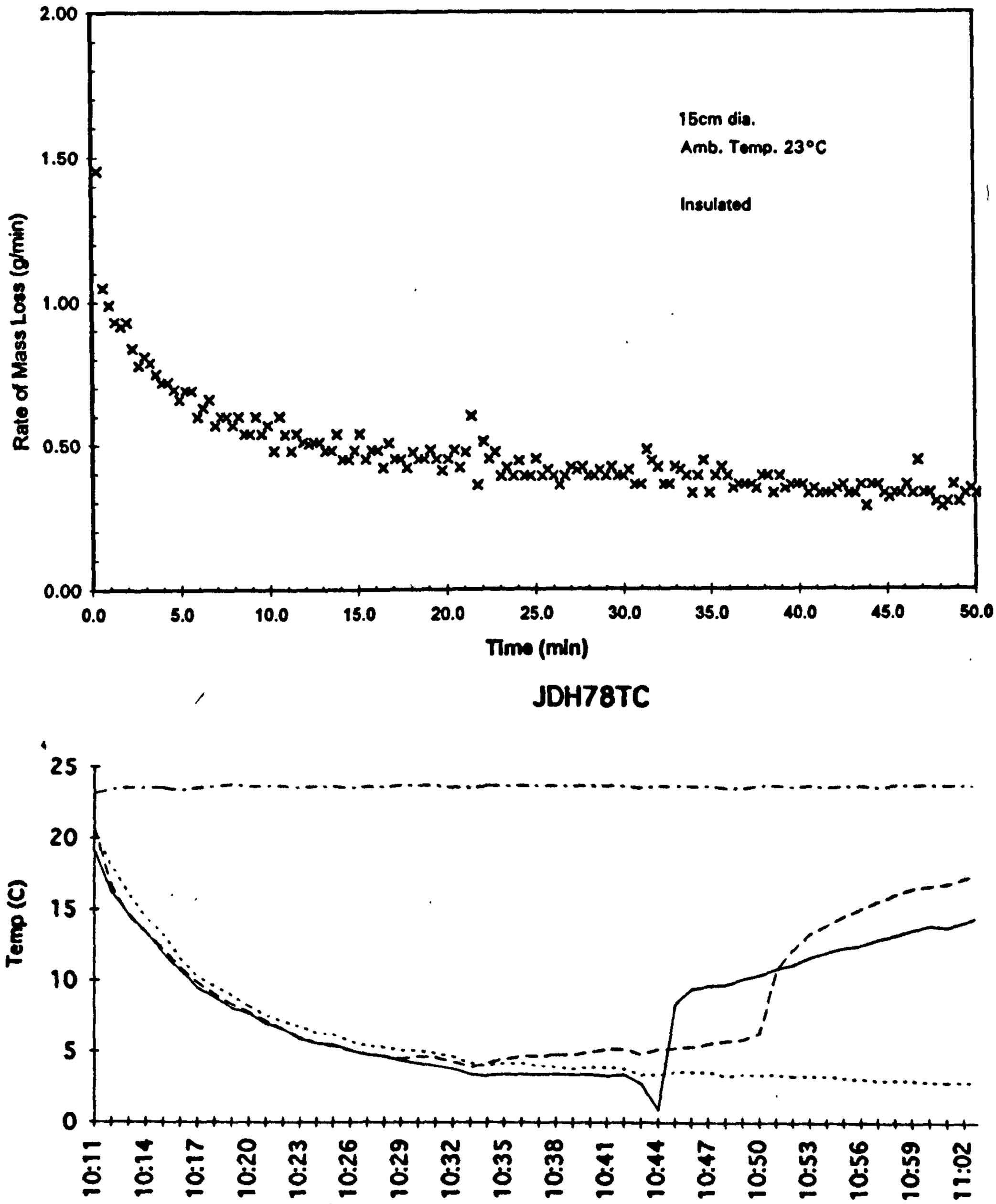

Figure 3.8.3.10: A repeat of the shallow pool experiment (Fig. 3.8.3.9) demonstrates the same rapid drop in temperature throughout the pool. In this case, the thermocouples remained wetted by the pentane until the surface TC was released at 10:44 and another went "dry" in the bottom of the dish at 10:50. Compare to the accompanying mass loss plot.

2.5 – 3°C), and a remaining mass of 10% of the original.

Plotting mass loss rate versus the surface temperature of a typical 15cm pentane pool (12mm deep) yields a plot such as Fig.3.8.3.11. The relationship between the two values is as expected. (Discontinuities at very low mass loss rates are due to the uncertainties in calculating those numbers, where small variations in measurements result in large fluctuations.)

3.8.4 Thermodynamics of Evaporation from Matrices

Plotting the mass loss rates of pentane evaporating from sand- and aluminium granule matrices against surface temperature yields Figs. 3.8.3.12 and 3.8.3.13. The upward curve is similar to the curve obtained for pentane pool evaporation, but its slope varies at a different rate. All three vary in the same manner as vapour pressure v. temperature for pentane (Fig. 1.1) but the more pronounced "flattening" at lower temperatures may be the result of combined changes in vapour pressure, surface tension, and viscosity, all of which will affect mass transport within a matrix. This relationship will be explored in more detail in Sect. 4.8.4.

3.8.4.1 Thermodynamics of Evaporation from Carpets

Five tests were carried out pouring 100ml quantities of n-pentane on panels of synthetic carpet that had been glued with water-based contact cement to panels of 12mm thick rigid Styrofoam. The resulting wetted areas were measured and the panels observed with the Inframetrics IR

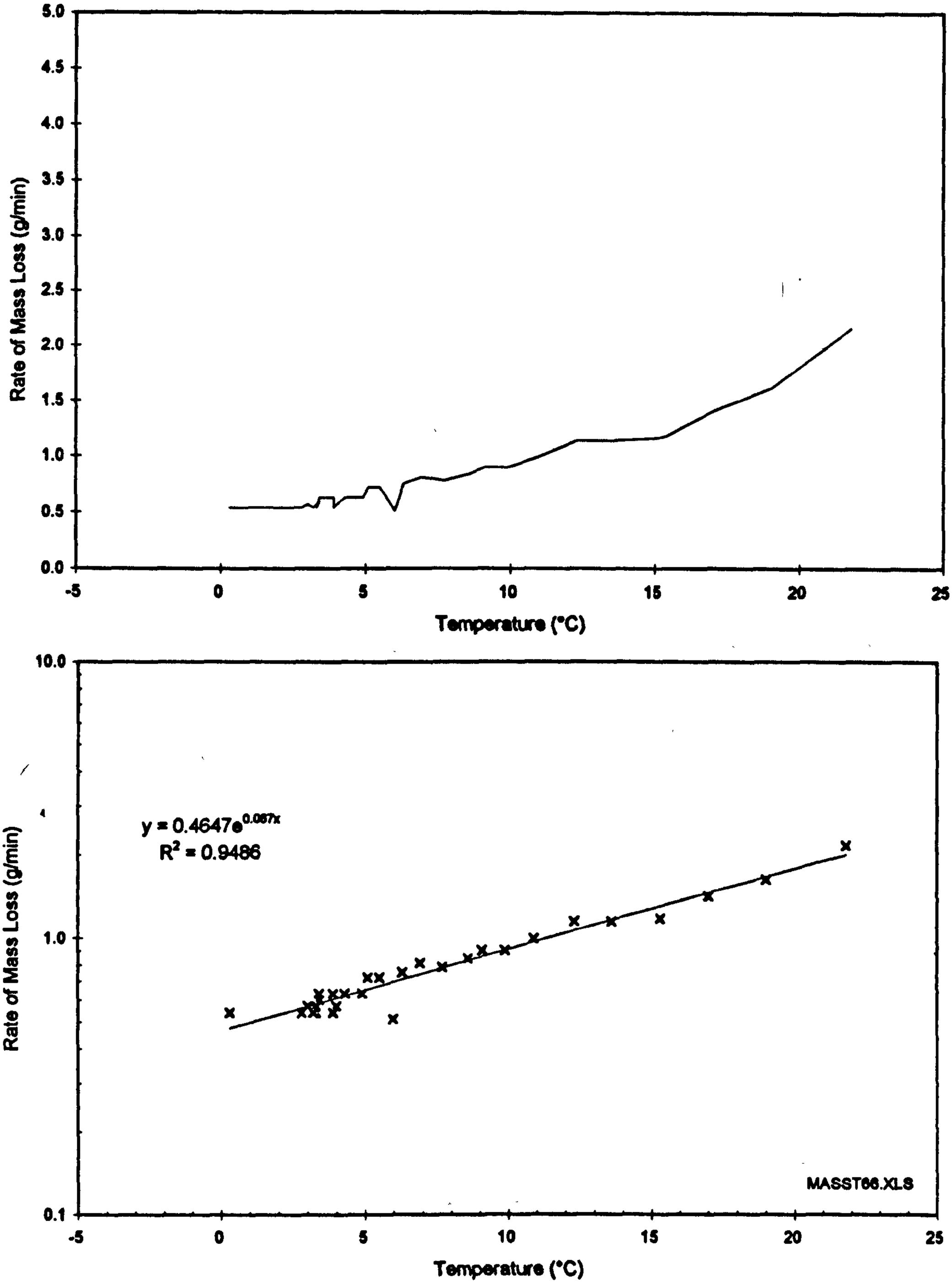

Fig. 3.8.3.11: (a) Plot of surface temperature v. mass loss rate for pentane pool evaporation. Note the direct relationship except at temperatures near ambient where the mass loss rate calculations are subject to large fluctuations.

(b) Semi-log plot of same data demonstrates relationship. Equation fitting line is of exponential form.

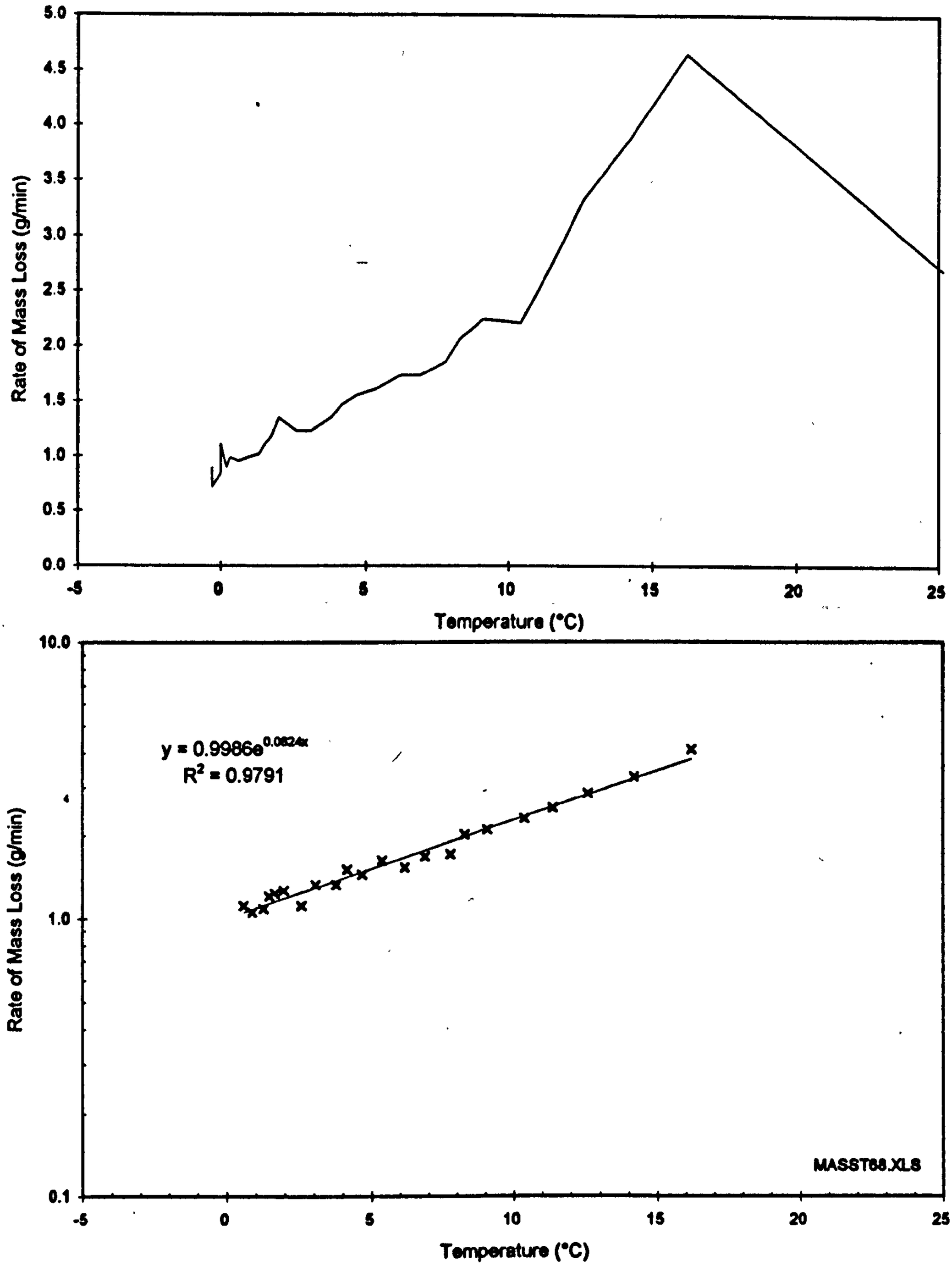

Fig. 3.8.3.12: (a) Plot of surface temperature v. mass loss rate for pentane/sand matrix. Plot exhibits the same relationship as in Fig. 3.8.4.11 but with a different y-axis intercept which suggests the substrate is affecting the mass loss rate.

(b) Semi-log plot of same data demonstrates relationship. Equation fitting line is of exponential form with a different multiplier and exponent from pentane.

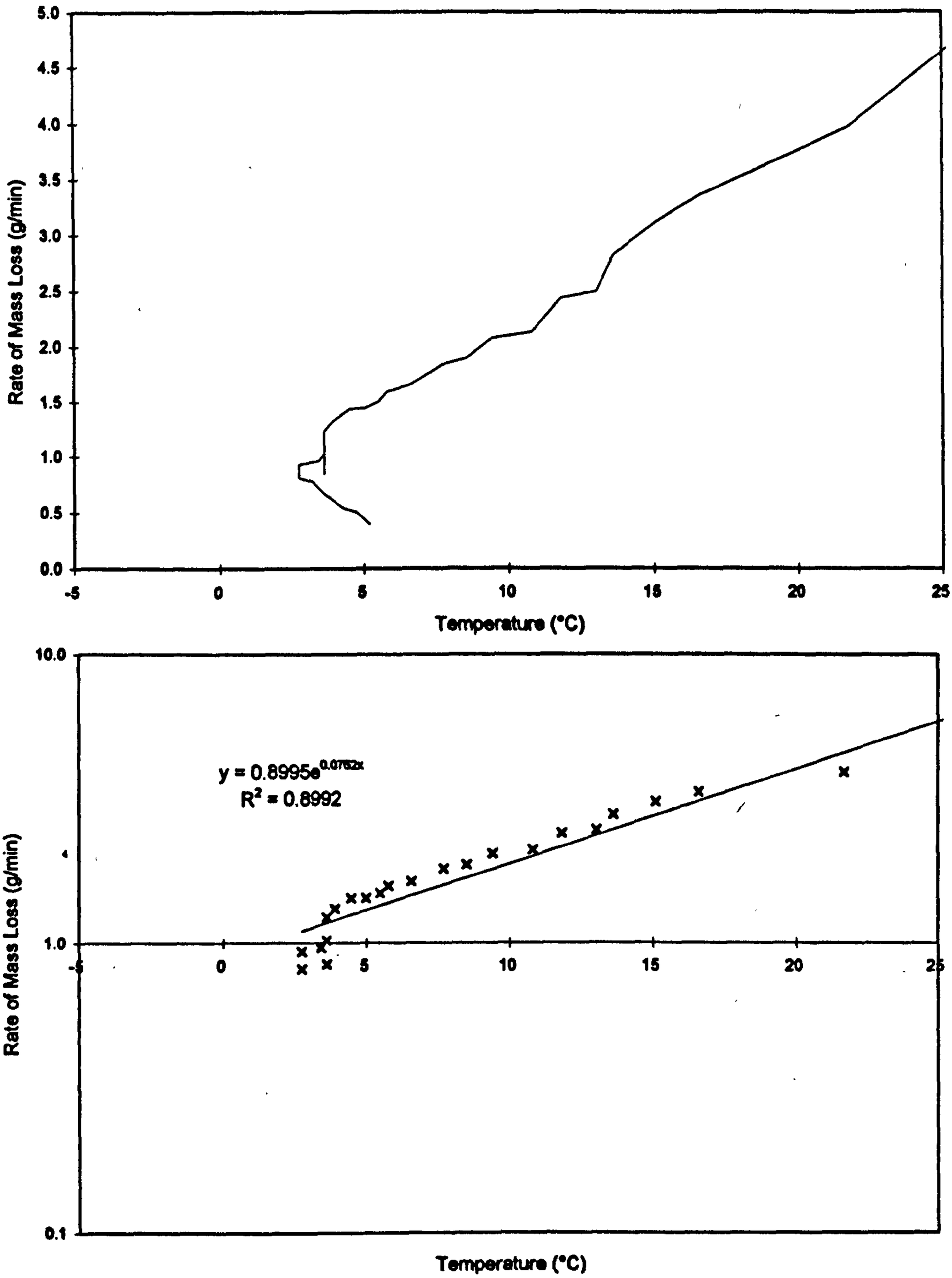

Fig. 3.8.3.13: (a) Plot of surface temperature v. mass loss rate for pentane evaporating from aluminium granules. The general shape is the same as that for pentane on sand (including the y-axis intercept) suggesting that the process is the same despite the difference in heat conductivity between sand and aluminium. The recurve near the end of the run is the result of the aluminium granules going to dryness and the temperature beginning to rise.

(b) Semi-log plot of same data demonstrates relationship. Equation fitting line is of exponential form with a different multiplier and exponent from pentane but very similar ones in value to those for pentane/sand matrix.

imaging system while the mass loss rate was measured using the electronic balance. The image sizes of pools from the Inframetrics videotape recording and ThermaGram® images were reconstructed by scaling according to the image sizes of the carpet squares (28x28cm). Temperatures were captured at three discrete points by the ThermaGram® system: ambient (measured at the corner of the carpet panel), the centre of pour pattern, and ≈10cm away from the centre.

Carpet A: Rubber-backed commercial-grade nylon loop pile carpet, 5mm pile height.

A pour of 100ml of n-pentane produced a 24cm pool (visibly wetted area), 0.044m2 in area. The surface temperature plot can be seen in Fig. 3.8.4.1. The temperature dropped by approximately 10°C in the first minute after pouring began (5.4s pour). The mass loss rate over the same period dropped from 8.15g/min to 6.27g/min. The surface temperature dropped continuously until 12 –14min, and then began to increase. At that point, less than 10g of the original 60g of pentane remained on the carpet. The mass loss rate was transitioning from 2.6g/min to 0. A false-colour still image made at 5min showed the centre of the pool to be generally uniform in temperature at 9 – 11°C, with its margins generally cooler, at 7 – 9°C. There was also a concentric ring of carpet extending an additional 4cm in all directions where there was no pentane but whose temperature was significantly lower than the ambient conditions, indicating heat was being drawn from adjoining areas of carpet.

Carpet B: Foam-backed commercial-grade polypylene loop pile carpet, 5mm pile height.

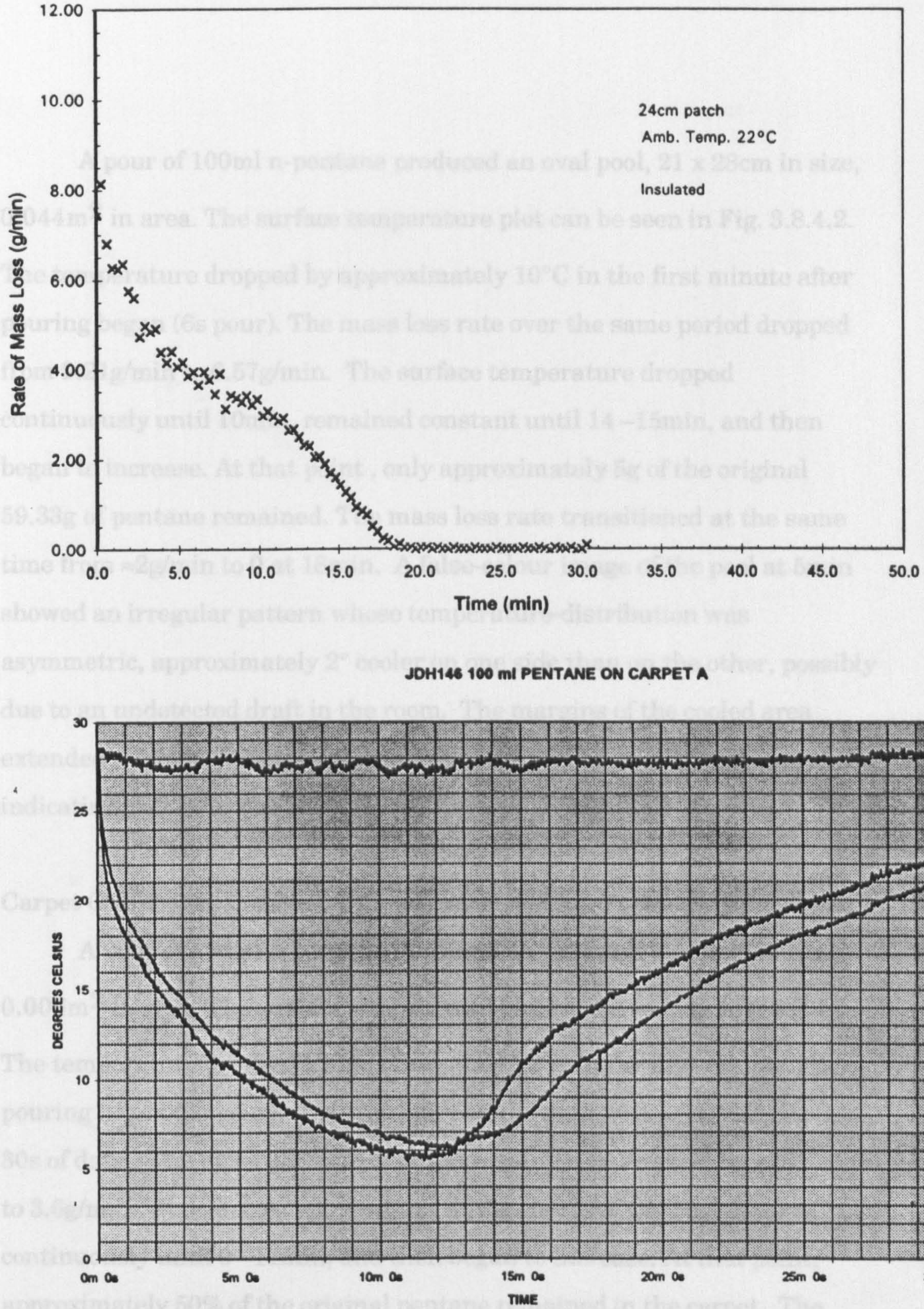

Fig. 3.8.4.1: Surface temperature (via Inframetrics system) v. time for n-pentane evaporating from a "free" pool on a 4mm pile carpet (wetted area 0.24m in diameter) and accompanying mass loss plot. Minimum temperature is 22°C below ambient. The temperature begins to rise at 12min as the mass loss rate drops dramatically towards zero as the pentane is exhausted.

A pour of 100ml n-pentane produced an oval pool, 21 x 28cm in size, 0.044m^2 in area. The surface temperature plot can be seen in Fig. 3.8.4.2. The temperature dropped by approximately 10°C in the first minute after pouring began (6s pour). The mass loss rate over the same period dropped from 9.21g/min to 6.57g/min. The surface temperature dropped continuously until 10min, remained constant until 14 –15min, and then began to increase. At that point , only approximately 5g of the original 59.33g of pentane remained. The mass loss rate transitioned at the same time from ≈2g/min to 0 at 18min. A false-colour image of the pool at 5min showed an irregular pattern whose temperature-distribution was asymmetric, approximately 2° cooler on one side than on the other, possibly due to an undetected draft in the room. The margins of the cooled area extended ≈2cm beyond the dimensions of the wetted area of the carpet, indicating that heat was being drawn from adjoining areas of carpet.

Carpet C: Unbacked residential-grade nylon carpet, 11mm deep plush pile.

A pour of 100ml n-pentane produced an oval pool 9 x 10cm in size, 0.006m^2 in area. The surface temperature plot can be seen in Fig. 3.8.4.3. The temperature dropped by approximately 10°C in the first minute after pouring began (6s pour). (Delayed start on the data system cut off the first 30s of data.) The mass loss rate over the same period dropped from 3.9g/min to 3.6g/min. The surface temperature at the centre of the pool dropped continuously until 9 –11min, and then began to increase. At that point, approximately 50% of the original pentane remained in the carpet. The mass loss rate continued to decrease steadily over the course of the run, ending at 0.5g/min. The surface temperature nearer the edge of the pattern

Test 147 - 100 ml Pentane on Carpet B

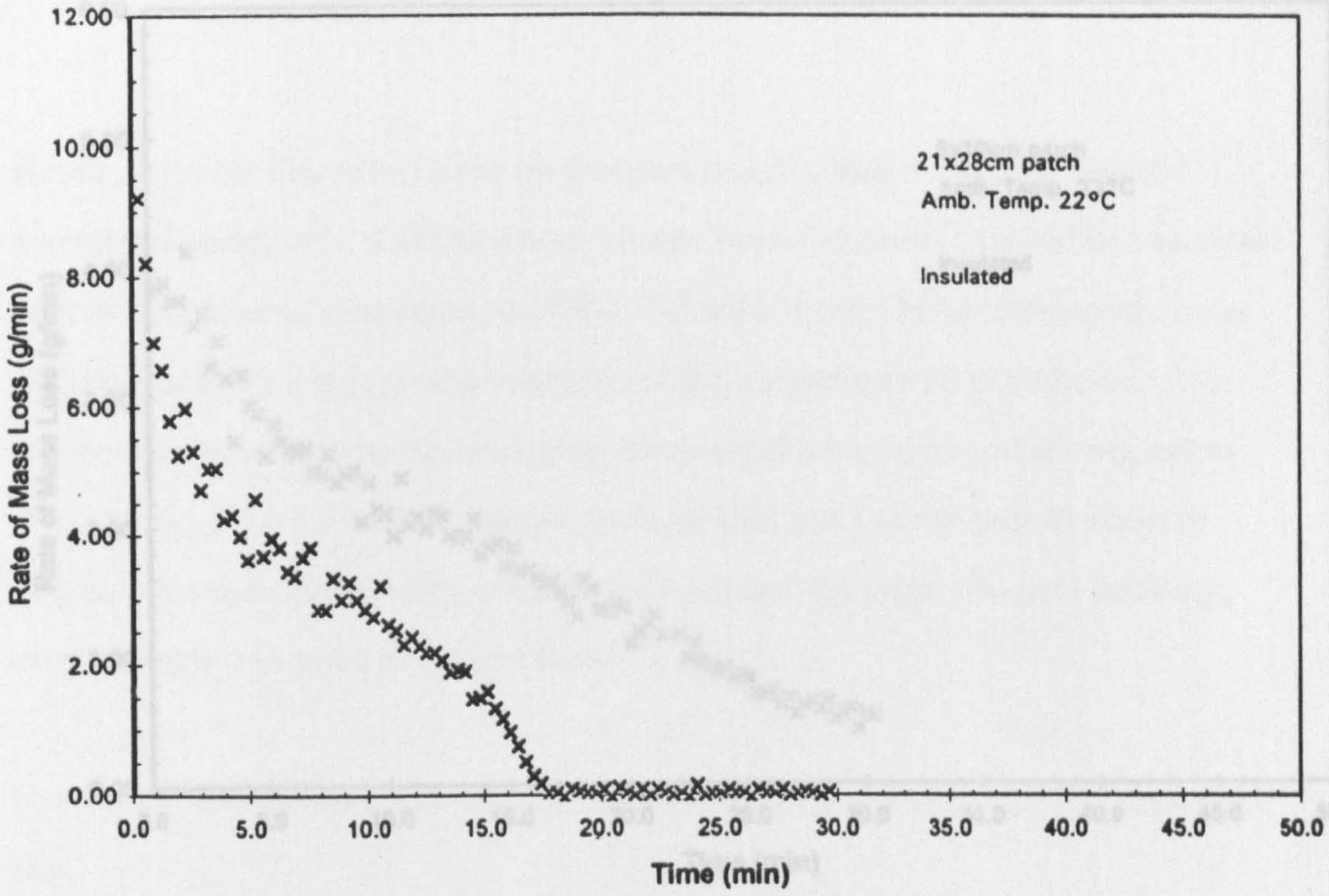

JDH147 100 ml PENTANE ON CARPET B

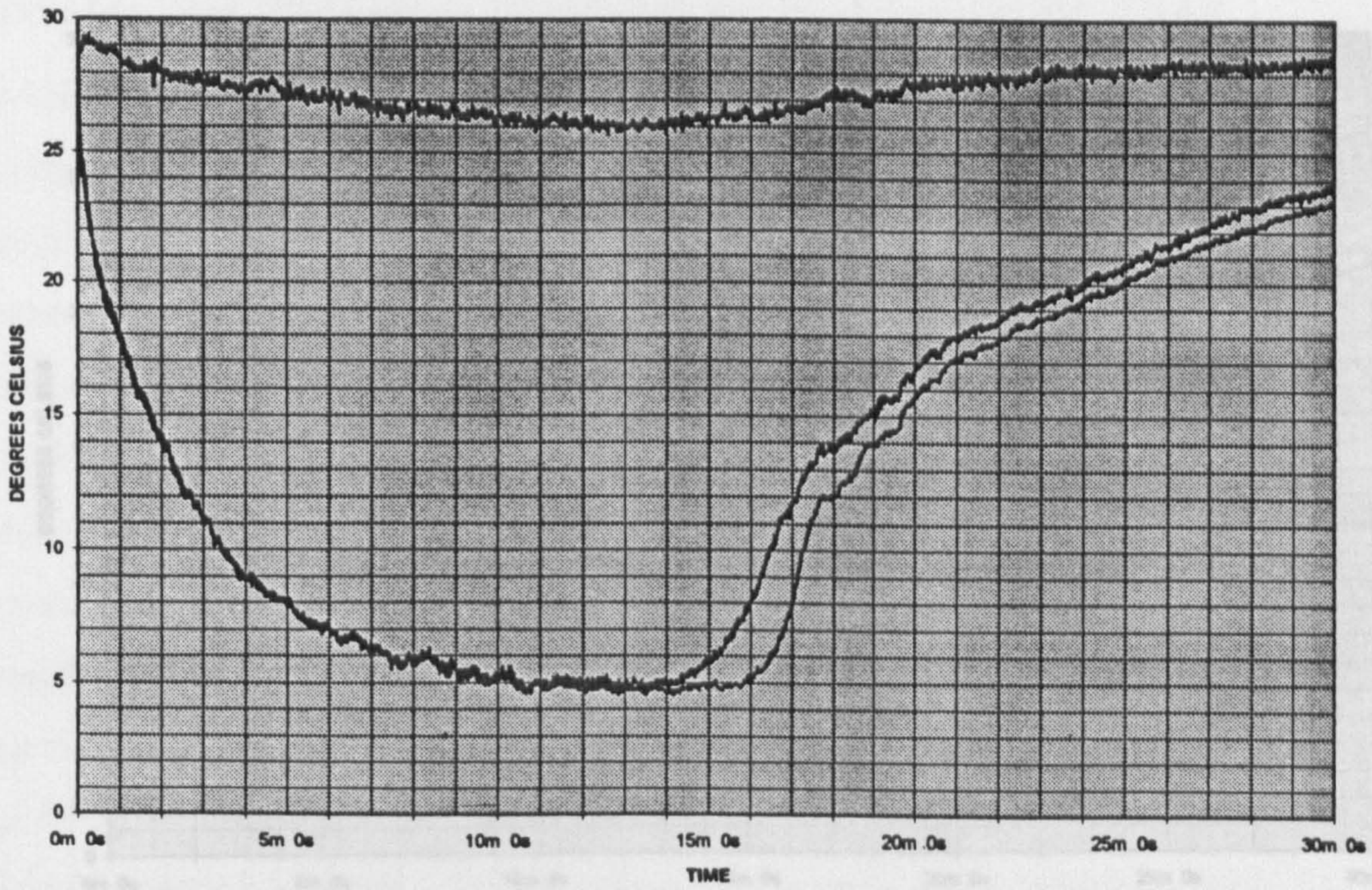

Fig. 3.8.4.2: Surface temperature (via Inframetrics system) v. time for n-pentane evaporating from a "free" pool on a 4mm pile carpet (wetted area 0.21 x 0.28m in size) and accompanying mass loss plot. Minimum temperature is 21°C below ambient, then begins to rise at 15min as the mass loss rate drops dramatically towards zero as the pentane is exhausted.

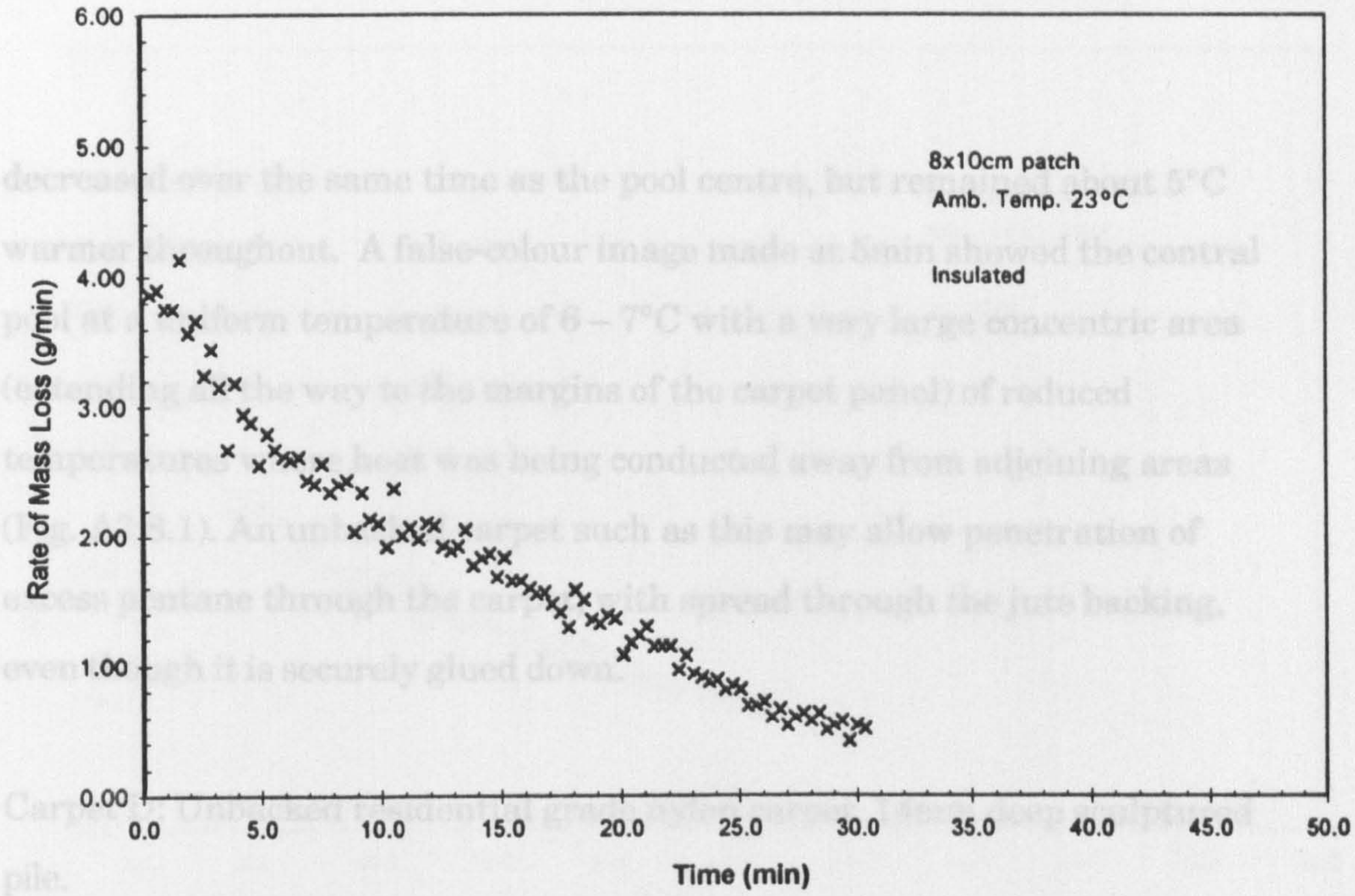

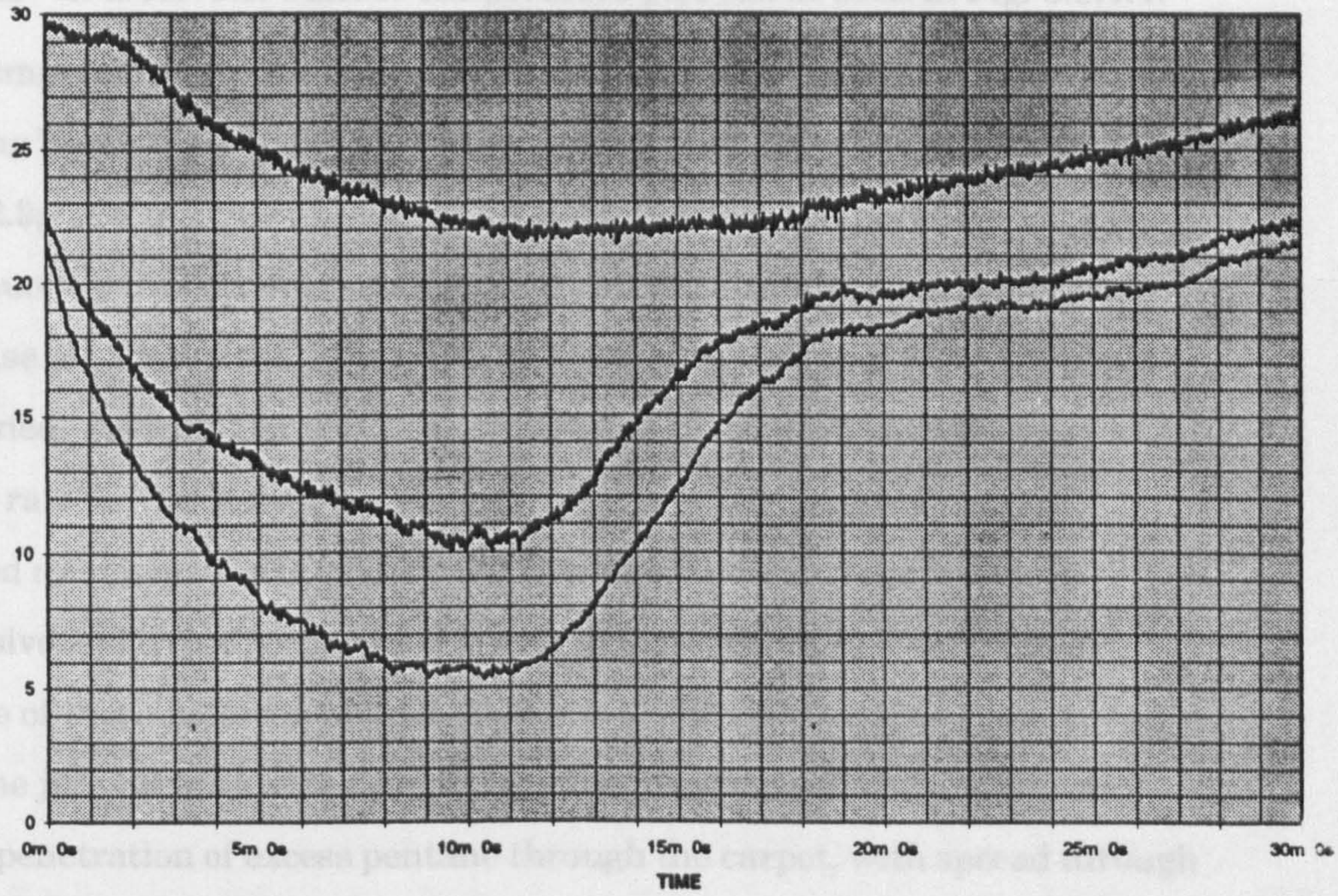

Fig. 3.8.4.3: Surface temperature (via Inframetrics system) v. time for n-pentane evaporating from a "free" pool on a 14mm pile carpet (wetted area 0.1m in diameter) and accompanying mass loss plot. The minimum temperature is 24°C below ambient, then begins to rise at 10min as the mass loss rate drops dramatically towards zero as the pentane is exhausted. Reference temperature decreased because of cold vapors accumulating on benchtop.

decreased over the same time as the pool centre, but remained about 5°C warmer throughout. A false-colour image made at 5min showed the central pool at a uniform temperature of 6 – 7°C with a very large concentric area (extending all the way to the margins of the carpet panel) of reduced temperatures where heat was being conducted away from adjoining areas (Fig. A3.8.1). An unbacked carpet such as this may allow penetration of excess pentane through the carpet, with spread through the jute backing, even though it is securely glued down.

Carpet D: Unbacked residential grade nylon carpet, 14mm deep sculptured pile.

A pour of 100ml of n-pentane produced an oval pool, 8 x 10cm in size, 0.005m^2 in area. The surface temperature plot can be seen in Fig. 3.8.4.4. The temperature dropped by approximately 12°C in the first minute after pouring began (3.5s pour). The mass loss rate over the same period dropped from 2.9g/min to 2.6g/min. The central-pool surface temperature dropped continuously until 4min, remained constant until 14min, and then began to increase. At that point, approximately 50% of the original 62.68g of pentane remained. As with Carpet C, the mass loss rate continued to decrease at a linear rate for the duration of the run. A false-colour image of the pool showed a central area of uniform 12°C temperature surrounded by an extensive and irregular pattern of reduced temperatures. The irregular nature of these patterns indicate that some of the pentane had penetrated into the jute backing of the carpet. An unbacked carpet such as this may allow penetration of excess pentane through the carpet, with spread through the jute backing, even though it is securely glued down.

Test 149 - 100 ml Pentane on Carpet D

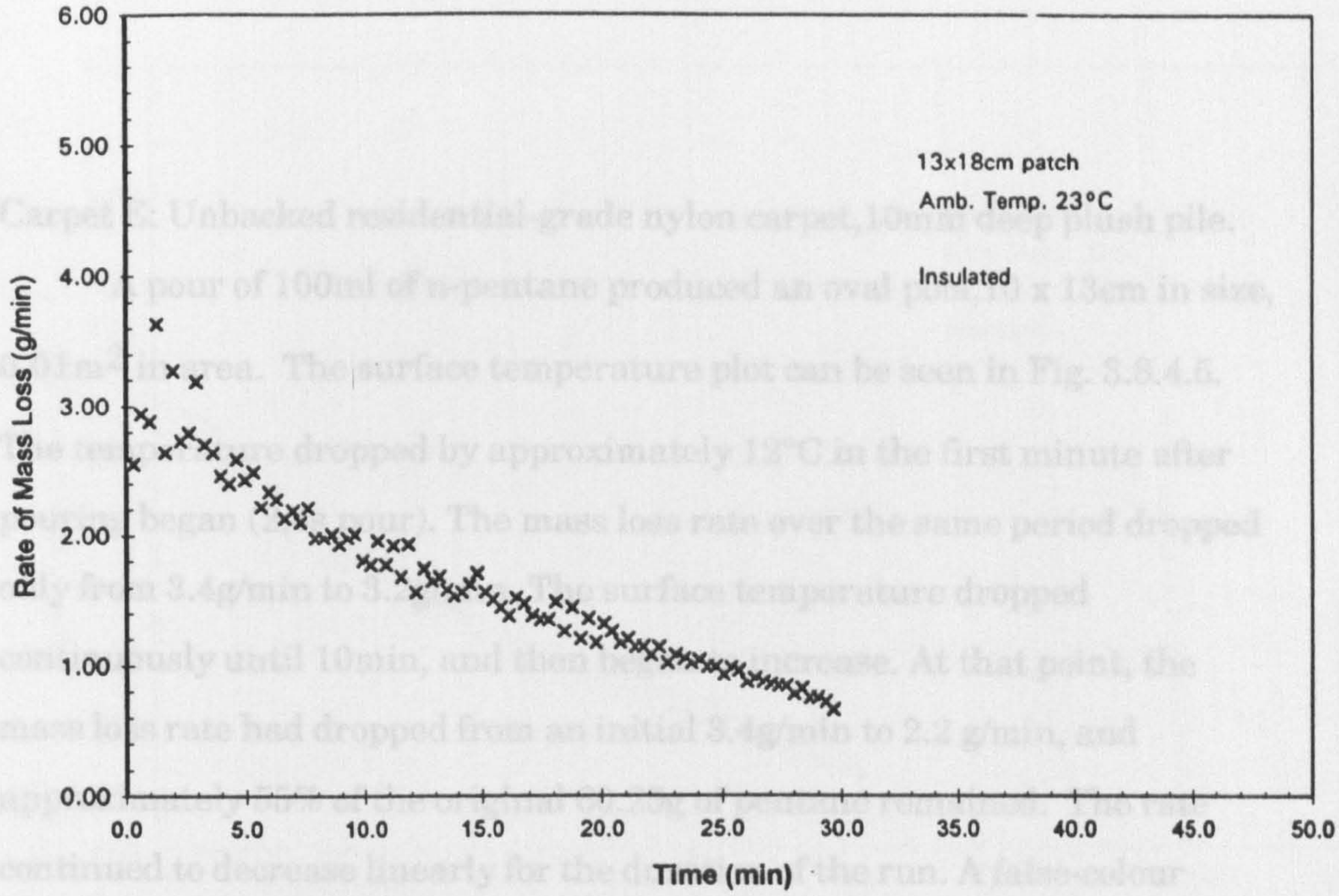

JDH149 100 ml PENTANE ON CARPET D

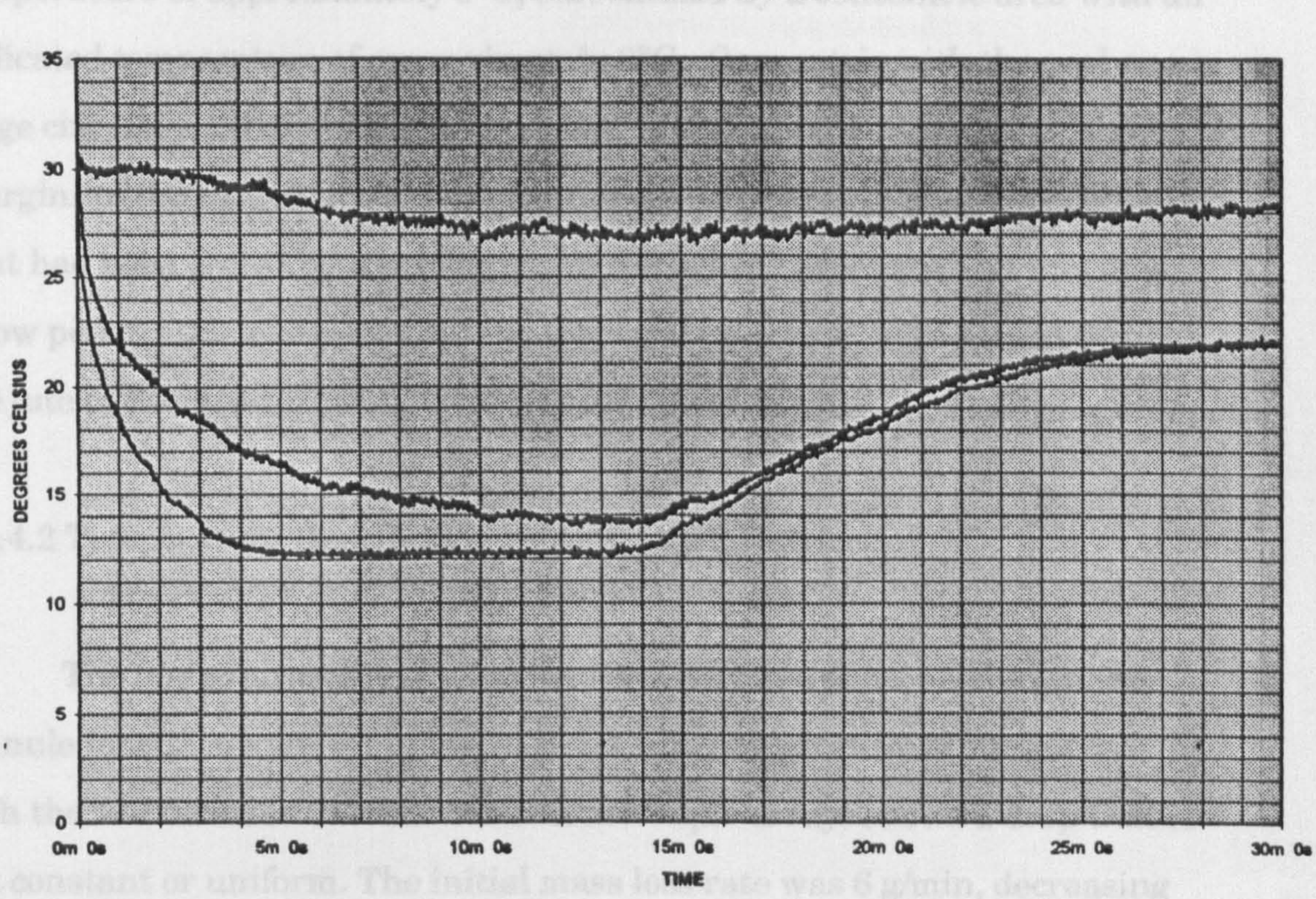

Fig. 3.8.4.4: Surface temperature (via Inframetrics system) v. time for n- pentane evaporating from a "free" pool on a 10mm pile carpet (wetted area 0.13 x 0.18m in size) and accompanying mass loss plot. The temperature begins to rise at 14min as the mass loss rate drops uniformly towards zero as the pentane is exhausted.

Carpet E: Unbacked residential-grade nylon carpet,10mm deep plush pile.

A pour of 100ml of n-pentane produced an oval pool,10 x 13cm in size, 0.01m^2 in area. The surface temperature plot can be seen in Fig. 3.8.4.5. The temperature dropped by approximately 12°C in the first minute after pouring began (2.4s pour). The mass loss rate over the same period dropped only from 3.4g/min to 3.2g/min. The surface temperature dropped continuously until 10min, and then began to increase. At that point, the mass loss rate had dropped from an initial 3.4g/min to 2.2 g/min, and approximately 55% of the original 60.25g of pentane remained. The rate continued to decrease linearly for the duration of the run. A false-colour image made at 5min shows a small central area with an average temperature of approximately 9°C, surrounded by a concentric area with an indicated temperature of approximately 8°C. Concentric with the pool was a large circular area of reduced temperatures extending all the way to the margins of the carpet panel. This indicated a large area of adjoining carpet that had been cooled by conduction. An unbacked carpet such as this may allow penetration of excess pentane through the carpet, with spread through the jute backing, even though it is securely glued down.

3.8.4.2 Temperature Distributions within other Matrices

The temperatures on the surface and within a pentane/aluminium granule matrix are shown in Fig. 3.8.4.6. The temperature of the surface (by both the IR trace and TC#3 of the thermocouple array) shows a drop that is not constant or uniform. The initial mass loss rate was 6 g/min, decreasing rapidly to ≈3g/min between 3 and 4min. The significant differences between

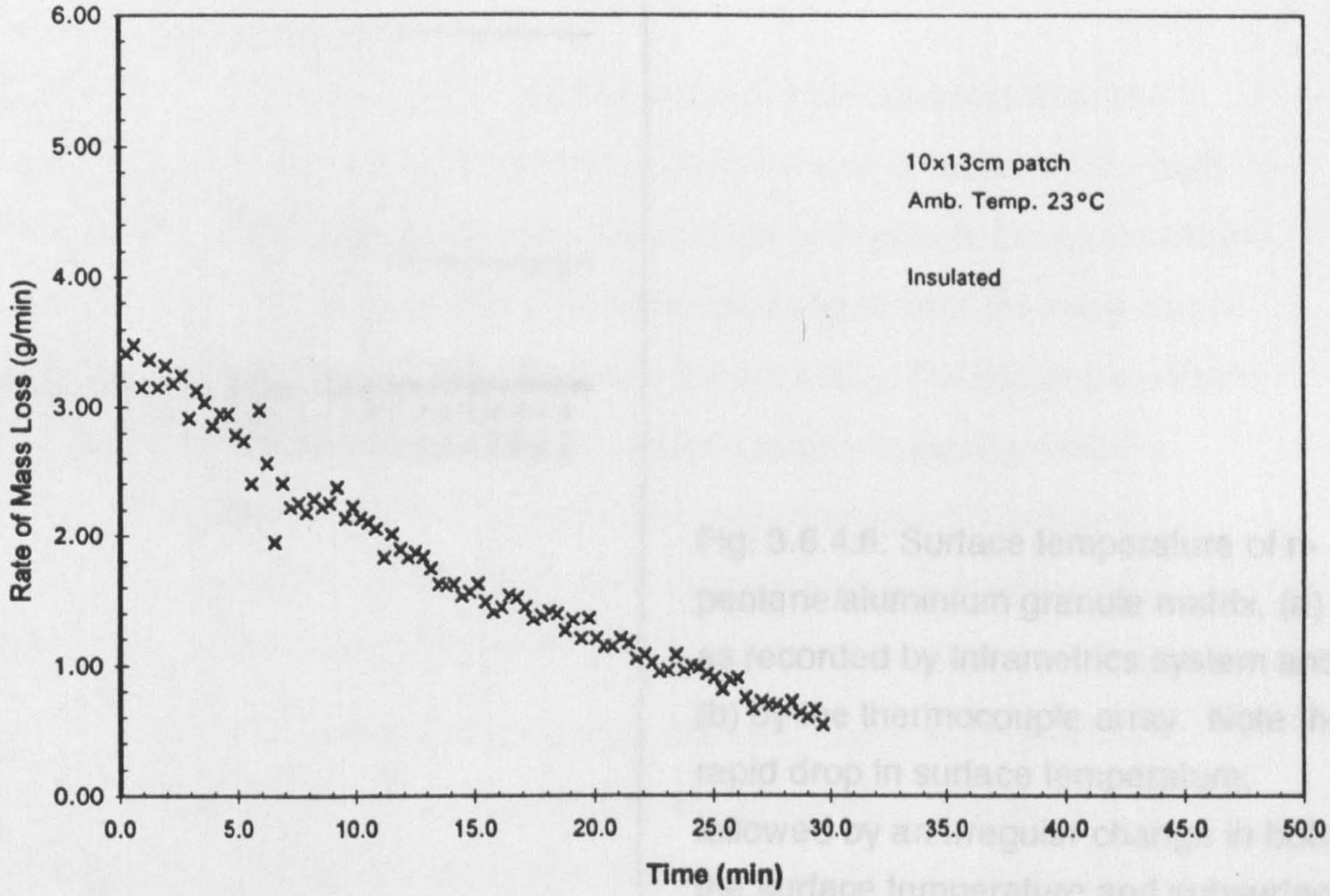

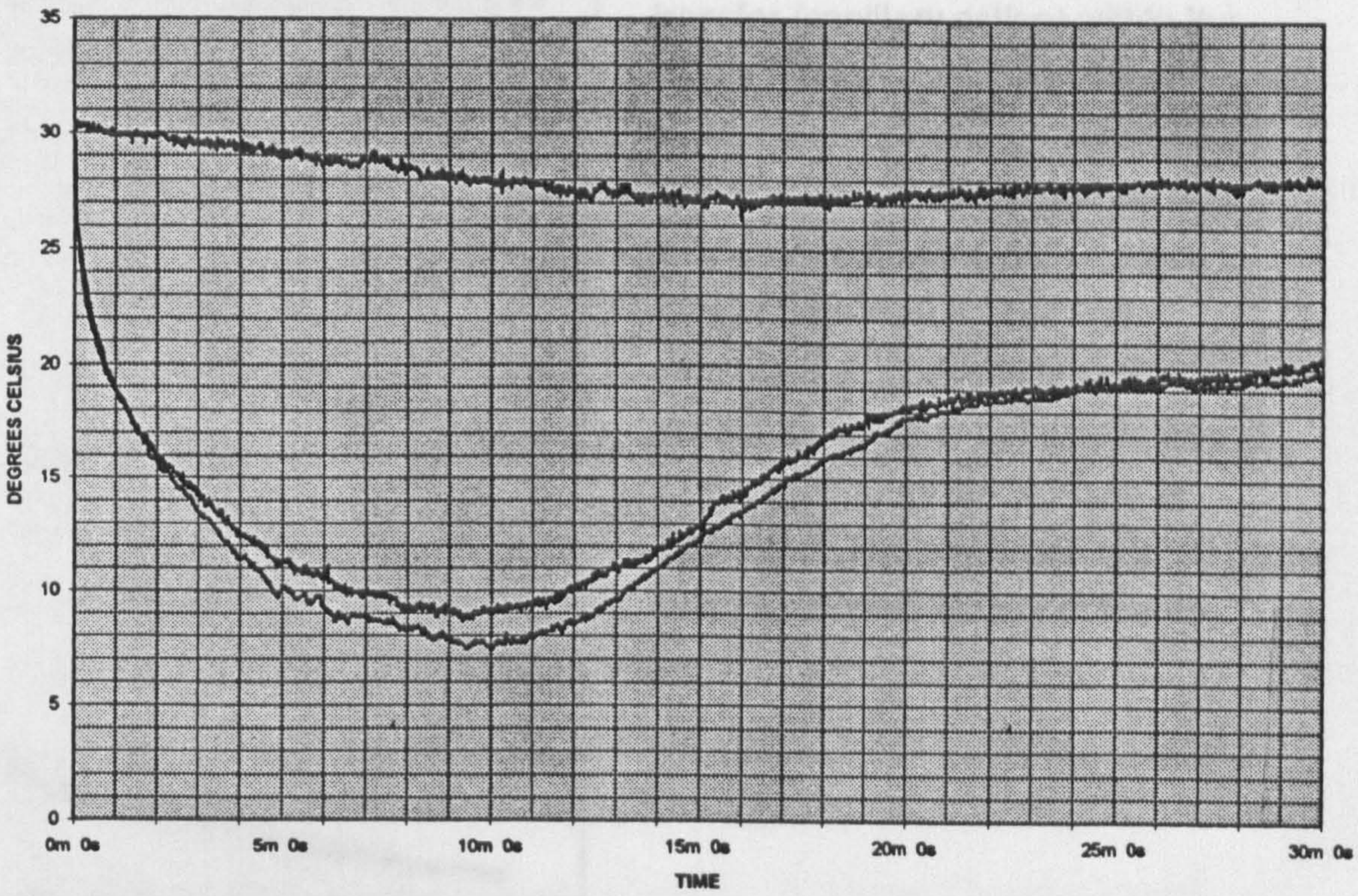

Fig. 3.8.4.5: Surface temperature (via Inframetrics system) v. time for n-pentane evaporating from a "free" pool on a 10mm pile carpet (wetted area 0.1 x 0.13m in size) and accompanying mass loss plot. The temperature begins to rise at 10min as the mass loss rate drops steadily towards zero as the pentane is exhausted.

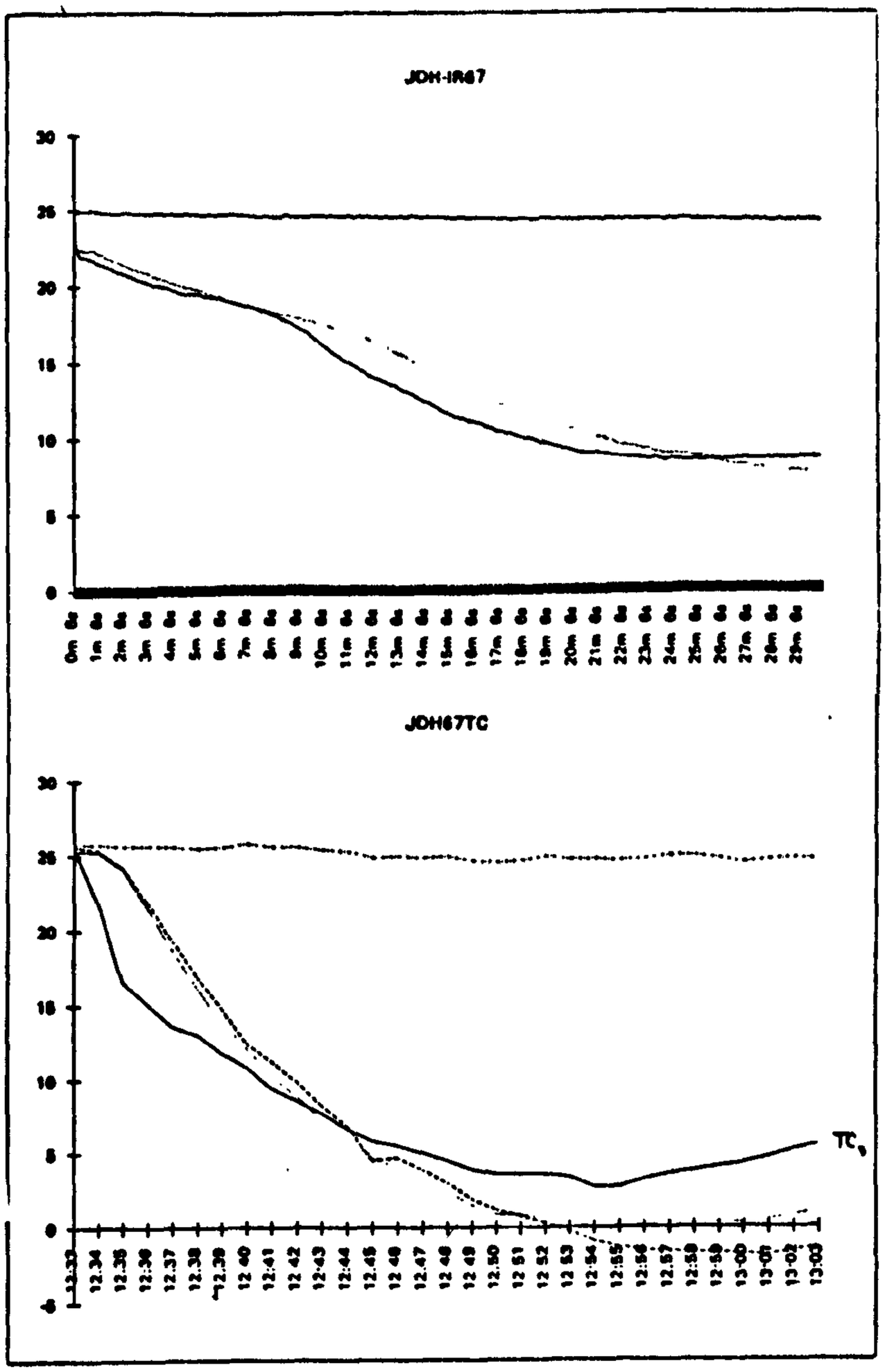

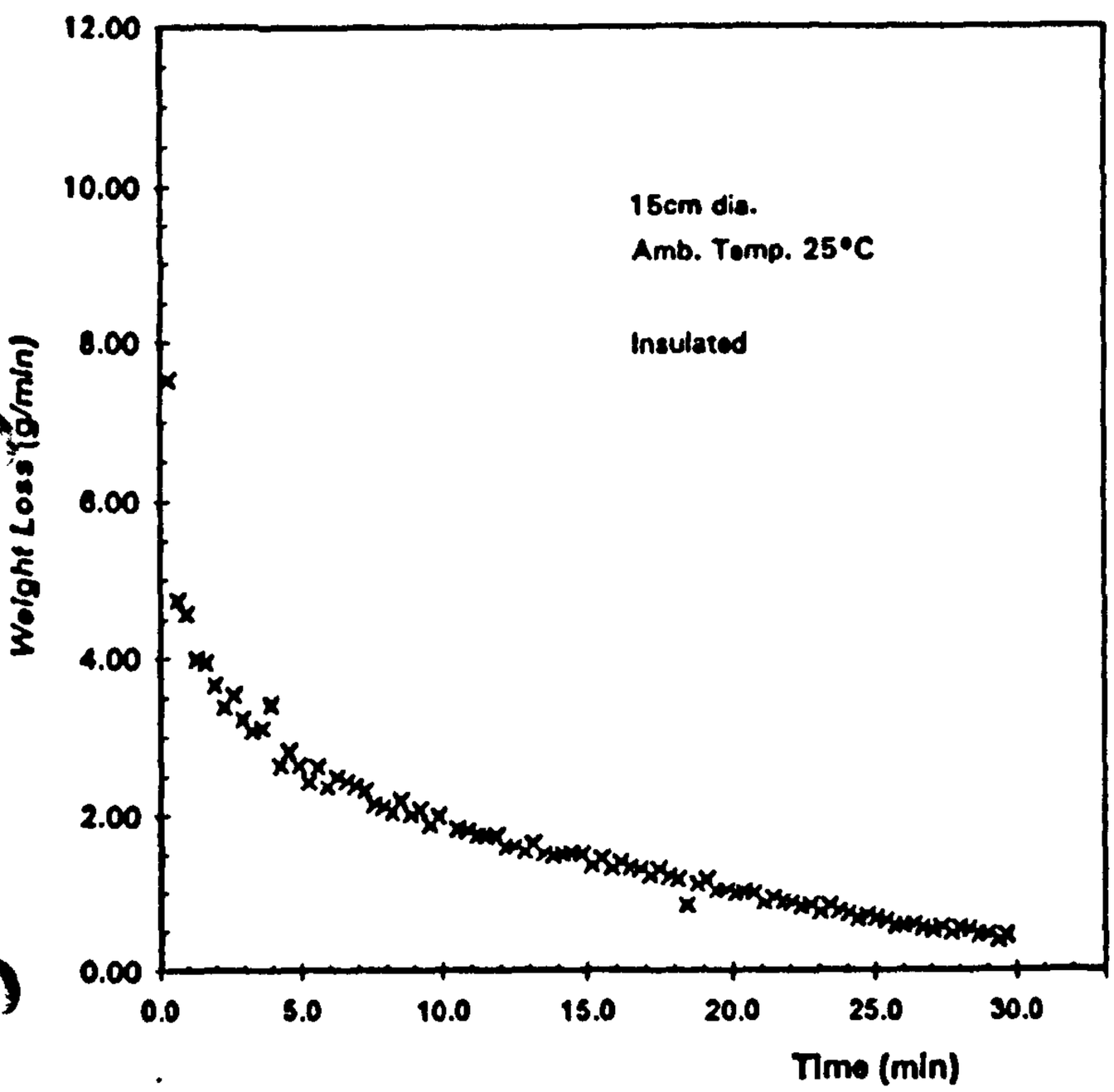

Fig. 3.8.4.6: Surface temperature of n-pentane/aluminium granule matrix, (a) as recorded by Inframetrics system and (b) by the thermocouple array. Note the rapid drop in surface temperature, followed by an irregular change in both the surface temperature and subsurface temperatures. This suggests a complex interaction of thermal transfer and mass transfer (capillary action) within the matrix. There is a substantial difference in temperature between surface and matrix at first. At 12min, the surface temperature and the bulk matrix temperature match. The bulk temperature continues to drop, but the surface temperature begins to rise at 21min (12:54) as the pentane is exhausted. The mass loss rate (c) drops steadily over the course of the run

surface and subsurface thermocouples indicate that heat lost from the surface is being replaced by heat from within the matrix (aided by the high conductivity of the aluminium). As the pentane is depleted, the temperature begins to rise, first at the surface where sensible heat from the room can be absorbed most readily, followed by areas deeper within the substrate (which are insulated from the room). The irregular changes suggest a complex interaction between thermal transfer and mass transfer via capillarity within this matrix. The mass loss rate decreases steadily, leveling off at 25min at ≈0.5g/min and a T_{sur} of 10°C.

A physically similar matrix with different thermal properties, pentane/sand, yields a thermal performance as shown in Fig. 3.8.4.7. Here, the behaviour is initially very similar to that of the aluminium granule matrix, with a very sharp decline in surface temperature (seen in both IR and thermocouple systems). This corresponds to a maximum mass loss rate of 5g/min. Due to the low thermal conductivity of sand (compared to that of aluminium) (see Table 3.8.4), there is a distinct lag in temperature loss from the deeper regions of the matrix. Over time, the bulk temperature approaches that of the surface just as it reaches its minimum and begins to rise (at ≈26min). At that time, there is still 18g (of the original 65g) of pentane present and evaporation is continuing to drop below 0.8g/min.

Concrete: The Inframetrics system was used to monitor the temperature of a smooth, unsealed concrete slab when 10ml of n-pentane was poured onto the slab. There was complete absorption into the concrete within 10s of completing the pour. In each case, the temperature at the centre of the pour dropped by 3 – 4°C within 10s, with a minimum temperature 5°C below ambient reached in 30s (20s in the test when an exhaust hood was left operating during the test). A typical ThermaGram®

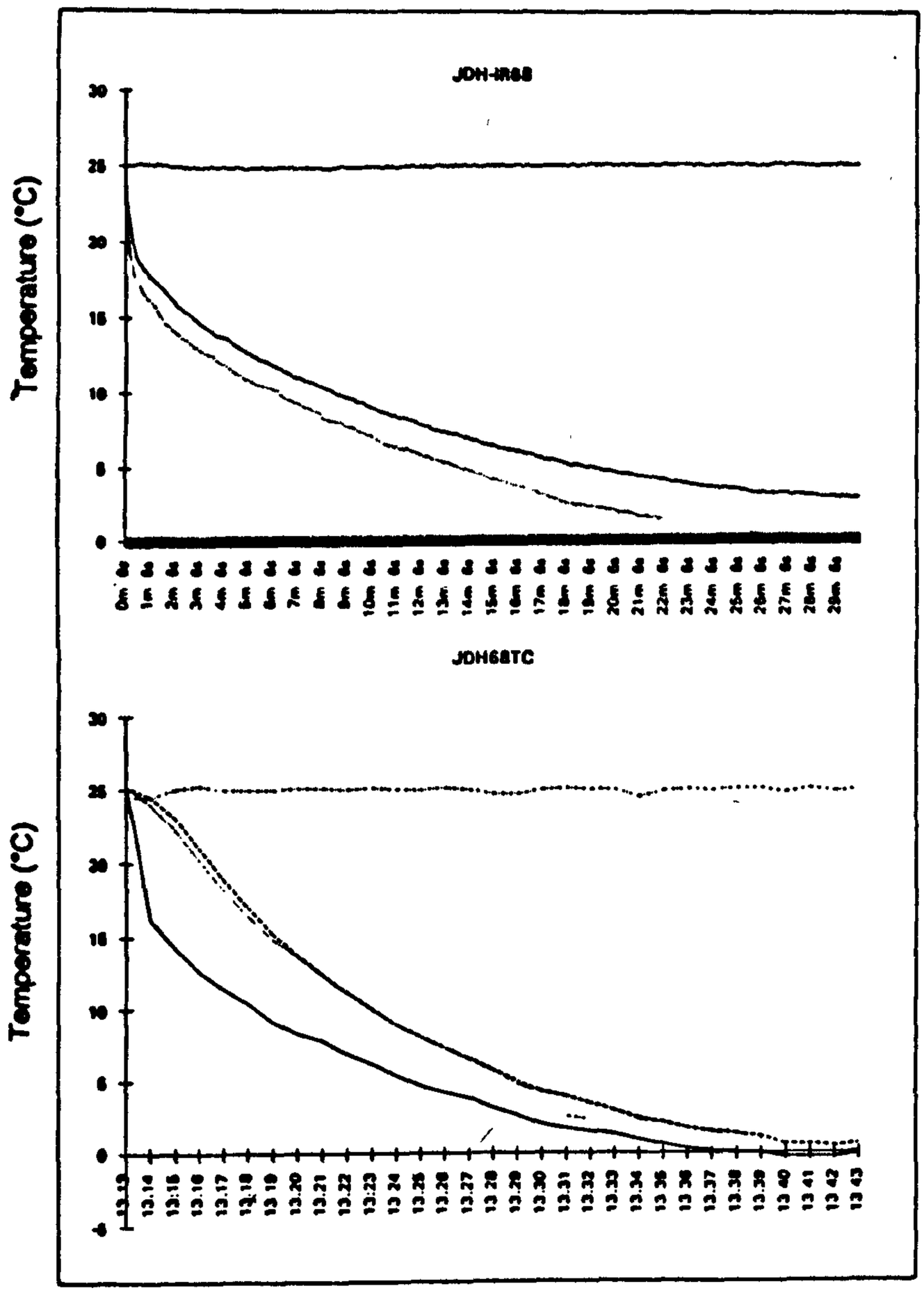

Fig. 3.8.4.7: Surface temperature of n-pentane/sand matrix, as recorded by (a) the Inframetrics system and (b) the thermocouple array. Note the same rapid drop in surface temperature, followed by a drop in the subsurface temperatures. The initial drop in surface temperatureis very similar to that for aluminium, but the temperature at the surface remains below that of the bulk for the entire run. This is due to the lower thermal conductivity for sand. The mass loss plot is almost identical to that for aluminium.

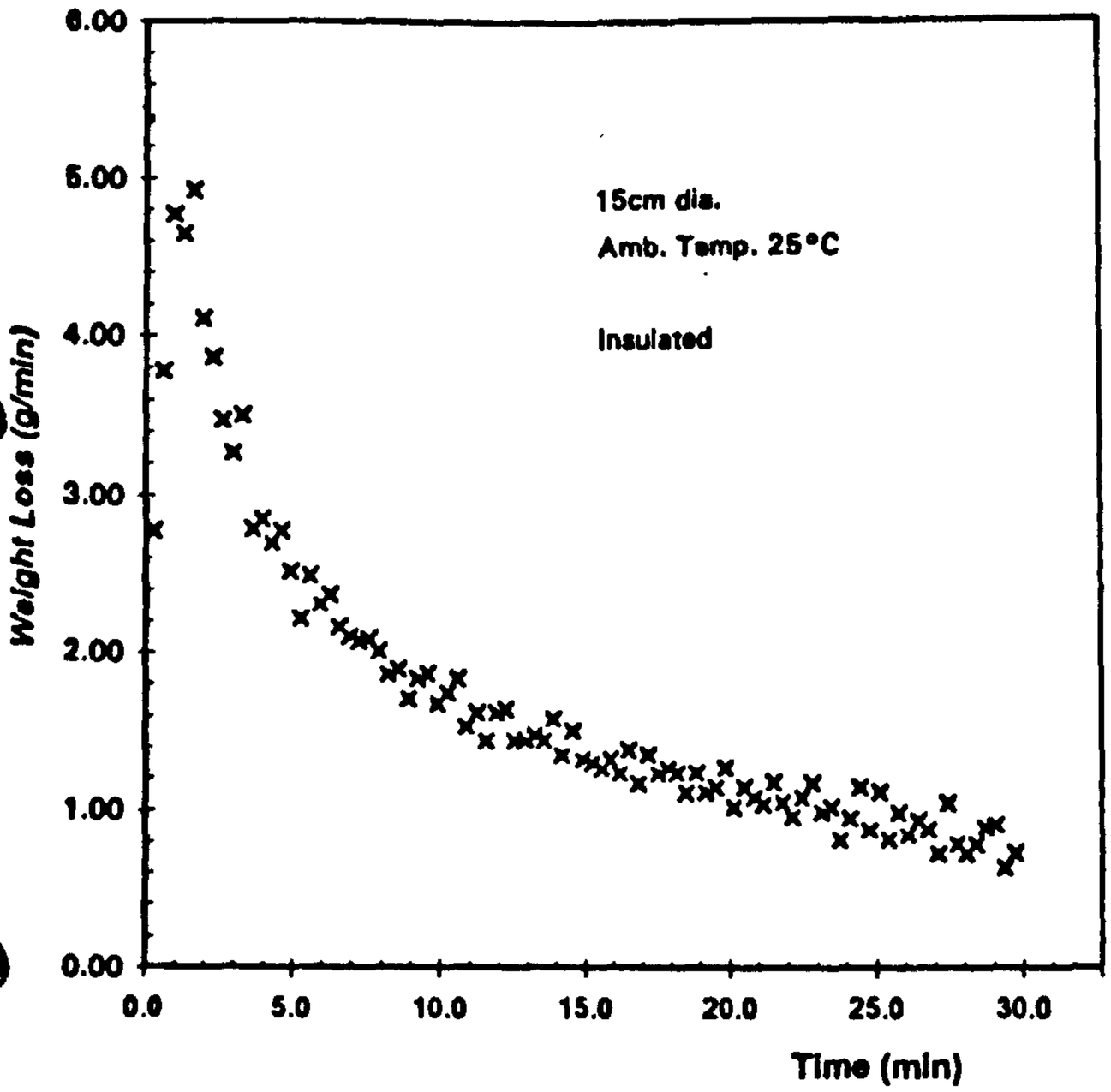

Table 3.8.4: Thermal Conductivities of Common Materials

Material	w/m. K	Material	w/m.K (@300K)
Sand (dry)	0.329	----	
Wallboard	0.048	----	
Linen	0.055	----	
Wool felt	0.052	----	
Cotton wool	0.042	----	
Gypsum (plaster)	0.433	Gypsum	0.48
Window glass	0.52 - 0.76	Plate Glass	0.76
Borosilicate	1.09	Pyrex	1.1
Mineral wool	0.042	----	
Animal wool	0.036	----	
----		Aluminum	273
----		Urethane	0.034
----		Silica	1.34
----		Nylon 66	0.4
----		Polyethylene	0.35 - 0.4
----		Air	0.026
[Perry, p.3-260]		[Drysdale, pp.4,36]	

plot is shown in Fig.3.8.4.8. In each test, the wetted area was completely dissipated by 1min, by which time the surface temperature had returned to within 1°C of ambient.

Vinyl Tile on Concrete: A similar test involving the pouring of 25ml of n-pentane onto a vinyl tile floor, resulted in a decrease of 8°C in 30s, followed by an immediate return to near-ambient temperature within 2min of pouring, as in Fig.3.8.4.9. This was accompanied by observation that the pool of liquid occupied an area of $0.1m^2$.

3.9 Evaporation of Pure Compounds v. Complex Mixtures

Two brands of unleaded, regular-grade petrol (automotive gasoline) and three different camping fuels were obtained from retail sources for evaporation tests. Each fuel was characterized by gas chromatographic (GC) analysis. Aliquots of each were injected onto a Hewlett-Packard 5890 gas chromatograph using a 15m x 0.1mm DB-1 (non-polar methyl silicone) capillary column with flame ionization detection (FID). Representative chromatograms are shown in Figs.3.9.1 – 3.9.3. The peaks were quantified by using the H-P data system to calculate the peak areas of all significant peaks (by integration). A sample quantitative print-out for a petrol analysis is shown in Fig.3.9.4, and one for a camping fuel is shown in Fig. 3.9.5. The peak areas over the retention time span appropriate for the compound, i.e., 0 – 5min for petrol and 0 – 4min for camping fuel, were then totalled. The peaks corresponding to certain key compounds were identified by their relative retention times against reference compounds and mixtures and the peak areas corresponding to those key compounds were normalized against the peak total. (A total of 60 – 65 peaks in the 0 – 4 min range were selected

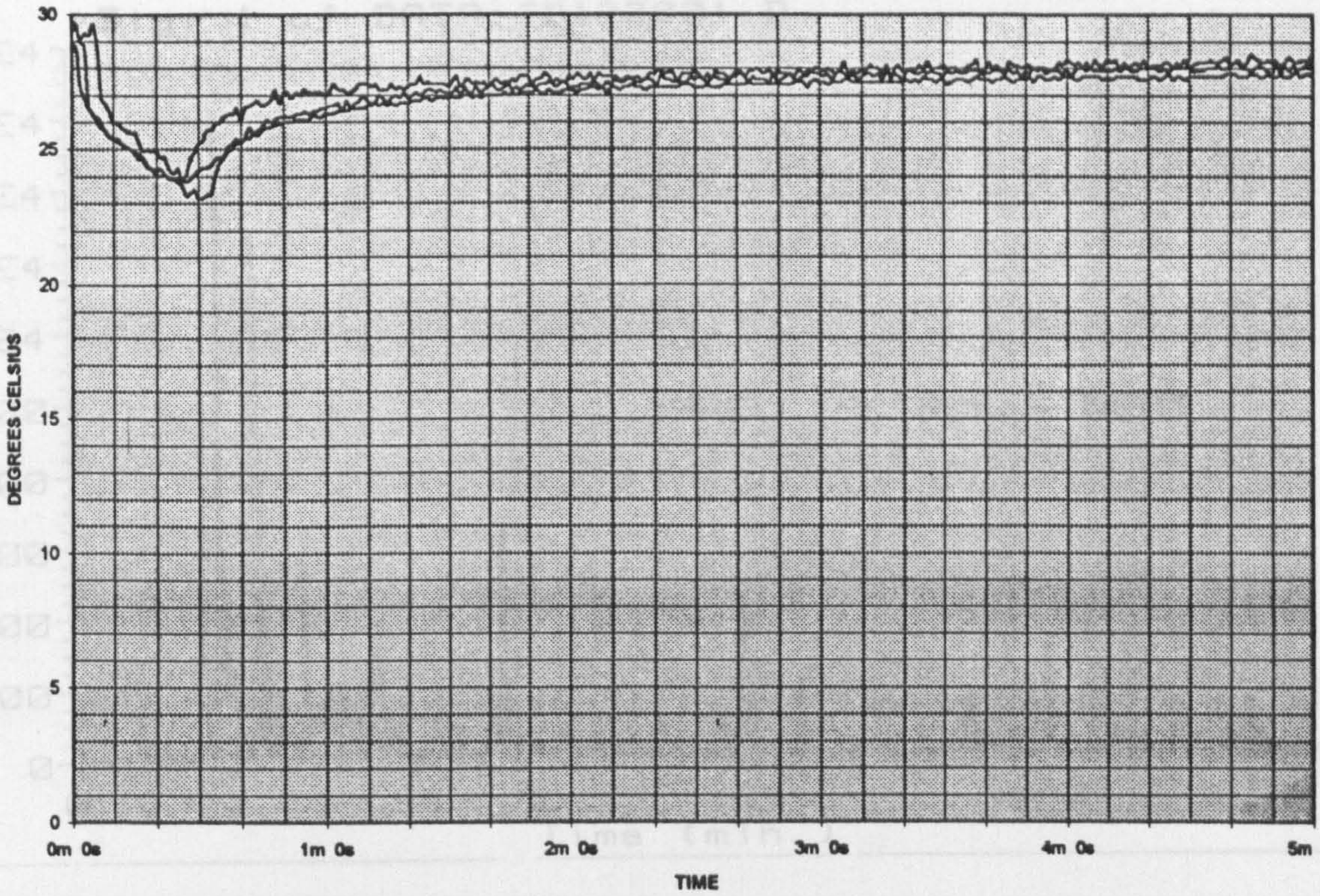

Fig. 3.8.4.8: Plot of surface temperature (by Inframetrics imaging) for a small (10ml) pour of n-pentane on concrete. There is the same rapid drop in temperature (6°C in 30s) followed by a rapid return to ambient temperature as the pentane is rapidly evaporated.

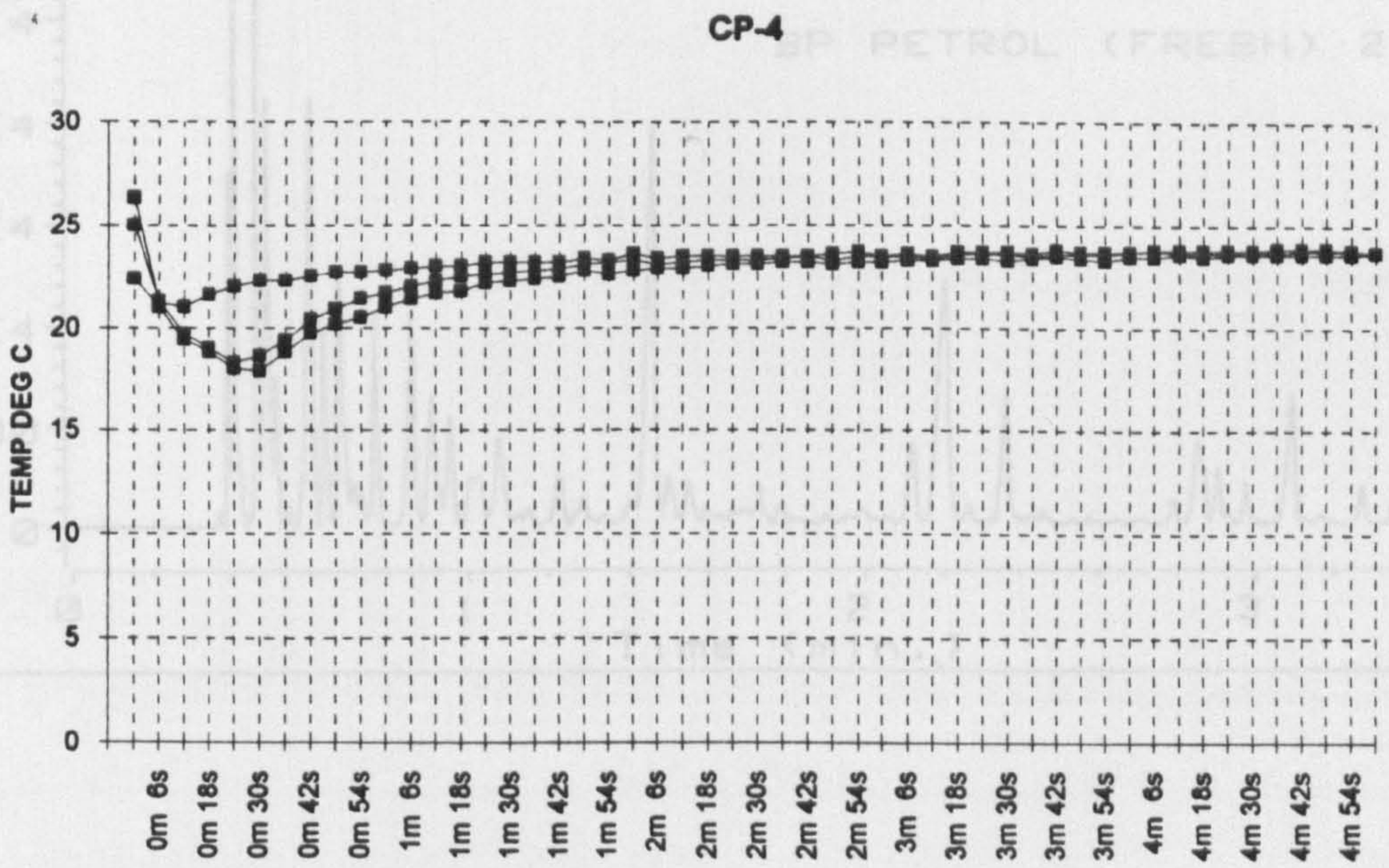

Fig. 3.8.4.9: Plot of surface temperature (by Inframetrics imaging) for a small (25ml) pour of n-pentane on vinyl tile over concrete. The same rapid drop in temperature (7°C in 30s) is followed by a rapid return to ambient as the pentane is rapidly evaporated. All three sampling points were included in the pour area.

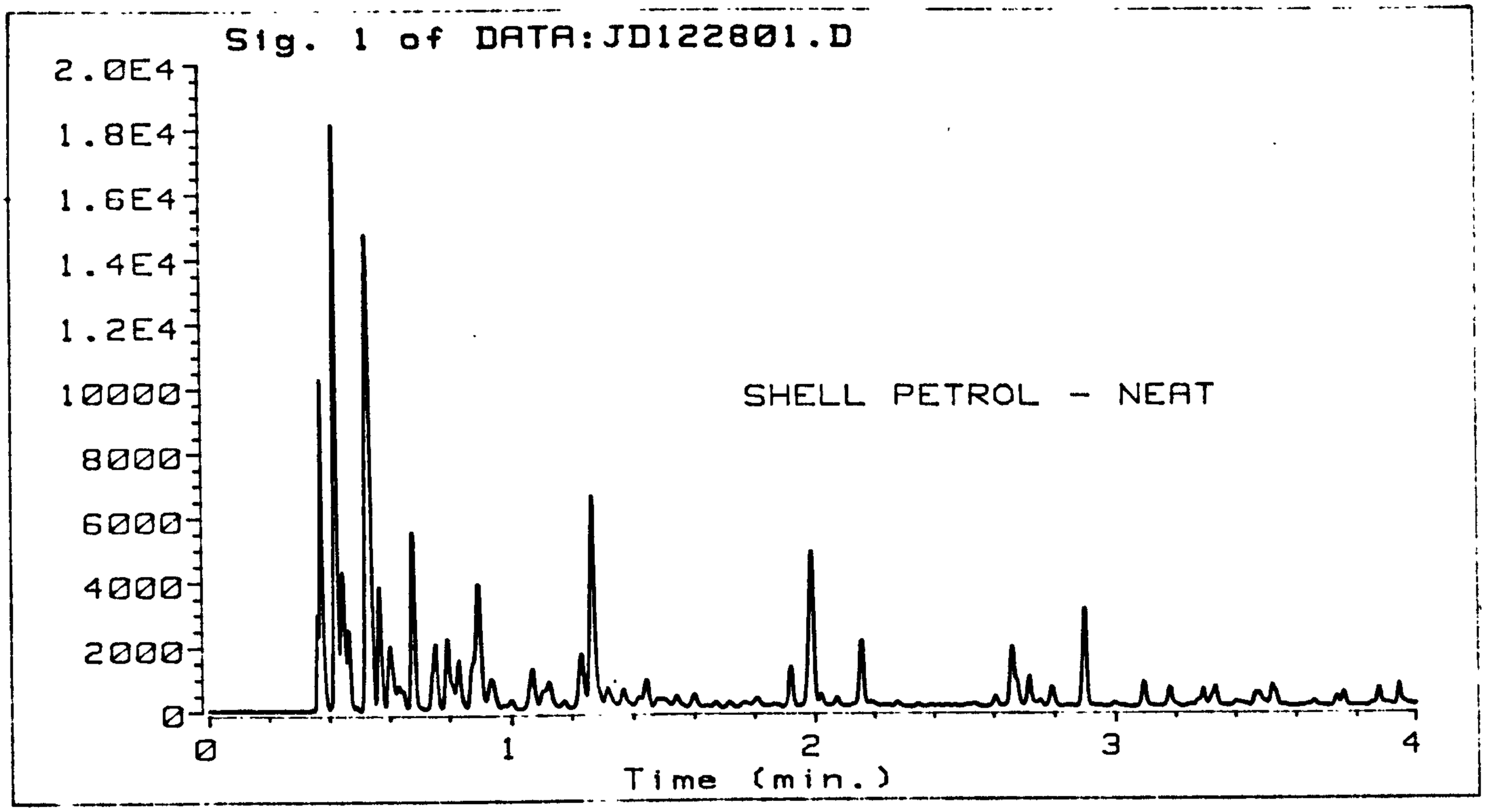

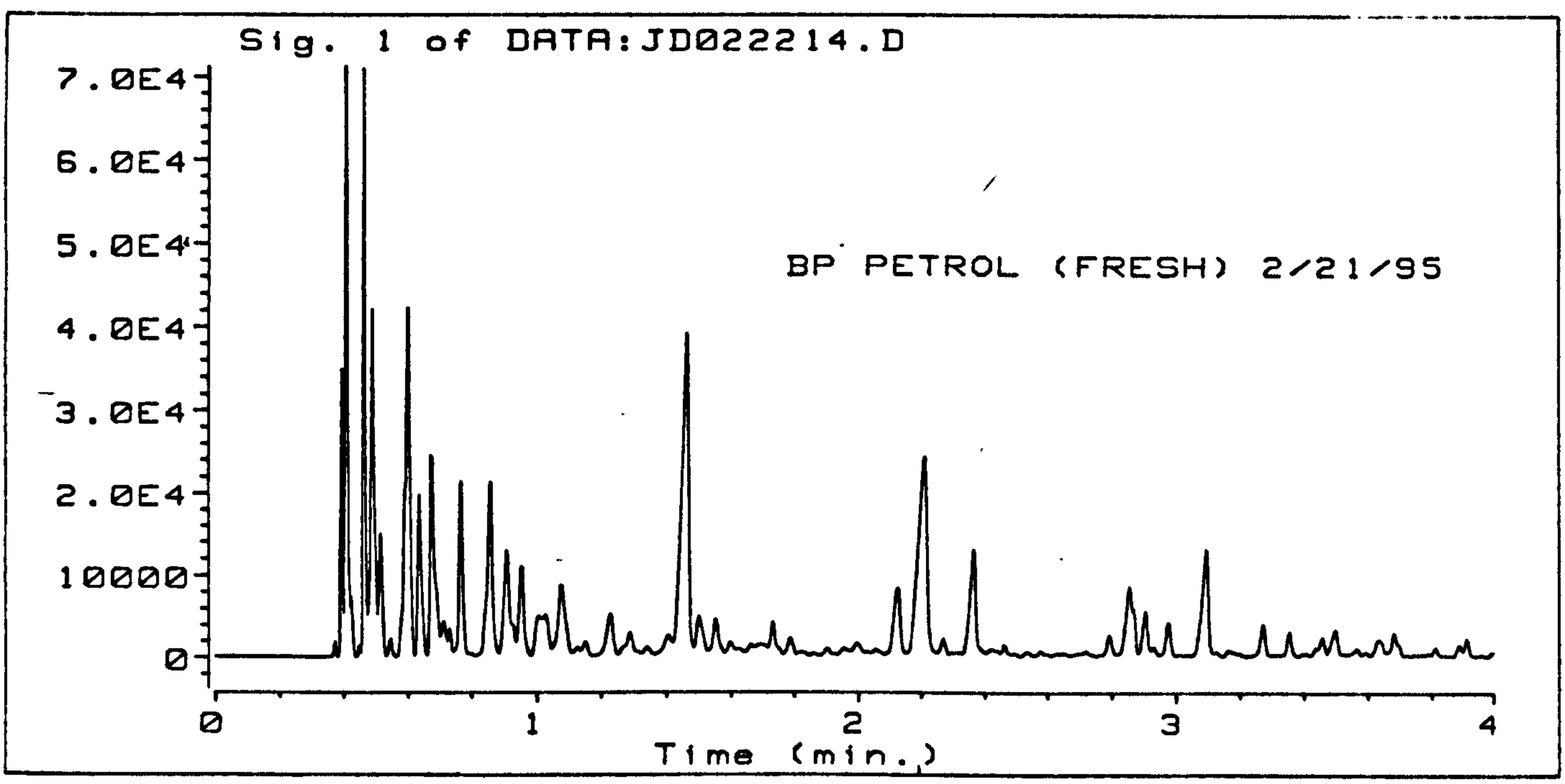

Fig. 3.9.1: Comparison of gas chromatograms of BP petrol and Shell petrol.

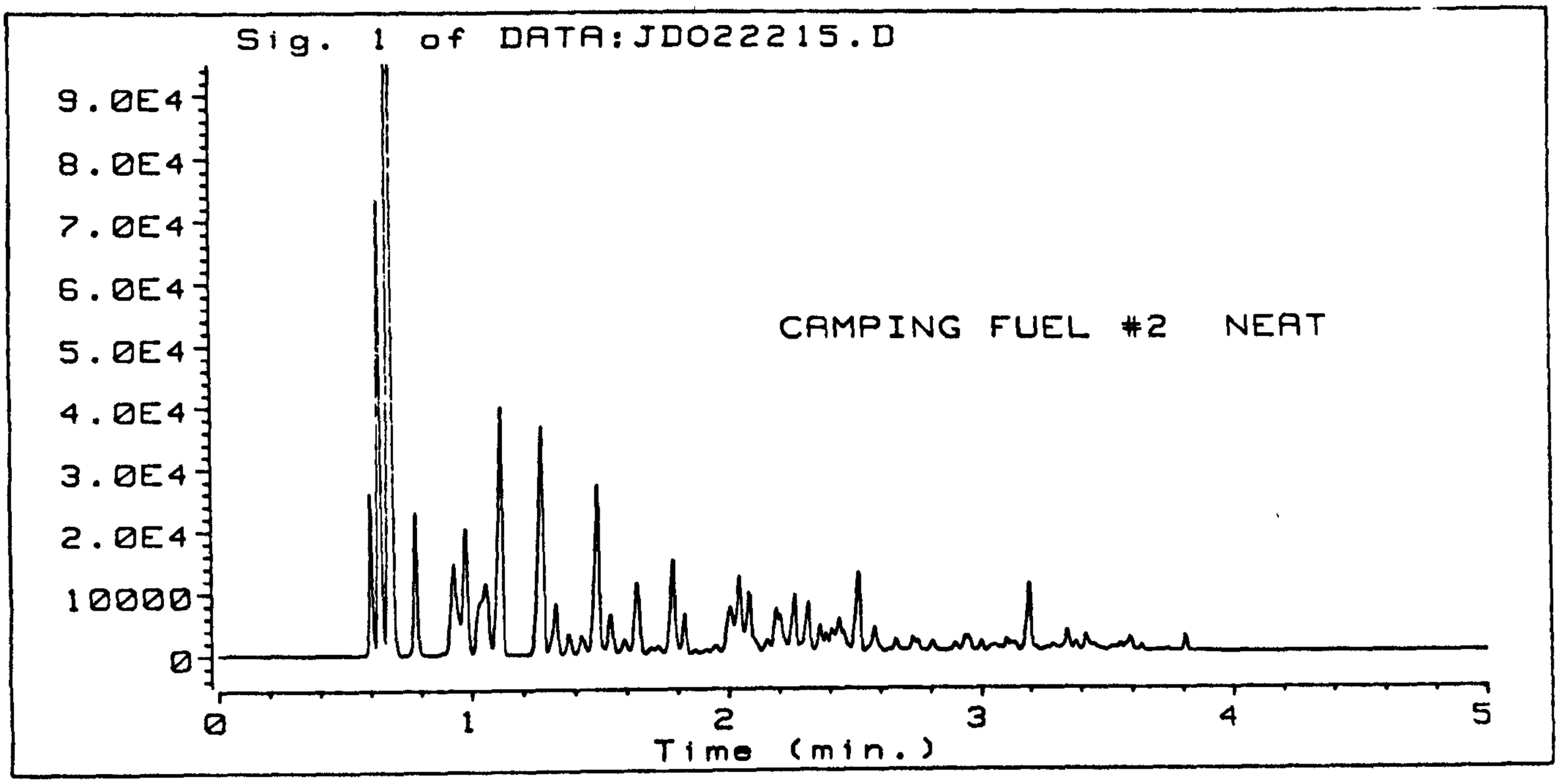

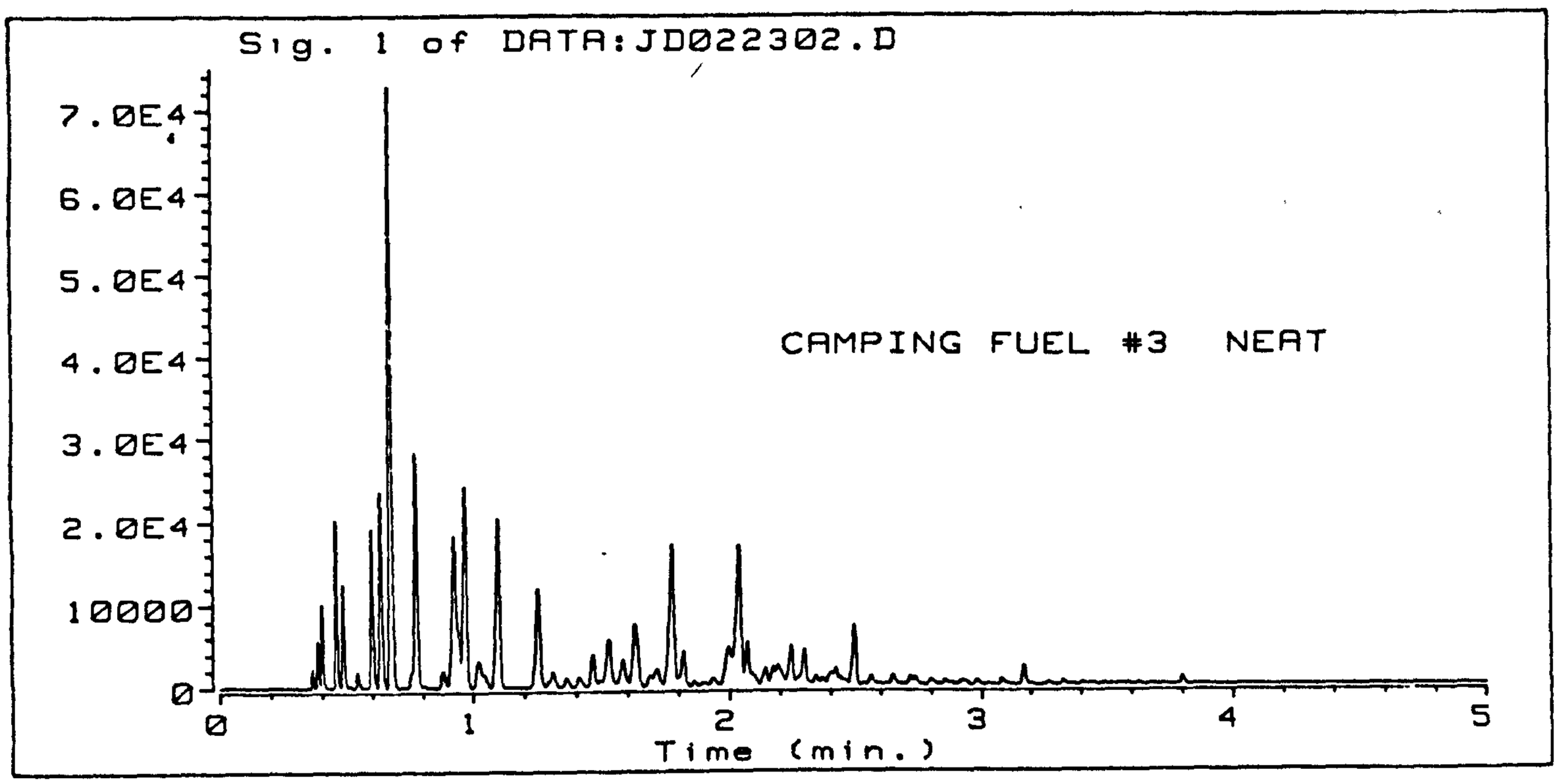

Fig. 3.9.2: Comparison of gas chromatograms of two camping fuels.

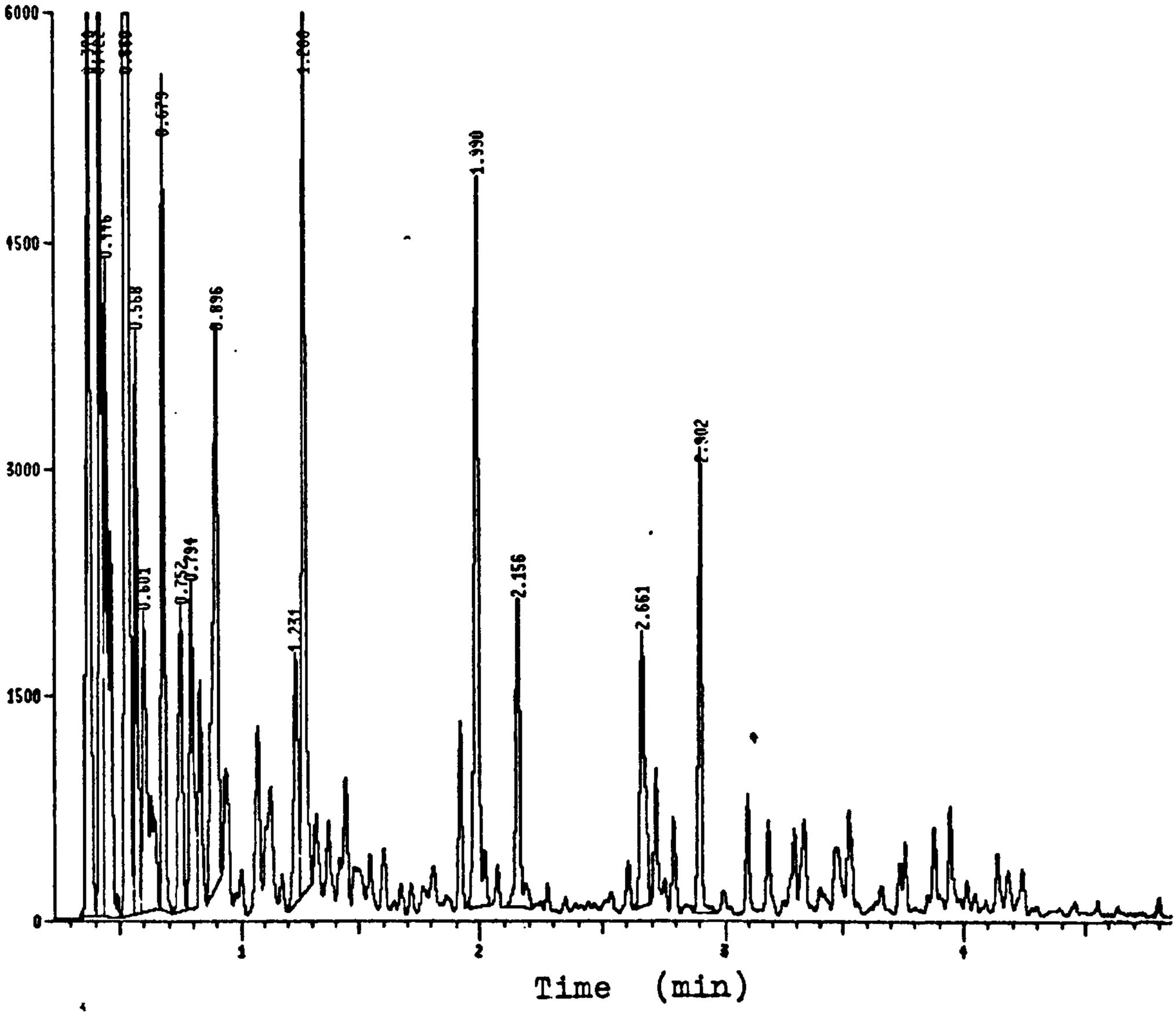

Fig. 3.9.3: Hewlett-Packard plot of petrol chromatogram showing assigned retention times and baselines added by quantitation program.

DATA:JD022214.D

Peak#	Ret Time	Type	Width	Area	Start Time	End Time
1	0.409	BV	0.019	588807	0.337	0.438
2	0.465	VV	0.009	389343	0.438	0.478
3	0.492	VV	0.017	329346	0.478	0.507
4	0.517	VV	0.012	111147	0.507	0.534
5	0.547	VV	0.011	14995	0.534	0.563
6	0.602	VV	0.015	439871	0.563	0.621
7	0.638	VV	0.014	166632	0.621	0.659
8	0.676	VV	0.018	252220	0.659	0.701
9	0.713	VV	0.027	73579	0.701	0.747
10	0.771	VV	0.020	183164	0.747	0.813
11	0.860	VV	0.018	233220	0.813	0.885
12	0.912	VV	0.021	183647	0.885	0.939
13	0.956	VV	0.016	117267	0.939	0.983
14	1.009	VV	0.026	74523	0.983	1.020
15	1.030	VV	0.020	64251	1.020	1.050
16	1.080	VV	0.026	145823	1.050	1.113
17	1.153	VV	0.025	33609	1.113	1.173
18	1.230	VV	0.022	76961	1.173	1.252
19	1.290	VV	0.027	54101	1.252	1.325
20	1.343	VV	0.022	16967	1.325	1.365
21	1.408	VV	0.026	45601	1.365	1.420
22	1.467	VV	0.026	614087	1.420	1.487
23	1.505	VV	0.021	70329	1.487	1.530
24	1.556	VV	0.020	61929	1.530	1.582
25	1.601	VV	0.025	24430	1.582	1.617
26	1.627	VV	0.023	13296	1.617	1.646
27	1.695	VV	0.044	51401	1.646	1.715
28	1.735	VV	0.020	57568	1.715	1.767
29	1.790	VV	0.021	30039	1.767	1.809
30	1.828	VV	0.029	9441	1.809	1.847
31	1.862	VV	0.020	5308	1.847	1.883
32	1.906	VV	0.027	15557	1.883	1.935
33	1.958	VV	0.029	17224	1.935	1.976
34	1.999	VV	0.032	35708	1.976	2.040
35	2.060	VV	0.029	16017	2.040	2.086
36	2.126	VV	0.023	124099	2.086	2.152
37	2.212	VV	0.028	472597	2.152	2.249
38	2.271	VV	0.018	26951	2.249	2.288
39	2.322	VV	0.036	12240	2.288	2.329
40	2.368	VV	0.033	179842	2.329	2.406
41	2.422	VV	0.037	20961	2.406	2.450
42	2.466	VV	0.021	23630	2.450	2.514
43	2.538	VV	0.023	10461	2.514	2.558
44	2.580	VV	0.028	14552	2.558	2.613
45	2.631	VV	0.022	6262	2.613	2.639
46	2.653	VV	0.021	7548	2.639	2.669
47	2.719	VV	0.039	21990	2.669	2.753
48	2.795	VV	0.020	36856	2.753	2.816
49	2.858	VV	0.027	157030	2.816	2.885
50	2.908	VV	0.024	75446	2.885	2.951
51	2.979	VV	0.017	47300	2.951	3.001
52	3.014	VV	0.040	7272	3.001	3.047
53	3.097	VV	0.026	178993	3.047	3.118
54	3.128	VV	0.020	8103	3.118	3.148
55	3.168	VV	0.033	20833	3.148	3.223
56	3.275	VV	0.019	50357	3.223	3.298
57	3.308	VV	0.017	3217	3.298	3.317
58	3.329	VV	0.018	3668	3.317	3.337
59	3.357	VV	0.018	32945	3.337	3.382
60	3.405	VV	0.029	9042	3.382	3.422
61	3.461	VV	0.025	37791	3.422	3.474
62	3.500	VV	0.024	52123	3.474	3.537
63	3.568	VV	0.028	18004	3.537	3.583
64	3.596	VV	0.019	7375	3.583	3.609
65	3.637	VV	0.028	39410	3.609	3.658
66	3.685	VV	0.025	50139	3.658	3.734
67	3.747	VV	0.019	4168	3.734	3.756
68	3.814	VV	0.038	30039	3.756	3.867
69	3.890	VV	0.018	17361	3.867	3.900
70	3.914	VV	0.025	25313	3.900	3.943
71	3.959	VV	0.031	5285	3.943	3.980
72	4.000	VV	0.018	7389	3.980	4.009
73	4.028	VV	0.025	36422	4.009	4.072
74	4.095	VV	0.022	47530	4.072	4.138
75	4.156	VV	0.021	14627	4.138	4.171
76	4.185	VV	0.026	13414	4.171	4.215
77	4.232	VV	0.025	10505	4.215	4.263
78	4.290	VV	0.017	28255	4.263	4.305
79	4.321	VV	0.024	18993	4.305	4.346
80	4.379	VV	0.025	23128	4.346	4.395
81	4.407	VV	0.018	5161	4.395	4.420
82	4.434	VV	0.020	5392	4.420	4.453
83	4.494	VV	0.032	8211	4.453	4.507
84	4.518	VV	0.033	7123	4.507	4.556
85	4.585	VV	0.028	10362	4.556	4.603
86	4.615	VV	0.031	5035	4.603	4.639
87	4.681	VV	0.029	12388	4.639	4.697
88	4.713	VV	0.027	4770	4.697	4.730
89	4.764	VV	0.031	11698	4.730	4.794
90	4.807	VV	0.019	3727	4.794	4.821
91	4.841	VV	0.023	3102	4.821	4.849
92	4.864	VV	0.023	5800	4.849	4.897
93	4.928	VV	0.021	22421	4.897	4.993
94	5.017	VV	0.018	8072	4.993	5.038
95	5.066	VV	0.020	3134	5.038	5.092
96	5.110	VV	0.023	1632	5.092	5.130
97	5.158	VV	0.025	1511	5.130	5.176
98	5.207	VV	0.041	2375	5.176	5.250
99	5.270	VV	0.027	782.07	5.250	5.281

Fig. 3.9.4: Typical quantitation of petrol chromatogram.

DATA:JD022208.D

Peak#	Ret Time	Type	Width	Area	Start Time	End Time
1	0.416	BV	0.008	2403	0.383	0.442
2	0.471	PV	0.014	184703	0.442	0.485
3	0.498	PV	0.009	142464	0.485	0.536
4	0.553	VV	0.018	26144	0.536	0.575
5	0.610	VV	0.013	355993	0.575	0.628
6	0.644	VV	0.013	351959	0.628	0.664
7	0.683	VV	0.013	859545	0.664	0.729
8	0.780	VV	0.024	527599	0.729	0.836
9	0.888	VV	0.024	113006	0.836	0.902
10	0.942	VV	0.031	1120238	0.902	0.961
11	0.988	VV	0.020	1055468	0.961	1.005
12	1.031	VV	0.028	221097	1.005	1.070
13	1.111	VV	0.022	693909	1.070	1.133
14	1.148	VV	0.020	3342	1.133	1.160
15	1.172	VV	0.020	2822	1.160	1.200
16	1.258	VV	0.020	384786	1.200	1.277
17	1.310	VV	0.024	84805	1.277	1.334
18	1.361	VV	0.020	58198	1.334	1.384
19	1.409	VV	0.022	69592	1.384	1.436
20	1.458	VV	0.019	41306	1.436	1.474
21	1.533	VV	0.035	385593	1.474	1.557
22	1.586	VV	0.032	189947	1.557	1.606
23	1.644	VV	0.028	462321	1.606	1.667
24	1.719	VV	0.038	195980	1.667	1.740
25	1.799	VV	0.029	908869	1.740	1.813
26	1.834	VV	0.017	157496	1.813	1.850
27	1.867	VV	0.016	25062	1.850	1.880
28	1.904	VV	0.026	24084	1.880	1.916
29	1.936	VV	0.027	43033	1.916	1.959
30	2.058	VV	0.034	972651	1.959	2.071
31	2.088	VV	0.026	277152	2.071	2.124
32	2.148	VV	0.020	88114	2.124	2.162
33	2.195	VV	0.037	191893	2.162	2.224
34	2.256	VV	0.025	204170	2.224	2.270
35	2.308	VV	0.022	211267	2.270	2.331
36	2.352	VV	0.021	66232	2.331	2.382
37	2.406	VV	0.023	73134	2.382	2.415
38	2.430	VV	0.030	137697	2.415	2.471
39	2.512	VV	0.021	301398	2.471	2.527
40	2.541	VV	0.017	11734	2.527	2.550
41	2.573	VV	0.021	56186	2.550	2.609
42	2.624	VV	0.019	9261	2.609	2.632
43	2.655	VV	0.019	59249	2.632	2.683
44	2.722	VV	0.032	85115	2.683	2.771
45	2.800	VV	0.025	35248	2.771	2.824
46	2.857	VV	0.025	22988	2.824	2.867
47	2.878	VV	0.020	16254	2.867	2.895
48	2.927	VV	0.030	50001	2.895	2.958
49	2.987	VV	0.022	23298	2.958	3.007
50	3.029	VV	0.029	16581	3.007	3.063
51	3.090	VV	0.029	48250	3.063	3.150
52	3.185	VV	0.022	78021	3.150	3.202
53	3.210	VV	0.019	7025	3.202	3.231
54	3.281	VV	0.033	28246	3.231	3.314
55	3.340	VV	0.022	22724	3.314	3.360
56	3.377	VV	0.022	9269	3.360	3.393
57	3.416	VV	0.022	18757	3.393	3.435
58	3.448	VV	0.029	18774	3.435	3.480
59	3.501	VV	0.023	13476	3.480	3.516
60	3.533	VV	0.020	8258	3.516	3.544
61	3.555	VV	0.016	5493	3.544	3.562
62	3.575	VV	0.017	7157	3.562	3.582
63	3.596	VV	0.021	11940	3.582	3.615
64	3.641	VV	0.024	14495	3.615	3.668
65	3.685	VV	0.029	8395	3.668	3.715
66	3.748	VV	0.028	9159	3.715	3.763
67	3.820	VV	0.026	38693	3.763	3.874
68	3.894	VV	0.022	3121	3.874	3.902
69	3.917	VV	0.027	5153	3.902	3.941
70	3.954	VV	0.023	3027	3.941	3.978
71	3.998	VV	0.019	2686	3.978	4.013
72	4.029	VV	0.018	1446	4.013	4.036
73	4.059	VV	0.024	4617	4.036	4.080
74	4.094	VV	0.034	4164	4.080	4.137
75	4.158	VV	0.031	3794	4.137	4.194
76	4.203	VV	0.020	1068	4.194	4.221
77	4.244	VV	0.026	1167	4.221	4.270
78	4.289	VV	0.021	693.07	4.270	4.305
79	4.327	VV	0.030	659.46	4.305	4.340
80	4.362	VV	0.034	1200	4.340	4.389
81	4.408	VV	0.019	1944	4.389	4.456
82	4.498	VV	0.024	690.94	4.456	4.517
83	4.589	VV	0.026	198.66	4.564	4.605
84	4.622	VV	0.027	192.56	4.605	4.645
85	4.668	VV	0.032	263.34	4.645	4.698
86	4.768	VV	0.026	237.52	4.733	4.790
87	4.923	VV	0.033	127.78	4.889	4.941
88	4.959	VV	0.017	210.19	4.941	4.993
89	5.476	VB	0.020	65.87	5.407	5.547

Fig. 3.9.5: Typical quantitation of camping fuel chromatogram.

by the integration system for each of the camping fuels. A total of 75 –100 peaks (in the 0 –5min range) were integrated for each of the petrol specimens.) While the FID response is not linear for all compounds, virtually all the compounds of interest here were hydrocarbons and the response was estimated to be linear enough for these purposes. Duplicate analyses showed good agreement, as shown in Table 3.9.1.

It is clear from these results that hydrocarbons ranging from butane to n-hexane constituted a large percentage of each of these petrols. It should be noted that both fuels were purchased during the winter months (for ambient temperatures of –10 to 25°C). Petrol blends are changed periodically to accommodate changes in the weather so as to maintain a predictable vapour pressure. No "summer blend" petrols were available at the time these experiments were conducted. However, Dale Mann of the Washington State Patrol Laboratory in Tacoma, WA, conducted extensive tests of evaporation using summer-blend fuels.[Mann-1994] A sampling of his quantitative GC results shows general agreement but a decreased percentage of butane and pentane fractions compared to those measured here.(Table 3.9.2) Such differences would be expected from fuels intended for operation at ambient temperatures of 20 – 40°C. Comparison of these results to analyses reported in the literature shows that the motor fuels of today are considerably different from those of 25 years ago, reflecting changes in vehicles, petroleum sources, and environmental requirements. [Sanders/Maynard]

It is also clear that there may be considerable differences between camping fuels, both between products and for a single product over time. These products are not blended specifically for this use. A petroleum fraction (generally $C_5 - C_{10}$) is purchased in bulk. The absence of aromatics and

Table 3.9.1 Quantitative Analysis of Flammable Liquid Fuels (Fresh, Neat)

Product	MeButane	Pentane	2-Me-C5	Hexane	Toluene	All ≤ C6	All≤C5
	%	%	%	%	%	%	%
Shell Petrol	9.5	4.6	13.1	1.9	5.9	38.3	21.2
Shell Petrol[1]	10.2	5.0	14.1	2.0	6.3	41.0	22.3
Shell Petrol	10.7	5.6	15.7	3.4	6.6	46.1	25.1
BP Petrol	6.2	5.2	7.0	4.0	9.7	36.4	20.8
BP Petrol	6.8	6.0	7.9	4.5	10.7	40.8	23.0
					C8/C10[2]		
Coleman©	1.6	1.2	3.1	7.4	7.9/0.7	16.6	3.1
(1990)	1.8	1.3	3.2	7.8	8.2/0.8	17.6	2.8
Coleman©	2.9	1.8	3.4	14.1	5.6/0.6	29.3	5.2
(1995)							
Camplite©	0	0	2.6	25.3	2.3/1.7	35.7	0
	0	0	2.9	25.8	2.5/1.9	37.5	0

Notes:

1: This analysis was a duplicate integration of the same chromatogram as the previous entry, conducted some three months apart. Some preset parameters (such as threshold) in the integration program were reset to separate the peaks of interest.

2: Camping fuels contain normal- and iso-alkanes, and no aromatics. n-octane and n-decane were selected as a representative mid-range compounds.

Table 3.9.2: Quantitative Analysis of Summer-Blend Petrols

Product	MeButane	Pentane	2-Me-C5	Hexane	Toluene	All ≤ C6	All≤C5
	%	%	%	%	%	%	%
Regular[1]	7.70	5.61	4.11	3.41	9.08	34.0	16.9
Regular[2]	7.32	5.28	4.34	3.7	11.34	31.5	15.2
Regular[1]	6.87	5.40	4.18	3.68	10.43	30.7	14.7
Regular[2]	5.71	4.24	3.74	3.18	10.99	25.0	11.5
Regular[1]	7.66	5.42	4.19	3.34	8.87	32.5	16.3
Regular[2]	6.41	5.18	4.84	4.4	14.71	30.0	12.9
Regular[1]	5.51	4.56	3.80	3.77	14.96	24.5	11.6
Regular[2]	7.58	5.27	4.46	3.97	15.35	29.6	14.5
Super[2]	5.65	1.98	2.12	1.34	12.86	20.9	11.6
Super[2]	4.75	2.14	2.24	1.75	14.45	20.6	12.2
Super[2]	7.69	1.44	2.68	1.31	12.78	23.2	12.4
Super[2]	4.37	2.46	2.42	1.94	13.75	21.7	9.2
Premium[1]	5.60	4.13	3.45	3.18	15.06	23.0	11.6
Regular[3]	7.88	7.27	3.85	3.50	5.92	36.1	20.6
Premium[3]	10.17	5.75	3.76	1.51	12.30	36.2	21.8

Notes:

1: Leaded varieties collected 6/92 (Mann 94)

2: Unleaded varieties collected 6/92 (Mann 94)

3: Leaded varieties reported 1968 (Sanders)

unsaturated hydrocarbons (which produce undesirable soot) are determined by analysis. Bulk physical properties such as vapour pressure, flash point, and odour are also determined. If these properties are within acceptable limits, a dye may be added and the product is packaged for retail sale. Variations in specific content are to be expected.

Once a baseline of composition was established for each of these products, evaporation studies could be carried out in the same manner as for evaporation rates of pure compounds. The rate of mass loss v. time was recorded for each of these products, as shown in typical graphs in Fig. 3.9.6. During each run, the aliquots of fuel removed were analyzed using the same GC method as described above. The peak areas corresponding to several key compounds were recorded and normalized against an internal standard. It was decided to use a compound already in each product that would be easily identified by its relative retention time and its relative size, and would be sufficiently non-volatile to not evaporate appreciably during the time of analysis. For petrol, 1,2,4-trimethyl benzene was selected; for camping fuels, n-decane was selected. The total mass loss corresponding to each sampling time was recorded from the raw data for each evaporation run. The results are shown in tabular form in Tables 3.9.3 and 3.9.4.

The loss of various components as a function of time is more easily seen when the tabular values above are plotted against time of evaporation, as in Figs.3.9.7 and 3.9.8. It can be seen that for petrol the most significant losses are from methyl butane, n-pentane, and other compounds of similar high vapour pressures until the evaporation process is well advanced. By extending the line connecting the data points, we can see that virtually all the n-pentane and lighter compounds will be evaporated from either petrol or camping fuel by approximately one hour. For camping fuels, while methyl

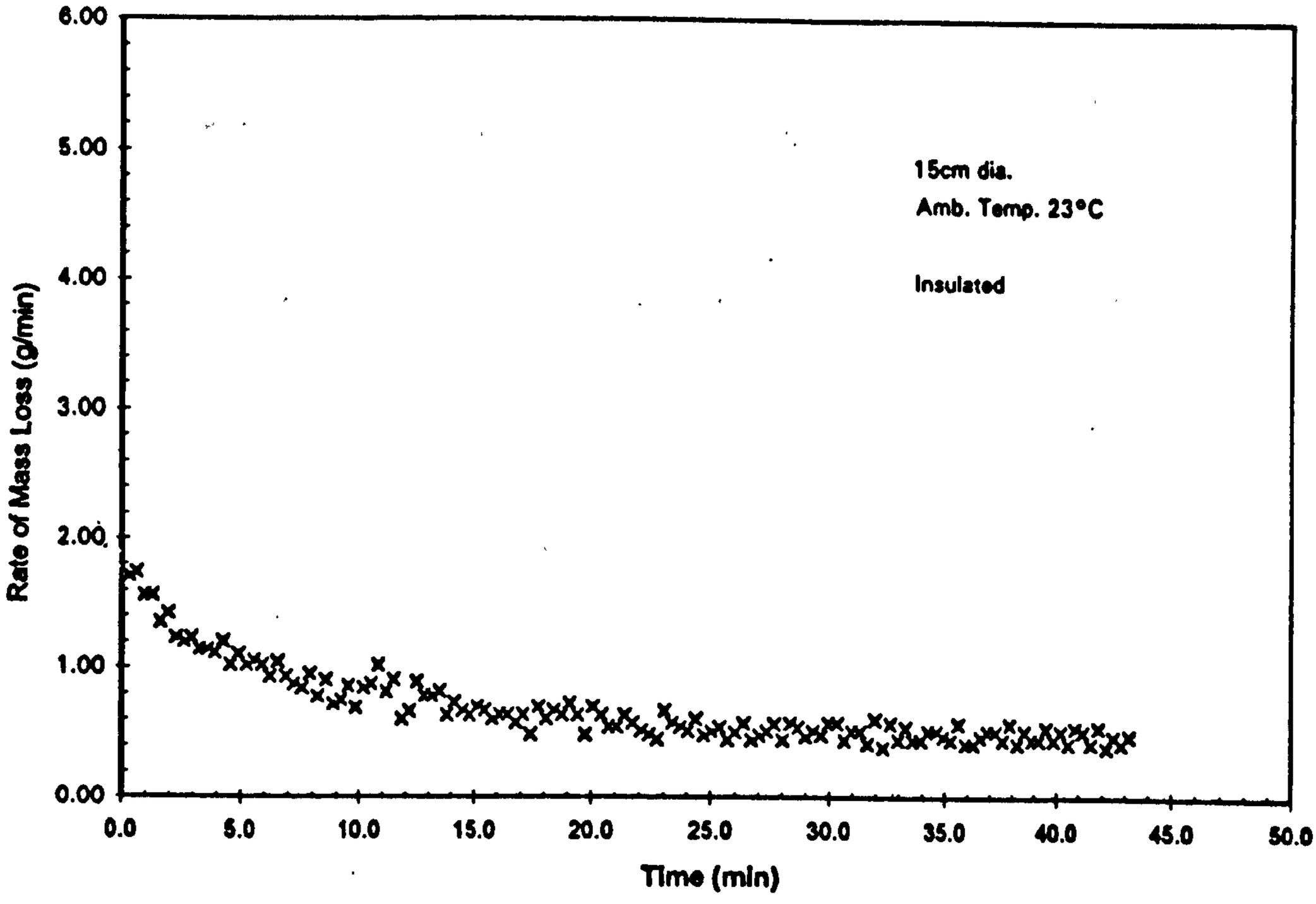

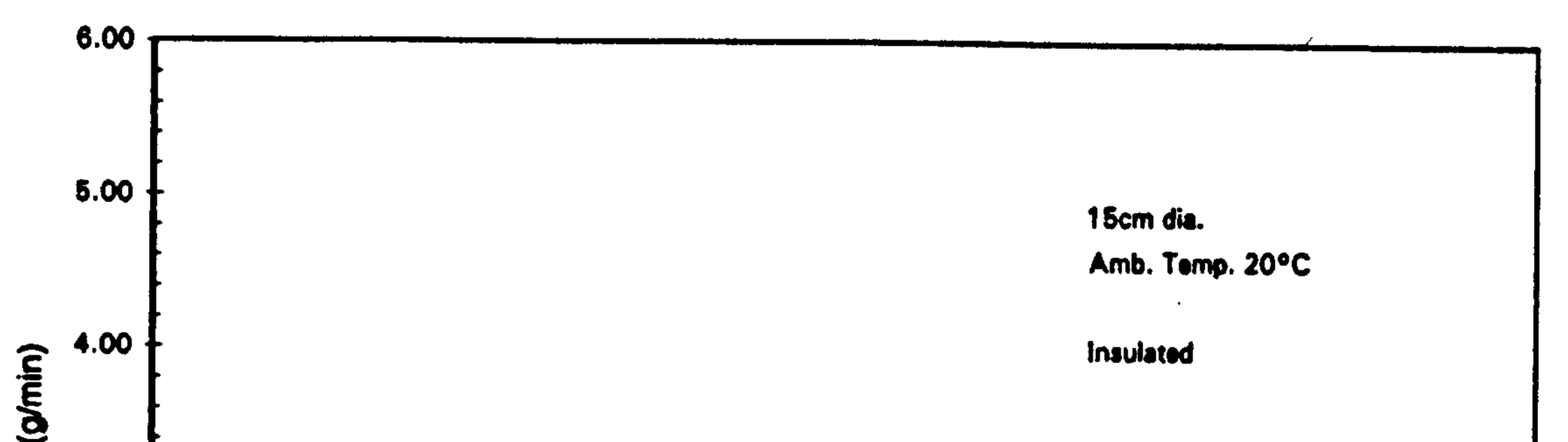

Fig. 3.9.6: Mass loss plots of petrol evaporating from a pool at 23°C. Upper one is with mass recorded every 20s. Lower one is mass recorded every 5s, showing considerable variation in mass as a result of the multi-component evaporation.

Table 3.9.3: Petrol Key Compound Peak Areas (normalized to 1,2,4-Trimethyl benzene)

Petrol	Time	%Mass Loss	MeButane	Pentane[1]	MeC5	C6	Toluene
Shell	0	0	3.86	1.89	5.31	0.76	2.39
	11	9.4	2.16	1.20	3.93	0.90	2.20
	20	13.1	2.50	1.34	4.52	0.65	2.31
	35	18.3	1.86	1.07	4.01	0.60	2.27
Shell	0	0	3.75	1.76	5.17	0.70	2.36
	5	6.8	3.26	1.62	4.88	1.04	2.32
	11	12.0	2.31	1.26	4.25	0.61	2.20
	20	17.6	2.03	1.22	4.45	0.66	2.38
	37	25.4	1.06	0.79	3.56	0.88	2.26
	60+[2]	50	0	0	0.75	0.21	1.93
Shell	5	6.1	2.96	1.47	4.53	0.97	2.24
	10	10.2	2.66	1.39	4.57	0.65	2.29
	20	16.9	1.63	1.06	3.75	0.57	2.17
	30	21.8	1.38	0.91	3.80	0.90	2.32
BP	0	0	2.33	2.83	2.71	1.56	3.67
	6	6.4	1.59	2.05	2.19	1.29	3.30
	20	14.6	1.05	1.57	1.95	1.21	3.24
	30	19.3	na[3]	0.42	1.88	1.54	3.35
	40	24.3	na[3]	0.28	1.68	1.10	3.13

Table 3.9.3: Petrol Key Compound Peak Areas (normalized to 1,2,4-Trimethyl benzene) Continued

Petrol Time	%Mass Loss	MeButane	Pentane[1]	MeC5	C6	Toluene
BP[4]	0	0	2.23	2.52	2.52	1.44	3.49
	8	28.8	0.62	0.16	1.27	0.96	3.35
	14	37.3	0	0.06	0.56	0.56	3.14
	24	46.9	0	0	0.12	0.21	2.65
	32	52.3	0	0	0.24	0.11	2.34

Notes:

1. Because peak resolution was not perfect, the integration program would not always discriminate between the n-pentane peak and a neighboring one (probably 1-pentene). As a result, sometimes there would be two peak areas reported and sometimes only one. To ensure reproducibility, when two separate areas were reported by the integration program, they were manually added together before being ratioed against TMB.

2. One of the petrol samples was allowed to evaporate with the aid of a forced draft until it had lost one-half its mass. This required more than 60 min but the precise time was not recorded.

3. The integration program reported a single peak where only a series of very small poorly resolved peaks were visible on the chromatogram itself. This meaningless "peak area" was not reported as it had no validity with respect to the experiment.

4. This petrol evaporation was conducted as a thin (≈ 2mm) film on water in a petri dish. Its loss of individual components is significantly different from the other petrol specimens which were analyzed as 12mm-deep pools in a Petri dish.

Table 3.9.4: Camping Fuel Key Compound Peak Areas (normalized to n-decane)

Fuel	Time	%Mass Loss	MeButane	Pentane[1]	MeC5	Hexane	n-Octane
#1	0	0	2.32	1.76	4.28	10.21	10.75
	6	2.0	1.91	1.57	4.12	9.93	11.37
	11	3.5	1.89	1.55	4.31	10.46	11.57
	24	6.7	1.07	1.02	3.55	9.16	11.34
	32	8.5	1.02	0.99	3.59	9.35	11.43
	45	10.3	0.70	0.76	3.31	8.79	11.70
#1[2]	0	0	2.34	1.80	4.51	10.88	11.50
	6	14.3	0.65	0.65	2.73	7.37	10.93
	11	23.6	0	0.12	1.45	5.11	11.08
	24	44.5	0	0	0.22	1.33	9.96
	30	52.1	0	0	0.15	0.75	9.37
	44	65.3	0	0	0	0	7.57
#2	0	0	0	0.003	1.55	15.16	1.40
	5	1.9	0	0.010	1.36	13.09	1.40
	12	4.5	0	0.003	1.40	13.53	1.29
	25	7.4	0	0.02	1.08	10.97	1.35
	35	11.0	0	0	1.06	11.02	1.20

Table 3.9.4 Camping Fuel Key Compound Peak Areas (Continued)

Fuel	Time	%Mass Loss	MeButane	Pentane[1]	MeC5	Hexane	n-Octane
#2	0	0	0	0.003	1.52	14.29	1.31
	6	2.3	0	0	1.40	13.27	1.26
	11	4.1	0	0.04	1.30	12.25	1.24
	20	6.9	0	0	1.15	11.35	1.18
	35	11.0	0	0	1.05	11.07	1.13
#3	0	0	4.76	3.37	5.59	22.82	9.03
	5	3.6	2.63	2.13	3.84	15.93	7.13
	10	5.7	3.09	2.57	4.77	18.99	8.75
	20	8.4	2.45	2.12	4.56	19.60	8.67
	30	10.3	1.62	1.28	3.51	16.03	7.20

KEY:

#1: Coleman© brand camping fuel, purchased 1990.

#2: Camplite© brand camping fuel, purchased 1995.

#3: Coleman© brand camping fuel, purchased 1995.

Notes:

1. Because peak resolution was not perfect, the integration program would not always discriminate between the n-pentane peak and a neighboring one (probably 1-pentene). As a result, sometimes there would be two peak areas reported and sometimes only one. To ensure reproducibility, when two separate areas were reported by the integration program, they were manually added together before being ratioed against n-decane.

2. This camping fuel evaporation was conducted as a thin (ca 2mm) film on water in a petri dish. Its loss of individual components is signifiantly different from the other camping fuel specimens which were analyzed as 12mm-deep pools in a Petri dish.

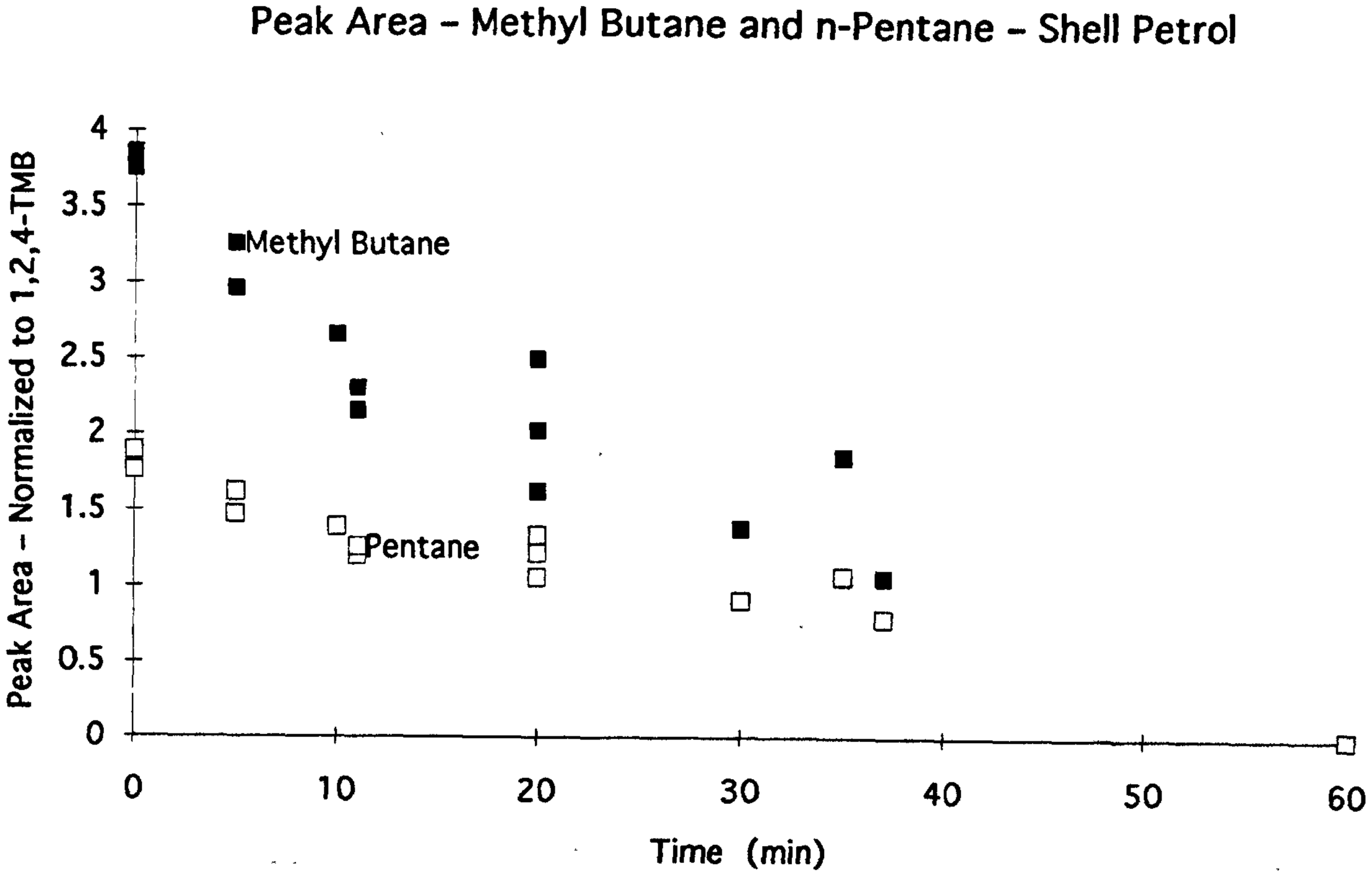

Fig. 3.9.7: Regression of methyl butane and n-pentane from Shell petrol evaporating as a pool (12mm deep) at 20-22°C [with peak areas normalized to 1,2,4-trimethylbenzene (TMB)]. (Three analytical runs)

REGRESSION: BP PETROL FILM AND POOL

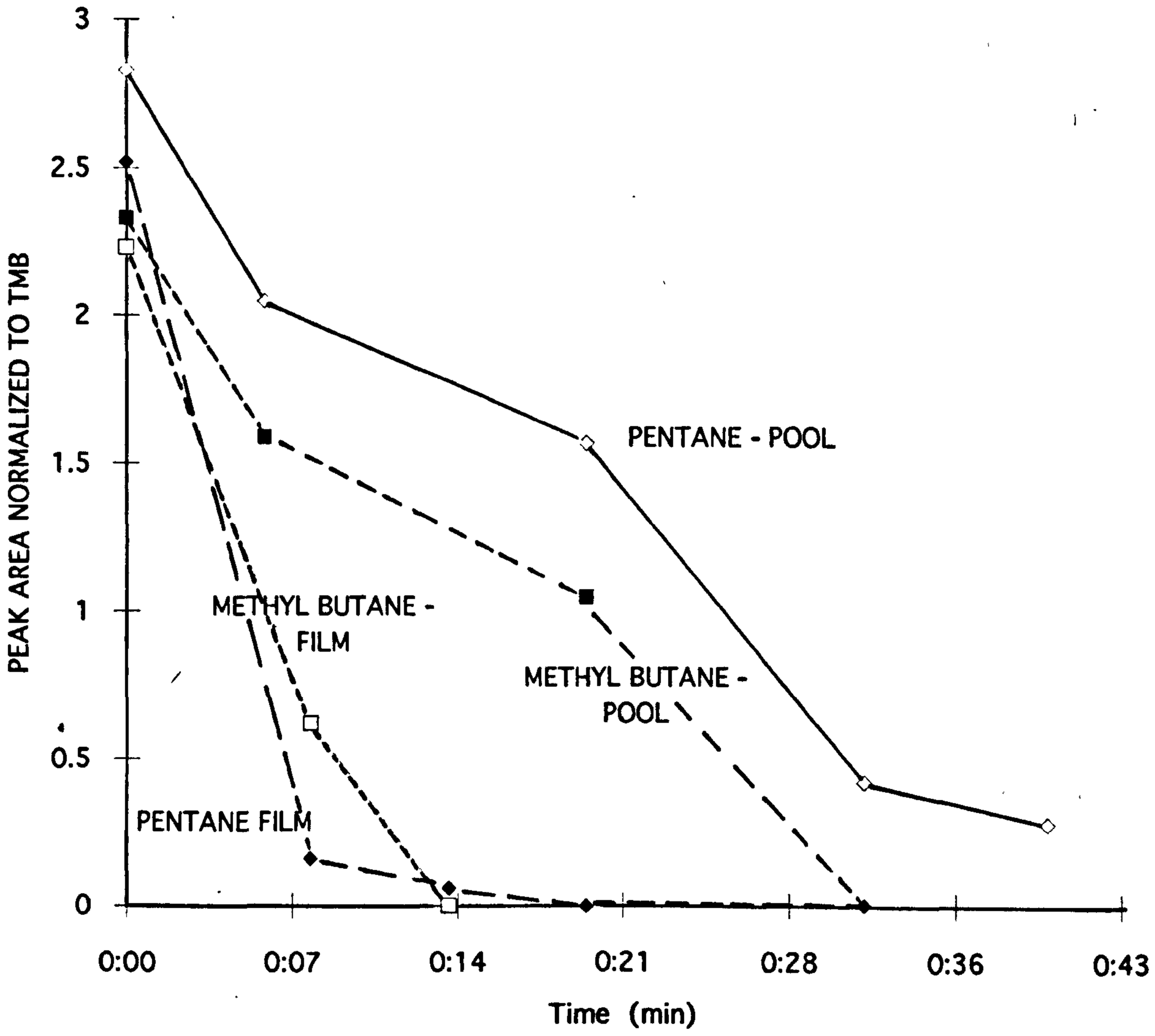

Fig. 3.9.8: Regression of methyl butane and n-pentane from BP petrol evaporating as a pool (12mm) and as a film (2mm on water) at 20-22°C [with peak areas normalized to TMB]. Note the faster rate for films, with a trend that matches ideal diffusion of one species into another. The slower rate demonstrates the effect of mass diffusion in the deeper pool as the species evaporating from the surface has to be replaced by eddy diffusion and circulation from the bulk liquid beneath.

butane and pentane are present (at least in Coleman© fuel), the most significant contributions are coming from methyl pentane and hexane (which alone constitutes between 7.5 and 25% of such fuels). The loss of n-hexane and methyl pentane from a typical camping fuel (both as a film and as a pool) is shown in Fig. 3.9.9.

When the mass loss rates for these products are compared against those of n-pentane and n-hexane, there are distinct similarities. The rate of evaporation for a typical petrol pool may be seen in Fig. 3.9.6(a). The initial rate is 2.4 g/min, which is the same as for n-pentane under the same conditions, and the slope of the mass loss v. time plot parallels that of n-pentane for about the first 5min of evaporation. The rate of mass loss of a typical camping fuel pool may be seen in Fig.(b)3.9.6. Its initial rate, 0.6 – 0.8 g/min, is very similar to that of n-hexane at the same temperature. The general trend of its evaporation rate as a function of time is similar to that of hexane for the first 10min.

Due to the multiple species evaporating, there is considerable scatter of the individual rate measurements from interval to interval. The same phenomenon is visible in the petrol evaporation rate plots. The scatter is more pronounced with time, presumably as an effect of the much more complex fuel chemistry. The behaviour of such complex fuels when evaporating as a thin film is very different from that of pure compounds, as can be seen in Figs.3.9.10 and 3.9.11. In deep pools, the mechanical diffusion of the evaporating species through the bulk of the pool to the surface may limit its rate of bulk loss. In a thin film, there is little diffusion necessary, and the evaporating species can reach the surface much more readily than in deep pools.

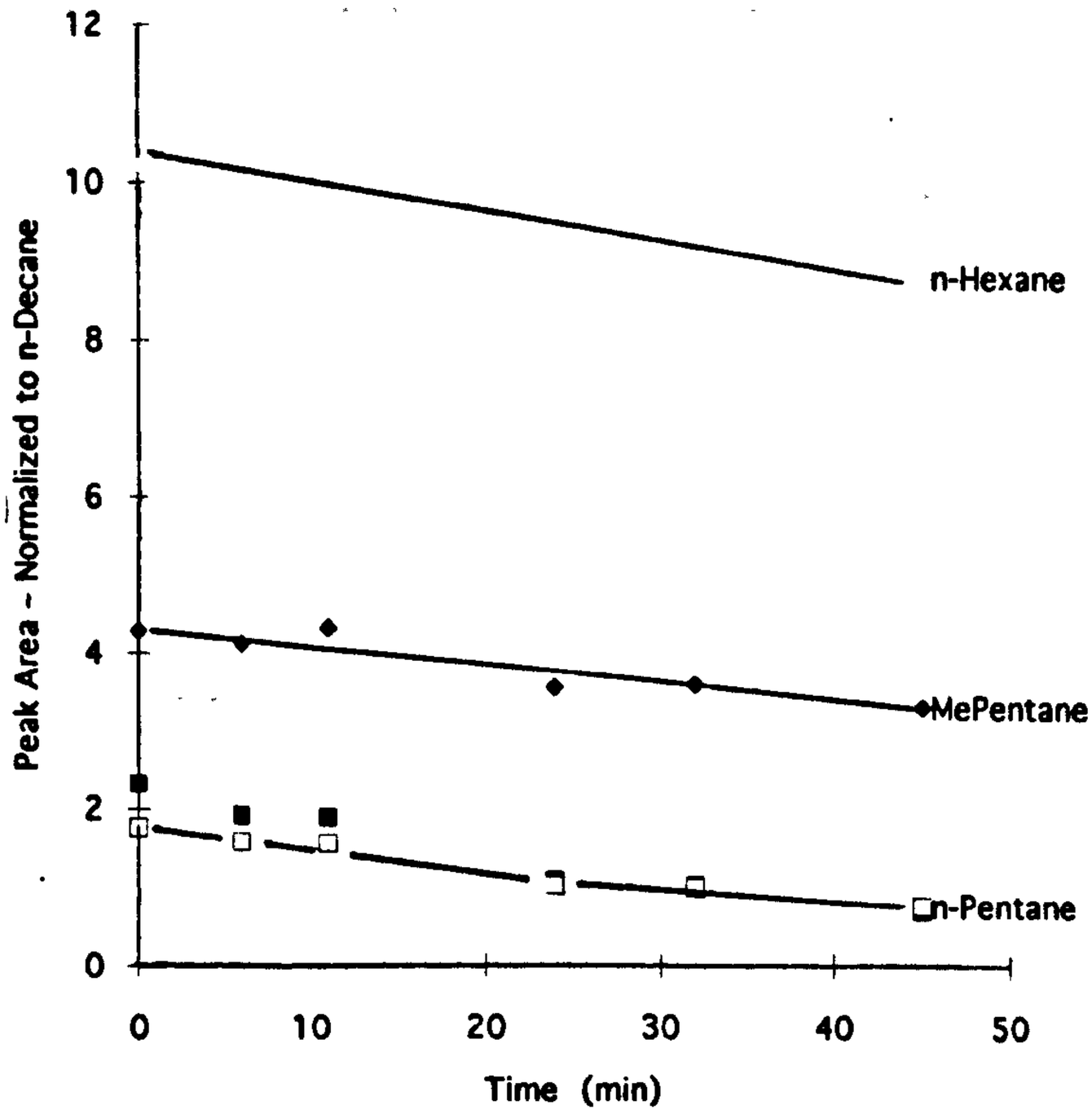

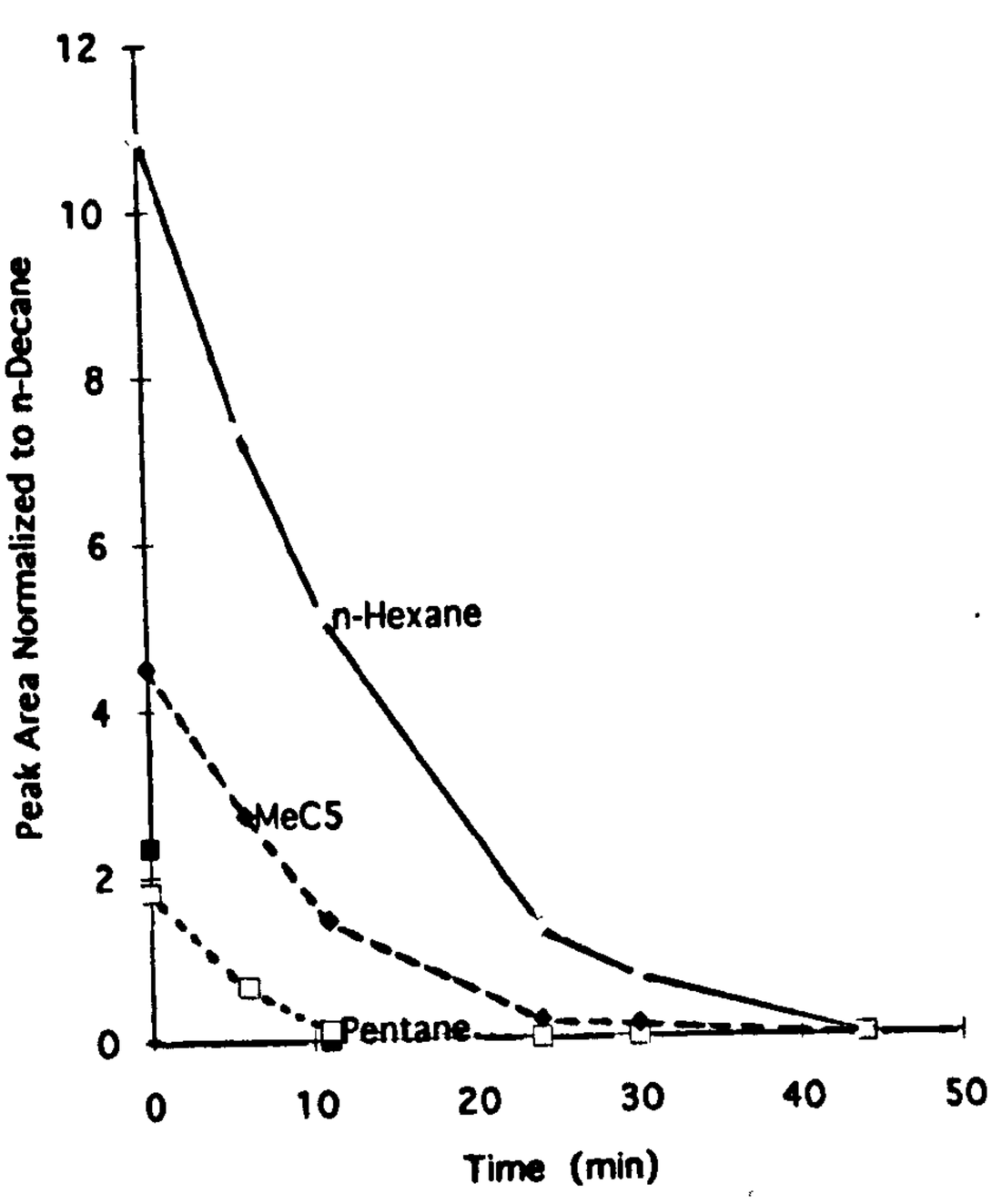

Fig. 3.9.9: Regression of hexane and methyl pentane from camping fuel #1, evaporating from a pool (12mm deep) and from a film (2mm deep). Peak area of hexane is normalized to that of n-decane to establish its relative loss with time. The loss from the film is much more rapid due to absence of mass transfer (diffusion) in the pool.

Test 219 - 38 ml BP Petrol Film

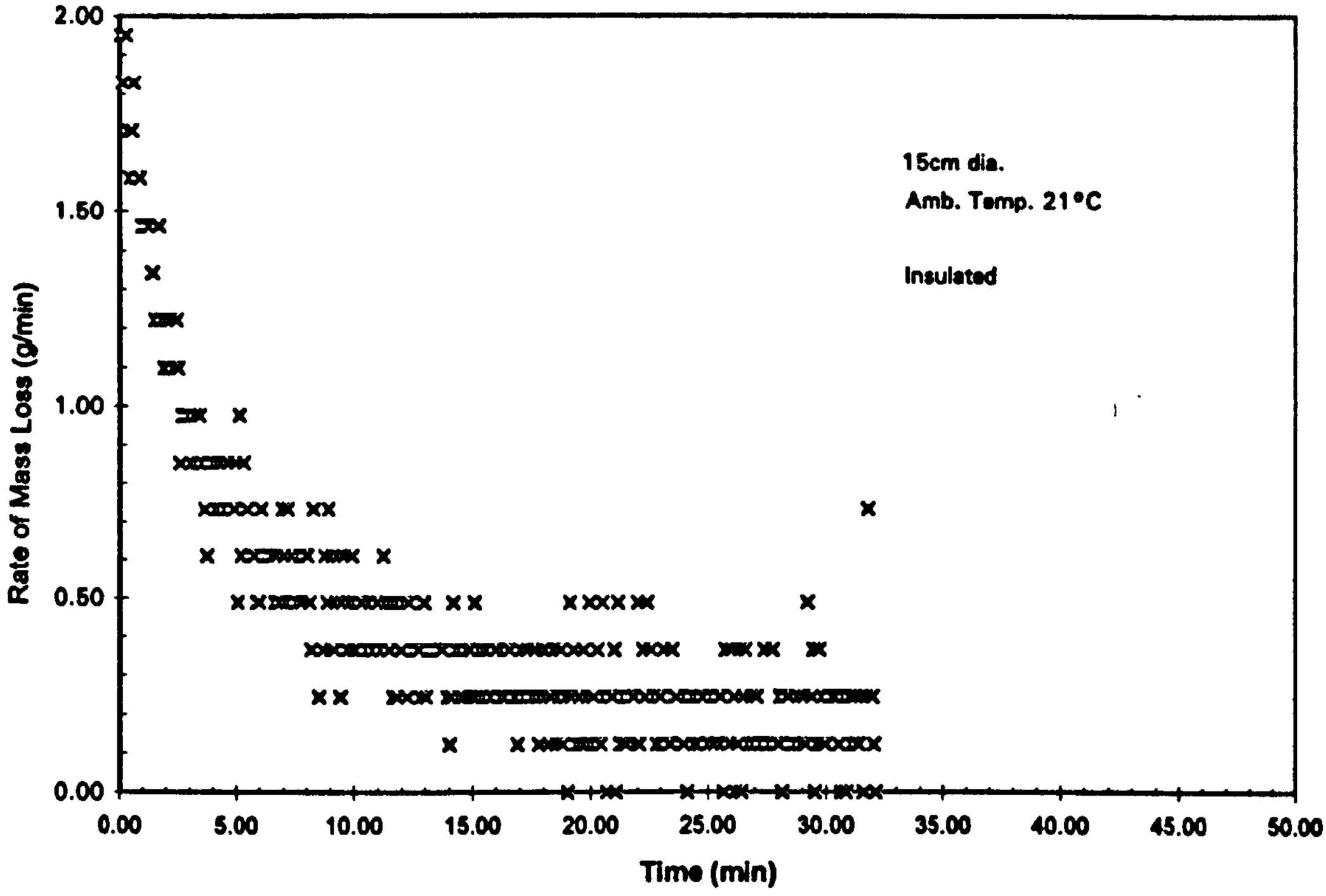

Test 221 - 190 ml BP Petrol Pool

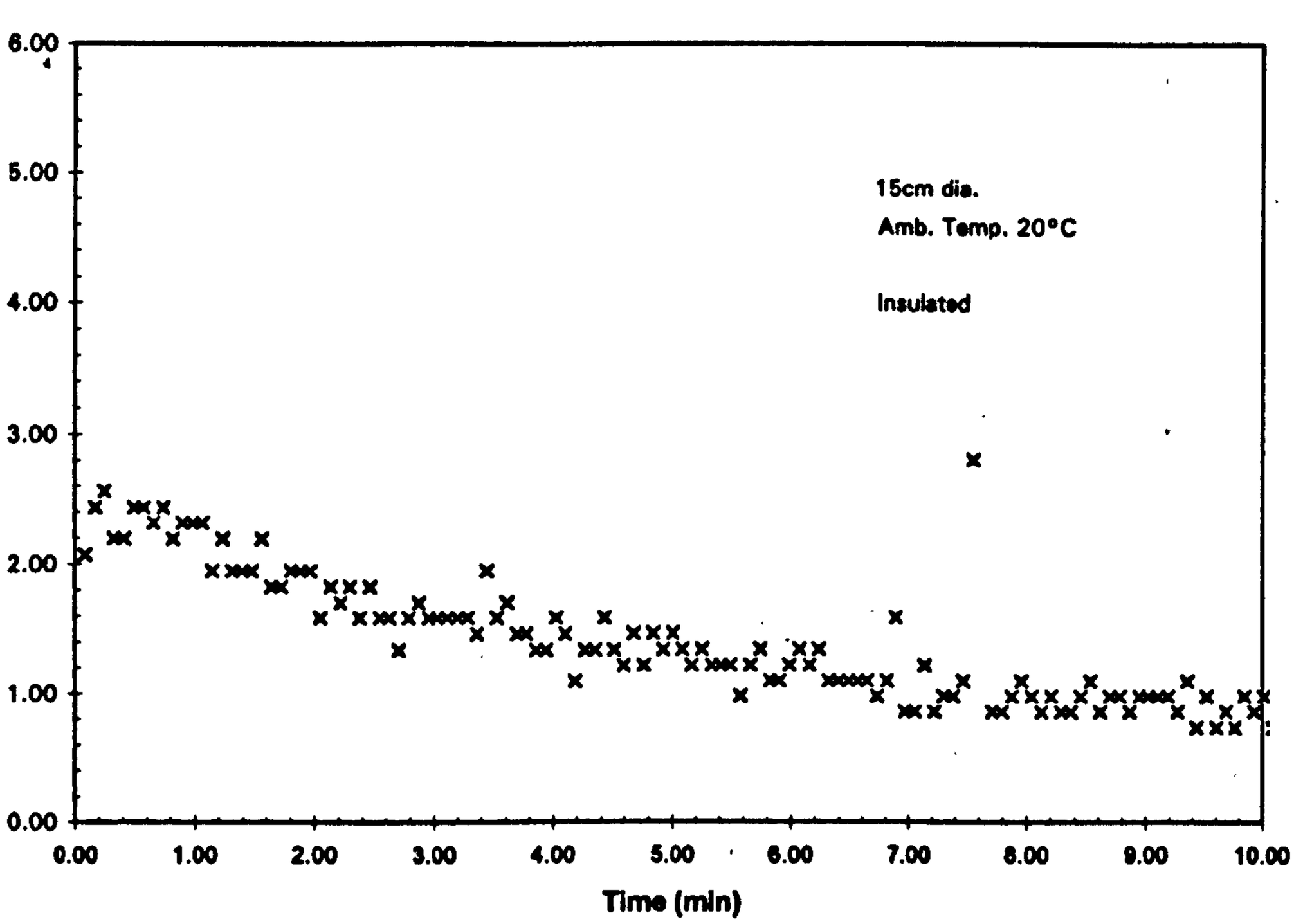

Fig. 3.9.10: Mass loss rate v. time for petrol evaporating from pool and film. The scatter visible in the calculated mass loss rate is the result of both diffusion and the competing species evaporating from a complex mixture.

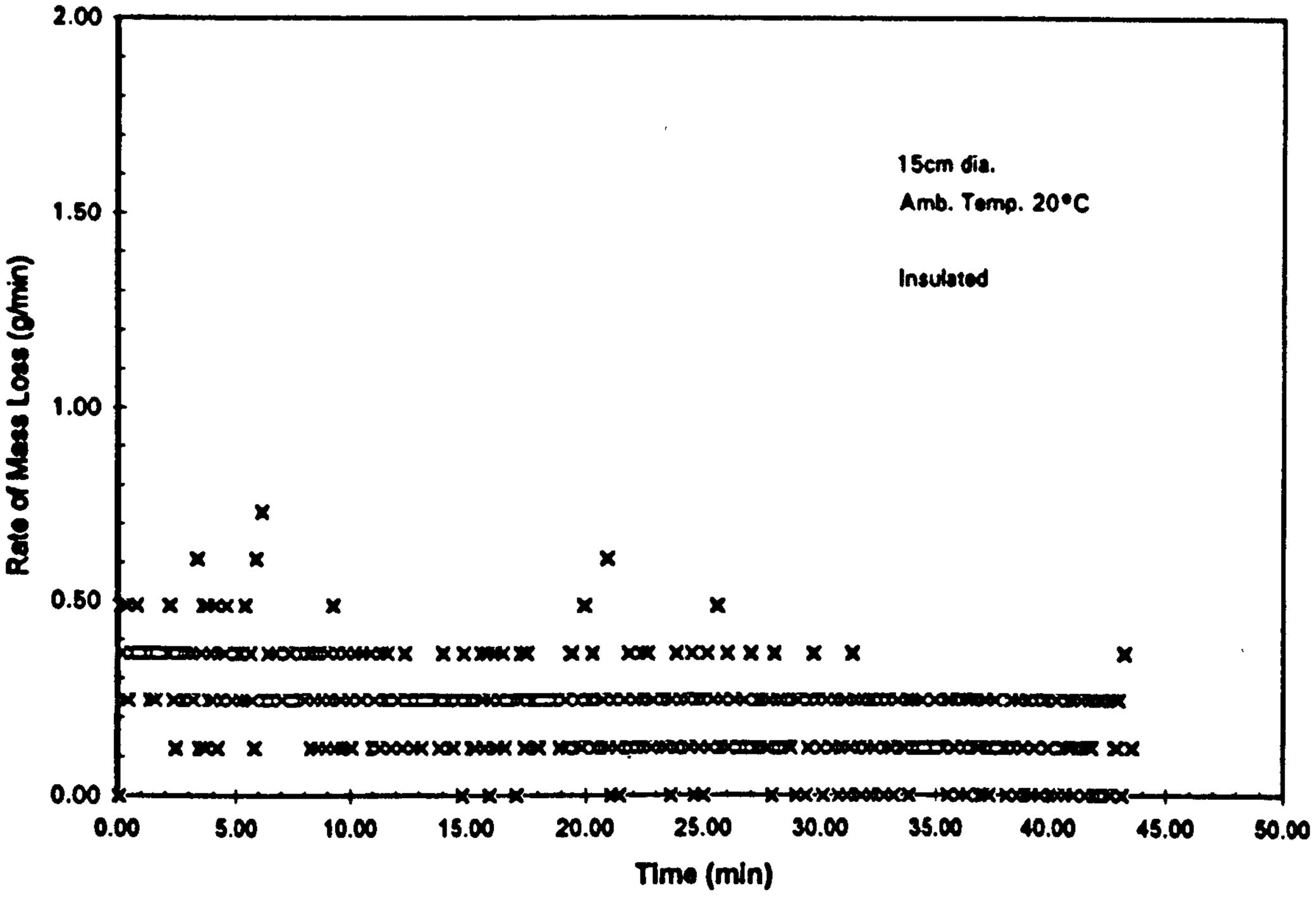

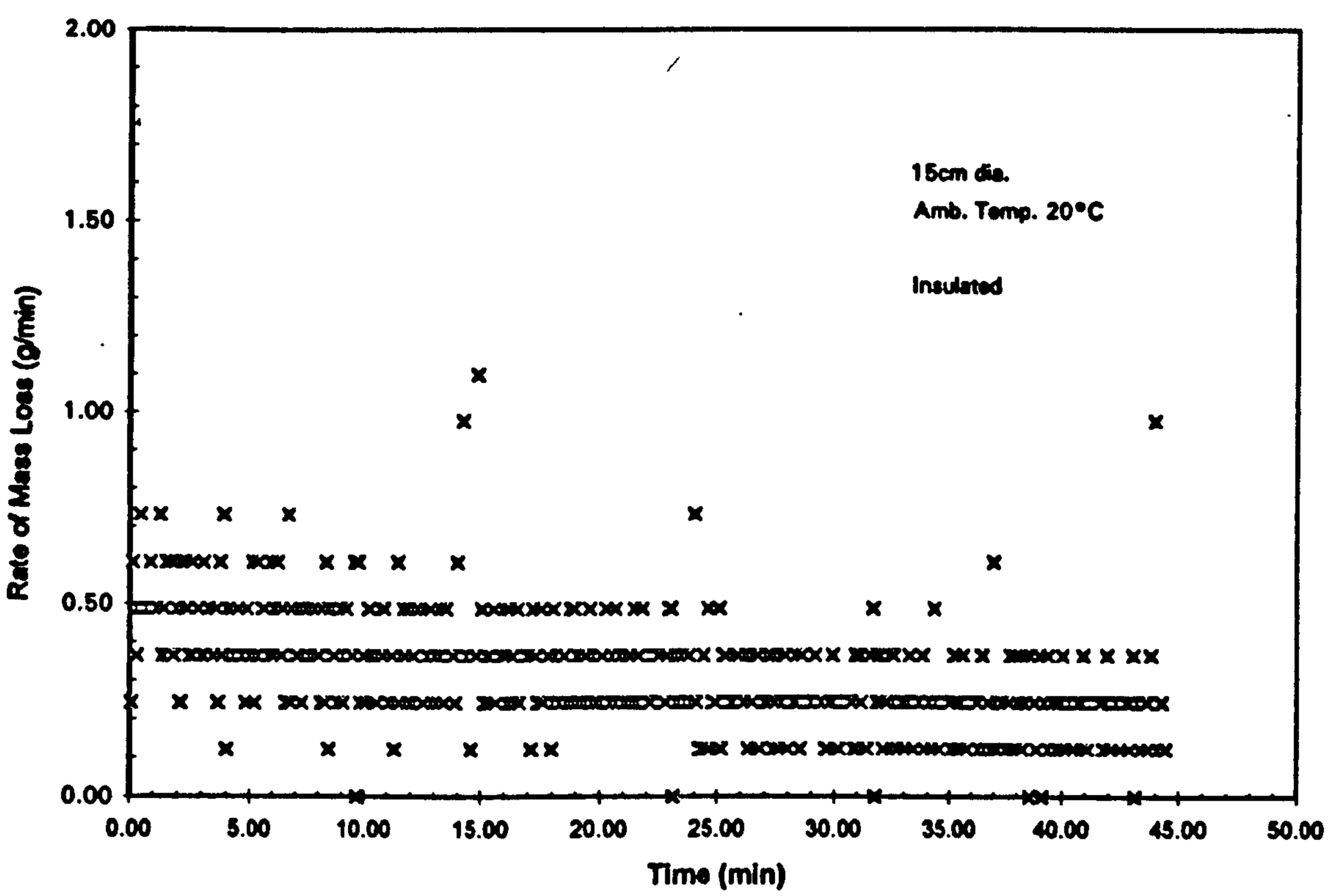

Fig. 3.9.11: Mass loss rate v. time for camping fuel evaporating from pool and film. The scatter visible in the calculated mass loss rate is the result of both diffusion and the competing species evaporating from a complex mixture.

3.10 Pool and Vapor Layer Characteristics and Fire Behavior

3.10.1 Pool Ignition Tests on Carpet

Test 1: One litre of methanol was poured on commercial-grade, acrylic short (3mm) loop pile carpet with integral foam rubber pad (worn). Ambient temperature: 15°C. Oval pool 74 x 86cm was ignited 5min 40s after pouring. Flames spread immediately across the pool. Clear yellow flames in a classical intermittent pool flame plume, 0.5 –1 m in total height were established (Fig. 3.10.1.1). A pronounced halo of charred carpet formed immediately outside the wetted area. All damage was external to pour area until 2 –3 min, then surface scorching and charring of central area occurred. Flames self-extinguished at 6 min.

Test 2: One litre of methanol was poured on commercial-grade, acrylic short loop-pile (3 – 4mm) carpet with integral foam rubber pad (worn). Oval pool 64 x 81cm ignited 6min after pouring. Ambient temperature: 15°C. Flames spread immediately across pool. Clear yellow flames in a classical intermittent pool flame plume, 0.5 –1 m in total height were established. A pronounced halo of charred carpet formed immediately outside wetted area. All damage was external to pour area until 2 –3 min, then surface scorching and charring of central area occurred. Flames self-extinguished after about 5 min.

Test 3: One litre of methanol was poured on commercial-grade, polypropylene short loop-pile carpet with foam rubber pad. Oval pool 66 x 89cm ignited 5min 20s after pouring. Ambient temperature: 15°C. Flames spread immediately across pool. Clear yellow flames in a classical, intermittent pool flame plume, 0.5 –1 m in total height were established. A pronounced halo of charred carpet formed immediately at edge of wetted

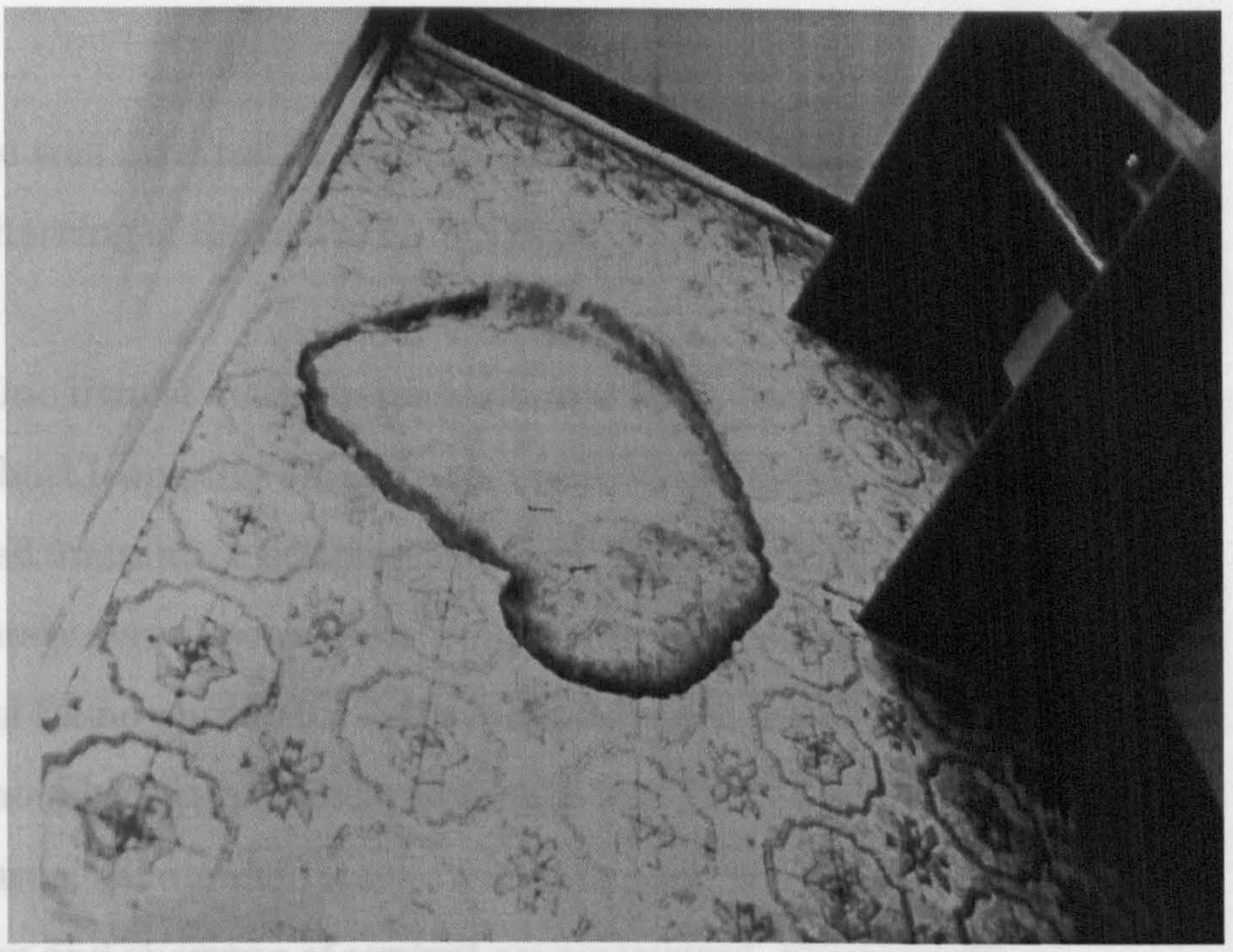

Fig. 3.10.1.1: Methanol pool fire on acrylic carpet (Test 1). Low luninosity flames are barely visible but the carpet has charred in a halo pattern around the margins of the pool. Some scorching of the carpet pile has begun in the lower right quadrant of the pool as the methanol evaporates.

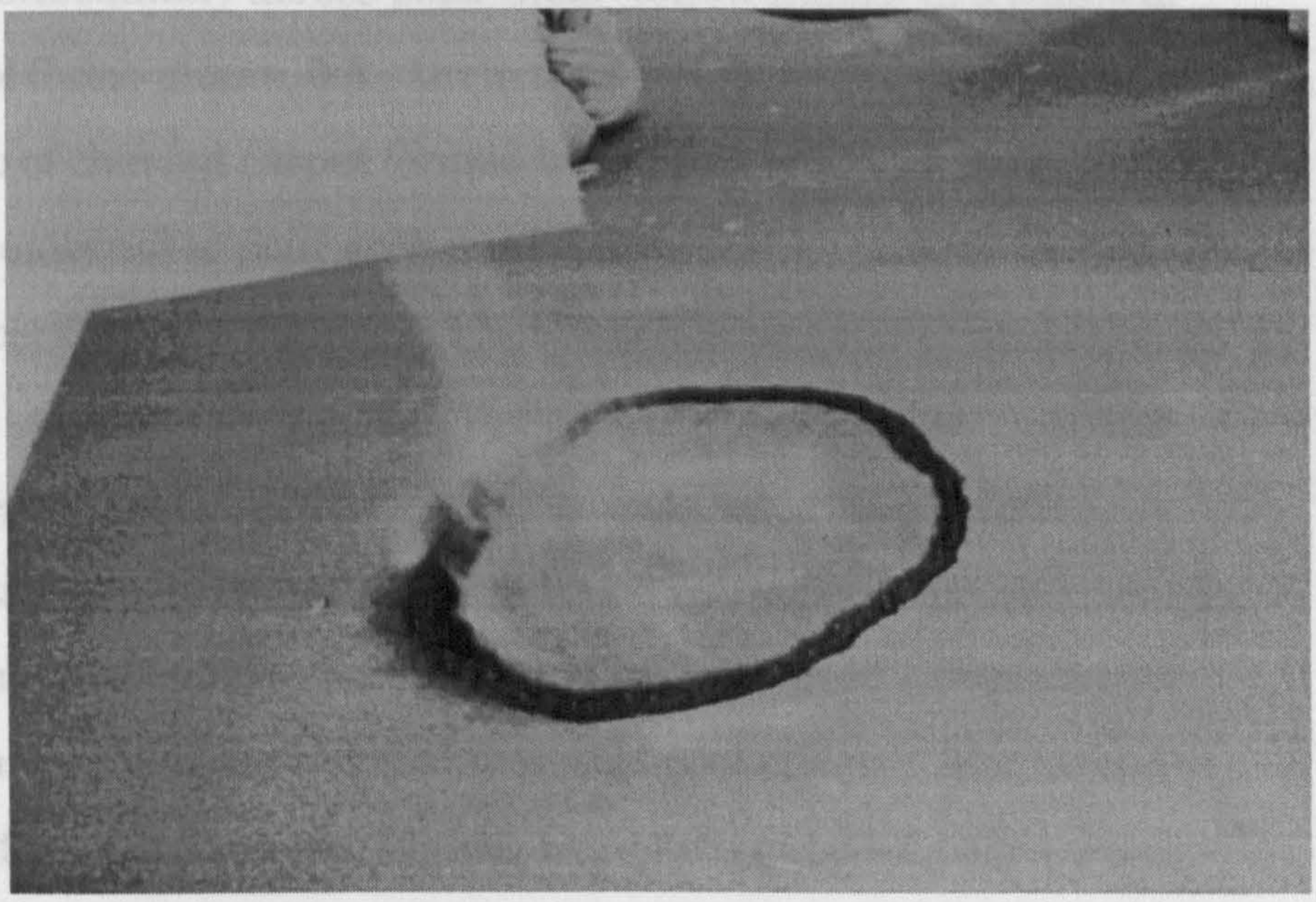

Fig. 3.10.1.2: Methanol pool fire on polypropylene loop-pile carpet (Test 4). Low luminosity flames are barely visible but the carpet has charred in a halo pattern around the margins of the pool. Flames are just visible. Photo taken approx. 1min after ignition.

area. All damage was external to pour area until 2 min, then surface scorching and charring of central area occurred. Flames self-extinguished at about 5 min.

Test 4: One litre of methanol was poured on commercial-grade, polypropylene short loop-pile (3mm) carpet with foam rubber pad. Oval pool 71 x 76cm ignited 5min after pouring. Ambient temperature: 15°C. Flames spread immediately across pool. Clear yellow flames in a classical intermittent pool flame plume, 0.5 – 1m in total height were established (Fig. 3.10.1.2). A pronounced halo of charred carpet was formed immediately outside wetted area. All damage was external to pour area until 2min, then surface scorching and charring of central area occurred. Flames self-extinguished after about 7min.

Test 5: One litre of methanol was poured on residential-grade, nylon short-shag (15mm) pile carpet with urethane foam rubber pad. Ambient temperature: 21°C. Circular pool 38 x 38 cm was ignited 5min after pouring. Flames spread immediately across pool. Clear yellow flames in a classical intermittent pool flame plume, 0.5 –1m in total height were established. Pronounced halo of charred carpet formed immediately outside wetted area. All damage was external to pour area until 2 –3min, then surface scorching and charring of central area occurred. Flames self-extinguished about 5 min after ignition.

Test 6/Test 7/ Test 8: Three tests were conducted on deep pile (15mm) synthetic carpet remnants over felt pad using petrol poured directly on the carpets in a pool-and-trailer pattern. Each produced a pronounced ring or halo of char external to the visibly wetted pool of liquid that extended slowly outward from the margins. Flames were extinguished with a water spray about one minute after ignition. There was virtually no damage to the

pile of the carpet in the central area of each pool.

3.10.2 Room Calorimeter Tests

Three tests were conducted in the room calorimeter facility at the California Bureau of Home Furnishings Laboratory, as follows:

Test 9: Camping Fuel, 1.9 litre on synthetic short-shag pile carpet.
Test 10: Camping Fuel, 1.9 litre on synthetic short-shag pile carpet with latex rubber pad.
Test 11: Camping Fuel, 1.9 litre on synthetic short-shag pile carpet with latex rubber pad.

In each test, the fuel was poured manually from a graduated cylinder at a central location, from a low (15cm) height to minimize splashing losses (Fig.A2.10.2.) There was no mechanical ventilation or excessive activity in the room between pouring the fuel and ignition. To allow some evaporation, 20 – 30s was allowed to elapse prior to ignition by direct application of an open flame. Each ignition caused a very rapid involvement of the entire surface wetted with fuel, taking less than 2s from ignition to full involvement. There was no "fireball" observed, merely a lateral rush of flame extending from the ignition source. The convective flame plume from the pool was observed to grow over a period of time and to reach the ceiling (2.4m) approximately 20 – 45s after ignition in each case (Fig. A3.10.2.1). Each fire was observed to diminish as quickly as it had grown, and within three minutes, was limited to consuming the carpet and pad, which had been ignited by the burning fuel. Until that occurred, there was very little smoke, and what there was was white or very light grey in color. Between 2 and 3

minutes, as the carpet became the predominant fuel, the smoke became darker in colour, reflecting the less complete combustion of the solid fuel.

The heat release rates (HRR) for the two open-door fires are shown in Fig. A3.10.2.2. Test 9 produced a maximum HRR of 1147 kW at 1min5s after ignition. Test 10 produced a maximum HRR of 892 kW at approximately 1min25s after ignition. The lower HRR and slightly longer time to maximum heat output was thought to be due to the thicker pad/carpet combination in Test 10 (resulting in a smaller pool) and slower combustion due to slower release of fuel from the fixed carpet/pad combination compared to the unpadded carpet, which allowed combustion to occur under the free edges.

The temperatures recorded are subject to the vagaries of measuring a turbulent process at a single fixed point and so should be considered averages over time and only approximate in actual value. The temperature data for all three tests is shown in Table A3.10.2.1. While the HRR itself could not be measured for Test 11 (closed door), the data in that table indicate that the two fires on padded carpet differed very little in performance. The maximum temperatures at both ceiling and mid-level are the same (to within measurement error). The higher temperatures recorded for Test 9 were probably the result of a larger pool of liquid on the unsecured,unpadded carpet, resulting in faster combustion.

The room concentrations of O_2 and CO_2 for tests 9,10 and 11 are recorded in Fig. A3.10.2.3. In Test 10 (open door), the normal oxygen level (20.9%) remained steady for only 20 – 30s after ignition (at 16s) and then started to fall very quickly as the flames grew larger. The CO_2 level began to grow at the same time and grew in complete symmetry with the O_2 consumption. After 1min19s , the CO_2 concentration began to drop as the

O_2 level continued to decrease. This appeared to be linked to a transition from a premixed vapour/air fire to a pool fire. The pool fire is much less efficient than the premixed phase, and a corresponding jump in the CO production rate occurred at about the same time (see Fig. A3.10.2.4). The CO level in the open-door test (#10) began to rise quickly 51s after ignition, reached a peak of 9522ppm after 1min16s and stayed high until after 3min, when the carpet was the predominant fuel burning.

It had been thought that the ignition of a similar quantity of flammable liquid in a closed room would consume the available oxygen so quickly that the dynamics would be significantly different. As can also be seen in Fig.A 3.10.2.3, the depletion of O_2 in the closed door test (#11) was almost exactly parallel to that of the open-door test (#10) until the O_2 level went off-scale (for this system) at 8.5%. The major difference between #10 and #11 occurred later when the O_2 level in Test 10 rose back above 8.5% at 1min52s, but in Test 11 it did not rise back above 8.5% until 3min30s (presumably when the the air leaking into the room around the door closure became adequate to support the small amount of combustion that was still occurring in the carpet).

The CO_2 level increased slightly faster in the closed door test (#11) than in the open-door but never reached the very high concentration noted in Test 10. It remained very high for the duration of the test due to the limited amount of O_2 available.

The CO levels for Tests 9, 10 and 11 are shown in Fig. A3.10.2.4. The CO level increased to virtually the same very high level (9000+ ppm) at approx. 1min30s in all three tests but the onset occurred slightly sooner in the closed-door test. It dropped very quickly in the open-door test but reached a second peak in the closed door test at 2min when the camp fuel

was almost entirely consumed and there was a transition of the predominant fuel to the carpet. The CO level, too, stayed very high for the duration of the test in the closed door scenario.

3.10.3 Room Tests (Non-Instrumented)

These tests were supplemented with three non-instrumented trials in full-size rooms where 2 – 3 litres of the same camp fuel was poured on a carpeted floor, allowed to stand with no forced ventilation for 30s, and then ignited by an electric match. The fires were recorded on videotape for later examination. In each case, the flames were seen to rapidly propagate horizontally throughout a layer near the floor (estimated depth ≈0.5m), extending from the ignition source to the walls (distance of approx. 2m) in 0.7 – 1.4s, with very short-lived vertical plumes in the vicinity of walls and furniture. A flash of extending away from the ignition source throughout the room and lasting 1.3 – 1.4s was seen in each case. The flames in the floor layer grew larger over 30 – 40s, producing white to very light grey smoke (both inside and outside the room). From a mass of clear, yellow flames, 0.6 – 1.2m in estimated height, each fire degraded to a series of isolated pool fires in the vicinity of the heaviest accumulations of liquid fuel. After 3 minutes, the fires were all very low (flame height estimated at 0.2 – 0.5m), and then became almost entirely carpet and furnishing fires, which burned to extinguishment (unless enough fuel became involved to trigger growth to flashover).

Infrared thermal imaging of two of these fires confirmed very rapid distribution of very hot (500°C or higher) gases as a result of the turbulence caused by the extremely rapid flame propagation interacting with the furnishings. Such intensely hot gases caused generalized scorching of some

wall surfaces and ignition of thin combustible fuels such as draperies. Within 5 –10s after ignition, these hot gases had cooled by contact with walls and ceilings or dissipated by convection through window and door openings. After that time, the room assumed its normal (non-accelerated) mode of progression: a hot gas layer only at the ceiling being supplied by the plumes of hot gases generated by the small pool fires burning on the fuel-soaked areas of the carpet. This hot gas layer grew deeper if there were fires of adequate heat release rate burning in both flammable liquid and in the ordinary combustibles ignited.

3.10.4 Post-Fire Indicators

Test 1: The carpet was deeply charred at the margins of the original pool. The surface of the carpet was uniformly scorched across the centre of the pool. The jute backing was penetrated in several isolated areas. Very limited fire extension outside the original halo took place so the dimensions of the char pattern indicate the size of the original pool. (Fig. 3.10.4.1)

Test 2: Results of this test were the same as Test 1. The carpet pile was badly worn prior to the fire and there was limited localized fire penetration of backing in the traffic-worn area. Very limited extension outside original halo was observed.

Test 3: There was very limited extension outside the original halo (≈76 x 92 cm). The char and melt damage was uniform across pattern. There were no penetrations of fire damage to jute backing. The post-fire char pattern is larger than the original pool by only 5 – 10%.

Test 4: There was limited extension outside original halo (≈ 92 x 92cm). The char and melt damage was uniform across pattern. There were

Fig. 3.10.4.1: Methanol pool on acrylic loop-pile carpet (Test 1) just as flames self-extinguish. Carpet is deeply charred at the margins of the original pool, less completely scorched across the centre, and penetrated in several isolated areas where the backing has failed.

Fig. 3.10.4.2: Methanol pool fire on polypropylene loop-pile carpet just after flames self-extinguished. Carpet is deeply charred at the margins of the original pool, less completely scorched across the centre, and not penetrated anywhere. this carpet exhibited less mechanical wear than that in Fig. 3.10.4.1.

no fire penetrations to jute backing. The post-fire char pattern is larger than the original pool by 10 – 15%. (Fig. 3.10.4.2)

Test 5: There was considerable extension outside original halo. The final char pattern was circular, 59cm in diameter (150% the original pool size). The pattern was uniformly melted and charred with small, isolated fire penetrations of the jute backing.

Tests 6,7, and 8: Unfortunately, these three tests were conducted on adjoining carpet remnants and there was considerable damage from the flames of adjacent burns. External wind caused distorted fire progression and significant radiant ignition of adjoining areas. There was virtually no damage to the pile of the carpet in the central area of each pool, with undamaged white carpet pile present (Fig. 3.10.4.3).

Tests 9,10, and 11 were allowed to burn to self-extinguishment. As a result, the carpet in each test was badly damaged by fire. The carpet in Test 9, which was unsecured and unpadded, burned nearly completely. There was none of the pile left undamaged, and the jute backing was completely carbonized to the point where it was not movable. It was reduced to a number of separate pieces of charred backing. The areas with the most complete damage did not match the areas where the fuel was poured. The carpet segments in Tests 10 and 11 were secured at their edges by metal bars and were laid over latex rubber padding. As a result, the carpet in each of those tests burned primarily on its upper surface, rather than on both upper and lower surfaces as it did in Test 9. Virtually all of its pile was consumed, with a very limited area at one end that was not completely consumed. The jute backing was charred but not completely carbonized and it could be removed with care. The butyl/latex rubber pad was charred on its upper surface but was still relatively intact. The pad was

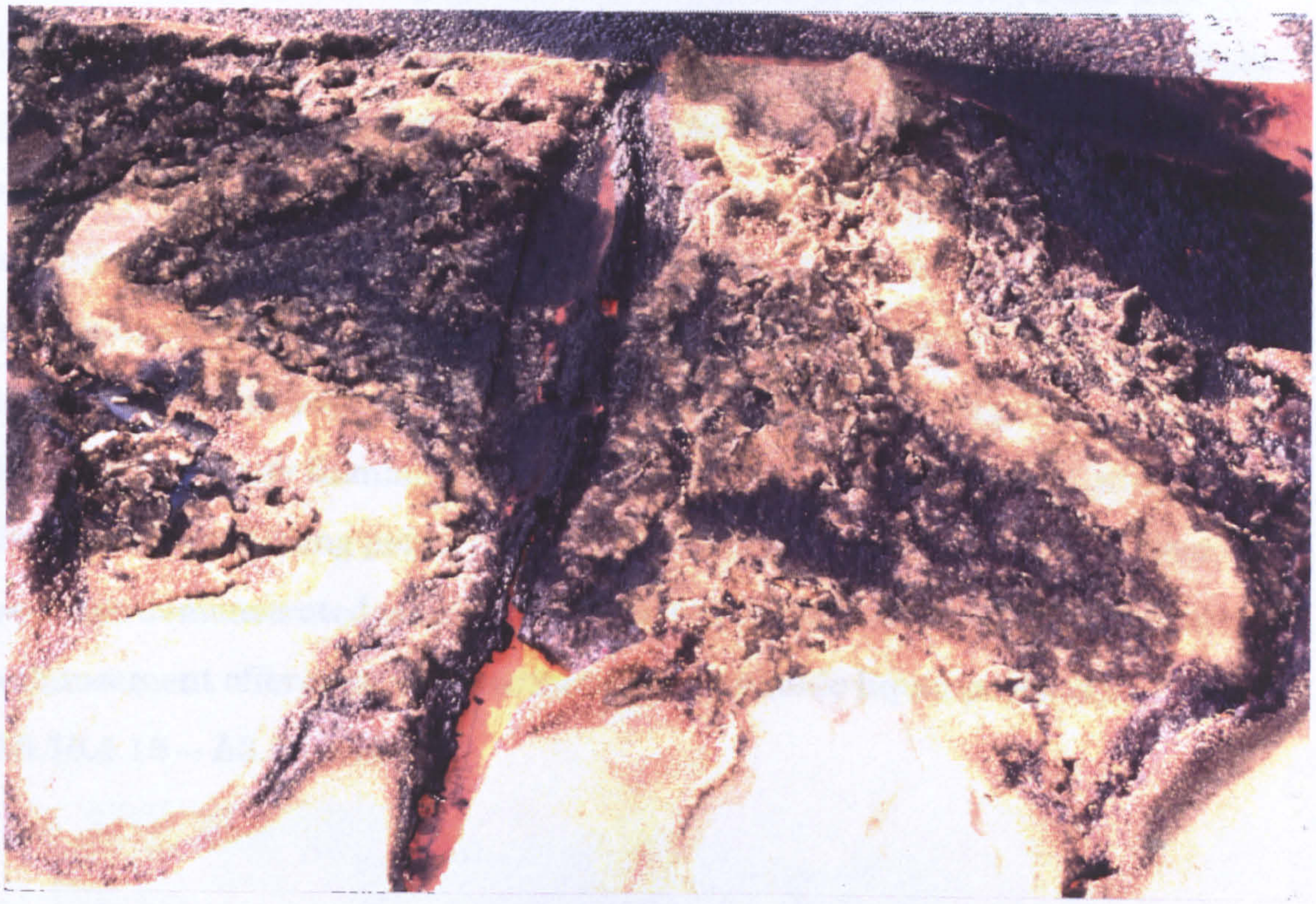

Fig. 3.10.4.3: Petrol pools on white deep (18mm) nylon plush pile carpet (Tests 6/7/8). Extinguished about 1min after ignition, the pool and "trailer" areas where the petrol was poured are clearly visible as protected areas. Surrounding areas heavily damaged by radiant heat from petrol flames.

completely penetrated only at the seam between pieces of pad. The pattern of most damage did not correspond to the pattern of pouring of the fuel. (Figs. 3.10.4.4 – 3.10.4.7)

The room fire tests were extinguished at the onset of flashover conditions prior to flaming ignition of the carpet. In each case, there was localized damage to each carpet in the vicinity of the poured fuel. The carpet pile was destroyed and there was some penetration of the jute backing in several places. Not all of the deep burns to the carpet co-incided with the location of the camping fuel. (See Figs. A3.10.4.8 – A3.10.4.13) In addition, a room fire test conducted under the same conditions, but which was allowed to progress to full-room involvement produced similar burn patterns despite the absence of any flammable liquid accelerant. (Figs. A3.10.4.14 and 15). Tests conducted using petrol or petrol/diesel fuel mixtures on various floor surfaces demonstrated considerable variation in the type of protection or enhancement offered to floor surfaces by flammable liquid pools. (Figs. A3.10.4.16 – A3.10.4.18)

Fig. 3.10.4.4: Nylon plush (16mm pile) carpet after ignition with 1.9 litres of camping fuel (Test 10) in a normally-ventilated room. Pile and backing largely destroyed by 7min of fire, especially at the end facing the ventilation source (door).

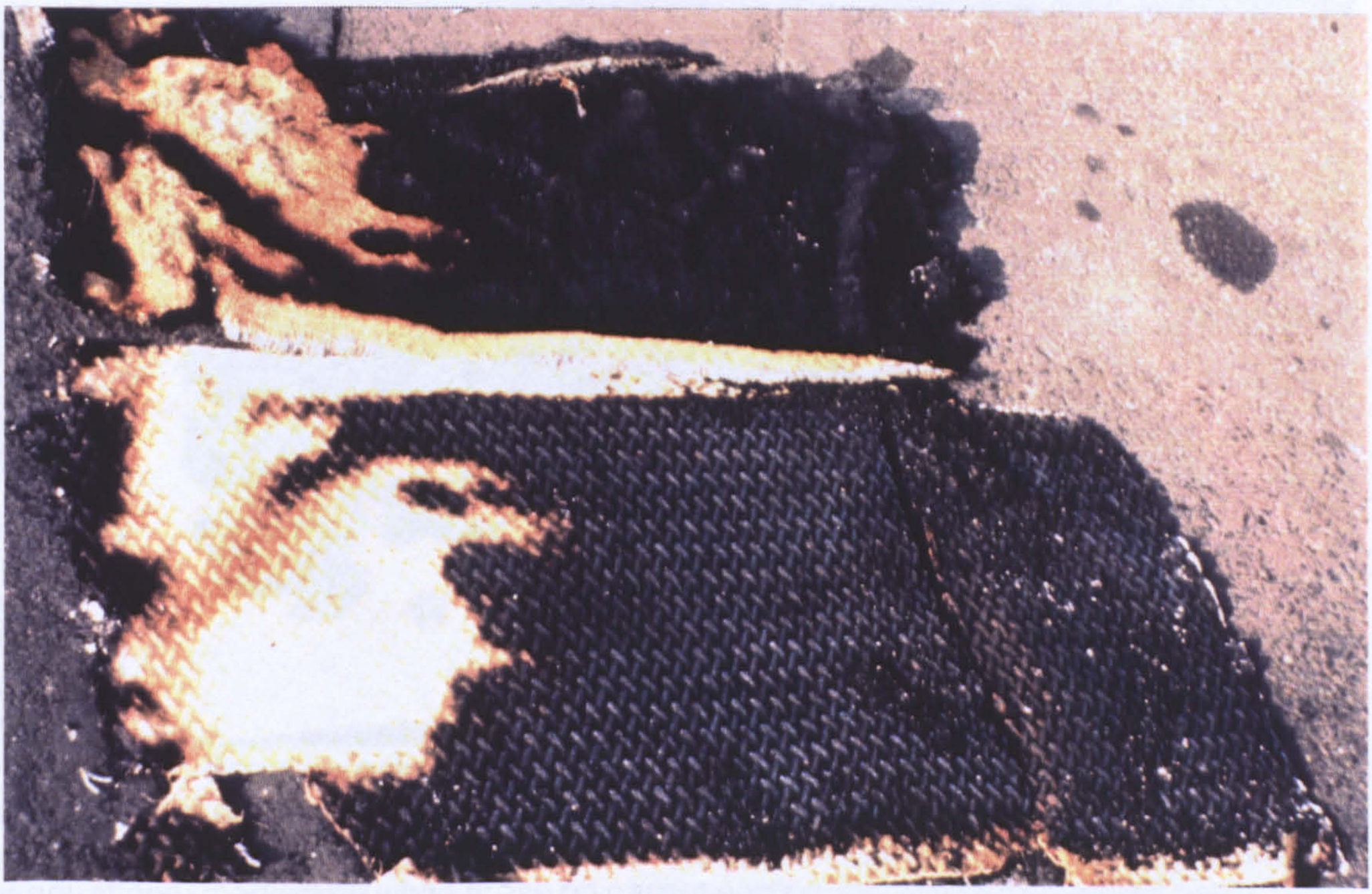

Fig. 3.10.4.5: Same carpet panel after reversal to reveal damage to rubber pad beneath. Most damage to pad cannot be linked to shape of original pour pattern.

Fig. 3.10.4.6: Fire damage to similar nylon pile carpet panel ignited with 1.9 litres of camping fuel, allowed to burn in a reduced ventilation condition for 5.5min, then allowed to burn for an additional 9min after door was opened (Test 11). Note generalized damage which was not readily identifiable with the original pour pattern.

Fig. 3.10.4.7: Same carpet panel after reversal to reveal damage to rubber pad beneath. Most of damage to pad cannot be linked to shape of original pour pattern. Note more extensive damage to carpet due to longer burning time. The H-shaped pattern of penetrations (marked by white areas on carpet and corresponding localized deep damage to pad) are in the shape and location of the pour pattern.

ANALYSIS AND DISCUSSION

Section 4

The results obtained in the preceding sections will be discussed in relation to their role in reconstructing the contribution of flammable liquid vapours to the ignition and spread of fire. These discussions will follow in the same order used in previous sections.

4.1 Pool Size v. Quantity

If we assume we are dealing with a non-volatile liquid with very low viscosity, the direct volume-to-area relationship for a one litre ($10^{-3}m^3$) pool with a uniform depth, z, at maximum pool size, could be calculated directly by dividing the volume by the depth as follows:

If: $z = 0.1mm$, area $= 10m^2$

$z = 0.2mm$, area $= 5.0m^2$

$z = 1.0mm$, area $= 1.0m^2$

$z = 5.0mm$, area $= 0.2m^2$

$z = 10mm$, area $= 0.1m^2$

$z = 14mm$, area $= 0.07m^2$

These values compare favourably with the corresponding pool sizes for liquids on various substrates observed in these tests (Table 3.1.1). If one assumes a pool depth of 0.2mm, the observed coverage of $2.5 - 4.0\ m^2/l$ on non-porous substrates is comparable to the theoretical coverage calculated above, i.e., $5m^2/l$. During the non-porous surface tests described in Sect. 3.1 estimates of pool depth were of the order of 0.2mm. Since the tests involved volatile liquids such as methanol or pentane, there must be some allowance

for evaporative losses. It was observed that pours in excess of 500ml on non-porous surfaces required 2 – 3min to achieve their maximum size, during which some evaporation was already well under way, reducing the available volume for spreading. While it would be possible to calculate the percentage of a volatile liquid lost during those first minutes (from the evaporation rate determined in later tests), for the purposes of assessment of vapour production it would be more appropriate to use the calculated maximum pool size. (The liquid that evaporates prior to the final formation of the pool is still contributing to the vapour layer and thereby to the ignition scenario; it does not really matter whether the vapour is produced during the actual spreading of the pool or after it reaches maximum size.)

For semi-porous substrates, assuming a depth of 1– 2mm yields an expected range of 0.5 – 1 m^2/l v. an observed range of 1.8 – 3.0 m^2/l on concrete and 1.3 – 2.2m^2/l on plywood. A depth of 1 – 2mm is consistent with that observed in the concrete penetration tests (Sect. 3.1.1). Here, the calculated area is smaller than that predicted by a factor of two. It was observed that the area covered was not directly proportional to the quantity for large volume pours. Doubling the quantity of liquid poured (from one litre to two, for example) did not double the area. In fact, quantities over one litre produced the lowest area coverage per litre. It was observed that the longer time required for the larger quantities to spread allowed for more penetration into the substrate and would also allow more time for evaporative losses from the still-spreading pool. While this was not measured directly, it was made evident by the visible wetting of substrates like plywood at the margins of the pool. Very small quantities (10ml) produced the largest equivalent pools because they reached their maximum area in such a short time that the substrate did not have time to absorb any significant quantity. Putting it another way, for small pour volumes, semi-porous substrates act

as non-porous ones, at least in terms of coverage. In terms of assessing the contributions of the evaporating liquid, the maximum area is most suitable as a part of a predictive model.

For porous carpets, using the pile depth of each of the carpets as an estimate for pool depth (z) results in:

4mm Carpet Pile — Expected : 0.25 m^2/l Observed: 0.3 – 0.5 m^2/l

10mm Carpet Pile — Expected: 0.1 m^2/l Observed: 0.08 – 0.1 m^2/l

14mm Carpet Pile — Expected: 0.07m^2/l Observed: 0.05 – 0.06 m^2/l

This good agreement demonstrates that, knowing the conditions of the floor covering prior to the fire, the investigator can estimate the area that can be covered by a given quantity of liquid using some basic assumptions and a very simple calculation.

The investigator must realize that there is a very range in the surface area that can be covered by a pool from a given volume of fuel. Pool areas can range from less than 0.1m^2/litre on deep carpet to as much as 4m^2/litre on a smooth vinyl floor.

If one is dealing with a flat, non-porous floor surface, one can assume a pool depth of 0.2mm and calculate accordingly. This is reasonable in light of experimental results obtained here for a variety of non-porous surfaces.

For semi-porous surfaces such as unpainted plywood or concrete, one can assume a pool depth of 1– 2mm and calculate accordingly. This estimate will not be as accurate for single-point pours of quantities over one litre which may require longer times to spread (thereby producing deeper penetrations and smaller final pools). Such situations would be balanced against the very small pools, which reach their maximum size before any absorption occurs. When liquids are being poured intentionally, they may be spread as a series

of small pools (less than 0.5m^2 in area) and narrow trails or streams between those pools or as a more-or-less continuous series of irregular discharges from the container. Observations of pours carried out during fire tests conducted as part of Sect. 3.9 indicate that a 1mm pool depth will tend to be a reasonable compromise assumption despite variations in pool size.

For absorptive substrates, maximum pool size is achieved very quickly as lateral spread by capillary action seems to be very limited for coverings such as carpets (at least in the time frames under consideration here, under 15min). Using the depth of the pile of the carpet as a guide to the depth of the pool is a useful means of calculating final pool size. Many carpets today have a sealed self-backing (synthetic rubber or urethane foam rubber). More carpets are being produced today with the pile bonded to a polypropylene mesh using a contact cement-like adhesive that seals the pile off from the backing. Older carpets with a porous jute backing will allow penetration of a liquid through the pile. If such carpet is laid over a foam pad with a vapour barrier, the penetration will stop there, with a relatively small influence on the effective depth of the substrate. If the carpet is laid over a traditional rag pad or over bare wood or concrete, there can be considerable penetration and the resulting pool will be much smaller than would result from absorption by the carpet pile alone. The investigator would be well advised to secure and retain a sample of both the carpet and the pad as a comparison sample, if an estimate of this type is thought to be likely.

Using the Melhem formula to calculate the radius of the pool:

$$r = [(r_0)^2 + (8g(1-s)V_0/\pi)\, t\,]^{0.5} \text{ [Melhem/Croce]}$$

requires an estimate of the shape factor, s, resulting from the profile of the pool edge. This shape factor has no applicable model other than to be

correlated with the results observed in this study. For a starting volume, V_0, of one litre and a starting radius of $r_0 = 10cm$, the pool area at time 60s can be calculated using that formula, substituting for various values of s:

where s = 0.5, Area = $20.7m^2$

s = 0.9, Area = $9.4\ m^2$

s = 0.99, Area = $3.1\ m^2$

For arbitrarily selecting s = 0.99, the Melhem model yields a projection close to the observed results for non-porous surfaces ($2.12 - 4.0m^2$). The effect of a very small starting radius, r_0, can be ignored, i.e., r_0 assumed to be 0. The Melhem formula, however, is valid only for instantaneous spills on non-porous surfaces and has no allowances for evaporation or absorption during the spreading process. In addition, the shape factor, s, cannot be readily established for pools spreading on or through porous substrates. It is much more straight-forward to use the pile depth of a carpet as the pool depth or to assume a uniform depth of 0.2mm on non-porous surfaces or 2mm on semi-porous surfaces to calculate maximum pool areas.

One interesting effect of this approach is apparent when one is dealing with infinitely deep porous substrates such as dry beach sand. In those cases, there is no substantial horizontal spread, and the pool is the same size as the contact patch of the original pour or spill. This has been observed when there has been a slow leak from a storage container that produces a laminar stream of small diameter. The resulting pool on dry sand or soil is the same diameter as the stream, often one centimetre or less in diameter.

4.2 Evaporation Rate v. Substrate

The evaporation rates observed in the pool tests in this study (Table 3.2.1.1) are generally comparable to the results of Kawamura and Mackay, as shown in Table 4.2.1. For insulated pools of n-pentane evaporating at 20 – 21°C, initial rates of 90 – 175 g/min/m^2 (and a norm of 143 – 150 g/min/m^2) were observed here. These are equal to 6 – 10.5kg/m^2/h. Their experiments were conducted in an exterior location with some wind and solar exposure, and generally at lower temperatures than those here (1 – 9°C). Their experimental results ranged from 6.84 to 10.52kg/m^2/h. These results are for bulk evaporations, which will undergo heat loss due to evaporative cooling (aided by mild wind in some cases), but will also sustain gains in heat by solar radiation, which did not take place in these experiments. In the experiments conducted here, there was no solar radiation and very limited ground conduction (the Styrofoam having a fairly low thermal conductivity). As a result, the pool temperatures dropped over the course of 10 –15min to 3 – 8°C, at which time the equivalent evaporation rate was 31 – 56g/min/m^2 (1.86 – 3.36 kg/m^2/h). Over that time interval, taking an average produces a result in the range 4 – 6 kg/m^2/h, which compares very favourably with the predictions of Kawamura and Mackay's direct evaporation model (4.19 – 7.22kg/m^2/h) as well as their surface temperature model (5.67 – 8.39kg/m^2/h) for those conditions. This would seem to be excellent correlation for the experimental results obtained here despite different thermal conditions. Actually, the difference between the rates obtained here

Table 4.2.1: Comparison of Pool Evaporation Rates v. Model of Kawamura and Mackay (1987)

Present Experiment	Kawamura/Mackay		
	Experimental	Direct Model	Surface Temperature Model
Pentane (at 21–22°C) (No wind or sun) (kg/m^2-h)	Pentane (at 1–9°C) (Wind and sun) (kg/m^2-h)	(kg/m^2-h)	(kg/m^2-h)
Initial Rate: 6–10.5 Final Rate: 4–6 (at 3–8°C)	6.84–10.52	4.19–7.22	5.67–8.39
Hexane (at 20–21°C) (No wind or sun) (kg/m^2-h)	Hexane (at 22°C) (Wind and sun) (kg/m^2-h)	(kg/m^2-h)	(kg/m^2-h)
Initial Rate: 1.9–3	10.88	10.9	13

for an insulated pool at 3 – 8°C (1.86 – 3.36kg/m^2/h) and their predicted values for an insulated pool exposed to sun and wind at the same ambient temperatures (4 – 8kgm^2/h) indicate the role that solar radiation and even a modest wind can play in pentane evaporation.

The correlation for hexane is not as good, however. The initial evaporation rates for hexane observed in these tests, 31 – 50g/min/m^2, are equivalent to 1.9 – 3kg/m^2/h. This is considerably lower than Kawamura and Mackay's experimental result of 10.88kg/m^2/h for a hexane pool and their model predictions of 10.9 – 13kg/m^2/h. It should be remembered that their pools, while of equivalent size to those tested here, were exterior pools subject to wind and solar radiation (which were not specified in their results). These sources of heat will all play a role in supporting evaporation. It may be that hexane, due to its lower heat of vaporization, is cooled less by evaporation. A hexane pool, then, would be maintained at a higher temperature and more easily evaporated by wind. Over the course of the tests conducted here, the pool temperatures for hexane evaporating at 20 –22°C were found to be 12.2 – 13.7°C at the end of the run. These temperatures are considerably higher than those observed for pentane pools under the same conditions (3 – 8°C) and would produce higher overall vapour pressures, as well as diffusivities, both of which would support faster evaporation. Some of the thermodynamics of these systems will be discussed further in Sect. 4.8.

The net effect of having a porous substrate is to increase the effective vapour pressure of the volatile liquid evaporating from it (Fig. 3.3.2.3). The surface texture of a substrate will affect the vapour pressure of any liquid

distributed on it by increasing the surface area and providing many small projections around which a film can assume a convex shape. Each of these surfaces here, however, are saturated with liquid at the start of each run. This means that there are no air/liquid interfaces offered within the fibrous interstices. This leaves surface texture to provide additional convex projections to encourage evaporation. This certainly accounts for the difference in rates between liquid pools and all matrices, but not for the differences observed between matrices.

While the texture of the surface of each of these substrates exhibits approximately the same degree of roughness, the differences between rates for sand/aluminium matrices and those of the other substrates indicate that a factor other than surface texture is affecting the vapour pressure and therefore the evaporation rate from substrates (Tables 3.2.2.1 – 3.2.2.4). If anything, the surface texture of each of the carpets tested could be described as rougher (having more coarse convolutions) than the surface of either sand or aluminium granules. Yet, carpet matrices exhibit lower initial evaporation rates than sand or aluminium granules and rates equivalent to those of smooth-textured plaster or urethane foam. Because these differences are observed at the start of evaporation before any significant heat transfer can take place, and because the initial rates for sand is the same as that for aluminium granules, it is clear that differences are not due to the heat capacity of the substrate. All liquids and substrates were at equilibrated to ambient temperature prior to the start of each run. While sand is not commonly encountered as a floor covering in fire investigations, it offered a porous structure which could be more easily classified (by mesh size) than could carpet pile. Aluminium granules were used to isolate the effect of capillarity from thermal conductivity by providing a structure with the same porosity (mesh size) but with a very different thermal conductivity.

The fundamental difference between the granular matrices and the other porous matrices is the nature of the contact between adjacent elements. Granulated substrates offer multiple surfaces for liquid to be trapped but also free to move by capillary action. It appears that the differences in surface tension and viscosity between hexane and pentane may account for the differences in transport in sand and granulated aluminium where the capillarity between the individual particles could play a role in enhancing mechanical transport of the liquid to the surface to replace that being lost by initial evaporation.

The capillarity of a bed of granular material may be characterized by a suction potential, i.e., the effective negative pressure that causes fluid in that bed to rise towards a surface from which the fluid is being lost by evaporation. The suction potential is a property of the matrix, that is, it is related to the properties of both the fluid and the bed or substrate, as in:

$$P_S = X\mu / r\, p\, g\,,$$

where P_S = suction potential (m of water) (*sic.*)

μ = surface tension (dynes/m) (*sic.*)

X = packing factor

r = radius of spherical elements (m)

p = density of liquid (kg/m^3)

g = acceleration due to gravity (m/s^2) (Porter, et al. in Perry)

It can be seen the smaller the radius of the elements or the larger the packing factor, the higher the suction potential. The radius and shape of the particles in the sand and aluminium granule matrices are very similar and we see that their effect on increasing effective vapour pressure and evaporation rate is similar.

Carpet, however, is not composed of closely packed spherical elements, but rather of cylindrical rods with considerable void space between adjacent elements. The packing density of such a material would be expected to be lower than that of sand, and we see, in fact, a lower evaporation rate for carpet than for sand. The lower the packing density is, the higher the void space. While neither property is easily measured with precision for substrates such as carpet, the void space can be approximated by examining the volume of liquid needed to fill the Petri dish used with various substrates in place. Substrates with a high packing density (low void space) such as sand and aluminium granules required only 90 – 100ml of pentane to fill the Petri dish to the rim, while those with a higher void space (carpet and foam) required 220 – 250ml to saturate the substrate to the rim. The carpet and foam matrices, while porous, have a large void space and, therefore, do not have the intimate and continuous element-to-element contact exhibited by the granular matrices. The suction potential they display by forcing more liquid to the surface is going to be reduced when compared to that of sand or aluminium granules. The evaporation rate for n-pentane from either fine-cell polyurethane foam or plaster of Paris is approximately 1.5 times the rate for a liquid pool under the same conditions. The observed rate for hexane on foam is about the same as for a pool (albeit for a very limited sample) while that on plaster is about twice the rate for a liquid pool. It may be that the higher viscosity for hexane offsets any increase in suction pressure that its higher surface tension would produce in some matrices.

The larger heat capacities offered by the insulated matrices studied here (especially those with sand and aluminium granules) will, of course, affect the cooling experienced by the liquids, but the marked differences

between matrices are observed at the very start of the evaporative process, before any cooling can take place. The thermodynamics of these matrices will be discussed in more detail in Sect. 4.8.

For purposes of reconstructing the events and time sequences of a fire, the relationship between the bulk properties and relative evaporation rates from pools, porous (but non-granular) matrices, and granular matrices appear to be valid. The investigator must be aware of the type of surface involved, not only to predict the size of the pool (or wetted area) that will result from the pouring of a given quantity of liquid, but also to predict how quickly that liquid will be vaporized from a given surface area of that pool.

The evaporation rate from a pool of volatile hydrocarbon liquid can be predicted from the vapour pressure of the liquid involved and the ambient temperature. The rates from porous substrates can be predicted from an evaluation of the porosity (void space) of the substrate.

4.3 Evaporation Rate v. Temperature

As would be expected from the basic relationship between temperature and vapour pressure (Fig. 1.1), the higher the temperature, the greater the evaporation rate. The data in Fig. 3.3.2.2 confirm Wade's prediction (Sect. 1.4) that:

$$e_s = K p_e^{1.25}.$$

Kawamura and Mackay's derivation, which is based on the relationship

$$E_a = (0.029u^{0.78}x^{-0.11}Sc^{-0.67}) Mp_s/RT)$$

would, at first glance seem to imply an inverse relationship between evaporation rate and temperature [Kawamura & Mackay]. Closer inspection shows that other factors are temperature dependent. The Schmidt number is the ratio of kinematic viscosity to diffusivity (which is dependent on $T^{1.5}$), and p_S, as we have seen, is directly dependent on T (by the Antoine relationship). Here, the Schmidt number is used in an inverse power, so the term $Sc^{-0.67}$ will increase with increases in diffusivity. In these present experiments, the wind velocity term is not zero but is very small due to the slow laminar movement of vapours away from the pool by advection. If we treat the effective wind velocity, u, and the pool dimension, x, as constants, we can test the relationship:

$$E \text{ proportional to } (D/\upsilon)Mp_S/T.$$

Using the diffusivities calculated in Sect. 1 (Table 1.2) and calculating DMp_S/T (in arbitrary units) for n-pentane and hexane at temperatures of 5, 20, and 35°C, then plotting the results against the evaporation rates (norms of ranges) observed in these experiments (from 12mm deep pools of $0.016m^2$ area), yields Fig. 4.3.1. It can be seen that there is excellent linearity even though the kinematic viscosity term of the Schmidt number has been disregarded. Over the temperature range here, the kinematic viscosity decreases in essentially a linear fashion, so incorporating it would only change the slope of the plots, not their linearity. Such approximations may not be true for temperatures much higher or much lower than those under consideration here. It is very rarely that fires start in buildings whose ambient temperatures fall outside the range of 5 – 35°C. For the purposes of fire reconstruction, the evaporation rate is directly dependent on the term $(D/\upsilon)Mp_S/T$ as predicted by Kawamura and Mackay.

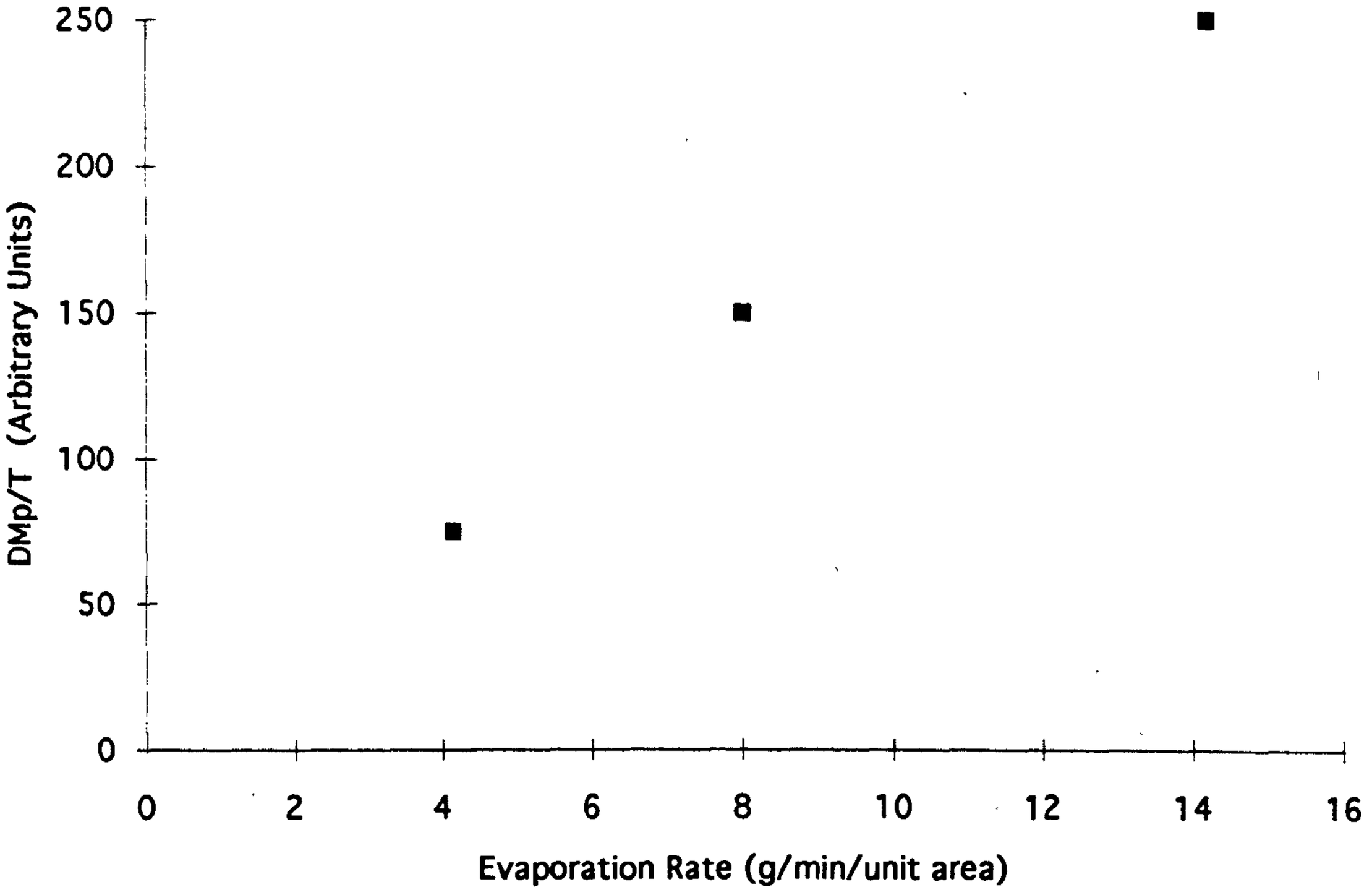

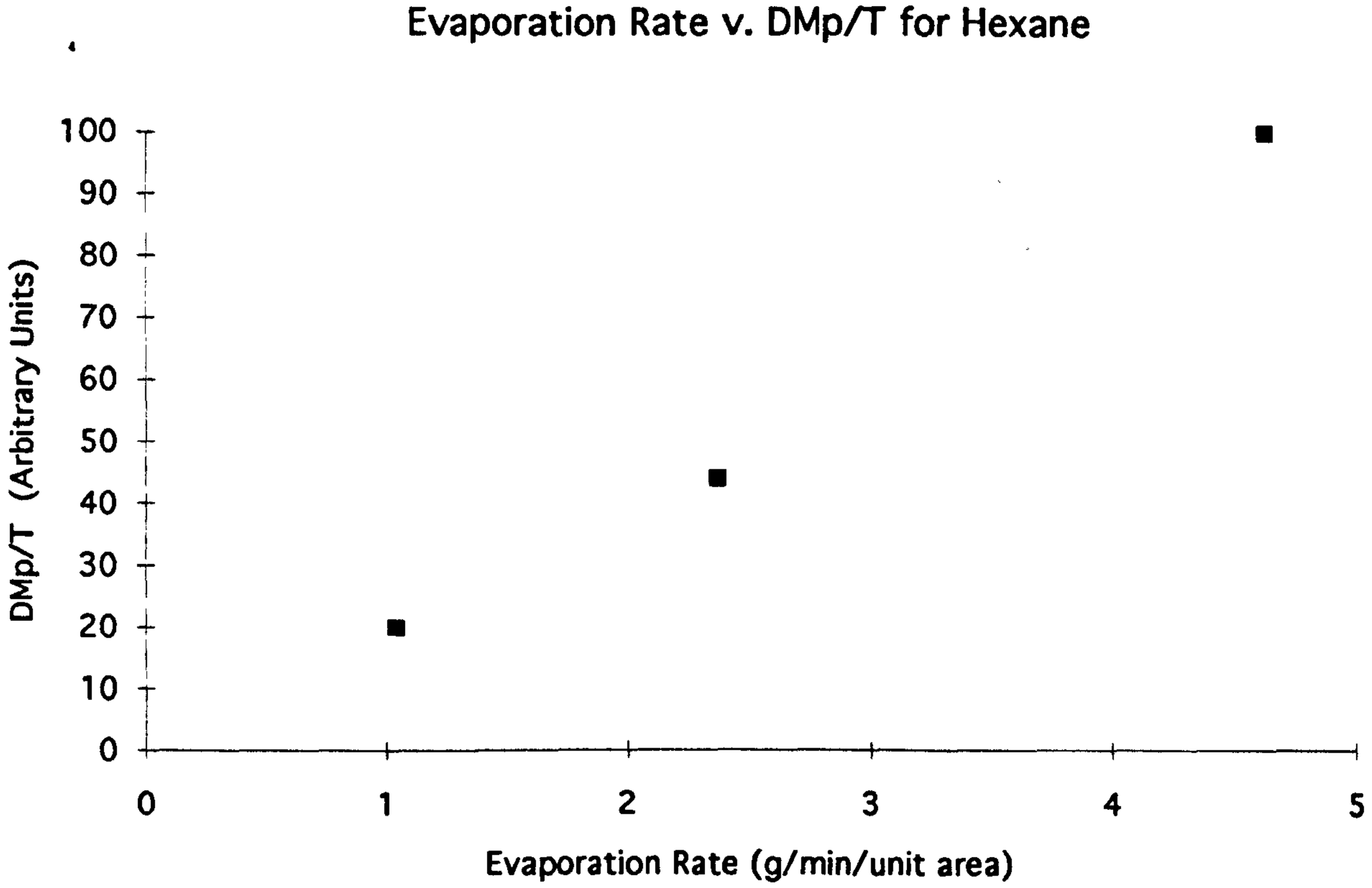

Fig. 4.3.1: Initial evaporation rates of n-pentane and hexane v. Dmp/T at starting ambient temperature of 5,20, and 35°C

The influence of temperature on evaporation rate over the range of 5 – 35°C can be predicted with reasonable accuracy. The relationship between surface temperature and evaporation rate will be further discussed in Sect. 4.10.8.

4.4 Rates v. Pool Size

Intuitively, one would expect that there would be a direct, linear relationship between the area of an evaporating pool and the corresponding mass loss rate. It would also be expected that as pool area approaches zero, the mass loss rate and evaporation rate would also approach zero. The plot of mass loss rate v. pool area (Fig. 3.4.1) demonstrates a relationship that is not constant and does not approach zero for very small pools. The marked departure from linearity for pools of area $\leq 0.01 m^2$ (diameter $\leq 0.12m$) occurs in both liquid pools and carpet matrices, but is much more pronounced in the carpet matrix (Fig.3.4.2). This relationship between pool size and evaporation rate had been noted by Mackay and Matsugu in their early pool evaporation paper. [Mackay/ Matsugu] They plotted evaporation rate of water pools ($kg/m^2/day$) v. the logarithm of pool equivalent diameter (m) and demonstrated a straight-line relationship with a slope of -0.11. That correction was incorporated in their correlation for evaporation rate discussed in Sect. 4.3 in the form of the $x^{-0.11}$ term. Their study was limited to larger pools (diameter 0.3 – 20m) evaporating in open air and they cautioned that the relationship of mass transfer coefficient to diameter may not be extrapolated to very small pools (0.1m or less).

The Blinov/Khudiakov and Hottel studies of pool fires burning in various size pools [Drysdale] showed that the regression rate was

essentially constant for very large pools (D >1m), but became very high for very small pools (D ≤ 0.03m). (Fig.4.4.1). Pools in the intermediate diameter range of 0.03 –1.0 m exhibited much lower regression rates. It was pointed out that the same range was a transitional range between the laminar flames observed in very small pools and the fully turbulent flames observed in large pools. It was suggested that the evaporation from small pools is controlled predominantly by conductive heat transfer between the flames and the pool via the metal rim of the pan. The radiative heat input from the flames to the surface of the pool predominates if the diameter is very large. In evaporation studies, there are no flames to generate heat to be conducted into the pool by conductive pan rims, to be convected into contact with the surface, or to be radiated down onto the pool surface. In the present study, the pan rim was of glass, which has a relatively low heat conductivity compared to that of a metal pan rim. Considering an insulated pool, we can see that heat is initially available from the thermal capacity of the liquid and its container. Heat can enter the pool by radiation and by convection from the atmosphere, and can be conducted into the pool from the bottom and sides of the container. In the present studies, the pan and pool are insulated from the surroundings, but there is still some heat that can be conducted (albeit slowly) into the pool from adjoining areas of the Styrofoam panel. The regression rates shown in Figs. 3.4.3 and 3.4.4 show that the initial rates for pentane liquid pools increase with decreasing diameter but not nearly as dramatically as they do for pentane/carpet matrices. Examination of the thermal video images of carpet evaporation tests shows a fairly rapid contribution of heat from the adjoining areas of carpet immediately outside the pool. This occurs faster in carpet than in similar tests of Petri dish pools insulated by Styrofoam. The ratio of rim circumference v. pool area becomes

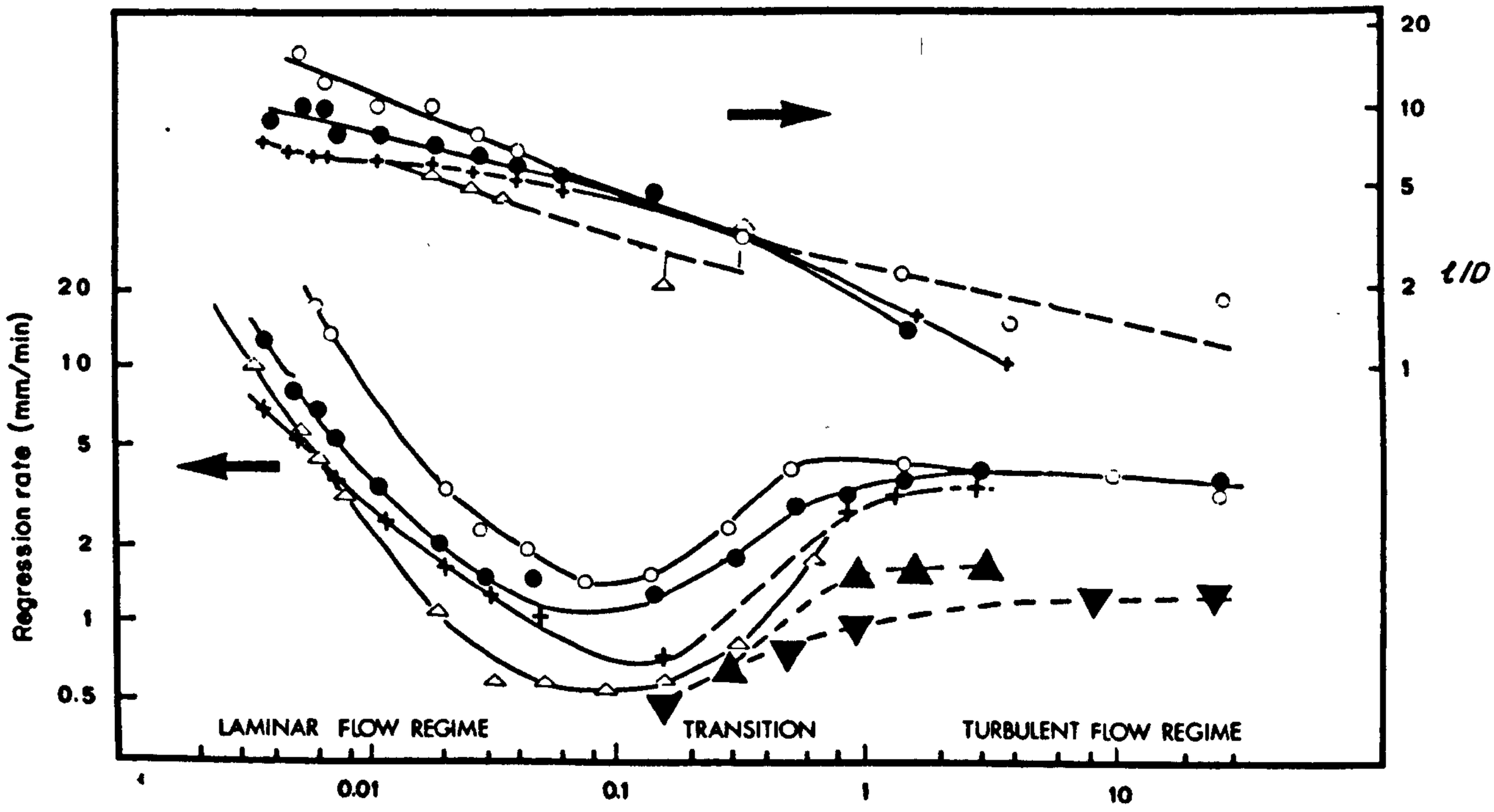

Fig. 4.4.1: Regression rates and flame heights for pool fires of various hydrocarbon fuels at diameters of 3.7×10^{-3} to 22.9m (from Drysdale).

much more significant for the smaller pools. If heat is being conducted out of the surrounding carpet via the circumference, it would be expected to play a more significant role in the smaller pools.

The regression rate measured here decreases with increasing diameter and appears to approach a constant rate of 0.1mm/min, for both free-standing pools and pools on carpet for pools with diameter greater than 0.3m. Data from the Blinov/Khudiakov pool fire tests [Drysdale] indicate that regression rates tend to reach a maximum for very small pools (radius $\leq$ 0.01m), reach a minimum near r = 0.1m, and then become constant above a particular threshold size, on the order of D $\geq$ 0.3m. It is indicated by the data here that the regression rates for evaporating pools under normal ambient conditions may become constant for all pools for which D $\geq$ 0.3m. Unfortunately, the limitations of the equipment available precluded the examination of pools greater than 0.35m in diameter. Fortunately, the pools produced by accidental and intentional spills may often be in this range of diameters.

The conduction of heat across the boundary between the liquid-saturated matrix and the dry substrate, or across the boundary between the Petri dish and the surrounding insulator, requires a temperature differential. When the liquid is poured, it is at the same temperature as the substrate, and its temperature drops very quickly as the initial evaporation takes place. This is confirmed by the videotape record of some of the tests recorded using the Inframetrics system. In those videos, the edge of the graduated cylinder can be seen as a faint outline in the thermal image but the liquid cannot be detected since it is at the same temperature as the substrate. A few seconds after pouring has begun, the growing outline of the pool beneath the lip of the graduated cylinder can be seen as the liquid begins to cool. The

initial mass loss rates used here to calculate the regression rates refer to the first 5 – 20s after pouring is completed, before the temperature of the bulk liquid drops appreciably. The carpet substrate is also a material with a low thermal conductivity, which will impede the transfer of heat from adjoining areas of the substrate. Clearly, there is another factor at work producing this differential of rates.

It should be noted that evaporation of a volatile liquid produces a layer of vapour that is at a lower temperature than the ambient air, as was seen in Sect.3.6. In the absence of wind, this layer remains above the pool, slumping sideways in a laminar viscous flow as it achieves a depth of a few centimeters, as revealed in Sect.3.7. (The production of such layers will be discussed in more detail in Sects. 4.6 and 4.7.) Such a layer will, however, exclude the normal air nearby, thereby precluding convective circulation that could supply some heat to the pool. In addition, this layer will tend to absorb atmospheric radiant heat. As a result, the role of heat conducted through the circumference becomes the dominant mechanism for contributing to the heat balance of an evaporating pool insulated from the ground. The thermodynamics of pools will be discussed further in Sect. 4.8.

The results of the same smoke tests described in Sects.3.6 and 3.7 reveal behaviour that is offered as the key to the problem of why pool area influences the evaporation rate even before conduction can play a significant role. During those tests it was observed that smoke laid down over the pool would remain static until it settled into the surface of the pool, while smoke laid down within 0.02 – 0.03m of the edge of the pool would be entrained and swept over the side of the Petri dish or pan. This was true for large and small pools but was most noticeable for pools of $D > 0.1$m. In those tests there would be a large central quiescent area above the centre of

the pool, and an annular area extending 0.02 – 0.03m inward from the edge where the smoke was swept outward. Tests above pools of $D \leq 0.06$m showed no central quiescent area. All smoke introduced above them was entrained and swept away from the edges of the pool. This behaviour would be expected to occur as soon as the vapour layer above the pool was formed, and would have the effect of making contributions from the edge of the pool much more significant than those from the area at the center of the pool. For very small pools ($D \leq 0.06$m), all of the surface would be contributing to the evaporation. For large pools, only the area of an annular ring corresponding to the outer diameter of the pool would be contributing significantly to the evaporation in still air.

This effect is confirmed by two observations from the evaporation rate tests conducted here. In the thermal images of large pools evaporating from carpet, which has a low thermal conductivity, an annular ring denoting a lower surface temperature can be seen in several of the tests (Fig. A4.4.2). A lower surface temperature at the margin of a large pool would be the expected result of more pronounced outward radial flow of the vapours due to the edge effect (as compared to the quiescent area in the center of such pools). In addition, evaporation rate tests from plaster substrates showed the formation of an annular ring where the wetted area of the plaster surface went to dryness some minutes before the central area of the plaster pool did. This occurred reproducibly when the entire surface of the plaster was flooded with pentane at the start of each run.

For the purposes of reconstruction of fires, it is not usually possible to know the size of flammable liquid pools (one exception being accidents involving catch trays or diked areas that will limit the pool size by design). In the case of intentionally set fires, it is rare for someone intentionally pouring

a flammable liquid to pour it all in one area, resulting in a single large pool. **Where arson fires involve a mixture of pools of various sizes connected by trails of liquid (whose width is dependent on the size of the pour spout of the container, but which are most often 0.05 – 0.1m in width in the opinion of this author) or a continuous pour, using the rate observed for 0.15m pools, 0.3 – 0.4mm/min, is probably justified. As can be seen from Fig. 3.4.4, such a rate is intermediate between that of the largest pool (studied here) and that of the smaller pools. This is true for both liquid pools and those on carpet. The size of the pool will affect the evaporation rate, the larger the pool the lower the rate (per unit area) over the diameter range of 0.05 –0.35m.**

However, the investigator is cautioned against applying these effects to pools significantly larger than those studied here. Kinetic mechanisms with competing factors (here, volume, spread time, evaporative losses, and absorptive effects) should not be extrapolated beyond the limits of reliable data.

It is interesting to note that Fig.4.4 also demonstrates a relationship between plume length (pl) and pool diameter (D) for pool fires involving a variety of liquid fuels. There it can be seen that flame plume behaviour of small pools is not constant with pool diameter. This relationship will be further explored in Sect. 4.10.3.

4.5 Losses from Pouring and Splashing

When a volatile fuel such as pentane or hexane is poured onto a horizontal surface, there will be some vaporization in advance of the formation of the pool. This vaporization will supplement that caused by pool

evaporation and must be included in any evaluation of vapour layer formation.

Table 3.5.1 shows that approximately 5% (by weight) of pentane poured from a height of 0.5m is lost immediately by evaporation, while 13% can be expected to evaporate if the same quantity is poured from 1m. Hexane, with its lower vapour pressure, is lost at a rate of approximately 2% from 0.5m and 5% from 1m. Moderately turbulent flows produce slightly higher rates than laminar flows at the same heights, but the rates are indistinguishable at 1m. As noted in Sect.3.5, laminar flows of low viscosity liquids such as these become turbulent within 0.25m of beginning their fall.

These data confirm that for reconstruction of intentional fires, where highly flammable liquid accelerants are usually poured from a height of 0.3 – 1.0m, it can be assumed that the pour involved was turbulent, with its corresponding losses of 5 – 13%. Highly turbulent pours, such as those that occur from metal cans with a typical 18 – 32mm opening, may double the losses produced by laminar pours at equivalent heights, 12% lost at 0.3m for highly turbulent pours versus 5% at 0.5m for laminar ones. Such a correction would mean that a highly turbulent pour of pentane from a height of one metre would result in approximately 25% of the original volume being vaporized before striking the floor. Unfortunately, it was not possible to test the losses from highly turbulent flows at heights greater than 0.3m, due to excessive splashing which resulted in a significant and non-reproducible quantity of the fuel falling outside the recovery pan. Due to weight limitations of the balance used, a larger diameter pan could not be fitted.

Splashing tests produced 6.5% losses for pentane pouring from 0.5m as compared to the 5% produced in the absence of splashing. Losses for hexane increased only to 2.5% for splashing pours, from 2.3% for non-splash. These differences were probably not statistically significant. For reconstructive purposes, the effects of splashing onto non-porous floors will have only a modest effect on the total amount of pentane in the vapour state, and no effect on the amount of hexane.

4.6 Vertical Diffusion of Hydrocarbon Vapours

Because the odours of volatile hydrocarbons are so readily detected in the vicinity of a pour or spill of liquid, it is often assumed that ignitable concentrations are readily created throughout a room by diffusion. In the absence of mechanical movement of the air in a room, diffusion may well be the predominant mechanism. The results of the tests conducted here demonstrate how slowly diffusion processes proceed.

The vertical barrier tests in Sect. 3.6.1 were expected to show that a cylindrical barrier 0.4m in diameter and 0.6m in height would significantly reduce the evaporation rate from a source within the barrier by forcing the vapours to be discharged from the top of the cylinder. The tests summarized in Table 3.6.1 showed that a 0.6m high barrier reduced pentane evaporation by 25 – 60% from the rates observed for pentane tests without a barrier. The effect was especially noticeable for matrix tests with sand and aluminium granules, where the rates were decreased by 50 – 60%. The mass loss rate for hexane, with its lower initial rate, was reduced by 30 – 40% for all types of pools. Octane saw its rate drop from an already low 0.1g/min at 20°C to 0g/min.

Increasing the height of the barrier was expected to reduce the mass loss rate even further. In one series of tests, hexane pools exhibited an equilibrium mass loss rate of 0.21 – 0.24g/min with a 0.6m high barrier. When the barrier was extended to 0.9m, the equilibrium mass loss rate was unchanged (0.22 – 0.25g/min). When the barrier was extended to 1.1m, the rate again remained unchanged, even after more than 55min had elapsed. Even placing an acrylic lid across the open top of the barrier served only to reduce the mass loss rate from a hexane pool to about 40% of its rate without any barrier at all. It was clear that the hexane vapours were unaffected by vertical stack height and that they were being lost from the barrier by some other mechanism.

The results of the IR-711 Hydrocarbon Detector in Sect. 3.6.2 revealed, at least in part, the mechanism. Starting with a pentane pool, tests of the hydrocarbon level at the open mouth of the 0.6m barrier were conducted every minute to 10min, with the results as seen in Table 3.6.2. It was clear from the very low levels detected at the top of the barrier that the vapours were not being discharged vertically despite the continuing mass loss from the pool. Tests at the base of the barrier revealed that vapours were being lost around the small gap in the barrier gasket (for power and data cables to the balance) and even through the urethane foam rubber gasket itself. This suggested that a significant percentage of the pentane vapours being generated were being dispersed not by diffusion but by a much stronger laminar flow of the vapours.

The smoke pen tests (Sect.3.6.3) revealed the formation of a distinct horizontal layer of vapour that exhibited strong convective flow, pentane vapours being at least 2.5 times the density of the surrounding air. The density of the stannic oxychloride "smoke" generated could not be measured,

but it was clear from the way it settled above an evaporating pool that it was encountering a fairly discrete boundary below which it could not settle. The formation of that boundary was consistent in height for both large and small pools of pentane. The boundary height for layers above hexane were lower than those observed for pentane. The ephemeral nature of the layers precluded direct measurement.

The thermocouple array data in Figs. 3.6.4.1 – 3.6.4.4 confirmed the production of a discrete layer that exhibited a significant thermal profile. This data demonstrated that, for pentane, a layer of vapour was generated that was denser than surrounding air due not only to its composition but also to its low temperature. The temperature gradient demonstrated here will serve to depress the vertical diffusion of the vapours. The temperature of a vapour generated by the evaporation of a liquid will be in thermal equilibrium with the surface of the liquid. As posited by Melhem and others, an evaporating liquid may be thought of as a very thin layer supported by the bulk of liquid beneath it. Since the diffusion process is so rapid immediately after initiation, the temperature of the thin layer drops very rapidly (as seen in the thermal image tests conducted in Sect. 3.8). The temperature of the vapour will also be reduced. In wind-driven evaporation, the cool vapour is quickly displaced by a fresh quantity of warmer air (with no vapour in it). The evaporation is enhanced and the temperature gradient is not very noticeable. In still air, the gradient is well-formed within two minutes of the onset of evaporation, and is controlled by the vapour layer slumping off to the sides of the pool (a process that will be further discussed in the following section). The gradient is more developed above pentane than above hexane due to its higher evaporation rate, and also more pronounced above sand matrices than above pools, again due to the higher evaporation rates from matrices.

All of this shows that diffusion plays a role in the vertical dispersion of flammable liquid vapours, but that its effect is much slower than sometimes thought. Using the Danckwerts relationship for diffusion discussed in Sect. 1.4.7, the error function can be applied to the diffusion of pentane vapours. Using the form

$$c_a/C_o = 1 - \mathrm{erf}\,(z/2(D_a t)^{0.5}$$

(since the initial concentration in the air is zero) and the diffusivity of $0.074 cm^2/s$ for pentane (at 20°C) calculated previously, the concentration can be calculated as a function of height (z) for various times (t). This concentration will be expressed as a fraction of the starting concentration (in the plane of the surface). Since that is the saturation vapour pressure of pentane in air at that temperature, the concentration can be expressed as a vapour pressure. Taking the vapour pressure of 15mmHg to represent the lower explosive limit of pentane in air as a critical threshold, the time-v.-concentration calculations can be sorted for the times required to diffuse enough vapour to achieve 15mmHg partial pressure. Plotting height v. time required to achieve 15mmHg partial pressure yields Fig. 4.6.1. From that plot it can be seen that LEL of pentane may be expected to reach only 6 – 7cm above the pool in the first 60s, while the LEL at 15cm may not be expected for 300s. The time required to reach LEL at 50cm (0.5m) will require 3600s (1 hour). Due to its lower diffusivity and lower saturation vapour pressure, hexane produces its LEL (12mmHg) more slowly (Fig. 4.6.2).

These results are comparable to the observations made in the experiments conducted. The minimal losses from the top of a 0.6m high barrier are in concert with the projected diffusion times for a test lasting less

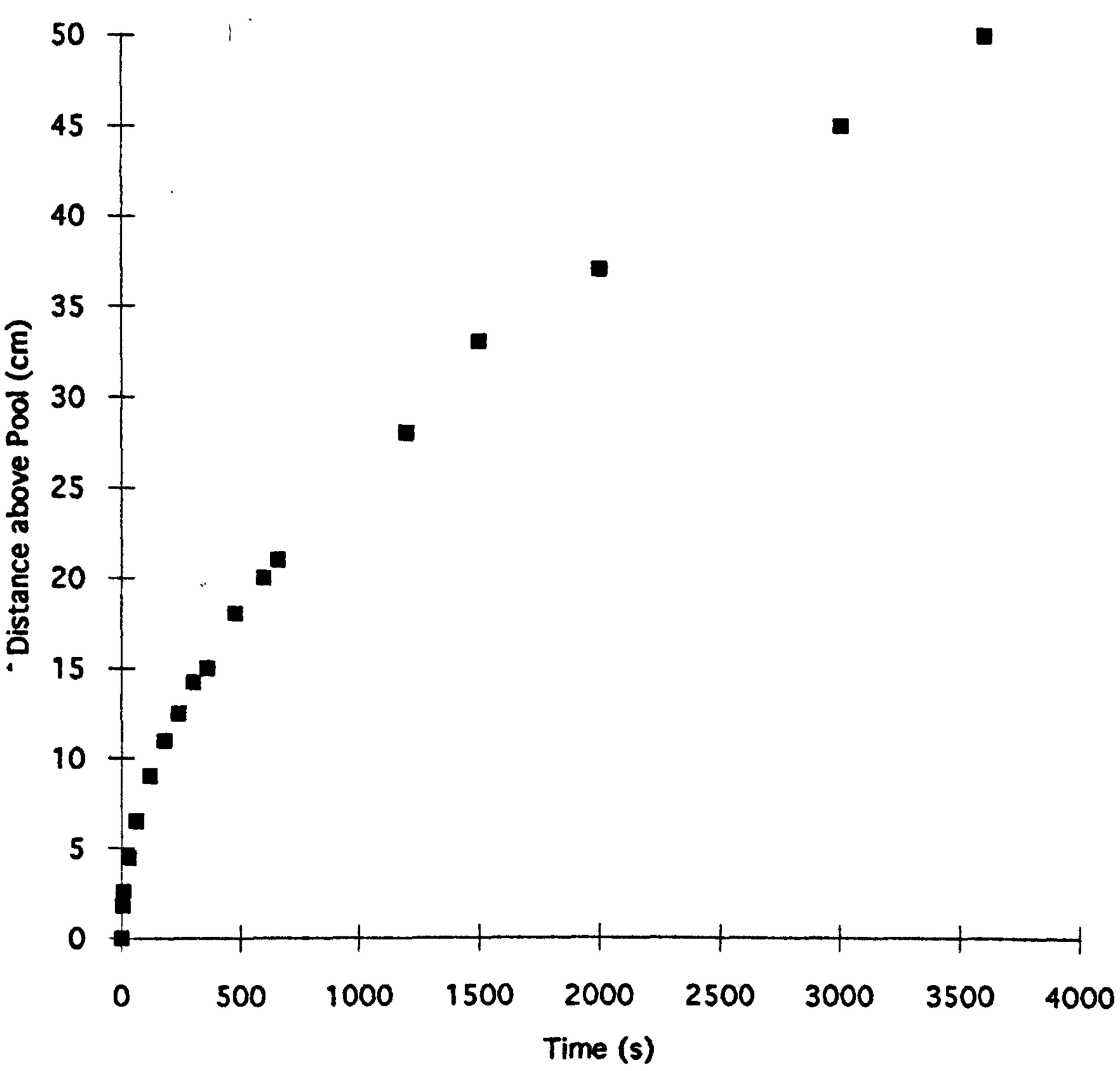

Fig. 4.6.1: Time to reach an n-pentane vapour concentration of 15mmHg (LEL) v. height above a source at saturation vapour pressure (C_o =440mmHg @ 20°C), based on error function calculation – $x/2(D_at)^{0.5}$, with $D_a = 0.074cm^2/s$.

Time to Reach 12mmHg Hexane Vapour Concentration

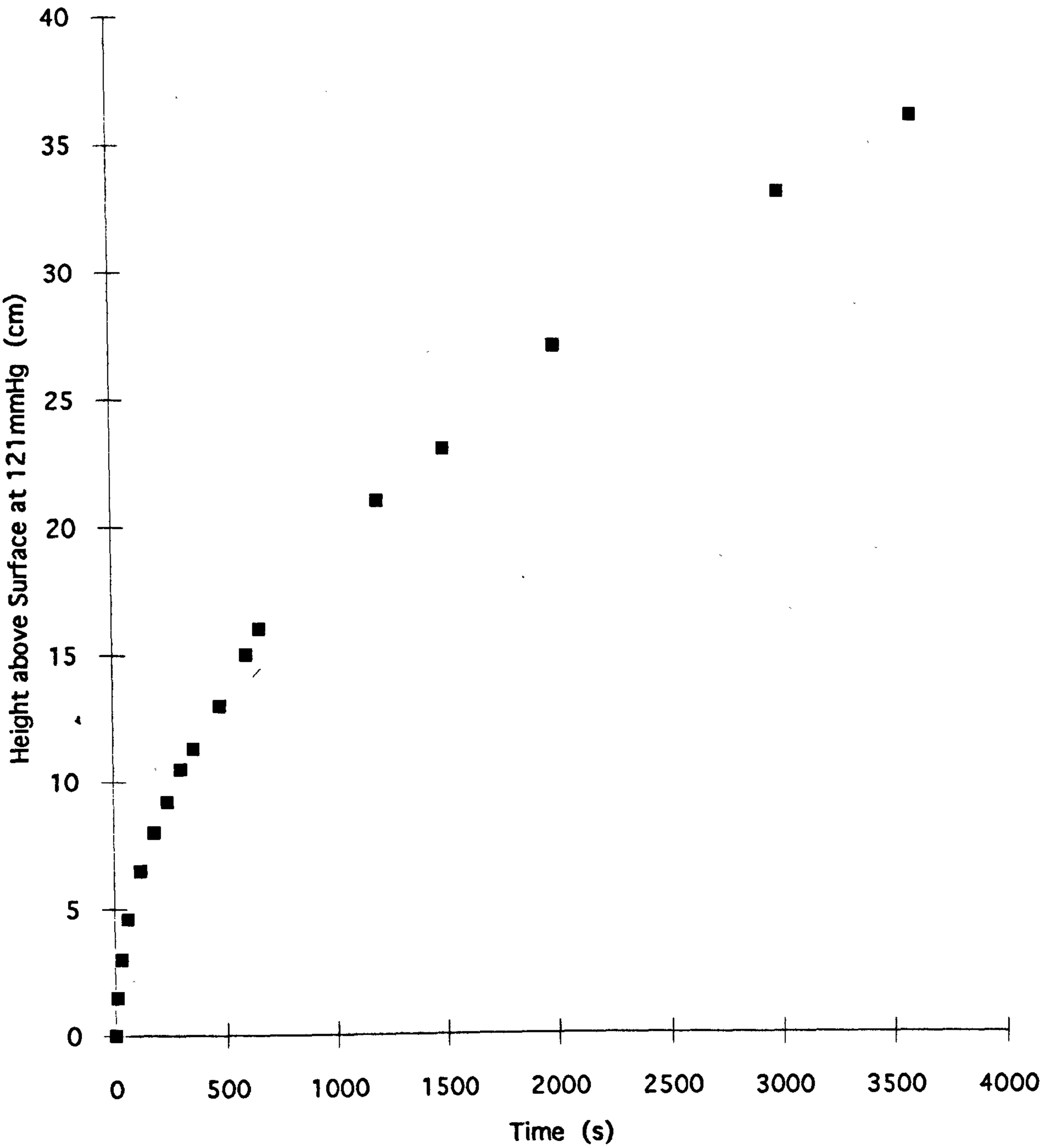

Fig. 4.6.2: Time to reach a hexane vapour concentration of 12mmHg (LEL) v. height above a source at saturation vapour pressure (C_o121mmHg @ 20°C), based on error function calculation – $x/2(D_at)^{0.5}$, with D_a = 0.067 cm^2/s. The same curve would apply to n-pentane evaporating from a pool at 5°C, however, C_o is 240mmHg for n-pentane at 5°C, so resulting concentrations will be twice those on y-axis.

than one hour. The production of a discrete layer that was more likely to spread horizontally by laminar viscous flow than to disperse vertically by diffusion was seen in the smoke pen tests (and in the hydrocarbons detected leaking out of the base of the barrier). The thermal gradient detected in the thermocouple tests would only serve to reduce further the diffusion (by imposing a gradient on the diffusivity of the vapours). This cold vapour layer would only be dispersed when heat from the overlying room air can be transferred to it by convection.

The implication for the fire investigator is significant. **The production of an ignitable layer in a room by evaporation of a flammable liquid whose vapours are being dispersed by diffusion processes alone will be very slow. It will be even slower if the room has a thermal gradient that can help maintain the gradient caused by the evaporation itself** (as Valentine and Moore showed). The height of the ignition source relative to the surface from which the evaporation is taking place will be critical. If the ignition source is at a low height, the elapsed time between production of the pool and its ignition can be very short. If it is much higher than the pool, the times can be very long. As Rabinkov points out, changes of room air will enhance the layering effect, further limiting the volume of space through which an ignitable vapour concentration is maintained.

4.7 Horizontal Transport–Advection

The results of the tests of Sect. 3.6 and discussed above demonstrated another mechanism for dispersion— laminar viscous flow or advection. The results of the tests in Sect. 3.7 indicated a slow, but perceptible flow from vapour sources. Melhem and Croce's formula for u,

the radial velocity of a vapor spreading from the release of an accumulation of vapour is:

$$u = [2\Delta (1 - s)z]^{0.5}$$

where $\Delta = g(1 - \rho_a/\rho_o)$ (acceleration due to gravity as modified for the buoyancy of the vapour with respect to air),

s = the shape factor as a function of the shape of the front, and

z = height of vapour cloud at the time of release.

By applying it to the data gathered in Sects. 3.6 and 3.7, we can test for various correlations. This formula is applicable to "top hat" shaped releases, but until now there was no way to estimate the starting height of the vapour cloud. From the information in Sect. 3.6, the height of the front of vapour issuing from a pool of pentane can now be estimated at 0.03 – 0.04m (3 – 4cm). The ratio of densities, ρ_a/ρ_o, is the inverse of the vapour density. For pentane, the density is 2.995g/l (2.995 kg/m^3) at 20°C, while that of air is 1.205kg/m^3. The ratio is then 0.4 and Δ becomes 0.6g. The shape factor is dependent on the viscosity and amount of mixing with air.

For heavier hydrocarbon vapours, where there is little mixing by diffusion, the simplified shape described by Van Ulden should be appropriate and the pool shape would look very much like a liquid of low viscosity spreading under the same conditions. If we assume s = 0.99 (the same s as for spreading of liquid pools discussed in Sect 4.1), and substitute the appropriate values, we get:

$$u = [2(9.8)(0.6)(0.01)(0.03)]^{0.5} = 0.059\text{m/s}$$

This is in good general agreement with the results in Tables 3.7.1 and 3.7.2 in which speeds of 0.02 – 0.08m/s were calculated. If a value of s = 0.9

is substituted, the same calculation gives 0.19m/s, which is much too high. It would appear that the assumption about the shape of the advancing front of vapour is appropriate. As the process continues, there will be some mixing of the pentane vapour with the air, and eventually, the buoyancy factor approaches zero, and the velocity reduces to zero, just as one would expect.

If we use Melhem and Croce's simplified formula for r, the radius of a pool of a spreading fluid for a continuous release of rate v (where $v_0 = 0$)

$$r = (2/3)^{0.5} [8\Delta(1 - s)v/\pi]^{0.25} t^{0.75},$$

and substitute the same values of $s = 0.99$ and $\Delta = 0.6g$, we get:

$$r = 0.816 (0.15 v)^{0.25} t^{0.75}$$

The rate of release (v) can be estimated from the mass loss rate. For a pentane pool with a maximum mass loss rate of 3g/min, at p of 2.995g/l, this mass loss rate becomes 1 l/min at 20°C which equals $1.6 \times 10^{-5} m^3/s$.

Then $r = 0.816 (4 \times 10^{-2}) t^{0.75} = 0.032 t^{0.75}$.

Substituting, for t = 30s r = 0.41m, and

for t = 60s r = 0.69m.

Both of these values are in good agreement with the time-to-spread values observed on the horizontal spread tests in Sect.3.7. This correlation shows that the values for z and s used are valid for pentane vapours spreading by advection. The radius estimate varies with the volume release rate to the 0.25 power. The equivalent calculation for hexane would be based on V.D. = 2.96, $\Delta = 0.66g$, but v typically for a $0.016 m^2$ pool would be only 0.7g/min. The equivalent volume rate at 3.84 g/l density would be 0.18 l/min or $3.0 \times 10^{-6} m^3/s$. Substituting in the above equation yields:

$r = 0.023\ t^{0.75}$, which gives the values for $t = 30s$, $r = 0.29m$

$t = 60s$, $r = 0.50m$

The estimate for u would be correspondingly smaller because z, the vapour pool depth is only 1 – 2cm for hexane, as shown in Sect. 3.6.

Once again, the implication for the reconstruction of a fire is significant. Diffusion in the vertical direction was considered in the previous section, but diffusion can only take place where there is a source of vapour at floor level. **In most fires, the pool of liquid will not occupy the entire floor surface of a compartment. The vapours will rise vertically from the pool only a few centimetres and will then slump laterally as a preferred direction. Vertical diffusion begins immediately above the pool surface but only when the floor area of the compartment has been covered with a layer of vapour can vertical diffusion begin in the rest of the compartment. It can be seen that the vapours from an isolated pentane pool will move laterally at about 0.05 – 0.08m/s in the absence of any wind, draught or mechanical circulation of air.**

Tests by the author of a variety of residential and commercial compartments using the smoke pens described earlier, show that, except in the immediate vicinity of doors, interior rooms have a negligible airflow (< 0.5m/s) in the absence of mechanical ventilation systems. Exterior rooms may have more significant airflows on the floors immediately beneath exterior windows depending on the relative temperatures inside and outside the building and the nature of the window (single- or double-pane). Typical bulk room air changes are of the order of 0.5 room change/hour for interior rooms, according to Melhem and Croce. [Melhem/Croce] If a pool of flammable liquid occupies only a small portion of the floor surface of the

room, the investigator must be aware of the time required for the vapours to cover the floor area before there can be vertical diffusion throughout the room. Vertical diffusion in the immediate vicinity of the pool will, of course, begin immediately. Once again the location of the ignition source relative to the pool will be an important consideration. An ignition source located some horizontal distance from the pool will not be likely to produce ignition within seconds of release of the pool unless the source itself can create a convective flow that can draw the vapours towards it. Such sources as fireplaces, water heaters, furnaces, gas or electric room heaters, kerosene lamps, even a candle in some circumstances, could all produce convective flows of various strengths that could entrain vapours from the spill and enhance their horizontal spread.

4.8 Thermodynamics of Evaporation from Pools

4.8.1 Thermal Imaging Calibration

The calibration of the infrared thermal imaging system is dependent on the setting of the emissivity level, which should match the emissivity of the target. Because these experiments are dealing with non-luminous sources at temperatures close to ambient and experimental conditions (room interiors) where there are no strong exterior sources of infrared, differences in emissivity or reflectivity of the targets involved (carpet, sand, liquid pool, aluminium granules) would not be expected to make a large difference in the temperatures observed. This experiment verified that assumption (Fig. 3.8.2.2). It can be seen that while there were minor variations between the temperatures measured for targets of different

reflectivity and emissivity, they were insignificant. In addition, the primary application of this system to the surface temperature measurements in these experiments is to record changes in temperature, rather than an absolute temperature.

4.8.2 Thermodynamics of Evaporating Liquids and Matrices

If we treat a pool of liquid in a Petri dish as an isolated (completely insulated) source of heat we can evaluate some of the various contributions to the heat balance of such a system. From Table 4.8.1 we can see that pentane has a heat capacity of 2.33 kJ/kg °C. A typical 15cm pool contained 0.117 kg of pentane, so the product would be 0.273 kJ/°C. (Decreasing the temperature by 10°C would require removing 2.73 kJ.) The insulated pool system, however, has a slightly larger heat capacity because the Petri dish has to be included. The glass base dish used for most of the pool tests weighed 80±2 g (0.08kg). According to Table 4.8.1, glass has a heat capacity of 0.84 kJ/kg°C. This, then, would add 0.067 kJ/°C to our system. If evaporation represents the only means of heat loss from the pool, we can examine the heat balance described in Sect. 1.4.4 with a limited set of terms: Q_{evap} and Q_{grd}. To evaluate Q_{evap}, heat lost from vaporization, we see from Table 4.8.2 that n-pentane has a heat of vaporization of 357 kJ/kg K. From the mass loss, we could calculate the kJ lost, and from the heat capacity of the system, calculate the expected temperature of the system. A comparison of this temperature against the observed temperature may reveal the nature of the heat balance for the pool. Fortunately, a number of mass loss runs were conducted during which the temperature of the system was measured continuously by thermocouple

Table 4.8.1: Specific Heat (Heat capacity) of Common Materials

(kJ/kg °C)

Pentane	2.331	~2.262	
Hexane	2.261	2.242	
Octane	2.181	2.202	
Cellulose		1.3392	~1.33
Petrol		2.2182	
Glass		0.8372	0.843
Sand		0.7952	
Urethane		1.402	~1.43
Water		0.6282	
Gypsum		1.0842	0.843
Air		1.0462	1.043
Polymers		~1.42	1.05 (PVC) –1.9 (LDPE)3
Aluminium		3.7742	

Notes: 1. Per Fire Protection Handbook [McKinnon]

2. Per Perry, p. 3-146 (Converted to kJ/kg K by 4.184)

3. Per Drysdale, p.4

Table 4.8.2: Heat of Vaporization of Pentane, Hexane, Octane
(kJ/kg-K at 30°C)

Pentane	357[1]	366.35[2]
Hexane	335[1]	366.1[2]
Octane	301[1]	363.2[2]

Notes: 1. Per Fire Protection Handbook, 19th Ed. [McKinnon]
2. Per Perry, p. 3-125.

array or by Inframetrics thermal imaging. The calculations for a variety of pools and matrices were carried out as follows.

4.8.2.1 Thermodynamics of Pools

The heat capacity of an insulated pool of pentane was calculated by multiplying the initial weight of pentane by its heat capacity (2.33kJ/kg-C) and adding to that the heat capacity of the Petri dish, 0.08 kg at 0.8 kJ/kg-K. From H_V =0.357 kJ/g for pentane, the ΔH_S of the system was calculated from the mass lost at one minute intervals (cumulative mass loss, cumulative ΔH, and cumulative ΔT were calculated). The mass losses were selected from the raw data for the evaporation runs that were monitored (by thermocouple or infrared) for temperature. The ΔH_S divided by the heat capacity of the system yields a calculated ΔT (ΔT_{calc}) which can be compared against the observed ΔT (ΔT_{obs}). The results are presented in Table 4.8.3 and Fig. 4.8.1.1. After three minutes, there is sufficient evaporative loss for the heat capacity of the insulated pool system to be reduced significantly due to the reduced mass of pentane. If the heat capacity of the system is recalculated based on this reduced mass for each minute, ΔT can be calculated for an extended time (30min). Doing this reveals a difference between ΔT_{calc} and ΔT_{obs} that grows greater with time(Fig. 4.8.1.2). The progressive nature of this plot is qualitatively similar to the error function calculations demonstrated earlier. Since that application is the same for thermal diffusivity as for mass diffusivity, it appears that heat conducted between the insulator and the pool (which will increase with time as the temperature difference becomes greater) is the primary source of heat to replace that being lost to evaporative cooling.

Table 4.8.3 Thermal Balance Calculations for Pentane Pools at 20 –21°C

Test	Ws	$H_C sys^2$	Time	Δm^1	ΔH^1	$\Delta T_{calc}{}^1$	$\Delta T_{obs}{}^1$
	kg	kJ/°C	min	g	kJ	°C	°C
47	0.085	0.198	1	2.32	0.828	3.1	3.1
			2	4.22	1.507	5.7	4.9
			3	5.88	2.099	7.9	7.5
			30	28.96	10.34	39	20
53	0.098	0.295	1	2.63	0.94	3.2	3.4
			2	4.61	1.64	5.6	5.1
			3	6.19	2.21	7.5	7.0
			30	27.14	9.69	32.8	19.1
65	0.069	0.235	1	1.27	0.45	2.0	3.1
			2	2.52	0.90	4.0	5.1
			3	3.57	1.27	5.6	7.3
			30	24.75	8.84	37.6	18.4
66	0.082	0.258	1	1.91	0.68	2.6	3.0
			2	3.43	1.22	4.7	5.0
			3	4.79	1.71	6.6	6.3
			30	24.38	8.70	33.7	19
70	0.113	0.330	1	1.84	0.65	2.0	4.6
			2	3.15	1.12	3.4	6.5
			3	4.33	1.55	4.7	8.9
			30	23.62	8.4	25.6	21

Table 4.8.3 Thermal Balance Calculations for Pentane Pools at 20 –21°C
Continued

71	0.108	0.319	1	2.10	0.75	2.4	2.6
			2	3.96	1.41	4.4	4.8
			3	5.61	2.00	6.3	6.6
			30	29.75	10.62	33.3	18.4
76	0.115	0.335	1	2.65	0.95	2.8	2.8
			2	4.76	1.70	5.1	5.0
			3	6.70	2.39	7.1	6.7
			30	32.9	11.7	35	21.3
77	0.03	0.20	1	1.14	0.41	2.0	2.5
			2	2.05	0.73	3.6	4.3
			3	2.86	1.02	5.1	6.0
			30	16.32	5.83	29.1	16.7
78	0.03	0.20	1	1.26	0.45	2.2	4.1
			2	2.20	0.79	3.9	6.1
			3	2.99	1.06	5.3	7.3
			30	15.48	5.53	27.6	16.8

Notes:

1: Δm, ΔT_{obs} and calculated ΔH, ΔT_{calc} were cumulative for the time period.

2: Includes pentane and Petri dish

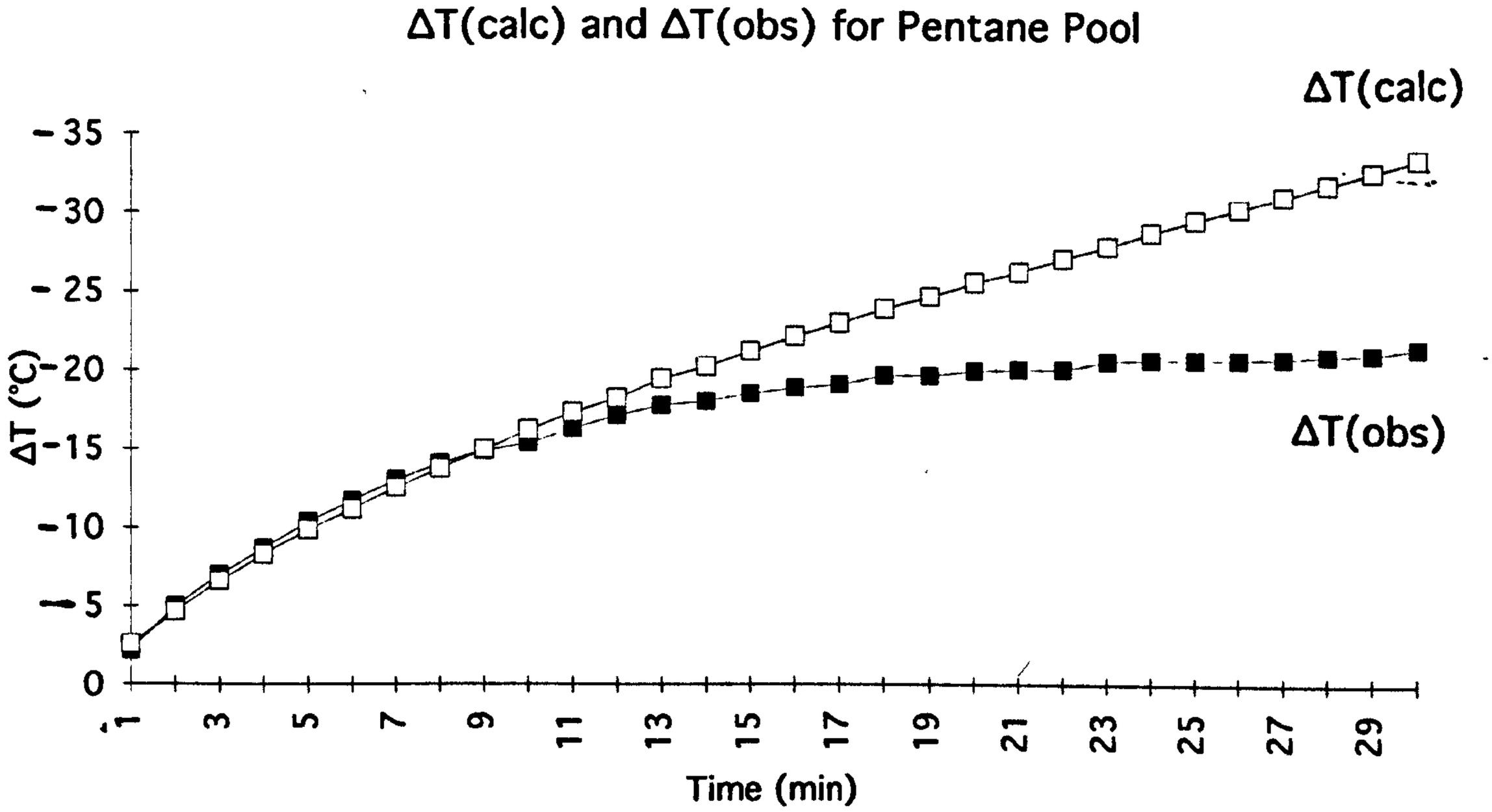

Fig. 4.8.1.1: ΔT as a function of time for a typical n-pentane pool. ΔT_{calc} (based on heat capacity of starting pool) becomes considerably higher than ΔT_{obs} for this pool after 7min due to heat conducted into pool from insulator.

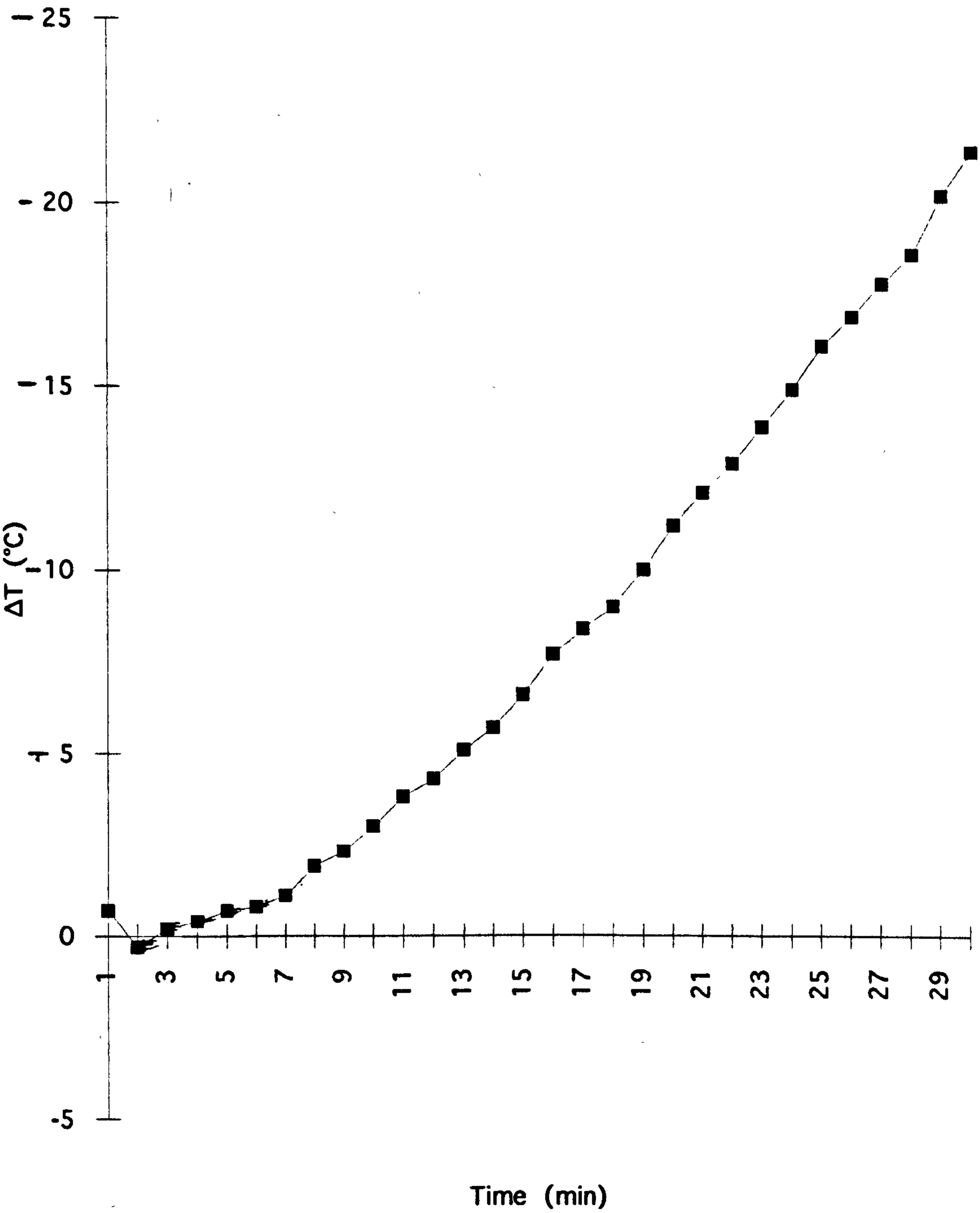

Fig. 4.8.1.2: Difference between ΔT_{calc} (with correction for decreasing heat capacity as pool evaporates) and ΔT_{obs} is apparent after 6min. The increasing slope of the the plot with time is consistent with heat conduction providing heat to maintain the pool temperature higher than is calculated.

The heat capacity of an insulated pool of hexane was similarly calculated by multiplying the initial weight of hexane by its heat capacity 2.24kJ/kg-C and adding to that the heat capacity of the Petri dish, 0.08 kg at 0.8 kJ/kg-K. From H_V =0.330 kJ/g for hexane, the ΔH_S of the system could be calculated. Results are presented in Table 4.8.4.

The heat capacity of an insulated pool of octane was similarly calculated by multiplying the initial weight of octane by its heat capacity (2.20kJ/kg-C) and adding to that the heat capacity of the Petri dish, 0.08 kg at 0.8 kJ/kg-K. From H_V =0.310 kJ/g for octane, the ΔH_S of the system could be calculated. The results are presented in Table 4.8.5.

4.8.2.2 Thermodynamics of Matrices

The heat capacity of an insulated pool of pentane on sand was calculated by multiplying the initial weight of pentane by its heat capacity (2.33kJ/kg-C), and adding to that the heat capacity of the Petri dish, 0.08 kg at 0.84 kJ/kg-K, and that of the sand (0.37 – 0.42kg) at 0.80kJ/kg-K. The results are presented in Table 4.8.6.

The heat capacity of an insulated pool of pentane on aluminium granules was similarly calculated by multiplying the initial weight of pentane by its heat capacity (2.33kJ/kg-C) and adding to that the heat capacity of the Petri dish, 0.08 kg at 0.84 kJ/kg-K, and that of the aluminium granules (0.37 – 0.4kg) at 3.77kJ/kg-K. The results are presented in Table 4.8.7.

The heat capacity of an insulated pool of pentane on carpet was calculated by multiplying the initial weight of pentane by its heat capacity (2.33kJ/kg-C) and adding to that the heat capacity of the Petri dish, 0.08 kg

Table 4.8.4 Thermal Balance Calculations for Hexane Pools at 20 –21°C

Test	W_s	H_{csys}[2]	Time	Δm[1]	ΔH[1]	ΔT_{calc}[1]	ΔT_{obs}[1]
72	kg	kJ/°C	min	g	kJ	°C	°C
	0.125	0.347	1	0.95	0.31	0.9	0.9
			2	2.05	0.68	2.0	1.4
			3	3.11	1.03	2.9	1.9
			30	19.11	6.31	18.2	7.8
73	0.126	0.349	1	0.91	0.30	0.8	0.6
			2	2.23	0.74	2.1	1.2
			3	3.53	1.16	3.3	1.9
			30	23.75	7.84	22.4	9.1

Notes:

1: Δm, ΔT_{obs} and calculated ΔH, ΔT_{calc} were cumulative for the time period.

2: Includes hexane and Petri dish

Table 4.8.5 Thermal Balance Calculations for Octane Pools at 20–21°C

Test	W_s	H_csys^2	Time	Δm^1	ΔH^1	ΔT_{calc}^1	ΔT_{obs}^1
	kg	kJ/°C	min	g	kJ	°C	°C
51	0.101	0.289	1	0.16	0.05	0.2	0
			2	0.31	0.10	0.3	0
			3	0.45	0.14	0.05	0
			30	3.09	0.96	3.3	1.4
74	0.130	0.353	1	0.15	0.05	0.1	0
			2	0.33	0.10	0.3	0
			3	0.51	0.16	0.4	0
			30	6.0	1.86	5.3	0
75	0.113	0.316	1	0.13	0.04	0.1	0
			2	0.22	0.07	0.2	0
			3	0.32	0.10	0.3	0
			30	2.25	0.7	2.2	0

Notes:

1: Δm, ΔT_{obs} and calculated ΔH, ΔT_{calc} were cumulative for the time period.

2: Includes octane and Petri dish

Table 4.8.6 Thermal Balance Calculations for Pentane/Sand Matrices at 20 – 21°C

Test	W_s	H_csys	Time	Δm^1	ΔH^1	$\Delta T_{calc}{}^1$	$\Delta T_{obs}{}^1$
	kg	kJ/°C	min	g	kJ	°C	°C
48	0.054[2]	0.126	1	5.59	2.00	4.1	7.0
	0.37[3]	+0.294	2	8.43	3.01	6.2	8.8
		+0.067	3	11.01	3.93	8.1	10.2
	Total	0.487	30	24.01	8.57	17.6	24.3
68	0.065[2]	0.151	1	3.73	1.33	2.4	9.2
	0.4[3]	+0.338	2	8.21	2.93	5.3	11.2
		+0.067	3	11.75	4.19	7.5	12.8
	Total:	0.556	30	50.45	18.01	32.4	25.5
142	0.071[2]	0.165	1	4.40	1.57	2.8	1.2
	0.4[3]	+0.320	2	8.19	2.92	5.3	3.6
		+0.067	3	11.87	4.24	7.7	6.1
	Total:	0.552	30	66.28	23.66	42.9	26.1

Notes

1: Δm, ΔT_{obs} and calculated ΔH, ΔT_{calc} were cumulative for the time period.

2: Mass of pentane at start

3. Mass of sand

Table 4.8.7 Thermal Balance Calculations for Pentane/Aluminium Matrices at 21°C

Test	W_s	H_{Csys}	Time	Δm^1	ΔH^1	ΔT_{calc}^1	ΔT_{obs}^1
	kg	kJ/°C	min	g	kJ	°C	°C
49	0.056[2]	0.130	1	4.60	1.64	1.0	2.6
	0.37[3]	+1.402	2	8.36	2.98	1.9	3.6
		+0.067	3	11.64	4.16	2.6	4.0
	Total:	1.599	30	50.74	18.11	11.3	19.4
67	0.056[2]	0.130	1	5.54	1.98	1.2	3.8
	0.40[3]	+1.500	2	9.41	3.36	2.0	8.9
		+0.067	3	12.74	4.54	2.7	10.4
	Total:	1.697	30	48.71	17.39	10.2	24.5
141	0.073[2]	0.170	1	5.21	1.86	1.1	0.5
	0.40[3]	+1.500	2	8.99	3.21	1.8	3.5
		+0.067	3	12.94	4.62	2.7	6.0
	Total:	1.737	30	68.4	24.42	14.0	29.4

Notes

1: Δm, ΔT_{obs} and calculated ΔH, ΔT_{calc} were cumulative for the time period.

2: Mass of pentane at start

3: Mass of aluminium granules

at 0.84 kJ/kg-K, and that of the carpet, 0.026 kg at 1.4kJ/kg-K. Results are presented in Table 4.8.8.

It can be seen from these results that for the first three minutes, the temperature changes (ΔT) predicted by assuming that the only heat being lost was being lost to evaporation and that $Q_{grd} = 0$, i.e., that the insulated pool was isolated, are very accurate for pools of pentane, hexane, and octane. For times beyond three minutes, the calculated temperature change is increasingly larger than that actually observed, as can be seen in a typical plot, Fig. 4.8.1.1. In some cases, the ΔT calculated for t = 3min, is already higher than the observed ΔT. This indicates that heat is entering the system by other means: either heat conducted through the bottom and sides of the Petri dish, or heat being convected or radiated into the pool from the room environment. Despite the low thermal conductivity of Styrofoam (on the order of 0.030 W/m K), once the temperature of the pool drops, some heat will be conducted from adjoining areas of the insulating block. This effect was seen in the Inframetrics videotapes of the pool tests where a "halo" of colour changes grew outward from the rim of the Petri dish as each test proceeded. At the conclusion of each test, the surface temperature of the Styrofoam under the Petri dish was found to be palpably cooler than ambient. This conducted heat would be expected to take some time to become established, and this co-incides with the three minute period during which the heat balance is controlled almost exclusively by evaporative cooling. As time goes by and the temperature of the pool drops, the amount of heat conducted into the pool will increase, contributing to the significant difference between ΔT_{calc} and ΔT_{obs} for later times. For times greater than 3min, there is sufficient mass lost by evaporation that the heat capacity of the pool is decreased. If the heat capacity is recalculated for the

Table 4.8.8 Thermal Balance Calculations for Pentane/Carpet Matrices at 20 – 21°C

Test	W_s	H_{csys}	Time	Δm^1	ΔH^1	$\Delta T_{calc}{}^1$	$\Delta T_{obs}{}^1$
	kg	kJ/°C	min	g	kJ	°C	°C
50	0.146[2]	0.340	1	3.85	1.37	3.1	5.7
	0.026[3]	+0.036	2	6.98	2.49	5.6	8.1
		+0.067	3	9.84	3.51	7.9	10.2
	Total:	0.443	30	49.91	17.82	40.2	27.2

Notes:

1. Δm, ΔT_{obs} and calculated ΔH, ΔT_{calc} were cumulative for the time period.
2. Mass of pentane at start
3. Mass of carpet

reduced mass of pentane remaining, and ΔT_{calc} is determined for times to 30min, the difference between ΔT_{calc} and ΔT_{obs} becomes progressively greater with time. If the difference is plotted as a function of time, the result is shown in Fig. 4.8.1.2. The progressive difference is of the type which would be expected from a diffusion or conduction mechanism being responsible for the additional heat input. Heat being conducted from the surrounding mass would produce this effect, its rate being, in part, dependent on the difference in temperature between the liquid and its surroundings.

Radiative and convective transfer from the room air could be expected to contribute to the heat balance. However, the radiative component would be expected to be very small in an interior exposure (unlike an exterior exposure where solar radiation could be very significant). The results of the experiments in Sect. 3.6 revealed the presence of a laminar distribution of cold vapour above the pool. The effect of this gradient would be to protect the pool itself from convective transfer from the room air. This is confirmed by the agreement between ΔT_{calc} and ΔT_{obs} seen for the pentane pool tests when convective and radiative contributions were disregarded. For hexane and octane pools, ΔT_{calc} is always higher than T_{obs}. Since the heat losses by evaporative cooling are lower for these liquids, the contributions made via radiation and convection are more significant. The very low evaporation rate of n-octane, for instance, produces such inconsequential cooling that there is little conduction and the radiative and convective processes are sufficient to maintain the temperature of the pool almost unchanged even for long periods (Table 4.8.5). In addition, the equilibrium temperatures for barrier tests of pentane are significantly higher than for non-barrier tests as the barrier retains a deep layer of vapour in the vicinity of the pool. This deep layer suppresses the

evaporation rate, reducing the evaporative cooling; it would also protect the pool from radiative and convective heat input. The differences are less notable for hexane and octane pools in barrier tests.

The agreement between ΔT_{calc} and ΔT_{obs} does not appear to be as good for matrices, where there are significant discrepancies (Tables 4.8.6, 4.8.7, and 4.8.8). In the matrix tests, however, the ΔT_{calc} is consistently smaller than ΔT_{obs}. When the Inframetrics temperature data (which capture the surface temperatures of the matrix) and the thermocouple array data (which capture both surface and bulk temperatures of the matrix) are compared, the cause for this apparent discrepancy is detected. It will be remembered from Sect. 3.8.4 that temperatures of shallow liquid pools are quickly and uniformly distributed from surface to bottom (accomplished via convection and eddy diffusion within the liquid). Figs. 3.8.4.6 and 3.8.4.7 demonstrated the large discrepancies between surface temperature and the bulk temperature for pentane/aluminium and pentane/sand matrices. After a very rapid decrease in surface temperature, the bulk temperature of a matrix requires considerable time before it reaches equilibrium with it since there is no convective transfer. There is a considerable difference between surface temperature of the sand (which is very low due to the high mass loss rate) and the bulk temperature that equilibrates slowly due to the low conductivity of sand. If one plots the ΔT_{calc} for pentane/sand on such thermocouple data, (Fig.4.8.2.1, bottom) it falls midway between the surface and bulk temperatures for the first five minutes.

The same situation is seen when one examines the ΔT_{calc} values entered on the pentane/aluminium thermocouple data (Fig. 4.8.2.1, middle).

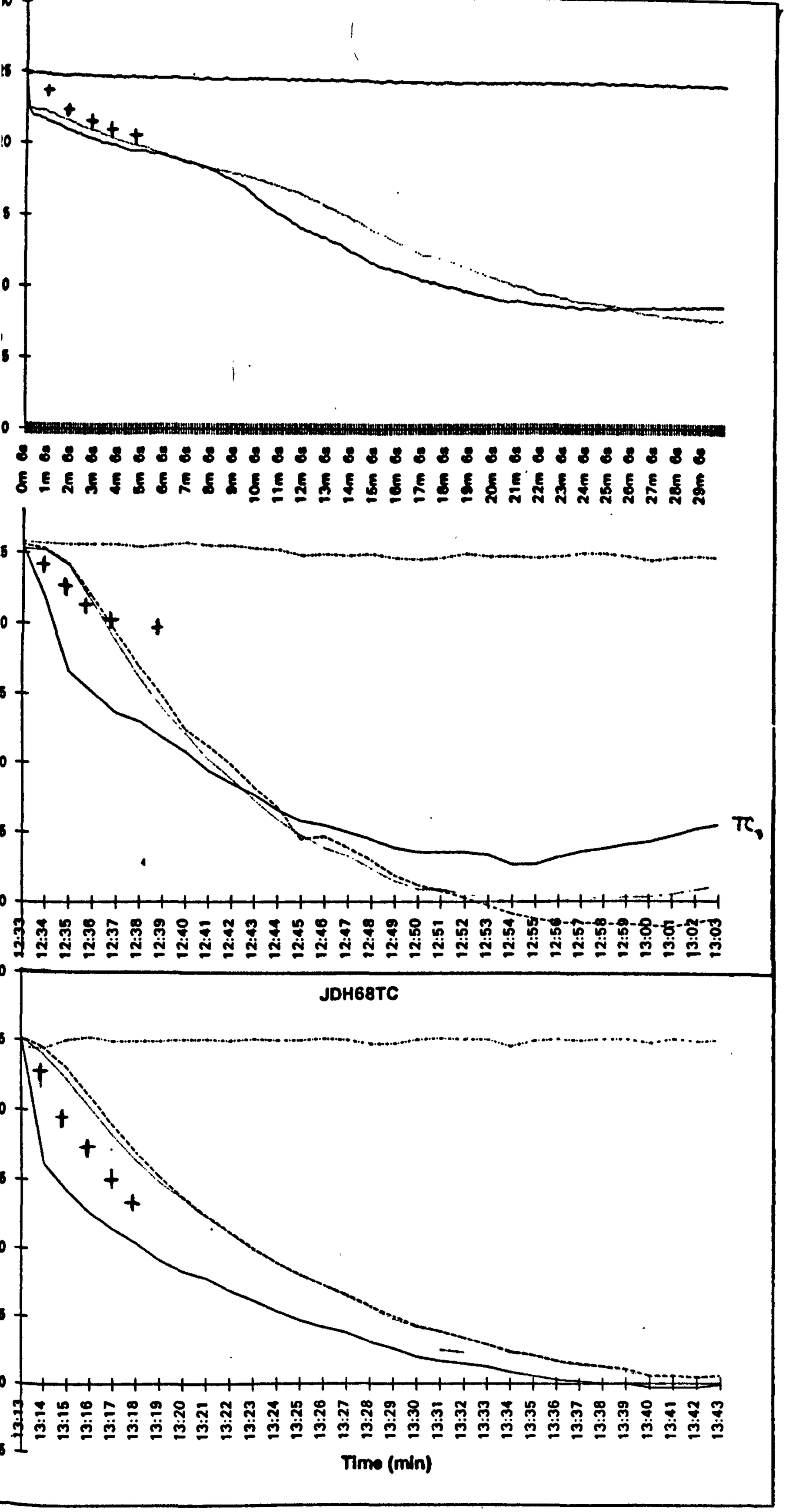

Fig. 4.8.2.1: (Top) Plot of surface temperature (via Inframetrics system) of pentane/aluminium matrix with ΔT_{calc} added.

(Middle) Thermocouple measurements of surface (TC3) and bulk temperatures of same matrix with ΔT_{calc} added.

(Bottom) Thermocouple measurements of pentane/sand matrix with ΔT_{calc} added.

The inital ΔT_{calc} values fall within the two temperatures (surface and bulk), but after 4min they no longer match either surface or bulk temperatures. Curiously, they agree better with the surface temperature of the aluminium granules as measured by the Inframetrics system (Fig. 4.8.2.1, top). The reason for the discrepancy between the infrared and thermocouple data for that matrix has not been identified, it may due to the high heat conductivity of aluminium and the low conductivity of the pentane.

The mass loss rate v. surface temperature plots for pentane, Figs. 3.8.3.11 – 3.8.3.13 were replotted in a semi-log form and a least-squares-fit curve is plotted, the result is a straight line with the general form as shown in those figures. The numerical solutions calculated for such lines are of the form:

$$dm/dt = \S\, e^{nT}$$

where: dm/dt = rate of mass loss

T = temperature in Celsius, and

§ and n = numerical values.

It was shown earlier that the evaporation rate is proportional to $D_a M p_s/T$, that D_a is proportional to $T^{1.5}$, and p_s is determined by $\log_{10} p_s = a - b/(T+c)$ so it should be expected that the relationship is logarithmic. For shallow pools of free liquid pentane of the type tested here, n is of the order of 0.07 and § is of the order of 0.47. When matrices are plotted, § changes due to the great increase in heat capacity of the system and n changes due to the competition between p_s, D, and the viscosity and surface tension of the liquid, which are all temperature dependent. Increases in viscosity caused by lower temperatures would be expected to reduce the mass transport of liquid within the matrix and, thereby, reduce its mass loss rate even further

than that which would result from lower vapour pressure. It should be remembered that the Schmidt number used by Kawamura and Mackay to characterize the mass transfer of liquids is the ratio of the diffusivity to kinematic viscosity. Due to the complexity of fluid interactions within a matrix, it is not possible here to relate the Schmidt number to the actual constant, n, obtained as the solution for the particular system under evaluation here.

4.9 Evaporation of Pure Compounds v. Complex Mixtures

As expected, evaporation of complex mixtures such as petrol and camping fuel produced complex results. The initial rate of petrol evaporating from a pool (12mm deep) is indistinguishable from that of n-pentane evaporating under the same conditions. Since the evaporation rate of a liquid is dependent on its vapour pressure, and the vapour pressure of petrol is very similar to that of n-pentane, this would be expected. [Rose/Cooper, 1977] The actual vapour pressure of a complex fuel depends on its composition, i.e., the vapour pressure contributions of its components are proportional to the mole fractions of each component. Due to the complexity of petrol, and the variability of its composition, calculating its vapour pressure from a comprehensive quantitative analysis of its components would be very difficult, and some reliance must be placed on published results. [Rose/Cooper] The quantitative analyses reported in Sect. 3.9 demonstrate that 20 – 40% by weight of a modern petrol is composed of hydrocarbons of molecular weight equal to or less than that of n-hexane, with a significant percentage of methyl butane, pentane, and compounds of similar vapour pressure. The compositions of even summer blend petrols

are, by weight, 9.2 – 16.9% compounds equal to or less than n-pentane in vapour pressure. The vapour pressure of such a mixture intuitively would be similar to that of n-pentane. At moderate temperatures, pentane and similar products would be expected to dominate the initial evaporation, as it seems to from these experiments. The mass loss rate of a petrol pool parallels that of pure n-pentane for the first 5min, at which time the bulk weight shows a loss of some 5 – 6% of the total mass of the sample. Quantitative analysis of the evaporating petrol (Table 3.9.2) shows a significant decrease in levels of methyl pentane, n-pentane, and methyl butane, but not for n-hexane or toluene. This strongly suggests that these lightest components are the only significant species present in the vapours being generated for the first 5min or more after a petrol is poured out at 20°C. After about 10 to 20min, the most volatile components are largely exhausted, and the less volatile components begin to dominate the vapour pressure and evaporation rate of the pool.

When camping fuel is evaporated, the initial mass loss rate is very similar to that of hexane. This would be expected from the composition of such fuels, being dominated by methyl pentane, n-hexane, and compounds of similar vapour pressure. Hexane continues to dominate the evaporative losses for 30min or more.

When a pure compound is being evaporated, the concentration of the evaporating species is uniform throughout the liquid phase (100%). When a multi-component mixture evaporates, there are two possible conditions that control the diffusion of the evaporating species. The first limiting condition would be one where there is perfect diffusion throughout the liquid – molecules evaporating from the surface are replaced immediately by an infinite diffusion rate (molecular or eddy) of that species in the liquid.

Thereby, the concentration of the species in the liquid does not change with depth, but its concentration drops uniformly throughout the bulk of the liquid with time. The other extreme is a condition where there is no diffusion at all in the liquid, and layers of a constant concentration are stripped off the surface of the pool while the composition of the pool remains constant with depth and with time. As Mackay and Matsugu point out, real-world evaporation of complex mixtures lies somewhere between these two conditions, and evaporation is controlled by a mass diffusion rate throughout the mixture, which results in a gradient of concentration with depth that changes with time. To explore the role that this plays in evaporation of petrol, a quantitative analysis was conducted of a petrol sample as it evaporated as a thin (2mm depth) film floated atop a quantity of water so as to maintain the same physical conditions as with a deep pool (surface flush with the surrounding rim of the Petri dish) and thermal conditions (thermal capacity of the water layer available to replace the heat lost to evaporation). The results (Table 3.9.2) show that the film evaporation occurs more quickly (possibly because of the greater thermal capacity of the water layer than an equal volume of petrol) but also that the thinner layer allows for more complete loss of the more volatile species than occurs in the deep pool. The methyl butane is lost completely by 14min (along with 37% of total mass lost). The pentane is exhausted by 24min (along with 46.9% of the total mass). The differences between pool and film evaporation clearly demonstrate the influence of mass diffusion rate on the loss of volatile species. These differences play a role in the evaporation of shallow pools from both non-porous and semi-porous surfaces.

The same behaviour is seen in the evaporation of camping fuels (Table 3.9.3). While the composition of such fuels is somewhat simpler than

that of petrol, there are too many components and too much variability between products to calculate successfully the vapour pressure of the finished product. According to one manufacturer, the Reid vapour pressure is 325mmHg at 38°C compared to a vapour pressure of 260mmHg for n-hexane at the same temperature.[May] We can see from the gas chromatographic results in Sect.3.9 that a significant percentage of the product (29 – 37% by weight) consists of components with volatility equal to or less than that of n-hexane. Unlike petrol, however, the highest concentrations in camping fuels are of the hexanes (n-hexane, methyl pentane, dimethyl pentane) and the percentages of methyl butane and n-pentane are very low compared to petrol (concentrations of those componds are zero in one brand). This would suggest that the evaporation rates of such fuels would be much more similar to that of n-hexane than to n-pentane. The initial rates of 0.7 – 1.1g/min evaporating from a deep pool of 0.016m^2 area (45 – 65g/min/m^2) are very similar to that of n-hexane under the same conditions. As with petrol, the evaporation from a thin (2mm) film of fuel on water is faster and the most volatile components are lost very quickly (Table 3.9.3.)

The mass loss rates for camping fuel evaporations (both as pools and as a film) demonstrate a more pronounced variation with time than petrol. The sampling interval of 5s recorded a considerable fluctuation in mass loss rate that may reflect the effects of turbulence within the liquid induced by eddy diffusion in the fuel as it evaporates. Such fluctuations were observed in nearly every experiment where a multi-component mixture was being evaporated but only very rarely when pure compounds were being evaporated.

From a reconstructive standpoint, for short periods of time (less than 10min) the evaporation of complex hydrocarbon fuels could be successfully modelled on the behaviour of the predominant species. **The data gathered here demonstrate that petrol evaporation is equivalent to n-pentane evaporation, especially for the first few minutes. It is in this time interval that ignition of vapours from a spilled fuel will be ignited in most fires. In terms of volume, it appears that one litre of petrol would produce the same quantity of vapours as 0.25litre of n-pentane would for the first 10–15 minutes. Over the next 45min, another 0.25litre of n-hexane would be equivalent. For camping fuels, the equivalent to one litre of a typical fuel would be 0.3litre of n-hexane for the first 30min or more.**

4.10 Pool and Vapour Layer Characteristics and Fire Behavior

It was noted during the room fire tests described in Sect. 3.10, that ignition of a layer of vapour produced characteristic flame behaviour – low flames extending rapidly through the lower volume of a compartment. Such fires may produce a detectable surface-scorch pattern throughout the volume of the room with more pronounced damage only in the lower reaches of the room. Such effects are more likely to be visible on thermally-thin fuels (paper, cloth, etc.) that might be present than on massive fuels such as painted walls or wood furnishings. Clothing of someone standing in the room at the time of ignition might well be more scorched (or even ignited) below knee level than above. If the fire proceeds to full room involvement, such minor effects may be obliterated and not detectable to a fire investigator. Such effects may well be visible to a witness, and such

witnesses should be sought out by the thorough investigator.

According to the Hottel and Blinov/ Khudiakov studies [Drysdale], the plume length (pl) developed when a pool of volatile fuel is ignited, is related to the diameter (D) of the pool (as in Fig. 4.4.1). The relationship, pl/D, is not constant and varies from 5 to 10 for pools of D = 0.01 – 0.1m, decreasing to ≈1.5 if D ≥ 1m. This would yield plumes 0.1m in height for a pool 0.01m (1cm) in diameter and 0.5m for a pool 0.1m (10cm) in diameter. This is exactly the plume height observed in the room tests conducted as part of this study, where the trail of fuel poured onto carpet was on the order of 5 –10cm wide. It is also consistent with the BHF tests where the flames from a single pool approximately 1m in diameter rose some 2m in the compartment (to ceiling level). This may represent a means of correlating fuel spread (both on the floor and in vapour layer) with observations made by eyewitnesses to the ignition.

The results of the post-fire observations indicate that unless the fire is extinguished within two or three minutes of ignition, the resulting char pattern may not be a reliable indicator of the size of the actual pool of fuel. Some carpets are especially susceptible to radiant heat ignition, and the flames ignited on the outside of the pool can advance some distance from the original margin. If the fuel produces low luminosity flames (as does methanol), this radiant heat-driven combustion will be much more limited than if the same fire involved petrol with its highly luminous flames. Correlation between fuel distribution and fire penetration of the carpet is not reliable as a guide to how much fuel was present prior to the fire. The interaction of flammable liquid fires on complex substrates such as carpet and pad is very complicated. Even replicate fires on padded carpets will sometimes produce penetrations and sometimes not. This is especially

true in fire scenes where the fire has progressed to near-flashover or post-flashover conditions. The radiant heat from a ceiling layer can induce significant damage to floor coverings, even in the absence of flammable liquid accelerants. In post-flashover fires, the turbulence of fully-involved rooms can create random damage that is not always traceable to the fuel load in the room or even to ventilation openings. Even in the absence of flashover, the damage which occurs in the minutes after the protective liquid pool is consumed may make it very difficult, if not impossible to estimate the area and shape of the starting pool. Obviously, in the absence of effective sprinkler systems few building fires are extinguished in the first two or three minutes after ignition. As a result, the investigator would be well-advised not to rely on burn patterns to estimate the quantity of liquid accelerant involved. It would be better to rely on the statements of witnesses (or even suspects) as to how much fuel was used as a starting point for reconstructing the fire. Evidence of containers in or near the fire may indicate the *maximum* amount of liquid fuel that was transported, but there is no guarantee that any or all were full when used.

4.11 Suggestions for Further Enquiries

4.11.1 Ignition tests

Tests of the ignitability of layers of hexane vapors are planned for the Fire Research Station – Cardington during 1995. These tests will involve the production of a floor-level layer of hexane vapour by evaporation from a $1 m^2$ pool at 20°C in the $20 m^3$ explosion test chamber. This vapour layer will be ignited via a sequence of electric match devices at heights of 0.5,

0.35, 0.15, and (if necessary) 0.05m. The pressures produced at various locations within the chamber will be monitored.

4.11.2 Visualization of vapour layers using gas imaging technology

It would also be informative to repeat some of the horizontal and vertical movement studies conducted here using an infrared laser gas imaging system developed for the monitoring of natural gas plumes. This system uses a Helium-Neon laser to illuminate a target with a strong source of infrared at 3.39μ. This wavelength is scattered back to the IR image converter system to produce a visual image, except where the IR is absorbed by hydrocarbon gases or vapours, which absorb very strongly at 3.39μ. Any such gas or vapour then produces a black image on the image-converter. It operates in real-time and would allow continuous monitoring of a developing plume or layer of hydrocarbon vapour from a pentane or hexane pool. At the present time, however, the prototype operational system of its kind is out of service, requiring expensive and time-consuming repairs. When it is returned to operational status, the proposed tests may be conducted.

4.11.3 Larger Pools

The experiments conducted in this study were limited to 0.35m in diameter because of limitations on the weight capacity of the electronic balance used. While the range of pool sizes studied is typical of pools produced in both accidental and intentional incidents, it would be potentially

useful to acquire data on the evaporation rates of pools of larger diameter, 0.3 to 1.5m in diameter. In light of the data on pool fires available in the literature, there may be a parallel threshold of diameter, above which rates remain constant.

4.12 Operational Model

The results of these studies may be used to help an investigator evaluate the competence of a suspected ignition and likely time factors given a known quantity of flammable liquid (or a hypothetical quantity). Since the data collected in this study involved still air environments and demonstrated sensitivity to forced ventilation or mechanical movement of air, their application to a real fire scene must be made with the awareness that most rooms are not draught-free. **The first steps are to measure the area of the room involved and to determine the nature of ventilation resulting from HVAC systems. This model is valid only for rooms with no mechanical ventilation, with minimal leakage due to exterior doors or windows, and that do not have significant human or vehicular traffic. It is most applicable to below-grade compartments with no exterior doors.** The temperature of the room at the time the spill occurred is very important. This model is applicable only to smooth, flat floor surfaces. Sloping or irregular floors will greatly affect the size of pools by mechanisms not studied here.

The type of floor must also be determined from the scene investigation; was the floor non-porous (vinyl flooring, sealed tile, painted concrete, terrazzo, or marble), semi-porous (unpainted concrete or wood), or porous (carpet)? A comparison sample of any carpet and pad should be

obtained so that the nature of the pile and backing and the pile height can be measured. Special cases such as a floor of dirt, sand, or sawdust will not be amenable to this model.

The maximum quantity of fuel used may be inferred from empty containers found at the scene (which may or may not have been full), based on the statements of eyewitnesses, or may simply be hypothesized to determine what quantity may fit the observed indicators. If a non-porous floor is involved, a pool depth of 0.2mm (0.0002m) is assumed. If a semi-porous floor is involved, a pool depth of 1–2mm (0.001 – 0.002m) is assumed. If a backed carpet is present, assume a pool depth equal to the pile depth of the carpet (in m). Divide the assumed pool depth into volume of liquid (expressed in m^3 – one litre = $0.001m^3$) to get maximum pool area.

If petrol is suspected to be the flammable liquid present, assume that an evaporating volume of 25% of the volume of petrol is present as pentane. If a camping fuel is suspected, assume that an evaporating volume of 30% of the volume is present as n-hexane.

From the calculated pool area, a total vapour generation rate at 20°C can be calculated by multiplying the area by one of the following vapour generation rates for pentane:

0.8 litres/s-m^2 can be assumed if non-porous surfaces are involved,

1.2 litres/s-m^2 can be assumed for unpainted concrete, wood, carpet, or plaster floor surfaces,

1.6 litres/s-m^2 can be assumed for sand or similar granular surfaces.

(The rates can be adjusted up or down if circumstances indicate a significantly higher or lower ambient temperature prevailed prior to the fire. Rates for pentane at 5°C are approximately 50% of the rate at 22°C, and

rates at 35°C are 50% higher than at 22°C. The same holds for hexane.)

The total vapour generation rate (in litres/s) can be used to calculate the minimum time to achieve a lower explosive limit if one assumes complete uniform mixing throughout the room. This time will be shortened if a turbulent pour is used, since an additional volume of vapour equal to 15% of the liquid volume will be generated by such pouring. Based on the experimental data in Sect. 3.5, a highly turbulent pour will generate a volume of vapour equal to that of 25% of the volume of pentane or its equivalent volume in other fuels.

Unless circumstances indicate otherwise, a pour centrally located in the room can be assumed. Since pentane vapours at 20°C will move horizontally at 0.05m/s, the time required to spread across the entire room can be calculated from the room dimensions. (As an example, the entire floor area of an average 3m x 4m room will be covered with a shallow (1 - 3cm deep) vapour layer within 30s of pouring.)

From the time the floor is covered with a saturated vapour layer, the fill rate of the room from evaporation alone (without diffusion) can be estimated from:

0.08cm/s maximum fill rate if all of the floor is covered with a liquid pool and stays at the same temperature, or

0.04cm/s average fill rate allowing for typical evaporative cooling.

For pools much smaller in area than the room, the rate can be approximated from the ratio of pool size to room size:

pool size (m^2)/ room size (m^2) x 0.08cm/s = maximum fill rate.

At any hypothetical time (t), the depth of the saturated layer is calculated from the rate equation above multiplied by t.

In addition to the saturated layer, there will be diffusion-driven dispersion. The diffusion layer to the lower explosive limit can be read off the chart Fig. 4.6.1 (for pentane at 20°C). The depth of the diffusion layer is added to the fill level to estimate the height of the lower explosive limit in the room. This model will only be applicable to rooms with no leaks. If there appear to have been significant leaks, a consistent layer 2 – 4cm deep can be established at the floor (all excess filling will be lost through the leaks). All filling of the room will be due to diffusion dispersion from floor level. A worked example is included in Appendix H.

Suitable corrections can be substituted if hexane or a hexane-like camping fuel is suspected. In such cases, the horizontal spread will be slightly slower, and the vapour generation rate is reduced to 1g/s-m^2 or 0.26 litre/s-m^2 at 20°C. This figure can be used to calculate the room filling rate. The diffusion rate for hexane vapours will be lower and the saturation (starting) vapour pressure will be 239mmHg. The total result will be that such fuels will produce threshold (LEL) concentrations at significantly lower heights than for pentane for the same times, and diffusion will be slower.

It should be noted that the regression rate (Fig. 3.4.4) when applied to the projections of pool depths on non-porous and semi-porous substrates, yields a maximum time over which the evaporation can take place. At an average regression rate of 0.1mm/min, it can be appreciated that a pool originally 0.2mm deep will be almost completely evaporated in 3min. This is confirmed by thermal imaging tests of pours on non-porous surfaces.

Similarly, a pool 2mm deep on a semi-porous surface will be essentially completely evaporated (or at least the most volatile components of it, if it is a mixture) within approximately 20min of the moment of pouring. This estimate is confirmed by direct observations as well as mass loss tests on surfaces such as plaster of Paris.

4.13 Conclusions

This study has explored the evaporation of simple, volatile hydrocarbon fuels and some of the factors that control evaporation and the propagation of the vapours produced as outlined in the statement of problem in Sect. 1.6.

The liquids form pools of predictable size depending on the nature of the surface on which they are poured. There is considerable variation in the pool sizes that will result from pours on different surfaces, the size being controlled by the pool depth formed on that surface. Most hydrocarbon fuels have sufficiently similar viscosities and surface tensions that they all will behave similarly. When volatile fuels like ethanol or isopropanol are involved, their higher surface tensions will reduce the equivalent pool sizes.

Pure compounds such as n-pentane and n-hexane will evaporate from pools of free liquid at a predictable rate per unit surface area that is the same both for films of 1 – 2mm and deeper pools of 12mm depth. There is more variation for deeper pools due to the random nature of eddy diffusion. The rates are surface dependent. Pentane and hexane will evaporate from a fully saturated porous substrate with a low packing density such as carpet or urethane foam at a rate approximately 50% higher than from a pool at the same temperature. They will evaporate from a saturated porous substrate with a high packing density such as sand at a rate 100% higher than from a free-liquid pool under the same conditions. This has the effect of raising the vapour pressure, i.e., the source strength, of a pool. The models previously reported do not reflect this difference.

The evaporation rate is temperature dependent for all surfaces studied here. For pentane, for instance, it was 50% lower at 5°C and 50% higher at 35°C than at 20°C for evaporation from a pool. The initial rate is determined by the temperatures of the fuel and that of the surface on which it is poured. This rate is not constant for shallow pools or films, however. As evaporation occurs, the temperature of the liquid will drop significantly, thereby reducing the evaporation rate.

The size of the pool as well as the nature of the surface will control the evaporation rate (mass loss rate per unit area). Smaller pools will evaporate at a higher mass flux rate than will large ones. Pools greater than 0.3m in diameter appear to have the same regression rate; pools less than 0.05m in diameter exhibit a regression rate several times higher than that for large pools. This effect is particularly apparent for pours on carpet.

Pouring volatile liquids can cause significant contributions to the vapour concentration in a compartment. Contributions equivalent to 10 – 25% of the starting volume of pentane can occur when the pour is very turbulent and from a height of one metre. Non-turbulent spills from a very low height (typical of accidental spills) will result in much smaller contributions to the vapour concentrations, equivalent to 5% or less. Less volatile fuels like hexane will contribute considerably less.

In still air the vapours form a dense layer that reaches a depth of only a few centimetres before slumping and spreading by laminar flow. The layer is accentuated by a pronounced thermal gradient above the pool that minimizes heat input from the room. A dense layer of vapours will fill a closed room from the floor upwards at a rate determined by the evaporation rate. In addition, the vapours will spread slowly throughout the space by diffusion at a rate controlled by the temperature and the species of fuel involved.

Co-incident with the vertical diffusion, there will be lateral spreading of the dense vapour layer by advection. The spread of pentane vapours has been measured here to be approximately 0.05m/s at normal ambient conditions. Such a slow rate is easily overwhelmed by air movement as the result of foot traffic or mechanical ventilation.

In the first few minutes after pouring, the evaporation of complex fuels like petrol are dominated by the loss of methyl butane, n-pentane, and species of similar vapour pressure. As a result, their evaporation may be modelled on the behaviour of n-pentane under the same conditions. Some 20 – 25% of modern petrol consists of such compounds. The evaporative behaviour of camping fuel is dominated by n-hexane and other hydrocarbons of similar vapour pressure. Their evaporation can be modelled on that of hexane for most time spans (less than 30min). Complex fuels evaporating from deep pools (greater than 12mm) will have lower overall evaporation rates over a long time due to the mass diffusion that must occur for the volatile species to reach the surface. For the purposes of fire reconstruction, the initial rates are usually the most important and they will be the same as for shallow pools or films of pentane.

Upon ignition of a vapour layer, the flame front will move through the layer and possibly create distinctive burn patterns that will survive an ensuing fire to allow their detection by an investigator. The flame front progression through the layer may be corroborated by eyewitness testimony or by damage to thin combustibles at various positions in the compartment. This information will be of use in reconstructing the distribution of the vapours. Unfortunately, the correlation between the size and location of the pre-fire pool and the post-fire burn patterns is not very high. An investigator should be very cautious about estimating the volume and distribution of a flammable liquid unless suppression occurs within moments

of ignition (such as in a sprinkler-protected building). The more extensive the fire damage is, the less useful the burn patterns are. This relationship has been confirmed through the observation of a number of room fires ignited with flammable liquids.

The final product, a model upon which to reconstruct the events of some compartment fires involving flammable or highly flammable liquids where draughts and ventilation are limited, will give investigators a better understanding of the many factors which contribute to these fires. It is better suited to the conditions commonly found in building fires — moderate temperatures, spills of small quantities of volatile fuels on semi-porous or porous surfaces and absence of wind and sun — than the models offered in the literature. The role of the substrate in the evaporation has never been recognized. The formation of a dense, laminar layer of vapour with its own thermal gradient in still air reduces significantly the spread of vapours throughout a compartment. The role of diffusion in spreading vapours in the absence of wind or mechanical circulation is much smaller than most investigators suspect. The location of an ignition source relative to the pool is the single most important factor in determining whether the vapours produced are going to be ignited and after what time has elapsed. Those are two critical factors in reconstructing fires involving flammable liquids, factors that can make all thedifference between an accidental fire and a deliberate one. While the ignition source may be identifiable from its physical remains after the fire, the elapsed time cannot. Time is the one factor which must be deduced from the physical evidence (including laboratory analysis to identify the flammable liquid present), the statements of witnesses, and a careful reconstruction based on a model such this one.

Cited References

Burgoyne, JH, *Free evaporation of pool petrol*, Ministry of Home Security, London, Dec. 1944.

Burgoyne, JH and Roberts, AF, *The spread of flame across a liquid surface II: steady state conditions*, Proc. Royal Society, London, Vol. A308, 1968, p.55.

Clancey, VJ, *The evaporation and dispersion of flammable liquid spillages*, Proc. Symp. on Chemical Process Hazards, Manchester,1974.

Clancey, VJ, *Dangerous clouds , their growth and properties*, Proc. of Symposium on Chemical Process Hazards, Manchester, 1977.

CRC, *Co-ordinating Research Council Aviation Handbook – Fuels and Fuel Systems*, Naval Air Systems Command (NASCOM), U.S. Navy, Washington, D.C., May 1967.

Danckwerts, PV, *Gas-Liquid Reactions*, McGraw-Hill, NY, 1970, p.32.

Dean, JA,Ed., *Lange's Handbook of Chemistry*, 14th Ed., McGraw-Hill, NY, p.5-30.

DeHaan, JD, *Laboratory aspects of arson*, Fire and Arson Investigator, Vol. 29, March 1979, p.46.

DeHaan, JD, *Kirk's Fire Investigation*, 3rd. Ed., Brady Publ.,1991.

DeHaan, JD and Greenfield, AR, *Evaporation rates of volatile hydrocarbons*, presented at American Academy of Forensic Sciences, New Orleans, LA, Feb.1992.

DeHaan, JD and Fultz, ML, *Gas chromatography in arson and explosives analysis*, in Tebbett,I (ed.),*Gas Chromatography in Forensic Science*, Ellis Horwood, Chichester, UK, 1992.

Drysdale, DD, *Introduction to Fire Dynamics*, John Wiley & Sons, NY, 1985.

Estepp, MH,Prince George's County Fire Dept., Landover, MD, personal communication, 17 Feb.1993.

Feng, CC, Lam, SDH, and Glassman, I, *Flame propagation through layered fuel-air mixtures* , Comb. Sci. and Tech., Vol.10, 1975, p.70.

Fleischer, MT, *SPILLS – An evaporation / air dispersion model for chemical spills on land*, Shell Development, Houston, TX, Dec. 1980.

Fried, V, Hameka,HF, and Blukis, U, *Physical Chemistry*, MacMillan, NY,1977, p.169.

Gardiner, M, Northwest Fire Investigation Unit, London Fire Brigades, Acton, personal communication, 3 March 1995.

Glasstone, S, *Textbook of Physical Chemistry*, D.Van Nostrand, NY, 1946, p.256.

Harris, RJ, *The Investigation and Control of Gas Explosions in Buildings and Heating Plant*, E & FN Spon, NY, 1983, p.7.

Hirano, T, Suzuki, T,Mashiko,I, and Iwai,K, *Flame propagation through mixtures with concentration gradient* , 16th Symp. on Combustion, MIT, Aug.1976, Combustion Institute, 1977, pp1307-1315.

Home Office Standing Conference on Crime Prevention, *Report of the Working Group on the Prevention of Arson*, 1988, p.22.

Ishida, H and Iwama, A, *Some critical discussions on flash and fire points of liquid fuels* , Proc. First Internatl. Symp. on Fire Safety Sciences, 1982, p.219.

Kanury, AM, *Introduction to Combustion Phenomena*, Gordon and Breach Science Publishers, New York, 1984, p.154.

Kaptein, M and Hermance,CE, *Horizontal propagation of laminar flames through vertically diffusing mixtures above a ground plane* , 16th Symp. on Combustion, MIT, Aug.1976, Combustion Institute, 1977, pp1295-1306.

Karter, MJ, *Fire Loss in the US in 1993*, NFPA Journal, Sept./Oct 1994, p.59.

Kawamura, PI and Mackay, D, *The evaporation of volatile liquids*, J Haz. Materials, Vol.15, 1987, p.344.

Kirk-Othmer Concise Encyclopedia of Chemical Technology, John Wiley & Sons, New York, 1985.

Kreith, F, *Principles of Heat Transfer*, Intext Educational Publishers, New York, 1973.

Lewis, A, Fire Protection Association, London, personal communication, 21 Feb. 1995.

Lide, DR, Ed. *CRC Handbook of Chemistry and Physics*, CRC Press, Boca Raton, 1991.

Lide, DR, Ed. *CRC Handbook of Chemistry and Physics*, CRC Press, Boca Raton, 1994. Viscosity: p.8-64, Surface Tension, pp6-151-154.

Mackay, D, and Matsugu, *Evaporation rates of liquid hydrocarbon spills on land and water*, Can J of Chem Engineering, Vol 51, Aug 1973, pp434-439.

Mann, DC, *Gasoline residue: evaporation or combustion?*, Paper presented at American Academy of Forensic Sciences, Cincinnati, OH, Feb. 1990.

Mann, DC, Washington State Patrol, Tacoma WA, personal communication,
1 Dec 1994

Marshall, JG, *The size of flammable clouds arising from continuous releases into the atmosphere*, Proc. Symposium on Chemical Process Hazards, Manchester, 1977.

Mason, EA and Evans, RB, *Graham's Laws: Simple demonstrations of gases in motion*, J Chem Educ., Vol.46, No.6, June 1969, pp358-364.

Mason, EA and Kronstadt, B, *Graham's laws of diffusion and effusion*, J.Chem. Educ., Vol. 44, #12, Dec. 1967.

May, R, Coleman Corp., Wichita, KS, Personal comunication, 6 March 1995.

McKinnon, GP, Ed., *National Fire Protection Handbook*, 14th Ed., NFPA, Boston, MA, 1976, Table 3-11A.

Melhem, GA, Personal communication, 24 Nov. 1992.

Melhem, GA and Croce, PA, *Advanced Consequence Modeling: Emission, Dispersion, Fires and Explosions*, Van Nostrand-Reinhold,NY, In Press (1995).

Miller, Allison, *The US Home Product Report*, NFPA, Quincy, MA, Feb.1994, p.80.

Pasquill, F. *Evaporation from a plane, free-liquid surface into a turbulent air stream*, Proc. Royal Society London, Vol.182, June 1944, p.84.

Perry, RH and Green, D, *Perry's Chemical Engineers' Handbook*, 6th Ed., McGraw-Hill, NY, 1984. p.3-260

Powell, Trans. Instn. Chem Engrs., 13, 175. Cited in Pasquill.

Rabinkov, VA, *The distribution of flammable gas concentrations in rooms*, Fire Safety J., Vol.13, 1988, p.212.

Reed, W., Los Angeles Co. Fire Dept., Arson Unit. Personal communication, 3 Feb. 1993.

Reid, R.C., Prausnitz,J.M., and Poling, B.E., *The Properties of Gases and Liquids, 4th Ed.*, McGraw-Hill, NY, 1987.

Rose JW and Cooper,JR, *Technical Data on Fuels, 7th Ed.* , Halsted Press, John Wiley & Sons, NY, 1977.

Sanders, WN and Maynard, JB, *Capillary gas chromatographic method for determining the C3–C12 hydrocarbons in full-range motor gasolines*, Anal Chem, Vol. 40, No.3, Mar 1968,pp 527-535.

Shaw,P and Briscoe, F, *Vaporization of spills of hazardous liquids on land and water*, UKAEA, May 1978.

Sherwood, TK and Pigford, RL, *Absorption and Extraction*, McGraw-Hill, NY, 1952, p.8.

State Fire Marshal, Sacramento, California. CFIRS Report, 6 Feb. 1995.

Sutton, OG, *Wind structure and evaporation in a turbulent atmosphere*, Proc. Royal Society of London, Vol. 146, Oct. 1934, pp 701 – 722.

Suzuki, T, Mashiko,I et al., *Flame jumping over obstacles on the surface of a flammable liquid and superflash temperatures* , Combustion in Reactive Systems, 1981, p.741.

Szekely, J, and Themelis, NJ, *Rate Phenomena in Process Metallurgy*, John Wiley & Sons, New York, 1971.

U.S. Treasury Dept., *Explosives Incidents Report - 1993*, July 1994, p.11.

Valentine,RL and Moore, RD, T*he transient mixing of propane in a column of stable air to produce a flammable but undetected mixture*, Amer Soc of Mech Engrs, NY, 1974.

Van Ulden, AP, *On the spreading of a heavy gas released near the ground*, Royal Netherlands Meteorological Institute, De Bilt, Neth., p.221.

Wade, SH, *Evaporation of liquids in currents of air*, Proc. Inst. Chem. Engineers, Jan.1942.

Welty, JR, Wicks, CE, and Wilson, RE, *Fundamentals of Momentum, Heat, and Mass Transfer*, Second Ed., John Wiley & Sons, New York, 1979.

List of Figures

List of Tables:

3.6.5	Hydrocarbon Detection above pentane pool
3.7.1	Smoke pen tests - advection
3.7.2	Hydrocarbon detection - advection
3.8.1	Bulk Temperature vs Equilibrium Mass Loss rate
3.8.2	IR correlation
3.8.4	Thermal conductivities of common materials
3.9.1	Quantitative Analysis of Petrol/Camping Fuel
3.9.2	Quantitative Analysis of Summer-Blend Petrols (Mann)
3.9.3	Key Compound Peak Ratios - Petrol
3.9.4	Key Compound Peak Ratios - Camping Fuel
3.10.2.1	Temperature data for room calorimeter camping fuel tests
4.2.1	Comparison of Evaporation Rates
4.8.1	Specific Heat (Heat Capacity) of Common Materials
4.8.2	Heat of Vaporization of Pentane, Hexane, Octane
4.8.3	Thermal Balance Calculations for Pentane Pools
4.8.4	Thermal Balance Calculations for Hexane Pools
4.8.5	Thermal Balance Calculations for Octane Pools
4.8.6	Thermal Balance Calculations for Pentane/Sand Matrices
4.8.7	Thermal Balance Calculations for Pentane/Aluminium Matrices
4.8.8	Thermal Balance Calculations for Pentane/Carpet Matrix

Appendices

Contents:

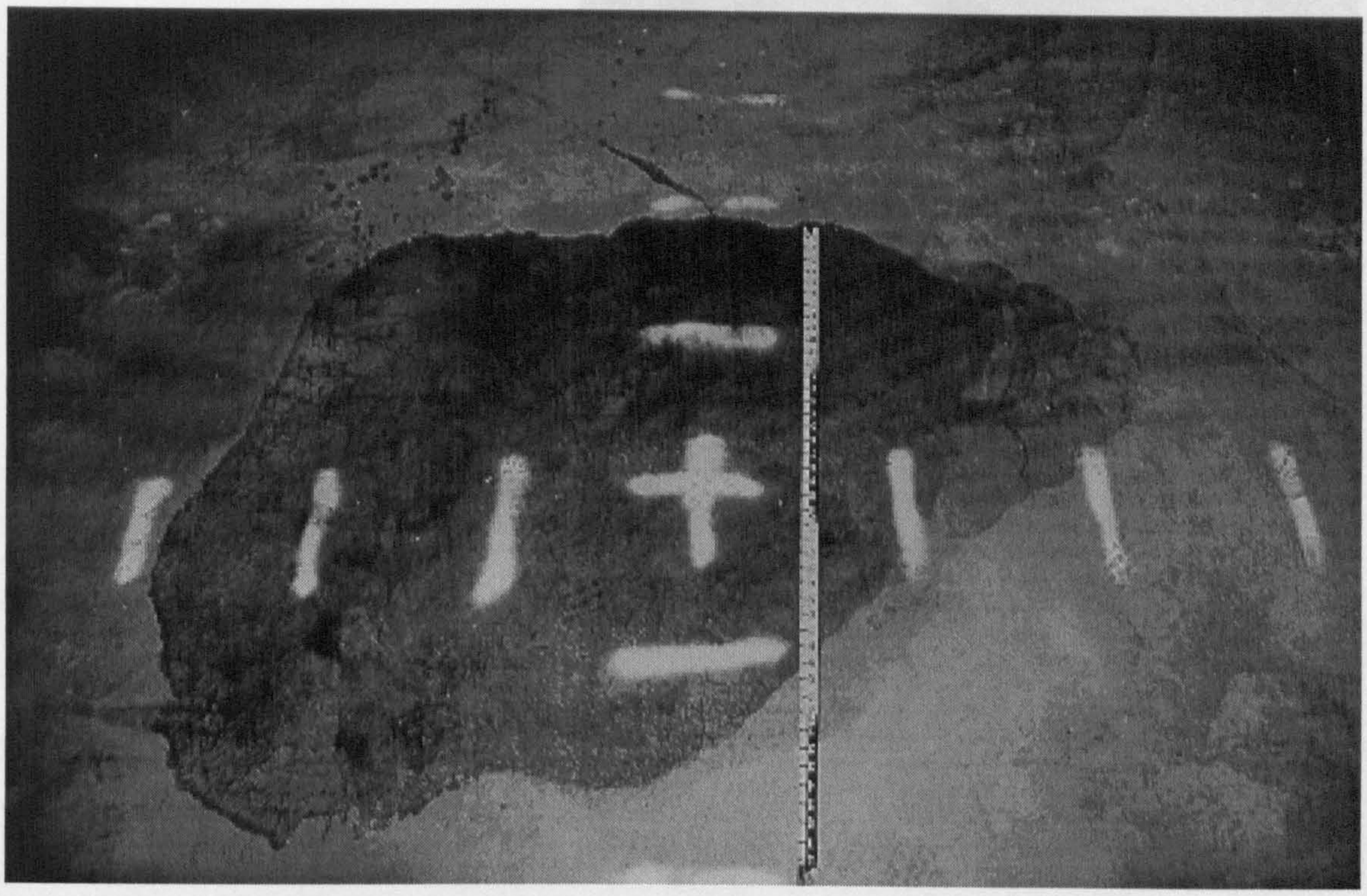

Fig. A.2.1.1: Typical pour test on concrete.

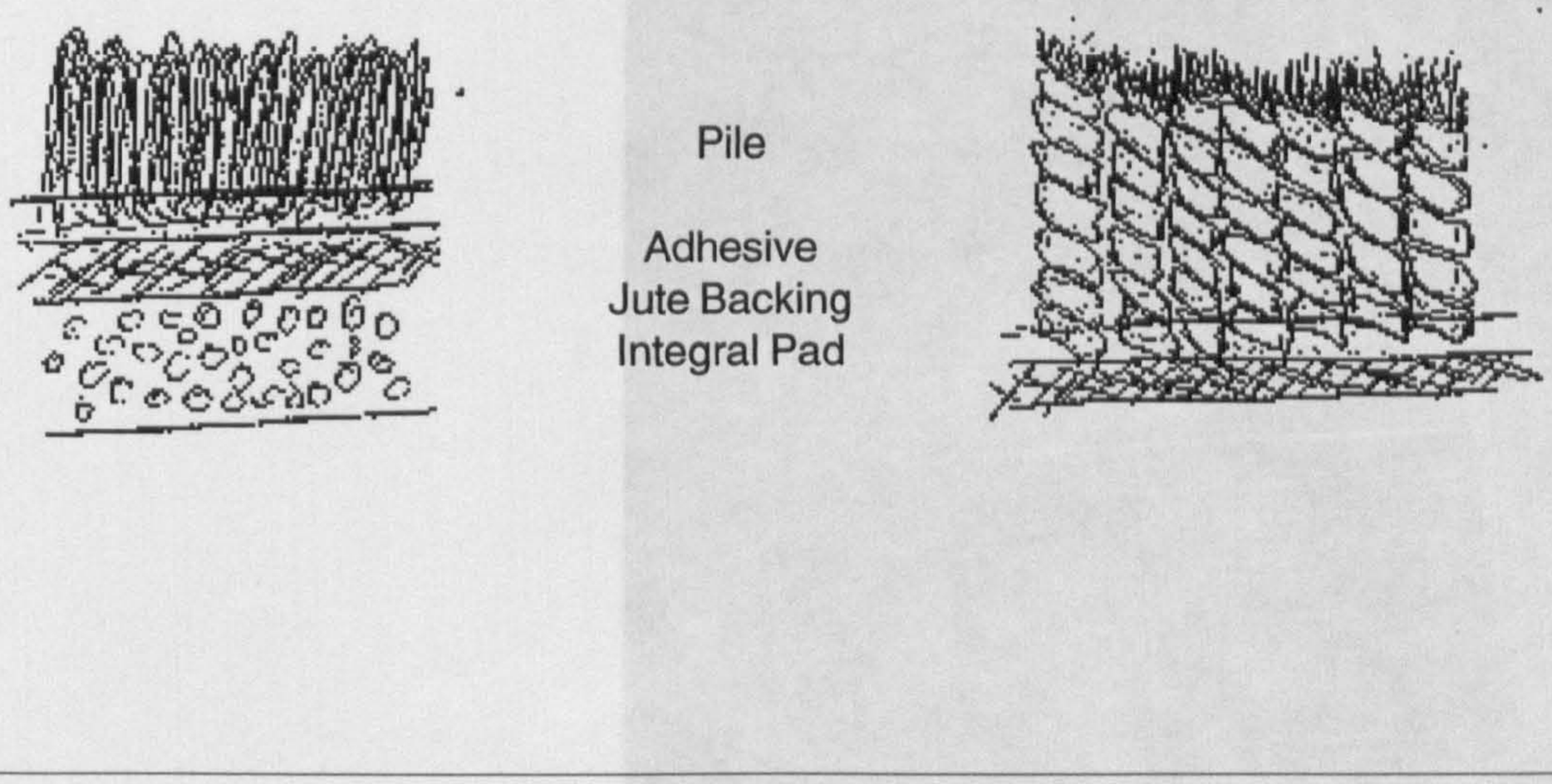

Fig. A.2.1.2: Cross-sections of common carpet types.

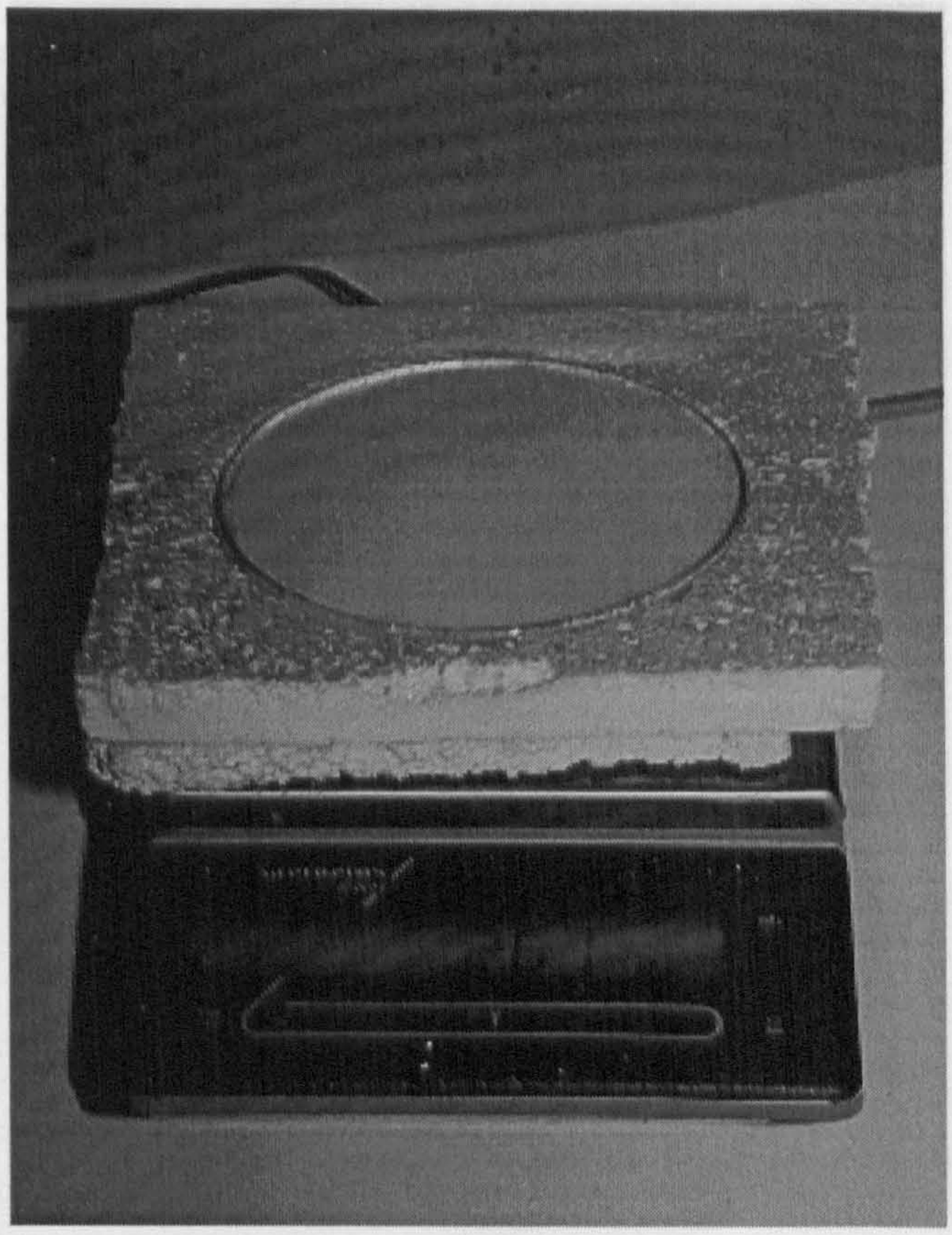

Fig. A.2.2.2.1(a): Balance with insulated Petri dish and polyurethane foam substrate.

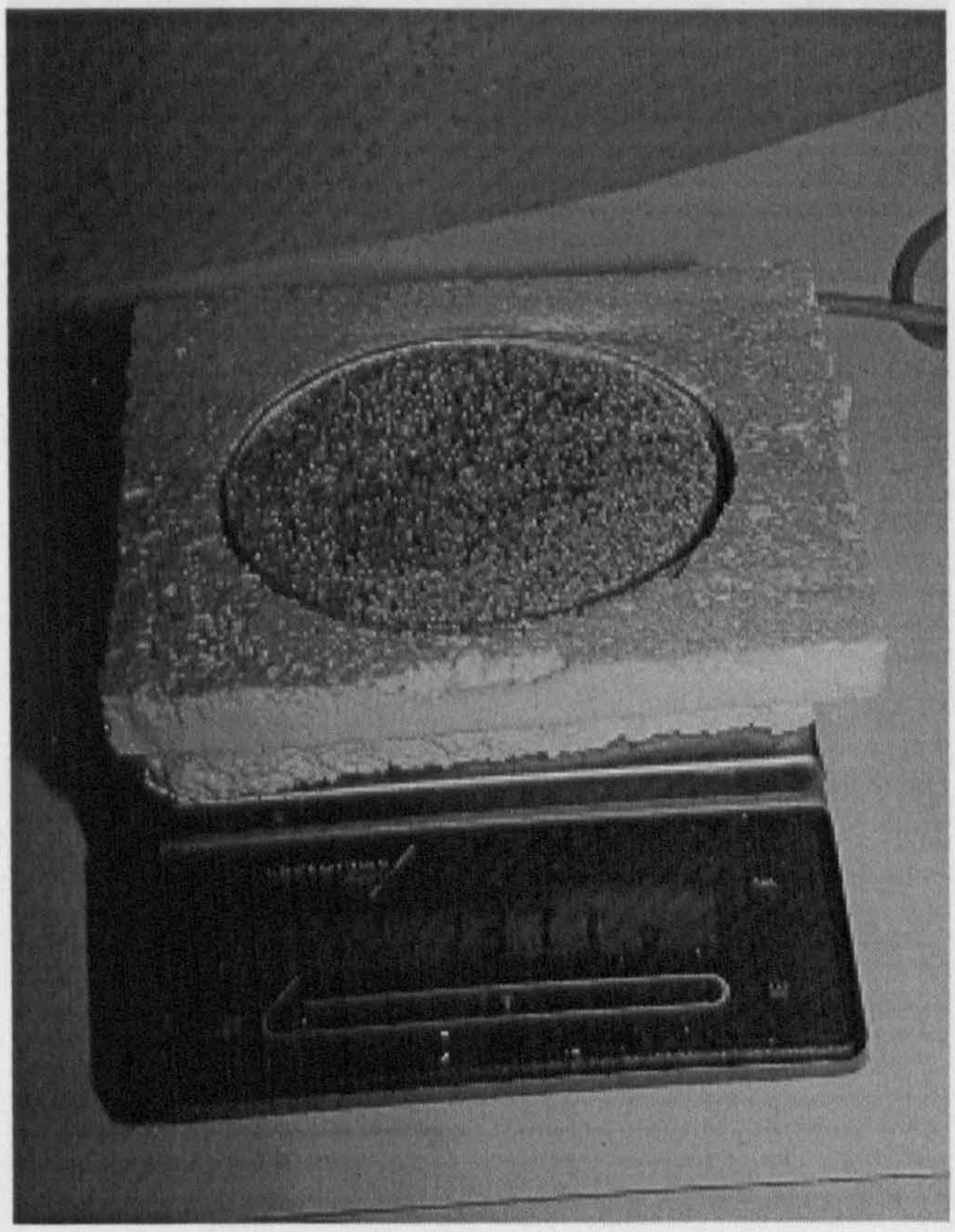

Fig. A.2.2.2.1(b): Balance with insulated Petri dish and sand (20-30 mesh) substrate.

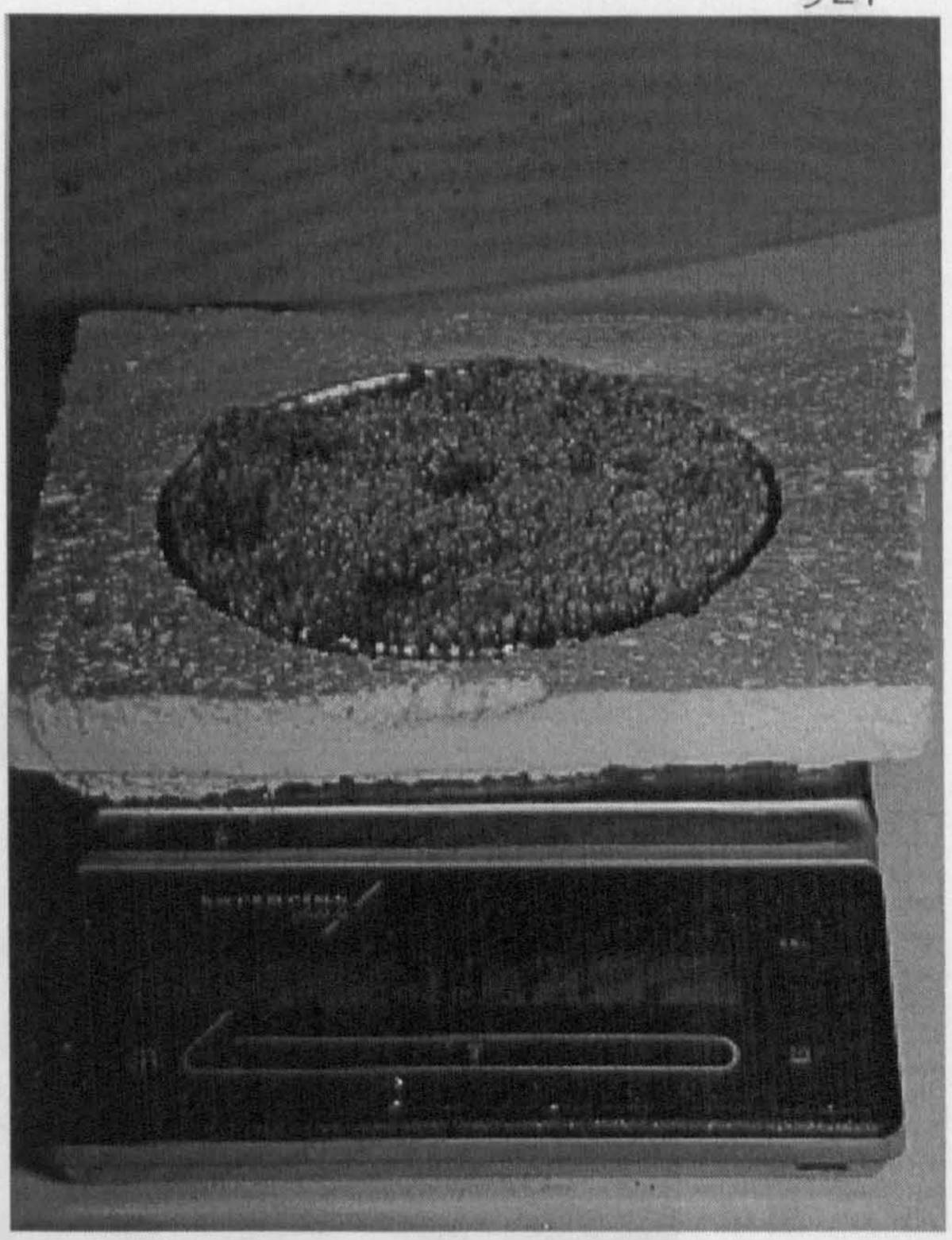

Fig. A.2.2.2.1(c): Balance with insulated Petri dish and carpet substrate.

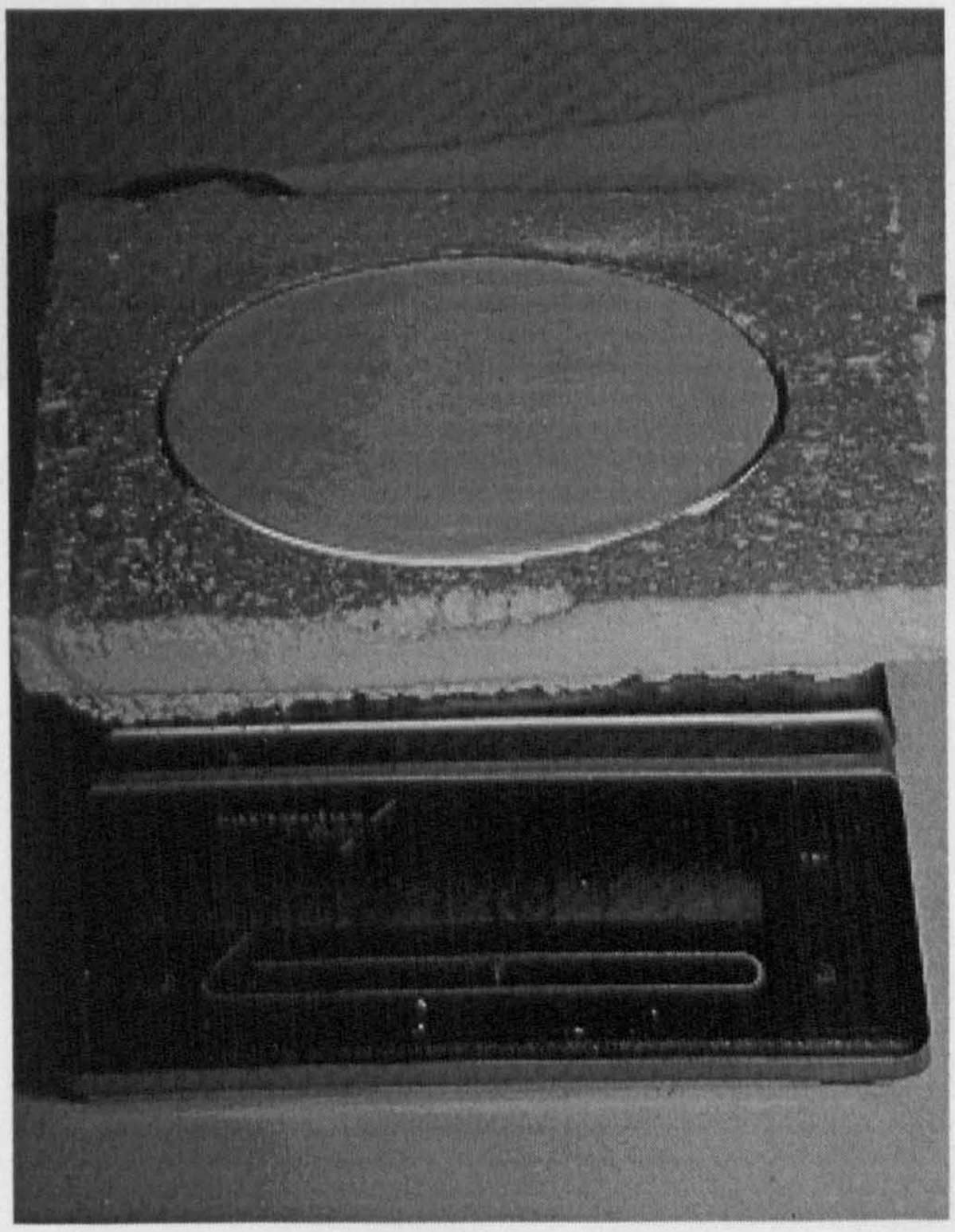

Fig. A.2.2.2.1(d): Balance with insulated Petri dish and plaster of Paris substrate.

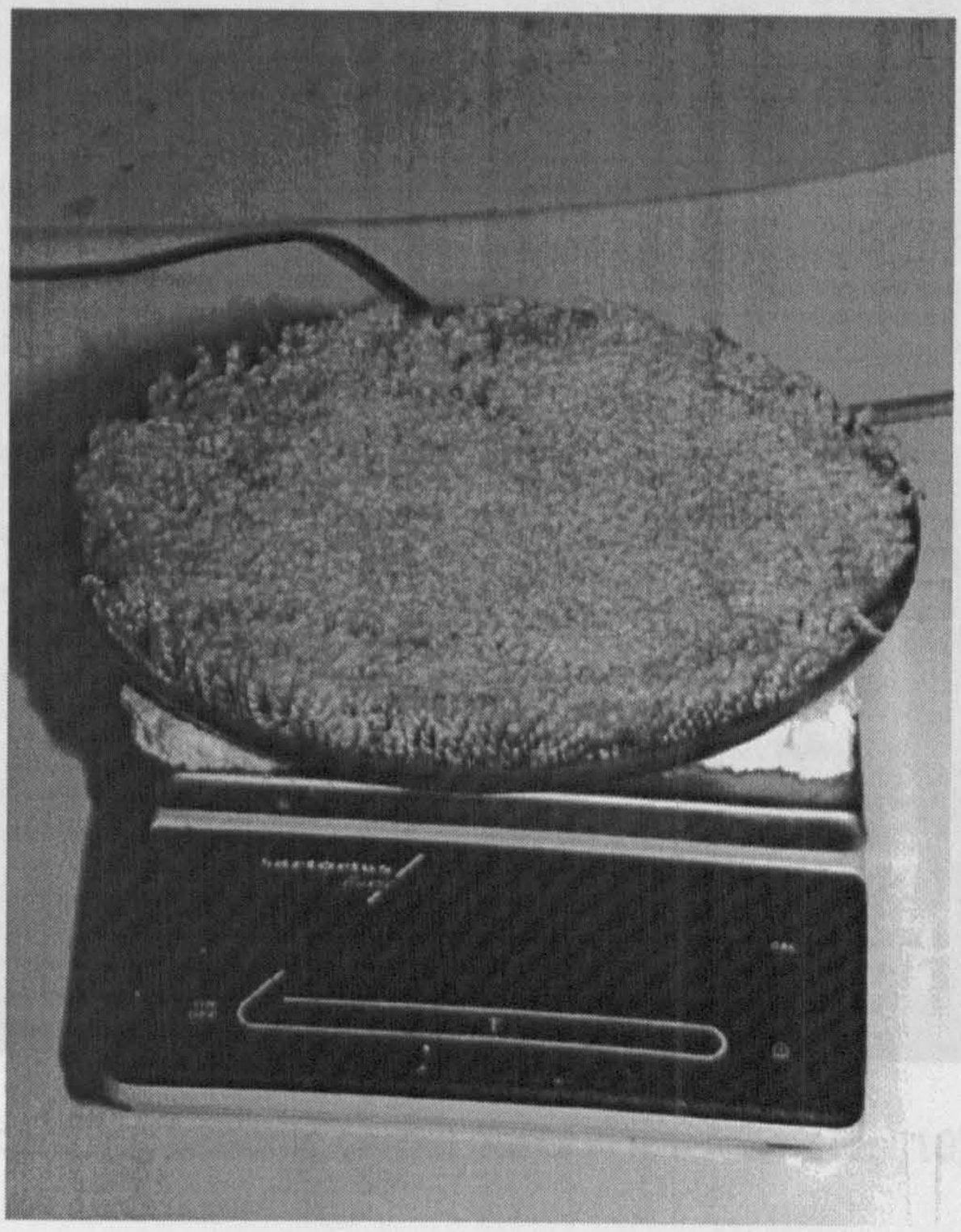

Fig. A.2.4.1: Large (0.3m) pan with carpet.

Fig. A.2.10.2: Pouring camping fuel onto carpet panel in test room (Test 10).

Table A3.10.2.1: Temperatures and Gas Concentrations, Camping Fuel on Carpet

Test	Ceiling Temp Max (°C)	4 Ft. Temp Max (°C)	O_2 Min. (%)	CO_2 Max (%)	CO Max (ppm)
9	939 (@ 0:43)	975	8.5 (0:42 -1:18)	12.4 (0:34)	9388(O:48)
10	753 (1:03)	502	8.5 (1:25-1:47)	16.2 (1:08)	9522 (1:17)
11	776 (1:14)	503	8.5 (1:44-3:11)	12.5 (1:40)	9251 (1:36) 9384 (1:53)

Numbers in parentheses denote actual elapsed time (in min:sec) from ignition

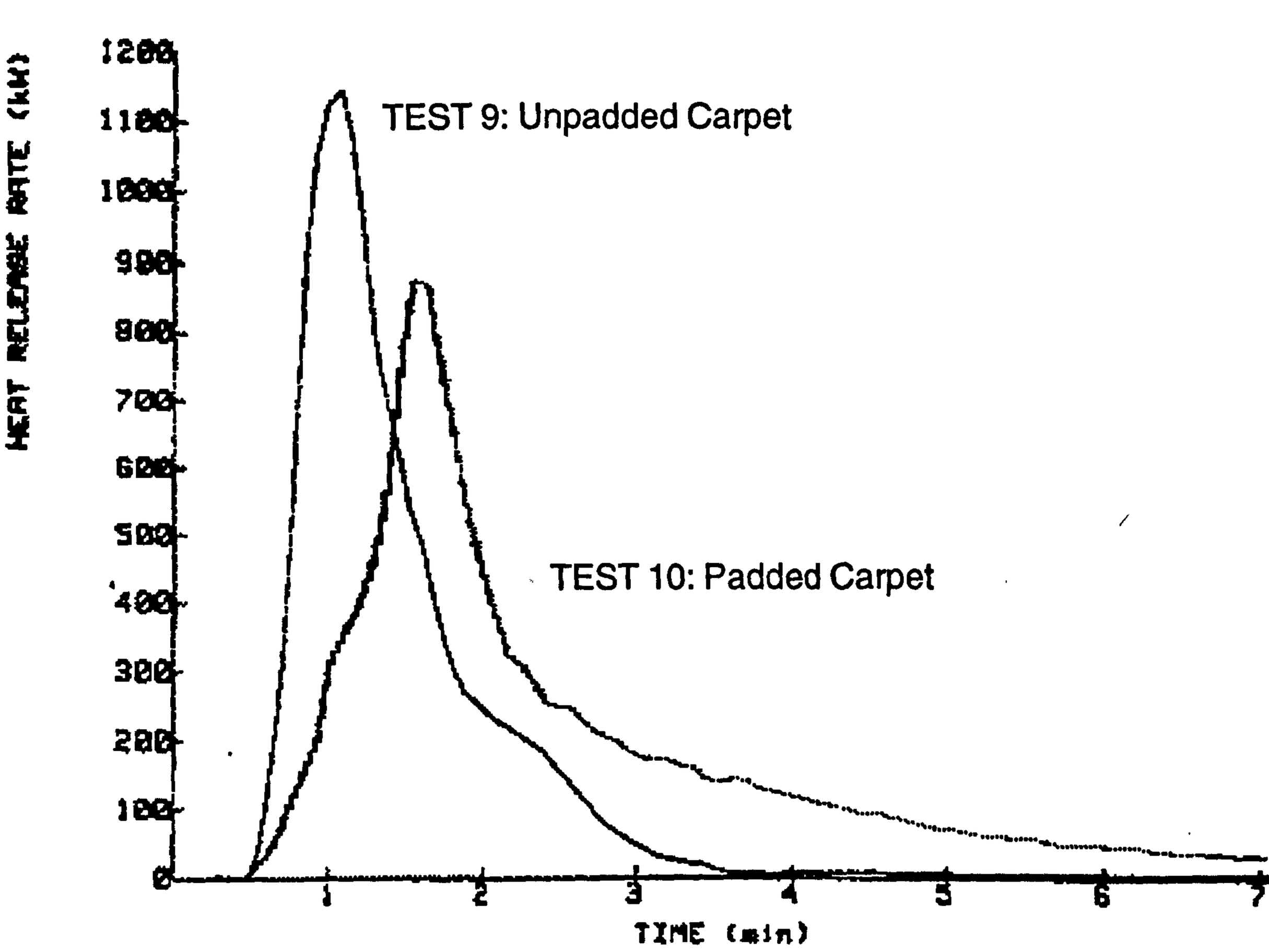

Fig. A 3.10.2.2: Heat release rates for 1.9litres of camping fuel pooled on nylon carpet, as measured in a 3m x 4m room calorimeter.

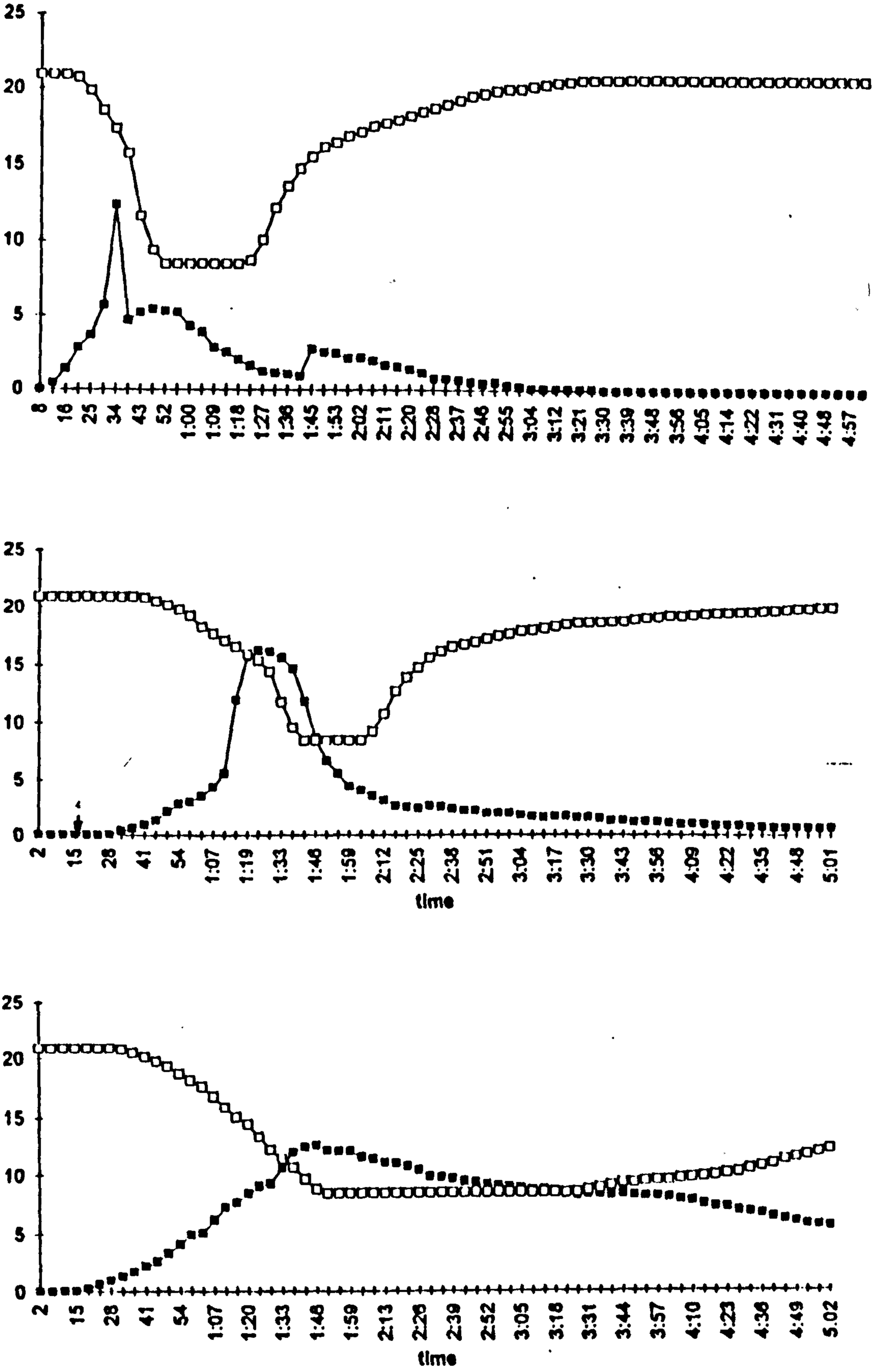

Fig. A3.10.2.3: Oxygen and carbon dioxide levels measured in the room calorimeter tests with 1.9 litres of camping fuel on carpet. Top – Test 9, carpet only (no pad), door open throughout test. Middle – Test 10, carpet and pad, door open throughout test, delayed ignition at 0:16. Bottom – Test 11, carpet and pad, door closed for first 5.5min then opened.

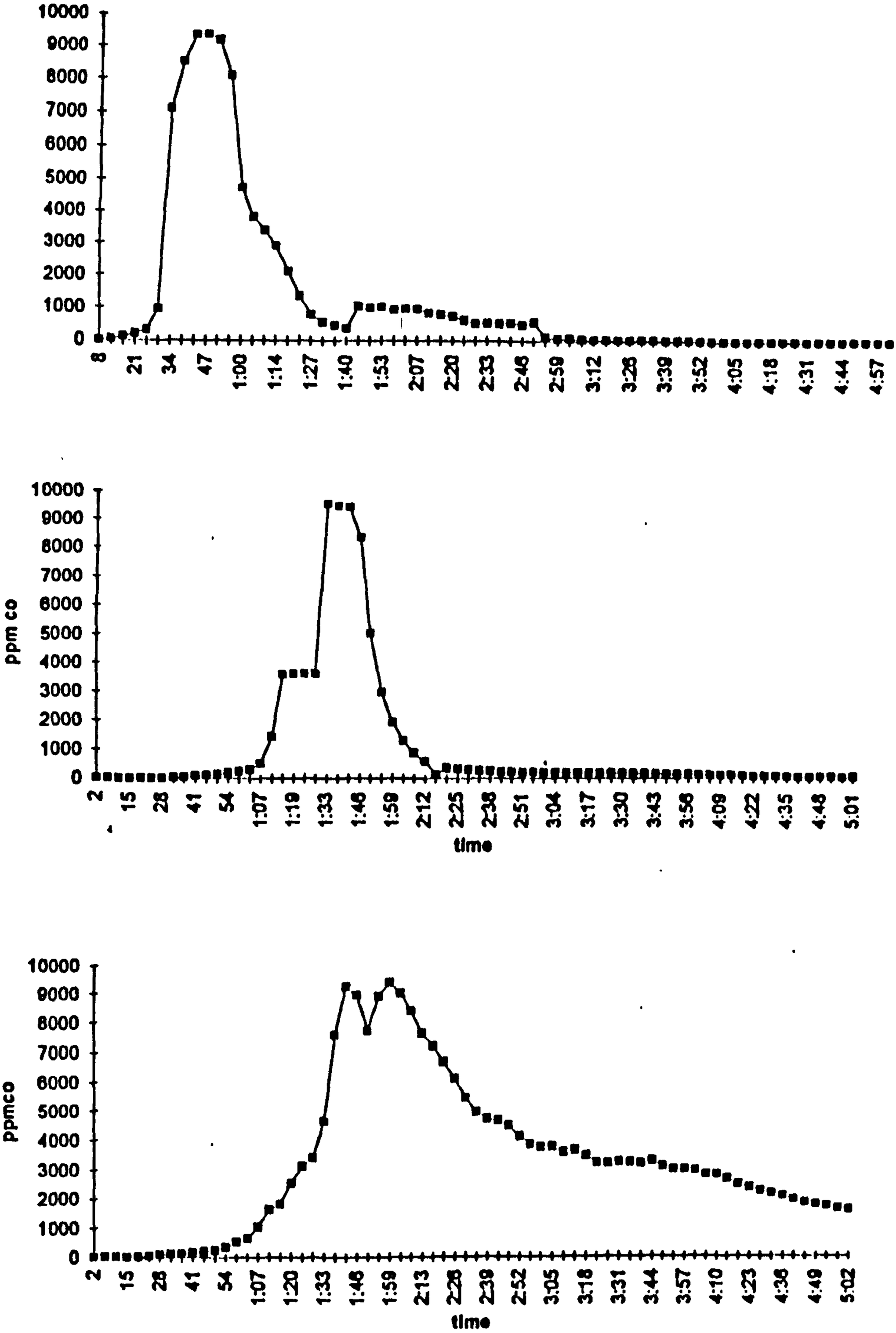

Fig. A3.10.2.4: Carbon monoxide levels measured in the room calorimeter tests with 1.9 litres of camping fuel on carpet. Top – Test 9, carpet only (no pad), door open throughout test. Middle – Test 10, carpet and pad, door open throughout test, delayed ignition at 0:16. Bottom – Test 11, carpet and pad, door closed for first 5.5min then opened.

Fig. A.3.10.2.1: Typical flame plume above camping fuel on carpet (Test 10). Height estimated at 1.2m. Photo taken approx. 1min after ignition.

Fig. A3.10.4.3: Results of room test (3 x) where 2litres of camping fuel was dispersed in a random pattern across a furnished carpeted room. The carpet has been removed to exposed the damage to the underlying chipboard and vapour barrier. The vehicle pattern in the centre of the room and the rectangular area parallel to the far wall co-incide with the pour pattern. The areas involved are much wider than the pour pattern (on a 6–7mm deep nylon pile carpet). These are also undamaged areas where fuel was known to have been splashed.

Fig.A3.10.4.8: Results of room test (B3) where ~2litres of camping fuel was poured in a random pattern across a furnished, carpeted room and ignited 40s after pouring was completed. Resulting fire was allowed to grow to flashover and then extinguished. Furniture has been removed to reveal damage to carpet. Extensive surface charring not associated with pour pattern is visible. Some localized deeper damage is visible in the centre of the room. Portions of that penetration co-incide with the pour pattern.

Fig. A3.10.4.9: Results of room test (B3) where ~2litres of camping fuel was poured in a random pattern across a furnished, carpeted room. The carpet has been removed to exposed the damage to the underlying urethane pad (with vapour-barrier). The circular pattern in the centre of the room and the rectangular area parallel to the far wall co-incide with the pour pattern. The areas involved are much wider than the pour pattern (on a 6–7mm deep nylon pile carpet). There are also undamaged areas where fuel was known to have been splashed.

Fig. A3.10.4.10: Results of the same room test (B3) where ~2litres of camping fuel was poured in a random pattern across a furnished, carpeted room, showing an isolated burn in the corner where some fuel was splashed.

Fig. A3.10.4.11: Results of the same room test (B3) showing the corresponding area of damage to the underlying carpet pad. The location of the pour pattern is detectable, but the size is larger than the original pool.

Fig. A3.10.4.12: Results of room test (B4) where ~3litres of camping fuel was poured in a random pattern across a furnished, carpeted room and ignited. The fire was extinguished less than 3min after ignition so the room was not allowed to proceed to flashover. Large areas of undamaged carpet are visible. The deep, localized damage is in the same area as the primary pour of fuel but is larger than the pool that could be produced from the quantity of fuel actually poured.

Fig. A3.10.4.13: Another view of the same room showing heavily damaged areas of carpet that co-incide with the location of the fuel pour, but not size (area).

Fig. A3.10.4.14: A furnished, carpeted room (B1) similar to that used in previous tests was ignited with direct flame applied to the bed with no flammable liquid accelerants present. Fire proceeded to flashover at ~46min after ignition and was extinguished as flashover progressed. The charred areas of carpet in the centre of the room were the result of radiant heat from the ceiling layer and from adjacent items of clothing and furnishings. Large unburned areas were the result of protection offered by those other fuels.

Fig. A3.10.4.15: The carpet from the same room test removed to make the burn patterns more visible. Localized deep charring in centre and left side were not produced by accelerant. The complete combustion of the carpet in the right rear corner was the result of the prolonged fire in the bed (which represented the primary fuel load in the room throughout much of the fire).

Fig. A3.10.4.16: Results of pour tests on carpet segments using 50/50 petrol/diesel fuel mixture. Burn time was approximately 5min. Large protected area in centre of rear carpet was the result of protection of carpet by wide pool (trail) of fuel. Continuous pour onto adjacent carpet segment (foreground) produced extensive destruction of carpet. Reference samples of carpet were not taken prior to test so fibre content and carpet type are unknown.

Fig. A3.10.4.17: Result of 4 litres of petrol on concret slab (exterior). Portions of outline of fuel pool are discernible due to soot deposited on adjacent unprotected areas of concrete. As pool was consumed, some soot was deposited on areas where there was fuel originally. Neither the soot deposits nor the limited "spalling" of the concrete surface yield an accurate estimation of size of original petrol pool.

Fig. A3.10.4.18: Result of one litre of 50/50 petrol/diesel fuel mixture poured on a wooden floor and allowed to burn to self-extinguishment (approx. 2min.). The wooden floor is more heavily scorched than would occur with a pool of petrol alone due to higher temperatures convected to the surface via higher-boiling-point constituents and the longer combustion times of diesel fuel. Portions of the margins of the pool are clearly delineated by the scorching but other portions are not so visible. after ignition, the margins of the pool were observed to spread due to the reduction of surface tension as temperature increases. This resulted in a larger pool than was present prior to ignition.

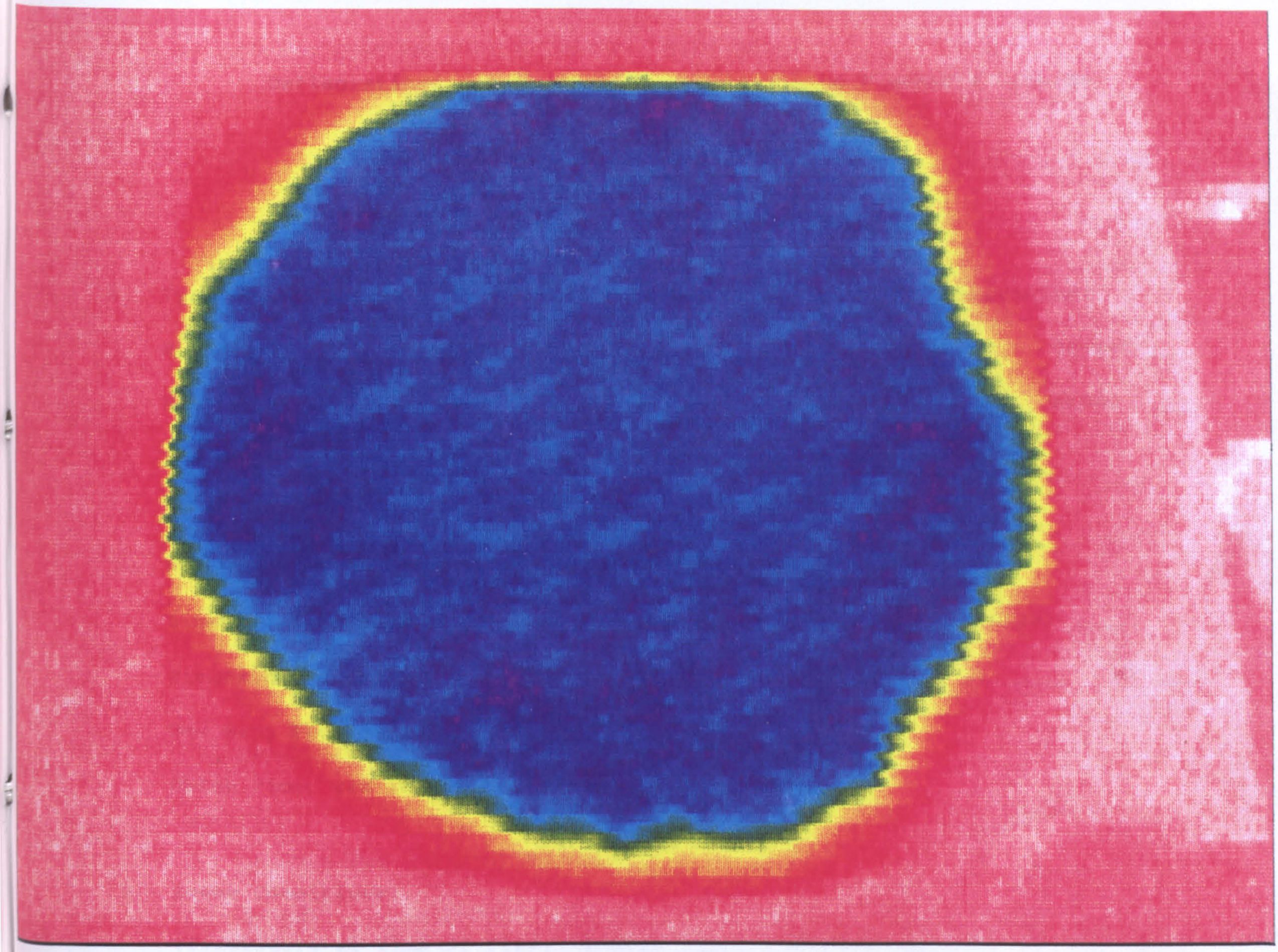

Fig. A4.4.2: False-colour image Inframetrics image of large (D = 28cm) pool of pentane evaporating from loop-pile carpet. The cooling effect on adjoining (non-wetted) areas of the carpet can be seen from the dark red and yellow haloes, which represent temperatures of 4° and 7°C below ambient (29°C). The cooling of an annular ring of carpet within the wetted area induced by the advective flow can be seen as the difference between the central area with a temperature of 11 – 12°C and the darker annular ring where the surface temperature is of the order of 9 – 10°C. The central area lies under a quiescent zone of vapour.

Deflagrations: A Study of Fires Involving Flammable Liquids

1. Type of Occupancy:

Business ____ Manufacturing _____

Residence ____ Other _____

Storage _____

Type of Construction:

Wood frame ____ Street ___

Masonry ____ Other ___

Concrete ___

2. Was the Fire Confined to the Room of Origin? ____

Dimensions of Room of Origin: Length _____ Width _____ Height ____

Dimensions of Building (if more than one room involved): L: _____ W: ____

How Many Floors? ____

Which Floor was Identified as Origin? ____

3. Scene Conditions:

Temperature at Time of Fire: Indoor _____ Outdoor ____

How Were Those Facts Established? _____

Weather: Windy _____ Still _____ Rainy _____ Unknown ____

Do you consider these conditions to have contributed to the fire? _____

If so, please describe: _____

_____

4. Witnesses:

Did Witnesses Report a Sound? _____ (Describe if Possible): _____

Whoosh ____ Thump ____ Bang ____ Boom ____ Other ___

Did Witnesses Report a Flash or Glow? _____

5. Type of Fuel Used: _____

How Was That Fact Established? Confession ____ Odor ____

Witness ____ Estimate ____

Container ____ Other ____

Lab Analysis ____

How Confident Are You of That Conclusion? _____

_____

6. How Much Fuel Was Poured/Spilled? _____

How Was That Fact Established? Confession ____ Container ____

Witness ____ Other ____

7. How Was the Fuel Applied?

Accidental Spill ____ Spray/Aerosol ____ Device ____

Deliberate Pour or Splash ____ Other ____

8. On What Was the Fuel Applied?

Carpet ____ Wood ____

Concrete ____ Soil ____

Tile ____ Other ____

9. How Large an Area Was Covered With Liquid? _____

How Was This Established? _____

10. What Was the Means of Ignition? Source: Appliance ____

Flame ____ Firesetter ____

Spark/Arc ____ Unknown ____

Hot Surface ____ Other ____

Unknown ____

How Was This Established? _____

11. How Far Was the Ignition Source From Pour/Spill? _____

How Was This Established? _____

12. Was the Ignition Source - Higher? _____ Lower? _____ or Same Level? _____

as Spill or Pour? _____ Describe: _____

13. Time Delay Between Pour and Ignition (If Known): _____

How Was That Fact Established? _____

14. Damage to Building:

Fire Only _____

Confined to Room of Origin _____

Confined to Floor of Origin _____

Structural Damage:

Windows Broken ____

Doors/Walls Cracked/Breached ____

Walls/Floors/Roof Collapsed ____

Other ____

15. Injuries: Firesetter: _____ Describe Severity & Distribution on Body: ___

Occupant: _____ _____

Other: _____ _____

16. Date of Incident: _____ Time of Incident: _____

17. Other Comments: _____

_____

18. Is It Possible To Obtain A Copy Of The Incident Report? _____

Source: _____

Thank you for your time and assistance.

Upon Completion, Return (by October 1993) to:

John D.DeHaan
2301 Alameda Street, Vallejo, CA 94590 USA

SartoWedge™

Version 1.0

Sartorius Systems, Ltd.
140 Wilbur Place
Bohemia, NY 11716
(516) 563-5120

[redacted]

sartorius

WHAT IS A WEDGE?

A "WEDGE" is normally a hardware device that connects between a computer's CPU and its keyboard to allow data input from an external device as if it were entered directly through the terminal's keyboard. Most wedges use an RS232 serial port to accommodate an external device. Since most electronic data output devices (including bar code scanners, card readers, scales, measuring instruments and portable data collection devices) are available from the manufacturer with an RS232 port and because almost all Personal Computers already have an RS232 port, the additional hardware wedge is not necessary and can be eliminated by using The Sarto Wedge™ instead.

WHAT IS THE SARTO WEDGE™?

The Sarto Wedge™ is a RAM resident (TSR) PC program that emulates a hardware wedge on any MS or PC DOS computer. With The Sarto Wedge™, any RS232 output device can be connected directly to your PC's RS232 (serial) port and data from the device can be inputted directly into any application program running in the PC that is expecting keyboard input; including LOTUS 123, Dbase, and all other PC application programs. The PC's keyboard is not disabled in any way and may also be used for input as in normal operation.

HARDWARE REQUIREMENTS

The Sarto Wedge™ is designed to run on any MS or PC DOS computer (IBM PC, XT, AT, PS2 or 386/486 PC or clone) that is equipped with an RS232 serial port. The only requirement for your input devices is that they must be capable of outputting ASCII data through an RS232 standard serial interface. No other hardware is required.

FEATURES

Version 1.0 of The Sarto Wedge™ contains many powerful features that were designed to allow data to be inputted from virtually any RS232 input device connected to any DOS computer running any DOS application program. These features include:

1. Support for any COMM port. The Sarto Wedge™ can be installed for any serial adapter available in your PC.
2. Data Parsing capabilities. If your input data consists of more that one data field, you can parse out data that you need and ignore any data that is not needed.
3. Numeric Filtering capabilities. The Sarto Wedge can be configured to filter out non numeric characters from any data field in your input data records.
4. Keystroke Macro Insertion. The Sarto Wedge™ can be configured to add a series of user defined keystrokes (macros) at the beginning or end of each data field in an input data record—up to 50 keystrokes before or after each field up to 450 keystrokes per data record.
5. Automatic Date and Time Stamping. Keystroke Macros may contain special date and time stamp functions generated automatically by The Sarto Wedge™.
6. Selectable Buffer Transfer Rate. You may select the rate at which characters are transferred from the serial input buffer to the DOS keyboard buffer.
7. Hot Key Data Requests. The Sarto Wedge™ can be configured to either send a string out the serial port or lower the DTR signal line for 100 ms whenever a special Hot Key is pressed on your PC's keyboard. With many types of input devices, these actions can be used to request data from the device.
8. Device Initialization String. You can configure The Sarto Wedge™ to send an initialization string out the serial port to your input device when The Sarto Wedge is first loaded into your PC's memory.
9. Input Data Translation Table. The Sarto Wedge™ allows you to translate any incoming character to either another character or to a specific keystroke. This feature can also be used to ignore specific characters or further filter incoming data.

WHY IS THE SARTO WEDGE™ BETTER THAN A HARDWARE WEDGE?

The advantage of The Sarto Wedge™ is that it does not take up any desk space; it simplifies the process of connecting an alternate input device; it is fully programmable and can parse and filter incoming data as well as add user specified keystroke macros to the input data; it is much less expensive than a hardware wedge; and it will never break. In addition, The Sarto Wedge™ buffers all input data and then transfers it to your application programs only when they are ready for it—unlike a hardware wedge that has no way to tell when your programs are ready to receive more data ("Keyboard Buffer Overrun" is a common problem with hardware wedges). The Sarto Wedge™ can also be used on a laptop or palmtop PC that does not have a detachable keyboard whereas a hardware wedge cannot.

The Sarto Wedge™ functions much faster than a hardware wedge and it may also be installed for each available serial port, allowing you to attach more than one serial input device to a single PC. If you are running Windows 3.0 in 386 Enhanced Mode, you can even have The Sarto Wedge™ running in the background in one or more windows, collecting data while you are working with another program in the foreground. True Multi Tasking!

Plain and simple—Sarto Wedge™ is smaller, faster, cheaper, more powerful, more portable, more versatile, and much easier to set up and use than any hardware wedge available.

C A U T I O N

Before operating this instrument it is important that the user read through this manual to insure efficient and safe operation.

IR-711

Portable Hydrocarbon Analyzer

with Arson Probe Adapter

OPERATIONS MANUAL

This manual describes the operation and calibration of the Infrared Industries, Inc. Model IR 711 Portable Hydrocarbon Analyzer.

INFRARED INDUSTRIES, INC.

Mailing Address

P.O. Box 989, Santa Barbara, California 93102

Shipping Address

6307 Carpinteria Ave., Carpinteria, California 93013

(805) 684-4181 Telex 658-480

S E C T I O N O N E

Introduction

1.1 GENERAL DESCRIPTION

The Infrared Industries, Inc. Model IR 711 Portable Hydrocarbon Analyzer is a non-dispersive infrared (NDIR) gas analyzer for monitoring the concentration of hydrocarbon vapors. The IR 711 has a dual range analog readout.

Features include internal rechargeable battery, adjustable audio alarm, solid state detector, direct reading display, calibration checks and corrosion resistant sample chamber.

1.2 SPECIFICATIONS

Ranges -

High	0-100% LEL
Low	0-1000ppm
Calibration gas	propane
Accuracy	5%
Resolution	
High Range	2.5% LEL
Low Range	25ppm

Drift (1hr: after 20min warm-up)	
High Range	2.5% LEL
Low Range	25ppm
Drift (8hrs: after 20min warm-up)	
High Range	5% LEL
Low Range	50ppm
Precision of Span Temperature Compensation (0° to 50°C)	2%
Response Time for Temperature Compensation	2min
Weight, Total	9 lb. (4 kg)

Warning:

The Model IR 711 is calibrated for monitoring the presence of the heavier alkanes such as found in the hydrocarbon fuels: gasoline, JP-4, kerosene, or JP-5. The response to methane will be limited. The IR 711 should not be used to monitor the presence of methane. A lower than true LEL indication will result. To monitor methane, the Model IR 712 should be used.

Note:

Probes and control boxes are not interchangeable without following lab calibration procedure, Section 4.2.

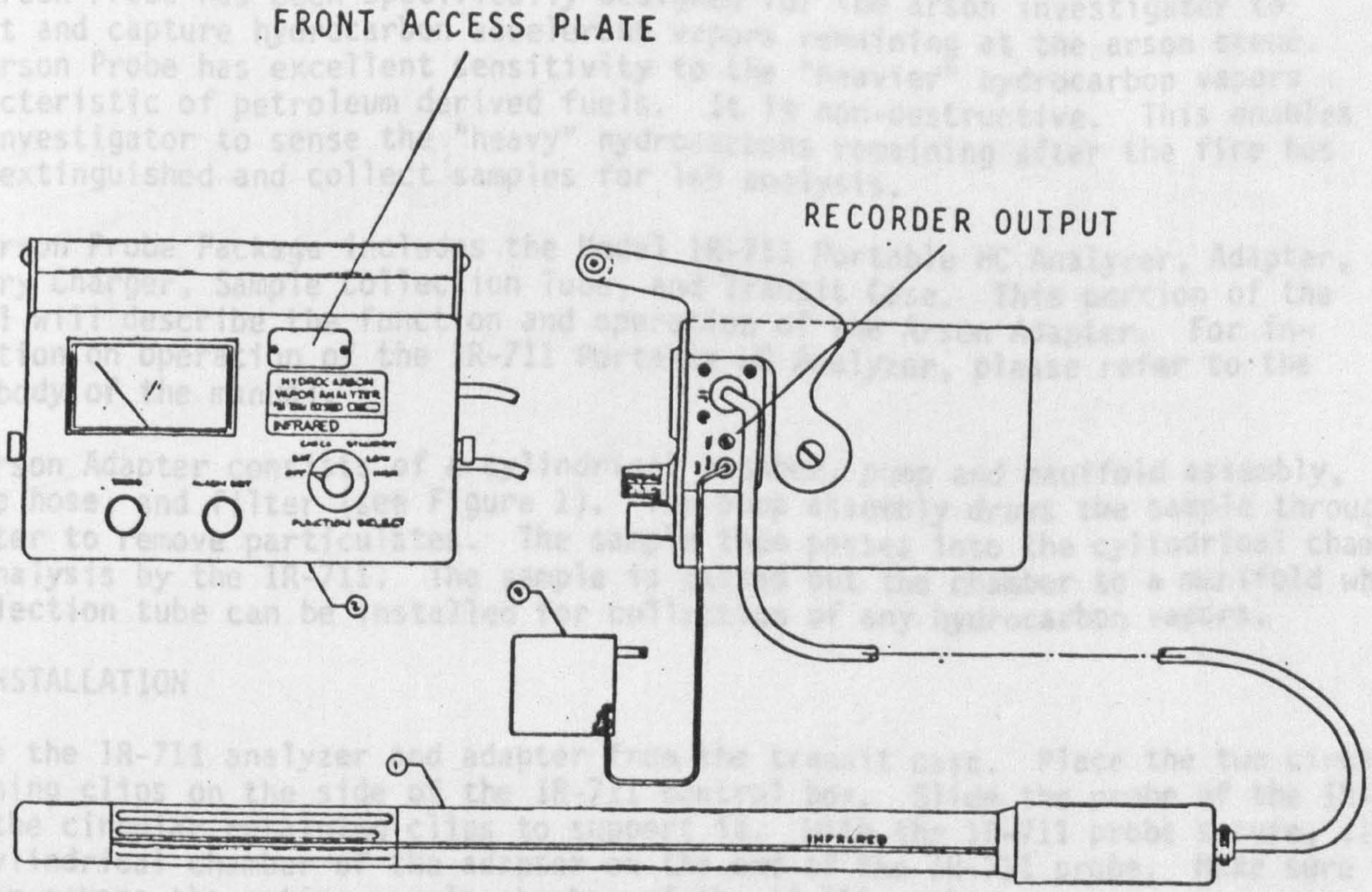
FRONT ACCESS PLATE
RECORDER OUTPUT
HYDROCARBON VAPOR ANALYZER
INFRARED
FUNCTION SELECT
INFRARED

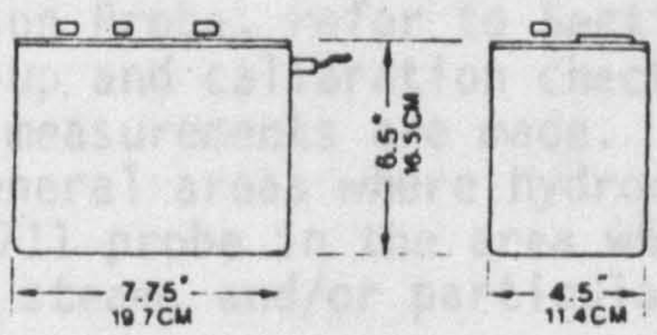
6.5"
16.5CM
7.75"
19.7CM
4.5"
11.4CM

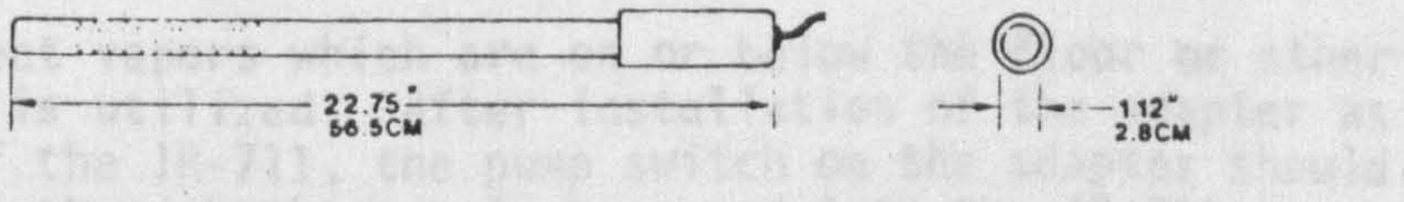
22.75"
56.5CM
1.12"
2.8CM

ARSON PROBE ADAPTER

I INTRODUCTION

The Arson Probe has been specifically designed for the arson investigator to detect and capture hydrocarbon accelerant vapors remaining at the arson scene. The Arson Probe has excellent sensitivity to the "heavier" hydrocarbon vapors characteristic of petroleum derived fuels. It is non-destructive. This enables the investigator to sense the "heavy" hydrocarbons remaining after the fire has been extinguished and collect samples for lab analysis.

The Arson Probe Package includes the Model IR-711 Portable HC Analyzer, Adapter, Battery Charger, Sample Collection Tube, and Transit Case. This portion of the manual will describe the function and operation of the Arson Adapter. For information on operation of the IR-711 Portable HC Analyzer, please refer to the main body of the manual.

The Arson Adapter consists of a cylindrical chamber, pump and manifold assembly, sample hose, and filter (see Figure 1). The pump assembly draws the sample through a filter to remove particulates. The sample then passes into the cylindrical chamber for analysis by the IR-711. The sample is passed out the chamber to a manifold where a collection tube can be installed for collection of any hydrocarbon vapors.

II INSTALLATION

Remove the IR-711 analyzer and adapter from the transit case. Place the two circular retaining clips on the side of the IR-711 control box. Slide the probe of the IR-711 into the circular retaining clips to support it. With the IR-711 probe secure, slide the cylindrical chamber of the adapter on the end of the IR-711 probe. Make sure the adapter covers the entire sample chamber of the IR-711 probe.

The Arson Probe is now ready for operation.

III OPERATION

Before operating the Arson Probe, refer to Section 3.3, "Operating Procedure". This describes the warm-up and calibration checks for the IR-711. These must be accomplished before any measurements are made. The IR-711 can be utilized without the adapter to locate general areas where hydrocarbon vapors are present. This is done by placing the IR-711 probe in the area where vapors are suspected. Avoid heavy amounts of smoke, steam, and/or particulates; they will cause false readings of the instrument.

To detect and collect vapors which are on or below the floor or other hard to reach areas, the adapter is utilized. After installation of the adapter as described earlier and warm-up time of the IR-711, the pump switch on the adapter should be turned on. This draws a sample through the sample hose and into the IR-711 for analysis. The metal tip at the end of the hose should be probed in the areas of suspected hydrocarbon vapors.

To collect a sample for lab analysis, the collection tube should be utilized. The ends of the tubes must be broken off to allow for flow-through of the sample. Once the ends are removed, the tube should be installed into the collection tube manifold. (See Figure 1, Adapter configuration). The adapter is now ready to collect a sample

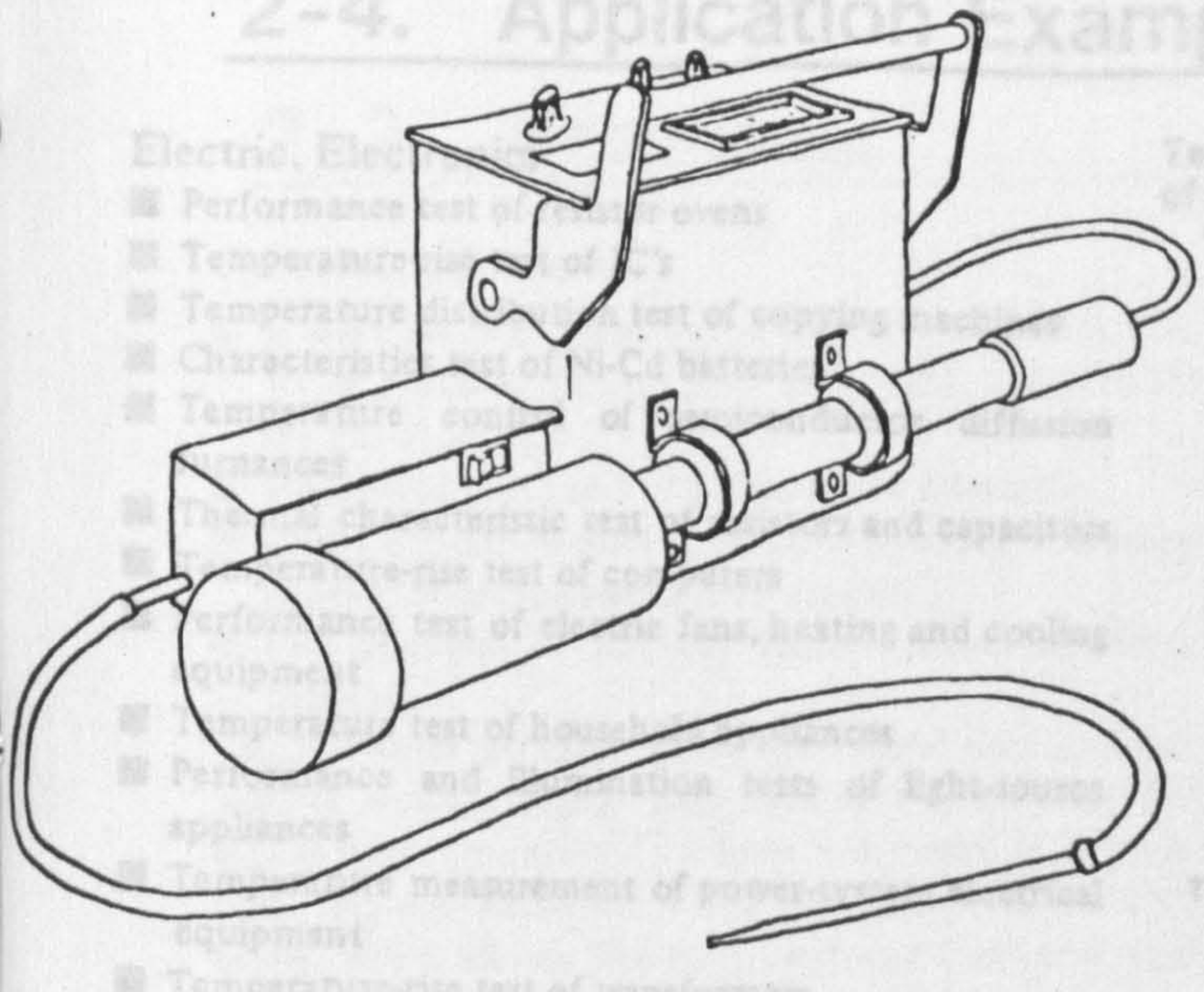

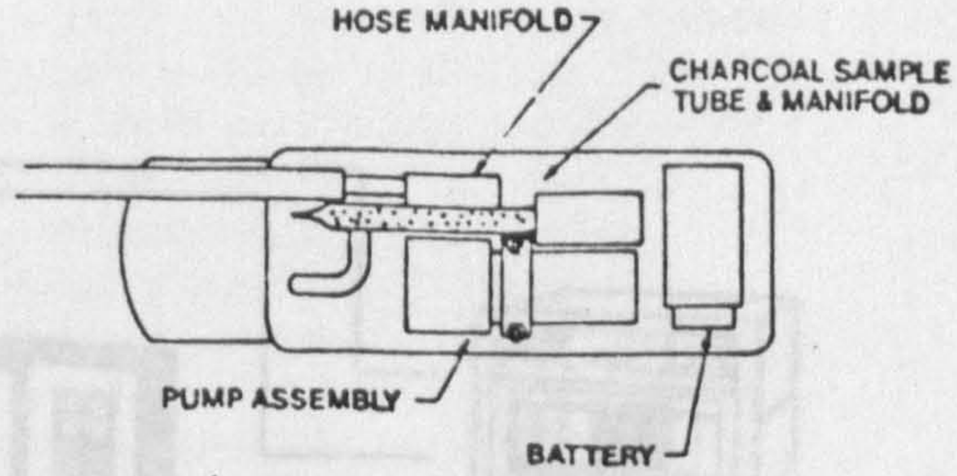
HOSE MANIFOLD
CHARCOAL SAMPLE TUBE & MANIFOLD
PUMP ASSEMBLY
BATTERY

ADAPTER

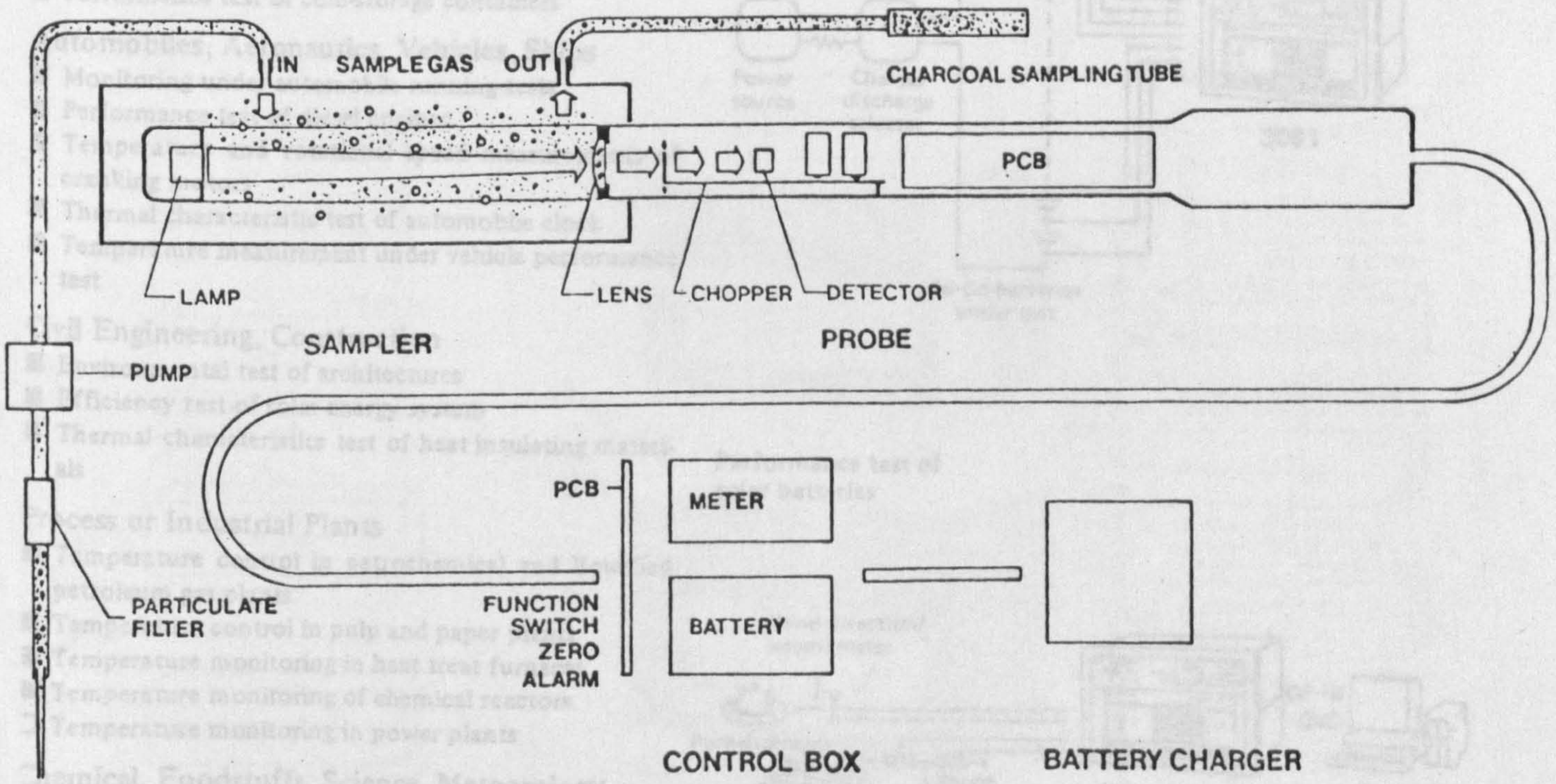
IN SAMPLE GAS OUT
CHARCOAL SAMPLING TUBE
PCB
LAMP
LENS
CHOPPER
DETECTOR
SAMPLER
PROBE
PUMP
PCB
METER
BATTERY
PARTICULATE FILTER
FUNCTION SWITCH ZERO ALARM
CONTROL BOX
BATTERY CHARGER

2-4. Application Examples.

Electric, Electronics

- Performance test of resistor ovens
- Temperature-rise test of IC's
- Temperature distribution test of copying machines
- Characteristics test of Ni-Cd batteries
- Temperature control of semiconductor diffusion furnances
- Thermal characteristic test of resistors and capacitors
- Temperature-rise test of computers
- Performance test of electric fans, heating and cooling equipment
- Temperature test of household appliances
- Performance and illumination tests of light-source appliances
- Temperature measurement of power-system electrical equipment
- Temperature-rise test of transformers
- Charge/discharge tests of batteries
- Continuous running tests of motors
- Performance test of air-conditioners
- Temperature distribution test of temperature ovens

Machinery

- Performance test of machine tool shafts
- Temperature-rise test of motor-operated appliances
- Temperature test of boilers
- Performance test of cold-storage containers

Automobiles, Aeronautics, Vehicles, Ships

- Monitoring under automobile running tests
- Performance test of diesel engines
- Temperature and rotational speed measurements of cranking motors
- Thermal characteristic test of automobile clock
- Temperature measurement under vehicle performance test

Civil Engineering, Construction

- Environmental test of architectures
- Efficiency test of solar energy system
- Thermal characteristics test of heat insulating materials

Process or Industrial Plants

- Temperature control in petrochemical and liquefied petroleum gas plants
- Temperature control in pulp and paper plants
- Temperature monitoring in heat treat furnaces
- Temperature monitoring of chemical reactors
- Temperature monitoring in power plants

Chemical, Foodstuffs, Science, Meteorology

- Temperature control in food warehouses
- Performance test of solar batteries
- Weather data monitoring systems
- On-line temperature control in glass plants

Temperature distribution test of temperature ovens

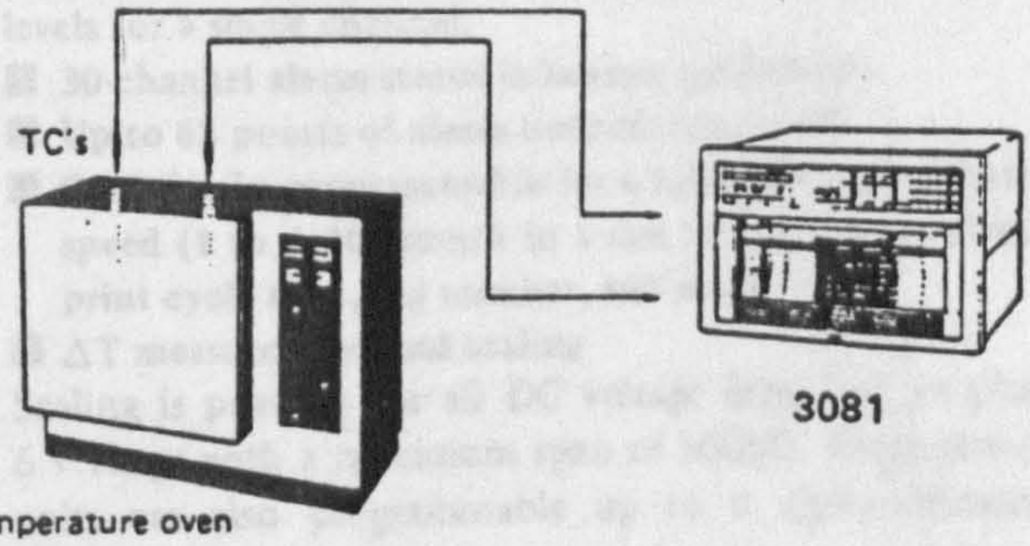

Characteristics test of Ni-Cd batteries

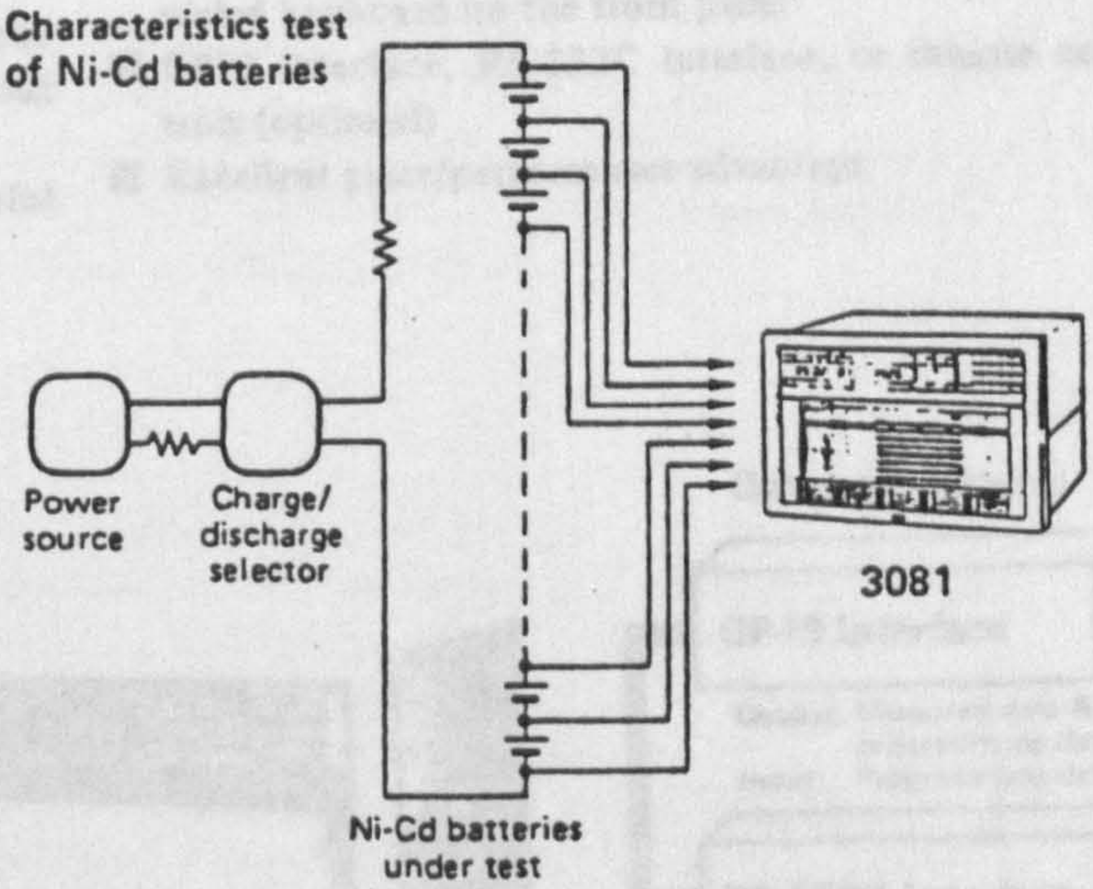

Performance test of solar batteries

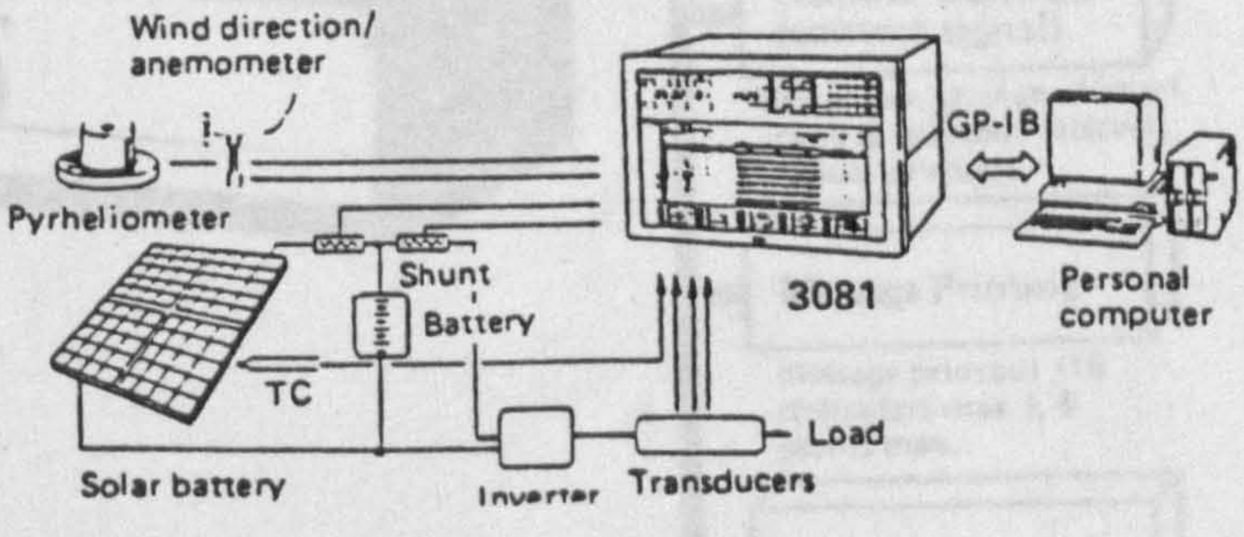

2-2. Features.

Convenient Features

- **A wide range of input types – DC V (±20 mV to ±50 V), 9 types of TC's (ANSI, DIN, JIS), and/or RTD (Pt 100 Ω, 50 Ω)**
- **High-speed printout – 30 channels in 6 seconds**
- **Clear, distinct 6-color printout by using a maintenance-free multi-color ribbon cassette**
- **Full selection of printout formats including ZONE printing**

TREND mode provides analog and digital data printout with or without digital scale data, and LOG mode is a digital logging printout. To meet a diversity of applications, Hybrid Recorder is also provided with a ZONE mode, which allows free programming of left and right end printout positions for each channel.

- **Versatile printout modes – PRINT ON ALARM, CHANGE ON ALARM**

On alarm of any channel, CHANGE ON ALARM mode automatically changes the chart speed or printout interval.

- **Maximum versatility through a wide range of useful alarm (up to 6 levels/channel)**

The variety of alarm types includes high, low, high-rate of change, low-rate of change, delta high, and delta low. Any mixture of alarm types is programmable up to 6 levels for a single channel.

- **30-channel alarm status indicators (standard)**
- **Up to 68 points of alarm outputs (optional)**
- **Completely programmable for a full-scale range, chart speed (1 to 1,200 mm/h in 1 mm steps), alarms, skip, print cycle time, tag number, and more.**
- **ΔT measurement and scaling**

Scaling is possible for all DC voltage input ranges plus 6 V range with a maximum span of 30000. Engineering units are also programmable up to 6 alphanumerics characters.

- **Simple to read printout (4081 equipped with internal illumination)**
- **Simplified programming and operation via membrane-sealed keyboard on the front panel**
- **GPIB interface, RS-232C interface, or remote controls (optional)**
- **Excellent price/performance advantage**

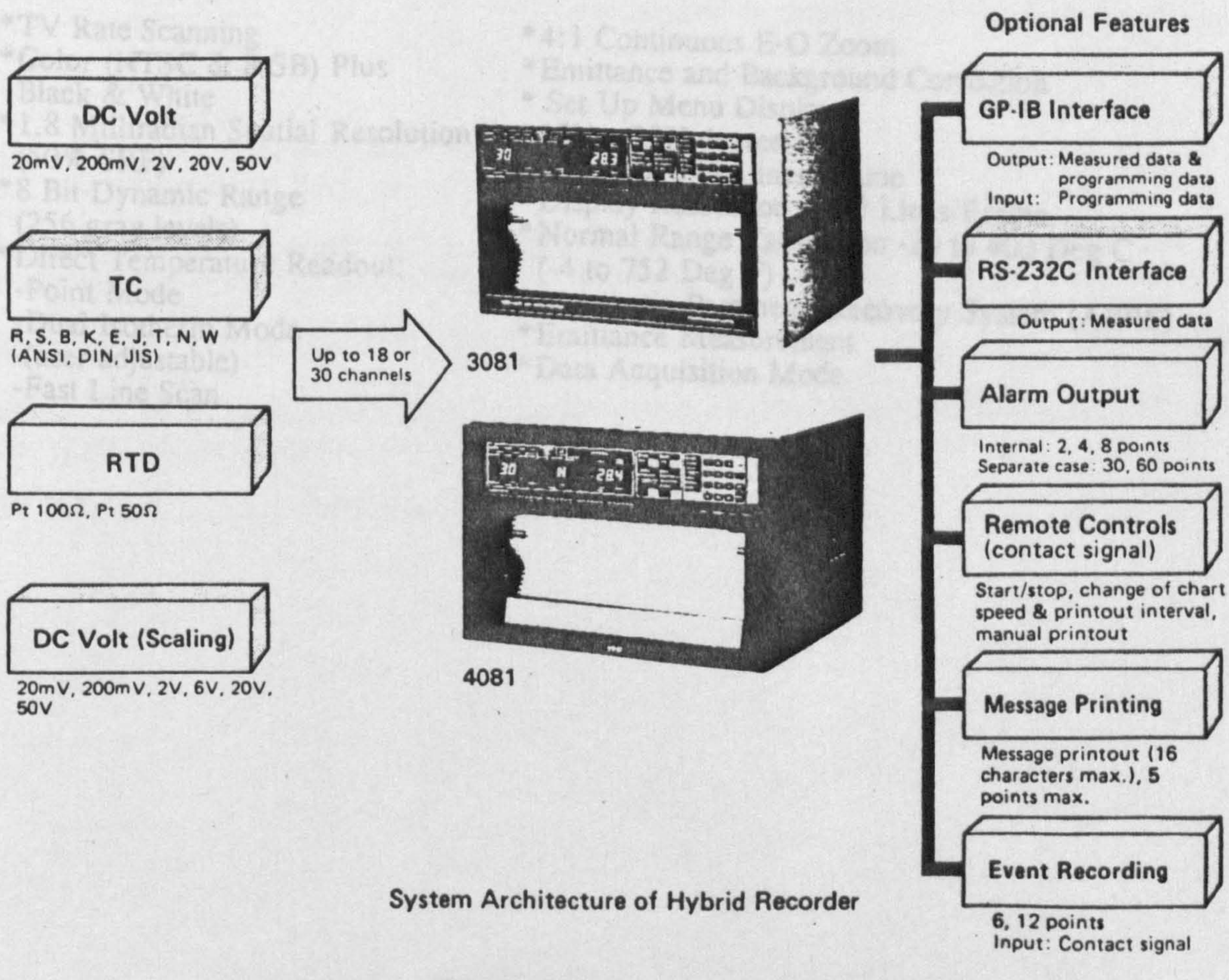

System Architecture of Hybrid Recorder

inframetrics

700 SERIES RADIOMETER SYSTEMS AND ACCESSORIES

April 1, 1992
(Rev 2, August 12, 1992)

Domestic Price List

TERMS: Net 15; Subject to Inframetrics Credit Approval and Purchase Conditions

FOB: No. Billerica, MA

SYSTEMS

(07559-206) **MODEL 740 *(8-12um)*** **$48,900.00**

The high resolution microprocessor based system features direct temperature readout with color and black and white display. A multi-purpose system for use in the field and in the laboratory.

Includes:

- *8-12um Spectral Response
- *Scanner and Control Electronics
- *1X Standard FOV Lens
- *AC Power Supply
- *Operations Manual
- *1.25M Scanner Cable
- *Shipping/Carrying Case
- *Inframetrics Closed Cycle Microcooler
- *Integral 3.5" Digital Image Recorder
- *Integral 4" Color LCD Monitor (displays live or digitally stored images)

Standard features include:

- *TV Rate Scanning
- *Color (NTSC & RGB) Plus Black & White
- *1.8 Milliradian Spatial Resolution (50% SRF)
- *8 Bit Dynamic Range (256 gray levels)
- *Direct Temperature Readout:
  - -Point Mode
  - -Dual Isotherm Mode (user adjustable)
  - -Fast Line Scan
- *4:1 Continuous E-O Zoom
- *Emittance and Background Correction
- * Set Up Menu Display
- *15V x 20H degree FOV
- *200 Active IR Lines/Frame
- *Display Resolution: 400 Lines/Frame
- *Normal Range Calibration -20 to 400 Deg C (-4 to 752 Deg F)
- *Automatic Parameter Recovery System (APRS)
- *Emittance Measurement
- *Data Acquisition Mode

(07559-200) **MODEL 760 *(8-12um)*** **$59,900.00**

The high resolution microprocessor based system features direct temperature readout with color and black and white display. A multi-purpose system for use in the field and in the laboratory.

Includes:

- *Scanner and Control Electronics
- *1X Standard FOV Lens
- *AC Power Supply
- *Operations Manual
- *Shipping/Carrying Case
- *Inframetrics Closed Cycle Microcooler
- *Integral 3.5" Digital Image Recorder
- *Integral 4" Color LCD Monitor (displays live or digitally stored images)
- *1.25M Scanner Cable

Standard features include:

- *TV Rate Scanning
- *Color (NTSC & RGB) Plus Black & White Display
- *1.8 Milliradian Spatial Resolution (50% SRF)
- *8 Bit Dynamic Range (256 gray levels)
- *Direct Temperature Readout:
  - -Point Mode
  - -Dual Isotherm Mode (user adjustable)
  - -Line Scan
  - -Fast Line San (8Khz)
- *Remote Control Interface - RS 232 Serial Communication Port
- *Sync Signal Connector
- *Digital Output Connector
- *4:1 Continuous E-O Zoom
- *Emittance and Background Correction
- *Extended Measurement Range (to 1500 Degree C)
- *Line Scan Integrator with Variable Time Constant)
- *Set Up Menu Display
- *15V x 20H degree FOV
- *200 Active IR Lines/Frame
- *Display Resolution: 400 Lines/Frame
- *Automatic Parameter Recovery System (APRS)
- *Emittance Measurement
- *Data Acquisition Mode

The Model 760 is also available with a 3-12um Broadband Detector for an additional $1,000. Wide band spectral coatings are used on the system optics to provide high optical throughput from 3-12 micrometers.

(07559-202) **MODEL 760 *(3-12um)*** **$60,900.00**

The Model 760 is also available with a 3-5um Shortwave Detector for an additional $1,000. The HgCdTe detector is peaked for response from 2.5-5um.

(07559-201) **MODEL 760 *(3-5um)*** **$60,900.00**

THE MODEL 760 INFRARED THERMAL IMAGING AND MEASUREMENT SYSTEM

Inframetrics' advanced technology makes infrared temperature measurement the reliable tool it should be for demanding research, monitoring, QC/QA and maintenance applications.

The highly versatile Model 760 infrared imaging system from Inframetrics brings new convenience, versatility, and accuracy to infrared thermal imaging and measurement. Built by the company that developed high resolution longwave imaging, the Model 760 reflects more than 15 years' experience in refining advanced infrared technology.

Simplicity of operation, functional controls and displays, exceptionally flexible data storage and management, and portability are among the designed-in advantages of these state-of-the-art Inframetrics systems. In the demanding environments of condition monitoring, testing and research, the Model 760 measures up with consistently reliable and easily obtainable results.

Modular system design and carrying vest optimize field portability.

Application-driven technology

Inframetrics pioneered high resolution infrared technology and patented the dual resonant scanning system that sets the Model 760 apart from conventional systems.

Equally important, these Inframetrics' systems are the product of "real world" input by IR users and experts, from R&D and NDT lab managers to electric power predictive maintenance teams, to process control and QC/QA professionals. In these and scores of other applications, Inframetrics' IR technology has long demonstrated its ability to measure up to demanding and diverse requirements. Now the advanced Model 760 system responds directly to user needs for next-generation measurement and imaging performance.

The result is a market-driven combination of high scan speed, excellent spatial resolution, temperature measurement accuracy and image display uniformity, as well as exceptional ruggedness. Extensive software capability makes the Model 760 even more versatile in demanding measurement analysis and long-term monitoring applications.

Another important innovation is Inframetrics' patented, NASA Space-qualified microcooler, which eliminates liquid nitrogen as a detector cooling medium, while actually improving system sensitivity and accuracy. Electric cooling gives the Model 760 the total mobility needed for large, multi-facility installations or utility surveys, and makes the system more convenient for laboratory use.

With this advanced technology, problem sources or anomalies are readily identified for timely monitoring or correction. "False positives" from solar reflections in outdoor predictive maintenance surveys — which often restrict IR systems without longwave capabilities to nighttime use — are eliminated. The Model 760 system provides 24-hour productivity. And there is no wasted time and expense spent tracking down problems that don't exist. Longwave systems are also less susceptible to image degradation from atmospheric humidity, indoors or out. You can depend upon the Inframetrics Model 760 to provide sharp, clearly superior images and accurate measurements in virtually any environment.

Optional cart with Model 760 system using 8mm VCR display unit.

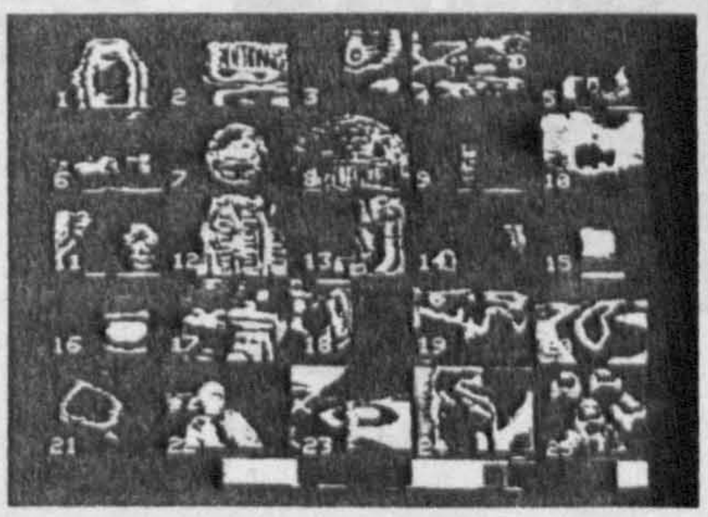

Image comparison and analysis capability is enhanced by integral disk drive 25-image directory.

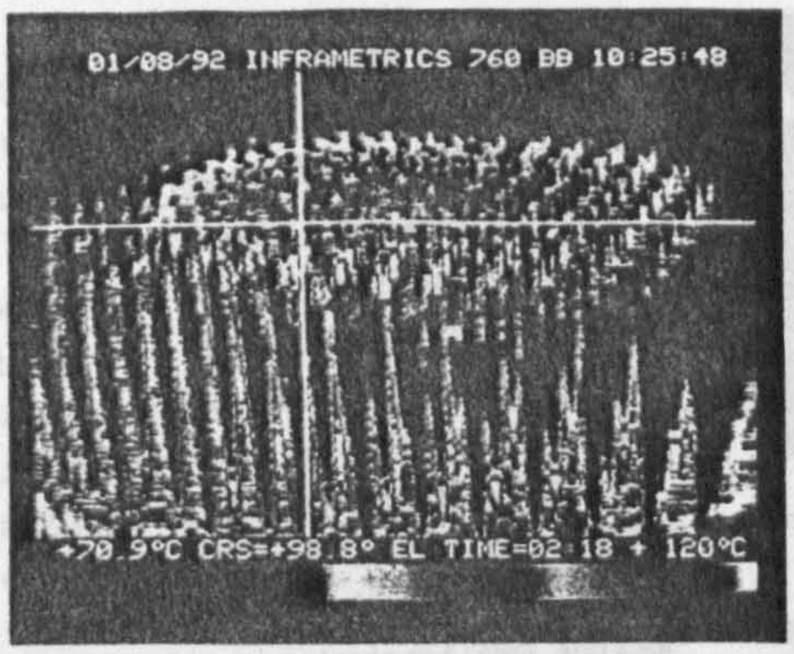

High resolution infrared images enhance R&D analysis.

Features That Enhance Performance and Ease of Use

Much more than just a thermal imaging system, the Inframetrics Model 760 *records and stores* precise measurements and high resolution images on an integral 3.5-inch floppy disk for instant, full color data analysis in the field. Multiple images can be captured and analyzed on the spot.

For increased storage and real-time image post processing capability, the Model 760 accommodates user-friendly, broadly compatible ThermaGRAM® software. Together they constitute the most flexible recording, reporting, and comparison capability in the industry. ThermaGRAM is the only image processing system that lets you load images from floppy disk, VCR, or video camera. Featuring a multiplicity of image manipulation, evaluation and data management options, ThermaGRAM also includes a full array of HELP menus, and twice the speed and resolution of conventional software packages.

With ThermaGRAM the user may compare multiple images, track and measure high-speed thermal transients, view thermal gradients, statistically analyze temperatures, and perform image subtraction. Unlike conventional programs, which may obscure as much as 50% of the screen with text, this exclusive Inframetrics program maximizes the image area. Information is logically arranged and presented. ThermaGRAM generates industry-standard files so you can export data and images to other programs for report generation and analysis. And a wide selection of optional, application-focused software modules further enhance productivity and performance.

From emittance correction and mapping to time vs. temperature plotting of dynamic thermal events to image archiving, database management and report generation, Inframetrics software options add exceptional value and versatility.

Digitally stored images from the Model 760 may be processed with user-friendly TherMonitor® software. Operating within the Windows® environment, TherMonitor features post image analysis, graphical trending and custom report generation capabilities.

For high digital storage and retrieval capability, the Model 760 is compatible with D*STAR, a specialized computer system that will capture up to twenty minutes of continuous full frame digital imagery and store it directly to disk. (For complete information on Inframetrics software modules, including our set-up and system test service, request our ThermaGRAM, TherMonitor or D*STAR brochure(s).)

Because the ability to look at thermal measurements from a variety of perspectives can significantly enhance its usefulness, the Model 760 offers more in-field measurement modes than any other system. Both absolute temperatures and temperature rise information can be determined quickly and easily in the field. And the user can "toggle" instantly from a stored image to a live image for immediate field comparisons.

Moreover, instead of a conventional monochrome (black and white) viewfinder the Model 760 features a large integral LCD display for color imaging in the field, and a temperature threshold palette that provides immediate "hot spot" identification during the survey. In addition,

Extensive post-processing options facilitate image comparison, trend analysis and report generation for condition monitoring and other research applications.

Model 760 flexibility: more measurement modes than any other system.

a) Black and White. Image can be displayed with or without alphanumerics. A 4:1 continuous zoom capability allows image enlargement. Complete image and alphanumeric data can be recorded for review and post-processing.

b) Color. Choose from eight color palettes, with display of up to 20 colors.

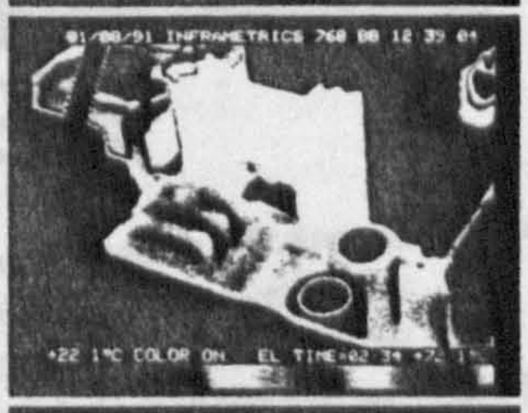

c) Point. Measure temperatures at any point on the subject selected by movable crossbairs; temperature at the intersection (CRS) is displayed in real time.

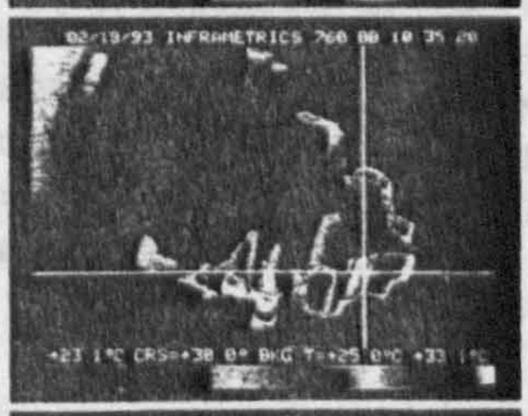

d) Line Select/Line Scan. In the Line Select mode, choose a horizontal cursor to obtain a quantitative temperature graph.

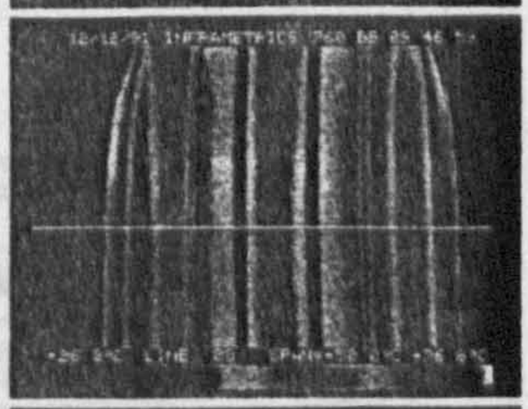

Line Scan capability presents a corresponding temperature graph across 256 points on the cursor chosen in Line Select mode.

In addition, a Fast-Line Scan mode analyzes events at 125 microsecond intervals.

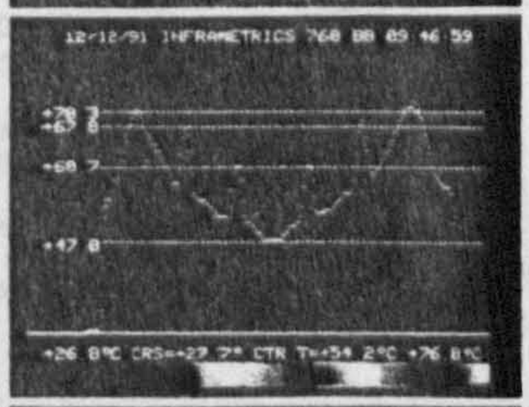

e) Dual Isotherm. Highlighted solid black and white regions identify corresponding temperatures. Ideal for comparison measurements.

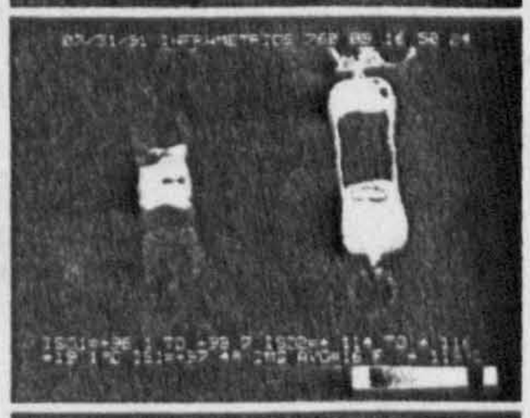

f) Area. (Average). Displays the average temperature of the region within the user-defined box.

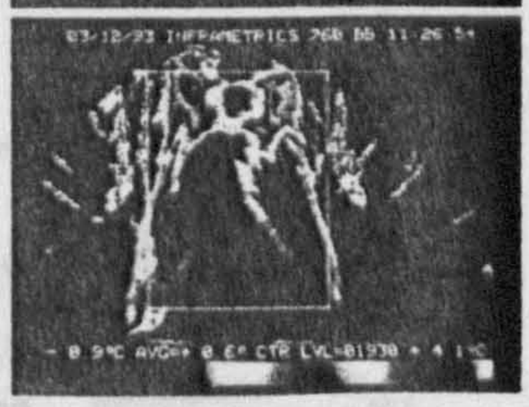

Images shown a) Gear; b) Heat Sink; c) Spindle; d) Rubber Tire; e) Resistor; f) Jacket

with the 4" LCD screen instead of a viewfinder, images are fully visible to other members of the maintenance team, or training personnel.

The Model 760 system is not only highly portable, but also provides a margin of safety for the operator, who does not have his vision limited –one eye on a viewfinder and the other eye shut– as he works in what are often constricted or hazardous spaces. An ergonomically-designed vest carries compact system components, distributing weight for operator comfort and leaving both hands free for convenience and safety. And especially important when measurements must be made in constricted areas, the system's modular concept allows the scanner to fit into tight spaces, while controls and display remain with the operator.

Still other advantages include new, highly compact optics, a filter wheel that accepts standard stock 1" filters, low power consumption and high RF resistance.

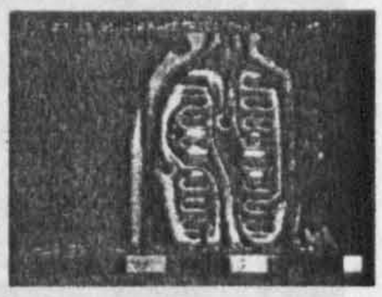

Inframetrics accuracy helps maintain high QC/QA standards in component board and IC testing.

Inframetrics: Not just systems, solutions.

There is virtually no limit to infrared measurement and imaging applications. And since each application has its own special requirements, the Model 760 is designed to be responsive to the widest array of IR measurement environments and techniques.

Part of that responsiveness is in the flexibility built into the systems and software. But IR technology is only as productive as the knowledge with which it's used. For example, knowing when to correct for emittance characteristics of certain materials and how to interpret images obtained under adverse conditions requires an understanding of infrared measurement theory and practice. That's why Inframetrics features applications support and training programs unmatched in the industry. As the only major manufacturer with fully-equipped customer training facilities, Inframetrics provides detailed 3-day instructional seminars for Model 760 users. And our highly experienced applications engineers are always available to work with you in refining your IR application protocols, or in finding ways to adapt Model 760 technology to specific needs.

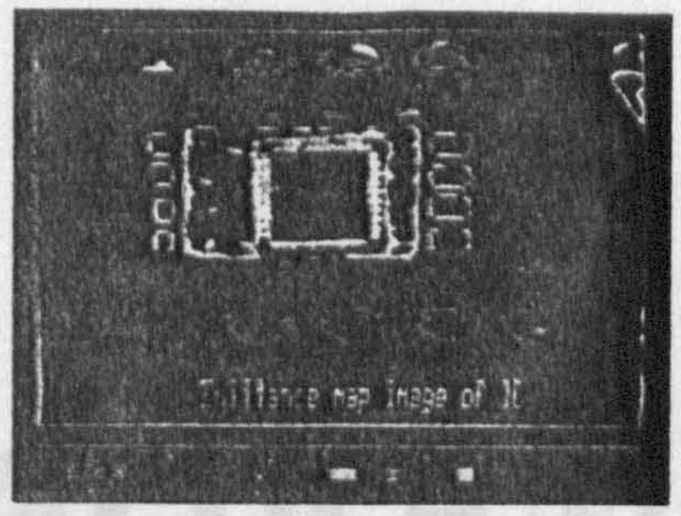

Model 760 with CIRPASS software shows calculated emittances from 0 to 100% on integrated circuit.

With the Inframetrics Model 760, you're buying not only the most advanced and flexible IR measurement and imaging system, but also the services of an exceptional customer training and technical support team. To put this team and a Model 760 system to work for you, call 508-670-5555.

Windows® is a registered trademark of Microsoft. ThermaGRAM® and TherMonitor® are registered trademarks of Thermoteknix Systems, Ltd.

IMAGING PERFORMANCE	
HFOV (DEG)	20
VFOV (DEG)	15
RESOLUTION EL. @ 50% SRF (mrad)	1.8
RESOLUTION ELEMENTS PER LINE	194
IMAGE FIELD RATE	60 Hz RS-170/NTSC or 50 Hz CCIR/PAL
ELECTRO-OPTICAL ZOOM	4:1 CONT.
DYNAMIC RANGE (BITS)	8
FOCUS RANGE	4.7" to infinity (12 cm to infinity)
MDT @ 30°C (Amb)	< 0.1°C
IR LINE RATE	7866 Hz RS-170/NTSC or 7812 Hz CCIR/PAL
VIDEO OUTPUT	RS 170/NTSC or CCIR/PAL

ENVIRONMENTAL	
OPERATING TEMP RANGE	-15 to 50°C (5 to 122°F)
POWER REQUIREMENTS	95 to 250 VAC/47 to 63 Hz or 11 to 17 VDC
VIBRATION	
OPERATING (Hz @ in DOUBLE AMPLITUDE)	5 to 22 Hz @ 0.03" (0.76 mm)
OPERATING (Hz @ G PEAK)	23 to 500 Hz @ 1.0 G
NON-OPERATING (Hz @ in DOUBLE AMPLITUDE)	5 to 22 Hz @ 0.085" (2.16 mm)
NON-OPERATING (Hz @ G PEAK)	23 to 500 Hz @ 2.0 G
NON-OPERATING (Hz @ G^2/Hz POWER SPECTRAL DENSITY)	5 to 50 Hz @ 0.04 G^2/Hz - 6 db/oct 50 to 500 Hz
SHOCK (HALF SINE 11 msec PULSE)	
OPERATING	15 G PEAK
NON-OPERATING	40 G PEAK

PHYSICAL CHARACTERISTICS	
SCANNER DIMENSIONS W/HANDLE AND W/O LENS	8.5 x 5.0 x 7.1" (21.6 x 12.7 x 18 cm)
SCANNER WEIGHT W/O LENS	6.6 lbs (3 kg)
CONTROL ELECTRONICS DIM.	10.4 x 9.3 x 6.7" (26.4 x 23.6 x 17 cm)
CONTROL ELECTRONICS WEIGHT	12.2 lbs (5.6 kg)
MONITOR DIMENSIONS	4" (10 cm) diagonal EMBEDDED
POWER SUPPLY DIMENSIONS	6.5 x 3.7 x 2.8" (16.5 x 9.5 x 7 cm)
POWER SUPPLY WEIGHT	1.5 lbs (0.7 kg)
1X LENS DIM	2.2" dia x 2.4" long (5.4 cm dia x 6.0 cm long)

FEATURES	
AUTO CENTER LEVEL	YES
FLOPPY DISK IMAGE CAPACITY	DIR + 25 IMAGES - RS/170/NTSC or DIR + 20 IMAGES - CCIR/PAL
IMAGE ANALYSIS FROM DISK	YES
GRAY SCALE IN IMAGE	YES
AUTO PARAMETER ENCODING	YES
IMAGE FREEZE	YES
MAN-PORTABLE KIT	OPT.

MEASUREMENT	
TEMP MEASUREMENT	
NORMAL	-20 to 400°C (-4 to 752°F)
EXTENDED	20 to 1500°C (68 to 2732°F)
EMITTANCE & BACKGROUND COR.	YES
FILTERS (MAX POSSIBLE)	4 OPTIONAL
ACCURACY	± 2% or 2°C

DETECTOR	
DETECTOR TYPE	HgCdTe
SPECTRAL RANGE (μm) std.	8-12
SPECTRAL RANGE (μm) opt.	3-12, 3-5

Inframetrics is committed to ongoing advancement of the state-of-the-art infrared imaging and measurement. Consequently, system specifications are subject to change.

inframetrics

The Infrared Specialists

Corporate Headquarters
16 Esquire Road
North Billerica, MA 01862
Tel: 508/670-5555
Fax: 508/667-2702

Inframetrics Brussels
Mechelse Steenweg 277
B-1800 Belgium
Tel: 32 2 252 5712
Fax: 358 200 740 760 or 32 2 252 5388

6 93 MS 10M

inframetrics

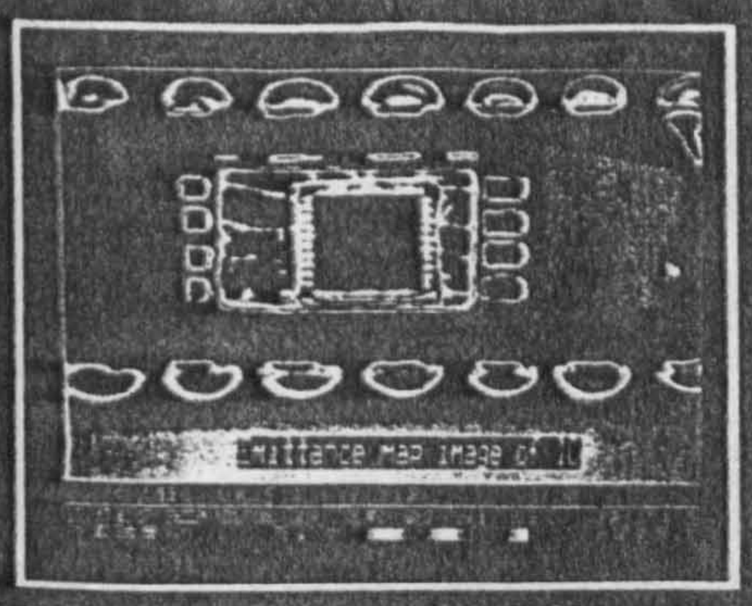

CirPASS software module displays calculated emittances from 0 to 100% on integrated circuit.

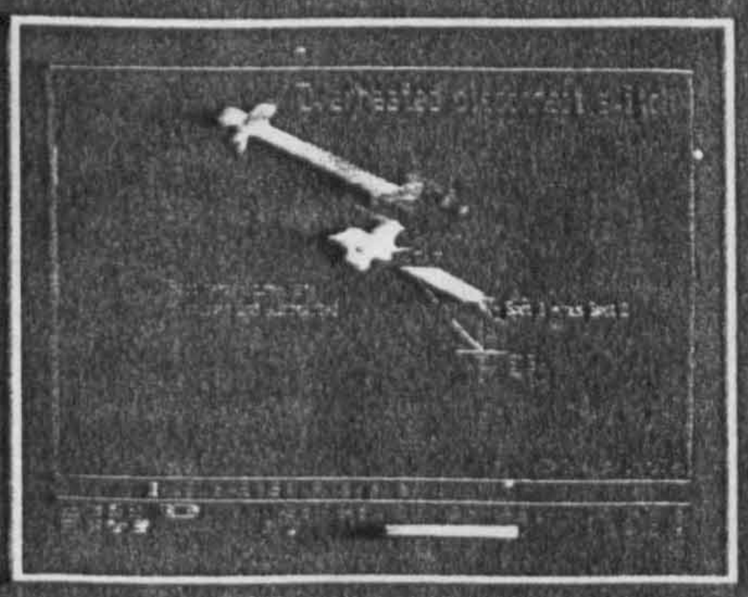

***Spot** function displays differences of up to ten temperature points or boxed areas.*

***Convolution Filtering** provides smoothing and edge enhancement on thermal patterns created by windshield defroster.*

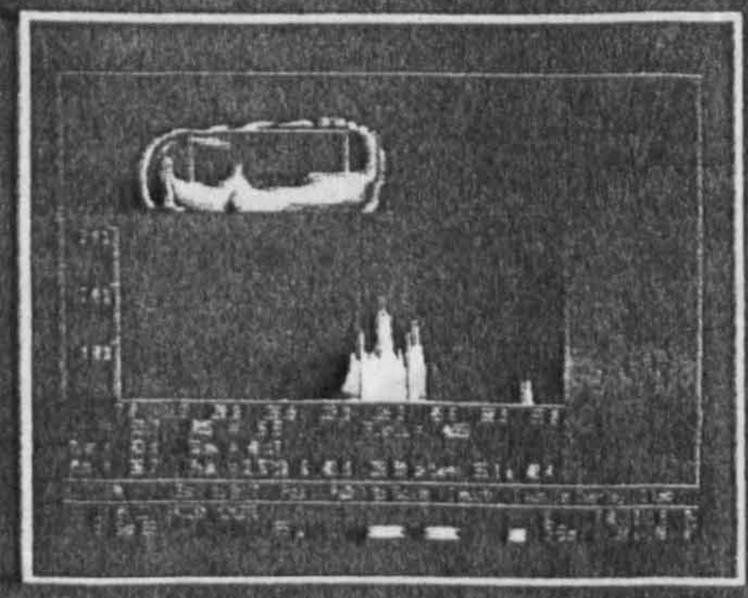

***Histograms** of up to ten areas of interest may be displayed simultaneously in real time or statically. Above, a histogram of compressor cylinder head.*

ThermaGRAM®

Thermal Image Processing System

ThermaGRAM® Thermal analysis for when you need to know all the answers.

Since 1975, when Inframetrics entered the world of infrared imaging and measurement, its thermal imaging radiometers have continued to set new standards to which others still aspire. As its microprocessor-based technology has evolved, more and better ways *to see, to quantify and to understand* have become integral to Inframetrics systems.

But despite the built-in capabilities of these remarkable systems, it soon became clear that much more data could be extracted from the wealth of information embedded in every image. An image processing program of enormous strength, virtually infinite depth and tremendous sophistication was required . . . *yet it had to run on a perfectly ordinary personal computer . . . and be easy for everyone to use and understand.*

Thus was the instant success called ThermaGRAM® created by Thermoteknix of England especially for Inframetrics. A real-time image processing system specifically designed to work with microprocessor-based thermal imaging radiometers, it is a completely integrated software/hardware package contained in an IBM compatible PC.

Infrared images from the scanner or video cassette recorder are digitized and displayed in black and white or color on a high resolution RGB monitor. All radiometer settings are encoded within the image and incorporated automatically into all temperature measurements. Everything is menu-driven With support from HELP screens at any time.

And what happens from there is dramatic and crystal clear.

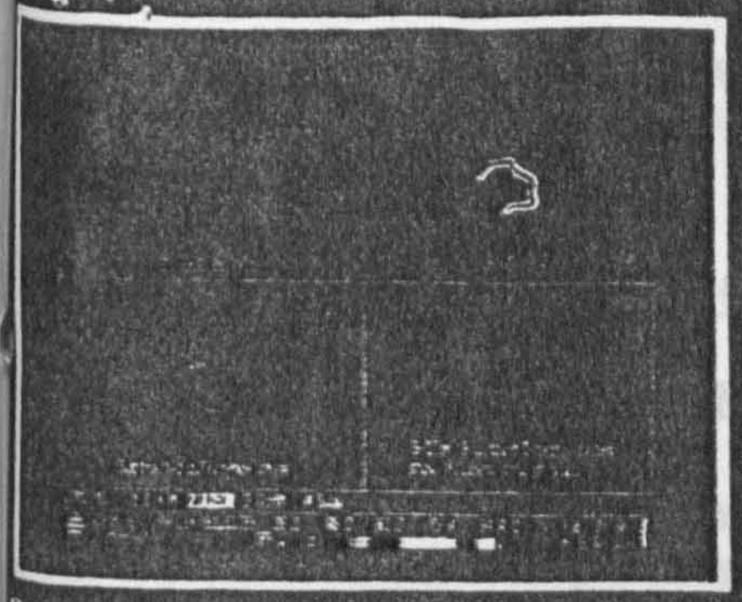

Static Image Subtraction *allows subtraction of one thermal image from another and the display of the difference.*

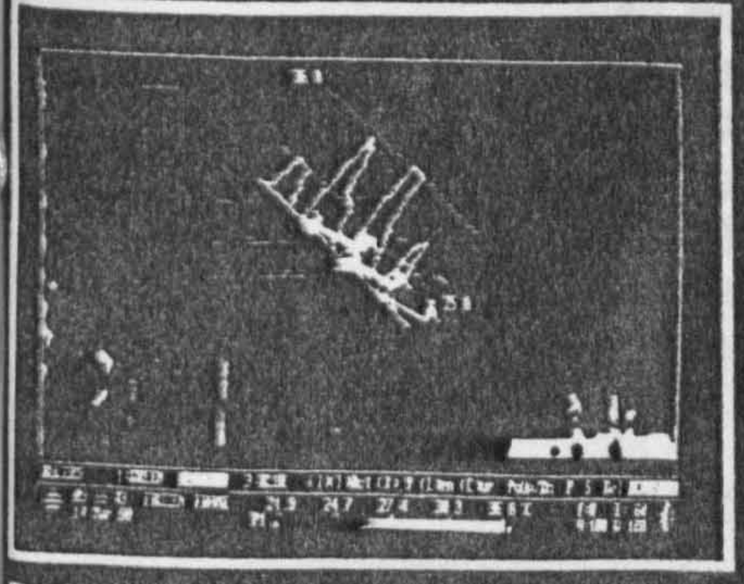

Ruler *function provides three independent rotatable line scan temperature profiles. Each ruler can also be used for measuring object sizes.*

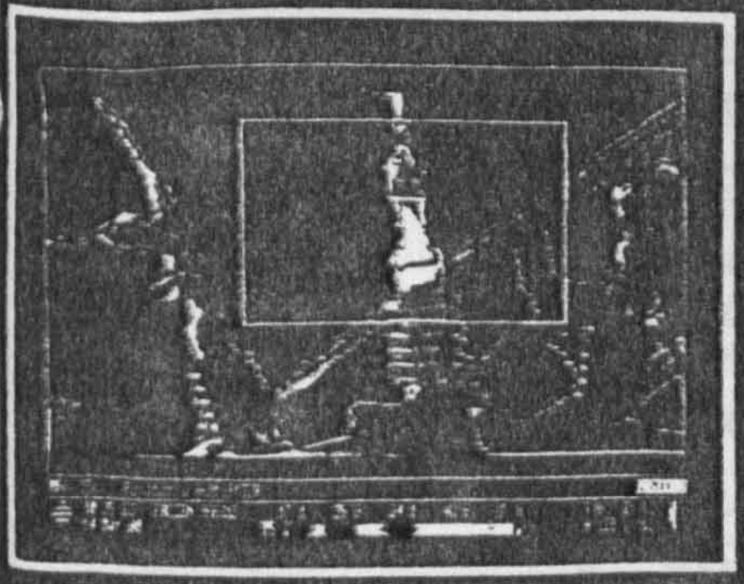

Magnification(select) *of an area anywhere within the displayed image can be accomplished by first defining area with variable size box.*

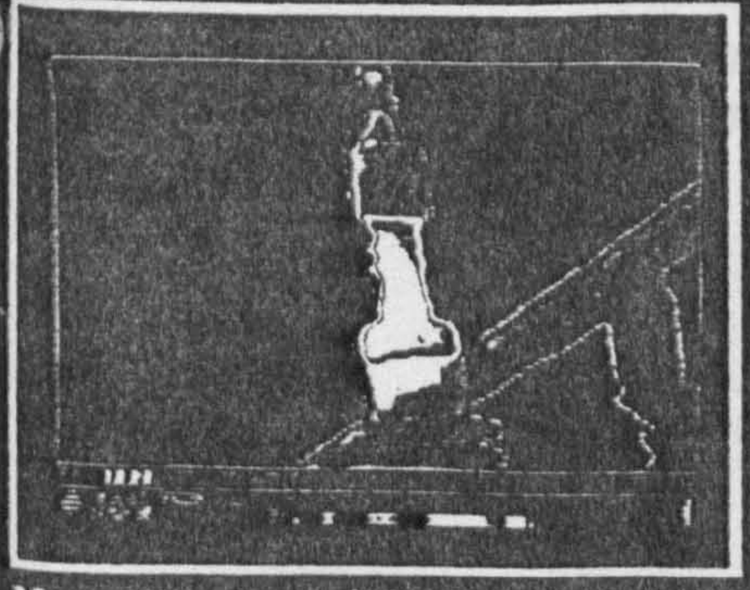

Magnification *of image area selected above with pixel interpolation.*

More features . . . more functions . . . more useful information.

The first thermal image is only the beginning. The need to analyze data after you've gathered it is ever-present. Special applications have special needs and ThermaGRAM® meets them all. You can compare multiple images, track and measure high-speed thermal transients, see a thermal gradient, perform statistical analysis of temperatures and dynamically subtract part of an image from the rest. You can see the image in 3-D. And ThermaGRAM® doesn't stop there — it takes you further than ever before in thermal analysis.

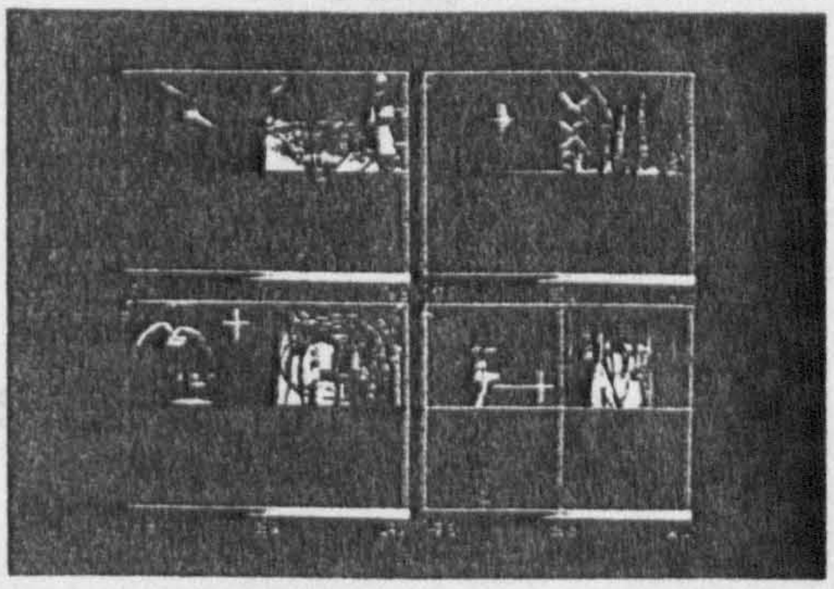

PictureBASE *shows four quadrant images, corresponding database information is displayed on an alternate screen. Each quadrant has both the thermal (IR) and visual image displayed.*

You can freeze any portion of the image while maintaining dynamic imaging throughout the remainder of the display. You may display multiple images in a quadrant for simple comparisons, while the program compensates for different images recorded at differing ranges. Thermal or visual images may be transferred from a floppy disk, VCR, VDR or still camera. All or part of an image may be magnified for fine detail. You can select from black-and-white or 128 colors (out of a possible 4096), including ten pre-defined palettes.

And if that's not enough, ThermaGRAM® offers optional software modules that allow you to tailor your equipment to your special needs more precisely than ever before.

Easier to understand, easier to use.

While other systems clutter as much as a third of their screens with data — greatly reducing the size and resolution of the image itself — ThermaGRAM® has been specifically designed to maximize the image area.

We created logical, easy-to-read layouts for the clearest of presentations. We placed spot and area measurements, logically, right next to the spots and areas being measured and added context-sensitive Help menus throughout the program. All of which adds up to ease of use second to none, and far less prone to operator error.

Compatible with a wide range of computer hardware, software and peripherals.

ThermaGRAM® meets most of the industry standards you're likely to come across. For instance, it generates standard ASCII files, so you can analyze data in other programs like Lotus 1-2-3 and MathCAD. It also supports more printers and printer features than competitive systems, including the HP Paintjet, the Canon PJ1080 and other HP printers.

Also, since ThermaGRAM® operates off of a standard video signal you can load visual images from a video or still camera, such as the Canon XAP Shot, for side by side comparison with the corresponding thermal image.

THERMAL IMAGE PROCESSING

(07560-200) THERMAGRAM SC VERSION 5.0 W/486-33 Computer & Monitor $20,900.00
$19,900.00[1]

The ThermaGRAM System is a real-time image processing system designed to work with the Inframetrics 760, 740, 600, 600L or 610 imaging radiometers. Infrared images from the scanner or video cassette recorder are digitized and displayed in black and white or color on a high resolution RGB monitor. All radiometer settings are encoded with the images and incorporated automatically into all temperature measurements. When used with a 610, only one channel at a time may be analyzed. ThermaGRAM is a completely integrated software/ hardware package contained in an IBM PC-AT compatible computer.

The system includes:

* Desktop computer with 486-33 MHz microprocessor (120/240 V 50/60 Hz)
* 8 Mb RAM
* Hard Disk: 200 Mb
* Floppy Disk Drives: 1.2 Mb 5 1/4" and 1.44 Mb 3.5"
* Super VGA graphics card: 1024 x 768 with 1Mb memory
* DOS 5.0
* Windows 3.1
* Microsoft mouse
* Excel for Windows
* 13" high resolution multisync monitor (VGA compatible)
* Thermoteknix GRAM Card with 380 x 480 (NTSC)

  or 380 X 576 (PAL) x 8 bit image and
* 760 x 480 (NTSC) or 760 x 576 (PAL) graphics resolution
* Thermoteknix ThermaGRAM V5.0 Image Processing software
* Software instruction manual
* Connecting cables

Please refer to product data sheet for complete details

Sample Calculation

In a room 3m x 4m x 2.5m in height with an unfinished wood floor, 2 litres ($0.002m^3$) of pentane is poured quietly onto the floor at an ambient temperature of 20°C. From Sect. 3.1, a pool depth of 2mm (0.002m) can be expected on raw wood. The expected pool size can be calculated by dividing the volume poured by the depth:

$$\text{Area} = \text{Volume/depth} = 0.002m^3/0.002m = 1m^2$$

On semi-porous surfaces, a maximum release rate for pentane at 20°C of 1.2 litre/s-m^2 is expected for pools on wood.

Complete (Ideal) Distribution

For a pool of $1m^2$ in area, the release rate would be 1.2litre/s. The room has a volume of $30m^3$ (30,000litres). Assuming perfect circulation and diffusion, the time required to produce a 2% concentration throughout the entire volume would be calculated from:

2% x Volume ÷ release rate = 0.02 x 30,000 litres ÷ 1.2 litre/s = 500s

Horizontal Spread

Horizontal spread can be calculated from the data in Sect. 3.7 which showed a horizontal rate for pentane of 0.05m/s. Assuming a centrally-located pour of $1m^2$ in a 3m x 4m room, the vapour layer will reach the farthest wall 1.5m away from the pool edge in 1.5m/0.05m/s , or 30s.

Filling

For filling a layer at the floor, if the entire floor ($12m^2$) were covered with fuel, the fill rate would be:

Filling rate = Area x rate/ pool area = $12m^2$ x 1.2 litre/s-m^2 = 14 litre/s

Assuming there are no floor-level leaks in the room (under doors), the time to fill a 1cm (0.01m) deep layer with a 100% pentane vapour would be:

Time = Depth x Area ÷ total vapour production rate = 0.01m x $12m^2$ ÷ 14litre/s

Time = $0.12m^3$ (= 120 litres) ÷ 14 litre/s = 8.6s

This reflects a fill rate of 0.12cm/s (0.0012m/s).

If the pool is only $1m^2$ in area, the fill rate would be proportional to pool area÷ floor area, or $1m^2/12m^2$. This produces a fill rate of only 0.01cm/s (0.0001m/s).

Filling a $12m^2$ room to 15cm (0.15m) depth with 100% vapour layer would require 1500s.

Diffusion

Over these time intervals, diffusion is occurring. If an ignition source is located at a far wall at floor level, ignition would be expected as soon as the horizontal advective flow would carry it there (30s or less after pouring). If the ignition source is located 15cm above the floor, diffusion will generate an ignitable vapour/air mixture above the saturated (100%) vapour layer. From Fig. 4.6.1, the time required to reach 2% concentration 15cm above a saturated pentane vapour layer can be estimated to be 400s.

Total Time

The total time between pouring and ignition under these conditions would then be:

Total time = horizontal spread to walls + time to establish 1cm layer across entire floor + time to diffuse to LEL = 30s + 100s + 400s = 530s

Conditions and Cautions

Because these processes are slow and easily affected by environmental features. Leaks at floor level will reduce the overall contribution to the developing layer. Reductions in ambient temperature (or allowances for evaporative cooling) will reduce the evaporation rate. The use of camping fuel will reduce evaporation rate. Draughts, a turbulent pour, or mechanical movement in the room will all increase the amount of vapour in the room and produce localized (and unpredictable) distributions of vapour/air mixtures. If these localized plumes of vapour occur in the vicinity of a competent ignition source, there can be ignition before the time predicted here.